


# Detailled Program-Book of abstracts

# Contents


**1 Sunday, 20th July** **3**

**2 Monday, 21st July** **4**

**3 Tuesday, 22nd July** **7**

**4 Wednesday, 23rd July** **10**

**5 Thursday, 24th July** **13**

**6 Friday, 25th July** **16**

**7 Speaker List** **17**

**8 Abstracts of oral presentations** **20**

**9 Program of Poster Session #1** **93**

**10 Program of Poster Session #2** **177**

**11 Program of Poster Session #3** **258**

**12 Program of Poster Session #4** **340**

# Sunday, 20th July

**17:00–21:00**

**Welcome Reception,**
**Conference Material Distribution,**
**Key Collection for Dormitory Rooms**
**Room:** Grand Hall Pouillon

# Monday, 21st July

**08:15–09:10**

**Welcome and Opening Ceremony:**

- Laurence Mouret, Dean of the Faculty of Sciences;
- Sander Nijdam, Chair of ICPIG 2025 ISC
- Gilles Cartry, Chair of ICPIG 2025 LOC

**09:10–09:55**

**Room:** Amphitheatre Portalis
**Session Chair:** Sander Nijdam

- **General invited lecture**
  Speaker: Jean-Paul Booth
  *In-situ measurement of surface reaction probabilities in low-pressure plasmas*

**09:55–10:25**

**Coffee Break** (outdoor plaza)

## Parallel session #1 – 10:25–12:15

**Room:** Amphitheatre Mirabau
**Chair:** Jean-Paul Booth

**10:25–10:55**

- **Topical invited lecture**
  Speaker: Alexandre Nominé
  *The Rising Importance of Sustainability: Opportunities for Plasma Processes*

**10:55–11:15**

- Speaker: Sophie Bois
  *Experimental and numerical study of* $CO_2/H_2$ *DC glow and pulsed RF discharges*

**11:15–11:35**

- Speaker: Fitriani Sukma Wahyu
  *Application of Machine Learning for Plasma Enhanced Chemical Vapor Deposition of Thin Film*

**11:35–11:55**

- Speaker: Agnès Granier
  *Time-resolved diagnostics of misty plasmas used for nanocomposite thin film deposition*

**11:55–12:15**

- Speaker: Naik Bibekananda
  *Hydrogen Negative Ion Production in an ECR-Based Large-Area Plasma Source for Fusion Applications*

## Parallel session #2 – 10:25–12:15

**Room:** Amphitheatre Portalis
**Chair:** Gerard Van Rooij

**10:25–10:55**

- **Topical invited lecture**
  Speaker: Judith Golda
  $H_2O_2$ *production in atmospheric pressure plasmas for plasma-assisted biocatalysis*

**10:55–11:15**

- Speaker: Inagaki Yoshinobu
  *Relative reaction constants of hydrated electrons in the region below the plasma-water interface*

**11:15–11:35**

- Speaker: Tiago C. Dias
  *The role of liquid layers as a circuit element in plasma activated solution chemistry*

**11:35–11:55**

- Speaker: Pankaj Pareek
  *Transient spark discharge and ozone-based nitrogen fixation: the study of reaction pathways*

**11:55–12:15**

- Speaker: Calum Ryan
  *Uncovering the Role of multi-Phase electro-hydrodynamics in plasma-induced liquid flows*

**12:15–13:45**

**Lunch Break** (outdoor plaza)
**ICPIG ISC Meeting** (council room)

**13:45–15:45**

**Room:** Grand Hall Pouillon
**Poster session #1**

**15:45–16:05**

**Coffee Break** (outdoor plaza)

## Parallel session #3 – 16:05–18:35

**Room:** Amphitheatre Mirabau
**Session Chair:** Zoltan Donkó

**16:05–16:35**

- **Topical invited lecture**
  Speaker: Suzuki Haruka
  *3D reconstruction of plasma emission and sheath structures based on tomography using multi-view images*

**16:35–17:05**

- **Topical invited lecture**
  Speaker: Kawaguchi Satoru
  *Electron transport in O2 and O2-Ar mixtures: electron collision cross section set of O2 and Monte Carlo simulation*

**17:05–17:35**

- **Topical invited lecture**
  Speaker: Gwenael Fubiani
  *Particle-In-Cell Modelling of Low Temperature Plasmas*

**17:35–18:05**

- **Topical invited lecture**
  Speaker: Tsanko Tsankov
  *Machine-learning-aided spectroscopy of low-temperature plasmas*

**18:05–18:35**

- **Topical invited lecture**
  Speaker: Ursel Fantz
  *Challenges of negative hydrogen ion sources for ITER's neutral beam systems*

## Parallel session #4 – 16:05–18:35

**Room:** Amphitheatre Portalis
**Session Chair:** Rémi Dussart

**16:05–16:35**

- **Topical invited lecture**
  Speaker: Milan Şimek
  *Transient plasmas in liquid water and at the liquid-gas interfaces: from fundamental discharge physics to nitrogen fixation*

**16:35–17:05**

- **Topical invited lecture**
  Speaker: Martina Modic
  *Atmospheric pressure air plasma for removal and detoxification of emerging genotoxic wastewater pollutants*

**17:05–17:35**

- **Topical invited lecture**
  Speaker: Nevena Puac
  *Influence of Plasma Activated Water (PAW) chemistry on physiology of plant calli and on bacterial susceptibility to antibiotics*

**17:35–18:05**

- **Topical invited lecture**
  Speaker: Luca Matteo Martini
  *Understanding the role of the catalyst support in plasma-catalysis*

**18:05–18:35**

- **Topical invited lecture**
  Speaker: Paolo Francesco Ambrico
  *From Spark to Sprout: Diagnostic Pathways in Plasma-Enabled Agriculture*

# Tuesday, 22nd July

**08:30–09:15**

**Room:** Amphitheatre Portalis
**Session Chair:** Isabel Tanarro

- **General invited lecture**
  Speaker: Davide Mariotti
  *Bulk to atoms and back*

**09:15–10:00**

**Room:** Amphitheatre Portalis
**Session Chair:** Isabel Tanarro

- **General invited lecture**
  Speaker: Zoltan Donkó
  *Secondary electron emission effects in low-pressure discharges*

**10:00–10:30**

**Coffee Break** (outdoor plaza)

## Parallel session #5 – 10:30–12:20

**Room:** Amphitheatre Mirabau
**Chair:** Shinichi Namba

**10:30–11:00**

- **Topical invited lecture**
  Speaker: Ryo Ono
  *Laser-based characterization of single filament streamers: A novel approach tos treamer discharge analysis*

**11:00–11:20**

- Speaker: Alexandra Brisset
  *VUV absorption spectroscopy for ultrafast TALIF calibration and mw plasma jet characterisation*

**11:20–11:40**

- Speaker: Nikita Lepikhin
  *A Laser Optical Loop for faster laser based measurements*

**11:40–12:00**

- Speaker: Dimitros Stefas
  *Advanced optical studies on a pin-dielectric-plane air discharge*

**12:00–12:20**

- Speaker: Marios Kounalakis
  *Probing the dynamics of high-pressure nanosecond pulsed discharges with non-linear non-resonant laser diagnostics*

## Parallel session #6 – 10:30–12:20

**Room:** Amphitheatre Portalis
**Chair:** Stvetlana Starikovskaia

**10:30–11:00**

- **Topical invited lecture**
  Speaker: Gerard Van Rooij
  *Plasma Chemistry for the Energy and Materials Transition of the Process Industry*

**11:00–11:20**

- Speaker: Cas Van Deursen
  *Preheating applied on a 915 MHz $CO_2$ Microwave Plasma: Unlocking the Potential for heat recycling in plasma systems*

**11:20–11:40**

- Speaker: Christain Busch
  *Nanosecond resolved $CO_2/N_2$ vibrational kinetics in a pulsed discharge investigated experimentally and by modeling*

**11:40–12:00**

- Speaker: Zdenko Machala
  *Indoor air decontamination by non-thermal DBD plasma and photocatalysis*

**12:00–12:20**

- Speaker: Anton Nikiforov
  *Plasma-generated atomic oxygen for contactless cleaning of cultural heritage objects*

**12:20–13:45**

**Lunch Break** (outdoor plaza)
**PSST AE meeting** (council room)

**13:45–14:30**

**Room:** Amphitheatre Portalis
**Session Chair:** Lénaïc Couëdel

- **General invited lecture**
  Speaker: Isabelle Regner

**14:30–16:10**
**Room:** Grand Hall Pouillon
**Poster session #2**

**16:10–16:30**
**Coffee Break**

## Special session– 16:10–18:35

**Room:** Amphitheatre Portalis
**Chairs:** Deborah O'Connell and Timo Gans

**16:30–16:55**

- **Topical invited lecture**
  Speaker: Deborah O'Connell and Timo Gans
  *Tribute to Bill Graham*

**16:55–17:20**

- Speaker: Tom Morgan
  *Professor Bill Graham: His Science Over Five Decades [Abridged Version]*

**17:20–17:45**

- Speaker: Cormac Corr
  *Diagnosing Technological Plasmas: A tribute to Professor Bill Graham*

**17:45–18:10**

- Speaker: Pascal Chabert
  *Iodine Plasmas: from Belfast to Space*

**18:10–18:35**

- Speaker: Tomoyuki Murakami
  *Plasma Chemistry and its Biological Applications: Always Passion.*

# Wednesday, 23rd July

## Parallel session #7 – 08:30–10:10

**Room:** Amphitheatre Mirabeau
**Chairs:** Davide Mariotti

**08:30–09:00**

- **Topical invited lecture**
  Speaker: Eduardo Ahedo
  *Numerical investigation of open problems in Hall thruster physics*

**09:00–09:30**

- **Topical invited lecture**
  Speaker: Svetlana Starikovskaia
  *Measurements of G-value at high electric fields in pulsed nanosecond discharge*

**09:30–09:50**

- Speaker: Julien Herbelot
  *EFILE: a diagnostic to measure electric field in a magnetized plasma column*

**09:50–10:10**

- Speaker: Takenao Sato
  *Phase-Resolved Measurement of electric-field-induced second harmonics for determining electric field polarity*

## Parallel session #8 – 08:30–10:10

**Room:** Amphitheatre Portalis
**Chairs:** Vasco Guerra

**08:30–09:00**

- **Topical invited lecture**
  Speaker: Francisco J Gordillo-Vazquez
  *Streamer corona electrical discharges in thunderclouds: New discoveries and possible impact in the atmosphere*

**09:00–09:30**

- **Topical invited lecture**
  Speaker: Shinichi Namba
  *Generation of high-density Ar cascade arc plasma for plasma window and its application to electron beam engineering in air*

**09:30–09:50**

- Speaker: Thomas Orriere
  *High-speed Particle Image Velocimetry of ionic wind generated between two plates in air at atmospheric pressure*

**09:50–10:10**

- Speaker: Ivan Tsonev
  *Re-defining the minimum energy cost for nitrogen fixation into NO in atmospheric pressure air plasma*

**10:10–10:40**

**Coffee Break** (outdoor plaza)

## Parallel session #9 – 10:40–12:00

**Room:** Amphitheatre Mirabeau
**Chairs:** Gwenael Fubiani

**10:40–11:00**

- Speaker: Mark Kushner
  *Particle Distribution Functions in EUV Produced Plasmas*

**11:00–11:20**

- Speaker: Laurent Garrigues
  *Simulation of magnetized RF capacitively coupled plasma discharges using 3D sparse Particle-In-Cell algorithms*

**11:20–11:40**

- Speaker: Inna Orel
  *Experimental derivation of electrical characteristics of a* $He/N_2$ *RF APPJ compared with PIC/MCC simulation*

**11:40–12:00**

- Speaker: Emilie Despiau-Pujo
  *Multiscale hybrid modeling of DF-CCP* $CF_4$ *plasmas for carbon resist microlens etching*

## Parallel session #10 – 10:40–12:00

**Room:** Amphitheatre Portalis
**Chairs:** Milan Şimek

**10:40–11:00**

- Speaker: Toshiro Kaneko
  *Analysis of short-lived reactive nitrogen species using gas-liquid interfacial plasma with high-speed liquid flow*

**11:00–11:20**

- Speaker: Arora Garima
  *Optical and Electrical Characteristics of Bipolar Nanosecond Electrical Discharge at the Water-Air Interface*

**11:20–11:40**

- Speaker: Lex Kuijpers
  *Microwave plasma-based dry reforming of methane: showing the role of radical reactions in the afterglow*

**11:40–12:00**

- Speaker: Maria Mitrou
  *In-situ nanoparticle size characterization in an arc discharge using coherent Rayleigh-Brillouin scattering*

**12:00–13:30**

**Lunch Box**

## Excursions – 13:30–19:00

**13:30–19:00**

ITER visit #1

OR

**13:30–19:00**

Boat Tour in the Callanques

# Thursday, 24th July

**08:30–09:15**

**Room:** Amphitheatre Portalis
**Session Chair:** Francisco J Gordillo-Vazquez

- **General invited lecture**
  Speaker: Toyoda Hirotaka
  *Diagnostics of high-energy species in plasma*

**09:15–10:00**

**Room:** Amphitheatre Portalis
**Session Chair:** Francisco J Gordillo-Vazquez

- **General invited lecture**
  Speaker: Isabel Tanarro
  *Ion chemistry in C2H2/Ar cold plasmas: the dramatic effects of* $N_2$ *addition*

**10:00–10:30**

**Coffee Break** (outdoor plaza)

## Parallel session #11 – 10:30–12:10

**Room:** Amphitheatre Mirabau
**Chair:** Suzuki Haruka

**10:30–11:00**

- **Topical invited lecture**
  Speaker: Vladimir Kolobov
  *Self-organization processes in low-temperature plasmas*

**10:30–11:30**

- **Topical invited lecture**
  Speaker: Matjaz Panjan
  *Illuminating plasma self-organization of magnetron sputtering discharges*

**11:30–11:50**

- Speaker: Chris Phong Van Nguyen
  *Millimeter-scale 3D Plasma Sheath Lenses*

**11:50–12:10**

- Speaker: Charlie Kniebe-Evans
  *Spatially resolved cavity ringdown spectroscopy studies on low pressure oxygen plasmas*

## Parallel session #12 – 10:30–12:10

**Room:** Amphitheatre Portalis
**Chair:** Judith Golda

**10:30–11:00**

- **Topical invited lecture**
  Speaker: Chen She
  *Investigating Plasma-Catalyst Synergy via Multi-Diagnostic Techniques*

**11:00–11:30**

- **Topical invited lecture**
  Speaker: Vasco Guerra
  *Delayed CO2 dissociation in nanosecond discharges*

**11:30–11:50**

- Speaker: Igor Adamovich
  *Kinetics of Excited Metastable Species and Ionization in a Ns Pulse Discharge Afterglow*

**11:50–12:10**

- Speaker: Luka Hansen
  *Vacuum UV spectroscopy at atmospheric pressure plasmas utilizing silicon nitride membranes*

**12:10–13:40**

**Lunch Break** (outdoor plaza)
**ESCAMPIG ISC Meeting** (council room)

**13:40–15:40**
**Room:** Grand Hall Pouillon
**Poster session #3**

**15:40–16:00**
**Coffee Break**

## Parallel session #13 – 16:00–17:40

**Room:** Amphitheatre Mirabau
**Chair:** Tsanko Tsankov

**16:00–16:30**

- **Topical invited lecture**
  Speaker: Rémi Dussart
  *Plasma interactions with a surface cooled to a cryogenic temperature*

**16:30–17:00**

- **Topical invited lecture**
  Speaker: Andrey Starikovski
  *Physics and chemistry of nonequilibrium plasma formation in pulsed discharges*

**17:00–17:20**

- Speaker: Kunihiro Kamataki
  *Effects of Rectangular Amplitude Modulated Radio Frequency Capacitively Coupled Plasma on Electron Heating: Simulations and Experiments*

**17:20–17:40**

- Speaker: Feng Chan
  *Field reversals in low pressure capacitively coupled plasma discharges driven by tailored voltage waveforms*

## Parallel session #14 – 16:00–17:40

**Room:** Amphitheatre Portalis
**Chair:** Luca Matteo Martini

**16:00–16:30**

- **Topical invited lecture**
  Speaker: Karol Hensel
  *Removal of hydrocarbons by plasma-catalysis, catalysts regeneration and reuse*

**16:30–17:00**

- **Topical invited lecture**
  Speaker: Hae June Lee
  *High-performance particle-in-cell plasma simulation for the investigation of the nonlinear sheath dynamics and its effect on plasma uniformity in RF capacitively coupled plasmas*

**17:00–17:20**

- Speaker: Thomas Vazquez
  *NRP Discharge Temperature Evolution in a $CH_4/N_2$ mixture*

**17:20–17:40**

- Speaker: Emile Carbone
  *Nanosecond Discharge with Droplet: fundamental and synthesis of silver Nanomaterials*

**17:40–18:25**

**Free time**

**18:25–19:55**

**Art exhibition**
**Apéritif**
**Location:** Hôtel de Caumont

**19:55–23:55**

**Lyric concert**
**Gala diner**
**Location:** Hôtel de Caumont

# Friday, 25th July

**09:30–11:15**
**Room:** Grand Hall Pouillon
**Poster session #4**

**11:15–11:30**

**Coffee Break**

**11:30–12:15**

**Room:** Amphitheatre Portalis
**Session Chair:** Toyoda Hirotaka

- **Von Engel and Franklin prize lecture**
  Speaker: Ute Ebert
  *Understanding streamer discharges: where do we stand?*

**12:15–12:45**

**Poster Prize and Closing Ceremony:**

**12:45–13:30**

**Lunch Box**

## Excursions – 13:30–19:00

**13:30–19:00**

ITER visit #2

# Speaker List


- Igor Adamovich ..... 21
- Eduardo Ahedo ..... 22
- Paolo Francesco Ambrico ..... 23
- Naik Bibekananda ..... 24
- Sophie Bois ..... 25
- Jean-Paul Booth ..... 26
- Alexandra Brisset ..... 27
- Christain Busch ..... 28
- Emile Carbone ..... 29
- Pascal Chabert ..... 30
- Feng Chan ..... 31
- Cormac Corr ..... 32
- Emilie Despiau-Pujo ..... 33
- Cas Van Deursen ..... 34
- Tiago C. Dias ..... 35
- Zoltan Donkó ..... 36
- Rémi Dussart ..... 37
- Ute Ebert ..... 38
- Ursel Fantz ..... 39
- Gwenael Fubiani ..... 40
- Arora Garima ..... 41
- Laurent Garrigues ..... 42
- Judith Golda ..... 43
- Francisco J. Gordillo-Vazquez ..... 44
- Agnès Granier ..... 45
- Vasco Guerra ..... 46
- Luka Hansen ..... 47
- Suzuki Haruka ..... 48
- Karol Hensel ..... 49
- Julien Herbelot ..... 50
- Toyoda Hirotaka ..... 51

- Kunihiro Kamataki ..... 52
- Toshiro Kaneko ..... 53
- Charlie Kniebe-Evans ..... 54
- Vladimir Kolobov ..... 55
- Marios Kounalakis ..... 56
- Lex Kuijpers ..... 57
- Mark Kushner ..... 58
- Hae June Lee ..... 59
- Nikita Lepikhin ..... 60
- Zdenko Machala ..... 61
- Davide Mariotti ..... 62
- Luca Matteo Martini ..... 63
- Maria Mitrou ..... 64
- Martina Modic ..... 65
- Tom Morgan ..... 66
- Tomoyuki Murakami ..... 67
- Shinichi Namba ..... 68
- Chris Phong Van Nguyen ..... 69
- Anton Nikiforov ..... 70
- Alexandre Nominé ..... 71
- Ryo Ono ..... 72
- Inna Orel ..... 73
- Thomas Orrière ..... 74
- Matjaz Panjan ..... 75
- Pankaj Pareek ..... 76
- Nevena Puac ..... 77
- Isabelle Regner ..... 78
- Gerard Van Rooij ..... 78
- Calum Ryan ..... 79
- Takeneo Sato ..... 80
- Kawaguchi Satoru ..... 81
- Milan Şimek ..... 82
- Chen She ..... 83

- Svetlana Starikovskaia ..... 84
- Andrey Starikovski ..... 85
- Dimitros Stefas ..... 86
- Isabel Tanarro ..... 87
- Tsanko Tsankov ..... 88
- Ivan Tsonev ..... 89
- Thomas Vazquez ..... 90
- Fitriani Sukma Wahyu ..... 91
- Inagaki Yoshinobu ..... 92

# Abstracts of oral presentations

# Kinetics of Excited Metastable Species and Ionization in a Ns Pulse Discharge Afterglow

S. Raskar[1], H. Telfah[1], and I. V. Adamovich[1]

[1] *Department of Mechanical and Aerospace Engineering, The Ohio State University, Columbus, OH, USA*

Time-resolved, absolute populations of metastable nitrogen molecules, $N_2(A^3\Sigma_u^+,v=0,1)$, nitrogen atoms, $N(^2D,^2P)$, and molecular ions, $N_2^+(X^2\Sigma_g^+,v=0)$, as well as gas temperature, are measured in nitrogen in a heated plasma flow reactor, at T=300-1000 K. The measurement results are compared to kinetic modeling predictions, illustrating kinetic processes controlling the energy transfer and ionization in the afterglow.

Associative ionization processes of air species in nonequilibrium plasmas, involving metastable states, have been studied extensively in the past [1]. However, time-resolved experimental data on the kinetics of these processes are relatively scarce [2]. In the present work, the kinetics of ionization are studied in a pulsed discharge sustained in a high-pressure plasma flow reactor, which generates metastable species that serve as ionization precursors in the afterglow. Measurements of excited species over a range of temperatures, at well characterized conditions, are critical for the quantitative insight into plasma chemistry. The focus of the present study is the generation of the excited metastable states of nitrogen, as well as nitrogen molecular ions. The main objective is to produce N atoms, both in the ground electronic state and excited metastable states, and to isolate the associative ionization processes generating $N_2^+$ ions.

Time-resolved, absolute populations of metastable nitrogen molecules, $N_2(A^3\Sigma_u^+,v=0,1)$, nitrogen atoms, $N(^2D,^2P)$, and molecular ions, $N_2^+(X^2\Sigma_g^+,v=0)$, as well as the gas temperature, are measured in nitrogen in a heated plasma flow reactor with optical access for laser diagnostics, at T=300-1000 K. $N_2(A)$ populations are also measured in $N_2$-NO mixtures. The flow in the reactor is excited by the ns pulse discharge bursts operated at a high pulse repetition rate, up to 100 kHz, generating a diffuse plasma with well-defined boundaries. The measurements are made by the cw Tunable Diode Laser Absorption Spectroscopy (TDLAS) [3] and pulsed UV Cavity Ring Down Spectroscopy (CRDS) [4]. Metastable atoms are measured by the Atomic Resonance Absorption Spectroscopy (ARAS), using the vacuum UV emission near 149 nm and 174 nm, produced by a probe ns pulse discharge. The measurement results are compared to the kinetic modeling predictions, illustrating the underlying kinetic processes. The $N_2(A)$ populations decay significantly during the burst, mainly due to quenching by the ground state N atoms, generating $N(^2D,^2P)$ atoms. The metastable atoms, $N(^2D,^2P)$, accumulate during the burst and decay in the afterglow due to quenching by $N_2$ and N atoms. Time-resolved $N_2^+$ measurements in the afterglow exhibit a transient rise with a subsequent decay, most likely controlled by the shift of quasi-equilibrium in the $N_2^+ - N_4^+$ ion conversion reaction. On this time scale, the effect of associative ionization on the electron and ion density appears insignificant. Future work will include metastable species and ionization measurements in $N_2$-$O_2$ mixtures.

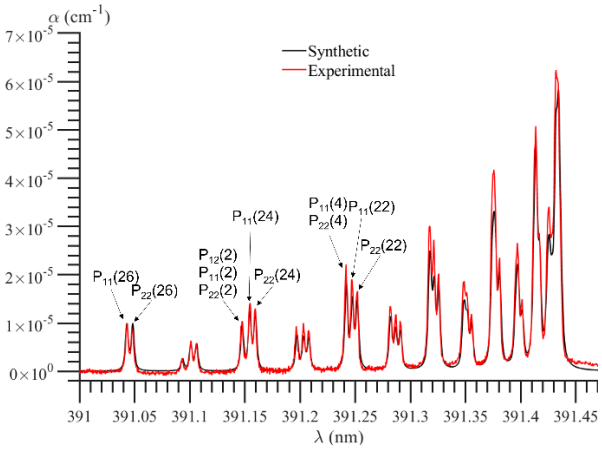



Figure 1. CRDS spectrum of $N_2^+(v=0)$. Nitrogen, P=100 Torr, T=1000 K, 15 μs after a 60-pulse, 100 kHz discharge burst.

The support of the US Office of Naval Research is gratefully acknowledged.

## References

[1] Popov, N.A., *Plasma Physics Reports* **35** 436-449 (2009)

[2] Sadeghi, N., Foissac, C., and Supiot, P., *Journal of Physics D: Applied Physics* **34** 1779-1788 (2001)

[3] Jans, E.R., Raskar, S., Yang, X., and Adamovich, I.V., *Plasma Sources Science and Technology* **30**, 025003 (2021)

[4] Yalin, A.P., Zare, R.N., Laux, C.O., and Kruger, C.H., *Applied Physics Letters* **81** 1408-1410 (2002)

# Numerical investigation of open problems in Hall thruster physics

E. Ahedo, A. Marín-Cebrián, G. Cuerva-Lázaro

*Universidad Carlos III de Madrid, Departamento de Ingeniería Aeroespacial, Leganés 28911, Spain*

The complex plasma physics in the Hall effect thruster discharge are still not fully understood, hindering the development of predictive and efficient simulation tools. The main open problems are related to the weak-collisionality of the discharge and the presence of several instabilities. Both affect much thruster performances. A particle-in-cell 2D code is used to investigate these phenomena.

The Hall-effect thruster (HET), which belongs to the family of electromagnetic plasma thrusters, is becoming the dominant technology for in-space propulsion, including the ambitious plans for missions to the Moon and Mars [1]. Despite its successful flight history and brilliant perspectives, some relevant physics of the HET plasma discharge are still not well understood. This is preventing the development of predictive models and codes, which are very necessary for improving new prototypes and fundamentally to shorten their qualification in long and costly test campaigns, a serious bottleneck in new thrusters with high power requirements and long lifetime.

Since several decades, the main open problems are related to the weak collisionality of the discharge and the non-linear saturation of plasma instabilities. Weak plasma collisionality implies that plasma species are not in thermodynamic equilibrium. Therefore, kinetic formulations are necessary to obtain their velocity distribution functions and accurate determination of plasma losses into the thruster walls. The large relative drift between the magnetized electrons and unmagnetized ions in the azimuthal direction of the HET is a source of several families of plasma instabilities, typical of ExB plasmas. Some of them give rise to an anomalous electron transport that affects much the thruster performances.

This lecture will discuss our recent findings with PICASO. This is a 2D-3V particle-in-cell code designed to tackle the above two problems in two different configurations: axial-radial (2Dzr) to determine plasma-wall interaction and macroscopic behaviour, and axial-azimuthal (2Dz$\theta$) to investigate instabilities and the related anomalous transport. In both cases, the focus is on electron dynamics, which play the central roles. Numerical challenges, such as dealing with the very thin Debye length and the very slow neutral dynamics will be addressed too [2].

The 2Dzr simulations of the thruster and near plume show a non-Maxwellian electron response, including a partial depletion of the tails of the electron VDF due to wall collection. Finite Larmor radius effects, disregarded in classical drift-diffusive formulations, are found to be relevant in the azimuthal momentum equation. A study of the energy flux vector reveals that the resulting heat flux vector is far from classical Fourier-type models. Additionally, plasma transport is very dependent on the details of the complex magnetic topology implemented in HET.

The 2Dz$\theta$ simulations show the development and saturation of plasma instabilities, leading to enhanced cross field electron transport. The main azimuthal instabilities seem to pertain to the electron-cyclotron drift type [3,4]. Nonetheless, the plasma response is very sensitive to simulation parameters. A proper characterization of these instabilities and the induced transport has not been achieved yet. Meanwhile, it has been shown the relevance of (i) including the losses to radial walls (making the problem 3D, in fact) (ii) the possible presence of a longitudinal ion transit time (ITT) instability.

## References

[1] Adamovich, I., Agarwal, S., Ahedo, E., Alves, L. L., Baalrud, S., Babaeva, N., ... & von Woedtke, T. (2022). The 2022 Plasma Roadmap: low temperature plasma science and technology. *Journal of Physics D: Applied Physics*, *55*(37), 373001.

[2] Marín-Cebrián, A., Bello-Benítez, E., Domínguez-Vázquez, A., & Ahedo, E. (2024). Non-Maxwellian electron effects on the macroscopic response of a Hall thruster discharge from an axial–radial kinetic model. *Plasma Sources Science and Technology*, *33*(2), 025008.

[3] Adam, J. C., Héron, A., & Laval, G. (2004). Study of stationary plasma thrusters using two-dimensional fully kinetic simulations. *Physics of Plasmas*, *11*(1), 295-305.

[4] Bello-Benítez, E., Marín-Cebrián, A., & Ahedo, E. (2025). Effect of injection conditions on the non-linear behavior of the ECDI and related turbulent transport. *Physics of Plasmas*, *32*(1).

# From Spark to Sprout: Diagnostic Pathways in Plasma-Enabled Agriculture

D. Aceto, M. Ambrico, G. Dilecce and P.F. Ambrico

*CNR ISTP sede di Bari, c/o Dipartimento Interateneo di Fisica, via Amendola 172, 70126 Bari, Italy*

In this talk we report on our findings in the field of plasma agriculture. We believe that the way of the full understanding of the mechanisms involved in the interaction between plasma and biological tissues proceeds through the application of advanced plasma diagnostics techniques. Some insight on new results will be also presented.

The pursuit of a sustainable, circular agricultural economy is inspiring the development of innovative technologies such as Non-Thermal Plasma (NTP) and plasma-activated media (liquids, fog, or mist). Plasma agriculture has shown promising results in various areas. NTP treatments can enhance seed germination and promote plant growth by stimulating biochemical processes[1,2]. Plasma can effectively reduce microbial contamination on seeds and crops, leading to healthier plants [3–7]. Plasma-Activated Water (PAW) can improve nutrient uptake in plants, boosting their overall productivity representing a new alternative to conventional fertilizers [8,9]. Moreover, PAW has also been demonstrated to be effective in reducing contamination by fungi both *in vivo* and *in vitro* experiments[10].

Although promising, these technologies are still in their early stages, with a thorough understanding complicated by factors like plant species differences, growth conditions, and varied plasma parameters. Many applications utilize atmospheric air at ambient pressure, making them a competitive alternative to traditional chemical methods. Several factors, such as reactive oxygen and nitrogen species (ROS and RNS), ultraviolet radiation, and electric fields, should be accounted for to explain the observed effects. These components interact with biological tissues, triggering physiological and biological effects. Research efforts have mainly focused on quantifying the plasma treatment effects through gas phase spectral emissions (indicating temperatures and molecular signatures), electrical characteristics (current, charge, voltage), discharge effluent composition ($O_3$, $NO_x$), and PAW chemical makeup ($H_2O_2$, $NO_2^-$, $NO_3^-$). Greater attention is needed on the detection of plasma's short- and long-lived species.

To gain a better understanding of the mechanisms of action on biological systems of the aforementioned species, several diagnostics could be applied to plasma discharges. Among them, we applied:

- Emission Spectroscopy: used to study the spectral emissions from plasma, providing insights into gas temperatures, electric fields and the presence of specific atoms, radicals, and molecules.
- Fourier Transform Infrared (FTIR) Spectroscopy: applied for *in situ* analysis of plasma interactions, such as seed treatment or bacterial decontamination.
- Laser-Induced Fluorescence (LIF): utilized for detecting reactive species like OH radicals and NO, though its effectiveness can be limited by quenching effects in certain environments.
- Electric Field Induced Second Harmonic Generation (EFISH): measures electric fields in plasma with temporal and spatial resolution, both during and after discharge phases.
- Spatially Enhanced EFISH (SEEFISH), an improved version of EFISH, to address challenges like non-uniform plasma behaviour.

Moreover, the composition of PAW, including reactive species like hydrogen peroxide ($H_2O_2$), nitrites ($NO_2^-$), and nitrates ($NO_3^-$) was studied by standard analytical techniques and Electrical Impedance Spectroscopy.

We believe that these diagnostics are crucial for understanding plasma's interaction with biological tissues and optimizing its implementation in agriculture.

**References**

1.Ambrico, P.F. et al. *J Phys D Appl Phys* **50**, 305401 (2017).
2.Ambrico, P.F. et al. *J Phys D Appl Phys* **53**, 104001 (2020).
3.Ambrico, P.F. et al. *Sci Rep* **10**, 1–17 (2020).
4.Ambrico, P.F. et al. *Appl. Sciences* **12**, 4711 (2022).
5.Waskow, A. et al., *Int J Mol Sci* **22**, (2021).
6.Ibba, L., et al., *Plasma Chem Plasma Process*. **44**, 785–805 (2024).
7.Rotondo,P.R.et al. *Plasma Chem Plasma Process.***43**, 1819–1842 (2023).
8.Aceto,D.et al., *Front Phys* **12**:1399910. doi: 10.3389/fphy.2024.1399910.
9.Aceto, D., F., *Front Phys* **12**:1455481. doi: 10.3389/fphy.2024.1455481 (2024).
10. Rotondo, P. R. *et al., Sci Rep* **15**, 5536 (2025).

# Hydrogen Negative Ion Production in an ECR-Based Large-Area Plasma Source for Fusion Applications

Bibekananda Naik[1], S. Sharma[1], R. Narayanan[1], D. Sahu[1], M Bandyopadhyay[2,3], A Chakraborty[2], M J Singh[2,3], A. Ganguli1, R. D. Tarey[1]

[1] [1]*Indian Institute of Technology Delhi, Hauz Khas, New Delhi, Delhi-110016*
[2]*Institute for Plasma Research, Gandhinagar, Gujarat,382428*
[3]*Homi Bhabha National Institute, Mumbai, Maharashtra 400094*

Experiments were conducted with Hydrogen plasma produced in a large cylindrical plasma chamber (Height/ Dia ~ 1 m.) with the help of an electron cyclotron resonance (ECR) plasma source. The ECR region within the plasma source chamber was generated using three concentric NdFeB permanent ring magnet that produces a diverging field within the expansion chamber aiding plasma flow. Plasma characterizations with Langmuir probe were performed at the downstream region of the expansion chamber which indicated a moderately uniform plasma over a diameter ~ 60 cm with low electron temperature ($T_e$ ~ 1 eV) favouring the production of $H^-$ ions through volume reactions. Mass spectrometry studies performed using the low-pressure probe of a molecular beam mass spectrometer (MBMS) provides useful information regarding the mass and energy distributions of the negative $H^-$ as well as positive ($H^+$, $H_2^+$, $H_3^+$) ions in the ECR plasma. The results signify the capability of this source for large area $H^-$ production for fusion applications.

## 1 Introduction

The hydrogen negative ion ($H^-$) is a vital species in hydrogen plasma, with applications in plasma-based material processing, accelerator physics, and most importantly in thermonuclear fusion. In fusion research, $H^-$ ions are essential for heating and current drive in magnetically confined fusion reactors [1]. Presently, most $H^-$ ion sources used in fusion rely on inductively coupled plasma (ICP) systems powered by radio frequency (RF) with power ~ 1 MW. These systems depend on collisional power coupling, which is less efficient than resonant coupling methods. Electron cyclotron resonance (ECR) offers a more efficient alternative, yet its use in large-area, high-current sources remains underexplored. This paper presents investigations into an ECR-based large-volume plasma system, for the efficient volume production of $H^-$ ions.

## 2 Experimental Setup & Diagnostics

The experiments were conducted in a cylindrical expansion chamber, known as ECR based Large Negative Ion Beam Source (ELNIBS), with a height and diameter ~ 1 m. Plasma was generated using a compact ECR plasma source (CEPS) [2]. Plasma characterizations were performed with the help of axial and radial Langmuir probes (LP) under varying microwave power (400 - 600 W) and gas pressure (1 - 3 mTorr) with the plasma source mounted onto the centre of the top dome of the expansion chamber, ELNIBS. The magnetic field configuration of the source decays exponentially into the plasma expansion chamber aiding plasma flow. Additional permanent ring magnets were installed around the periphery of the expansion region to reduce wall-loss. Mass spectrometry studies were conducted using a low-pressure plasma sampling probe (PSM) of Hiden HPR-60 quadrupole molecular beam mass spectrometer (MBMS). Measurements were conducted under two distinct configurations: one with the PSM probe aligned with the plasma flow and the other with it oriented transversely to the plasma flow.

## 3 Results and Discussion

The LP results indicate a uniform plasma with density $n_e \sim 10^{11}$ cm$^{-3}$ and $T_e \sim 1$ eV at a distance of 37.5 cm away from the source mouth. Plasma density improved with the presence of additional magnets at the sidewall reducing the plasma wall losses. These conditions favour the volume production of $H^-$ ions, which were detected through MBMS measurements. The mass as well as the energy spectra of both positive and negative hydrogen ions were obtained for the two configurations mentioned earlier. Effect of positive ion distributions on production of $H^-$ ions along with the variation with microwave power and gas pressure will be presented.

**References**

[1] Takeiri, Y. Negative ion source development for fusion application. *Rev. Sci. Instrum.* 81, 02B114 (2010)

[2] Ganguli, A. et al. Development and studies on a compact electron cyclotron resonance plasma source. *Plasma Sources Sci. Technol*. 25, no. 2(2016):025026

# Experimental and numerical study of $CO_2/H_2$ DC glow and pulsed RF discharges

S. Bois[1], E. Baratte[1], M. Budde[1], V. Guerra[2], T. Silva[2] and O. Guaitella[1]

[1] *Laboratoire de Physique des Plasmas, CNRS, UMR 7648, Univ. Paris-Saclay, SorbonneUniversité, Ecole Polytechnique, France*
[2] *Instituto de Plasmas e Fusão Nuclear, Instituto Superior Técnico, Universidade de Lisboa, Portugal*

In this work, the electronic and chemical kinetics of $CO_2/H_2$ plasmas, that is essential for any hydrogenation process of $CO_2$, has been investigated through quantitative comparison of experiment and numerical simulation. First, a DC glow discharge was studied. It has the advantage of being homogeneous along the positive column, allowing for line of sight integrated measurements and quantitative comparison with a simple 0D kinetic model. A pulsed RF discharge in a batch reactor was then used to further validate the model by monitoring the gas composition from initial mixture until steady state.

## 1. Introduction

The kinetics of $CO_2/H_2$ plasmas are generally studied for methanation processes and, consequently, almost always in the presence of catalysts. The high complexity of the chemistry induced in these mixtures prevents the identification of the major reactions. Building on our previous work in pure $CO_2$ and $CO_2/CH_4$, this work aims to identify a minimal kinetic scheme capable of quantitatively reproducing the molecular densities, as well as the reduced field measured experimentally in model discharges of $CO_2/H_2$ at reduced pressure (a few mbar).

To achieve this, two complementary types of discharges are studied: (i) a DC glow discharge, whose homogeneity of the positive column allows for effective validation of the electron kinetics by comparing the experimental and simulated electric fields, in addition to molecular densities, (ii) a pulsed RF discharge in a 'batch' reactor (i.e. without gas flow) where the evolution of the gas mixture is tracked from the initial composition to a steady state. The model developed in this work uses the 0D LoKI simulation tool [1]. LoKI provides a 0D Boltzmann solver and a solver of the volume average rate balance equations for heavy species in the plasma. The cross sections for elastic collisions, electronic excitation, vibrational excitation and dissociation used in this work were taken from [2] and [3] where they had been validated against swarm parameters.

## 2. Results in glow and RF discharges

The glow discharge is generated in a glass tube with an inner diameter of 2 cm. The field is measured by floating potential probes, and the gas temperature by emission spectroscopy. Fig. 1 illustrates a typical result comparing the densities of molecules measured by FTIR at the outlet of the plasma reactor (points) and simulations (solid lines), plotted in function of the initial percentage of $CO_2$ in the mixture.

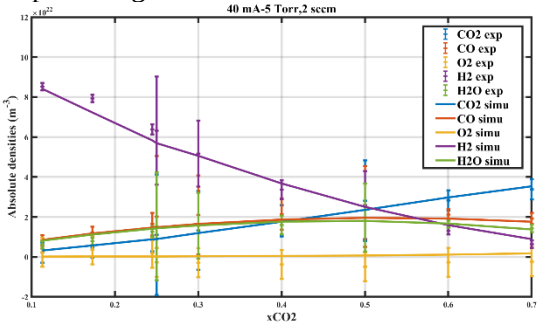



**Fig 1:** typical simulation (solid lines) and experimental (points) results

Such good agreement was obtained for variations in pressure, current and total gas flow rate, validating the electron kinetics and the main $H_2O$ formation processes. Under these experimental conditions, a significant portion of the gas is renewed by the gas flow. The pulsed RF discharge allows operation in a 'batch' reactor. In this experiment, consecutive RF plasma pulses are ignited while the densities of IR-reactive molecules are monitored in time by infra-red absorption. Playing with the plasma pulse duration and frequency enables to investigate the influence of processes with different characteristic times. In particular, the key role of water adsorption to the wall, and consequent $CO_2$ losses are evidenced.

### References

[1] A. Tejero-del-Caz et al Plasma Sources Sci. Technol. 28 (2019) 043001
[2] A F Silva et al, Plasma Sources Science and Technology (2020).
[3] M. Budde, et al. Journal of Physics D: Applied Physics (2022).
[4] Baratte, Edmond et al. Plasma Chemistry and Plasma Processing 44.3 (2024): 1237-1286

IPFN activities were supported by the Portuguese FCT-Fundação para a Ciência e a Tecnologia, under funding to IPFN, DOI: 10.54499/LA/P/0061/2020, 10.54499/UIDB/50010/2020, 10.54499/UIDP/50010/2020, and 10.54499/PTDC/FIS-PLA/1616/2021)

# In-situ measurement of surface reaction probabilities in low-pressure plasmas

J-P. Booth[1], S. Zhang[1], G. Curley[1]

[1] *Laboratoire de Physique des Plasmas (LPP), CNRS, Sorbonne Université, École Polytechnique, Institut Polytechnique de Paris, Palaiseau, 91120, France*

Surface-catalysed recombination is often the dominant loss process for reactive atoms and free radicals created in low-pressure plasmas in molecular gases. However, ab-initio theoretical methods to estimate the rates of these processes are far from mature, in part due to the complexity of the chemical composition and morphology of surfaces subjected to energetic ion bombardment. Therefore, reliable in-situ measurements are essential to understand the chemical kinetics of these systems. A number of experimental techniques to measure surface reaction rates have been developed, and will be reviewed in this talk. However, analysis of these experimental results has historically relied on simplifying assumptions, notably that of constant surface reaction probability, $\gamma$. However, high-quality data from improved experimental techniques combined with systematic measurements in simplified model systems has shown that this assumption is far from correct in many circumstances. More sophisticated surface models are therefore necessary.

The simplest way to estimate the surface loss probability of a species X in a plasma chamber is to make time-resolved measurements of the density, [X](t) during modulation of the plasma density. The density can be monitored using optical emission actinometry (only only possible when the plasma is on, so either the power is partially modulated [1, 2], or the discharge is turned off for variable delays before re-ignition[3]). Active spectroscopic techniques, such as Laser-Induced Fluorescence (LIF[4]), Two-Photon Absorption Laser Induced Fluorescence (TALIF[5]), or Cavity Ring Down Spectroscopy (CRDS[6]) are need to make measurements in the afterglow of fully-modulated plasmas.

If the surface reaction probability can a) be described by a constant value, $\gamma$, and b) the transport of X to the surface is described by a constant and spatially uniform diffusion coefficient, D, then the density [X] will decay exponentially in the afterglow (or the lower-power period) with a time constant, $\tau$, from which $\gamma$ can be deduced using the formula of Chantry[7]. This method has been widely employed, and has been very useful to provide initial estimates of $\gamma$. However, whether these assumptions are valid may be hidden by mediocre experimental signal-to-noise ratio. Alternatively, at intermediate gas pressures $\gamma$ can be deduced from measurements of the spatial gradient next to a surface, using LIF [4] or TALIF, but this technique is complex to implement.

We have studied the kinetics of oxygen using CRDS of the forbidden $^1D_2 \leftarrow {}^3P_2$ transition at 630nm[6]. The atom density in cw DC glow discharge in pure $O_2$ (0.5-4 Torr) shows significant (reversible) drifts over several hours, which can only be explained by changes in the state of the glass tube surface. Faster time-resolved measurements in pulsed discharges show decays that slow with time in the afterglow (the effective value of $\gamma$ reduces with time), most marked at high pressure and current. This effect can be explained by the recombination occurring at both chemisorbed and physisorbed sites, the latter dominating with high atoms fluxes. Analogous measurements in an aluminium RF CCP in $O_2$ over the same pressure range showed superficially similar behaviour. However, in this case the non-exponential decay was most marked at low pressure and high RF power, and was even more marked in $O_2$/Ar mixtures. This provides clear evidence that energetic ion bombardment causes a significant increase in $\gamma$, with the surface recovering within fractions of a second, leading to the observed slowing decays.

**References**

[1] Booth J P and Sadeghi N *Journal of Applied Physics* 1991 **70** 611-620
[2] Booth et al. *Plasma Sources Science and Technology* 2019 **28** 055005
[3] Bouchoule A and Ranson P *Journal of Vacuum Science & Technology A* 1991 **9** 317-326
[4] Booth J P, Hancock G, Perry N D and Toogood M J *Journal of Applied Physics* 1989 **66** 5251-5257
[5] Jolly J and Booth J P *Journal of Applied Physics* 2005 **97** 103305
[6] Booth et al. *Plasma Sources Science and Technology* 2023 **32** 095016
[7] Chantry P J *J. Appl. Phys.* 1987 **62** 1141

# VUV absorption spectroscopy for ultrafast TALIF calibration and mw plasma jet characterisation

A. Brisset[1], C. Pascual-Fort[1], N. de Oliveira[2], G.D. Stancu[1]

[1]*Laboratoire EM2C, CNRS, CentraleSupélec, Université Paris-Saclay, 3 rue Joliot Curie, 91192, Gif-sur-Yvette, France*

[2]*Soleil, l'Orme des Merisiers, St. Aubin BP 48, 91192 Gif-sur-Yvette, France*

This study is aimed at performing VUV-absorption to *i)* improve the calibration accuracy of the ultrafast Two-photon Absorption Laser Induced Fluorescence (TALIF) diagnostic under high laser intensity conditions (i.e. $TWcm^{-2}$), *ii)* investigate the generation of atomic radicals in microwave (mw) plasma jets. Traditional rate equations are invalid in the high-intensity TALIF regime, requiring calibration with a source of known atomic density. A DC plasma was employed as a reference source for atomic O, H and N, where absolute densities were measured by Vacuum Ultraviolet (VUV) absorption spectroscopy at the SOLEIL synchrotron. The accuracy was improved by choosing operating conditions with non-saturated absorption lines and negligible molecular spectral overlap. VUV absorption was applied to characterize a low-pressure mw plasma jet in Ar:$O_2$ mixtures. Resonant broadening and hysteresis effects were observed in these experiments.

## 1 Context of the study

The extreme laser intensity and mode-lock features of ultrafast lasers make the fluorescence signal in TALIF dependent on the ground and excited state populations, as well as novel phenomena like Stark detuning and coherent excitation, and therefore, not correctly described by the classical rate equations. To overcome these challenges, it was suggested in [1] to perform the calibration of the fluorescence signal using a source of known density of the same reactive atom as the probed one. A DC discharge characterised by high resolution VUV absorption spectroscopy [2] is used to serve as the calibration cell. Since the fluorescence becomes dependent only on the laser characteristics (e.g. rates of laser induced processes are much larger than the plasma quenching rates), the atomic spectroscopic properties and their ground state densities, the calibration reduces to a factor that only depends on the ratio of fluorescence signals in the cell, $S_F^{calib}$ and in the plasma of interest, $S_F$. Using the same laser beam, the density of the probed species $X$ in the plasma of interest ($n_X$) is related to the density of $X$ in the calibration cell ($n_X^{calib}$) through: $n_X = C \times \frac{n_X^{calib}}{S_F^{TALIF}} \times S_F$ with $C$, a constant accounting for potential changes, such as different transmission coefficients of fluorescence collection windows of the two plasma reactors.

## 2 Results

Means to improve the accuracy of the VUV-calibration method (e.g. source design, gas dilution, increase spectral resolution) were obtained. For example, N density in plasma was evaluate with a total uncertainty of ~20% which is appreciably better compared to traditional nanosecond TALIF. Among findings, we can cite the importance of laser dispersion and photon statistic effects on the TALIF signals.

VUV absorption was also performed for H and O generated in the calibration cell (see Figure 1) and in a low-pressure mw plasma jet (1-100 mbar).

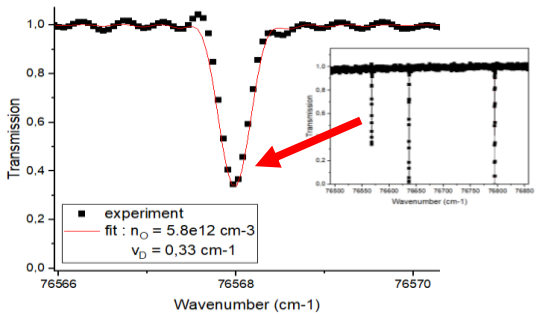



Figure 1: VUV absorption spectrum of O in the DC plasma cell at 6.5 mbar, Ar:$O_2$ = 5000:1 and 7 mA.

Mw plasma jet measurements revealed, for instance, a complex broadening of O lines at 130 nm and a hysteresis power dependence for oxygen radical production.

### Acknowledgments

This research was funded by ANR, ULTRAMAP project (ANR-22-CE51-0027), Soleil, project 20231659 and IdF SESAME, project DIAGPLAS.

### References

[1] Dumitrache C. *et al. Plasma Sources Sci. Technol.* **31** 015004 (2022)

[2] de Oliveira N. *et al. J. Synchrotron Radiation*, **23** 887 (2016)

XXXVI ICPIG, July 20–25, 2025, Aix-en-Provence, France

# Nanosecond resolved $CO_2/N_2$ vibrational kinetics in a pulsed discharge investigated experimentally and by modeling

Christian A. Busch[1], Tiago Silva[2], Vasco Guerra[2], Inna Orel[1], Nikita D. Lepikhin[1], Dirk Luggenhölscher[1], Uwe Czarnetzki[1]

[1] *Ruhr University Bochum, Institute for Plasma and Atomic Physics, Bochum, Germany*
[2] *Institute for Plasmas and Nuclear Fusion, Instituto Superior Técnico, University of Lisbon, Lisbon, Portugal*

The vibrational kinetics of $CO_2/N_2$ mixtures are studied in a ns-pulsed discharge, which separates in time different energy transfer processes for the vibrational excitation and de-excitation, using quantum-cascade laser absorption spectroscopy (QCLAS) and coherent anti-Strokes Raman scattering. The results are compared to a state-of-the-art kinetic model (LoKI).

## Introduction

The vibrational kinetics of $CO_2$ and $CO_2/N_2$ mixtures are crucial for the conversion of $CO_2$, for $CO_2$ lasers or atmospheric reentry in $CO_2$ rich atmospheres such as that of Mars. A full understanding of the vibrational kinetics is complicated due to the large number of states and reactions involved. In order to separate the different processes such as electron-vibrational (e-V), vibrational-vibrational (V-V) and vibrational-translational (V-T) transfer in time to allow for their independent study, a ns-pulsed discharge in $CO_2/N_2$ mixtures is used. The densities of vibrationally excited states are measured with the required ns-resolution using quantum-cascade laser absorption spectroscopy (QCLAS) [1] and coherent anti-Stokes Raman scattering (CARS).

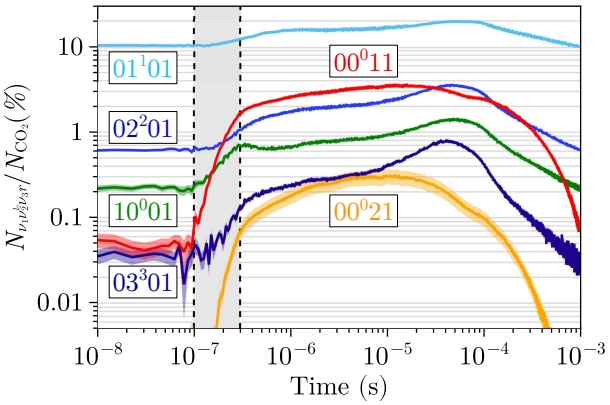



Figure 1: Time evolution of the vibrational populations of $CO_2$ molecules in selected vibrational states at a pressure of 150 mbar with a gas mixture of 10% $CO_2$ and 90 % $N_2$ and applied voltage of 3 kV. The duration of the discharge is marked by the gray bar [1].

## Results

The evolution of the vibrational populations of $CO_2$ on different time scales is shown in figure 1 highlighting the rapid electron impact excitation during the discharge and the subsequent V-V and V-T transfer in the afterglow. A non-equilibrium between the symmetric stretch mode and bending mode of $CO_2$, which are usually assumed to be in equilibrium, was observed for the first time to the best knowledge of the authors. The experimental results are compared to a state-of-the-art kinetic model (LoKI [2, 3]) for the validation of rate coefficients. This further reveals that a commonly used scaling law for the electron impact excitation of the $CO_2(\nu_3)$ states leads to erroneous results.

## Funding acknowledgments

The work is supported by the DFG funded SFB1316 Project ”Transient atmospheric plasmas - from plasmas to liquids to solids”.
IPFN activities were supported by FCT - Fundação para a Ciência e Tecnologia under projects UIDB/50010/2020 (https://doi.org/10.54499/UIDB/50010/2020), UIDP/50010/2020 (https://doi.org/10.54499/UIDP/50010/2020), LA/P/0061/202 (https://doi.org/10.54499/LA/P/0061/2020) and PTDC/FIS-PLA/1616/2021 (https://doi.org/10.54499/PTDC/FIS-PLA/1616/2021)

## References

[1] C. A. Busch et al 2025 J. Phys. D 58 065202
[2] IPFN - IST The LisbOn KInetics - LoKI. (available at: https://nprime.tecnico.ulisboa.pt/loki/)
[3] A. Tejero-del-Caz et al Plasma Sources Sci. Technol. 28 (2019) 043001

# Nanosecond Discharge with Droplet: fundamental and synthesis of silver Nanomaterials

L. Sebih[1,2], E. Carbone[1], A. Hamdan[1]

[1] *Département de physique des plasmas, Université de Montréal, Montréal, Canada*
[1] *Institut National de la Recherche Scientifique, CEMT, Varennes, Québec, Canada*

Herein, we study the impact of electrical conductivity of water droplet and voltage amplitude on the dynamics of a nanosecond discharge and the obtained modes. Streamer or spark discharges can be produced, and their interaction with a droplet that contains $AgNO^3$ lead the formation of Ag nanomaterials. Fine tuning of the experimental conditions allowed formation of 2D Ag nanostructure, which opens the way for substrate-free synthesis of nanostructures.

## 1 Introduction

Discharges in air with the presence of liquid droplets is an interesting setup for fundamental investigation as well as technological applications. For instance, the presence of a droplet in or near the interelectrode gap affects the propagation pathway of the discharge [1]. Such a property is of interest because it enhances plasma-liquid interactions. In the context of material synthesis, metal salts can be added to the droplet and nanomaterial can be synthesized in the droplet after plasma-droplet interaction. As the experimental parameters (e.g. droplet electrical conductivity and applied voltage) allowed the establishment of various discharge modes (e.g. streamers and sparks), it is expected that different types of nanomaterials can be produced in the droplet. This study aims to elucidate the mechanisms of discharge dynamics under various experimental conditions and their role in driving nanomaterial synthesis.

## 2 Experiments and Results

We conducted nanosecond discharges in a pin-droplet-pin setup using three different configurations: anodic-, cathodic- and floating-droplet setups. The droplet's electrical conductivity (EC) varied between 10 µS/cm (i.e. distilled water) to 5 mS/cm by adding salts, namely KCl and $AgNO_3$. High voltage pulses with width (between 100 and 500 ns) and magnitude (10-20 kV) are applied to the electrodes. The discharges were characterized electrically and by ICCD imaging. In the case of droplets made from $AgNO_3$ solution, the synthesized materials were analyzed using UV-Visible; TEM was used to investigate the characteristics of the synthesized nanomaterials.

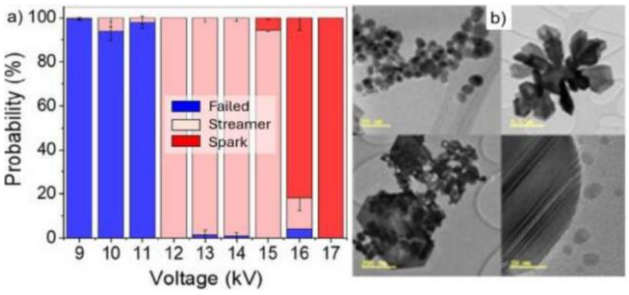



**Fig. 1.** a) The probability to obtain streamer or spark discharge modes as a function of the voltage [4]. b) A selection of the different nanostructures obtained.

The results show that EC significantly impacts the dynamics of the discharge, in particular its mode as streamer or speak. Figure 1a shows the probability to obtain streamer or spark discharge modes as a function of the applied voltage. The data (obtained for a 6-mm droplet, 9-mm gap, and EC of 5 mS/cm) shows that streamers are dominant for an applied voltage between 12 and 15 kV, while sparks dominate for higher voltage. Time resolved images are also acquired, and the various propagation modes as well as streamer-to-spark transition will be presented [2]. After discharge under specific conditions (i.e. mode) with $AgNO_3$ droplet, Ag-based nanostructures were synthesized (Fig. 1b). As the main mechanism of synthesis is the reduction of Ag ions by electrons, the diversity of the structures may be explained by different charge fluxes on the droplet that occur in different discharge modes. Notably, under a specific condition, Ag nanosheets are synthesized. Such 2D nanostructure is usually obtained when a substrate is used. The lack of a substrate in our setup highlights the role of the droplet-air interface as a surrogate substrate, which opens the way for substrate-free synthesis of oriented nanostructures.

**References**

[1] Hamdan et al. JPhysD **56** 215202 (2023).
[2] Sebih, et al. J Phys D ***58*** 045206

# Iodine Plasmas: from Belfast to Space

P. Chabert

[1] *LPP, CNRS, Ecole Polytechnique, 91128 Palaiseau, France*

Professor W.G. (Bill) Graham has been fascinated by plasmas containing negative ions during his entire career. In the late seventies/early eighties, he spent a short sabbatical at Ecole Polytechnique to work with Martha Bacal on hydrogen plasmas used as negative ion sources for fusion. In the beginning of the twenty-first century, he investigated chlorine plasmas used in plasma processing in the semiconductor industry. When I told Bill I was interested in iodine plasmas for space propulsion, he proudly told me that they had been studied in Belfast, just after World War II, by Karl George Emeleus! This paper will be on iodine plasmas for space propulsion, but it will also be on what I learned from Bill, not only in plasma physics.

Plasmas containing negative ions, often called electronegative plasmas, are quite fascinating, and they certainly caught Bill's attention. His first visit to Ecole Polytechnique was in the late seventies, and at this time he worked with Martha Bacal on negative ion sources for fusion. They were interested in the production mechanisms of $H^-$ and the detection of $H^-$ by laser-induced photodetachment [1]. Their work has had a strong impact and Bill later used the photodetchment technique in other types of plasmas, for instance chlorine plasmas used in semiconductor etching [2,3].

Electronegative plasmas have unique properties and behave differently from usual electropositive plasmas. They are intrinsically unstable, and transport phenomena are severely affected by the presence of heavy negatively-charged particles. Negative ion sources are based on magnetic filtering, a technique that leads to ion-ion (electron free) plasma formation. Negative ions may be extracted from these ion-ion plasmas and accelerated to produced negative ion beams that are neutralized for energetic atom injection in fusion reactors. It was also shown that alternative acceleration of positive and negative ion beams from ion-ion plasmas may be used for charge free etching in microelectronics and/or neutralizer-free plasma thrusters. In the case of thrusters, iodine was identified as the best candidate, because it is both heavy and easy to ionize, and it was used in the so-called PEGASES Thruster [4]. Iodine plasmas are now intensively studied in the context of plasma propulsion. Basic diagnostics used by Bill and co-workers in hydrogen or chlorine plasmas (Langmuir probes, Laser-induced photodetachment, laser-induced fluorescence) have recently been successfully applied to iodine plasmas [5,6].

Bill was pleased to see research in iodine plasmas and he proudly told me that they had been studied in Belfast, just after World War II, by Karl George Emeleus. [7]. In 2021, iodine plasmas were used in space for the first time in a small satellite mission [8]. From Belfast to space, the adventure continues!

**References**

[1] Bacal M, Bruneteau A M, Graham W G, Hamilton G W and Nachman M "Pressure and electron temperature dependence of $H^-$ density in a hydrogen plasma" *J. Appl. Phys.* **52** (1981) 1247

[2] C. S. Corr, P. G. Steen, W. G. Graham, Temporal phenomena in inductively coupled chlorine and argon–chlorine discharges. *Appl. Phys. Lett.* **86**, 141503 (2005).

[3] C S Corr, E Despiau-Pujo, P Chabert, W G Graham, F G Marro and D B Graves, "Comparison between fluid simulations and experiments in inductively-coupled argon/chlorine plasmas", *J. Phys. D*, **41** (2008) 185202

[4] A. Aanesland, D. Rafalskyi, J. Bredin, P. Grondein, N. Oudini, P. Chabert, D. Levko, L. Garrigues, and G. Hagelaar, "The PEGASES Gridded Ion-Ion Thruster Performance and Predictions", IEEE TRANS. ON PLAS. SCIENCE, 43 (2015) 321-326

[5] B. Esteves, F. Marmuse, C. Drag, A. Bourdon, A. Alvarez Laguna, P. Chabert, "Charged-particles measurements in low-pressure iodine plasmas used for electric propulsion", *Plasma Sources Sci. Technol.* **31** (2022) 085007

[6] B. Esteves, C. Blondel, P. Chabert, C. Drag, "Two-photon absorption laser induced fluorescence (TALIF) detection of atomic iodine in low-temperature plasmas and a revision of the energy levels of I I", Journal of Physics B: Atomic, Molecular and Optical Physics, 56 (2023) 055002

[7] Alan Garscadden, "Karl George Emeleus", Physics Today, NOVEMBER, 1990, page 106

[8] D. Rafalskyi, J. M. Mart´ınez, L. Habl, E. Zorzoli Rossi, P. Proynov, A. Bor´e, T. Baret, A. Poyet, T. Lafleur, S. Dudin, et al., In-orbit demonstration of an iodine electric propulsion system, *Nature* **599**, 411 (2021).

# Field reversals in low pressure capacitively coupled plasma discharges driven by tailored voltage waveforms

Chan Feng[1], De-Qi Wen[1*], Jon Tomas Gudmundsson[2,3], John P Verboncoeur[4,5], Julian Schulze[6], You-Nian Wang[1]

[1] *School of Physics, Dalian University of Technology, Dalian, 116023, China*
[2] *Science Institute, University of Iceland, Dunhaga 3, IS-107 Reykjavik, Iceland*
[3] *Division of Space and Plasma Physics, School of Electrical Engineering and Computer Science, KTH Royal Institute of Technology, SE-100 44 Stockholm, Sweden*
[4] *Department of Electrical and Computer Engineering, Electrical and Computer Engineering, Michigan State University, MI, 48824, USA*
[5] *Department of Computational Mathematics, Science and Engineering Michigan State University, MI, 48824, USA*
[6] *Chair of Applied Electrodynamics and Plasma Technology, Faculty of Electrical Engineering and Information Sciences, Ruhr University Bochum, Bochum, Germany*

## 1 General

Capacitively coupled plasma (CCP) discharges are widely applied for etching processes in the microelectronics industry. In recent work, using experimentally validated kinetic particle-in-cell Monte Carlo collisional simulations [1,2], we reported the sheath electric field reversal in low pressure CCPs, driven by a radio-frequency voltage source, when the driving voltage amplitude is up to 1000 V [3]. Due to the symmetry in geometrically symmetric single-frequency driven CCPs, the field reversal appears within each sheath adjacent to each electrode. In this work, we demonstrate the presence of field reversals in CCPs driven by tailored voltage waveforms. For a CCP with one electrode grounded and another electrode powered by a peaked or valley-type waveforms composed of 13.56 MHz sinusoidal waveform and its harmonics, a strong reversed sheath field is found only in one sheath that has the prominent sheath collapse phase shift. However, when the capacitive discharge is driven by a high frequency (60 MHz) voltage source on one electrode and a very low frequency (0.6 MHz) composed peak-type waveform on another electrode as shown by figure 1, multiple strong field reversals are found when the sheath collapses near the low frequency source driven electrode, a few weak field reversals are observed near the high frequency source-driven electrode due to secondary electron emission. In addition, the effect of a reversed sheath field on the electron/ion energy distribution incident on the electrodes will also be discussed in detail.

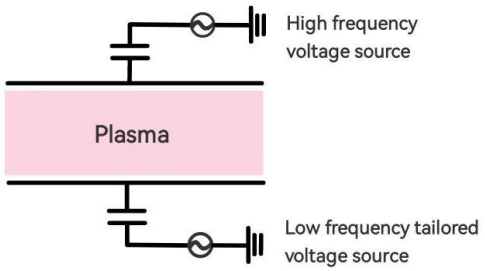



Fig. 1: Schematic of the capacitive discharges with one electrode driven by a high frequency voltage source and another electrode driven by a low frequency tailored voltage waveform.

**Acknowledgments**

This work was partially supported by the Fundamental Research Funds for the Central University (Grant No. DUT24RC(3)115) and the Air Force Office of Scientific Research (AFOSR) MURI Grant FA9550-21-1-0367 and NSF-DOE Partnership Grant for DE-SC0022078.

**References**

[1] D.-Q Wen, J Krek, J.T Gudmundsson, E Kawamura, M.A Lieberman, P. Zhang and J P Verboncoeur, Plasma Sources Sci. Technol. 32 (2023) 064001

[2] D. A Schulenberg, I Korolov, Z Donkó, A Derzsi and J Schulze Plasma Sources Sci. Technol. 30 (2021) 105003

[3] D.-Q Wen, J Krek, J. T Gudmundsson, E Kawamura, M A Lieberman, P Zhang, and J P Verboncoeur, Appl. Phys. Lett. 123, (2023) 264102

# Diagnosing Technological Plasmas: A tribute to Professor Bill Graham

Cormac Corr

*Research School of Physics, Australian National University, Canberra, Australia*

Professor W.G. (Bill) Graham has made significant advancements to the study of low-temperature plasmas, with an emphasis on diagnostic techniques and modelling to explore their fundamental properties and practical applications. Bill's research applied diagnostic methods such as Thomson scattering, electrostatic probes, laser photodetachment and emission spectroscopy to provide detailed insights into the behaviour of low-temperature technological plasmas for various applications, ranging from ion sources to surface modification and plasma medicine. In this presentation, I will provide a snapshot of Bill's contributions to diagnosing these plasmas and his energetic scientific approach that has inspired many in the community.

After years of research in atomic and molecular collision processes, in the early 1980s Professor Bill Graham focused his research on the physics and chemistry of low-pressure negative ion sources and their application for neutral beam heating of fusion devices. In collaboration with Martha Bacal, they made a comparison between experimental data obtained via laser photodetachment measurements and theoretical predictions with results suggesting that the production of negative hydrogen ions primarily occurs through electron attachment to vibrationally excited hydrogen molecules [1]. Further experiments by Bill using vacuum ultraviolet (VUV) emission spectroscopy, supported these results and emphasized the role of vibrational excitation in enhancing negative ion production [2]. Langmuir probe-based measurements over many years with Mike Hopkins provided detailed insights into electron energy distribution functions in these plasmas [3]. Throughout, Bill stressed the need for the development of models and comparison with experimental data [4].

Following this foundational work on hydrogen plasmas, in the mid 1990s Bill's research interests focussed on RF driven plasma processing devices [5, 6]. Research topics included capacitive to inductive transition; atomic oxygen and chlorine measurements; negative ion measurements; instabilities in electronegative plasmas; atomic oxygen sticking probabilities; and textile processing [7]. At that time, Bill's research group had developed a suite of diagnostic techniques such as laser induced fluorescence, Thomson scattering, laser photodetachment, Langmuir probes, optical emission spectroscopy and current-voltage probes. In the 2000s, and in character with Bill's research approach and desire to keep advancing knowledge, his focus shifted towards atmospheric pressure plasmas and plasmas created in liquids with applications in medicine, catalysis and surface modification [8]. This research involved developing and employing a broad array of diagnostic tools, computer simulations, modelling techniques, and various plasma sources.

Whether it was negative ion sources for fusion, RF plasmas for material processing or plasmas created in liquid, Bill wanted to understand the fundamental physics and chemistry that initiate and sustain these plasmas, with an aim to exploiting the research findings for various applications.

## References

[1] Bacal M, Bruneteau A M, Graham W G, Hamilton G W and Nachman M "*Pressure and electron temperature dependence of $H^-$ density in a hydrogen plasma*" 1981 J. Appl. Phys. **52** 1247

[2] W G Graham "*Vacuum ultraviolet emission and H- production in a low-pressure hydrogen plasma*" 1984 J. Phys. D: Appl. Phys. **17** 2225

[3] M B Hopkins and W G Graham "*Electron energy distribution function measurements in a magnetic multipole plasma*" 1987 J. Phys. D: Appl. Phys. **20** 838

[4] W G Graham "The kinetics of negative hydrogen ions I in discharges" Plasma Sources Sci. Technol. 1995 **4** 281492

[5] Bill Graham "Technological Plasmas" 2001 Phys. World **14** (3) 31

[6] W.G Graham, C.M.O Mahony, P.G Steen "Electrical and optical characterisation of capacitively and inductively coupled GEC reference cells" Vacuum **56** (1) 3-8

[7] S. Gomez, P. G. Steen, and W. G. Graham "Atomic oxygen surface loss coefficient measurements in a capacitive/inductive radio-frequency plasma" 2002 Appl. Phys. Lett. **81**, 19–21

[8] W G Graham and K R Stalder "*Plasmas in liquids and some of their applications in nanoscience*" 2011 J. Phys. D: Appl. Phys. **44** 174037

# Multiscale hybrid modeling of DF-CCP CF4 plasmas for carbon resist microlens etching

E. Despiau-Pujo[1], P. Ducluzaux[1,2] , D. Ristoiu[1,2], G. Cunge[1]

[1] *LTM, Univ. Grenoble Alpes, CNRS, 17 avenue des Martyrs, 38054 Grenoble, France*
[2] *STMicroelectronics, 850 Rue Jean Monnet, 38920 Crolles, France*

This paper investigates the etching of carbon resist microlenses performed in DF-CCP reactors using CF4 chemistry. Multiscale hybrid simulations (fluid-kinetic, Monte-Carlo) are performed to investigate the impact of operating conditions (LF and HF RF powers, pressure, wall conditions) on the plasma composition, the flux and IEAD of species at the wafer, as well as the etching of blanket wafers and spherical microlenses. Plasma gas-phase simulations show that, as expected, the low-frequency (13,56 MHz) power controls the ion energy while the high-frequency (40.68 MHz) power controls the ion flux at the wafer, while pressure modifies the structure and electronegativity of the plasma. In most of the conditions explored, the multiscale model developed provides a better understanding of the mechanisms involved in the etching of resist microlenses.

## 1 . Introduction

Low-temperature plasmas have been used in the semiconductor industry since the 1960s to process materials and miniaturize devices. Over the past decade, the development of image sensors used in smartphones has focused on reducing pixel size to improve photography resolution. Microlenses are a key component of these sensors, as they focus the incident light on the photodiode, enhancing the sensor's quantum efficiency. However, the fabrication of resist microlenses requires an etching step performed in low-pressure fluorocarbon plasmas, in which plasma-resist interaction are not well understood and can lead to a final 3D shape difficult to control.

In this paper, we investigate the influence of operating conditions on the etching of carbon resist microlenses in CF4 plasmas, to better understand the transfer mechanisms. Using a 2D hybrid fluid-kinetic model, we simulate the CF4 plasma gas-phase in a DF-CCP industrial reactor, as well as the flux and IEAD of plasma species on the wafer. These data are then used as entry parameters for a Monte Carlo etch profile model. We investigate the impact of pressure (30-200 mT), LF and HF RF powers (100-1500 W) on the plasma composition, the IEADF at the wafer, as well as the etch characteristics of resist blanket wafers and spherical microlenses. Results are compared to experimental data (ellipsometry, TOF-SIMS, SEM) to validate the model predictions.

## 2. Model of the DF-CCP CF4 plasma

A schematic of the reactor used in this study is shown in figure 1. The lower electrode is a metal substrate powered through a blocking capacitor by the two RF frequencies (13.56 and 40.68 MHz). The $CF_4$ plasma is simulated using the Hybrid Plasma Equipment Model (HPEM) described in [1]. 14 species are included in the simulation: e-, $CF_{x\ (x=1-4)}$, $F_2$ and F radicals, $CF_x+_{(x=1-3)}$, $F_2$+, F+, CF3- and F- ions. The model includes volume reactions (e.g. inelastic electron impact, charge exchange, neutralization, etc.) directly affecting these species densities, as well as surface reactions (neutral recombination or reflection, ion neutralization, etc.) described using global reaction probabilities.

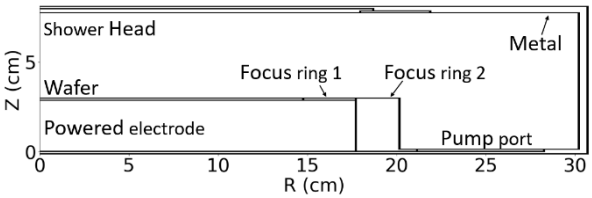



Figure 1: Schematic of the DF-CCP reactor

## 3 Results and discussion

In base-case conditions, CF3+ and F- are shown to be the primary ions in the gas-phase, while F, CF, CF3, CF2, and F2 as the predominant radicals (by decreasing density). It is also found that increasing the surface recombination coefficient of F radicals into F2 at the reactor walls, $\gamma$(rec,F>F2), has a strong impact on the final plasma composition, decreasing CF and F densities while increasing CF3, CF2 and F densities. The LF power (100-900 W) is shown to substantially modify the IEDF owing to sheath voltage changes, while the HF power (100-1500 W) strongly impacts the ion flux at the wafer due to HF voltage fluctuations. Increasing the pressure from 30 to 200mTorr increases the electronegativity by a factor 4, strongly impacts the plasma structure and widens the ion angular spread, potentially influencing etch uniformity. The impact of operating conditions on the etching of carbon resist blanket wafers and spherical microlenses will be discussed in details during the presentation and provide insights into the chemico-physical mechanisms involved.

## References

[1] Kushner MJ, J. Phys. D: Appl. Phys. 42, 194013 (2009)
[2] Ducluzaux P, Ristoiu D, Cunge G, Despiau-Pujo E, J. Vac. Sci. Technol. A 42, 013002 (2024)

# Preheating applied on a 915 MHz $CO_2$ Microwave Plasma: Unlocking the Potential for Heat Recycling in Plasma Systems

C.F.A.M. van Deursen[*1], and E.R. Mercer[*2], F.J.J. Peeters[1], F.M.A. Smits[3], W.A. Bongers[1], A. Bogaerts[2] and M.C.M. van de Sanden[4]

*Dual first authorship

[1] *Research Group PSFD, Dutch Institute for Fundamental Energy Research, Eindhoven, The Netherlands*

[2] *Research group PLASMANT, Department of Chemistry, University of Antwerp, Antwerpen, Belgium*

[3] *Department of Mathematics and Physical sciences, Leiden university, Leiden, The Netherlands*

[4] *Eindhoven Institute of Renewable Energy Systems, Eindhoven University of Technology, Eindhoven, The Netherlands*

**Abstract:** In this work, we present an investigation of the influence of heated input flows on a $CO_2$ microwave discharge. Our study explores the benefits of heat recycling for enhancing conversion and energy efficiency in future industrial applications of plasma-based $CO_2$ conversion. Effluent composition, plasma size, thermal losses and plasma temperatures were investigated. We demonstrate that recycling less than 10% of the input power (1000 W) to preheat $CO_2$ ($T_{inlet}$ = 700 K) can increase $CO_2$ conversion and energy efficiency by up to ~74% at quasi-atmospheric pressure (700 mbar). Spectroscopic and thermographic measurements show that the increase in performance is due to an increase in the 'reactive volume' (i.e. the high temperature region surrounding the plasma) and changes to flow dynamics.

## 1 Introduction

Microwave (MW) plasmas offer a promising approach for splitting $CO_2$ with high energy efficiencies, approaching the thermal limit of ~50% [1,2]. In these reactors $CO_2$ is rapidly heated to temperatures of >3000 K, driving thermal dissociation. However, a large part of the input energy is lost as heat in the effluent [3]. Recuperation of heat using a heat exchanger is a well-known method to increase process efficiency in industry, leading to the question whether or not there is a benefit in utilizing heat recovery in $CO_2$ plasma reactors.

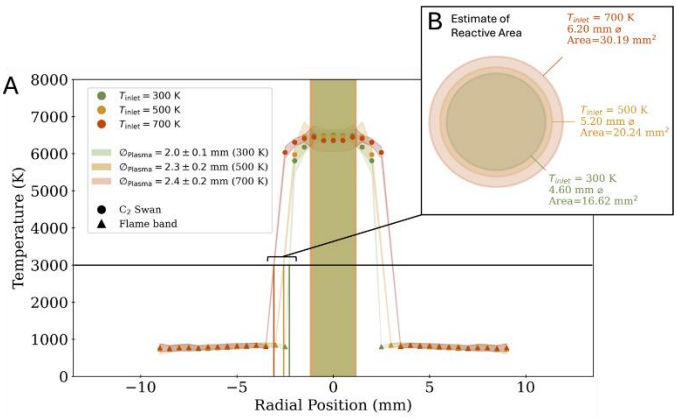



Figure 1: Reactive area ($T_g$ > 3000 K) for a 1000 W, 10 ln/min, 700 mbar plasma at different inlet temperatures.

## 2 Methods

Experiments took place in a 915 MHz MW plasma reactor. An FeCrAl spiral heater was used to preheat the injection flow to temperatures up to 850 K. Conversion and energy efficiencies were determined using gas chromatography. Plasma sizes were determined using the atomic oxygen 777 nm emission profile, and the plasma temperature profile was determined using optical emission spectroscopy, utilizing the $C_2$ Swan band. Thermal losses through the wall were measured using IR thermography.

## 3 Results and Discussion

Conversions and energy efficiencies were determined for a 1000 W, 10 slm $CO_2$ plasma at different pressures, showing a relative increase of up to 74 % at near-atmospheric pressure (700 mbar) by preheating the inlet gas to $T_{inlet}$ = 700 K. CCD imaging of the oxygen 777 nm line shows little change to the plasma diameter with increasing $T_{inlet}$; however, spectroscopic measurements of the $C_2$ Swan bands show that the reactive volume (i.e. the region in which temperatures are sufficiently high to dissociate $CO_2$) increases with $T_{inlet}$, as shown in Figure 1. Further analysis using IR thermography shows stark changes in heat loss near the wall, indicating changes to flow dynamics, as well as increased CO+O recombination.

## 4 Conclusions

This work presents results of a preheated 915 MHz $CO_2$ plasma reactor, showing increased conversion and energy efficiencies as a function of $T_{inlet}$. Spectroscopic measurements reveal that this increase is likely caused by enlargement of the reactive volume. Present work shows that heat recovery in $CO_2$ plasma reactors is a viable strategy for increasing the system-level efficiency of these reactors.

**References**

[1] A. Hecimovic et. al., J. $CO_2$ Util., **57**, 101870 (2022)

[2] W.A. Bongers et. al., Plasma Processes and Polymers, **14**, 1600126 (2017)

[3] C.F.A.M. van Deursen et. al., J. $CO_2$ Util., **88**, 102952 (2024)

# The role of liquid layers as a circuit element in plasma activated solution chemistry

Tiago C. Dias, Jisu Jeon and Mark J. Kushner
*Dept. Electrical Engr. & Computer Science, University of Michigan, Ann Arbor, MI 48109-2122 USA*

Plasma activated solution chemistry leverages atmospheric-pressure plasmas to chemically modify liquids. The liquid layer is an active element in the electrical circuit that produces the activation. We investigate the consequences of liquid thickness, conductivity, substrate material, and circuit impedance on the strength and propagation of surface ionization waves (SIWs) across the liquid. Computational results show that higher liquid capacitance boosts SIW intensity and extent, while higher liquid conductivity confines the SIW to the center. The substrate material is also relevant, as it contributes to the overall capacitance between the plasma and the ground electrode.

Plasma activated solution chemistry, one example being plasma-driven solution electrochemistry (PDSE), leverages atmospheric pressure plasmas (APPs) in contact with solutions to modify their chemical composition [1]. Energetic plasma species (electrons, ions, photons, and radicals) impinge on the liquid surface, initiating physicochemical processes at the gas/liquid interface and within the liquid phase. Since these interactions can trigger the consumption or generation of new species, APPs can be used both for liquid decontamination (such as removing PFAS molecules from water) and for synthesis of materials (such as silver nanoparticles) as in PDSE.

In many such applications, the plasma on the surface of the solution takes the form of a surface ionization wave (SIW) which hugs the surface. The strength of the SIW depends, among other factors, on the impedance of the liquid and its container, as this determines how much charge can be deposited onto the liquid surface, thereby influencing the resulting electric field of the SIW. The impedance of the driving circuit couples to the impedance of the liquid to affect reactive fluences to the surface.

In this work, we performed a computational investigation of the electrical parameters of the treated liquid, such as its capacitance, conductivity, and container material, and the impedance of the driving circuit, to quantify their impact on SIWs. Results are discussed for APPs sustained in $Ar/H_2O$ mixtures impinging onto thin water layers. The model used in this investigation is *nonPDPSIM*, a 2-dimensional plasma hydrodynamics model executed on an unstructured mesh, which can address both gas and liquid phases [2]. For the results discussed here, the plasma is sustained in an $Ar/H_2O$ = 98/2 gas mixture flowing through a 2 mm-wide tube. The thickness of the water layer varies from 1.2 to 5.0 mm. The water conductivity varies from 0.01 to 0.5 mS/cm, controlled by adjusting NaCl concentration. The material below the water can be either grounded metal or a dielectric. A -18 kV pulse of 100 ns duration with a 5 ns rise time was applied to the powered electrode to generate the plasma. The gap between the powered electrode and the liquid surface is 5 mm.

Electron densities near the liquid surface after 40 ns for liquid thicknesses of 1.2, 2.4, and 5.0 mm are shown in Fig. 1. The surface below the liquid is a grounded metal. As the liquid capacitance varies inversely with thickness, thinner liquids enable higher surface charging, generating stronger SIWs, both in terms of the electron density and the maximum extent of the wave. However, the material containing the liquid is also important, since if it is not a grounded metal, the overall capacitance is defined by the series impedance of the liquid and the container. The liquid conductivity is another key parameter. SIWs interacting with high-conductivity liquids propagate slower across the liquid, being focused at the center, as current can also flow through the liquid volume.

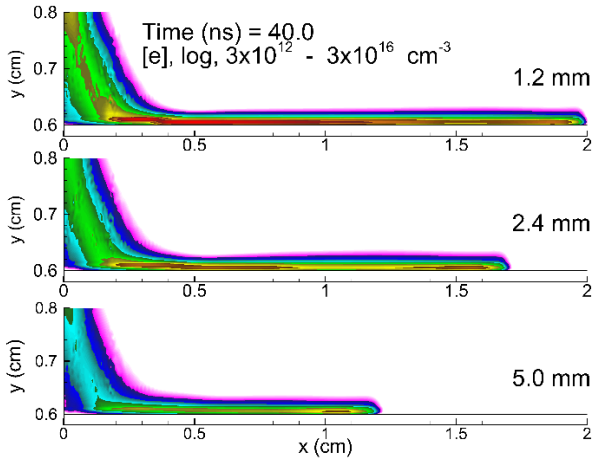



**Figure 1:** Electron density near the liquid surface for liquid thicknesses of 1.2, 2.4 and 5.0 mm.

**Acknowledgements:** Work supported by US Dept. of Energy (DE-SC0020232), Army Research Office (W911NF-20-1-0105), National Science Foundation (2032604) and 3M Company.

**References**

[1] P. Bruggeman *et al. J.Chem.Phys.* **162**, 071001 (2025).
[2] S. Doyle *et al. Plasma Sources Sci. Technol.* **34**, 035004 (2025).

# Secondary electron emission effects in low-pressure discharges

Z. Donkó[1]

[1]*HUN-REN Wigner Research Centre for Physics, Budapest, Hungary*

The emission of secondary electrons may have a significant influence of the operation of gas discharges. The talk will review these effects and report on recent efforts that focused on the in-situ determination of the effective secondary electron yield in low-pressure capacitively coupled plasmas.

## 1 Introduction

The emission of secondary electrons from the electrodes of gas discharges is indispensable for the self-sustained direct-current (DC) discharges and is often important as well in radiofrequency (RF) plasmas. While in the majority of studies ion-induced electron emission is considered exclusively, like in the fundamental Paschen theory of gas breakdown, in reality, additional species: metastable atoms, fast ground-state atoms – originating from ion-atom collisions – and ultraviolet photons may induce the emission of secondary electrons, too [1]. In [2], in the revision of the classical Paschen theory, the contributions of these species have been quantified for discharges characterized by a homogeneous electric field (i.e., for Townsend discharges) in argon gas. The results of this study were shown not to be directly applicable to DC glow discharges with an inhomogeneous electric field [3], where the importance of the fast neutrals was quantified in [4]. The effects of secondary electrons in RF capacitively coupled plasmas (CCP) were also addressed in some studies. The most spectacular of these effects is perhaps the "α-γ mode transition" [5], when the power absorption by the secondary electrons via their acceleration in the sheath electric field becomes dominant over the energy gain of bulk electrons in the ambipolar field near the sheath edge. In cases when multiple species contribute to electron emission, the use an effective secondary electron yield (the ratio of the electron to the ion flux at the electrode) is appropriate.

One has to note, that some of the secondary electron yield data in the literature originate from surface physics experiments carried out under ultrahigh vacuum conditions and with carefully prepared samples. As these conditions differ significantly from those of usual discharge physics experiments, data originating from surface physics experiments are usually not directly applicable in gas discharge modelling.

## 2 Recent works

During the past years, a number of studies have targeted the in-situ determination of the effective secondary electron yield in low-pressure CCPs. The studies quoted below were all based on synergistic combinations of experiments and simulations. The authors of [6] developed a computationally assisted spectroscopic technique ($\gamma$-CAST) that is based on the comparison of measured and computed spatio-temporal excitation maps for atomic transitions, obtained, respectively, by phase resolved optical emission spectroscopy (PROES) and particle-in-cell / Monte Carlo collisions (PIC/MCC) simulations. This approach was subsequently extended to a wider range of operating conditions [7] and to various electrode materials [8]. In [9], measurements / computations of the ion energy distributions at the electrodes and in [10], the dependence of the DC self-bias voltage developing in a CCP under dual-frequency excitation were utilized for the determination of the effective secondary electron yield under actual discharge operation.

**References**

[1] Little, P. F. "Secondary Effects" in *Encyclopedia of Physics* **XXI**, Ed. Flügge, S. (1956).
[2] Phelps, A. V., Petrovic Z. Lj., *Plasma Sources Sci. Technol.* **8**, R21 (1999).
[3] Phelps, A. V., Pitchford, L. C., Pedoussat, C., Donkó, Z. *Plasma Sources Sci. Technol*. **8**, B1 (1999).
[4] Donkó, Z. *Phys. Rev. E* **64**, 026401 (2001).
[5] Belenguer, Ph., Boeuf J.-P., *Phys. Rev. A* **41**, 4447 (1990).
[6] Daksha, M., Berger, B., et al. *J. Phys. D* **49**, 234001 (2016).
[7] Schulenberg, D. A., Korolov I., et al. *Plasma Sources Sci. Technol*. **30**, 105003 (2021).
[8] Beckfeld, F., Masheyeva R., et al. *Plasma Sources Sci. Technol.* **34**, 035009 (2025).
[9] Schulze, C., Donkó, Z., Benedikt, J. *Plasma Sources Sci. Technol*. **31**, 105017 (2022).
[10] Masheyeva, R., Hartmann, P., et al. *J. Phys. D* **58**, 045208 (2024).

# Plasma interactions with a surface cooled to a cryogenic temperature

R. Dussart[1], T. Tillocher[1], L. Becerra[1], P. Lefaucheux[1]

[1]*Université d'Orléans, CNRS, GREMI UMR 7344, Orléans, France*

Although it seems quite counterintuitive, cooling the substrate to a very low temperature can increase the chemical reactions during plasma-surface interaction and significantly improve the process efficacy. Many examples clearly show the benefits of decreasing the temperature for different processes of plasma etching, plasma enhanced chemical vapour deposition (PECVD) or physical vapour deposition (PVD). In this paper, we discuss the involved mechanisms that have been highlighted in different examples of cryogenic etching.

## 1 Introduction

It is a well known effect, which was highlighted a long time ago by the cryo-chemistry community, that chemical activity can be heaved when a material sample is cooled or frozen to a very low temperature [1,2]. This effect is of interest for cryogenic plasma processes for thin film deposition or etching. For example, sputtering deposition experiments at cryogenic temperature was performed to form microcrystalline structures. [3] Carbon nitride deposition by reactive sputtering on a temperature range from -130°C to 600°C was also reported by another team. [4] Cryo-etching was introduced more than 35 years ago by a Japanese team. [5] Today, cryoetching is attracting renewed interest from companies, particularly for dielectric deep etching. [6] In this paper, we will discuss the involved mechanisms, which make the cryo-processes attractive.

## 2 Chemical activity at low temperature

To illustrate the effect of surface temperature, an example of etch rate (ER) of $SiO_2$ versus $H_2$ content in $SF_6/H_2$ plasma is provided in figure 1 for substrate temperatures of +20 and -130°C. An ICP reactor was used for this experiment. High source power (2000W) and high bias power (200W) were used to achieve a high etch rate. The effects of temperature and chemical reactions are clearly established in this example: The addition of $H_2$ enhances the chemical activity, but only at low temperature. The formation of HF and its longer residence time can explain this higher ER value.

Another example is given in $SiF_4/O_2$ plasma to form a $SiO_xF_y$ layer on Si, $Si_3N_4$ or $SiO_2$ surface. Using this plasma mixture, a very different chemical composition of the $SiO_xF_y$ layer is obtained if the substrate is cooled to a very low temperature. In particular, in-situ XPS analysis showed that fluorine content was much higher at low temperature. This effect can be explained by the enhanced physisorption of radicals at lower temperature.

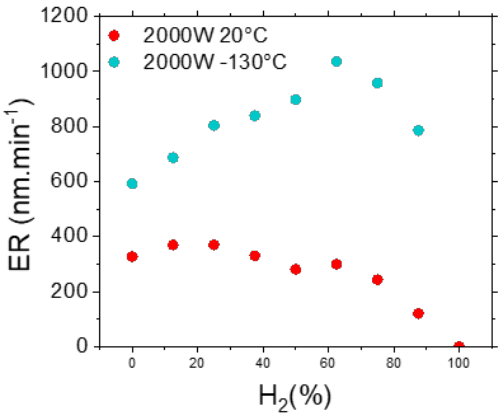



Figure 1: Etch rate of $SiO_2$ versus $H_2$ content in $SF_6/H_2$ plasma for temperatures of +20 and -130°C

## 3 Conclusion

Cooling the substrate to a very low temperature can significantly modify the chemical activity at its surface. Other examples will be detailed at the conference.

**References**

[1] McGee, H. A. and Martin W. J. Cryochemistry. *Cryogenics*, vol2 (5) 257 (1962).
[2] An, L.-Y. et al. Molecules 26 750 (2021)
[3] Chambers, D. L. et al. Surface and Coatings Technology 36 893–900 (1988)
[4] Khabashesku, V. N. et al. Thin Solid Films 381 62–8 (2001)
[5] Tachi, S. Tsujimoto, K. and Okudaira S. Appl. Phys. Lett. 52 616–8 1988
[6] Oehrlein, G. S. et al. J. Vac. Sci. Technol. B 42(4), 041501 (2024).

# Understanding streamer discharges – where do we stand?

Ute Ebert[1]

[1] *Group Multiscale Dynamics, Centrum Wiskunde & Informatica (CWI), Amsterdam, The Netherlands*
[2] *Dept. Applied Physics, Eindhoven University of Technology, Eindhoven, The Netherlands*

Streamers generically appear in the early stage of gas discharges, both in plasma technology and in nature. They transform neutral gas into weakly ionized plasma, and their high energy electrons can drive non-equilibrium chemistry as well as high energy radiation. I will review the state of approach and understanding, and the many puzzles that remain.

Streamer discharges appear in nature in the early stages of lightning and in blue jets and sprite discharges above thunderclouds, and they contribute to generating terrestrial gamma-ray flashes. They also appear in numerous fields of technology such as in plasma medicine, in plasma agriculture, or in high voltage grids for electrical transmission.

There has been much progress in recent years on high resolution measurements and on multiscale modelling of streamer propagation and branching, on verification and validation and on model reduction. General features are:

- Positive streamers can start at lower background fields than negative ones. This makes them more relevant for applications.
- In contrast, in radio measurements of intracloud lightning mostly negative streamers are detected.
- Radius and velocity can vary by orders of magnitude.
- Streamers can propagate into background fields below the breakdown value due to the local field enhancement at their tips.
- Streamer heads leave a conducting plasma trail behind.

But … all these statements are valid for streamers in air, but not in general! Very different behaviour is observed in pure nitrogen or in insulating gases for high voltage technology.

I will discuss how this different behaviour depends on gas properties such as photoionization and electron attachment rates.

There are plenty more questions:

- How do discharges consisting of thousands of streamers behave collectively?
- How much do they change the chemical composition of the gas?
- How do they contribute to the emission of high energy radiation (> 1MeV) in thunderstorms?
- How do streamers move in strong magnetic fields?

I will sketch my view on the current understanding of streamer dynamics.

I acknowledge the long term collaboration on the topics of this talk with Sander Nijdam and Jannis Teunissen, and with my, their, and our PhD students and postdocs.

# Challenges of negative hydrogen ion sources for ITER's neutral beam systems

U. Fantz for the IPP NNBI Team

[1] *Max-Planck-Institut für Plasmaphysik, IPP, Garching, Germany*

The challenges of developing a large and powerful low temperature plasma to deliver the required current of extracted negative hydrogen ions ($H^-$, $D^-$) for heating and current drive of the international fusion experiment ITER are enormous. Limiting parameters are the reduction of the co-extracted electrons and thus the electron density in front of the extraction apertures, their homogeneity over the large ion source area (1 m × 2 m) and the temporal stability, which depends strongly on the caesium that is injected to achieve the required negative ion densities at the pressure of 0.3 Pa. Physical insights and technology developments paved the way for the recent world record values in hydrogen achieved with the half-size ion source at ELISE reaching the ion source performance for ITER's first operation phase with NBI.

## 1 Introduction

Large and powerful negative hydrogen ion sources ($H^-$, $D^-$) will be used at the international fusion experiment ITER to deliver after acceleration and neutralization energetic beams of neutral particles (H, D) to the tokamak. These beams will be used for heating and current drive, but also for plasma diagnostics [1]. The inductively coupled plasma source (ICP) operates at a frequency of 1 MHz and at low gas pressure (0.3 Pa) using a total RF power of 800 kW to illuminate an area of 1 m × 2 m. The production of negative ions relies on the surface conversion of hydrogen atoms and positive ions at a converter surface with a low work function, for which caesium is injected into the low-temperature plasma.

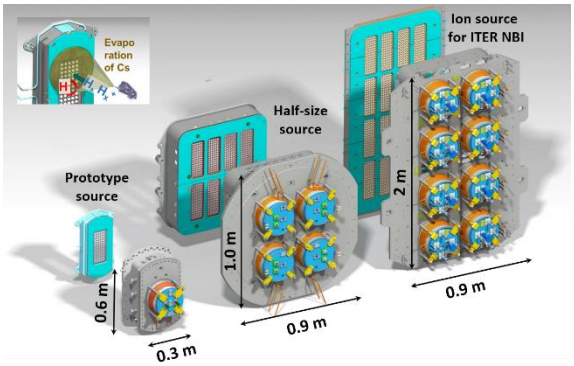



**Figure 1: Size scaling route of the modular ICP system. Each cylindrical driver is powered with an RF power of up to 100 kW. The surface conversion process is illustrated in the small inset.**

Within the European step ladder approach the size scaling from the prototype source towards the full-size source of ITER NBI is complemented by the half-size system (Figure 1) [2]. The corresponding test facilities BATMAN Upgrade and ELISE, equipped with the prototype and the half-size source, both at IPP Garching, as well as the full-size source from SPIDER and MITICA at the Neutral Beam Test Facility hosted by Consorzio RFX, Padua, Italy contribute to achieving the required target parameters and reliable operation.

## 2 Challenges and current status

The ion source must deliver a current of up to 60 A of homogeneously extracted negative ions for one hour. Additionally, the unavoidable co-extracted electron current must be reduced to prevent damage to the extraction system. Injecting caesium into the source introduces a temporal component and together with the required magnetic filter field, a spatial component into the otherwise stable and homogeneous plasma. Plasma diagnostics and modelling provide valuable insights into various aspects of plasma physics in these electronegative plasmas. The technological implementation of the knowledge gained made it possible to achieve world-record pulses at the ELISE test facility, which represent a milestone towards operating ITER NBI during its first DT campaign [3].

**References**

[1] Hemsworth R. et al. Overview of the design of the ITER heating neutral beam injectors. *New J. Phys.* **19** 025005 (2017).

[2] Fantz, U. et al. Contributions of the extended ELISE and BATMAN Upgrade test facilities to the roadmap towards ITER NBI. *Nucl. Fusion* **64**, 086063 (2024).

[3] Wünderlich, D. et al. ITER-relevant 600 s steady-state extraction of negative hydrogen ions at the test facility ELISE. *Nucl. Fusion* **65**, 014001 (2025).

# Particle-In-Cell Modelling of Low Temperature Plasmas

G. Fubiani[1], N. Savard[2,3], L. Garrigues[1], F. Gaboriau[1] and M. Dehnel[4]
[1] *LAPLACE, Université de Toulouse, CNRS, Toulouse, France*
[2] *TRIUMF, 4004 Wesbrook Mall Vancouver, BC V6T 2A3 Canada*
[3] *D-Pace, Suite 305, 625 Front Street Nelson — British Columbia — Canada V1L 4B6*
[4] Selkirk Ion-source Research Centre (SIRC), 2950 Highway Drive, Trail, BC, Canada V1R 2T3

Particle-In-Cell (PIC) models are effective in simulating low-pressure plasmas, but they face challenges due to the need to resolve both small and large scales, like plasma sheaths and instability wavelengths, within devices that are typically tens of centimeters in size. Standard explicit PIC methods require fine grids and small time steps to resolve the electron Debye length and plasma frequency, often necessitating parallel 3D computations. Advanced approaches, such as fully implicit charge- and energy-conserving algorithms, have relaxed these constraints by enabling larger, non-uniform grid sizes tailored to local physics. Another promising method uses sparse grids, which significantly reduce the number of grid nodes and macro-particles, thus accelerating convergence. This review critically examines these techniques, highlighting their strengths, limitations, and applications in low-temperature plasma physics research.

## 1 Overview

PIC simulations approximate the Boltzmann equation for a plasma by modeling particles as macro-particles and solving Maxwell's equations on a discrete grid [1]. The explicit leap-frog method is commonly used due to its simplicity, but it has notable limitations. The grid spacing $\Delta x$ must be smaller than the electron Debye length $\lambda_{De}$ to avoid finite-grid instability. Additionally, $\sim 100$ macro-particles per cell are required to minimize statistical noise, and the time step $\Delta t$ must satisfy the CFL condition $\Delta t < \Delta x/(\lambda_{De}\omega_{pe})$, where $\omega_{pe}$ is the plasma frequency. To overcome these constraints, fully implicit, energy-conserving methods were developed, coupling particles and fields nonlinearly [2]. These methods were also made charge-conserving and capable of using non-uniform grids [3, 4]. Implicit schemes are unconditionally stable, allowing for $\Delta t > \omega_{pe}^{-1}$ and $\Delta x \gg \lambda_{De}$. Recent work have studied its applicability to model low electron temperature bounded plasma discharges and found that the complexity of the algorithm combined with the need for a large number of macro-particles per Debye sphere for convergence results in a runtime in 1D often comparable to the performance of explicit models. Another promising development in the field of kinetic modelling is the so-called sparse grid particle-in-cell PIC technique [5]. It associates sparse grids with the so-called "combination technique" to improve the computational efficiency of PIC simulations. By utilizing sparse grids, the method allows for a significantly smaller amount of cell nodes in multi-dimensional PIC simulations. This approach reduces the overall computational cost while maintaining accuracy, as it only incurs a minor increase in grid-based error. The result is a faster and more efficient simulation framework for modelling plasma dynamics. We will review these different techniques providing a critical assessment of the advantages and limitations of each using as examples simulations of Hall Thrusters (HT), Penning, Radio-Frequency (RF) and Capacitively Coupled Plasma (CCP) discharges, respectively.

## References

[1] Charles K. Birdsall and A. Bruce Langdon. *Plasma physics via computer simulation*. Institute of Physics Pub., 2005.

[2] Stefano Markidis and Giovanni Lapenta. The energy conserving particle-in-cell method. *Journal of Computational Physics*, 230(18):7037–7052, 2011.

[3] L. Chacón, G. Chen, and D.C. Barnes. A charge- and energy-conserving implicit, electrostatic particle-in-cell algorithm on mapped computational meshes. *Journal of Computational Physics*, 233:1–9, 2013.

[4] D. Eremin. An energy- and charge-conserving electrostatic implicit particle-in-cell algorithm for simulations of collisional bounded plasmas. *Journal of Computational Physics*, 452:110934, 2022.

[5] L. Garrigues, M. Chung-To-Sang, G. Fubiani, C. Guillet, F. Deluzet, and J. Narski. Acceleration of particle-in-cell simulations using sparse grid algorithms. i. application to dual frequency capacitive discharges. *Physics of Plasmas*, 31(7):073907, 07 2024.

# Optical and Electrical Characteristics of Bipolar Nanosecond Electrical Discharge at the Water-Air Interface

Garima Arora[1], Jiří Fujera[1], Petr Hoffer[1], and Milan Šimek[1]

[1] *Institute of Plasma Physics of Czech Academy of Sciences, U Slovanky 2525/1a, 18200Prague, Czech Republic*
e-mail: arora@ipp.cas.cz

## 1 Introduction

The interaction between low-temperature plasma and water brings dramatic changes in the water's properties, leading to the generation of highly reactive nitrogen and oxygen species (RONS). This field of study has gathered considerable attention due to its promising applications, especially in the innovative area of plasma-activated water (PAW)[1-3]. In our recent work, we have introduced a unique design for producing plasma-activated water, where the discharge effectively propagates along the air-water interface, significantly enhancing nitrogen fixation in water [4]. The reactor is a 3D-printed plastic vessel, divided into three distinct compartments by plastic blades consisting of a high-voltage (HV) middle electrode and two grounded electrodes. The comprehensive analysis of the discharge phases and their characteristics using ultrafast imaging and optical emission spectroscopy was conducted in conjunction with its electrical properties. Our findings indicate the formation of a distinct discharge morphology, characterized initially by a diffusive streamer phase that transitions into a spark phase with filamentary behaviour. A study of the discharge morphology demonstrates that initially a diffuse streamer phase is formed, followed by a spark phase with the formation of several dominant filaments. The properties of these two phases were studied in two different conductivities of water [5-6]. The time-resolved emission spectra were recorded at the centre of the blade and found that the streamer phase is characterized by molecular bands of nitrogen followed by atomic lines emission in the spark phase.

### Results and Discussion

In this work, we present a detailed investigation of the spatial characteristics of the plasma-induced emission within all three compartments—HV, ground, and centre of the blade—using various optical diagnostics, including fast photomultiplier tubes (PMTs), intensified charge-coupled imaging devices (ICCDs), and emission spectroscopy. The results indicate that emission intensity is significantly higher at the blade compared to both the grounded area and the HV region. Furthermore, the effect on optical characteristics with the polarity of the applied voltage will be discussed. Our preliminary findings reveal a strong variations of electric field E/N whereas the spectra suggest that only atomic line emissions are present in the negative polarity regime. This work not only elevates our understanding of plasma-liquid interactions but also establishes a clear pathway for practical advancements in the field of plasma-activated water and nitrogen fixation.

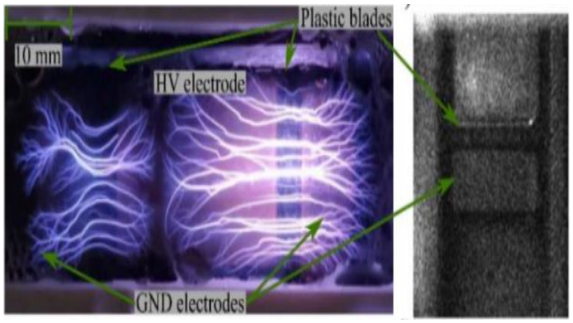



Fig1. Picture of the whole reactor showing the three compartments.

### References

[1] Adamovich, I., Agarwal, S., Ahedo, E., Alves, L. L., Baalrud, S., Babaeva, N., ... & von Woedtke, T. *Journal of Physics D: Applied Physics* ***55*****(37)**, 373001 (2001).

[2] Weltmann, K. D., Kolb, J. F., Holub, M., Uhrlandt, D., Šimek, M., Ostrikov, K., ... & Becker, K. , Plasma Processes and Polymers **16(1)** 1800118 (2019).

[3] Guo, D., Liu, H., Zhou, L., Xie, J., & He, C. *Journal of the Science of Food and Agriculture* ***101*** **(12)** 4891-4899 (2021).

[4] Hoffer, P., Niedoba, K., Jirásek, V., Prukner, V., & Šimek, M. **43(6)** 1531-1547 (2023).

[5] Hoffer, P., Prukner, V., Arora, G., & Šimek, M. *Plasma Sources Science and Technology*, ***32*****(9)**, 09LT01 (2023).

[6] Arora, G., Hoffer, P., Prukner, V., Bílek, P., & Šimek, M. Plasma Sources Science and Technology, **33(2)**, 025025 (2024).

### Acknowledgement

This study was supported by the Grant Agency of the Czech Republic (grant number: GA24-10903S).

# Simulation of magnetized RF capacitively coupled plasma discharges using 3D sparse Particle-In-Cell algorithms

L. Garrigues[1], G. Fubiani[1] and M. Lobet[2]

[1] *LAPLACE, Université de Toulouse, CNRS, INPT, UPS, Toulouse, France*
[2] *Maison de la Simulation, CEA, CNRS, Université Paris-Sud, UVSQ, Université Paris-Saclay, Gif-sur-Yvette, France*

3D Particle-In-Cell (PIC) simulations in the context of low temperature plasma surveys are very time consuming. The combination of sparse methods with PIC algorithms can drastically reduce the computational time while maintaining a minimum error between standard and sparse PIC approaches. We illustrate a comparison between the two approaches in the context of magnetized radio-frequency (RF) capacitively coupled plasma (CCP) discharge.

## 1 Introduction

The radio-frequency (RF) capacitively coupled plasmas (CCP) are widely used in the semiconductor industry for etching and deposition [1]. The electrostatic Particle-In-Cell (PIC) method, which is based on the coupling between a Lagrangian description of the charged particles transport and a Eulerian approach to resolve the Poisson's equation on a prescribed computational grid, has been largely employed to study the effect of the voltage waveform and frequency applied on the RF electrode (see e.g.[2]), the plasma chemistry [3], etc.

The introduction of a magnetic field to enhance the plasma density has revealed the existence of instabilities that modify the plasma uniformity studied with 2D PIC simulations [4]. We have performed 3D PIC simulations of magnetized RF CCP using sparse PIC algorithms.

## 2 Sparse PIC approaches

In a standard discretization of a uniform square Cartesian grid of $M$ meshes for a dimension $d$, the number of freedom is $M^d$. The objective of sparse algorithms is to compute a hierarchy of anisotropic grids with a coarser resolution, hence reducing the total number of degrees of freedom lower than $M^d$. Coupling sparse method with PIC algorithms leads to reduce the total number of cells and consequently the total number of particles for a same statistical error than the standard PIC algorithms [5]. This results in a faster calculation time.

Ricketson and Cerfon [6] have firstly demonstrated the interest of the sparse PIC method in the context of Landau damping and diocotron instability. More recently, the sparse PIC approach has been applied in the context of 2D simulations of low temperature plasmas, including collisions, ion motion, appropriated boundary conditions, for unmagnetized RF capacitively coupled plasma discharge [7], and for partially magnetized plasmas [8].

## 3 Results

We will show at this conference the comparisons between standard and sparse PIC approaches in the context of 3D simulations of magnetized RF CCP discharges.

**Acknowledgments**
This research was funded by l'Agence Nationale de la Recherche (ANR), project ANR-22-CE46-0012. This work was granted access to the HPC resources of TGCC/Joliot Curie under the allocation A0162B13923.

**References**

[1] P. Chabert and N. Braithwaite, *Physics of Radio-Frequency Plasmas*, Cambridge University Press, Cambridge, UK, 2011.
[2] Z. Bi, Y. Liu, W. Jiang, X. Xu, and Y. Wang, *Curr. Appl. Phys.* **11**, S2–S8 (2011).
[3] Q. H. Yuan, C. Ye, Y. Xin, X. J. Huang, Z. Y. Ning, and G. Q. Yin, *Appl. Phys. Lett.* **93**, 071503 (2008).
[4] S. S. Ganta, K. Bera, S. Rauf, I. Kaganovich, A. Khrabov, A. T. Powis, D. Sydorenko, and L. Xu, *Phys. Plasmas* **31**, 102107 (2024).
[5] F. Deluzet G. Fubiani, L. Garrigues, C. Guillet, and J. Narski, *ESAIM: Math. Model. Numer. Anal.* **56**, 1809 (2022).
[6] L. F. Rickeston and A. J. Cerfon, *Plasma Phys. Control. Fusion* **59**, 024002 (2017).
[7] L. Garrigues, M. Chung-To-Sang, G. Fubiani, C. Guillet, F. Deluzet, and J. Narski, *Phys. Plasmas* **31**, 073907 (2024).
[8] L. Garrigues, M. Chung-To-Sang, G. Fubiani, C. Guillet, F. Deluzet, and J. Narski, *Phys. Plasmas* **31**, 073908 (2024).

# $H_2O_2$ production in atmospheric pressure plasmas for plasma-assisted biocatalysis

J. Golda[1], S. Schüttler[1], T. Dirks[2], S. Klopsch[2], A.L. Schöne[3], A.R. Gibson[4] and J. Bandow[2]

[1] *Plasma Interface Physics, Ruhr University Bochum, Bochum, Germany*
[2] *Applied Microbiology, Ruhr University Bochum, Bochum, Germany*
[3] *AEPT, Ruhr University Bochum, Bochum, Germany*
[4] *University of York, York, UK*

This study explores the integration of low-temperature plasmas into catalytic processes for renewable energy storage and industry electrification. We focus on biocatalysis, where enzymes selectively oxidize carbon atoms, offering a green alternative to metal catalysis. Atmospheric pressure plasmas produce necessary reactants, but biocatalysts require mild, stable conditions. We present a method to tune plasma and liquid chemistry for biocatalysis, using multiple plasma sources for scale-up. Our setup involves a capillary plasma jet delivering $H_2O_2$ to enzymes, with diagnostics and simulations to optimize production and transport. Results show tailored $H_2O_2$ delivery and improved energy efficiency through plasma pulsing.

## Motivation

The integration of low-temperature plasmas into catalytic processes has gained attention for storing renewable energy in chemical forms, aiding industry electrification in response to the climate crisis. Biocatalysis, using enzymes for selective oxidation of carbon atoms, offers a green alternative to metal catalysis. Enzymes are highly selective, reducing side product formation and simplifying downstream purification. Production in atmospheric pressure plasmas is one way to provide these reactants [1].

However, biocatalysts are biological macromolecules requiring mild and stable operating conditions which often include the supply of substrates and reactants within a narrow concentration range. Additionally, some plasma-produced species might also be harmful to the enzymes. Thus, a selective tuning of the plasma chemistry is required. Here, we present a rational approach to tuning plasma and liquid chemistry for biocatalysis combining biotechnology, experimental, and computational plasma science expertise.

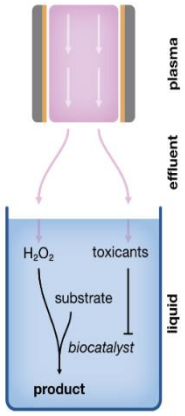



**Figure 1: Setup for plasma-assisted**

## Setup

The setup is schematically shown in Fig. 1. The enzyme unspecific peroxygenase (UPO) requires $H_2O_2$ delivered from the plasma to catalyze ethylbenzene into R-1-phenylethanol. The atmospheric pressure plasma jet used was a capillary plasma jet developed by Winzer et al. [2]. It is comparable to the COST reference plasma jet [3] and was operated using RF excitation in humid helium.

## Results

We used various gas and liquid diagnostics such as mass spectrometry, Fourier transform infrared, laser-induced fluorescence, and mass spectrometry compared to simulations to understand the production and transport of $H_2O_2$ for biocatalysis.

Our measurements show that the $H_2O_2$ reaching the enzymes is almost entirely produced in the plasma by recombination of OH. By varying plasma parameters and treatment distance, we can tailor the $H_2O_2$ concentration to reach the enzymes in the liquid. The solution in the liquid obeys Henry's law taking into account a thin interface layer at the liquid's surface [4]. While at higher gas flows, convection is dominating in the liquid, smaller gas flow rates lead to diffusion-dominated liquid transport.

By pulsing the plasma source, the energy efficiency of $H_2O_2$ production can be increased. Additionally, the plasma chemistry can be shifted between hydrogen and oxygen chemistry [5].

## Acknowledgments

This work is supported by the DFG within CRC 1316 (Project B11, project number 327886311).

## References

[1] A. Yayci et al., ChemCatChem **12**, 5893-5897 (2020).
[2] T. Winzer et al., J. Appl. Phys. **132**, 183301 (2022).
[3] J. Golda et al., J. Phys. D: Appl. Phys. **49**, 084003 (2016)
[4] H.-F. Poggemann et al., J. Phys. D: Appl. Phys. **58**, 135208 (2025)
[5] S. Schüttler et al., submitted to PSST (2025)

# Streamer corona electrical discharges in thunderclouds: New discoveries and possible impact in the atmosphere

F. J. Gordillo-Vázquez[1], F. J. Pérez-Invernón[1], S. Soler[1], T. Neubert[2] and N. Ostgaard[3]

[1] *Instituto de Astrofísica de Andalucía (IAA-CSIC), Glorieta de la Astronomía s/n, 18008 Granada, Spain*
[2] *National Space Institute, Technical University of Denmark (DTU Space), Denmark*
[3] *University of Bergen, Department of Physics and Technology, Bergen, Norway*

Recent results indicate that, in addition to hot lightning, kilometer scale corona electrical (cold) discharges formed by hundreds of millions of streamers are common in thunderclouds around the globe. However, their genesis, dynamics and probable atmospheric chemistry impact ($N_2O$, $O_3$) remain not well understood. In this talk I will overview some of our recent findings [1]-[6] on optical measurements by the Atmosphere-Space Interactions Monitor (ASIM) at the International Space Station (ISS). Cloud coronas are observed in a narrow (3 nm) near UV band centered at 337 nm (key spectral band of the $N_2$ second positive system also seen in laboratory corona optical spectra), with no simultaneous activity at 777.4 nm (considered a strong lightning emission line). I will also present our findings on the altitudes of storm coronas, their polarity, number of streamers and length. Finally, we will describe the procedures we developed to include storm coronas in global chemistry-climate models to describe their global distribution in the Earth atmosphere during the present and future (end of 21st century) warmer climate scenario [6].

## 1 General

Recent research results indicate that, in addition to lightning (hot discharges), corona electrical (cold) discharges formed by hundreds of millions of streamers are common in thunderclouds around the globe. In this talk, I will present some results of our research during the last five years (2019-2024) using data of ASIM in the ISS exploring key properties and geographical distribution of cloud coronas around the world. The ASIM mission (launched April 2018) has found a significant number of Blue Luminous Events (BLUEs) at an annual average rate of ~ 4 events per second [1]-[3]. BLUEs are optical single (or multi) pulses of different shapes distinctly showing strong 337 nm signal, associated with cloud corona streamer discharges, and lacking the 777.4 nm emissions indicating the absence of hot lightning leaders. Combined radio and optical studies have found that Narrow Bipolar Events (NBEs), characterized by a very impulsive radio signature, often have a BLUE counterpart [1]. NBEs normally occur in isolation (usually located close to cloud tops) but a small fraction of them, named initiation-type NBEs (normally found deeply inside thunderclouds) are the initial event of a lightning flash [5].

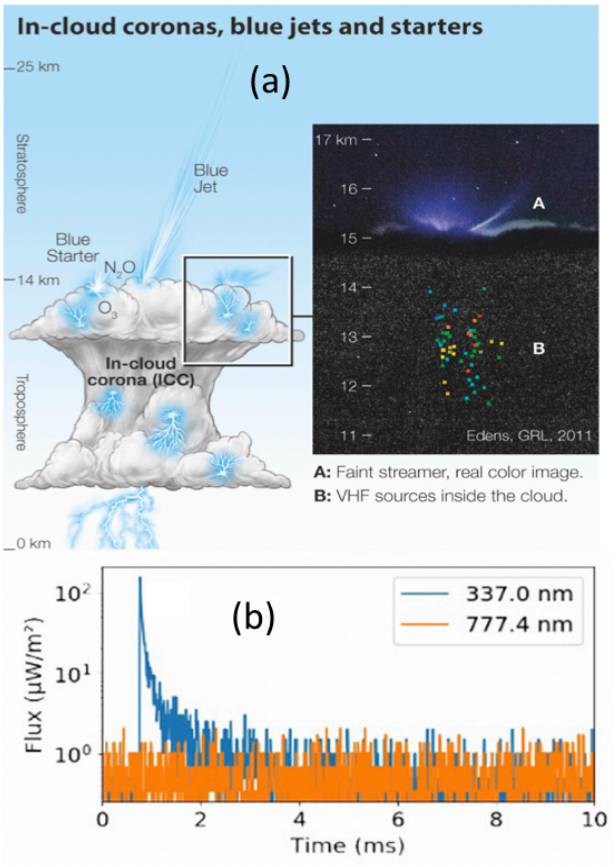



**Figure 1: (a)** Representation of cloud corona activity in a thundercloud together with possible concurrent Blue Jet and/or Blue Starter (left). Real color image of a cloud corona (right). Faint streamers are visible together with VHF sources–colored in time from blue (earlier) to red (later) – inside the cloud recorded at Langmuir Observatory (New Mexico). Real color image of the blue starter reproduced from Edens (2011). Adapted from Gordillo-Vázquez and Pérez-Invernón, Atmospheric Research 2021. **(b)** Shallow corona discharge light curve recorded by ASIM 337.0 and 777.4 nm photometers. Note that the 777.4 nm signal is at noise level. Adapted from Soler *et al.*, GRL 2021.

### References

[1] Soler, S., Pérez-Invernón, F.J., Gordillo-Vázquez F.J., *et al.*, JGR-Atm, (2020), doi: 10.1029/2020JD032708.
[2] Li, D. *et al.* (incl. Gordillo-Vázquez, F.J. ), JGR-Atm, (2021), doi: 10.1029/2021JD035913.
[3] Soler, S., Gordillo-Vázquez, F.J. *et al.*, JGR-Atm, (2022), doi: 10.1029/2022JD037535.
[4] Husbjerg, L. S. Neubert, T. *et al.*, GRL (2022), doi: 10.1029/GL099064
[5] López J. A., *et al.*, (incl. Gordillo-Vázquez, F.J.), Atmospheric Research, (2022), doi: 10.1016/j.atmosres.2021.105981.
[6] Soler, S., Gordillo-Vázquez, F. J. *et al.*, ACP, (2024), doi: 10.5194/acp-24-10225-2024.

# Time-resolved diagnostics of misty plasmas used for nanocomposite thin film deposition

A. Granier[1], S. Chouteau[1,3], A Durocher-Jean[3], J. Chevet[1], A. Goullet[1], M. Richard-Plouet[1], R. Clergereaux[2] and L. Stafford[3]

[1] *Nantes Université, CNRS, Institut des Matériaux de Nantes Jean Rouxel, IMN, - NANTES (France) IMN*
[2] *Laplace, Université de Toulouse, CNRS, UPS, INPT, F-31062 Toulouse cedex 9*
[3] *Département de Physique, Université de Montréal, Québec, Canada*

Time resolved diagnostics of misty plasmas used for the deposition of inorganic nanocomposite thin films in a low pressure rf inductively coupled plasma are investigated in order to get better insight in the plasma/liquid interactions in the plasma and the nanocomposite thin film deposition kinetics.

Misty plasmas have recently emerged as a promising tool in the context of nanocomposite (NC) multifunctional thin films deposition. Among the many strategies aiming for the growth of high quality nanocomposite thin films, combining sol-gel-synthesized nanoparticles and plasma has been shown to be quite attractive [1]. In these 'misty' plasma experiments, liquid colloidal solutions are injected as droplets during matrix deposition, as a direct supply of nanoparticles (NPs). We recently developed such a hybrid reactor, operating in the mTorr range, for the growth of inorganic NC thin films with $TiO_2$ (anatase) or ZnO (wurtzite) NPs embedded in a $SiO_2$ matrix [2-3]. The NPs were provided by a colloidal solution and a $O_2$/HMDSO (hexamethyldisiloxane) mixture was used to deposit the $SiO_2$ matrix.

In this work, 1-ms pulses or a sequence of N 1-ms pulses of the colloidal solution were injected in the diffusion plasma of a 3-mTorr inductively coupled rf plasmas (ICP). Plasma pressure measurement, time-resolved optical emission spectroscopy (TROES) and *in situ* real time spectroscopic ellipsometry were used to control the pulsed injection of the solution in the plasma and to investigate NC film deposition kinetics.
Additional TROES measurements were performed in argon/solvent ICP plasmas. Time-resolved measurements of metastable Ar density, electron temperature and density were determined from radiation trapping analysis and particle balance equations of selected Ar 1s and 2p levels.

The plasma/liquid interactions in the plasma and the nanocomposite thin film deposition kinetics are investigated by coupling the information derived from the time resolved diagnostics of the plasma and of the growing film.
In the case of NC deposition conditions it is shown that the sharp pressure increase following pulsed liquid injection lowers the electron temperature and density, which mitigates the matrix deposition rate as the nanoparticles are supplied to the film. This effect creates alternating matrix-rich and nanoparticles-rich deposition periods, which can be used as an additional knob for judicious control of the nanoparticle fraction in the film and hence its macroscopic properties [3].
In the case of argon-based plasmas, the pulsed liquid injection is found to induce a sudden drop in metastable density and electron temperature, and an increase in electron density. These results are attributed to the lower ionization thresholds of the injected molecular species compared to the one of argon [4].

Acknowledgement for the financial support of CNRS, Université de Montréal and Nantes Université through their contributions to the International Research Network on Controlled Multifunctional Nanomaterials and the French ANR through the project LuMINA ANR-21-CE08-0011

**References**

[1] Mitronika M. *et al*. Hybrid Approaches coupling sol-gel and plasma for the deposition of oxide-based nanocomposite thin films: A review SN Appl. Sci. 3, (2021)
[2] Mitronika M. et al, $TiO_2$-$SiO_2$ Nanocomposite thin films deposited by Direct Liquid Injection of colloidal solution in an $O_2$/HMDSO low-pressure plasma, J. Phys. D : Appl. Phys 54, 085206 (2021)
[3] Chouteau S. *et al*. Kinetics driving nanocomposite thin film deposition in low-pressure misty plasma processes J. Phys. D: Appl. Phys. 55 (2022)
[4] Chouteau S. *et al*, Time-resolved analysis of Ar metastable and electron populations in low-pressure misty plasma processes using optical emission spectroscopy, Plasma Sources Sci Technol 33, 075016 (2024)

# Delayed $CO_2$ dissociation in nanosecond discharges

T. C. Dias,[1] L. M. Martini,[2] P. Tosi[2] and V. Guerra[3]

[1] *Electrical Engineering and Computer Science Department, University of Michigan, Ann Arbor, USA*
[2] *Department of Physics, University of Trento, Italy*
[3] *Instituto de Plasmas e Fusão Nuclear, Instituto Superior Técnico, Universidade de Lisboa, Portugal*

In this work we develop a 0D model to describe recent experimental observations of delayed $CO_2$ dissociation in nanosecond discharges at atmospheric pressure, *i.e.*, the dissociation fraction peaks with a time-delay in relation to the power pulse, when the electron density is already negligibly small. It is shown that dissociation is well described by thermal chemistry driven by gas heating.

## 1 Introduction

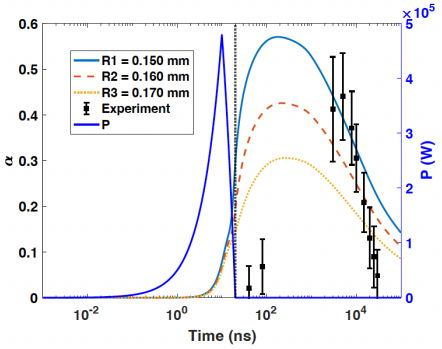
Nanosecond pulsed discharges in $CO_2$ are gaining increasing attention due to their potential in sustainable energy and environmental applications [1]. Indeed, these discharges offer unique pathways to control the excitation and ionization processes, as well as chemical reactions to convert carbon dioxide into value-added chemicals and fuels. $CO_2$ dissociation in gas discharges is often the outcome of direct electron impact. However, other $CO_2$ dissociation mechanisms were proposed and studied in the literature. In particular, vibrational-induced dissociation [2] and thermal dissociation [3] were invoked to explain observed dissociation degrees in MW and RF discharges. Recent work by Montesano *et al* [4] evinced a delayed dissociation mechanism in nanosecond discharges at atmospheric pressure, that is likely a signature of any of these additional dissociation mechanisms. In this work, we develop a zero-dimensional model to study the results of Montesano and co-workers.

## 2 Results and discussion

The experimental conditions from [4] involve large currents in a short time interval, leading to a local pressure increase, to the propagation of a pressure wave and to discharge expansion into the surrounding medium. We assume that any pressure increase/decrease in the discharge volume leads to a radial expansion/contraction of the discharge at the sound speed. The equations for conservation of mass and energy were revisited and adapted to a 0D formulation, as the volume under study is not fixed in time. The chemical kinetics is based on the thermal chemistry set from [5].

The power pulse used as input to the calculations, together with the calculated and measured dissociation fraction, $\alpha = \frac{[CO]}{[CO]+[CO_2]}$, are shown in the figure.

There is a general good agreement between the simulation predictions and the experimental data, strongly suggesting the observed delayed dissociation is driven by thermal chemistry. Future work will address the impact of the detailed vibrational kinetics, that is likely to bring the growth of $\alpha$, which is too fast in the present calculations, closer to the experimental observations.




## Acknowledgements

IPFN activities we supported by the Portuguese FCT-Fundação para a Ciência e a Tecnologia, under funding to IPFN (https://doi.org/10.54499/LA/P/0061/2020, https://doi.org/10.54499/UIDB/50010/2020, https://doi.org/10.54499/UIDP/50010/2020, and https://doi.org/10.54499/PTDC/FIS-PLA/1616/2021)

## References

[1] L. D. Pietanza *et al*. *Eur. Phys. J. D*, **75**, 237 (2021).
[2] V. A. Legasov *et al*. *Dokl. Akad. Nauk*, **243**, 323 (1978).
[3] D. C. van den Bekerom *et al*. *Plasma Sources Sci. Technol.*, **28**, 055015 (2019).
[4] C. Montesano *et al*. *J. Phys. Chem. C*, **127**, 10045 (2023).
[5] L. Vialetto *et al*. *Plasma Sources Sci. Technol.*, **31**, 055005 (2022).

# Vacuum UV spectroscopy at atmospheric pressure plasmas utilizing silicon nitride membranes

L. Hansen[1,2], G. Bilgin[1] and J. Benedikt[1,2]

[1] *Institute of Experimental and Applied Physics, Kiel University, Kiel, Germany*
[2] *Kiel Nano, Surface and Interface Science KiNSIS, Kiel University, Kiel, Germany*

Vacuum ultraviolet (VUV) radiation produced by different atmospheric pressure plasma jets was successfully measured down to wavelengths of 58.4 nm utilizing a 20 nm thin $Si_3N_4$ membrane to transfer the radiation into a vacuum monochromator. This novel transfer method allows to measure VUV spectra without disturbing the plasma or the spectra themselves. Filling the monochromator with Helium revealed absorption in the 59 nm to 61.8 nm region as a result of photo-induced excimer formation, proving that the assumption of He being transparent at wavelength above 50.48 nm (except for the He resonance absorption at 58.4 nm) is not justified.

Vacuum ultraviolet (VUV) radiation corresponds to the wavelength region from 10 nm to 200 nm (124 eV to 6.2 eV) and is crucial for several applications. In the biomedical field, VUV radiation is used for disinfection, water treatment and part of the synergistic effect of plasma medicine. Further exemplary applications include lithography, material modification, and photocatalysis.

A fundamental problem is the transfer of VUV radiation produced in an atmospheric pressure plasma into the vacuum for further analysis, as ambient species absorb the VUV photons. Typical window materials like $MgF_2$ or LiF are not suited for the vacuum transfer due to their cut-off wavelength at 110 nm [1]. Different approaches via pneumatic valves [2] or differential pumping [3,4] have been pursuit in the past to overcome the transfer problem, but have different drawbacks. The plasma itself is either not operated at atmospheric pressure or it is unclear, whether the plasma may be extending into the vacuum environment.

Another approach was based on an aerodynamic window [5] by transferring the VUV photons through a pure Helium atmosphere, which was assumed to be transparent for VUV photons with wavelengths above 50.48 nm (except for He resonance absorption) [6,7].

A new approach presented in this contribution is utilizing a 20 nm thin $Si_3N_4$ membrane as entrance window. Its low thickness allows transmittance in the order of 10 % in the wavelength region from 55 nm to 120 nm [7], while being stable enough to withstand the pressure gradient of one atmosphere.

The capillary jet [8] was used as plasma and VUV photon source and placed close to the $Si_3N_4$ membrane. Spectra resolving the He resonance line (58.4 nm), as well as the $He_2$* excimer continua (58-64 nm, 64-100 nm) were taken. The monochromator was stepwise filled with He and absorption in the 59-61.8 nm region became visible. Photo-induced excimer formation is the origin of this absorption and will be explained based on the potential energy curves of $He_2(X)$ and $He_2(A)$.

The new setup was utilized to measure the VUV spectra of the commonly used COST-Jet and kINPen, which will also be shortly presented.

**References**

[1] Gerasimova, N. G. $CaF_2$, $MgF_2$, $SiO_2$, SiC, LiF, $BaF_2$, and $ZrO_2$ optical single crystals used in studies in the VUV spectral region. *Instrum. Exp. Tech.* **49**, 408 (2006).
[2] Ryberg, D. *et al.* System for time-discretized vacuum ultraviolet spectroscopy of spark breakdown in air. *Rev. Sci. Instrum.* **85** 103109 (2014).
[3] Kurunczi, P. *et al.* Excimer formation in high-pressure microhollow cathode discharge plasmas in helium initiated by low-energy electron collisions. *Int. J. Mass Spectrom.* **205** 277 (2001).
[4] Liu, F. *et al.* Atmospheric plasma VUV photon emission. *Plasma Sources Sci. Technol.* **29** 065001 (2020).
[5] Golda. J. *et al.* Vacuum ultraviolet spectroscopy of cold atmospheric pressure plasma jets. *Plasma Process. Polym.* **17** 1900216 (2020).
[6] Lee, P., Weissler, G. L. Absorption Cross Section of Helium and Argon in the Extreme Ultraviolet. *Phys. Rev.* **99** 540 (1955).
[7] Henke, B. L., Gullikkson, E. M., Davies, J. C. X-Ray Interactions: Photoabsorption, Scattering, Transmission, and Reflection at E = 50-30,000 eV, Z = 1-92. *At. Data Nucl. Data Tables* **54** 181 (1993).
[8] Winzer, T. *et al.* RF-driven atmospheric-pressure capillary plasma jet in a He/O2 gas mixture: Multi-diagnostic approach to energy transport. *J. Appl. Phys.* **132** 183301 (2022).

# 3D reconstruction of plasma emission and sheath structures based on tomography using multi-view images

H. Suzuki[1,2]

[1] *Graduate School of Engineering, Nagoya University, Nagoya, Japan*
[2] *Center for Low-temperature Plasma Sciences, Nagoya University, Nagoya, Japan*

Tomographic techniques are applied to evaluate the three-dimensional structure of process-plasma emission and sheath. A capacitively coupled plasma is generated, and the 3D distribution is reconstructed using images taken from multiple directions with or without a telecentric lens and a bandpass filter. The *r*-*z* spatial distribution information of electron energy is evaluated from the ratio of Ar to Ne emission intensity. The spatial structure of the plasma emission and sheath is evaluated by intentionally generating a non-uniform plasma. As a result, the spatial structures of the plasma emission and sheath are well reproduced.

## 1 Introduction

The increasing process complexity associated with the miniaturization and stacking of semiconductor devices has made yield improvement more challenging. Current process development primarily focuses on the evaluation of processed wafers. However, this approach is challenged by the enormous time, cost and environmental impact associated with energy consumption. Therefore, incorporating real-time process plasma monitoring information, such as three-dimensional (3D) emission distribution and sheath structure, into process development is important.

In this study, we report 3D reconstruction of plasma emission structures from multi-view images using tomography technique.

## 2 Experimental setup

A disk-shaped RF electrode (100 mm in diameter) is placed in the center of a vacuum vessel. Discharge gases are introduced into the vessel, and RF power is applied to the electrode. The emission from the plasma is observed from multiple directions using CMOS cameras with or without a bandpass filter through an observation window on the side of the vessel. To investigate the feasibility of evaluating 3D plasma structures from 2D images, a non-uniform plasma is intentionally produced by covering part of the electrode with a dielectric. Due to the limited number of accessible viewing ports, three cameras are placed, and multidirectional 2D images are obtained by rotating the dielectric position instead of moving the cameras.

To reconstruct the plasma profile between the electrodes, the reconstruction space is assumed to be a rectangular space of 22 cm long, 22 cm wide, and 4 cm high, and the space is divided into voxels of 1 $cm^3$ cubes. When the emission information vector of each voxel is $\boldsymbol{f}$, the captured image emission information vector is $\boldsymbol{g}$, and the camera parameter matrix is $H$, the relationship is expressed as follows.

$$H\boldsymbol{f} = \boldsymbol{g}$$

The spatial structure of the plasma is analyzed using Tikhonov-Phillips regularization

$$\boldsymbol{f} = (H^{\mathrm{T}} H+R)^{-1} H^{\mathrm{T}}\boldsymbol{g}$$

where $R$ is a regularization term in the reconstruction. The camera parameter $H$ is evaluated experimentally by photographing a checkerboard.

## 3 Results and discussion

A plasma was generated using an Ar/Ne gas mixture, and images were taken from two directions, perpendicular to each other at 90 degrees, through a telecentric lens and a bandpass filter. Assuming an axisymmetric plasma, the R-Z spatial distribution information of electron energy was evaluated by taking the ratio of Ar and Ne emission intensity. The results showed that high-energy electrons existed near the electrode, which reproduced the characteristics of CCP well.[1]

To investigate the feasibility of 3D plasma structure evaluation from 2D images, the emission structure was reconstructed from 2D images of an intentionally generated non-uniform plasma in eight azimuthal directions. As a result, the inhomogeneous shapes were well reproduced.

These results indicate that this technique can be used to evaluate the emission profiles of 3D plasma structures.

**References**

[1] M. Kyuzo, K. Harada, R. Izumi, H. Suzuki and H. Toyoda, *Jpn. J. Appl. Phys.* **63**, 056004 (2024).

# Removal of hydrocarbons by plasma-catalysis, catalysts regeneration and reuse

K. Hensel, J. Kšanová, R. Cimerman
*Faculty of Mathematics, Physics and Informatics, Comenius University Bratislava, Slovakia*

Removal of toluene and naphthalene by dielectric barrier discharge (DBD) reactor filled with various pellet catalysts is discussed with respect with catalyst properties. Regeneration of pellets by various methods (plasma, ozonation, heat) is carried out and regenerated catalysts are repetitively tested. The results show a potential of plasma for effective both removal of hydrocarbons and regeneration of deactivated catalysts.

Plasma catalysis is an effective method for the removal of hydrocarbons. Their removal often leads to formation of various undesirable gaseous and solid products. Solid carbon-containing products (coke deposits) may gradually accumulate on the surface of catalysts and cause their deactivation. Thus their effective regeneration is needed. This work deals with the experimental removal of a model hydrocarbons - toluene and naphthalene - using plasma catalysis in a dielectric barrier discharge (DBD) reactor filled with various pellet catalysts [1,3]. We studied the effect of pellets material properties on removal process [2] and their regeneration by various methods and subsequent re-use [3]. Gaseous and solid products of toluene and naphthalene decomposition were analysed by means of FTIR, TGA, GC-MS, SEM, EDX.

In case of napthalene, the effect of the pellets of various catalytic activity (glass, $Al_2O_3$, $Pt/Al_2O_3$, $TiO_2$, $BaTiO_3$, $ZrO_2$), shape and size (spherical, cylindrical, 3-8 mm), dielectric constant (5-4000) and specific surface area (35-250 $m^2/g$) in various carrier gases on removal efficiency and $CO_2$ selectivity were investigated. The experiments were carried out at low temperature (<150°C) and with relatively high initial concentrations (5000 ppm). In case of toluene, removal efficiency, accumulation of coke deposits on pellet catalysts ($Al_2O_3$, $Pt/Al_2O_3$, $Pd/Al_2O_3$, $TiO_2$). followed by their gradual deactivation were investigated. Deactivated catalysts were regenerated using various methods - by plasma generated in a similar DBD reactor filled with the pellets, by ozonation or by heat. The initial concentrations of toluene (2,770 ppm).

With respect to the pellet materials, the highest naphthalene removal efficiency (RE) was obtained with $TiO_2$ catalyst (88%, 320 J/L), and slightly lower with $Pt/Al_2O_3$ (78%), but much higher $CO_2$ selectivity suggesting its best oxidation abilities compared to other materials. The RE for other materials followed a sequence: $ZrO_2$ (72%)> $Al_2O_3$ (66%)> glass (64%)> $BaTiO_3$ (51%). The RE increased with increasing material surface area. Shape and size of pellets were found also important: higher RE was found for cylindrical and smaller pellets. Surface analysis of materials revealed differences in distribution of coke deposits on the surface for different pellets as result of dominant discharge mode. Besides the main gaseous products ($CO_2$, CO, $H_2O$ and HCOOH), several other complex gaseous and solid by-products were identified (phthalic anhydride, maleic anhydride, benzoquinone naphthoquinone, etc).

Toluene removal by plasma catalysis as well as subsequent pellet catalyst regeneration were tested on pellets of various catalytic properties. Removal efficiency, selectivity and carbon balance were evaluated. The RE of toluene followed a sequence: $Pd/Al_2O_3$ (76%, 760 J/L)> $Pt/Al_2O_3$ (74%)> $Al_2O_3$ (65%)> $TiO_2$ (56%). These results were affected not only by catalytic properties of materials, but also dielectric constant and specific surface area. $Pd/Al_2O_3$ exhibited the highest toluene RE and the lowest energy demand [kWh/kg]. All catalysts showed the highest selectivity for $CO_2$ and smaller for CO, HCOOH. $Al_2O_3$ had the worst carbon balance.

The used pellets materials were regenerated by three different methods - by DBD discharge plasma, by ozone (8,000 ppm) and by heat (at 100°C). The results show $O_3$ had negligible effect, and the heat regeneration was completely ineffective. Plasma regeneration was the best although still only partial and spatially non-uniform. It was further improved by mixing pellets in DBD reactor in with several shorter sequences that allow more uniform and effective treatment of the pellet surface with plasma. Regenerated catalysts were further tested exhibiting higher toluene RE after each cycle than those non-regenerated (by 7%, after 3 cycles with $Pt/Al_2O_3$).

Funded by NextGenerationEU through the Recovery and Resilience Plan projects 09I03-03-V03-00033 and 09I03-03-V04-00092 and APVV-20-0566.

**References**

[1] Cimerman R. et al., JPD: AP. 51, 274003 (2018)
[2] Cimerman R. et al. Catalysts 10, 1476 (2020)
[3] Kšanová J. et al. Hakone XVII, Padova (2024)

# EFILE: a diagnostic to measure electric field in a magnetized plasma column

J. Herbelot[1], S. Ferri[1], V. Gonzalez-Fernandez[2], A. Escarguel[1], L. Chérigier-Kovacic[1],
[1] *Aix-Marseille Université, CNRS, PIIM UMR 7345, Marseille, France*
[2] *Dpto. De Optica, Universidad Complutense deMadrid, Av. Arcos del Jalon 118, E-28037 Madrid*

We will present electric field measurements obtained with the EFILE diagnostic in the MISTRAL plasma device. The measurement principle and the precision range will be discussed extensively.

## 1 General

Measuring electric and magnetic fields in a plasma remains a significant challenge.
We introduce Electric Field Induced Lyman-α Emission (EFILE), a diagnostic method based on measuring the Lyman-alpha emission intensity from a beam of hydrogen atoms in the metastable 2s state when subjected to electric or magnetic fields. Our objective is to develop a robust and versatile diagnostic for measuring electric and magnetic fields in complex and turbulent plasma environments.

EFILE has already demonstrated its effectiveness in measuring static electric fields, both in vacuum and in low-density plasma sheaths [1], as well as oscillating (radiofrequency) electric fields [2], in the absence of a magnetic field. In magnetized plasmas, however, interpreting the signal requires a specific quantum mechanics-based theoretical framework. To address this, we developed a predictive model for the expected Lyman-α emission, incorporating Stark, Motional Stark, and Zeeman effects along the beam path. The model was validated against experimental results from a custom-designed setup, achieving strong agreement with the observed data.

Currently, EFILE is being tested in MISTRAL [3,4] a device producing a low-temperature, magnetized plasma column with a 200 G magnetic field and an ion density of $10^9$ $cm^{-3}$. A calibration procedure for the optical system has been developed and implemented. When coupled to the Lyman-α emission model, it ensures quantitative measurements of the electric field.

We will present measurements obtained under various plasma conditions, along with the principles of the measurement and a detailed discussion of the diagnostic's precision range.

**References**

[1] Chérigier-Kovacic, L. Lejeune, A. Doveil, F Debye shielding measurements in a multipolar plasma with a stark quenching of a metastable atomic hydrogen beam technique. *31st International Conference on Phenomena in Ionized Gases*, (2013).

[2] Poggi, C. Guillaume, T. Doveil, F. Chérigier-Kovacic, L. Estimation of the lyman-α signal of the efile diagnostic under static or radiofrequency electric field in vacuum. P*lasma Science and Technology*, **20(7),** 074001 (2018).

[3] Barni, Ri Riccardi, C. Pierre, T. Leclert, G. Escarguel, A. Guyomarc'h, D. Quotb, K. Formation of spiral structures and radial convection in the edge region of a magnetized rotating plasma, *New Journal of Physics*, **7(1),** 225 (2005).

[4] Escarguel. A, Optical diagnostics of a low frequency instability rotating around a magnetized plasma column. *The European Physical Journal D*, **56(2),** 209–214, (2010).

# Diagnostics of high-energy species in plasmas

H. Toyoda[1,2]

[1]*Department of Electronics, Nagoya University, Nagoya, Japan*
[2]*Center for Low-temperature Plasma Sciences, Nagoya University, Nagoya, Japan*

In various plasma processes using biased electrodes, energetic particles are often produced by various mechanisms. These energetic particles may or may not be generated intentionally and may have beneficial effects or cause problems. In the talk, after briefly surveying my works related to diagnostics of high energy species in magnetron plasma sources, energy-resolved angular distribution measurement of high-energy ions impinging on RF-biased electrode will be presented.

## 1 High energy neutral and negative ions in magnetron plasmas

In magnetron discharge, high energy species are produced, and film quality is degraded by defect formation or interface mixing. One example of high energy species is high energy neutrals from the target. In magnetron discharge, high energy rare gas ions impinge on the sputter target and, after neutralized on the surface, backscatter into the gas phase. In our work, such high energy neutrals were indirectly detected by measuring high-energy rare gas ions produced by charge-exchange or heavy particle collisions ($Ar_f$ + Ar -> $Ar^+_f$). [1,2] Another example of high-energy particle production is high-energy $O^-$ ions produced from oxide targets. Spatial variation of high energy $O^-$ were measured.[3] Furthermore, origin of the fine-structure of the $O^-$ energy distribution in RF magnetron plasma was clarified.[4]

## 2 Energy-resolved angular distribution measurement of ions impinging on RF-biased electrode

In high-aspect ratio etching of semiconductor devices, angular distribution (AD) of ions impinging on the RF electrode is always one of concerns. In our work, the AD of ions impinging on the RF electrode was observed by directly connecting an electric-field-free drift tube to an orifice-installed RF electrode. Using a micro-channel plate which was installed at the end of the drift tube, angular-broadened ion profile was observed using a phosphor plate and an ICCD camera. Both in single- and dual-frequency capacitively-coupled plasmas, monotonic decrease in the angular width with the bias potential was clearly observed.[5,6]

Furthermore, energy-resolved AD was measured by using time-of-flight method. In the measurement, a pair of deflection plate was placed in the drift tube and polarity of the deflection voltage was momentarily reversed, resulting in the trajectory change of ions depending on the ion position in the deflector. From time-resolved measurement of the phosphor plate image, energy-resolved AD was obtained at different pressures while keeping the sheath thickness and plasma density.[7] The AD had tail component and its increase with the pressure was observed, suggesting scattering of ions in the sheath.

**References**

[1] Matsui H., *et al.*, High-energy ions and atoms sputtered and reflected from magnetron source for deposition of magnetic thin films, *J. Vac. Sci. Technol.*, **A23**, 671-675 (2005).
[2] Takagi Y., *et al.*, Suppression of high-energy backscattered particles in magnetron plasma using cylindrical cathode, *Jpn. J. Appl. Phys.*, **46**, 7865-7869 (2007).
[3] Ishijima T. *et al.*, Spatial variation of negative oxygen ion energy distribution in RF magnetron plasma with oxide target, *Jpn. J. Appl. Phys.*, **48**, 116004 (2009).
[4] Toyoda H. *et al.*, Fine Structure of $O^-$ Kinetic Energy Distribution in RF Plasma and Its Formation Mechanism, *Appl. Phys. Express* **2**, 126001-1-3 (2009).
[5] Ichikawa K. *et al.*, Angular distribution measurement of high-energy argon neutral and ion in a 13.56 MHz capacitively-coupled plasma, *Appl. Phys. Express* **14**, 126001-1-5 (2021).
[6] Kawamura S. *et al.,* Effect of collisions in a sheath on angular distributions of high-speed particles incident on an RF electrode from a dual-frequency capacitively-coupled plasma, Abst. 44th Int. Symp., Dry Process G-1 (2023).
[7] Kawamura S. *et al.*, Energy-resolved measurement of ion angular distribution in dual-frequency capacitively-coupled Ar plasma incident on an RF electrode, Abst. 45th Int. Symp., Dry Process H-1 (2024).

# Effects of Rectangular Amplitude Modulated Radio Frequency Capacitively Coupled Plasma on Electron Heating: Simulations and Experiments

K. Kamataki, Y. Yamamoto, Y. Sato, Y. Kurosaki, D. Wakita, K. Nagamine, D. Yamashita, T. Okumura, N. Itagaki, K. Koga, M. Shiartani

*Graduate School and Faculty of Information Science and Electrical Engineering, Kyushu Univ. Japan*

The behavior of electron temperature and high-energy electrons in capacitively coupled plasmas driven by rectangular amplitude-modulated (Rect-AM) discharges was investigated through experiments and PIC-MCC simulations. Unlike pulsed discharges, the low-voltage phase (VL) in Rect-AM discharges suppresses the time-averaged electron density drop, stabilizing the plasma. At a modulation frequency of 100 kHz, the bulk electron temperature rises approximately 1.8 times within 10 μs after entering the high-voltage phase (VH). By exploiting differences in electron density and temperature response times, independent electron temperature control is achieved by adjusting the modulation frequency. The heating effect persists under high-pressure conditions, showing Rect-AM discharges' potential to improve radical control, enhancing plasma etching selectivity and PECVD film quality.

## 1 Introduction

The rise of AI and IoT has driven increased semiconductor demand, advancing miniaturization. Plasma processes are essential in semiconductor manufacturing, requiring precise control of ions, electrons, and radicals. Radical generation, critical in RIE and PECVD, depends on feed gas-electron reactions, whose rates are influenced by electron energy. Thus, electron temperature control is crucial in plasma processing. We investigated the effect of AM discharge on plasma parameters [1]. In this study, we achieved partial independent electron temperature control using Rect-AM discharges, where voltage amplitude is modulated in a rectangular waveform. Like PTM plasmas, rapid voltage rise in Rect-AM induces a transient $T_e$ increase. The sheath during the low-voltage phase sustains heating while maintaining electron density and ion flux, ensuring stable operation.

## 2. Setup

Simulations used a 1D3V PIC/MCC code developed by PEGASUS, widely applied in CCP studies[2]. To validate $T_e$ dynamics in Rect-AM discharges, OES measurements were conducted in a CCP reactor [3] with two electrodes (85 mm diameter, 26 mm gap). An RF power at 13.56 MHz modulated at 100 Hz to 300 kHz was applied to the bottom electrode. Ar (5 sccm) was used at 10 mTorr. Emission spectra at 750.4 nm (2p1 → 1s2, Eth = 13.48 eV) and 425.9 nm (3p1 → 1s2, Eth = 14.74 eV) were recorded with a spectrometer. The line ratio indicates $T_e$ changes.

## 3. Results and Discussion

Simulation results show that the time-averaged $T_e$ in the plasma bulk for Rect-AM discharge is higher than that for the CW discharge. To confirm $T_e$ rise during Rect-AM discharge, OES measurements were performed. $T_e$ rises rapidly after the voltage increase, then stabilizes to the steady-state CW discharge value. Figure 1 shows the Rect-AM frequency dependence of the two-line emission intensity ratio of Ar excited species ($I_{425nm}/I_{750nm}$) derived from OES measurements, and the probability of the presence of electrons with energies above 14.7 eV obtained from simulation results of EEDF. Here, the value of 14.7 eV corresponds to the threshold energy for Ar I emission at 425.9 nm. These results show good agreement between the Rect-AM frequency dependence of the emission intensity ratio from OES measurements and the proportion of high-energy electrons from the simulations. Both dependencies exhibit a peak around the Rect-AM frequency range of 50–100 kHz. Details are presented at conference.

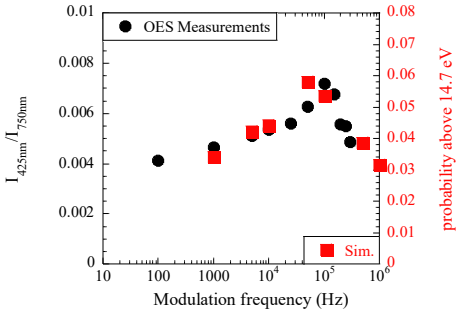



Fig.1 Rect-AM frequency dependence of Ar emission intensity ratio ($I_{425nm}/I_{750nm}$) and probability of electrons with energies above 14.7 eV.

This work was partly supported by JSPS KAKENHI (Grant No. JP23K03368 and JP24H00205)

## References

[1] K. Kamataki, *et al.*, *Applied physics express,* **4,** 10, 105001 (2011).
[2] I. Nagao *et al.*, *MRS Advances*, **7**, 911 (2022).
[3] M. Otaka, *et al.*, *Japanese Journal of Applied Physics*, **63**, 7, 076001 (2024).

# Analysis of short-lived reactive nitrogen species using gas-liquid interfacial plasma with high-speed liquid flow

T. Kaneko[1], K. Takeda[1] and S. Sasaki[1]

[1] *Graduate School of Engineering, Tohoku University, Sendai, Japan*

A combined experimental and modeling study was conducted on plasma-generated interfacial $NO_x^-$ chemistry using an atmospheric-pressure plasma system with high-speed liquid flow. This setup enables the observation of the decay of short-lived $NO_2^-$ precursors. The measurements indicate that more than 40% of the total $NO_2^-$ production is mediated by precursor species without simultaneous $NO_3^-$ formation. Analysis of $NO_x^-$ precursor pathways suggests that $N_2O_3$ is the dominant $NO_2^-$ precursor. Consequently, the results demonstrate that at least 40% of the total $NO_2^-$ is generated via $N_2O_3$.

## 1 Introduction

Recently, atmospheric-pressure plasmas (APPs) interacting with liquids have been extensively studied in the context of life sciences [1]. When a liquid is exposed to APPs, reactive oxygen and nitrogen species (RONS) are transferred into the liquid phase across the plasma-liquid interface through various physicochemical processes. Since the primary reactions induced by APPs typically occur near this interfacial region, understanding and controlling the transfer of RONS at the interface remain critical challenges for advancing plasma-based applications.

In this study, we experimentally evaluate the transfer process of RONS, such as $N_xO_y$, using the APP system in contact with a high-speed liquid flow [2]. This axisymmetric system ensures a relatively uniform plasma-liquid interface in the circumferential direction. Additionally, the high-speed advection system minimizes APP-induced convection effects, enabling the experimental detection of short-lived RONS.

## 2 Experimental setup

The experimental setup is shown in Fig. 1. APP is generated inside the quartz tube and pure water jet passing through the central axis of plasma region over the speed of 10 m/s. In order to track the transferred liquid-phase RONS, aqueous chemical reagent flow is mixed with the plasma-exposed water flow. The mixing position of reagent flow ($d_g$) is controlled with 1-mm or better resolution. Owing to high-speed liquid flow, a spatial resolution of 1 mm corresponds to a temporal resolution of 0.1 ms.

## 3 Results and discussion

To detect the $NO_x^-$ precursor, p-HPA solution is used as the $NO_x^-$ precursor scavenger. We assume that $NO_x^-$ precursor is scavenged by the p-HPA at the mixing position, resulting in the decrease of

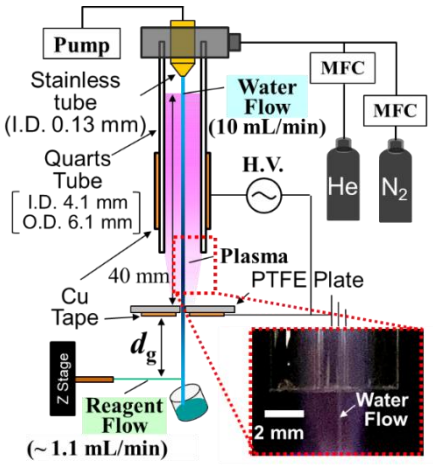



Fig.1 Experimental setup.

$NO_2^-$ concentration equivalent to the $NO_x^-$ precursor concentration. The estimated value is calculated from the difference from $NO_2^-$ or $NO_3^-$ concentration without p-HPA.

A significant decrease in $NO_2^-$ concentration, with no notable decrease in $NO_3^-$ concentration right after plasma exposure, indicates the presence of short-lived nitrogen-containing precursor species that lead to $NO_2^-$ rather than $NO_3^-$. The estimated cross-sectional average concentration of the $NO_2^-$ precursor at $d_g$=1 mm reached 0.7 µM, corresponding to up to 40% of total $NO_2^-$ (1.5 µM).

While various pathways contribute to $NO_x^-$ generation, those involving $NO_2^-$ precursors in the liquid phase are limited, primarily to $HNO_2$ dissolution and $N_2O_3$ hydrolysis. The high $NO_2^-$ generation ratio supports the conclusion that $N_2O_3$ hydrolysis plays a key role in $NO_2^-$ formation.

**References**

[1] Kaneko, T., Takashima, K. and Sasaki, S. *Plasma Chem. Plasma Process.* **44**, 1165–1201 (2024).

# Spatially resolved cavity ringdown spectroscopy studies on low pressure oxygen plasmas

C. Kniebe-Evans[1], R. Peverall[1], G. Hancock[1], and G. A. D. Ritchie[1]

[1] *Department of Chemistry, University of Oxford, South Parks Road, Oxford, OX1 3QZ, United Kingdom*

Advances in semiconductor etching depend on reliable plasma modelling and quantitative knowledge of near-surface behaviour of key reactive species. In this research, diode laser spectroscopic techniques are utilised to determine number densities, translational temperatures, and lifetimes of key species in technologically relevant low pressure ICPs of pure oxygen. 2D-axisymmetric simulations are performed and compared with experimental data in order to enhance reactive chemistry sets and refine simulation parameters

Diode laser based Cavity ring-down spectroscopy (CRDS) is an absolute, high resolution, calibration-free experimental technique for sensitive measurements of plasma species number densities and temperatures. Selective transitions have been studied in a low pressure inductively coupled plasma to characterise the important reactive species in a pure oxygen plasma. These studies are extended into the plasma-surface boundary layers to quantify absolute number densities and translational temperatures as a function of height in the region 20 mm directly above a non-driven electrode.

Two spin forbidden $O(^1D_2) \leftarrow O(^3P_J)$ transitions around 630 nm are used to investigate the major reactive product, $O(^3P)$. The spin-orbit states are determined to be in thermal equilibrium and thus total $O(^3P)$ densities can be calculated solely from $O(^3P_2)$ measurements using statistical mechanics. Figure 1 shows absorption profiles recorded for the $O(^3P_2)$ and $O(^3P_1)$ states, at a distance of $1.8\,\mathrm{mm}$ above a grounded electrode surface. These results yield a total $O(^3P)$ density of $3.67 \times 10^{14}\,\mathrm{cm}^{-3}$ and a translational temperature of $322\,(\pm 20)$ K, which correspond to an $\approx 6\%$ degree of dissociation.

$O(^3P)$ densities and translational temperatures are further quantified in the near surface region. Translational temperatures are observed to decrease as the water-cooled surface is approached, whilst a modest increase in number density is observed, consistent with gas dilation. The number density of the dominant anion, $O^-$ is also inferred via its photodetachment continuum at several nearby wavelengths in a modulated oxygen plasma. The spatially resolved anion densities show that $O^-$ density decreases as the electrode surface is approached, closely following modelled trends in electron density.

$O(^3P)$ lifetimes obtained in the plasma bulk are contrasted with near-surface lifetimes at a series of pressures. Surface recombination is the dominant loss process for $O(^3P)$ and experimental results show that lifetimes are thus shortest at lower pressures where drift-diffusion is fastest and in regions closer to the electrode surface. Knowledge of surface loss parameters is an essential component of plasma modelling simulations and thus it is important to accurately quantify these surface parameters for our chamber. Spatially resolved measurements of several plasma species across a range of conditions enables careful refinement of our plasma modelling simulations.

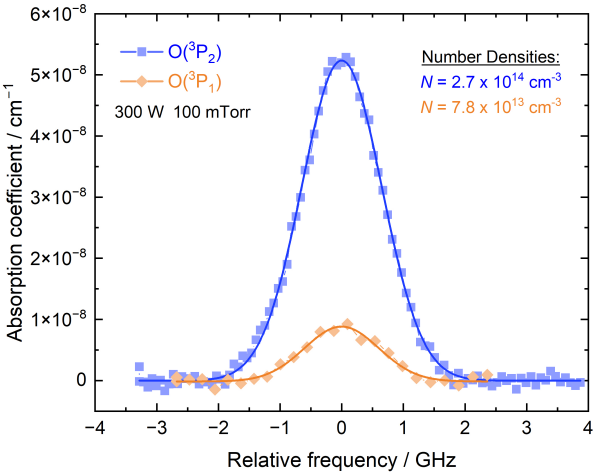



Figure 1: Absorption profiles recorded for the $O(^3P_2)$ and $O(^3P_1)$ spin states under plasma condition of 300 W and 100 mTorr, 1.8 mm above the electrode surface.

## References

[1] S. D. A. Rogers, C. Kniebe-Evans, R. Peverall, G. Hancock, B. Rhodes, and G. A. D. Ritchie. Measurements of $N_2^+$ ions in an inductively coupled plasma using saturated cavity ringdown spectroscopy. *Plasma Sources Sci. Technol.*, **33**, 125002 (2024).

# Self-organization processes in low-temperature plasmas

Vladimir I. Kolobov

*The University of Alabama in Huntsville, Huntsville, AL, USA*

Nonlinear and nonlocal effects control self-organization processes in low-temperature plasma. The disparity of time scales explains how transient and non-local kinetic effects ensure the high efficiency of ionization processes in plasma in dynamic regimes and self-pulsing of Townsend discharges. Plasma stratification reveals non-local and non-linear electron kinetics in noble gases. In our presentation, we review recent progress in understanding self-organization processes in laboratory plasmas, including self-pulsing phenomena, stratification, filamentation, and pattern formation at electrodes.

## 1 General

Self-organization processes in low-temperature plasmas (LTP) often obey the principle of minimal power [1]. Although the fundamental laws of physics do not imply this principle, a detailed analysis typically reveals why nature tends to follow this path. Nonlinear and nonlocal effects are responsible for self-organization processes in LTP, often justifying the realization of a plasma state maintained at minimal electric power. The nonlinearity appears because small groups of energetic electrons usually control the ionization processes. The number of these electrons depends strongly on the ratio of the electric field to gas density, *E/N*. Under certain conditions, the ionization rate can also depend nonlinearly on electron density due to stepwise ionization and Coulomb collisions. Furthermore, the disparity of time scales makes particle and energy transport in plasma amazingly sophisticated.

### 1.1 Dynamic discharges

A broad class of phenomena can be unified under the concept of **dynamic discharges** [2]. An electric field binds electrons and ions together in plasmas on a fast timescale ensuring **ambipolar** diffusion. Heat transport occurs rapidly on the timescale of **free** electron diffusion. In alternating current (AC) discharges, plasma density remains constant within a specific range of driving frequencies, whereas electron temperature, ionization rate, and chemical reactions exhibit significant temporal variations. These variations make plasma generation and maintenance more efficient.

### 1.2 Self-pulsing phenomena

In the absence of quasi-neutrality, the ion and electron transport decouple. Subnormal oscillations in DC discharges, self-pulsing of dielectric barrier discharges, and the Trichel pulses in the corona are consequences of decoupled electron and ion transport [3].

### 1.3 Plasma stratification

The plasma of noble gases is usually stratified. Moving striations in DC discharges [4] and standing striations in AC discharges [5] are both types of ionization waves of a common nature. Stratification at high plasma densities is due to non-linear effects associated with Coulomb collisions among electrons. The disparity in time scales between slow ambipolar diffusion, which occurs at the ion time scale, and electron kinetics, which occurs at the fast free electron diffusion time scale, produces complicated fluxes in the coordinate-energy phase space responsible for the stratification. Recent papers [4,5] emphasize the need for the non-local kinetic approach to stratification phenomena in noble gases.

**References**

[1] V.I Kolobov and Y.B Golubovskii, The principle of minimal power, Plasma Sources Sci. Technol. **31**, 094003 (2022)

[2] N A Humphrey and V I Kolobov, Electron kinetics in a positive column of AC discharges in a dynamic regime, Plasma Sources Sci. Technol. **32**, 085017 (2023)

[3] S. Thagunna, V.I. Kolobov and G.P. Zank, Self-pulsing of dielectric barrier discharges at low driving frequencies, Phys. Plasmas **31**, 053507 (2024)

[4] V.I. Kolobov and R.R. Arslanbekov, Ionization waves in low-current DC discharges in noble gases obtained with a hybrid kinetic-fluid model, Phys. Rev. E **106**, 065206 (2024)

[5] V.I. Kolobov and R.R. Arslanbekov, Plasma stratification in AC discharges in noble gases at low currents, Phys. Rev. E **111**, 015203 (2025)

# Probing the dynamics of high-pressure nanosecond pulsed discharges with non-linear non-resonant laser diagnostics

M. Kounalakis[1], G. Trayner[2], P. Bruggeman[2], M.S. Simeni[2] and A. Gerakis[1]

[1] *Luxembourg Institute of Science and Technology (LIST), 4422 Belvaux, Luxembourg*
[2] *Department of Mechanical Engineering, University of Minnesota, Minneapolis, MN, 55455, USA*

We present working progress towards probing the dynamics of nanosecond plasma discharges upon the application of high-voltage pulses between two pin electrodes at atmospheric pressures. Using non-linear and non-resonant laser diagnostics, in particular coherent Rayleigh Brillouin scattering complemented by coherent anti-Stokes Raman scattering, the gas velocity distribution function will be directly probed leading to a better understanding of the overall dynamics during the formation and decay of the arc discharge.

Nanosecond pulsed discharges find unique technological applications, e.g. by enabling the removal of pollutants that are harmful for the environment, increasing the efficiency in plasma-enhanced combustion, or assisting in sterilization of biomedical equipment [1]. They are characterized by a high degree of ionization and reactivity, as well as transient non-trivial dynamics [1,2]. Under certain conditions, high-pressure nanosecond pulsed discharges exhibit ultra-high electron number densities (>$10^{18}$ $cm^{-3}$) and may lead to ultrafast gas heating (5000–50000 K), a behaviour that is not fully understood at a fundamental level [3-6].

Recent theoretical simulations predict that the formation of this *thermal spark* regime arises due to strong Coulomb coupling between ions leading to local thermal equilibrium (LTE) at sub-nanosecond timescales, which was experimentally observed via Optical Emission Spectroscopy (OES), although without conclusive evidence [6,7]. Moreover, OES measurements are heavily model-dependent and rely on the assumption of LTE to extract useful quantities.

Here, we present progress on experimentally probing such plasma discharges created by nanosecond high-voltage pulses between two pin electrodes (see Fig. 1), at different gases using non-linear and non-resonant laser diagnostics. Coherent Rayleigh Brillouin scattering (CRBS) spectroscopy will allow us to directly probe the gas velocity distribution function during the discharge, without relying on the LTE hypothesis. As an example, Fig. 1(d) shows a CRBS spectrum obtained in pure $CO_2$ at 1 bar, in the absence of a discharge. These measurements will be complemented by coherent anti-Stokes Raman scattering (CARS) spectroscopy. Fig.1(c) shows a CARS measurement at 100 ns from the beginning of a 10 kV, 300 ns pulse, in pure $N_2$ at 800 mbar, showcasing a non-equilibrium rotational energy spectrum with an estimated temperature rise of ~200 K during the discharge. Using both CARS and CRBS will enable the extraction of both translational and ro-vibrational gas temperatures during the formation and decay of the arc discharge, thereby directly testing the validity of the LTE hypothesis during this process.

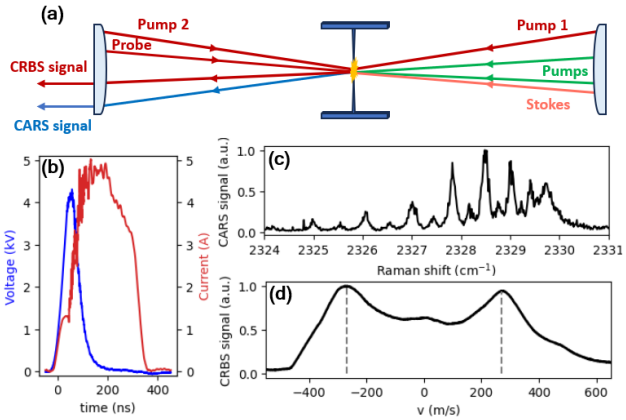



Fig.1. **(a)** Schematic of the experimental setup for CRBS and CARS spectroscopy at the centre of the plasma discharge. **(b)** Voltage and current waveforms measured directly at the electrode during the discharge for a 10 kV, 300 ns pulse in pure $N_2$ (800 mbar), and **(c)** corresponding CARS spectrum measured at 100 ns from the beginning of the pulse. **(d)** Measured CRBS spectrum showcasing the velocity distribution of molecules in $CO_2$ gas (1 bar).

## References

[1] I. Adamovich, *et al.*, *J. Phys. D: Appl. Phys.* **55**, 373001 (2022).
[2] D.Z. Pai, D.A. Lacoste, and C.O. Laux, *J. Phys. D: Appl. Phys.* **107**, 093303 (2010).
[3] R.M. van der Horst, *et al.*, *J. Phys. D: Appl. Phys.* **45**, 345201 (2012).
[4] A. Lo, *et al.*, *Plasma Sources Sci. Technol.* **26**, 045012 (2017).
[5] T. Orrière, E. Moreau and D.Z. Pai, *J. Phys. D: Appl. Phys.* **51**, 494002 (2018).
[6] N. Minesi, *et al.*, *Plasma Sources Sci. Technol.* **29**, 085003 (2020).
[7] M.D. Acciarri, C. Moore and S.D. Baalrud, *Plasma Sources Sci. Technol.* **31**, 125005 (2022).

# Microwave plasma-based dry reforming of methane: Showing the role of radical reactions in the afterglow

L. Kuijpers[1], C.F.A.M. van Deursen[1], Q. Shen[1], W.A. Bongers[1], E.J. Devid[1], and M.C.M. van de Sanden[1,2]

[1]*Plasma Solar Fuel Devices, Dutch Institute For Fundamental Energy Research, Eindhoven, Netherlands*
[2]*Eindhoven Institute for Renewable Energy Systems, Eindhoven University of Technology, Eindhoven, Netherlands*

In this contribution we present an investigation of methane addition to $CO_2$ microwave discharges. Experimental results include the effluent gas composition, core plasma temperature and optical emissions. Addition of only 1% $CH_4$ is found to diminish the $CO_2$ conversion and decrease the energy efficiency significantly, while barely changing discharge characteristics. A quasi-1D chemical kinetic model is implemented for the afterglow, which shows that the overall chemistry is nearly completely controlled by hydrogen-containing radical reactions in the cooling trajectory.

## Introduction

In the dry reforming of methane (DRM), methane is reacted with $CO_2$ to directly produce synthesis gas. It has promising uses in the context of methane valorisation, carbon capture and utilisation, and biogas reforming. Especially warm plasmas have shown promising results in terms of energy efficiency and conversion [1-3], showing great improvements in comparison to direct $CO_2$ dissociation. Additionally, previous work has shown complete oxygen removal from the effluent with only 5% $CH_4$ addition [1].

## Methods

The addition of 0-30% methane to a $CO_2$ vortex-stabilised 2.45 GHz microwave discharge is studied. Three pressures are tested (150, 400 and 900 mbar). The power and total flow are kept constant at 1000 W and 9.4 SLM. The effluent composition is measured using gas chromatography. The plasma core gas temperature is determined from the Doppler broadening of the atomic oxygen emission triplet at 777 nm. The same emission line is used to determine the plasma size. A quasi-1D chemical kinetic model is implemented for the afterglow.

## Results and Discussion

Figure 1 shows the conversion of $CH_4$ and $CO_2$ as a function of $CH_4$ addition. $CO_2$ conversions of 45% are reached, with a related energy efficiency of 70%. The $CO_2$ conversion diminishes with only 1% $CH_4$ addition, while it is found that the discharge characteristics (i.e. gas temperature and optical emissions) show nearly no changes. Additionally, the $CO_2$ conversion appears insensitive to pressure variations, while the gas temperature in the core and the plasma size have a strong pressure dependence.

The afterglow model shows that hydrogen-containing radicals catalyse the recombination of CO and $O_2$ for small $CH_4$ additions. Additionally, they are found to drive the water gas shift (WGS) reaction in the afterglow for higher methane additions (10-30%). The afterglow model can accurately reproduce the experimentally obtained selectivity. A sensitivity analysis on the selectivity shows no influence of the initial temperature, and minimal influence of the cooling rate and pressure.

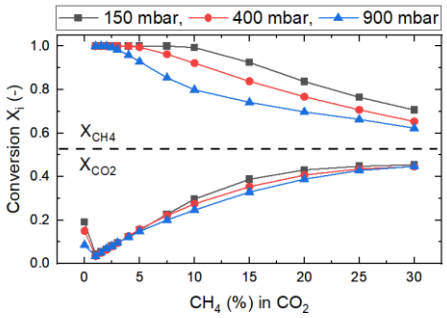



**Fig. 1**. Conversion of $CO_2$ and $CH_4$ as a function of $CH_4$ addition to $CO_2$ plasmas.

## Conclusion

It is shown that the overall chemistry of discharges with 1% to 30% methane is nearly completely controlled by the chemical kinetics of the afterglow. This is driven by hydrogen-containing radicals, that are found to both catalyse the recombination of CO and $O_2$, as well as drive the WGS equilibrium reaction.

## Acknowledgements

This work is partially funded by NXTGEN HT under the Energy domain, project 03: Plasma conversion of methane.

## References

[1] O. Biondo et al., Green Chem., **25,** 10485 (2023).
[2] S. van Alphen et al., ACS Sustainable Chem. Eng., **12**, 15715-15728 (2024).
[3] B. Wanten et al., J. CO2 Util., **56**, 101869 (2022).

# Particle Distribution Functions in EUV Produced Plasmas

Tugba Piskin and Mark J. Kushner

*Electrical Engineering and Computer Science, University of Michigan, Ann Arbor, MI 41809-2122 USA*

Photolithography for semiconductor fabrication uses EUV photon sources for photoresist exposure. The most widely used lithography system produces 13.5 nm radiation by laser ablation of tin droplets. The chamber is often filled with $H_2$ resulting in an EUV generated plasma. Results from a computational investigation of electron and ion distributions produced by pulsed 13.5 nm EUV sources will be discussed.

## 1. EUV Plasma Sources

The decrease in feature size in semiconductor manufacturing has been enabled by higher resolution photolithography resulting from a decrease in wavelength. Current photolithography tools use extreme-ultra-violet (EUV) photons which enable sub-10 nm feature sizes. A widely used EUV source produces 13.5 nm (92 eV) photons by laser ablation of tin droplets. To reduce damage to optics by ablation debris, the chamber is often filled with 10s to 100s mTorr of $H_2$. The EUV flux photoionizes the $H_2$ generating a diffuse plasma while also producing H atoms which etch deposited Sn. The photoelectrons have energies up to 77 eV, which cascade through the $H_2$ gas producing additional ionization. EUV fluxes onto the walls produce energetic secondary electrons.

In this presentation, results from a computational investigation will be discussed for EUV produced plasmas in $H_2$, Ar and Ar/$H_2$ mixtures. The chamber is patterned after the ASML photolithography tool which has a nearly point source of EUV photons [1].

## 2. Description of Model

The computations were performed with an updated version of the Hybrid Plasma Equipment Model (HPEM) [2]. Radiation transport is addressed with a Monte Carlo simulation which generates photoionization sources and EUV fluxes to surfaces. Electron transport is divided into two groups – a high energy group which is kinetically tracked using a Monte Carlo simulation and a bulk low energy group that is represented by fluid equations. Space charge resulting from the high energy photo-electrons and their progeny are included in solution of Poisson's equation for the electrostatic potential.

## 3. Charged Particle Densities & Distributions

A 5 kW pulsed EUV source (60 ns pulse length) operating at 3.3 MHz is centered in a 30 cm diameter, 30 cm tall cylindrical chamber filled with 75 mTorr of $H_2$. EUV photons reflect off the bottom collector and are focused on axis at the top. Bulk electron density, high energy photo- and secondary electrons and plasma potential are shown in Fig. 1 during the 4th EUV pulse. Plasma densities of several $10^{11}$ $cm^{-3}$ are generated. Photo-electron emission from chamber walls produce energetic secondaries. Loss of high energy photo-electrons result in a plasma potential of 28 V. Electron energy distributions of photo-electrons are shown in Fig. 2 at the beginning, end and 50 ns after the EUV pulse. Photoelectrons slow during the interpulse period while highly energetic electrons are lost from the plasma.

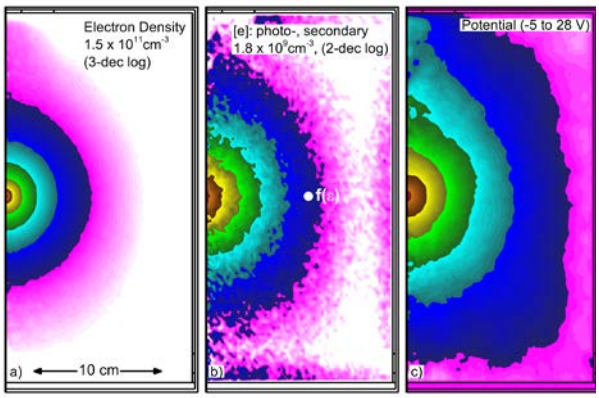



Figure 1 – Plasma properties during 4th EUV pulse. a) Bulk electron density, b) high energy photo- and secondary electrons, and c) plasma potential.

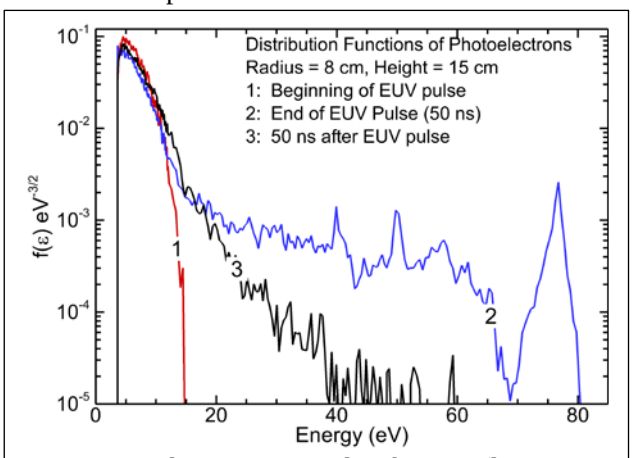



Figure 2 – Electron energy distributions (location in Fig. 1b) of photo-electrons during 4th EUV pulse.

## References

[1] K. Hummler, et al., Proc. SPIE 12953, Optical & EUV Nanolithography XXXVII, 129530V (2024)

[2] S. J. Doyle, et al., J. Phys. D **57**, 435202 (2024).

# High-performance particle-in-cell plasma simulation for the investigation of the nonlinear sheath dynamics and its effect on plasma uniformity in RF capacitively coupled plasmas

Hae June Lee

*Department of Electrical Engineering, Pusan National University, Busan 46241, South Korea*

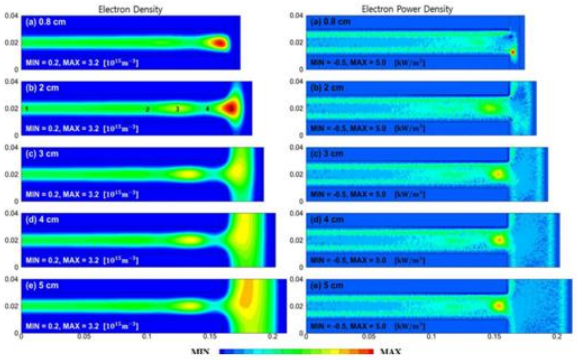
Plasma processing technology utilizing low-temperature plasma has played a crucial role in semiconductor manufacturing. However, the analysis of plasma processing equipment has typically relied on two-dimensional fluid-based simulations or one-dimensional particle-in-cell (PIC) simulations. In contrast, two-dimensional PIC simulations have not been widely utilized. Recently, however, advances in computational science, particularly in parallelization techniques, and rapid improvements in computer hardware performance have significantly enhanced the capabilities of two-dimensional PIC simulations. As a result, their application to semiconductor processing equipment research is increasingly being reported. In this presentation, we introduce a GPU-accelerated particle-in-cell simulation code developed to analyse RF plasma equipment. We report the effects of structures and driving frequency on the plasma uniformity.

## 1.1 The necessity of 2D PIC Simulation

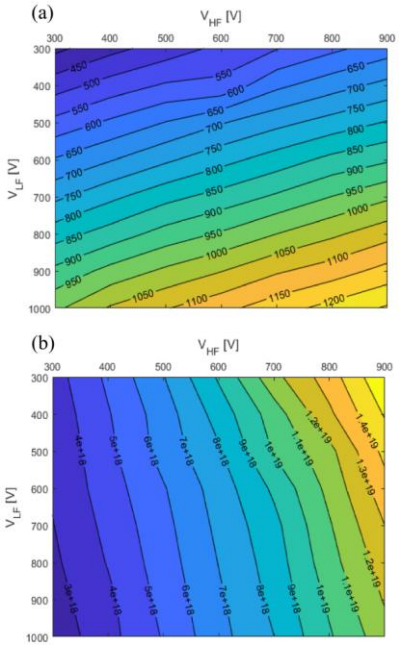
- The limitation of a fluid model assuming the electronic energy distribution function (EEDF) results in errors for the nonlinear and transient kinetic effects.
- For LTPs, most PIC simulations were performed in low pressure or micro-scale 1D systems because of a limitation in computation time.
- 2D fluid models are commonly used to analyse low-temperature plasmas (LTPs) and chemical reactions as a reaction-diffusion system with fast convergence.
- The non-local electron kinetics caused by the sidewall effect in the asymmetric structure were analysed using the particle trajectory analysis in the 2D GPU-PIC simulation [1-5].
- The ion trajectories are analysed for the dual frequency CCPs to understand the formation mechanism of the ion energy and angle distribution (IEAD) [6].

## 1.2 Simulation Results

### 1.2.1 Nonlocal kinetics and sidewall effect [5]




### 1.2.2 Independent control of ion energy and flux in DF CCPs [6]




## References

[1] J. S. Kim et al., *J. Phys. D: Applied Phys.* **51**, 104004 (2018).
[2] C. H. Kim et al., *J. Appl. Phys.* **126**, 173301 (2019).
[3] C. H. Kim et al., *Plasma Sources Sci. Technol*. **30**, 065031 (2021).
[4] C. H. Kim et al., *Plasma Sources Sci. Technol*. **30**, 075005 (2021).
[5] C. H. Kim et al., *Plasma Process Polym.* **19**, e2100196 (2022).
[6] H. H. Kim et al., *J. Vac. Sci. Technol. A* **41**, 023004 (2023).

# A Laser Optical Loop for faster laser based measurements

N. D. Lepikhin[1], D. Luggenhölscher[1], U. Czarnetzki[1]

[1] *Institute for Plasma and Atomic Physics, Ruhr University Bochum, D-44780 Bochum, Germany*

A Laser Optical Loop (LOL) approach is introduced which allows to reuse single laser shots in laser based experimental techniques, increasing the effective repetition rate of the laser and thus accelerating measurements. Experimental methods which require high energy laser pulses in particular benefit, since those lasers usually suffer from low repetition rates. Several optical schemes for E-FISH, TALIF and Thompson scattering are proposed. The feasibility of the suggested method is demonstrated using the example of the E-FISH technique.

## 1 Introduction

The typical repetition rate of commercially available lasers of 10 Hz makes laser experiments extremely time consuming due to large number of laser shots required to achieve high signal-to-nose ratio. Here, we introduce a Laser Optical Loop (LOL) approach, allowing for multiple use of a single laser shot by a simple optical arrangement consisting of a small number of optical elements.

## 2 Experimental setup

As it follows from the name, the idea of the Laser Optical Loop is to trap the laser emission between a set of highly reflective mirrors to minimize the laser energy losses. The proposed optical arrangement for trapping the laser light based on frequency conversion is shown in figure 1 for the example of the E-FISH diagnostic.

## 3 Results

To demonstrate that the LOL approach can be used to perform Rapid E-FISH (RE-FISH) measurements, the rising edge of a high voltage pulse is used. The pulse is applied to an capacitor-like electrode arrangement in ambient air. The measurement results are shown in figure 2. The measured electric field waveform agrees well with the field value calculated as the voltage over the gap ratio, $U/d$ (Laplacian field). The LOL approach in the present case allows to measure the electric field at 8 time points separated by 12 ns simultaneously. In another words, the temporal profile of the electric field shown in figure 2 has been obtained 8 times faster than it would be done by ”normal” E-FISH.

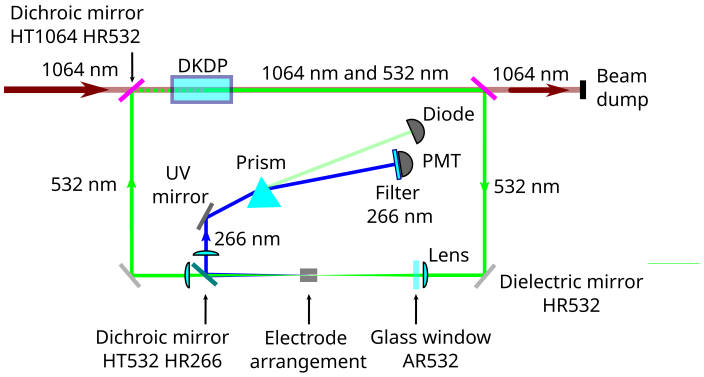



Figure 1: The experimental setup used to demonstrate the Laser Optical Loop approach feasibility using the example of the E-FISH diagnostic. DKDP denotes a deuterated potassium dihydrogen phosphate crystal used to generate 532 nm emission from the 1064 nm laser pulse. Then the trapped 532 nm light is used as a pump beam to generate the E-FISH signal at 266 nm.

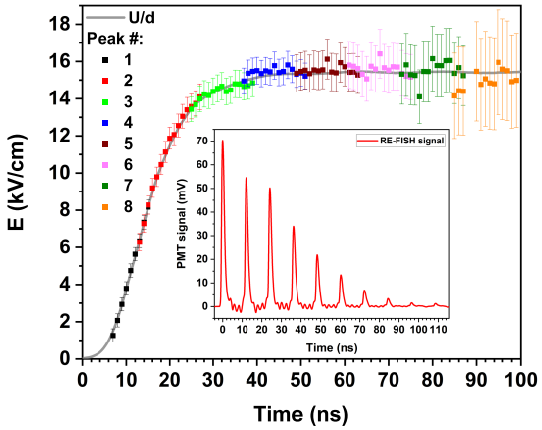



Figure 2: Test results of the RE-FISH measurements obtained by the LOL approach (symbols). Different colors correspond to the peaks in the E-FISH signal waveform shown in the inset. The gray solid line represents the Laplacian field waveform calculated as the voltage over the gap ratio, $U/d$, used to validate the measurement results.

## Acknowledgements

The work is supported by the DFG funded SFB1316 Project ”Transient atmospheric plasmas - from plasmas to liquids to solids”.

# Indoor air decontamination by non-thermal DBD plasma and photocatalysis

T. Vazquez[1], A. Destrieux[1], A. Lavrikova[1], D. Wiederman[2], J. Babic[2], M. Palko[2,3], M. Palko[2,3], M. Janda[1], K. Hensel[1], and Z. Machala[1]

[1]*Faculty of Mathematics, Physics, and Informatics, Comenius University Bratislava, Slovakia*
[2]*IQ Capital s.r.o., Banská Bystrica, Slovakia*
[3]*Faculty of Mechanical Engineering, Technical University Košice, Slovakia*

Indoor air contains harmful chemical and biological contaminants. We use non-thermal atmospheric plasma of a dielectric barrier discharge and UV-induced photocatalysis for the treatment of polluted indoor air. The combination of these two technologies is their capability to destroy and completely mineralize the contaminants. The main challenge of this study is to target chemical pollutants, fine and ultrafine particles, and pathogenic bio-aerosols at high gas flow rates (>300 L/min) for a real scale use.

## 1 Introduction

Indoor air contains many harmful contaminants (chemical pollutants, bacteria, pathogenic aerosols, tobacco smoke, etc.) that can cause respiratory, cardiovascular, and oncological diseases under long-term exposure. Hospital-acquired infections are also spread through air contaminants. Finding an innovative technology that would efficiently remove all airborne pollutants without producing harmful by-products and with a low energy cost would be a major advance for public health. It would also help to prevent the spread of airborne pathogens such as the recent COVID-19 pandemic. Contrary to traditional filters that just trap the contaminants, the goal of this work is to develop non-thermal plasma DBD technology combined with UV-induced photocatalysis for the removal of volatile organic compounds (VOC) [1], fine and ultrafine particulate matter, and inactivation of aerosol-borne bacteria at high gas flow rates relevant for real indoor settings.

## 2 Experimental

We designed an indoor air decontamination device that combines a DBD and a $TiO_2$ coating activated on-demand by UV-C lamps or UV-A LEDs. The device uses a very short residence time of the pollutant in the reactor: the gas flow rate is >300 L/min and uses a single-pass method to determine the pollutant reduction.

The chemical analysis of the VOC contaminants (e.g. formaldehyde) and the gaseous species produced by the DBD was performed by FTIR absorption spectroscopy. The water aerosol-borne bacteria *E. coli* and *S. aureus* were collected after a single-pass on Petri dishes and evaluated by thermostatic cultivation.

## 3 Results

The removal efficiency of 40% was reached for formaldehyde with >300 L/min flow rate in the single pass. We monitored the concentration of ozone generated by the DBD, which must be decomposed by the photocatalytic process before exiting the device. The obtained decontaminations of bio-aerosols are very promising: 3.73 log (99.98%) and 3.32 log (99.95%) inactivation of water aerosol-borne *E. coli* and *S. aureus*, respectively [2].

## 4 Summary

We developed a new device for indoor air decontamination efficient for chemical (VOC and fine and ultrafine particles) and biological decontaminantion. It employs combined effects of DBD plasma and UV activated $TiO_2$ photocatalysis. The device can operate at high gas flow rates (>300 L/min). High inactivation of both organic chemical pollutants and airborne bio-pathogens was achieved at a low specific input energy. This combined NTP-photocatalysis technology can be applied in multiple indoor settings, such as hospitals and public spaces, as well as in potential manned space missions.

**Acknowledgment**
Funded by the EU NextGenerationEU through the Recovery and Resilience Plan for Slovakia under the project 09I03-03-V03-00033, and Slovak Research and Development Agency grants APVV-22-0247 and APVV-20-0566.

**References**

[1] Zhang Y et al. *Catalysis Communications* 172, 106535 (2022)
[2] Vazquez T. et al. *J. Electrostat., under review* (2025)

# Bulk to atoms and back

D. Mariotti

[1] *University of Strathclyde, Department of Design, Manufacturing & Engineering Management-DMEM, Glasgow, UK*

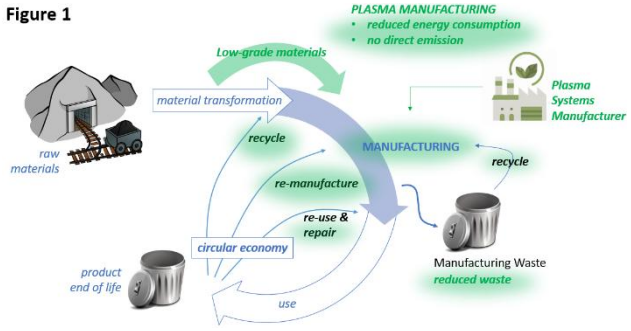
## 1 Introduction

Materials processing and manufacturing rely on the ability of manipulating chemical elements in all their different forms. We often transform bulk materials into atoms and build them back into a new useful and functional bulk form (think of film deposition by sputtering for instance). In other cases, we may stop short of re-building a bulk material and produce nanoparticles instead. Alternatively, the process may follow the '*reversed*' path, from molecular precursors to semi-bulk materials (think of molecular beam epitaxy).

Plasmas, and more specifically electrical discharges, can *break-down* through kinetic energy, using charged species. The advantage of a '*kinetic*' approach is the reduced requirement for chemical energy, which necessarily introduce '*foreign species*' (chemical energy carriers) that are then necessarily transformed into by-product or waste. Plasmas processes are therefore inherently conducive to sustainable manufacturing, in addition to being electrified and therefore amenable to be powered by renewable energy sources.

This lecture will provide examples of atmospheric pressure plasmas that exemplify the journey of sustainably *breaking-down* and *building-back*, focused on metal-based materials. However, the journey from '*bulk to atoms and back*' is today far more relevant than just for plasma manufacturing (figure 1). Plasmas' features are ideal for contributing to resolve sustainability challenges. We could therefore ask ourselves: are synthesis and deposition really different from recycling and re-manufacturing?

Figure 1




## 2 Example: metal cluster and cluster doping

Microplasmas have demonstrated great opportunities to synthesize ultra-small nanoparticles [1, 2]. The ability to synthesize even smaller '*particles*', i.e. *clusters*, is scientifically intriguing as well as important. The formation of clusters can be also one of the steps leading to the nucleation and growth of larger particles. The lecture will report on the synthesis of clusters and their role into the formation mechanisms of nanoparticles in atmospheric pressure plasmas [3].

## 3 Example: plasma exsolution

Exsolution has demonstrated great opportunities to deliver well-dispersed nanoparticles on oxide supports with chemical and mechanical stability. Plasmas are particularly suited for exsolution as they can produce surface oxygen defects through physical means. The lecture will discuss recent results in plasma-based exsolution [4, 5].

## 4 Example: metal-oxide nanoparticles, from manufacturing to applications

Microplasmas represent a viable synthesis platform for tuning the synthesis of metal-oxide nanoparticles, achieving an exquisite control of the size, composition and defects. The lecture will discuss the synthesis and properties of metal oxide nanoparticles spanning a wide range of chemical compositions [6, 7, 8] and will report on the application and manufacturing opportunities [9, 10].

## 5 Going '*back*': plasma sustainability

Plasma technologies hold a significant potential for conversion of wastes into valuable products. Thermal plasmas allow reaching high temperatures and therefore can be used for instance as alternative method to pyrometallurgical smelting. Non-thermal plasmas offer new beneficial advantages, in particular when interfaced with liquids. As electrical energy is directly used to generate highly reactive species without the need of additional heat or chemicals, plasmas can make a substantial contribution to overcoming sustainability challenges.

## References

[1] Haq, A. U. et al. *Nature Comm.* **10**, 817 (2019)
[2] Askari, S. et al. *Nanoscale* **8**, 17141 (2016)
[3] Haq, A. U. et al. *Nanoscale Horiz.* **9**, 2042 (2024)
[4] Khalid, H. et al. *Adv. Energy Mater.* **12**, 2201131 (2022)
[5] Haq, A. U. et al. *Adv. Sci.* **11**, 2402235 (2024)
[6] Tarasenka, N. et al. *Small Methods* **8**, 2400481 (2024)
[7] Buerkle, M. et al. *J. Phys. Chem. Lett.* **15**, 4185 (2024)
[8] Padmanaban, D. B. et al. *Green Chem.* **23**, 3983 (2021)
[9] Padmanaban, D. B. et al. *Adv. Eng. Mater.* **26**, 2400826 (2024)
[10] McGlynn, R. et al. *Small Methods* **8**, 2300710 (2023)

# Understanding the role of the catalyst support in plasma-catalysis

F. Spadoni[1], S. Perina[1,*], G. Castellani[3], P. Tosi[1], P. Fornasiero[3], V.M. Sglavo[2] and L.M. Martini[1]

[1] *University of Trento, Department of Physics, Trento, Italy*
[2] *University of Trento, Department of Industrial Engineering, Trento, Italy*
[3] *University of Trieste, Department of Chemical and Pharmaceutical Sciences, CNR-ICCOM, CENMAT, Trieste, Italy*
[*] *Present address: Maastricht University, Maastricht, The Netherlands*

Plasma catalysis combines plasma's ability to promote high-energy chemistry at mild conditions with the speed and selectivity of catalysis. However, plasma catalysis needs a deeper understanding of its fundamental mechanisms, as evidenced by the differing results reported in the literature regarding the true synergy between plasma and the catalytic material. The interaction between the catalyst and its support and the plasma is critical and requires thorough investigation.

## 1 Introduction

Plasma catalysis is an emerging research area that aims to combine catalysis with non-thermal plasmas. Unlike thermal catalysis, in plasma catalysis, dissociation also occurs in the gas phase, and the presence of the electric field, charged particles, and radicals can lead to different pathways unique to the specific environment [1]. In addition, complex chemical and physical interactions arise between the catalyst support, the catalyst, and the discharge that are not well known and understood. Adding a catalyst does not necessarily improve the activity of the plasma, and, in some cases, it can be detrimental to the performance [2]. In most plasma catalysis studies, the procedure for preparing the catalyst (and the catalyst support) is not standardized, making it problematic to understand and reproduce the experiments. In this contribution, we examine the plasma-catalytic ammonia synthesis process to gain insights into the role of support preparation.

## 2 Experimental methods

Two different types of discharge have been chosen: a dielectric barrier discharge and a nanosecond repetitively pulsed discharge, while alumina beads and alumina monoliths serve as support for silver, the active material. The ratio between $N_2$ and $H_2$ flows is set to 1:3 for both reactors. The ammonia production is inferred from FTIR absorption spectra. To reveal the influence of the preparation process of the support, we use bare alumina beads as a control group. These beads underwent the same preparation steps as the silver-impregnated beads (drying, impregnation with or without stirring, and calcination), except that silver was not added. The same procedure has been applied to monoliths of $\gamma$-$Al_2O_3$ on $\alpha$-$Al_2O_3$ except that monoliths do not require stirring. Supports have been studied using BET, SEM, EDXS, and XRD.

## 3 Results

The catalyst support significantly affects the ammonia production. In particular, the treatment of the support required to load the catalyst strongly impacts ammonia production, as demonstrated by the comparison between treated and untreated support. This difference can be attributed to the combination of stirring (for beads) and the heat treatment that the supports undergo during preparation. The addition of silver, which is not active in thermal catalysis, enhances the production of ammonia when loaded on the supports in both discharges compared to the performance of the correct reference group (i.e., unloaded supports processed similarly to the loaded ones).

## Acknowledgement

Funded by the European Union under NextGenerationEU. PRIN 2022 Prot. n. 2022J5NBBN; European Union - FSE REACT-EU, PON Research and Innovation program 2014-2020.

## References

[1] Mehta P., Barboun P., Go D.B., Hicks J.C. and Schneider W.F. Catalysis enabled by plasma activation of strong chemical bonds: a review *ACS Energy Letters*, **4**, 1115–1133 (2019).

[2] Loenders B., Michiels R. and Bogaerts A. Is a catalyst always beneficial in plasma catalysis? Insights from the many physical and chemical interactions *J. Energy Chem.*, **85**, 501–533 (2023).

# *In-situ* nanoparticle size characterization in an arc discharge using coherent Rayleigh-Brillouin scattering

M. Mitrou[1], T.-H. Nguyen[2], D. Z. Pai[2] and A. Gerakis[1]

[1] *Luxembourg Institute of Science and Technology (LIST), 4422 Belvaux, Luxembourg*
[2]*Laboratory of Plasma Physics (CNRS), Ecole Polytechnique, Route de Saclay, 91128, Palaiseau, France*

This work reports on the progress in utilising non-resonant, four-wave-mixing optical diagnostics, in the form of coherent Rayleigh-Brillouin scattering (CRBS) to probe *in-situ* the spatio-temporal evolution of nanoparticle properties that are produced in an arc discharge. A novel method to calibrate CRBS with engineered nanoparticles suspended in an aqueous solution is presented.

## 1 Introduction

In the growing field of nanotechnology, the control and optimization of nanoparticle (NP) synthesis processes relies on having a solid understanding of the physical mechanisms that govern NP formation. In this direction, this work aims at a systematic exploration of carbon NP formation in a nanosecond-pulsed arc discharge for the first time by means of CRBS [1], a non-resonant four-wave-mixing optical diagnostic with proven applicability in characterizing atomic and molecular gases, gas flows, plasmas, and in detecting *in-situ* NPs [2]. Moreover, a novel calibration method for CRBS using NPs of known characteristics is demonstrated.

## 2 Experimental setup

CRBS consists of inducing an electrostrictive grating in a medium by the interference of two *pump* laser beams. A third *probe* beam is then Bragg-scattered to produce a fourth *signal* beam [1]. The CRBS signal is directed to a photodiode and subsequently recorded. To perform CRBS in this experiment a custom-made laser system is used with capabilities that have been described in detail in [3].

In this study, carbon NPs are produced in a small cubic reactor employing a concentric pin-to-disk electrode configuration. The spatio-temporal properties of the NP formation in the reactor are probed and are a function of operational parameters such as the amplitude of the applied high voltage pulse, its duration and frequency.

The calibration of CRBS signals is performed prior to these measurements by probing engineered NPs and verifying that the experimentally derived NP size matches that given by the manufacturer. To achieve this, a way to suspend the NPs in space was established which ensures limited agglomeration. In particular, a device was developed in which 20 nm gold NPs are suspended in an aqueous solution circulating through an aluminum nozzle creating a vertical, nearly laminar, liquid flow 0.15 μm thick. Fig. 1(a) depicts the implementation of CRBS in the liquid flow.

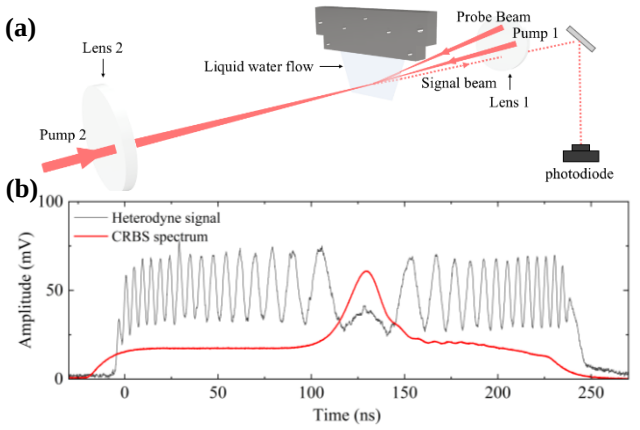



**Figure 1.** a) Schematic representation of the CRBS geometry used in this experiment, b) Heterodyne signal of the two pump beams and CRBS spectrum obtained from water; chirp frequency range: 0-220 MHz.

## 3 Preliminary results and conclusion

Fig. 1(b) showcases an example of a CRBS spectrum obtained from liquid water which is reported, to the best of our knowledge, for the first time. A prominent Rayleigh peak is distinguished at the zero-phase-velocity point of the spectrum. It is superimposed on a background signal attributed to the refraction of the pump and/or probe beams on the water surface resulting in a portion of them to be also detected on the photodiode. In a next step, with the introduction of NPs in the water another narrower peak is expected to appear on top of the existing one for water on account of the significantly larger mass of the NPs [2]. The CRBS measurements will be further complemented by Coherent anti-Stokes Raman spectroscopy (CARS) measurements performed in a similar setup.

## References

[1] Pan, X. *et al.* Coherent Rayleigh-Brillouin scattering, *Phys. Rev. Lett.* **89**, 183001-1 (2002).
[2] Gerakis, A. *et al.* Four-wave-mixing approach to in situ detection of nanoparticles, *Phys. Rev. Appl.* **9**, 014031 (2018).
[3] Bak, J. *et al.* Dual color, frequency, pulse duration and shape agile laser system for particle spectroscopy and manipulation, *Opt. Express* **30**, 41709 (2022).

# Atmospheric Pressure Air Plasma for Removal and Detoxification of Emerging Genotoxic Wastewater Pollutants

M. Modic[1], A. Kovačič[2], N. Hojnik[1], M. Štampar[3], B. Žegura[3], D. Heath[2], E. Heath[2], J. L. Walsh[4,1] and U. Cvelbar[1]

[1]*Department for Gaseous Electronics, Jozef Stefan Institute, Slovenia*
[2]*Department of Environmental Sciences, Jozef Stefan Institute, Slovenia*
[3]*Department of Genetic Toxicology and Cancer Biology, National Institute of Biology, Slovenia*
[4]*York Plasma Institute, University of York, United Kingdom*

Bisphenols, widely used in polycarbonate plastics, pose environmental and health risks due to their endocrine-disrupting, cytotoxic, and genotoxic properties. Wastewater discharge is a major contamination source, as conventional treatment methods fail to fully remove them. Various remediation techniques have been explored, with Cold Atmospheric Pressure Plasma (CAP) emerging as a promising alternative. CAP generates reactive oxygen and nitrogen species that aid in pollutant degradation. This study evaluated CAP's efficiency in degrading bisphenol-A (BPA) and bisphenol-S (BPS) in wastewater. High-resolution mass spectrometry identified transformation products, and toxicological analysis showed reduced toxicity post-treatment. These findings support CAP as an effective method for bisphenol removal.

Bisphenols comprise a diverse group of chemicals widely used in the production of polycarbonate plastics, commonly found in products such as plastic bottles, food and beverage containers, and sports equipment. Growing concerns about their potential endocrine-disrupting effects, cytotoxicity, and genotoxicity have heightened awareness of their environmental impact. Studies have identified wastewater discharges as a major source of bisphenol contamination, as conventional water treatment techniques—primarily biological and physiochemical processes—fail to fully eliminate them.

In response to these concerns, extensive research has been conducted on effective methods for removing bisphenols from the environment. Various approaches have been explored, including adsorption, membrane filtration, flocculation, UV irradiation, and advanced oxidation techniques such as ozonation, heterogeneous photocatalysis, and photo-Fenton treatments. More recently, Cold Atmospheric Pressure Plasma (CAP) has emerged as an innovative and promising technology for wastewater treatment. CAP generates intense electric fields that accelerate electrons to high energies, initiating collisions that produce ions, excited neutrals, and reactive ground-state species. In humid conditions, key reactive oxygen species (ROS) include hydroxyl radicals ($^{\cdot}OH$), atomic oxygen (O), ozone ($O_3$), and hydrogen peroxide ($H_2O_2$), while reactive nitrogen species (RNS) consist of nitric oxide (NO), nitrites ($NO_2^-$), nitrates ($NO_3^-$), and peroxynitrites ($ONOO^-$), all of which contribute to degradation processes.

This study aimed to assess the potential of CAP technology for degrading two commonly used bisphenols, bisphenol-A (BPA) and bisphenol-S (BPS), in wastewater [1]. Using high-resolution mass spectrometry (LC-MS/MS), we identified the primary transformation products and proposed possible degradation pathways for both compounds. Toxicological evaluation with an in vitro HepG2 cell model demonstrated that the transformation product mixture generated during CAP treatment exhibited lower toxicity than the parent compounds, BPA and BPS. These findings highlight the effectiveness of CAP as a promising method for the safe degradation of bisphenols [2].

**References**

[1] Kovačič et al. Degradation and toxicity of bisphenol A and S during cold atmospheric pressure plasma treatment. *Journal of Hazardous Materials*, **454**, 1-12 (2023).
[2] Kovacic et al. Degradation of bisphenol A and S in wastewater during cold atmospheric pressure plasma treatment. Science of the Total Environment. **837**, 1-7 (2022).

# Professor Bill Graham: His Science Over Five Decades [Abridged Version]

Tom Morgan[1,2]

[1] *Wesleyan University, Middletown, CT 06459, United States*
[2] *Queen's University Belfast, Belfast, Northern Ireland*

The talk highlights some of the many scientific accomplishments and achievements of Professor Bill Graham, Queens University, Belfast, Northern Ireland. The talk traces portions of his 50-year research career from his graduate school days at Queens up until retirement in 2018, showcasing his diverse scientific contributions, collaborations and colleagues, with emphasis on his research in the areas of atomic and molecular collision processes of importance in plasmas and ionized gases, $D^-$ and $D^0$ beam development of importance to neutral beam injection heating in fusion plasmas, and his work in the area of nanosecond laser induced plasma breakdown in gases and liquids.

# Plasma Chemistry and its Biological Applications: Always Passion

T. Murakami

*Seikei University, Musashino, Tokyo, Japan*

Professor W.G. (Bill) Graham has always been a passionate enthusiast who has taken on new challenges based on the knowledge and skills he has cultivated through his many achievements. In the 2000s, he focused on fundamental research into the unique physical chemistry of atmospheric pressure non-thermal plasma and plasma generated in liquids, as well as its biological and medical applications. This article looks back at the latter part of his career and shows how he was free to expand his interests.

In the 2000s, Professor Bill Graham's main research interests were in fundamental research into the unique physics and chemistry of atmospheric pressure non-thermal plasmas and plasmas generated in liquids, as well as their biological and medical applications.

The range of applications of plasmas in liquids, in contact with liquid surfaces, including droplets or vapours, was rapidly expanding in various technological fields. He became interested in the physical phenomena and plasma-induced chemical reactions in plasmas with electrodes immersed in liquids. Together with Ken Stalder, he studied the generation mechanism of water vapor plasma and chemical reactions at the interface with liquids from the viewpoint of the generation of highly reactive radicals. [1-3].

He became interested in the atmospheric pressure dielectric barrier discharge jet, which is now one of the classic examples of low-temperature plasma sources [4]. In most applications, the plasma jet operates in an open environment. The presence of moist air in the plasma jet can affect the plasma chemistry and lead to the generation of a greater variety of reactive species. He promoted the development of highly detailed numerical simulation models showing that the presence of moist air leads to the emergence of new species such as N, NO, H and OH radicals [5-7]. These species are now considered important in biomedical applications.

The chemistry of liquid and gas-phase plasmas sparked his interest in the field of plasma medicine. He collaborated with the School of Pharmacy to conduct research into the wide range of medical applications of plasma, including cancer cell therapy, bacterial inactivation and DNA therapy. [8-10].

Although the time the author spent with Bill in Belfast was short, his research group always had people from all over the world and we had a lot of fun. As you all know, many of them are now leading our community. There is no doubt that his "always passionate" attitude contributed to this.

## References

[1] W. G. Graham and K. R. Stalder, “Plasmas in liquids and some of their applications in nanoscience,” J. Phys. D: Appl. Phys. **44** 174037 (2011).
[2] L. F. Schaper, K. Stalder and W. G. Graham, "Plasma production in electrically conducting liquids," Plasma Sources Sci. Technol. **20** 034004 (2011).
[3] L. F. Schaper, K. Stalder and W. G. Graham, "Vapour layer formation by electrical discharges through electrically conducting liquids - Modelling and experiment," Plasma Sources Sci. Technol. **20** 034003 (2011).
[4] C. McDonnell, R. Irwin, S. White, W. G. Graham and D. Riley, "Optical diagnosis of a kHz-driven helium atmospheric pressure plasma jet," J. Plasma Phys. **88** 905880316 (2022).
[5] T. Murakami, K. Niemi, T. Gans, D. O'Connell and W. G. Graham, “Chemical kinetics and reactive species in atmospheric pressure helium–oxygen plasmas with humid-air impurities,” Plasma Sources Sci. Technol. **22** 015003 (2013).
[6] T. Murakami, K. Niemi, T. Gans, D. O'Connell and W. G. Graham, “Interacting kinetics of neutral and ionic species in an atmospheric-pressure helium–oxygen plasma with humid air impurities,” Plasma Sources Sci. Technol. **22** 045010 (2013).
[7] T. Murakami, K. Niemi, T. Gans, D. O'Connell and W. G. Graham, “Afterglow chemistry of atmospheric-pressure helium–oxygen plasmas with humid air impurity,” Plasma Sources Sci. Technol. **23** 025005 (2014).
[8] W. G. Graham. L. F. Schaper. M. F. Muir and F. Currell, "The Effect of Electrical Discharges in the Cell Media on Their Viability and DNA Damage and Comparison with the Effect of X-Rays," Plasma Med. **2** 169 (2012).
[9] A. R. Gibson, H. O. McCarthy, A. Ali, D. O'Connell and W. G. Graham, "Interactions of a Non-Thermal Atmospheric Pressure Plasma Effluent with PC-3 Prostate Cancer Cells," Plasma Process. Polym. **11** 1142 (2014).
[10] P. B. Flynn, A. Busetti, E. Wielogorska, O. P. Chevallier, C. T. Elliott, G. Laverty, S. P. Gorman, W. G. Graham and B. F. Gilmore, "Non-thermal Plasma Exposure Rapidly Attenuates Bacterial AHL-Dependent Quorum Sensing and Virulence," Sci. Rep. **6** 26320 (2016)

# Generation of high-density Ar cascade arc plasma for plasma window and its application to electron beam engineering in air

S. Namba[1], H. Okuno[2], and K. Yamasaki[1]

[1] *Graduate School of Advanced Science and Engineering, Hiroshima University, 1-4-1 Higashihiroshima, Hiroshima, 739-8527, Japan*
[2] *RIKEN, Nishina Center for Accelerator-Based Science, Wako, Saitama 351-0198, Japan*

In order to realize plasma windows as virtual vacuum interfaces, we have developed indirectly heated hollow cathode electrodes and cascade arc discharge apparatus. For windowless vacuum–atmosphere separation, a compact arc discharge source having a channel diameter of 3 mm is fabricated. An atmospheric high-density Ar thermal plasma (temperature: ~1 eV and density: $>10^{16}$ cm$^{-3}$) is generated, and plasma window creating 100 kPa and 76 Pa separation is demonstrated.

Plasma window (PW) has been paid attention as an innovative technique, by which a dense plasma can separate vacuum from atmosphere [1,2]. The promising applications of the plasma window enable us to transmit charged particles through plasma channel without significant beam scattering and attenuation. We have tried to weld/cut the substances by an electron beam in air. Note that the PWs make it possible to realize that the size of work piece for the welding is substantially mitigated, capable of applying this method to large structures that requires precise fabrications in air.

A cascade arc discharge plasma source has often been employed to generate atmospheric dense plasmas. However, the pressure difference between the plasma window was 100 kPa and ~100 Pa, so that further increase of the gas viscosity is essential to realize the practical plasma window. Thus, we have developed a cascade arc device to demonstrate the pressure separation of 100 kPa-1 Pa by improving the electrode structures. In particular, hollow-type $LaB_6$ cathode heated by a carbon fiber reinforced carbon composite was developed to emit the thermionic electrons [3].

Figure 1 shows a schematic view of the cathode. The cathode is constituted of three main parts, electron emitters, a heater, and a keeper electrode. The electron emitter is a hollow cylinder made of $LaB_6$, located inside a Mo tube. In hollow cathode discharges, ions are trapped with good efficiency inside the emitter and heat the emitter wall to approximately 2500°K, generating abundant thermionic electrons and the dense highly ionized plasma. Therefore, collision frequencies increase among electrons, ions, and neutrals, and high-gas temperature is achieved. Thus, the improvement of PW performance owing to an increase in gas viscosity can be expected in comparison to the conventional cathode. The heater and the Mo tube

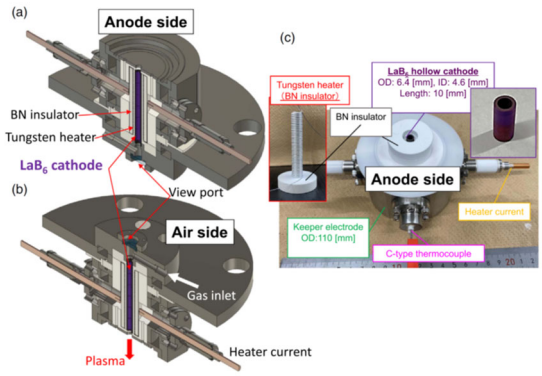



Fig. 1. Schematic of the cathode, (a) anode side, (b) cathode side. (c) cathode assembly, including the heater, keeper, BN insulator, and $LaB_6$ cylinder.

are electrically isolated by a BN tube. A keeper electrode made of Mo is electrically floating and with the role of expelling out electrons to outside from inside of emitters.

Performance of the PW was examined by the pressure gradient between the cathode and anode. At a 20-A discharge, we succeeded in significant pressure separation of 100 kPa and 76 Pa. On the other hand, passive and active spectroscopic measurements were conducted, showing that Ar atmospheric plasmas had a temperature of ~1 eV and density of $>10^{16}$ cm$^{-3}$.

In this presentation, we also discuss the electron beam transmission in Ar atmosphere channel without the discharge to understand how the electron beam is scattered and attenuated in the Ar gas.

## References

[1] A. Hershcovitch, Phys. Plasmas **5**, 2130 (1998).
[2] S. Namba *et al*, Phys. Plasmas **25**, 113511 (2018).
[3] K. Yamasaki *et al*., Jpn. J. Appl. Phys. **62** SL1009 (2023).

# Millimeter-scale 3D Plasma Sheath Lenses

C.P.V. Nguyen[1], E. Stamate[1]

[1] *National Centre for Nano Fabrication and Characterization (DTU Nanolab), Technical University of Denmark, 2800 Kongens Lyngby, Denmark*

Using microfabrication, we show for the first time discrete focusing effects by customized 3D plasma sheath lenses at the millimeter scale. When biased negatively and exposed to a plasma, we show that the exposed 1 mm × 1 mm structures are etched by a distinct pattern according to discrete focusing. We also observe this for an array of 2 mm × 2 mm square structures. This will provide deeper understanding of fundamental properties of the plasma-presheath-sheath-surface system, including potential applications in micro- and nanofabrication and plasma diagnostics.

## 1. Introduction and methodology

3D plasma sheath lenses based on the discrete and modal focusing effect could be used for ion extraction crucial for precise etching, ion implantation or deposition. [1,2] The samples are made from low resistivity 500 µm thick silicon wafers. We deposited 3.7 µm of $SiO_2$ on top of silicon, and etched structures of various dimensions and shapes into the $SiO_2$ layer, exposing the Si surface underneath. $SiO_2$ is an electrical insulator, which limits the sheath formation of the sample to the conducting area exposed to the plasma environment. This allows us to design precise 3D plasma sheath lenses of variable size and shapes potentially up to the micrometer scale. Our presented samples are diced into 20 mm × 20 mm squares, inserted into an electrical insulating ceramic mount, biased negatively, and then exposed to $Ar/SF_6$ plasma. The plasma is generated by a large area plasma source based on 12 multi-dipolar ECR plasma cells arranged in a 3×4 matrix configuration [3]. After short mild ion bombardment for native oxide removal, the presented samples are biased to −100V/−150V for 5 min in an Ar [10 sccm], $SF_6$ [2.5 sscm] plasma, for 1.7 mTorr discharge pressure and 300 W discharge power. The plasma parameters are monitored by mass spectrometry and Langmuir probe measurements (plasma potential $V_p$=5.7V, plasma density $n$=6.9×10$^{15}$ m$^{-3}$, and electron temperature $T_e$=2.3 eV).

## 2. Results and Discussion

The conducting electrode surface will attract positive ions, which bombard it according to the shape of the 3D plasma-sheath-lens and discrete focusing manifestation. [1]. We are reporting for the first time this effect on electrodes at dimensions smaller than 10 mm × 10 mm as presented in Fig. 1. Furthermore, we are reporting individual 3D plasma-sheath-lenses formation on a 3×3 matrix configurated pattern, with 2 mm × 2 mm square structures (see Fig. 2). Additional results on array structures designed in purpose to enlarge the plasma sheath of the individual squares to the point of individual lenses interference are considered.

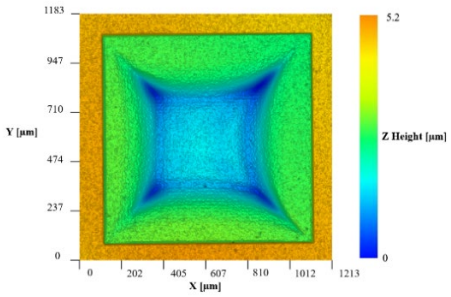



**Fig. 1** Optical profilometry of 1mm x 1mm silicon surface structure after plasma treatment (−100V).

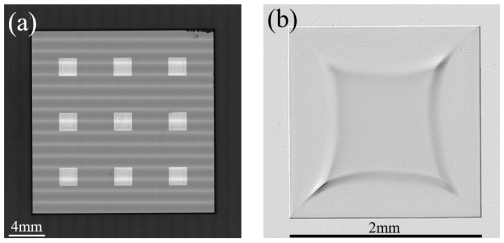



**Fig. 2** a) 3 × 3 square structure after plasma treatment (−150V). b) 2D optical profilometric image of the top left square.

**Acknowledgment**

This work was partially supported by the "Smart3D" project (2081-00011A) financed by Innovation Fund Denmark.

**References**

[1] Stamate, E. and H. Sugai, *Physical Review E* **72**, 036407 (2005)

[2] Stamate, E., *Plasma Physics and Controlled Fusion* **54**, 12, 124048. (2012)

[3] Stamate, E. and M. Draghici, *Journal of Applied Physics* **111**, 8, 083303 (2012)

# Plasma-generated atomic oxygen for contactless cleaning of cultural heritage objects

A. Nikiforov[1], Y. Song[1], L. Invernizzi[2], K. Gazeli[2], D. Stefas[2], G. Lombardi[2], M. Poupouzas[1,3], A. Sobota[3], R. Morent[1]

[1] *Research Unit Plasma Technology, Faculty of Engineering and Architecture, Ghent University, 9000, Ghent, Belgium*
[2] *Laboratoire des Sciences des Procédés et des Matériaux (LSPM—CNRS), Université Sorbonne Paris Nord, Villetaneuse, UPR 3407, F-93430, France*
[3] *Elementary Processes in Gas Discharges Group, Department of Applied Physics and Science Education, Eindhoven University of Technology, Eindhoven, The Netherlands*

Non-thermal generation of atomic oxygen (AO) emerged as a novel application in cultural heritage (CH) areas as a contactless cleaning approach capable of removing contaminants from treated objects. This is an entirely non-mechanical, solvent and liquid-free manner, without waste. Here, the concept of AO generation by the change of the discharge voltage waveform and results of various contaminates treatment are presented. The generation of AO in non-thermal RF plasma is investigated by optical spectroscopy and ps-/ns-TALIF capable of achieving high temporal and spatial AO mapping. It is revealed that the generation of AO can be tuned to specific requirements by controlling operational parameters including RF input power, voltage pulsing and harmonics, as well as the phase shift between RF harmonics.

## 1 Introduction

The removal of contaminants from heat-sensitive materials is a key challenge in different areas, including microelectronics, medicine, and cultural heritage (CH). Among others, carbon-based fire-born contaminants represent one of the most difficult contaminants to remove by traditional methods of "wet" chemistry in CH. Recently, a new contactless cleaning method has been proposed based on the reaction of highly oxidizing atomic oxygen (AO) with organic contaminants. AO can be effectively generated in conditions of non-thermal plasma where its generation rate and so the flux to the surface can be precisely tuned through the variation of plasma conditions.

## 2 Plasma diagnostics and results

The AO beam has been generated by RF low current non-thermal discharge in the axial geometry. The operational parameters of the source were adjusted to control the efficiency of AO generation. The effect of gas composition, input power, and RF harmonics on $O_2$ dissociation and gas heating were analysed and optimized for the needs of contactless cleaning. Both emission spectroscopy and ps-/ns resolved two photon absorption laser-induced fluorescence (TALIF) were applied for the diagnostics of AO generation and its transport towards the treated surface. The use of ps-TALIF helped to precisely measure the quenching rate of laser-excited O atoms whereas ns-TALIF was used to define the spatially resolved O density in the plasma effluent.

It was revealed that the optimal $O_2$ admixing in He gas is in the range of 0.15-0.3 vol.% whereas higher $O_2$ admixing results in undesirable formation of $O_3$. The key electrical parameters to control the production of AO were the RF power and RF harmonics. Interestingly, it is revealed that the presence of second harmonics of 27.12 MHz and, more specifically, phase shift between 1$^{st}$ and 2$^{nd}$ harmonics, can strongly enhance O production. The change of the phase from 90° to 270° at the same RF power of 7 W results in highest increase of the AO flux at the effluent region located at 10 mm from the nozzle with little increase of the gas heating.

The proposed method of atomic oxygen generation was applied to samples mimicking fire-born contaminants on CH objects. It was demonstrated that AO can selectively remove soot with negligible impact on the substrate. As such, the method of contactless cleaning developed here empowers CH conservators in diverse specializations with a new technology that resonates with the urgent need to refine cleaning methodologies.

### Acknowledgements

The research is supported by EU Horizon "MOXY" project, Grant 101061336, and FWO "PlasmArt" project G0C2822N. The authors thank ANR ULTRAMAP Project (ANR-22-CE51-0027), Labex SEAM Project (ANR–10–LABX–0096; ANR–18–IDEX–0001) and IDF project SESAME DIAGPLAS.

# The Rising Importance of Sustainability: Opportunities for Plasma Processes

A. Nominé[1,2,3], Adrián Benedit-Cárdenas[1], Janez Zavašnik[3,4], Valentin Milichko[1], Stéphanie Bruyère[1], Thierry Belmonte[1], Uroš Cvelbar[3]

[1] *Institut Jean Lamour, Université de Lorraine – CNRS, Nancy, France*
[2] *University of Lorraine, Mines Nancy, Nancy, France*
[3] *Department of Gaseous Electronics, Jožef Stefan Institute, Ljubljana, Slovenia*
[4] *Max Planck Institute for Sustainable Materials, Düsseldorf, Germany*

The concomitant green and digital transitions will generate unprecedented demand for materials, raising legitimate concerns about whether existing material resources can meet these requirements. While circular economy practices offer partial solutions through improved recycling and reuse, they alone may prove insufficient. A complementary approach involves discovering novel materials with properties equivalent to current standards but with enhanced sustainability profiles [1].

To substitute critical materials (e.g., platinum, gallium, germanium) two main approaches have emerged. As detailed by Raabe *et al*. [2], one strategy leverages compositional complexity through alloying, which can produce synergistic effects leading to enhanced properties. However, Rousseau et al. . [3] have demonstrated that there exists an optimal "golden number" of alloying elements (typically 3 to 6). While increasing the number of elements exponentially expands possible combinations, it simultaneously increases the probability for any single element to fail (shortage). A complementary strategy focuses on microstructural complexity, where properties are enhanced and tuned through controlled introduction of structural features like lattice distortions, grain boundaries, and twinning defects. This latter approach is particularly dependent on the synthesis method employed, making processing techniques increasingly critical in materials development.

Plasma processes represent a particularly valuable tool in this materials revolution due to their inherently non-equilibrium character. This unique property enables the synthesis of materials that remain largely inaccessible through conventional manufacturing routes [4,5]. The non-equilibrium conditions created by plasma processes allow for exploration of vast regions of the materials space that remain largely unexplored.

This presentation will highlight the immense untapped potential within the materials space and demonstrate specific examples where plasma processes have significantly enhanced material properties. For instance, Beneditt *et al*. demonstrated that the Curie temperature of SiMn materials can be significantly increased—by a factor five —through plasma synthesis techniques. This dramatic enhancement results from the plasma process's ability to generate metastable phases and introduce specific defects that would be unattainable through conventional synthesis methods. [6]. Similar results are observed in the fields of plasmonics, non-linear optics or catalysis.

These examples illustrate how plasma-based synthesis approaches can unlock novel material functionalities while simultaneously addressing sustainability concerns through reduced reliance on critical raw materials.

**References**

[1] Wiederrecht G, *et al.* Nanomaterials and Sustainability *ACS Energy Letters*, **8**, 3443–3449, (2023)

[2] Raabe D. The Materials Science behind Sustainable Metals and Alloys *Chemical Reviews*. **123**, 2436–2608 (2023)

[3] Rousseau F., Nominé A., Zavašnik J. , Cvelbar U., Is alloying a promising path to substitute critical raw materials? *Materials Today* **83**, 1-8 (2025).

[4] Nominé AV, *et al.* Mixing gold and iron in nanoparticles by electrical discharges in liquid: A new approach *Nano-Structures & Nano-Objects* **35** 100996 (2023)

[5] Belmonte *et al.* Submerged Discharges in Liquids for Nanoobject Synthesis: Expectations and Capabilities *Plasma Chemistry and Plasma Processing* **44**, 1109–1164, (2024)

[6] Benedit-Cárdenas *et al.* Kinetics vs. thermodynamics: walking on the line for a five-fold increase in MnSi Curie temperature *Materials Horizons* **11** 460-467 (2024)

# Laser-based characterization of single filament streamers: A novel approach to streamer discharge analysis

R. Ono[1], S. Mok[1], Y. Inada[2], K. Tomita[3] and Y. Nakagawa[4]

[1] *The University of Tokyo, Tokyo, Japan*
[2] *Saitama University, Saitama, Japan*
[3] *Hokkaido University, Sapporo, Japan*
[4] *Tokyo Metropolitan University, Tokyo, Japan*

Streamer discharge is a low-temperature plasma generated in atmospheric-pressure air. We perform comprehensive laser diagnostics to investigate its reaction mechanisms, measuring electric field, electron density, EEDF, reactive species, and temperatures. To overcome challenges in diagnosing branching streamers, we developed a non-branching, quasi-2D single filament streamer, enabling precise measurements and validation of 2D simulations.

## 1 Introduction

Streamer discharge is a representative low-temperature plasma generated in atmospheric-pressure air. Investigating its reaction mechanisms is crucial for a deeper understanding of atmospheric-pressure air plasmas. To achieve this, comprehensive laser diagnostics of streamer discharge are conducted.

High-precision laser diagnostics of branching streamer discharges pose significant challenges. To overcome this, we have developed a non-branching, quasi-2D single filament streamer discharge [1], which allows for more precise measurements. Its axisymmetric 2D nature also enables the obtained data to be used for validating 2D simulations.

## 2 Experimental setup and results

A single filament streamer is generated between a 13-mm, pin-to-plate electrode in atmospheric-pressure air, the same as in [1]. High-voltage pulses (20 to 30 kV) are applied at 2 pps. The electric field is measured using electric-field-induced second harmonic generation (E-FISH) with a femtosecond laser (1030 nm, 190 fs) [2]. The electron density is measured using a Talbot interferometer with 408 and 785 nm continuous-wave diode lasers [3]. The electron energy distribution function (EEDF) is measured using laser Thomson scattering (LTS) with the second harmonics beam of an Nd:YAG laser (532 nm) [4]. Reactive species (OH, $O_3$, and O) are measured using laser-induced fluorescence (LIF), photofragmentation LIF, and two-photon absorption LIF (TALIF), respectively [1, 5, 6].

The spatiotemporal evolution of these parameters was measured and compared with simulation results developed by Komuro [1]. Some agreements and discrepancies were observed. We are also planning to measure positive ion densities using LIF, negative ion densities using LTS with laser detachment, and vibrational and translational temperatures using laser Raman scattering.

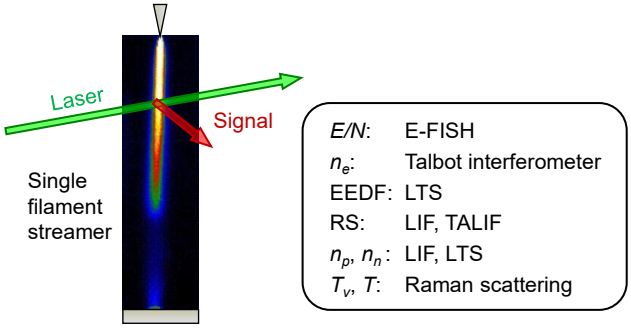



Fig. 1. Single-filament streamer and measured parameters with measurement methods. $n_e$: electron density, RS: reactive species, $n_p$ and $n_n$, positive and negative ion densities.

### References

[1] R. Ono and A. Komuro, *J. Phys. D: Appl. Phys.* **53**, 035202 (2020).
[2] Y. Inada, T. Shioda, R. Nakamura, M. Maeyama, A. Kumada, S. Nakamura, and R. Ono, *J. Phys. D: Appl. Phys.* **55**, 385201 (2022).
[3] Y. Inada, A. Komuro, R. Ono, A. Kumada, K. Hidaka, M. Maeyama, *J. Phys. D: Appl. Phys.* **52**, 185204 (2019).
[4] K. Tomita, Y. Inada, A. Komuro, X. Zhang, K. Uchino, and R. Ono, *J. Phys. D: Appl. Phys.* **53**, 08LT01 (2020).
[5] R. Ono, X. Zhang, and A. Komuro, *J. Phys. D: Appl. Phys.* **53**, 425201 (2020).
[6] Y. Nakagawa, T. Kawakita, S. Uchida, and F. Tochikubo, *J. Phys. D: Appl. Phys.* **53**, 135201 (2020).

# Experimental derivation of electrical characteristics of a He/$N_2$ RF APPJ compared with PIC/MCC simulation

I. Orel[1], N. D. Lepikhin[1], D. Luggenhölscher[1], U. Czarnetzki[1] and Z. Donkó[2]

[1] *Faculty of Physics and Astronomy, Ruhr-University Bochum, Bochum, Germany*
[2] *Institute for Solid State Physics and Optics, HUN-REN Wigner Research Centre for Physics, Budapest, Hungary*

A COST-jet-like RF atmospheric pressure plasma jet operated in a He/$N_2$ mixture is investigated by Electric Field Induced Second Harmonic generation (E-FISH) electric field measurement and by Particle-in-Cell / Monte Carlo Calculation (PIC/MCC) simulation results.

## 1 Introduction

The so-called COST-jet [1] is a standardized RF driven atmospheric pressure plasma source that allows to accumulate a large wealth of experimental data on various radicals and excited species. To the best of our knowledge, no model independent data exist on the electric field and the charge densities in the jet. In this work we report for the first time experimental measurements of these basic plasma parameters. The results are in excellent agreement with those obtained from PIC/MCC simulations. Both experiment and simulation confirm a recent theory on the non-neutrality of the RF APPJ discharge [2].

## 2 Methods

The COST-jet-like discharge has an inter-electrode gap width of 1.5 mm, is operated in a vacuum chamber filled with 1 slm He with 0.5 % $N_2$ admixture at 950 mbar. It, unlike the COST-jet, easily allows an application of a laser driven diagnostic of the electric field, E-FISH. The discharge is also investigated by PIC/MCC simulation. The details can be found in [3].

## 3 Results and Discussion

In Fig. 1, the space and time resolved electric field obtained experimentally is compared with the simulation results. Using first principle derivation, these data are evaluated to determine the space and time resolved total, displacement and conduction current densities, electron and ion densities. All these data are in excellent agreement with the PIC/MCC simulation predictions. The period averaged electron and ion density in the center of the discharge are shown in Fig. 2. The required electric field dependent mobility is calculated using the local Boltzmann solver BOLSIG+ [4]. Finally, the charged species' density data illustrate clearly, experimentally as well as by the simulation, the non-neutral character of the atmospheric pressure RF discharge.

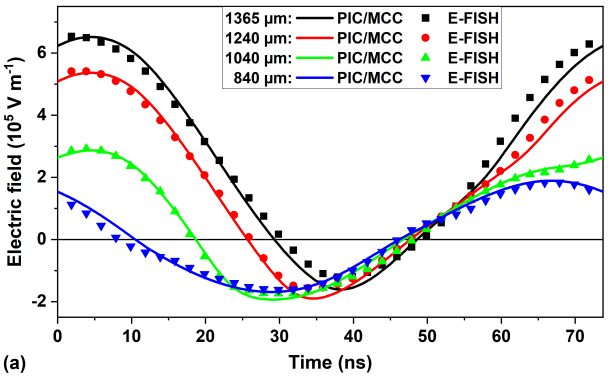



Figure 1: Electric field at different positions from the powered electrode.

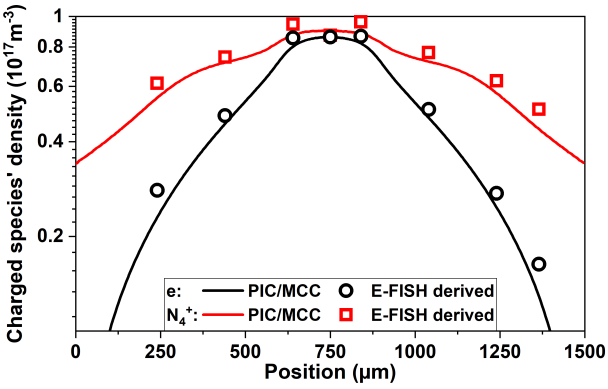



Figure 2: Period-averaged electron and main ion specie, $N_4^+$, densities.

### Acknowledgements

The work is supported by the DFG funded SFB1316 Project 'Transient atmospheric plasmas – from plasmas to liquids to solids' and by Hungarian Fund for Research, Development, and Innovation, via the grant NKFIH 134462.

## References

[1] Golda, J. *et al*, *JPhysD*, **49**, 084003 (2016).
[2] Klich, M. *et al*, *PSST*, **31**, 045003 (2022).
[3] Orel, I. *et al*, *sumbitted to PSST*
[4] Hagelaar, G. J. M. *et al*, *PSST*, **14**, 722 (2005).

# High-speed Particle Image Velocimetry of ionic wind generated between two plates in air at atmospheric pressure

T. Orrière[1]

[1] *Institut PPrime, Université de Poitiers-ENSMA, CNRS, UPR 3346, Poitiers, France*

This study investigates ionic wind generation between two parallel plates using a nanosecond repetitively pulsed microplasma. The microplasma was generated within a cavity on one plate, while a DC electric field was applied across the plates. In this configuration, gas flows with velocities up to $4m.s^{-1}$ were produced and characterized using 2D2C high-speed Particle Image Velocimetry (PIV) at a 10 kHz sampling rate. Voltage, current, and the DC current through the plate were measured simultaneously. By correlating the recorded current with gas acceleration data from high-speed PIV, the transport properties of charged species migrating from the microplasma to the opposing plate were determined.

Ionic wind has a wide range of applications, including cooling systems, combustion enhancement, propulsion, and aerodynamic flow control [1]. Typically, ionic wind is generated in configurations where the electric field is highly non-uniform, such as wire-to-cylinder geometries commonly used in propulsion systems. In these setups, a corona discharge is initiated at the sharper electrode (e.g., the wire), producing electrical charges that drift toward the opposing electrode. The ionic wind arises as these charges transfer their momentum to neutral gas molecules during their migration. However, increasing the voltage in such setups often triggers streamer-to-spark transitions in air at atmospheric pressure. A plate-to-plate geometry offers a potential solution by providing a more uniform electric field and avoiding streamer formation.

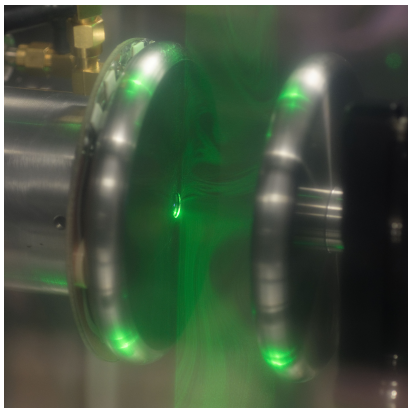


Figure 1: Picture illustrating the experimental setup.

In this study, we build upon a concept introduced in prior work [2]. As illustrated in Figure 1, a nanosecond repetitively pulsed microplasma serves as a charge supplier and is positioned within a 1 mm diameter cavity on a 80 mm diameter plate. A second 80 mm diameter plate, biased at a high voltage of 40 kV, is placed 30 mm away. The microplasma is generated between a 0.5 mm diameter rod inside the cavity, supplied with 6 kV pulses at 1 kHz, and the grounded plate. Under these conditions, PIV reveals an impinging jet-like flow, with a maximum velocity of approximately $2m.s^{-1}$ near the high-voltage plate, as shown in Figure 2. The time resolved measurements indicates the transport properties of the charged species.

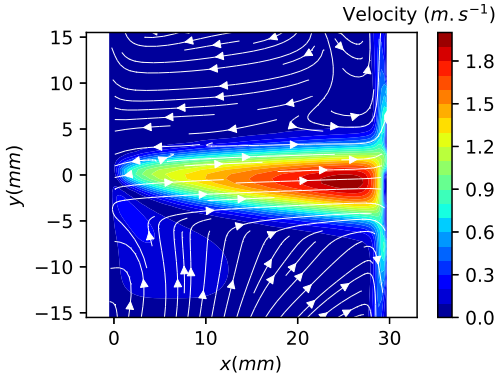



Figure 2: Average velocity field of the ionic wind generated between the two plates with a repetition frequency of 1 kHz. The microplasma is positionned at $x = y = 0mm$.

## References

[1] Johnson, M. J., & Go, D. B. Recent advances in electrohydrodynamic pumps operated by ionic winds: a review. *PSST* **26(10)**, 103002 (2017).

[2] Orrière, T., Moreau, É., & Pai, D. Z. Electric wind generation by nanosecond repetitively pulsed microplasmas. *J. Phys. D* **52(46)**, 464002 (2019).

# Illuminating plasma self-organization of magnetron sputtering discharges

Matjaž Panjan[1]

[1] *Jožef Stefan Institute, Jamova 39, 1000 Ljubljana, Slovenia*

In magnetron sputtering discharges, plasma is not azimuthally homogenous instead it forms dense, localized regions known as spokes or ionization zones. These structures are observed across all magnetron sputtering regimes (DCMS, RFMS and HiPIMS), various geometries (planar and cylindrical) and for a wide range of discharge conditions typically used in the deposition of thin films. The ubiquitous presence of spokes demonstrates that plasma self-organization is an intrinsic phenomenon in magnetron discharges. The talk will provide an overview of the spoke phenomenon and examine spoke behavior under varying discharge conditions—pressure, current, and cathode voltage—across all magnetron regimes.

Magnetron sputtering is a widely used plasma-based deposition method for the fabrication of high-quality thin films. The technique is classified based on the type of voltage applied to the cathode, with magnetron operation regimes defined as DCMS for continuous voltage, HiPIMS for high-power pulsed voltage, and RFMS for oscillatory voltage.

The crossed magnetic and electric field configuration of a magnetron device is essential for the formation of plasma above the cathode. This configuration causes electrons to gyrate around the magnetic field lines, bounce off the sheath, and drift in the **E**×**B** direction. Electric and magnetic fields confine electrons near the target and extend their trajectories in the azimuthal direction. This increases the probability of ionization and leads to the formation of a dense, torus-shaped plasma above the cathode.

Since electric and magnetic fields affect the motion of electrons and ions differently – electrons exhibit **E**×**B** drift and ions move along the **E**-field, this leads to a spatial separation of charges. In turn, the plasma appears concentrated in dense, localized regions known as spokes [1-3], which often form periodic or semi-periodic patterns (Figure 1).

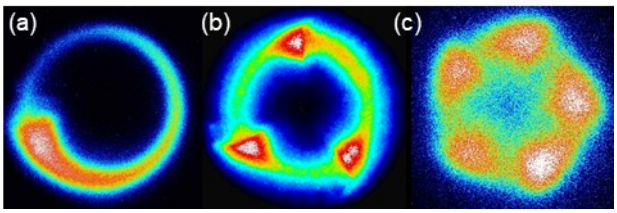



**Figure 1** Typical spokes patterns in (a) DCMS, (b) HiPIMS and (c) RFMS discharges

The properties of spokes depend on the type of magnetron operation, working gas pressure, cathode voltage, discharge current and magnetic field strength of the magnetron. In all regimes, number of spokes increases with the pressure. At lower currents – both in DCMS and HiPIMS regimes – spokes exhibit an elongated arrowhead-like shape and rotate in the direction opposite to electron drift (i.e., **-E**×**B** direction). Their velocity depends on the pressure, current growth rate and number of spokes. Spoke velocity increases with decreasing pressure and higher current growth rates. A single spoke rotates faster than two or more spokes.

At higher currents in HiPIMS discharges, spokes form short triangular spokes that rotate in the **E**×**B** direction. The velocity of spokes is unaffected by both the discharge current and the number of spokes but is influenced by pressure – at lower pressures, spokes rotate faster than at higher pressures (e.g., in a 3-inch magnetron with an Al target the velocity ranges from 9 km/s at 0.25 Pa to 6 km/s at 2 Pa).

In this talk, I will present the latest insights into plasma self-organization in magnetron discharges. The discussion will explore the formation, dynamics and various distributions related to spokes as a function of discharge current, gas pressure, cathode voltage and magnetic field of a magnetron.

## Acknowledgments

The research was supported by the Slovenian Research Agency (project J2-2509 and P2-0082).

## References

[1] M. Panjan *et al.*, Non-uniform plasma distribution in DC magnetron sputtering: origin, shape and structuring of spokes, *Plasma Sources Sci. Technol.*, **24** 065010 (2015).

[2] M. Panjan, Self-organizing plasma behavior in RF magnetron sputtering discharges, *J. Appl. Phys.*, **125** 203303 (2019).

[3] M. Panjan, Plasma dynamics of individual HiPIMS pulses: imaging study using high-frame-rate camera, *Plasma Sources Sci. Technol.*, **33** 055015 (2024).

# Transient spark discharge and ozone-based nitrogen fixation: The study of reaction pathways

P. Pareek, G. Selvaraj, K. Hensel, and M. Janda

*Faculty of Mathematics, Physics and Informatics, Comenius University, Bratislava, Slovakia*

This study investigated the conversion of NO and $NO_2$ produced by transient spark (TS) discharge into more soluble species, such as $N_2O_5$ and $HNO_3$, using TS-treated air combined with ozone (400 ppm). In-situ spectroscopic diagnostics were employed to examine the solvation of these species in water and the subsequent formation of $NO_2^-$ and $NO_3^-$. Water exposed to TS-treated air alone and TS-treated air with ozone was compared. The results underscore the importance of soluble species in plasma-based nitrogen fixation, elucidating the chemical pathways leading to $NO_2^-$ and $NO_3^-$ formation.

## 1. Introduction

Cold plasma is widely employed for liquid treatment, generating highly activated solutions known as plasma-activated water (PAW) [1]. In agricultural applications, reactive nitrogen species (RNS) within PAW are crucial for plant growth [2]. Therefore, understanding the chemical pathways and generation mechanisms of RNS, specifically $NO_2^-$ and $NO_3^-$, is essential.

This study utilized transient spark (TS) discharge to generate NO and $NO_2$ in dry synthetic air. These gases were then mixed with $O_3$-enriched air to produce more soluble species like $N_2O_5$ and $HNO_3$. Gas-phase reactive species were measured using infrared spectroscopy and compared with chemical kinetic modelling. The gas mixture was subsequently passed through a cuvette containing 3 mL of deionized water, where in-situ UV-VIS absorption spectroscopy was used to analyse $NO_2^-$ and $NO_3^-$ formation. Post-treatment, changes in pH and conductivity were monitored.

## 2. Results

Transient spark discharge in dry air produced NO (100–490 ppm) and $NO_2$ (90–160 ppm), with concentrations increasing linearly with discharge power (3.5–7.5 W). The mutual reaction of NO and $NO_2$ led to $NO_2^-$ formation in the liquid phase, governed by the reaction (1), while concentration of generated $NO_3^-$ was negligible.

$$NO_{(aq)} + NO_{2\,(aq)} \rightarrow 2NO_{2\,(aq)}^- + H^+ \qquad (1)$$

When TS-generated NO and $NO_2$ were mixed with $O_3$-enriched air, with $O_3$ concentration of ~ 400 ppm, $N_2O_5$ (1–100 ppm) and $HNO_3$ (1–15 ppm) were produced in the gas phase depending on the discharge power. Significant concentrations of $N_2O_5$ were observed exclusively when the initial NO concentration was lower than the $O_3$ concentration. Conversely, if the NO concentration surpassed the $O_3$ level, the dominant reaction pathway became the conversion of NO to $NO_2$.

Chemical kinetic modelling revealed that $N_2O_5$ formation primarily occurs through a two-step process. First, $O_3$ oxidizes NO to $NO_2$. If the initial NO concentration is below the $O_3$ level, the remaining $O_3$ oxidizes a portion of the $NO_2$ to $NO_3$, which then reacts with $NO_2$ to form $N_2O_5$. The presence of $N_2O_5$ in the gas phase led to a significant increase in $NO_3^-$ concentration in the liquid phase governed by reaction (2), accompanied by a rapid decline in pH:

$$N_2O_{5\,(aq)} + H_2O \rightarrow 2NO_{3\,(aq)}^- + 2H^+_{(aq)}. \qquad (2)$$

The introduction of $O_3$ to TS spark-treated air resulted in an approximately fourfold increase in nitrogen fixation energy efficiency relative to the absence of ozone. To summarize, the quantification of reactive species in both the gaseous and liquid phases, coupled with the analysis of treated water characteristics, provided a comprehensive understanding of the chemical pathways leading to the formation of $NO_2^-$ and $NO_3^-$.

**Acknowledgment**

Funded by:

1. EU NextGenerationEU through the Recovery and Resilience Plan for Slovakia under the project No. 09I03-03-V03-00033
2. APVV SK-SRB-23-0043

**References**

[1] P. Bruggeman *et al.*, "Plasma–liquid interactions: A review and roadmap," *Plasma Sources Sci. Technol.*, vol. 25, no. 5, 053002, 2016.

[2] G. B. Ndiffo Yemeli *et al.*, "The effect of water activated by nonthermal air plasma on the growth of farm plants…," *Plasma Process. Polym.*, vol. 18, no. 1, 2000205, 2021.

# Influence of Plasma Activated Water (PAW) chemistry on physiology of plant calli and on bacterial susceptibility to antibiotics

N. Puač[1], M. Milutinović[2], S. Živković[2], B. Toljić[3], N. Milivojević[3], O. Jovanović[1], M. Miletić[3], D. Vuković[4] and N. Škoro[1]

[1] *Institute of Physics, University of Belgrade-National Institute of Republic of Serbia, Pregrevica 118, 11080 Belgrade, Serbia*
[2] *Institute for Biological Research "Siniša Stanković"- National Institute of Republic of Serbia, University of Belgrade, Bulevar despota Stefana 142, 11000 Belgrade, Serbia*
[3] *School of Dental Medicine, University of Belgrade, dr Subotića starijeg 8, 11000 Belgrade, Serbia*
[3] *Faculty of Medicine, University of Belgrade, dr Subotića starijeg 8, 11000 Belgrade, Serbia*

We present the effects of Plasma Activated Water (PAW) on plant cells and antibiotic-resistant bacteria. PAW induced significant physiological and metabolic changes in Daucus Carrota calli, stimulating growth, metabolic activity and enhancing antioxidant enzyme activity. For antibiotic-resistant bacteria, PAW increased susceptibility to antibiotics through its bactericidal effects and amplification of antibiotic efficacy.

## 1 Introduction

By adjusting plasma parameters, the properties of cold atmospheric plasmas (CAPs) and types of produced reactive oxygen and nitrogen species (RONS) can be controlled. Plasma generated RONS can be introduced in the cells during the direct treatments or by applying the Plasma Activated Water (PAW) [1]. Here we will present the results of the application of PAW on plant cells and on antibiotic resistant bacteria strains. The influence of PAW on plant calli cells was studied through changes in morphology and physiology of two different varieties of *Daucus Carrota* calli. In case of bacteria strains we have used the antibiotic-resistant strains and investigated if pretreatment with PAW can increase the susceptibility of bacteria to antibiotics.

## 2 Experimental setups

Treatments of deionized water samples were performed by using pin atmospheric pressure plasma jet (APPJ). A detailed description of the pin APPJ has been provided in a previous study [2]. As feeding gas we used Argon and the ground electrode was 15 mL of deionized water (Milli-Q, pH 7.3) sample, placed in a plastic Petri dish. For Calli samples we have used PAW samples obtained with 5 min and 20 min plasma treatments and for bacteria - 10 min plasma treatment.

Morphological changes and metabolic status of PAW treated carrot calli was determined together with profile of specific metabolites and activity of antioxidant enzymes. As a second case study we have investigated the potential of PAW to affect susceptibility of multidrug-resistant bacterial pathogens (*K. pneumoniae* and *E. faecalis*) to conventional antibiotics.

## 4 Results and conclusion

We have shown that PAW treatment induced significant physiological and metabolic changes in calli of carrot varieties. The growth of the black calli can be stimulated by using the PAW rich in RONS and oxidative stress was generally more pronounced after the PAW treatment with an increase in the activity of antioxidant enzymes and changes in metabolites. The antibacterial efficacy of the PAW was demonstrated through a) its bactericidal effects; and b) its potential to enhance the effects of certain antibiotics against multidrug-resistant bacteria. These aspects of the antibacterial efficacy of the PAW were further examined by detecting intracellular concentrations of RONS in bacteria exposed to the PAW treatment.

***Acknowledgments:*** *This work was supported by the SF (7739780, APPer-TAin- BIOM) and by MSTDI, Republic of Serbia (Grants 451- 03- 66/2024- 03/200024, 451-03-65/2024-03/200129 and 451-03-65/2024-03/200110).*

**References**

[1] Puač, N. and Škoro, N. Plasma–Liquid Interaction for Agriculture—A Focused Review, Plasma Processes and Polymers, (2024)

[2] Kumar, A., Škoro, N., Gernjak, W., Povrenović, D. and Puač, N. Direct and Indirect Treatment of Organic Dye (Acid Blue 25) Solutions by Using Cold Atmospheric Plasma Jet, Front Phys 10, 1–14, (2022).

# Plasma Chemistry for the Energy and Materials Transition of the Process Industry

GJ van Rooij, the CCE plasma group

*Circular Chemical Engineering (CCE), Faculty of Science and Engineering, Maastricht University, PO Box 616, 6200 MD Maastricht*

A carbon neutral and circular economy must rely on utilization of waste materials and biomass as feedstock for the production of new materials. Its energy input must be of zero carbon footprint, which essentially is intermittent electricity. Some of the challenges encountered in the transition towards such an economy can potentially be addressed by plasma technology. Particularly its compatibility with (intermittent) sustainable energy and unique opportunities for efficiency and/or selectivity in reactions with $CO_2$, $N_2$, and $CH_4$ inspire our research in the context of the process industry at Chemelot. This presentation discusses the use cases of $CH_4$ valorisation via carbon coupling to illustrate the plasma opportunity. These insights are used to draft a roadmap for industrial implementation of the technology for direct production of ethylene ($C_2H_4$), an important building-block for the chemical industry.

## 1 General

The chemical industry in the Netherlands as well as in Europe must be climate-neutral by 2050. The use of green electricity plays a key role here. The Maastricht University plasma group collaborates with Sitech, TNO, and the Brightlands Chemelot Campus within the Brightsite partnership to unlock the potential of plasma technology as an efficient electrical process for splitting and synthesizing sustainable molecules in this context. The ambitious goal of Brightsite is demonstration of industrial viability for cracker fuel gas conversion into acetylene and/or ethylene with plasma.

A long-standing challenge of the chemical industry is a robust means of direct methane coupling to ethylene. Ethylene is the highest volume traded synthetic commodity chemical as it is used as a building block for plastics, textiles and chemicals, with a demand of 185 million tons/year in 20213. 90% of the CO2 emissions from ethylene production occur by combustion of fuel gas, used to heat the crackers to drive the strongly endothermic reaction6. Fuel gas is the mix of waste gases produced as a by-product from the naphtha cracker and is composed predominantly of methane.

Electrical crackers (e-crackers) should replace these conventional fossil crackers. The e-crackers use industrial heat pumps powered by renewable electricity to substitute the gas-fired furnaces (combustion), circumventing emissions from methane combustion. Also, pyrolysis oil from end-of-life plastics will become a feedstock to naphtha crackers.

Due to this decarbonisation of crackers, huge volumes of excess methane (by-product of naphtha cracking) will become available and burning it would result in $CO_2$ emissions. Thus, it is essential to find a way to valorise this huge amount of excess methane with the least environment impact as possible.

## 2 Results

Methane pyrolysis in commonly explained through the Kassel mechanism which runs at high (>1500 K) temperature:

$$2CH_4 \rightarrow C_2H_6 \rightarrow C_2H_4 \rightarrow C_2H_2 \rightarrow C(s)$$

The strategy within the Hüls process to achieve acetylene selectivity is to quench the process at ms timescale, faster than its polymerization produces significant amounts of C(s), soot [1]. Our research expands on this work and investigates how well selectivity towards ethylene is achievable. We present systematic studies on the effects of plasma residence time via flow control and plasma pulsing, and of radical chemistry via dilution with hydrogen.

**References**

[1] Fincke, J. R., Anderson, R. P., Hyde, T. A. & Detering, B. A. *Ind. Eng. Chem. Res.* **41**, 1425–1435 (2002).

# Uncovering the Role of Multi-Phase Electro-Hydrodynamics in Plasma-Induced Liquid Flows

Calum T. Ryan[1,2,3], Mariska Schalk[1], Anton A. Darhuber[1,3], Hanneke Gelderblom[1,2,3], Ana Sobota[1,2,3]

[1] *Department of Applied Physics and Science Education, Eindhoven University of Technology, The Netherlands*
[2] *Institute for Complex Molecular Systems, Eindhoven Unviersity of Technology, The Netherlands*
[3] *J. M. Burgers Centre Research school for Fluid Mechanics, The Netherlands*

Plasma-induced liquid flow is a fundamental part of plasma-liquid interactions. However, there is very little currently known about the flow in plasma-liquid interactions. Any flows present will influence the transport of species produced by the plasma through the liquid, meaning controlling plasma-induced flow can control liquid phase species distribution. We demonstrate that in the interaction of a plasma jet with water, electro-hydrodynamic forces are one of the main processes behind the liquid flow. In floating liquids, electro-hydrodynamics in the plasma affluent will drive faster gas flows, inducing stronger viscous shear stresses as a result. The results demonstrate that by tuning parameters of the system, more efficient distribution of reactive species through the liquid can be achieved, leading to the potential improvement of any plasma-liquid application.

## 1 General

During plasma-liquid interactions, the desired distribution of reactive oxygen and nitrogen species (RONS) in a solution will be different depending on the application; in applications like the activation of water a homogeneous distribution of RONS is preferred, whereas in applications like plasma medicine, RONS are preferred to efficiently transport across a layer of bodily fluids (e.g. sweat, blood) onto an underlying layer of damaged tissue. The ability to control the distribution of RONS through a liquid would therefore improve the efficiency of plasma-liquid interactions, and one possible method of doing this is through plasma-induced liquid flow (PILF) [1].

While a fundamental part of plasma-liquid interactions, very little is currently known about the driving mechanisms of PILF. Ionisation produces flow effects that will not exist without plasma. One force exerted by the plasma is electro-hydrodynamic (EHD) forces [2]. EHD occurs when charged particles, accelerated across an electric field, collide with neutral molecules and thereby induce a flow. During the presence of direct current electric fields, the EHD force is dominated by the Coulomb force resulting in the following form;

$$\vec{\mathbf{f}}_{EHD} = \rho_i \vec{\boldsymbol{E}},$$

where $\rho_i$ is the free charge density in C m$^{-3}$, and $\vec{\boldsymbol{E}}$ is the electric field vector in V m$^{-1}$. EHD exists in both the gas and liquid phases of plasma-liquid interactions. In both the gas phase and directly at the gas-liquid interface, an EHD force arises from charged particles produced by the plasma sheath colliding with the surrounding neutral gas molecules and the liquid surface. The gas-phase EHD will drive faster gas flows that will change the strength of the gas-liquid viscous shear stress and normal forces. In the bulk liquid, an EHD force arises in conductive liquids (such as saline) that exhibit local free charge density through plasma and electrolytic reactions (while generally maintaining liquid quasi-neutrality) [2].

Here, we uncover the effects of EHD and how it dominates the induced flow of plasma-liquid interactions. In floating de-mineralised water, particle image velocimetry results align with theoretical predictions of PILF dominated by gas-phase EHD. When a grounded electrode is placed into the liquid, the alignment with gas phase EHD dominating PILF breaks down, and the driving forces become less clear. Our results demonstrate the ability to tune the intensity of PILF, and proves that for applications the improved mixing of RONS can be controlled.

**References**

[1] Kawasaki, T. et al. Instant Switching Control Between Two Types of plasma-driven liquid flows. *Jpn. J. Appl. Phys.* **62**, 060904 (2023).

[2] Ryan, C. T. et al. Electrical Properties Determine the Liquid Flow Direction. *Sci. Rep.* **14**, 17152 (2024).

# Phase-Resolved Measurement of Electric-Field-Induced Second Harmonics for Determining Electric Field Polarity

T. Sato[1], T. Umemoto[1], M. Sato[1], T. Fujii[1] and A. Kumada[1]

[1] *Department of Electrical Engineering and Information Systems, The University of Tokyo, Japan*

The electric-field-induced second-harmonic generation (E-FISHG) method has gained attention as a non-contact, non-invasive, and highly sensitive technique for measuring electric fields. In this method, the electric field profile along the laser path influences the second harmonic (SH) signal and must be carefully characterized. We successfully measured the E-FISH phase distribution using the interference fringes formed by the E-FISH beam and reference light, while varying the electric field polarity.

## 1 Introduction

In recent years, methods based on electric-field-induced second-harmonic generation (E-FISHG), which utilize nonlinear optical effects, have attracted attention as optical techniques for non-invasive and non-contact electric field measurements [1]. The E-FISHG method employs the signal generated by second-harmonic generation (SHG) when a laser is irradiated onto a medium subjected to an external electric field. Recent study has demonstrated the determination of electric field polarity using interference fringes formed by E-FISH and the reference light [2]. Additionally, obtaining phase information from E-FISH could lead to even higher precision in electric field estimation. In this paper, we report the results of measuring the phase distribution of E-FISH by varying the electric field polarity while acquiring interference fringes as the electrodes were moved.

## 2 Experimental Method and Results

The experimental setup is shown in Fig. 1. A Ti:sapphire laser (Spectra-Physics, Solstice Ace, repetition rate: 1 kHz, central wavelength: 800 nm, pulse width: 200 fs) was used as the light source. The laser beam was split into two optical paths using a beam splitter. One beam, with an energy of 50 μJ, was used as the fundamental wave to generate E-FISH light. The other beam was directed into a β-BBO crystal to generate second-harmonic light, which served as the reference beam.

After combining the fundamental wave and the reference beam, they were focused using a lens with a focal length of 1 m and then collimated using another lens with the same focal length. The fundamental wave was then removed, and the interference fringes produced by the generated E-FISH light and the reference beam were amplified using an image intensifier (Hamamatsu Photonics, C9016-03) and recorded with a camera (Nikon, D5600). The parallel rod electrodes (φ20 mm, gap length: 10 mm, ±14 kV) were moved downstream of the optical path.

We successfully measured the E-FISH phase distribution at ±14 kV. The interference fringes at the focal point are shown in Fig. 2. It was observed that the E-FISH phase varies with the polarity.

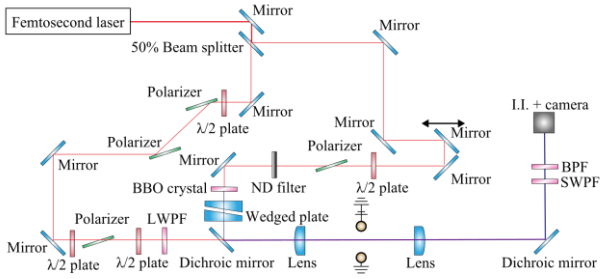



Fig.1. Experimental setup.

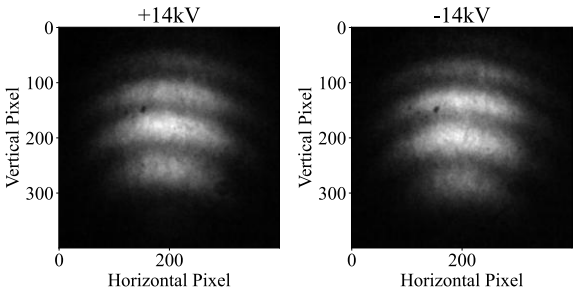



Fig.2. Changes in interference fringes due to polarity.

**References**

[1] A. Dogariu. *et al*. Species-Independent Femtosecond Localized Electric Field Measurement. *Phys. Rev. Applied* **7**, 024024 (2017).

[2] J. B. Billeau. *et al*. Coherent homodyne detection for amplified cross-beam electric-field induced second harmonic, Appl. Opt. 63, 19, 5203–5207 (2024).

# Electron transport in $O_2$ and $O_2$-Ar mixtures: Electron collision cross section set of $O_2$ and Monte Carlo simulation

S. Kawaguchi[1], K. Takahashi[1] and K. Satoh[1]

[1] *Muroran Institute of Technology, Muroran, Hokkaido, Japan*

A complete and consistent set of electron collision cross sections of molecular oxygen ($O_2$) is developed. Electron swarm parameters in $O_2$ and $O_2$-Ar mixtures are calculated by Monte Carlo simulation and the consistency of the developed cross section set is validated by comparing measured and calculated electron swarm parameters. Then, electron transport properties in $O_2$ and $O_2$-Ar mixtures are examined.

A complete and consistent set of electron collision cross sections is necessarily for interpreting and modelling the diverse phenomena in plasmas. Such a cross section set includes adequate and accurate cross sections for elastic, excitation, ionization, and electron attachment collisions to describe the gain and loss of electron number, momentum, and energy in a gas. Furthermore, the validity of the cross section set should be confirmed by its ability to reproduce measured electron swarm parameters over a wide range of reduced electric fields. In this talk, a complete and consistent cross section set for molecular oxygen ($O_2$) recently developed by our group [1] is presented. Then, electron transport properties in $O_2$ and $O_2$-Ar mixtures are examined.

Table 1 summarizes the reactions between an electron and a $O_2$ molecule considered in the present cross section set. The shapes and magnitudes of the cross sections for these reactions were determined to reproduce measured electron swarm parameters in $O_2$ and $O_2$-Ar mixtures. Experimentally measured and theoretically calculated electron collision cross sections are respected as far as possible. The ionization cross section for producing $O_2^+$ was resolved into four ionization cross sections corresponding to different excited states of $O_2^+$ using measured photoemission cross sections and branching ratios [2, 3]. The numerical data for the present cross section set will be available in the MuroranIT database on LXCat [4].

Electron drift velocity, ionization coefficient, electron attachment coefficient, excitation coefficients for $O_2(a^1\Delta_g)$ and $O_2(b^1\Sigma_g)$, and longitudinal diffusion coefficient in $O_2$ and $O_2$-Ar mixtures are calculated using Monte Carlo simulation. The calculated electron swarm parameters show good agreement with measured data over a wide range of reduced electric fields. Transitions from the Herzberg states of $O_2$ ($c\ ^1\Sigma_u^-$, $A'^3\Delta_u$, and $A^3\Sigma_u^+$) to $O_2(b^1\Sigma_g)$ and the generation of $O_2(b^1\Sigma_g)$ through quenching of $O(^1D)$ by $O_2$ are important to reproduce the measured excitation coefficient for $O_2(b^1\Sigma_g)$. Comparison results suggest that up to 40% of $O_2$ molecules excited to the Herzberg states may dissociate and that more than 80% of $O(^1D)$ quenched by $O_2$ results in the formation of $O_2(b^1\Sigma_g^+)$.

**Acknowledgement**

This study was partly supported by JSPS KAKENHI JP17J11124.

**References**

[1] S. Kawaguchi et al. Plasma Sources Sci. Technol. (submitted)

[2] C. A. Terrell et al. J. Phys. B: At. Mol. Opt. Phys. **37**, 1931 (2004)

[3] J. P. Dorering and J. Yang J. Geophys. Res. **102**, 9691 (1997)

[4] https://www.lxcat.net/contributors/#d836

**Table I.** Reactions between electron and $O_2$ considered in the present cross section set.

| Type of collision | Reaction |
|---|---|
| Elastic | $O_2 + e \rightarrow O_2 + e$ |
| Rotational excitation | $O_2(J = J') + e \rightarrow O_2(J = J' + 2) + e$ ($J' = 1, 3, \dots, 29$) |
| Rotational de-excitation | $O_2(J = J') + e \rightarrow O_2(J = J' - 2) + e$ ($J' = 3, \dots, 31$) |
| Three-body attachment | $O_2(X\ ^3\Sigma_g^-) + M + e \rightarrow O_2^-(^2\Pi_g, v' \leq 3) + M$ |
| Electron attachment | $O_2 + e \rightarrow O^-(^2P) + O(^3P)$ |
| Vibrational excitation | $O_2(v=0) + e \rightarrow O_2(v= v') + e$ ($v' = 1, 2, 3, 4$) |
| Electronic excitation | $O_2 + e \rightarrow O_2(a\ ^1\Delta_g) + e$ |
| Electronic excitation | $O_2 + e \rightarrow O_2(b\ ^1\Sigma_g^+) + e$ |
| Electronic excitation[(a)] | $O_2 + e \rightarrow O_2(c\ ^1\Sigma_u^-) + e$ |
| Electronic excitation[(a)] | $O_2 + e \rightarrow O_2(A'\ ^3\Delta_u) + e$ |
| Electronic excitation[(a)] | $O_2 + e \rightarrow O_2(A^3\Sigma_u^+) + e$ |
| Electronic excitation[(b)] | $O_2 + e \rightarrow O_2(1\ ^3\Pi_g) + e$ |
| Electronic excitation[(b)] | $O_2 + e \rightarrow O_2(B^3\Sigma_u^-) + e$ |
| Electronic excitation[(b)] | $O_2 + e \rightarrow O_2(8.87\ eV) + e$ |
| Electronic excitation[(b)] | $O_2 + e \rightarrow O_2(E^3\Sigma_u^-(v'=0)) + e$ |
| Electronic excitation[(b)] | $O_2 + e \rightarrow O_2(E^3\Sigma_u^-(v'=1)) + e$ |
| Electronic excitation[(b)] | $O_2 + e \rightarrow O_2(10.5eV) + e$ |
| Neutral dissociation | $O_2 + e \rightarrow O(^3P) + O(^3P) + e$ |
| Neutral dissociation | $O_2 + e \rightarrow O + O + e$ |
| Ion-pair formation | $O_2 + e \rightarrow O^+ + O^- + e$ |
| Ionization | $O_2 + e \rightarrow O_2^+(X^2\Pi_g) + 2e$ |
| Ionization | $O_2 + e \rightarrow O_2^+(a^4\Pi_u) + 2e$ |
| Ionization | $O_2 + e \rightarrow O_2^+(A^2\Pi_u) + 2e$ |
| Ionization | $O_2 + e \rightarrow O_2^+(b^4\Sigma_g^-) + 2e$ |
| Ionization | $O_2 + e \rightarrow O^+ + O + 2e$ |
| Ionization | $O_2 + e \rightarrow O^{2+} + O + 3e$ |

[(a)] Up to 40% of excited $O_2$ molecules dissociate into $2O(^2P)$.
[(b)] All excited $O_2$ molecules dissociate into $O(^3P) + O(^1D)$.

# Transient plasmas in liquid water and at the liquid-gas interfaces: from fundamental discharge physics to nitrogen fixation

M. Šimek[1], P. Bílek[1], G. Arora[1], J.Fujera[1], V. Prukner[1], and P. Hoffer[1]

[1] *Institute of Plasma Physics of Czech Academy of Sciences, U Slovanky 2525/1a, 18200 Prague, Czech Republic*

Understanding the basic mechanisms responsible for the emergence of discharges in/with liquids and determining the corresponding plasma parameters still appear to be a rather demanding task, which is important for the development of many potential applications based on plasma-liquid interactions. Several unresolved issues related to the generation of high-voltage electrical discharges in/with liquids pose a non-trivial challenge and are therefore still the subject of research efforts. In this presentation, nanosecond discharges in liquid water and at the water-air interface will be discussed in terms of basic mechanisms, plasma properties and corresponding diagnostic strategies.

Transient plasmas in or with liquids produced by high-voltage pulses of nanosecond duration appear to be very complex systems and represent a significant challenge in the attempt to experimentally determine the most important plasma parameters and properties.

The dynamics of such systems is largely determined by the rate of increase/collapse of the electric field. Plasma formation generally involves the multiplication of free electrons through various ionization processes, while the electrons lose their energy through collision processes, which in turn lead to the production of large amounts of radiation. As a result, analysis of the radiation produced is often the diagnostic tool of first choice in an attempt to obtain primary microscopic information as a necessary complement to the basic electrical characteristics. In addition, more advanced diagnostics (e.g. laser-based) can be used to obtain further detailed information.

In addition to their inherent stochastic and often microscopic nature, transient discharges in/with liquids involve phase transitions, the simplest example being the enhanced heating/evaporation of water at the plasma-water interface. This can typically occur in the case of streamer-spark plasma filaments developing at the air-water interface. A much more complex case may be the "direct" transition from the "liquid" to the "plasma" phase via an electrostriction-driven nanovoid mechanism (which has been predicted long ago but has not yet been consistently experimentally confirmed).

However, in both cases (in/with liquid), the initial development of the (micro)discharge is so fast (morphological changes can be similarly fast) that the use of optical diagnostics often gives meaningful results only if it allows sub-nanosecond and sub-micron resolution. Furthermore, to avoid errors caused by the stochastic nature of the studied discharge events, statistical averaging during data acquisition (e.g. images or spectra) is often excluded. A proper data mining strategy then requires repeated registration of images, spectra and other characteristics from individual discharge events (and statistical methods should be applied only in the post-processing phase).

We have recently successfully applied the above strategies to the study of nanosecond discharges both in water [1,2] and on the water surface [3,4]. In this presentation, we will discuss imaging and spectrometric techniques based on (a) four-channel ICCD imaging and ICCD imaging spectrometry, which provide (sub)nanosecond and micrometre resolution, and (b) interferometric, shadow and Kerr techniques using a 532 nm laser with tens of picosecond resolution.

We will show that such proper techniques help reveal information that might otherwise remain hidden, such as the distinct dark and luminous phases in the case of nanosecond discharge in water or the formation of bidirectional filamentary streamers from an initial homogeneous glow on the water surface.

Acknowledgements: *Supported by the Czech Science Foundation (GA24-10903S).*

**References**

[1] Šimek, M., Hoffer, P., Prukner, V. and Schmidt, J. *Plasma Sources Sci. Technol.* **29,** 095001 (2020).
[2] Hoffer, P., Prukner, V., Schmidt, J. and Šimek, M. *J. Phys. D: Appl. Phys.* **54**, 285202 (2021).
[3] Hoffer, P., Prukner, V., Arora, G., and Šimek, M. *Plasma Sources Science and Technology*, **32**, 09LT01 (2023).
[4] Arora, G., Hoffer, P., Prukner, V., Bílek, P., and Šimek, M. *Plasma Sources Science and Technology*, **33**, 025025 (2024).

# Investigating Plasma-Catalyst Synergy via Multi-Diagnostic Techniques

Mengbo Li[1], She Chen[1], Linlin Liu[1], Feng Wang[1], Chijie Zhuang[2]

[1] *College of Electrical and Information Engineering, Hunan University, Changsha, China*
[2] *Department of Electric Engineering, Tsinghua University, Beijing, China*

Plasma catalysis technique shows great potential in various fields, promoting environmental sustainability. Understanding plasms-catalyst interactions offers critical insights into enhancing the performance of this method, addressing its lower conversion efficiency compared to conventional industrial approaches and improving its competitiveness as a potential alternative. The advancement of diagnostic techniques and simulations provides opportunities to investigate the characteristics of the plasma catalysis environment, further promoting the elucidation of synergistic mechanisms. Our work provides a concise overview of our research on characterizing plasma catalysis through various diagnostic techniques and simulations, including electric field distribution, particle concentration quantification, and reaction-sensitive analysis under different plasma catalysis conditions.

## 1 Introduction

Investigating the synergistic mechanisms of plasma catalysis offers valuable insights for enhancing its performance, encompassing studies on both plasma characteristics and catalytic properties [1]-[3]. In this study, we aim to quantify key characteristics of plasma catalysis, including fundamental electrical parameters and species concentrations in both the plasma phase and on the catalyst surface, through diagnostic techniques. By analyzing these results, we seek to elucidate the reaction processes and optimize external conditions to steer the reactions toward the desired pathway more effectively.

## 2 Results

### 2.1 Electrica field measurement for simplified nanosecond pulsed In-plasma catalytic reactor in air

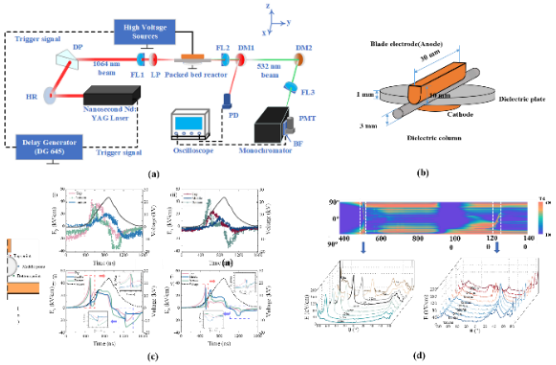



**Fig 1 (a) Experimental setups of EFISH; (b) Simplified IPC structure; (c)Comparison between measured electric field and simulation results; (d) Simulated electric field distribution on the surface of the dielectric column.**

In-Plasma Catalysis (IPC) configuration, as the direct and common way to couple non-thermal plasma and chemical catalysts. The electric field, a crucial parameter in plasma catalysis, regulates the plasma characteristics and affects the rates and pathways of chemical reactions. The measurement of the electric field will help reveal the coupling mechanism, but limited experimental results were obtained due to the existence of the catalysts. In our work, the electric field distribution in simplified IPC was obtained experimentally using EFISH for the first time. Meanwhile, a two-dimensional fluid model was also established to further investigate the IPC characteristic [4].

### 2.2 Multi-Diagnostic Approaches for Plasma Catalysis in Ammonia Synthesis

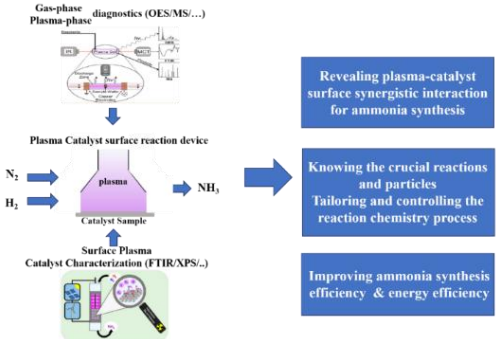



**Fig 2 Comprehensive diagnoses for revealing the synergistic interaction between plasma and catalysis surface under $N_2/H_2$ mixed gases**

A comprehensive diagnostic system integrating multiple techniques was established to investigate plasma-surface interactions in an $N_2$ /$H_2$ gas environment. Based on diagnostic results, the critical reaction pathways for ammonia synthesis were identified, enabling the regulation of reaction chemistry to enhance ammonia production while minimizing the loss of synthesized ammonia molecules. These strategies are expected to improve the energy efficiency of plasma-catalytic ammonia synthesis and provide valuable insights for material fabrication and plasma source design.

## Reference

[1] A Sobota. Diagnostic techniques for the interaction of non-thermal atmospheric pressure plasmas and targets. *J. Phys. D: Appl. Phys.* **58** 063005 (2025).
[2] I Adamovich. The 2022 Plasma Roadmap: low temperature plasma science and technology. *J. Phys. D: Appl. Phys.* **55** 373001 (2022).
[3] Dell'Orco, S. Exploring opportunities in operando DRIFTS and complementary techniques for advancing plasma catalysis. *EES. Catal.* **2**, 1059–1071 (2024).
[4] Mengbo Li. Experimental and numerical investigation of surface streamers in a nanosecond pulsed Packed Bed Reactor. *Plasma Sources Sci. Technol.* **32** 064002. (2023).

# Measurements of G-value at high electric fields in pulsed nanosecond discharge

Inna S. Orel[1,2], Youssef Haouchat[1], Tat Loon Chng[1,3], Nikolai A. Popov[4], Svetlana M. Starikovskaia[1]

[1]*Laboratory of Plasma Physics (CNRS, École Polytechnique, Univ. Paris-Sud, Observatoire de Paris, Sorbonne Université, Institut Polytechnique de Paris), Ecole Polytechnique, route de Saclay, 91128 Palaiseau, France*
[2] *Ruhr University Bochum, Institute for Plasma and Atomic Physics, 44780 Bochum, Germany*
[3] *Department of Mechanical Engineering, College of Design and Engineering, National University of Singapore, Singapore 117575*
[4] *Skobeltsyn Institute of Nuclear Physics, Moscow State University, Moscow, 119991, Leninsky gory, Russia*

This study suggests an experimental measurement technique for the G-value at a high reduced electric field of hundreds of Td. A high-voltage repetitively pulsed nanosecond discharge is used as a source of a diffuse plasma at high E/N. The G-value is obtained experimentally by combining consistent time synchronized measurements of electrical properties of the discharge (i.e., voltage on the electrodes, discharge current, specific energy delivered to the discharge (SED), electric field and emission radial distribution) with number density measurements of the specie of interest. The kinetic numerical modelling validates the suggested technique on the example of nitrogen dissociation.

The G-factor, or G-value refers to the number of species produced per 100 eV of deposited energy. In plasma chemistry, the G-value is used for comparative analysis of different discharge systems with respect to the selected chemical process. An experimental measurement of the G-value at a high electric field of hundreds of Townsend is challenging due to both SED and E/N measurements. The present work suggests a technique of measuring of G-values for the range of E/N = 100-300 Td for a broad range of gas mixtures and SED values in a discharge with a cylindrical symmetry.

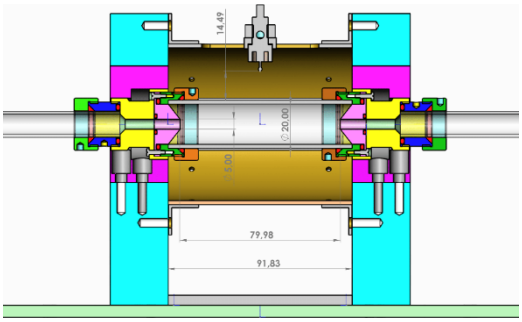



**Figure 1:** Schematic of the nanosecond discharge setup.

Fig. 1 displays a cross-sectional schematic of the experimental setup. The discharge with a typical voltage amplitude of 10-30 kV and pulse duration of 20-30 ns was used to obtain a diffuse plasma with a uniform E-field along the tube in the pressure range from ones to tens of mbar. For the present work, $N_2$ was selected as a feed gas although the discharge can be operated in a broad range of atomic and molecular gases and gas mixtures. The electrical properties of the discharge were measured by back current shunt (BCS) and capacitive probe (CP) techniques. Two-photon absorption laser-induced fluorescence (TALIF) with an absolute calibration in Kr was used to track the time evolution of the atomic nitrogen density in the centre of the discharge tube. The time resolved emission of the second positive system of $N_2$ (SPS) was measured with an ICCD camera.

It was found that the nanosecond discharge in $N_2$ has a cylindrically symmetrical profile with a clearly pronounced minimum on the tube axis. To account for the species' radial distribution, an in-house regularized Abel inversion algorithm was developed. The radial distribution of the electron density prior to the discharge initiation is assumed to replicate that of the SPS due to the direct electron impact excitation. For the kinetic numerical modelling, the experimentally measured electrical current waveform and the radial distribution of the electron density were taken as an input data. It was obtained that at reduced electric fields (180 ± 20) Td, the G-value is equal to 0.85 N-atoms/100 eV of the deposited energy.

## Acknowledgements

This work was partially supported by CEDINA Project (Merlion Program, Campus France and University of Singapore), by the Energy4Climate Interdisciplinary Center (E4C) of IP Paris and Ecole des Ponts ParisTech, Programme d'Investissements d'Avenir (ANR-18-EUR-0006-02). The work of S. M. Starikovskaia was partially supported by the European Union Project CAIPIRINH3A, under the GA number 101191768. The work of N. Popov was partially supported by the Russian Science Foundation, Project No. 23-17-00264.

# Physics and chemistry of nonequilibrium plasma formation in pulsed discharges

A. Starikovskiy[1]

[1] *Princeton University, Princeton, NJ, USA*

Contemporary plasmachemical applications increasingly demand enhanced selectivity and efficiency in media excitation. Beyond conventional applications such as laser and lamp-based optical sources and microelectronics [1], several emerging fields, including plasma-assisted flow control [2], plasma-assisted combustion [3], as well as plasma medicine and biology [4], represent highly promising research directions. For these advanced applications, selective excitation implies the capability to achieve maximal efficiency while maintaining minimal energy consumption [5,6].

Increased selectivity can be effectively realized by maintaining a prescribed level of the reduced electric field (*E/n*) within the discharge. Optimizing plasmachemical processes through precise *E/n* control necessitates transitioning from conventional quasi-stationary discharges, characterized by self-consistent electric fields, toward pulsed discharge techniques. These techniques ensure the required *E/n* conditions during moments of peak energy input [7].

Recent breakthroughs in solid-state electronics have significantly augmented the generation capabilities for ultra-short, high-voltage, and high-power pulses. Within a broad spectrum of media densities, the rapid establishment of strong electric fields at discharge initiation substantially enhances plasma homogeneity [7]. It also facilitates accurate regulation of the electric field strength, electron energies, and the distribution of energy among internal molecular degrees of freedom [2]. Such technological advancements have catalyzed the emergence and rapid development of a novel discipline within plasmachemistry – specifically, the plasmachemistry associated with nanosecond and picosecond discharge regimes.

Precise spatial and temporal control over plasma energy deposition becomes achievable within very short temporal intervals, typically below the electron multiplication timescale above the breakdown threshold, or recombination timescale below it. Under conditions of relatively low plasma conductivity, stable maintenance of the inter-electrode gap at predefined *E/n* levels becomes viable. Implementing short-duration, high-voltage pulses in combination with a sustained bias voltage enables highly non-equilibrium conditions, promoting extremely selective excitation of gaseous media. Critical pulse durations for high-voltage applications are strongly dependent upon gas-specific parameters, including density and composition. Practically relevant pulse durations are typically restricted to a few nanoseconds across a broad parameter range. Consequently, the capability for selective and controlled gas excitation via electric discharge is inherently linked to advances in ultra-short pulse generation technology.

This report aims to discuss the distinctive features and mechanisms underlying pulsed non-equilibrium plasma generation within diverse gaseous media, employing nano- and picosecond high-voltage discharges.

**References**

[1] A.Fridman. Plasma Chemistry. Cambridge University Press. 2008.

[2] A.Starikovskiy, N.Aleksandrov. *Plasma Aerodynamics and Flow Control by Superfast Local Heating.* In: Pulsed Discharge Plasmas Characteristics and Applications. Edited by T.Shao, Cheng Zhang. Springer Press. 2023.

[3] Y.Ju, A.Starikovskiy. *Plasma Assisted Combustion and Chemical Processing.* Taylor & Francis. 2025.

[4] A.Fridman, G.Friedman. *Plasma Medicine.* John Wiley & Sons. 2013.

[5] A.Starikovskiy. *High E/N Discharges: Applications.* In: Encyclopedia of Plasma Technology, edited by J. Leon Shohet. CRC Press. 2016.

[6] N.Anikin, S.Bozhenkov, D.Zatsepin, E.Mintoussov, S.Pancheshnyi, S.Starikovskaia, A.Starikovskiy. *Pulsed Nanosecond Discharges and Their Applications.* In: Encyclopedia on Low-Temperature Plasma. Ed: V.E.Fortov. V.VIII-I. Chemistry of Low-Temperature Plasma. Moscow, 2007.

[7] S.Starikovskaia, A.Starikovskiy. *Pulsed Discharges in a Wide Density Range: Plasma Development and Media Excitation.* In: Runaway Electrons Preionized Diffuse Discharges. Edited by: V.F.Tarasenko. NOVA Publishers. 2015.

# Advanced optical studies on a pin-dielectric-plane air discharge

D. Stefas[1], K. Giotis[2], Y. Agha[1], L. Invernizzi[1], H. Höft[3], P. Svarnas[2], G. Lombardi[1] and K. Gazeli[1]

[1] *Laboratoire des Sciences des Procédés et des Matériaux (LSPM), CNRS, Université Sorbonne Paris Nord, UPR 3407, F–93430 Villetaneuse, France*
[2] *High Voltage Lab., Electrical & Computer Eng. Dept., University of Patras, Rion, Greece*
[3] *Leibniz Instit. for Plasma Sci. and Technol. (INP), Greifswald, Germany*

Air dielectric barrier discharges (ADBDs) in pin-to-plane configurations generate non-thermal plasmas (NTP) with unique physical properties. However, the description of key reactive atoms in ADBDs is challenging because they suffer significant quenching from air species. To access their decay times and, thus, their absolute densities, optical diagnostics with exceptional temporal and spatial resolution are needed. Here, a stainless-steel needle is driven by a pulsed high voltage generating an ADBD in the gap between the needle and a grounded dielectric plate. The discharge dynamics are studied using ICCD imaging with ns temporal resolution. Furthermore, employing ps-TALIF and a streak camera allows directly accessing sub-ns decay times and absolute densities of reactive atoms produced, as it is exemplarily shown for N-atoms, which is a key species in ADBDs in general.

Pin-to-plane ADBDs offer a versatile approach to generating NTPs in atmospheric pressure air being characterised by a rich chemical activity. This motivates their fundamental studies for applications requiring controlled plasma chemistry.

This work focuses on the description of reactive atoms (N, O) generated in a pulsed-driven pin-plane ADBD. The ADBD consists of a stainless-steel needle electrode (Fig. 1) facing an AlN flat dielectric (0.1 mm tip radius) with a 1.5 mm gap between them. The discharge is ignited in ambient atmospheric pressure air, using a pulsed high voltage (HV; 200-1000 ns width, 10 kV amplitude, 10 kHz frequency, 60 ns rise time). Single shot ICCD imaging (Fig. 1; 200 ns gate) reveals deviations of the discharge channels from the vertical axis of propagation, and surface discharges expanding on the dielectric. Probing the decay times and absolute densities of atoms is done below the pin (where the laser is always interacting with the plasma) using ps-TALIF and a streak camera (Fig. 1) [1].

The collected raw N-atom ps-TALIF signals present sub-ns effective lifetimes, down to 100 ps, due to a strong collisional quenching of the laser-excited states occurring in atmospheric air (Fig. 2). Resolving these lifetimes makes necessary the use of sub-ns detector, e.g. a streak camera [1]. However, its utilisation is not straightforward, needing consideration of its instrumental function (Fig.2) to determine actual TALIF signals and, thus, correct atomic densities (on the order of $10^{15}$ $cm^{-3}$ in the present case) [1,2]. Time-resolved densities are determined different HV pulse widths. These results allow exploring the capacities of ps-TALIF and streak camera in studying transient behaviours of reactive atomic species in ADBD, advancing their fundamental understanding.

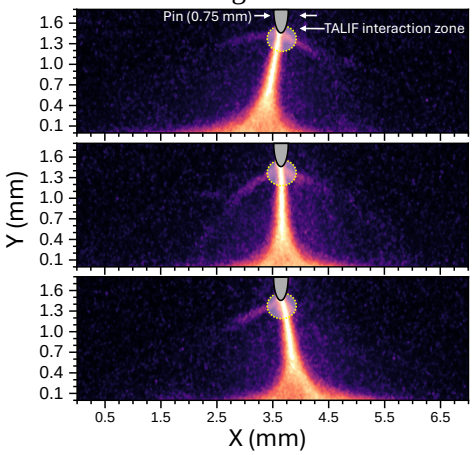



Fig. 1: Representative single-shot ICCD images (200 ns gate) of the discharge capturing a full period of the HV pulse (200 ns, 10 kV, 10 kHz).

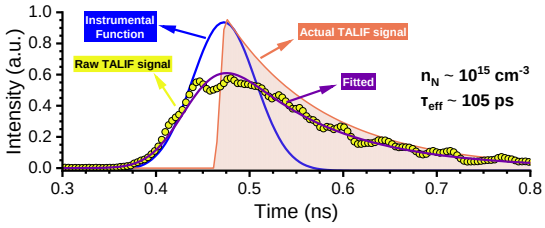



Fig. 2: ps-TALIF signal for N-atoms generated in a ADBD.

**Acknowledgements**

Labex SEAM (ANR-10-LABX-0096; ANR-18-IDEX-0001), ANR ULTRAMAP (ANR-22-CE51-0027), DFG d3DBD (project number 535827833).

**References**

[1] L. Invernizzi et al., Meas. Sci. Technol. 34, 095203 (2023).
[2] D. Stefas et al., AIAA SCITECH 2024 Forum, 2024-0806 (2024).

# Ion chemistry in $C_2H_2$/Ar cold plasmas: the dramatic effects of $N_2$ addition

I. Tanarro, R. J. Peláez and V. J. Herrero

*Instituto de Estructura de la Materia (IEM-CSIC), Madrid, Spain*

Relevant effects of increasing proportions of $N_2$ in the chemical composition of $C_2H_2$/Ar low pressure plasmas, in conditions of incipient polymerization, have been observed in a capacitively coupled RF discharge. The enrichment in $N_2$ causes the appearance of cyanopolyynes, as well as the global increase of anions and the depletion of cations, with changes in their relative concentrations spanning several orders of magnitude, although with very different tendencies for ions with and without nitrogen, and makes these plasmas strongly electronegative. All of the few anions detected thus far in the interstellar medium (ISM) and in the ionosphere of Titan appear in these discharges, and protonated cations of astrophysical interest stand out. This study can also shed some light on basic processes in plasmas of $C_2H_2$ with admixtures of $N_2$ used in the fabrication of advanced materials, in the generation of astrophysical dust analogues, and in kinetic models, which nowadays present some controversies related especially with the anion chemistry.

## General

From the >300 molecular species identified until now in the ISM or circumstellar shells, organic compounds containing C and H atoms dominate, being $C_2H_2$ one of the most abundant [1]. Moreover, many of the species found in the ISM contain C-N chemical bonds, of prime importance in prebiotic chemistry, like HCN, which is ubiquitous. Besides, the atmosphere of Titan, Saturn's satellite, is rich in these compounds, and a complex chemistry occurs in its ionosphere.

Low pressure glow discharges containing $C_2H_2$ and $N_2$ are efficient laboratory systems to characterize many of the neutrals and ions of interest in these media. They can be also good factories of carbonaceous materials containing heteroatoms, of great interest for advanced industrial applications and laboratory simulations of interstellar dust [2].

RF discharges of $C_2H_2$/Ar/$N_2$ are used in this work to study by mass spectrometry, light scattering, and optical emission spectroscopy, the neutral and charged species generated. The experimental set-up was described elsewhere [3,4]. On/off modulation at 100 Hz allows the detection of anions during the off part of the cycles. Different proportions of $N_2$, from <1% up to ~30% are investigated.

It is shown that the addition of $N_2$ produces a drastic effect in the diversity and concentrations of the different species, leading to a high enrichment and complexity in the plasma composition [3].

With the onset of the discharge, $C_2H_2$ dissociates quickly, almost completely, there is a steep rise in $H_2$ concentration and, irrespective of the $N_2$ content, a transient is observed, characterized by the sudden growth and decay of $C_{2n}H_{2m}$ (n, m = 1,2,3) products, and by the fleeting presence of dust, after which, the plasma become dust-free and ions begin to grow markedly. HCN and $HC_3N$ are also formed and survive in increasing concentrations with growing $N_2$ proportion. Atomic H, and the CH, $C_2$ and CN radicals are also observed.

Masses up to ~ 200 u could be detected for ions of both signs. Particularly interesting is the global loss of cations and large growth of anions with increasing $N_2$ ratio, especially of those anions presumably containing CN bonds. Among cations, protonated ones such as $H_3^+$, $ArH^+$, $NH_4^+$ or $N_2H^+$, present in the ISM, seem to dominate, together with pure hydrocarbon ions, whose mass distributions follow a regular pattern. As for anions, they follow a something different regular pattern but, interestingly, the few ones observed thus far in the ISM ($C_{2n}H^-$ and $C_{2n-1}N^-$ (n=1-4)) have also been found to be prominent in the plasmas of this work.

## Acknowledgements

This work was funded by the Spanish M. de Ciencia e Innovación, under grant PID2023-146415NB-I00.

## References

[1] https://cdms.astro.unikoeln.de/classic/molecules#

[2] Herrero, V. J. et al. Structure and evolution of interstellar carbonaceous dust. Insights from the laboratory *Frontiers in Astronomy and Space Sciences* **9**:1083288 (2022).

[3] Tanarro, I. et al. Drastic effects of $N_2$ addition in the composition of $C_2H_2$/Ar glow discharges. *Plasma Phys. Control. Fusion* **67**, 035014 (2025).

[4] Peláez, J R et al. Multi-diagnostic of dust growth in a capacitive Ar/$C_2H_2$ plasma. *Plasma Sources Sci. Technol.* **33**, 105006 (2024).

# Machine-learning-aided spectroscopy of low-temperature plasmas

Ts. V. Tsankov[1], T. Ben Slimane[1], C. Deltel[2], A. Woiselle[3]

[1] *Laboratoire de Physique des Plasmas (LPP), Ecole Polytechnique, CNRS, Palaiseau, France*
[2] *Safran Spacecraft Propulsion (SSP), Vernon, France*
[3] *Safran Electronics and Defense (SED), Massy, France*

The application of machine learning (ML) techniques can supplement the use of collisional-radiative models (CRM) for obtaining the plasma parameters from the emission spectrum. These techniques allow also the study of the correlation of the emission intensities with other parameters, such as the discharge current or voltage. These capabilities of ML go beyond what is achievable by a CRM and allow the design of feed-back controllers for adjusting the operation conditions of the discharge based on the spectral emission of the plasma. Various ML possibilities are applied to experimental and synthetic spectra and the tendencies are analyzed.

## 1 Introduction

Optical emission spectroscopy is often a preferred choice for simple, non-invasive diagnostics of discharges. The plasma parameters, such as electron density and temperature, are extracted by matching a synthetic spectrum from a collisional-radiative model (CRM) to experimentally measured spectrum. This requires multiple runs of the CRM. With machine learning (ML), an artificial neural network (ANN) can be trained on pre-generated synthetic spectra. This provides a rapid inference of the plasma parameters which makes it suitable for designing feed-back controllers. Previous studies investigated the use of ML methods for obtaining the electron energy distribution function (EEDF) [1] as well as the electron density and temperature [2] from emission spectra. The ability of an ANN to infer the discharge parameters (voltage, mass flow rate) from the emission intensities and the application as a feed-back controller have also been explored [3].

Here, ML techniques for unsupervised learning are used to study the correlations between the emission lines, allowing to select a reduced set of transitions that still contain sufficient information. A comparison of the correlations between the lines in the synthetic and experimental spectra allow for a benchmark of the CRM used. ML methods for supervised learning are then trained on the full and reduced set of lines.

## 2 Methods

Experimental spectra of Xe and Kr from Hall effect thrusters are recorded for various operation conditions. Synthetic spectra are generated from a CRM for Xe [2], extended to work also with Kr. The model accounts for the first 14 excited states (1s and 2p blocks in Paschen notation). The synthetic spectra are generated for a set of electron densities, temperatures and EEDF shapes. The emission lines are normalised to the total intensity in the spectrum. ANN with various architectures (number of layers and neurons, activation function) and random forest are trained on the data.

## 3 Results

A reduced set of lines is identified both for Xe and Kr. ML on the reduced set of transitions shows comparable performance as with the full set. Random forest methods generally perform better than ANN within the range of the training values.

## References

[1] Arellano, F. J., Kusaba, M., Wu, S., Yoshida, R., Donkó, Z., Hartmann, P., Tsankov, Ts. V., and Hamaguchi, S., Machine learning-based prediction of the electron energy distribution function and electron density of argon plasma from the optical emission spectra. *J. Vac. Sci. Technol. A*, **42**, 053001 (2024).

[2] Ben Slimane, T. Investigation of the Optical Emission of Hall Effect Thrusters using Collisional Radiative Model, Particle-In-Cell Simulations, and Machine Learning. *PhD thesis* (2023, IP Paris). https://theses.hal.science/tel-04572928

[3] Ben Slimane, T., Leduc, A., Schiesko, L., Bourdon, A., and Chabert, P., Analysis and control of Hall effect thruster using optical emission spectroscopy and artificial neural network. *J. Appl. Phys.*, **136**, 153302 (2024).

# Re-defining the minimum energy cost for nitrogen fixation into NO in atmospheric pressure air plasma

I.Tsonev[1,2], M. Albrechts [1,2] and A. Bogaerts[1,2]

[1]*Research group PLASMANT, University of Antwerp, Antwerp, Belgium*
[2] *Electrification Institute, Antwerp, Belgium*

The formation of NO in plasmas predominantly follows the Zeldovich mechanism, which can be enhanced through vibrational-translational (VT) non-equilibrium, where overpopulated vibrational states of $N_2$ reduce the reaction energy barrier. While early research by Rusanov *et al.* suggested an exceptionally low energy cost (EC) of 0.2 MJ/mol at low pressure, attributed to the vibrationally-enhanced Zeldovich mechanism, this result has never been reproduced. In this work, we re-evaluate the theoretical minimum EC for nitrogen fixation (NF) into NO, in atmospheric pressure air plasmas, more suitable for industrial applications. We use a new global model, incorporating recent VT relaxation rate coefficients and updated reaction kinetics from the Stellar database. Our model simulates both steady state and transient conditions to determine optimal parameters for NF at VT non-equilibrium..

## 1 Introduction

The value of 0.2 MJ/mol reported by Rusanov *et al.* [1] is largely considered the theoretical minimum EC at atmospheric pressure, but this result has never been reproduced. In this work we constructed a new global model incorporating recent rate coefficient data from the Stellar database and VT relaxation data based on the modified Landau-Teller approach [2, 3]. We present a novel global model, which solves for the gas temperature and vibrational temperature of $N_2$, $O_2$ and NO with considerable computational efficiency. The model is used to recalculate the minimum EC for NF in atmospheric pressure air.

## 2 Results

Figure 1 presents simulations at steady state, assuming a constant $T_g$, as well as $T_vO_2$, $T_vNO$ and $T_vN_2$ during the entire simulation, hence only the species continuity equations are solved. We can see that the EC generally decreases with rising gas temperature and reaches a minimum at 3100 K, after which it rises again, for all conditions except for $T_vN_2$ = 8000 K (green curve). For the thermal equilibrium condition, the minimum EC is 2.6 MJ/mol, while the lowest EC achieved in steady state is 2.09 MJ/mol for $T_vN_2$ = 6000 K. When taking into account the energy loss due to VT relaxation, hence not keeping $T_vN_2$ fixed, but solving the energy balance equations, the EC is 3 times higher, indicating that efficient NF by VT-nonequilibrium, is not possible under atmospheric pressure conditions.

In order to determine the potential of ns-pulsed plasmas for achieving very low EC, we set the initial $T_g$ at 3100 K, and we define an elevated temperature of $T_vN_2$ = 8000 K as initial condition (Figure 2). We can see that NO can be formed efficiently with EC of 2.17 MJ/mol after the relaxation of $T_vN_2$, indicating that chemical non-equilibrium in combination with fast gas heating can be an efficient pathway for NF instead of VT-nonequilibrium.

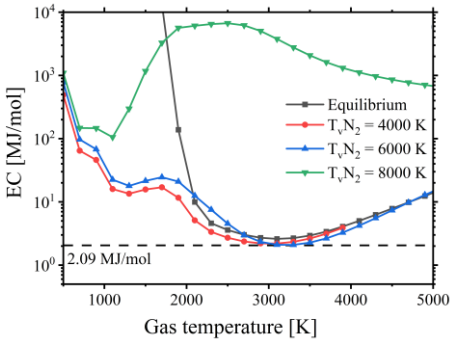



Figure 1. EC as a function of $T_g$, for $T_vN_2$ of 4000 K, 6000 K and 8000 K, as well as for thermal equilibrium.

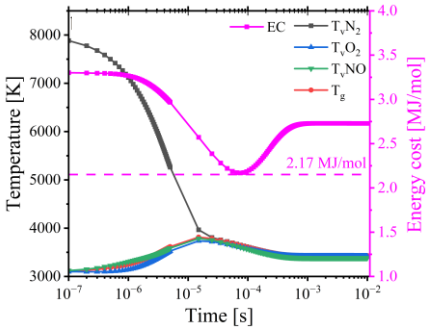



Figure 2. $T_vN_2$, $T_vO_2$, $T_vNO$, $T_g$ and the EC as a function of time for initial $T_vN_2$ of 8000 K and $T_g$ of 3100 K.

## References

[1] Rusanov V.D., The physics of a chemically active plasma with nonequilibrium vibrational excitation of molecules. *Soviet Physics Uspekhi*. **24**, 447, (1981).

[2] da Silva L., A multiquantum state-to-state model for the fundamental states of air: The stellar database. *ESA Special Publication*, **714**, 16. **(**2012).

[3] Oblapenko, G. Calculation of vibrational relaxation times using a kinetic theory approach. *J. Phys. Chem. A*, **122**, 9615-9625, (2018).

# NRP Discharge Temperature Evolution in a $CH_4/N_2$ mixture

T. Vazquez[1], L. Dakroub[2], M. Scherman[2], B. Tretout[2], C. Laux[1], S. McGuire[1]

[1]*Université Paris-Saclay, CNRS, CentraleSupélec, Laboratoire EM2C, 91190, Gif-sur-Yvette, France*
[2]*ONERA, The French Aerospace Lab, DPHY, Centre de Palaiseau, 91123 Palaiseau, France*

This study examines the temporal evolution of vibrational temperature of a nanosecond repetitively pulsed (NRP) discharge initiated in a $N_2$ /$CH_4$ mixture. We employ hybrid femtosecond/picosecond Coherent Anti-Stokes Raman Scattering (fs/ps CARS) for precise, time-resolved measurements. These findings shed light on ultrafast processes linked to the optimization of plasma-assisted combustion (PAC) for industrial applications.

## 1 Introduction

As the aviation and energy industries shift towards sustainable and carbon-neutral fuels, challenges such as combustion instability and NOx emissions remain obstacles. Plasma-Assisted Combustion (PAC) presents a promising approach to stabilize lean flames and lower emissions, making it a valuable tool for enhancing the performance of sustainable fuel-air mixtures [1]. This study focuses on applying nanosecond discharges to $N_2$ /$CH_4$ mixtures to isolate specific chemical kinetics of relevance involved in PAC.

We examine the time-dependent changes in the vibrational temperature of nanosecond repetitively pulsed (NRP) discharges in $N_2$ /$CH_4$ mixtures. NRP discharges deliver high-voltage pulses (~10 ns duration) at repetition rates of 10-100 kHz. We used a hybrid femtosecond/picosecond Coherent Anti-Stokes Raman Scattering (fs/ps CARS) setup developed at ONERA [2], that was adapted and synchronized with the NRP discharges.

## 2. Results

Results include CARS spectra obtained in a plasma initiated in air, $N_2$ and in a $N_2/CH_4$ mixture, all at 115 mbar. A recent refinement to the setup—shortening the focal length of the focusing lenses from 300 cm to 150 cm—has significantly improved the plasma CARS signal. This adjustment reduced the interaction volume, decreasing interference from surrounding air and enhancing the clarity and accuracy of the plasma measurements.

These findings contribute to a deeper understanding of the ultrafast processes involved in PAC, helping to overcome current limitations and paving the way for its broader adoption in sustainable and carbon-neutral fuel applications.

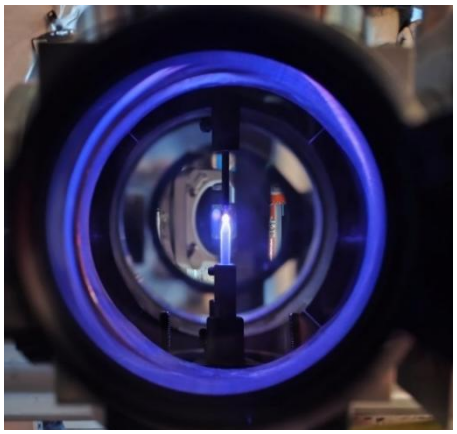


**Fig. 1**. Picture of the NRP discharge in air at 115 mbar.

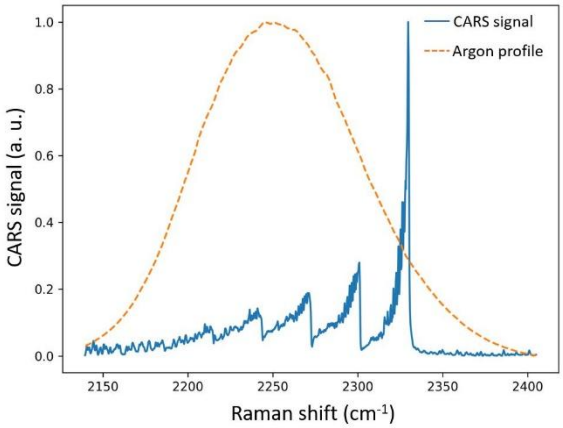



**Fig. 2**. CARS signal in air plasma at 115 mbar.

**Acknowledgement**
This work has received funding from the European Research Council (ERC) under the European Union's Horizon 2020 research and innovation program (grant agreement No. 101021538).

**References**

[1] Y. Ju and and W. Sun, Prog. Energy Combust. Sci. 48, 21–83 (2015).
[2] J. Barros, M. Scherman, E. Lin, N. Fdida, R. Santagata, B. Attal-Tretout, A. Bresson, Opt. Express 28, 34656-34664 (2020)

# Application of Machine Learning for Plasma Enhanced Chemical Vapor Deposition of Thin Film

S. W. Fitriani[1], K. Kamataki[2], Y. Sato[2], Y. Kurosaki[2], K. Koga[2] and, M. Shiratani[2]

[1] *Joint Graduate School of Mathematics for Innovation, Kyushu University, Fukuoka, Japan*
[2] *Graduate School and Faculty of Information Science and Electrical Engineering, Kyushu University, Fukuoka, Japan*

This work presents a prediction of plasma process for thin film deposition using an explainable machine learning based on plasma optical emission spectroscopy. The machine learning model provides insights into the contributions and correlations of different plasma species to the thin film deposition process. Furthermore, we leverage these findings to derive a mathematical model for predicting the deposition rate, demonstrating that optical emission spectroscopy can serve as a valuable tool for monitoring plasma output under varying deposition process conditions.

## 1 Introduction

Nowadays, around 80% of semiconductor manufacturing is dominated by plasma processes, e.g., $SiO_2$ thin film fabrication using plasma enhanced chemical vapor deposition (PECVD). However, in order to control the process variation and to deposit ultra-multi-layer thin film, it is required a high precision processes technology. To date, research development in this field has relied on a trial-and-error approach driven by experience and intuition due to the complexity of plasma reactions. As a consequence, there is a loss in energy, materials, and resources.

In the past few years, Machine Learning (ML) has been offering data-driven solutions to optimize plasma processes, enhance diagnostics and predict plasma-material interactions. Moreover, ML is a black box approaches that do not provide any information about the internal physical and chemical processes. In the present study, we proposed an explainable machine learning to predict the thin film properties deposited by PECVD.

## 2 Methods

The data sets ware prepared by fabricating $SiO_2$ thin film using plasma of TEOS/$O_2$/Ar. A gradient boosting decision tree model was employed to predict $SiO_2$ film deposition properties using optical emission spectroscopy. The hyperparameters of the model was optimized using Bayesian optimization by Gaussian process. Furthermore, we employed an explainable machine learning so-called SHapley Additive exPlanation (SHAP) to unfold the model prediction result. The performance of the model was evaluated by calculating the coefficient determination $R^2$, root mean square error (RMSE) and mean absolute error (MAE).

## 3 Results

Fig. 1 shows the performance of the model prediction. The deposition rate prediction result showed an agreement with the measured deposition rate, owning a coefficient determination $R^2$ of 0.93 ± 0.04; RMSE of 14.95 ± 6.20; MAE of 10.62 ± 4.60 for the training data, whereas the test data had a coefficient determination $R^2$ of 0.54 ± 0.32 and higher RMSE of 39.22 ± 12.69 and MAE of 31.75 ± 9.69. Furthermore, The SHAP result revealed that the deposition rate is significantly influenced by the following species, OH, CO, OI, ArI and ArII. It is suggested that these species are correlated to the TEOS dissociation process through electron impact, reaction with oxygen atoms and argon metastable [1].

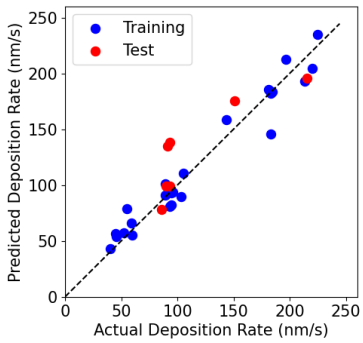



Fig. 1. ML model prediction performance of the thin film deposition rate [1]

**Acknowledgment**

This work was partly supported by JSPS KAKKENHI (Grant No. JP24H00205 and No. JP23K03368) and JST-ASPIRE (Grant No. 1234505)

**References**

[1] S. W. Fitriani et. al., Predictive Model for $SiO_2$ Film Properties Using Plasma Optical Spectra based on Machine Learning. *Surf. Coat. and Technol.* **504** 132029 (2025)

# Relative reaction constants of hydrated electrons in the region below the plasma-water interface

Y. Inagaki[1], Y. Kiniwa[1] and K. Sasaki[1]

[1] *Division of Applied Quantum Science and Engineering, Hokkaido University, Sapporo, Japan*

We have developed a new detection method for hydrated electrons in the interfacial region with plasmas. We tried to estimate relative reaction constants of hydrated electrons just below the plasma-water interface by using the new method and compared them with those in bulk water. As a result, we observed a proportional relationship between the measured and known reaction constants for $NO_2^-$, $NO_3^-$, and $Cu^{2+}$, whereas another proportional relationship was found for $H_2O_2$, $O_2$, and $H^+$.

## 1 Introduction

Hydrated electrons are generated by plasma-liquid interaction. However, there have been limited reports on the detection of hydrated electrons in liquids interacting with plasmas. The difficulty is caused by the fact that hydrated electrons generated by the plasma irradiation are localized in a narrow region with a thickness of several nanometers below the plasma-liquid interface. To overcome the difficulty, we have developed a method to detect hydrated electrons in the interfacial region [1]. Hydrated electrons in the interfacial region are converted to free electrons when they are irradiated with laser beam having a photon energy exceeding the solvation energy. Free electrons produced by the desolvation are transported to and detected in the gas phase. In a previous work, we suggested that hydrated electrons just below the plasma-water interface had a higher chemical potential and higher reactivity than those in the bulk region. In the present work, we tried to estimate relative reaction constants of hydrated electrons at the plasma-water interface and compared them with those in bulk water.

## 2 Experimental methods

A metal nozzle electrode having an inner diameter of 500 μm and a NaCl solution (0.3 g/L) were placed in a glass chamber, and a high voltage was applied between them to generate an Ar atmospheric-pressure dc glow discharge. A ballast resistor of 25 kΩ was connected in series between the dc power supply and an electrode, and a shunt resistor of 50 Ω was inserted between the other electrode and the ground potential. The voltage across the shunt resistor was measured using an oscilloscope to determine the temporal variation of the discharge current. We irradiated the liquid surface with Nd:YAG laser pulses at wavelengths of 266 nm. The irradiation of the laser beam from the bottom side of water resulted in the total reflection at the water surface, by which we avoided the production of free electrons in the gas phase by photodetachment of negative ions. Note that this method detects hydrated electrons only in the vicinity of plasma-water interface.

## 3 Results and Discussion

Figure 1 shows the relationship between $\Delta I$, which is defined as the amplitude of the pulsed current superposed on the dc discharge current, and the concentrations of chemicals in the water cathode. For example, hydrated electrons react with $NO_3^-$ as follows,

$$e_{solv}^- + NO_3^- \rightarrow N^{\cdot}O_3^{2-}.$$

The solid fitting curve illustrated in the figure is given by

$$\Delta I = \frac{\alpha}{\nu + k_{A_i}[A_i]},$$

where $[A_i]$ is the concentrations of $NO_3^-$, $\nu$ is the loss frequency of hydrated electrons due to mechanisms other than the reaction with admixed $NO_3^-$, and $\alpha$ stands for the proportional constant that includes the production rate of hydrated electrons. We estimated the relative value of reaction constant $k_{A_i}$ by the curve fitting. Figure 2 shows relative reaction constants for 7 chemical species ($H_2O_2$, $NaNO_2$, $NaNO_3$, $O_2$, $HCl$, $NiCl_2$, and $CuCl_2$) as a function of known reaction constants in bulk water. A proportional relationship was found between the measured and known reaction constants for $NO_2^-$, $NO_3^-$, and $Cu^{2+}$, whereas reaction constants for $H_2O_2$, $O_2$, and $H^+$ followed another proportional relationship. A unique proportional relationship was not obtained, suggesting that reactivity of hydrated electrons in the vicinity of the plasma-water interface is different from that in bulk water.

## References

[1] Y. Inagaki, and K. Sasaki, Plasma Sources Sci. Technol. 31, 03LT02 (2022).

[2] G. V. Buxton, et al., J. Phys. and Chem. Ref. Data 17, 513 (1988).

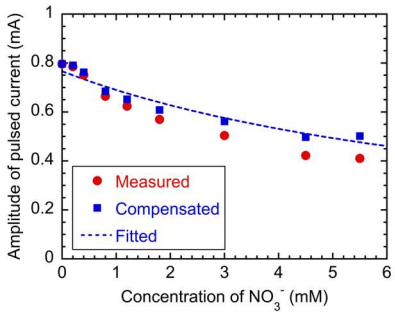



Figure 1. Amplitude of pulsed current as a function of the concentration of $NaNO_3$.

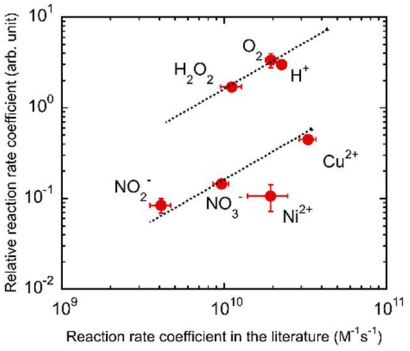



Figure 2. Relative reaction constants between hydrated electrons and 7 chemical species as a function of known reaction constants in bulk water [2].

# Program of Poster Session #1

| # | In Competition | Title | Speakers | Topic |
|---|---|---|---|---|
| M-1 | NO | Cross sections for H2 and NH3 relevant to N2-H2 plasma modelling | Baghel Shubham Singh | Elementary processes and fundamental data |
| M-2 | NO | Microwave Plasma CVD growth of Diamond for NV-Applications | Davis William | Plasma processing of surfaces and particles |
| M-3 | YES | Cold Atmospheric Pressure Plasma (CAP) Jet for Endodontic applications | Mishra Abhijit | Medical, biological, environmental and aeronautical applications |
| M-4 | YES | Fast Plasma Nanomodification of Graphitic Carbon Nitride by Amide and Carboxyl Groups for Enhanced Sulfamethoxazole Degradation in Wastewater: Detailed Experimental and DFT Study | Zažímal František | Plasma processing of surfaces and particles |
| M-5 | NO | Plasma-Activated Fog treatments as sustainable protective tool in post-harvest | Aceto Domenico | Medical, biological, environmental and aeronautical applications |
| M-6 | NO | Hold-Off Voltage Computation in Industrial Gas Insulation | Ferreira Nuno | Modelling and simulation techniques, Non-equilibrium plasmas and microplasmas at high pressure |
| M-7 | NO | Investigation of an $Ar/C_2H_2$ temporal plasma afterglow employing MCRS and LIP techniques | Salinaro Michela | Complex and dusty plasmas, ion-ion plasmas, mixed phase plasmas |
| M-8 | YES | Modeling of methane plasmalysis via NRP discharges | Goutier Pierre-Antoine | Non-equilibrium plasmas and microplasmas at high pressure |
| M-9 | NO | Enhanced UVC surface decontamination by mercury-free excimer lamp-phosphor systems | Maho Thomas | Medical, biological, environmental and aeronautical applications |

| # | In Competition | Title | Speakers | Topic |
|---|---|---|---|---|
| M-10 | NO | Quantitative evaluation of the thrust efficiency in a parallel-plate pulsed plasma thruster | Watanabe Masayuki | Medical, biological, environmental and aeronautical applications |
| M-11 | NO | Electron beam divergence and instability in ionospheric plasmas | Mori Koichi | Other applications such as low temperature plasma applications for magnetically confined fusion |
| M-12 | NO | CH4 plasma in water to produce H2 and hydrophilic carbon solids | Saito Atsushi | Plasma in/with liquids |
| M-13 | YES | Development of a Low-Pressure Hydrogen Dielectric Barrier Discharge | Salij Jörgen | Thermodynamics and transport phenomena, Low pressure plasmas |
| M-14 | NO | Atomic nitrogen versus vibrational excited molecular nitrogen in ammonia synthesis using low-pressure nitrogen-hydrogen plasma | Sasaki Koichi | Medical, biological, environmental and aeronautical applications |
| M-15 | NO | Modeling electron beam-induced evaporation of macroparticles in vacuum arc plasma | Litovko Iryna | Modelling and simulation techniques |
| M-16 | NO | Neutralization of Ion Beams at Low Background Gas Pressures | Hopkins Matthew | Other applications such as low temperature plasma applications for magnetically confined fusion |
| M-17 | NO | Study of rotating structures in E×B plasmas and their implications on charged particle transport | Stevens J. | Low pressure plasmas |
| M-18 | YES | Dynamics of CCRF argon plasma with aerosol pulsed injection | Valdovinos Aguilar Luis | Complex and dusty plasmas, ion-ion plasmas, mixed phase plasmas |
| M-19 | NO | Optical actinometry in CF4-containing plasmas | Silva Tiago | Low pressure plasmas |
| M-20 | NO | Automated Processing of High-Frequency Electrodeless-Lamp Spectra | Zorina Natalja | Plasma diagnostics methods |

| # | In Competition | Title | Speakers | Topic |
|---|---|---|---|---|
| M-21 | NO | Quantification of ammonia production in a surfaguide discharge over a wide pressure range | Wolf Vinzenz | Plasma processing of surfaces and particles |
| M-22 | NO | Mass spectrometry of plasma reactive species produced by a surface DBD source | Skoro Nikola | Plasma diagnostics methods |
| M-23 | NO | Influence of axial magnetic field on the ion flux uniformity in a VHF CCP | Eremin Denis | Low pressure plasmas |
| M-24 | NO | Disinfection of Bacteria- and Fungi-Contaminated Tap Water Using a Gliding Arc in Air with $CO_2$ Bubbling | Mobasher Mona | Medical, biological, environmental and aeronautical applications |
| M-25 | YES | Comparison of three plasma reactors in contact with water: application to micro-pollutant degradation | Ben Othmen Cyrine | Medical, biological, environmental and aeronautical applications, Plasma in/with liquids |
| M-26 | NO | Modeling approach for an atmospheric pressure, compressed air inductively coupled plasma torch with arbitrary geometry | Gils Anne Van | Modelling and simulation techniques |
| M-27 | YES | Quenching of a magnetically stabilized arc discharge at different pressures for CO2 conversion | Vasilev Veselin | Medical, biological, environmental and aeronautical applications |
| M-28 | NO | Modelling of diffusion and viscosity of carbon nanoparticles in low-temperature plasma | Kodanova Sandugash | Complex and dusty plasmas, ion-ion plasmas, mixed phase plasmas |
| M-29 | YES | Control of average ion energy and ion flux through incorporation of helium in inductively coupled and capacitively coupled hydrogen plasmas | Kellermann-Stunt Maximilian | Low pressure plasmas |
| M-30 | YES | Subcellular Visualization of Cold Atmospheric Plasma Effects on Living Cell Surfaces Using Scanning Ion Conductance Microscopy | Nguyen Han | Medical, biological, environmental and aeronautical applications |

| # | In Competition | Title | Speakers | Topic |
|---|---|---|---|---|
| M-31 | NO | An introduction to a series of linear plasma devices within CRAFT project in China | Yang Xin | Other applications such as low temperature plasma applications for magnetically confined fusion |
| M-32 | NO | Electron properties and non-thermal equilibrium in an 80 kV nanosecond discharge studied by incoherent Thomson scattering | Tardiveau Pierre | High frequency and pulsed discharges, Non-equilibrium plasmas and microplasmas at high pressure |
| M-33 | NO | Effects of ion irradiation on the structure of a-C:H films deposited using cumene plasma CVD | Eri Manato | Plasma processing of surfaces and particles |
| M-34 | YES | Temporal evolution of NO density after nanosecond repetitively pulsed discharges in plasma-assisted combustion | Gablier Renaud | High frequency and pulsed discharges |
| M-35 | YES | Study of a surface wave plasma under the influence of pulsed gas injections by rapid imaging | Brochier Jules | Low pressure plasmas |
| M-36 | YES | Experimental study and modelling of high temperature N2/CH4 plasma | Merhaben Cyrine | Non-equilibrium plasmas and microplasmas at high pressure |
| M-37 | NO | Evaluation of rice seed coat penetration characteristics of plasma-generated reactive oxygen species using the KI-starch | Shi Heping | Medical, biological, environmental and aeronautical applications |
| M-38 | YES | Numerical and theoretical investigation of the ECRIPAC accelerator concept | Cernuschi Andrea | Low pressure plasmas |
| M-39 | YES | Electron density measurements in a $H_2$/Ar microwave microplasma | Jeevan Joel | Plasma diagnostics methods |
| M-40 | YES | Study of the physical properties of different $\mu$m-scale He plasma jets | Agha Yanis | Non-equilibrium plasmas and microplasmas at high pressure |

| # | In Competition | Title | Speakers | Topic |
|---|---|---|---|---|
| M-41 | NO | Real-time tracking of emissive species and gas temperature in a pulsed MHCD during the deposition of h-BN on a Si substrate | Menacer Belkacem | Plasma diagnostics methods |
| M-42 | NO | Plasma irradiation to cytokines and immune cell in culture medium using a porous membrane plasma source | Nakamura Hinako | Medical, biological, environmental and aeronautical applications |
| M-43 | NO | Application of non-conformal triangular meshes in fluid modelling of low-temperature plasma discharges. | Semenov Igor | Modelling and simulation techniques |
| M-44 | NO | Optical Emission Spectroscopy of $Ar/CO_2/H_2O$ plasmas generated in a modified surfatron device | Rodero Serrano Antonio | High frequency and pulsed discharges, Non-equilibrium plasmas and microplasmas at high pressure |
| M-45 | NO | Active species in the afterglow of MW N2 plasma | Starostine Serguei | Plasma diagnostics methods |
| M-46 | NO | Streamer-to-spark transition: time-resolved imaging and time evolution of $n_e$ and $T_p$ | Hamdan Ahmad | Plasma in/with liquids |
| M-47 | NO | Measurement of the electric field distribution in streamer discharges | Nijdam Sander | Plasma diagnostics methods |
| M-48 | NO | The McWhirter criterion revisited for laser-induced plasmas | Bultel Arnaud | Non-equilibrium plasmas and microplasmas at high pressure |
| M-49 | NO | Production of durable superhydrophobic coatings using atmospheric pressure plasma | Kyrykbay Baglan | Plasma processing of surfaces and particles |
| M-50 | YES | Temperature measurements in methane NRP discharges | Delahaie Sara | High frequency and pulsed discharges |
| M-51 | YES | Effects of He addition to Ar/C2H2 PECVD on a-C:H film properties | Nagamine Kazuki | Plasma processing of surfaces and particles |
| M-52 | NO | Bridging structure and magnetism of diluted magnetic semiconductor films using nitrogen-mediated crystallization | Shiratani Masaharu | Plasma processing of surfaces and particles |

| # | In Competition | Title | Speakers | Topic |
|---|---|---|---|---|
| M-53 | YES | 2D spatial mapping of the fundamental properties of a microwave argon plasma jet in contact with surfaces | Khazem Fatima | Non-equilibrium plasmas and microplasmas at high pressure, Plasma diagnostics methods |
| M-54 | NO | The 2025 status report on the LXCat project | Carbone Emile | Elementary processes and fundamental data |
| M-55 | NO | Ionization Region Model (IRM) for Helium High Power Impulse Magnetron Sputtering (HiPIMS) with Mo target | Zakaria Belkaid | Modelling and simulation techniques |
| M-56 | YES | A hybrid FTIR system for process characterisation and in-situ plasma diagnostics for gas conversion reactors | Franco Francesco | Plasma diagnostics methods |
| M-57 | NO | Elucidation of the Nitrogen Blue Afterglow in Atmospheric Pressure Helium Plasma Jet | Enomoto Jun | Plasma diagnostics methods |
| M-58 | NO | Influence of air admixture in an Ar pin-jet on water treatment | Jovanović Olivera | Plasma in/with liquids |
| M-59 | NO | Controlling Pulsed Dielectric Barrier Discharges Using Shaped High-Voltage Waveforms | Van Oorschot Jeroen | Non-equilibrium plasmas and microplasmas at high pressure |
| M-60 | NO | Particle-In-Cell Study of Laser Wakefield Acceleration in a Gas Cell for GeV-Scale High-Quality Electron Beams | Maity Srimanta | Modelling and simulation techniques, Collective and nonlinear phenomena |
| M-61 | NO | Time and space dependence of iodine atomic density produced by laser photodissociation | Drag Cyril | Thermodynamics and transport phenomena |
| M-62 | YES | Measurement of N2(C) and N2(B) quenching rate constants | Du Garreau De La Mechenie Jean-Loup | Elementary processes and fundamental data |
| M-63 | NO | Synergestic effect of coupling Non thermal plasmas with perovskite-type membranes for oxygen permeation | Sadi Dihya | Low pressure plasmas |

| # | In Competition | Title | Speakers | Topic |
|---|---|---|---|---|
| M-64 | NO | Ion acceleration in a diverging magnetic nozzle : Laser Induced Fluorescence measurements and expansion model. | Pioch Romain | Thermodynamics and transport phenomena |
| M-65 | NO | Particle-in-Cell Modeling of EUV-Induced Plasma Dynamics in Lithography Exposure Chamber | Sharova Yulia | Plasma wall interactions, electrode and surface effects, Plasma processing of surfaces and particles, Low pressure plasmas |
| M-66 | NO | About the sensitivity of atomic hydrogen surface loss coefficients with respect to Si contamination | Remigy Alice | Plasma wall interactions, electrode and surface effects |
| M-67 | NO | Log-normal density scaling of species embedded in chemical network topology in low-temperature silane plasma | Sakai Osamu | Modelling and simulation techniques |
| M-68 | NO | Evidence for sputtering of D and O adsorbed on W(110) by a D2+ ion beam | Latournerie Matthieu | Plasma wall interactions, electrode and surface effects |
| M-69 | NO | ps-TALIF and streak camera system for measuring sub-ns decay times and densities of reactive atoms in collisional microplasmas | Gazeli Kristaq | Plasma diagnostics methods |
| M-70 | NO | Effects of material properties on Surface Semiconducting Barrier Discharges | Taihi Ayah Soundous | Non-equilibrium plasmas and microplasmas at high pressure |
| M-71 | NO | Electrohydrodynamic flows induced by DC and AC needle-to-liquid discharges | Frederic Dyson | Plasma in/with liquids |
| M-72 | NO | Similarities between formation of low-current self-sustained discharge and breakdown in industrial gas insulation | Almeida Rui | Modelling and simulation techniques, Non-equilibrium plasmas and microplasmas at high pressure |

| # | In Competition | Title | Speakers | Topic |
|---|---|---|---|---|
| M-73 | YES | Phenomenological description and numerical modelling of vacuum breakdown | Cró Camila | Modelling and simulation techniques, Plasma wall interactions, electrode and surface effects |

# Presenter Index


- **Aceto Domenico**: M-5
- **Agha Yanis**: M-40
- **Almeida Rui**: M-72
- **Baghel Shubham Singh**: M-1
- **Ben Othmen Cyrine**: M-25
- **Brochier Jules**: M-35
- **Bultel Arnaud**: M-48
- **Carbone Emile**: M-54
- **Cernuschi Andrea**: M-38
- **Cró Camila**: M-73
- **Davis William**: M-2
- **Delahaie Sara**: M-50
- **Drag Cyril**: M-61
- **Du Garreau De La Mechenie Jean-Loup**: M-62
- **Enomoto Jun**: M-57
- **Eremin Denis**: M-23
- **Eri Manato**: M-33
- **Ferreira Nuno**: M-6
- **Franco Francesco**: M-56
- **Frederic Dyson**: M-71
- **Gablier Renaud**: M-34
- **Gazeli Kristaq**: M-69
- **Gils Anne Van**: M-26
- **Goutier Pierre-Antoine**: M-8
- **Hamdan Ahmad**: M-46
- **Hopkins Matthew**: M-16
- **Jeevan Joel**: M-39
- **Jovanović Olivera**: M-58
- **Kellermann-Stunt Maximilian**: M-29
- **Khazem Fatima**: M-53
- **Kodanova Sandugash**: M-28

- **Kyrykbay Baglan**: M-49
- **Latournerie Matthieu**: M-68
- **Litovko Iryna**: M-15
- **Maho Thomas**: M-9
- **Maity Srimanta**: M-60
- **Menacer Belkacem**: M-41
- **Merhaben Cyrine**: M-36
- **Mishra Abhijit**: M-3
- **Mobasher Mona**: M-24
- **Mori Koichi**: M-11
- **Nagamine Kazuki**: M-51
- **Nakamura Hinako**: M-42
- **Nguyen Han**: M-30
- **Nijdam Sander**: M-47
- **Pioch Romain**: M-64
- **Remigy Alice**: M-66
- **Rodero Serrano Antonio**: M-44
- **Sadi Dihya**: M-63
- **Saito Atsushi**: M-12
- **Sakai Osamu**: M-67
- **Salij Jörgen**: M-13
- **Salinaro Michela**: M-7
- **Sasaki Koichi**: M-14
- **Semenov Igor**: M-43
- **Sharova Yulia**: M-65
- **Shi Heping**: M-37
- **Shiratani Masaharu**: M-52
- **Silva Tiago**: M-19
- **Skoro Nikola**: M-22
- **Starostine Serguei**: M-45
- **Stevens J.**: M-17
- **Taihi Ayah Soundous**: M-70
- **Tardiveau Pierre**: M-32

- **Valdovinos Aguilar Luis**: M-18
- **Van Oorschot Jeroen**: M-59
- **Vasilev Veselin**: M-27
- **Watanabe Masayuki**: M-10
- **Wolf Vinzenz**: M-21
- **Yang Xin**: M-31
- **Zakaria Belkaid**: M-55
- **Zažímal František**: M-4
- **Zorina Natalja**: M-20

# Cross sections for $H_2$ and $NH_3$ relevant to $N_2$-$H_2$ plasma modelling

S. S. Baghel[1], L. Marques[2] and L.L. Alves[1]

[1] *Instituto de Plasmas e Fusão Nuclear, Instituto Superior Técnico, Universidade de Lisboa, Portugal*
[2] *Centro de Física das Universidades do Minho e do Porto, Universidade do Minho, Braga, Portugal*

This contribution uses swarm analysis to propose complete and consistent electron-impact cross section sets for ground-state $H_2$ and $NH_3$. For hydrogen, we update the cross section set published in the IST-Lisbon database of LXCat, while for ammonia we propose a novel set of direct cross sections.

The efficient modelling of $N_2$-$H_2$ plasmas is key to understand the main kinetic pathways leading to plasma assisted synthesis and decomposition of $NH_3$ [1]. In low-temperature plasmas, electron collisions with atomic/molecular neutral-species are one of the most important kinetics mechanisms, and therefore complete and consistent sets of electron-neutral collisional cross-sections are essential data for modelling [2].

In this work, (i) we update the electron-impact cross section set for ground-state $H_2$ published in the IST-Lisbon database of the LXCat open-access website [3], and (ii) we propose an electron-impact cross section set for ground-state $NH_3$. Both sets of cross sections are complete and consistent, because they include the most relevant mechanisms for the electron-neutral exchange of energy and momentum, and because when used in a two-term electron Boltzmann solver they predict swarm parameters in agreement with experimental measurements, within less than 15%.

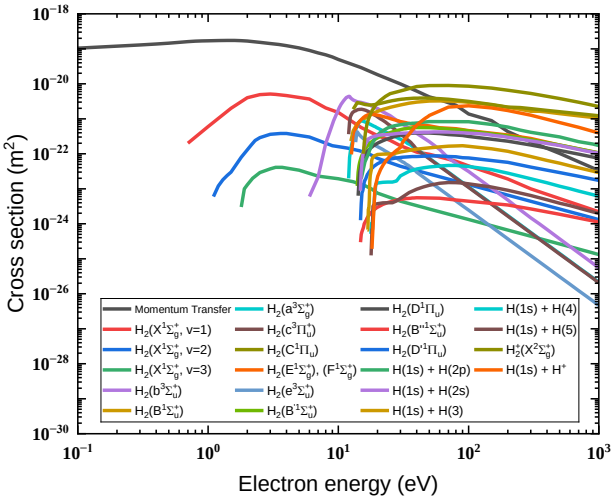



Figure 1: Final set of electron-impact cross sections proposed for $H_2(X^1\sum_g^+,v=0)$, including different processes viz. momentum-transfer, excitation, ionization.

The swarm analysis was carried out using the LisbOn KInetics Boltzmann solver (LoKI-B) [4], to calculate electron transport parameters (reduced mobility, characteristic energy, and drift velocity) as well as several reduced Townsend coefficients (ionization, dissociation, emission, attachment) from different cross-section sets [5-8]. Results were compared with the corresponding available measurements [9], and some cross sections were adjusted to improve the swarm predictions.

Figure 1 shows the final set of cross sections proposed for $H_2$. In this case, the most relevant updates are with the cross sections for the excitation to $H_2(B^1\Sigma_u^+)$ and $H_2(C^1\Pi_u)$ states, the dissociative excitation of $H_2(b^3\Sigma_u^+)$ state, and the dissociative ionization yielding H(1s) + $H^+$. For $NH_3$, the new cross section set was built from the Hayashi dataset on LXCat [8], which was updated with cross sections recommended by Snoeckx *et al.* [6]. Both cross section sets will be published on the IST-Lisbon database of LXCat.

## Acknowledgements

This work was funded by FCT - Fundação para a Ciência e a Tecnologia under projects UIDB/50010/2020(https://doi.org/10.54499/UIDB/50010/2020),UIDP/50010/2020(https://doi.org/10.54499/UIDP/50010/2020),LA/P/0061/202(https://doi.org/10.54499/LA/P/0061/2020) and 2022.04128.PTDC(https://doi.org/10.54499/2022.04128.PTDC).

## References

[1] Jiménez-Redondo, M. *et al.*, *Plasma Sources Sci. Technol.* **29**, 085023 (2020)
[2] Zhang, B. *et al.*, *J. Phys. D. Appl. Phys.* **56**, 134001 (2023)
[3] The IST-Lisbon database on LXCat www.lxcat.net/IST-Lisbon
[4] Tejero-Del-Caz, A. *et al.*, *Plasma Sources Sci. Technol.* **28** 043001 (2019)
[5] Celiberto, R. *et al.*, reference *At. Data Nucl. Data Tables.* **77** 161 (2001)
[6] Zammit, M. *et al.*, *Phys.Rev.A.* **95**, 022708 (2017)
[7] Snoeckx, R. *et al.*, *Plasma Sources Sci. Technol.* **32** 115020 (2023)
[8] Hayashi database on LXCat www.lxcat.net/Hayashi
[9] Dutton, A. *J. Phys. Chem. Ref. Data* **4** 3 (1975)

# Microwave Plasma CVD growth of Diamond for NV- Applications

W. Davis[1] and M.P. Bradley[1]

[1] *University of Saskatchewan, Saskatoon, SK, Canada*

Diamond thin films doped with nitrogen exhibit a specific type of vacancy, the diamond NV- centre, with unique optical and spin properties. The diamond NV- centre consists of a substitutional nitrogen atom (N) adjacent to a vacancy (V). Because of the $sp^3$ bonding of the diamond lattice, NV centres are vector in nature, with 4 possible alignment directions relative to the bulk crystal or crystallite in which they are embedded. NV centres can be neutral (designated $NV^0$) or negatively charged (designated $NV^-$) [1]. Only the NV- centre is relevant for magnetometry; this is a consequence of the spin-1 nature of the NV- defect. Optically pumped (typically at 532 nm) diamond NV- centres exhibit a spin-dependent fluorescence intensity at 637 nm. This opens the door to Optically Detected Magnetic Resonance (ODMR) [2]. ODMR of the diamond NV- centre has great potential for magnetometry in various applications, including geophysical exploration via magnetic surveys as well as pipe inspection etc. For this reason, careful study of the influence of different diamond growth conditions for diamond NV films is an important technology both for magnetometry applications as well as potential quantum information applications using NV- spin qubits.

In this work we report on recent studies of nitrogen-doped diamond thin films grown using microwave plasma chemical vapour deposition. The nitrogen content of the thin films was controlled by varying the concentration of nitrogen gas added to the feedstock gas (methane with a large excess of nitrogen). The effect of film growth time and nitrogen doping time is discussed.

**References**

[1] Hacquebard, L., Kuret, L. and Childress, L. Photo-induced charge state switching of the nitrogen-vacancy center in diamond, APS March Meeting 2017, abstract id. T1.013, bibcode 2017APS..MAR.T1013H.

[2] Sengottuvel, S. *et al*. Wide-field magnetometry using nitrogen-vacancy color centers with randomly oriented micro-diamonds. *Scientific Reports* **12**, Article number: 17997 (2022).

# Cold Atmospheric Pressure Plasma (CAP) Jet for Endodontic applications

Abhijit Mishra[1], Pravin Kumar[2] and Ram Prakash[1]

[1] *Department of Physics, Indian Institute of Technology Jodhpur, 342030, Rajasthan, India*
[2] *Department of Dentistry, All India Institute of Medical Sciences, 342005 Jodhpur, Rajasthan, India*

This study optimizes a cold atmospheric pressure plasma (CAP) jet for root canal treatment, focusing on smear layer removal and Enterococcus faecalis disinfection. A helium CAP jet, driven by a bipolar pulsed power supply, was optimized by varying voltage, frequency, and gas flow rate, with plasma parameters determined using a Collisional-Radiative model. The jet was applied to teeth samples for 2, 5, and 10 minutes, and its efficacy was validated through SEM imaging, log reduction analysis, and statistical evaluation.

## 1 Introduction

Cold atmospheric plasma (CAP) jets, also referred to as non-equilibrium plasma jets, have demonstrated significant potential for dental applications due to their ability to produce reactive oxygen and nitrogen species (RONS), radiation, and electromagnetic fields at temperatures close to the environment [1]. CAP has the unique ability to penetrate irregular cavities/fissures, like dentinal tubules or apical regions, effectively inactivating bacteria without damaging living tissues [2]. Additionally, CAP-induced surface modifications make it particularly relevant for endodontic applications.

Mechanical instrumentation invariably creates a smear layer (SL) on the root canal walls that blocks dentinal tubules, hindering medicament penetration and sealing. An infected SL promotes bacterial growth. While variety of chelating agents are in use, none of them meets the ideal criteria, prompting researchers to explore more in this field.

## 2 Methodology

In this ex-vivo study, the efficiency of bipolar pulsed powered helium CAP jets in removing the smear layer from intra-radicular dentin and disinfecting the root canal is investigated, targeting potential applications in endodontics. The developed cross-field configured CAP jet is a double dielectric barrier discharge (DBD) system operated by a bipolar pulsed power supply [3]. The discharge characteristics of the CAP jet is studied through electrical and optical characterizations. The collisional–radiative (CR) model coupled with Optical Emission Spectroscopy (OES) is employed to extract the plasma parameters like electron density ($n_e$) and electron temperature ($T_e$) and to identify the generated species from the spectra. 60 mandibular premolars, prepared with ProTaper Universal hand files, are divided into four groups and treated with Normal saline (control) and helium CAP jets for 2, 5, and 10 minutes. The smear layer removal efficacy is evaluated at coronal, middle, and apical thirds using SEM images, while statistical analysis is performed to analyse the differences among groups.

## 3 Results

The jet exhibited a transition from laminar to turbulent flow at helium flow rates exceeding 4 slpm, corresponding to a Reynolds number of ~400. OES analysis identified key reactive species, while the C-R model confirmed a non-equilibrium plasma regime with $n_e \sim 10^{13}$ $cm^{-3}$, $T_e \sim 0.35$ eV, and plasma gas temperature (Tg ~ 305 K) under optimized conditions (4 kV, 20 kHz, 4 slpm). Scanning Electron Microscopy (SEM) imaging and microbial disinfection analysis revealed substantial smear layer removal and an approximately 5-log reduction in *Enterococcus faecalis* count, suggesting their potential as chemical-free alternatives in dentistry with optimized exposure. The obtained results along with certain safety evaluation test results will be presented in details.

### References

[1] Mishra, A., Pandey, S., Kumar, P., & Prakash, R. Comparative analysis of disinfection effectiveness of Helium CAP jet, sodium hypochlorite and QMix in *Enterococcus faecalis* infected root canals. *Radiation Effects and Defects in Solids* **179**, 1009–1016 (2024).

[2] Borges, A. C. et al. Applications of Cold Atmospheric Pressure Plasma in Dentistry. *Applied Sciences* **11**, 1975 (2021).

[3] Mishra, A., Mishra, R., Siddiqui, Y. H., Jangra, S., Pandey, S., & Prakash, R. Analysis of discharge parameters of an argon cold atmospheric pressure plasma jet and its impact on surface characteristics of White Grapes. *Physica Scripta* **99**, 105615 (2024)

# Fast Plasma Nanomodification of Graphitic Carbon Nitride by Amide and Carboxyl Groups for Enhanced Sulfamethoxazole Degradation in Wastewater: Detailed Experimental and DFT Study

F. Zažímal[1], S. Atri[2], D. Plašienka[1], L. Vrána[1], A. Stýskalík[3], A. Vlk[4], M. Čaplovičová[5], M. Šob[3], O. Monfort[6], T. Homola[1,7]

[1]*Masaryk University, Department of Plasma Physics and Technology, Czech Republic*
[2]*Comenius University Bratislava, Department of Inorganic Chemistry, Slovak Republic*
[3]*Masaryk University, Department of Chemistry, Czech Republic*
[4]*Czech Academy of Sciences, Institute of Physics, Czech Republic*
[5]*Slovak University of Technology in Bratislava, STU Center for Nanodiagnostics, Slovak Republic*
[6]*Comenius University Bratislava, Centre for Nanotechnology and Advanced Materials, Slovak Republic*
[7]*Slovak University of Technology, Institute of Chemical and Environmental Engineering, Slovak Republic*

This study presents a plasma nanomodification strategy for graphitic carbon nitride (gCN) prepared from melamine (M-gCN) and 3-amino-1,2,4-triazole (3AT-gCN). For the first time, we report surface functionalization of gCN with amide ($CONH_2$), carboxyl (COOH), and amine ($NH_2$) groups using low-temperature plasma in open air. The process is rapid (4 minutes), non-destructive, and environmentally friendly, enhancing the photocatalytic performance of gCN. X-ray Photoelectron Spectroscopy (XPS) and Density Functional Theory (DFT) simulations were used to analyze the impact on electronic properties. The surface functionalization significantly improved the electronic properties of materials leading to enhanced charge carrier separation and migration and efficient sulfamethoxazole (SMX) degradation in wastewater in presence of peroxymonosulfate (PMS). SMX removal reached 88% (M-gCN-PT) and 76% (3AT-gCN-PT) after 2 hours in pure water, and 83% (M-gCN-PT) and 71% (3AT-gCN-PT) after 12 hours in municipal wastewater effluents.

The contamination of wastewater effluents with residues of antibiotics, such as SMX, poses a significant environmental and health risk. We present an innovative plasma nanomodification approach of gCN by DCSBD plasma to enhance its photocatalytic activity. The presence of these groups on the gCN surface was uncovered based on thorough analysis by XPS complemented by DFT calculations. The mechanistic study reveals the role of both radical and non-radical pathways in the degradation of SMX. The content of this work is illustrated in **Fig. 1**.

The gCN nanomaterial is a promising metal-free photocatalyst for environmental applications due to its unique structural and electronic properties. It is formed by heptazine-based polymeric networks, exhibits a medium bandgap (~2.7 eV), allowing for visible light absorption and photocatalytic activity. Additionally, it possesses high thermal and chemical stability, making it suitable for various applications, including pollutant degradation, hydrogen evolution, and $CO_2$ reduction. However, gCN suffers from limited charge carrier mobility and fast recombination of photogenerated electron-hole pairs, which restricts its photocatalytic performance. To overcome these limitations, various surface and structural modifications, including heteroatom doping, copolymerization, and functionalization with oxygen- and nitrogen-containing groups, have been explored.

Among various modification strategies, low-temperature plasma treatment has emerged as an environmentally friendly and efficient technique for surface functionalization of materials. DCSBD plasma offers a promising approach for tuning the catalytic properties of gCN elucidated in this study. Unlike wet-chemical functionalization methods, plasma modification does not require toxic reagents or prolonged processing times, making it a sustainable and scalable approach for nanomaterial modification.




Figure 1: Surface functionalization of gCN by low-temperature plasma. Enhanced SMX degradation in wastewater in presence of modified gCN and PMS. Promoted radical and non-radical pathway.

# Plasma-Activated Fog treatments as sustainable protective tool in post-harvest

Domenico Aceto[1], Daniele Chieffi[2], Palma Rosa Rotondo[3], Marianna Ambrico[1], Rita Milvia De Miccolis Angelini[3], Vincenzina Fusco[2], Paolo F. Ambrico[1]

[1] *Institute for Plasma Science and Technology, National Research Council of Italy (CNR-ISTP), 70126 Bari, Italy*
[2]*Institute of Sciences of Food Production, National Research Council of Italy (CNR-ISPA), 70126 Bari, Italy*
[3]*Department of Soil, Plant and Food Sciences, University of Bari Aldo Moro, 70126, Bari, Italy*

We propose Plasma-Activated Fog (PAF) as a novel tool in plasma-agriculture, involving water droplets nebulized within plasma effluent gases to enhance reactive species delivery. This approach to plasma-treated media was characterized and tested to decontaminate produce harbouring phytopathogenic and human pathogens. Preliminary results indicate significant reductions in pathogen load, highlighting PAF as a valuable asset in food safety and sustainability efforts.

## 1 Introduction

Low-temperature plasma (LTP) has gained attention in agriculture and food safety due to its eco-friendly antimicrobial properties and absence of chemical residues. Among indirect LTP applications, plasma-activated water (PAW) has been widely studied for plant irrigation and microbial decontamination [1, 2].

Here, we introduce Plasma-Activated Fog (PAF), a novel indirect method where water droplets are nebulized using plasma effluent gases, enhancing the delivery of Reactive Oxygen and Nitrogen Species (RONS). Unlike conventional PAW, PAF generates a fine mist (<5 µm droplets) that mixes efficiently with bioactive plasma species without wetting the product.

## 2 Reactor

The experimental setup consisted in a cylindrical coaxial DBD reactor, fed by 10 sLm of ambient air. The plasma afterglow was injected into a medical glass aerosol nebulizer loaded with double-distilled water. The produced PAF then saturated the treatment chamber where the substrates were positioned.

## 3 Results

PAF was characterized in its physicochemical properties, e.g. droplet dimension and RONS concentration in liquid and gas phase (Fig. 1). Furthermore, the plasma used to produce it was electrically and spectroscopically characterized.

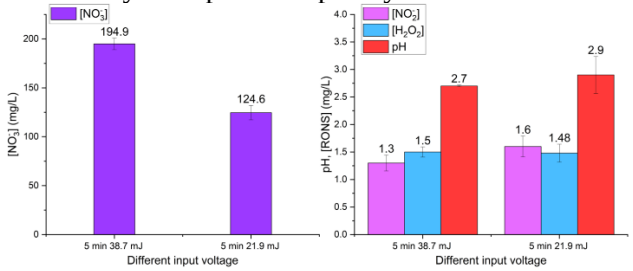



Fig. 1 – pH and RONS concentration in PAF produced using different input voltages.

PAF treatments were tested *in vitro* against major phytopathogenic fungi, significantly reducing spore germination Additionally, *Listeria monocytogenes*, a foodborne pathogen causing severe infections, showed a marked reduction in colony-forming units after PAF treatment. Preliminary *in vivo* tests proved effective against fungal rots on grape and strawberry fruits (Fig. 2). These results highlight PAF's potential as an effective, chemical-free decontamination tool for fresh produce, reducing food waste and losses with beneficial effects on productivity.

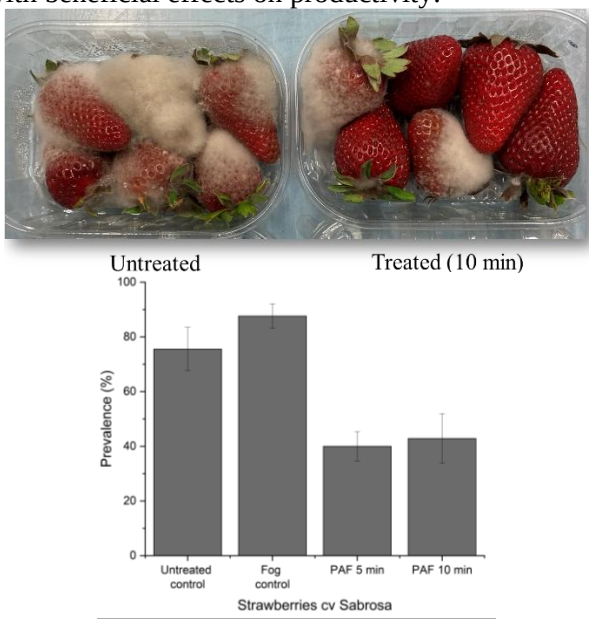



Fig. 2 - Efficacy of PAF against fungal rots on strawberries.

**References**

[1] Aceto D. *et al*, *Frontiers in Physics* **12** (2024), 10.3389/fphy.2024.1399910.

[2] Rotondo P. *et al*, *Scientific Reports* **15** (2025), 10.1038/s41598-025-88369-7.

**Acknowledgements**

DA thanks project NEFERTARI – CUP B53C22003070006, funded by the European Union under the National Recovery and Resilience Plan (NRRP) – NextGenerationEU.

# Hold-Off Voltage Computation in Industrial Gas Insulation

N. Ferreira[1,2], R. Almeida[1,2], P. Almeida[1,2], M. Benilov[1,2], H. Kaufmann[3], M. Koletzko[3], K. Benkert[3]

[1] *Departamento de Física, FCEE, Universidade da Madeira, Largo do Município, 9000 Funchal, Portugal*
[2] *Instituto de Plasmas e Fusão Nuclear, Instituto Superior Técnico, Universidade de Lisboa, 1041 Lisboa, Portugal*
[3] *Siemens Energy Global GmbH & Co. KG, Berlin/Erlangen, Germany*

This work employs a self-consistent method for computing the inception voltage of a low-current discharge in air, which in many cases of industrial relevance is virtually the same as the breakdown voltage. The conditions under study correspond to experiments specifically designed for investigation of breakdown in the exterior of vacuum interrupters. The method is very efficient and can be used in a vast range of conditions, providing as output the inception voltage of a specific setup. The modelling results are in good agreement with the experimental data for various air pressures.

## 1. Introduction

Vacuum interrupters in high-voltage circuit breakers are sometimes enclosed in a pressurized container with air. To prevent electric breakdown in air, sharp edges are avoided in the design and thus the degree of field nonuniformity is reduced. One can expect that the breakdown voltage, $U_b$, is close to the voltage of inception of self-sustaining discharges, $U_c$, in such conditions. In this work, $U_c$ is computed by the so-called resonance method [1] and is shown to coincide with the computed values of $U_b$ and to be in good agreement with experimental results.

## 2. Model and conditions

The numerical model of low-current discharges in high-pressure air employed in this work is detailed in [1]. Results reported in this communication refer to the electrodes being disks with 2 mm thickness and 41 mm radius, with a toroidal end of minor radius of 6 mm. A solid cylindrical dielectric ($\varepsilon$ = 9), radius of 34 mm and height of 22 mm, is placed between the electrodes. The air pressure is 1 to 6 bar.

## 3. Results and discussion

The computed value of $U_c$ for a dielectric with no surface charge present on its surface for 1 bar is 29.2 kV. Fig. 1 shows time variation of computed current for applied voltages equal to precisely this value and 1% higher. In the former case, the discharge extinguishes, and in the latter, breakdown occurs. This example shows that the inception voltage is very close to the breakdown voltage in these conditions.

Computed values of $U_c$ and measured values of $U_b$ are compared in Fig. 2. The agreement between the modelling and experiment is quite good up to $p$ = 4 bar. For higher $p$, the computed $U_c$ keeps increasing almost linearly, whereas the measured $U_b$ shows a kind of saturation. A possible reason for the latter is enhancement of the electron field emission (FE) from the negative electrode. Indeed, modelling with account of FE, assuming the filed enhancement factor $\beta$ equal to 100, shows a good agreement with the experiment also for $p$ > 4 bar.

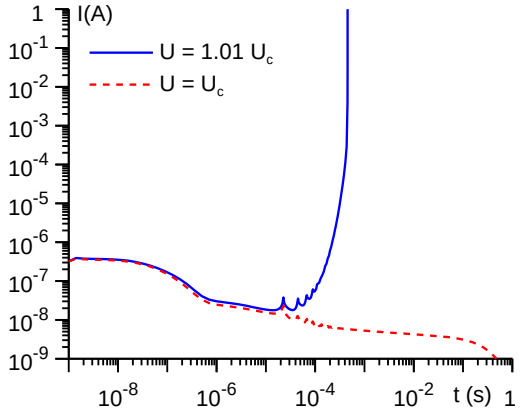



Figure 1: Time variation of current for different applied voltages. $p$ = 1 bar, $U_c$ = 29.2 kV, initial charge density $10^4$ cm$^{-3}$.

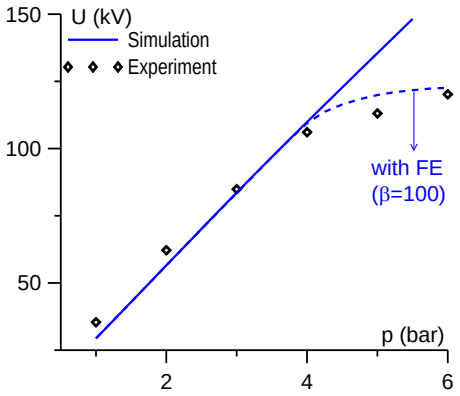



Figure 2: Dependence of the computed $U_c$ (lines) and the experimental $U_b$ (points) on pressure.

## 4. Acknowledgments

This work at UMa was supported by FCT of Portugal under Project Nr. IPFN/UID/50010/2025, and by Siemens Energy Global GmbH & Co. KG.

## References

[1] M. Benilov, P. Almeida, N. Ferreira, R. Almeida, and G. Naidis, *J. Appl. Phys.* **130**, 121101 (2021).

# Investigation of an $Ar/C_2H_2$ temporal plasma afterglow employing MCRS and LIP techniques

M. Salinaro,[1] T. Donders[1] and J. Beckers[1]

[1]*Eindhoven University of Technology, Eindhoven, The Netherlands*

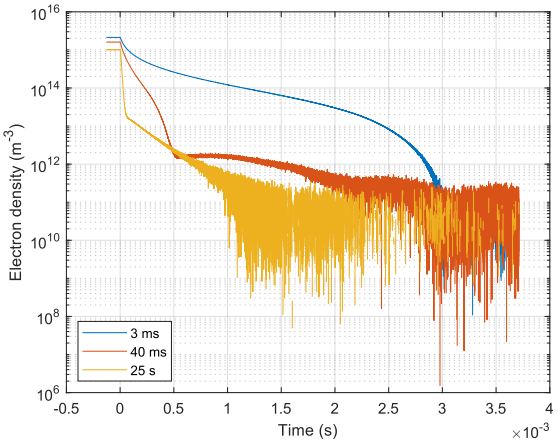
In the present research, the electron and negatively charged species densities of an Argon-Acetylene ($Ar/C_2H_2$) repetitively pulsed plasma afterglow, which are generated in a cylindrical cavity, are studied in detail.
Utilizing the *Microwave Cavity Resonance Spectroscopy* (MCRS), a minimally invasive diagnostic method, allows for the detection of free electrons within a cylindrical cavity. Furthermore, combining MCRS with *Laser-Induced Photodetachment* (LIP) provides an indirect method for detecting negatively charged species.

## 1 Overview

A fascinating aspect of plasma is the afterglow, which marks the transition back to the gas phase. In a temporal plasma afterglow, the power source is turned off, leading to a decrease in electron density.
In a complex plasma, dust particles can either be injected or, as in our case, spontaneously formed when the plasma is ignited in a reactive gas, such as acetylene.

MCRS technique provides a method to probe electrons inside a plasma using microwaves; the eigenfrequency of a cylindrical cavity shifts due to the presence of free electrons. This technique has been proved as an efficient method on timescales down to a few nanoseconds.
As a result of MCRS application, the decay of the electron density can be influenced by the pressure and by the pulse length. The decay time gets longer for higher pressures, while for a fixed pressure the decay time becomes much shorter for longer pulse times, as showed in the figure on the right. It is important to take into account the temperature rise and cavity cleanliness, due to the formation of dust, especially in longer measurements for profile shape corrections.

In combination with MCRS, LIP is an indirect method for the detection of negatively charged species. When laser photons strike, electrons can be detached from negatively charged species, converting them into electron-neutral pairs; the photon energy (hv) must exceed the electron affinity of the negatively charged species. This event causes a sudden local increase in electron density, detectable using MCRS as an additional temporal shift in resonance frequency.




Fixed pressure for different plasma-on times

### References

[1] Hasani, M. ; Marvi, Z. ; Beckers, J. / Probing negative ions and electrons in the afterglow of a low-pressure oxygen radiofrequency plasma using laser-induced photodetachment. In: Journal of Physics D: Applied Physics. 2021 ; Vol. 54, No. 49.

[2] Hasani, M. ; Donders, T.J.M. ; Beckers, J. / Temporal afterglow between two pulses of repetitively pulsed argon-acetylene plasma : measuring electron and negatively charged species densities. In: Journal of Physics D: Applied Physics. 2023 ; Vol. 56, No. 36.

# Modeling of methane plasmalysis by NRP discharges

P.-A. Goutier[1,2], S. Delahaie[1,2], S. McGuire[1], N. Q. Minesi[1], E. Pannier[2], and C. O. Laux[1,2]

[1] *Université Paris-Saclay, CNRS, CentraleSupélec, Laboratoire EM2C, 91190, Gif-sur-Yvette, France*
[2] *Spark Cleantech, 91190, Gif-sur-Yvette, France*

We model the conversion of $CH_4$ towards $H_2$ and $C_2H_2$ at atmospheric pressure via Nanosecond Repetitive Pulsed (NRP) discharges. The chemical kinetic mechanism includes species up to $C_2H_6$ with their corresponding ions. The reaction rate constants available in the literature are reviewed and compared to build a kinetic model valid on the temperature range of interest for plasmalysis of methane. The zero-dimensional kinetic model is then used in a closed constant-volume system to solve the temporal evolution of species concentrations, the gas (heavy) temperature and the electron temperature. This model also includes the interactions between the pulser, the transmission line (co-axial cable), and the load (plasma). The simulation provides the plasma resistance, which can then be used to design optimized pulsing strategies to increase the energy efficiency and yield of plasmalysis.

## 1 Introduction

To reduce the CO2 emissions of high- temperature industries (cement plant, steel mill, glassware, etc…), one solution is to replace fossil fuels with hydrogen. The H2 molecule can be synthesized using the so-called plasmalysis of methane: CH4 → C(s) + 2H2. Plasmalysis is less electricity intensive than water electrolysis (theoretically 5 kWh/kgH2 vs. 40 kWh/kgH2), produces a valuable byproduct (solid carbon), and emits as much greenhouse gas as the electrical energy injected.

The chemical conversion can be performed using a DC discharge to increase the gas temperature and achieve thermal conversion [1]. Cold nonequilibrium NRP discharges can also be employed to fine-tune the temperature, thereby improving the thermal efficiency or the carbon product properties [2]. Moreover, multiple regimes exist in NRP discharges (corona, glow, non-thermal spark, and thermal spark, in order of increasing pressure/current) and their chemical, thermal, and flow dynamic effects must be understood to design efficient reactors and pulsers.

## 2 Numerical model

Experiments with NRP spark discharges at atmospheric pressure show that $CH_4$ is converted mainly towards $C_2H_2$ and $H_2$ [2]. Thus, we first focus on modeling the neutral and electronic reactions and consider hydrocarbons up to $C_2H_6$, as well as their corresponding ions. A literature survey was performed to obtain the reaction rates and thermodynamic data, accounting for their temperature ranges of validity. The rate constants of electron-impact reactions are computed assuming a Maxwellian distribution of electrons. Reverse reaction rates between heavy species are calculated using the equilibrium constant, which requires accurate thermodynamic data.

The model is used to simulate the temporal evolution of species concentrations, gas temperature, and electron temperature over the first tens of nanoseconds, when the discharge can be assumed isochoric. The master equation is solved using Cantera [3], whereas the gas and electron energy equations are solved following the method of Aurora [4].

Special care is given to the injected power, which depends on the voltage applied to the plasma. The incident and reflected voltages along the transmission line are simulated by solving the telegraph equations [5] with a variable resistance as a boundary condition.

**References**

[1] Fulcheri L. *et al*, An energy-efficient plasma methane pyrolysis process for high yields of carbon black and hydrogen, *International Journal of Hydrogen Energy* **48**, 2920 (2023).
[2] Maqueo P. D. G. *et al*, Energy efficiency of a nanosecond repetitively pulsed discharge for methane reforming, *J. Phys. D: Appl. Phys*. **52**, 274002 (2019).
[3] Goodwin D. G. *et al*, Cantera: An Object-oriented Software Toolkit for Chemical Kinetics, Thermodynamics, and Transport Processes, (2024).
[4] Meeks E. *et al*, AURORA: A FORTRAN Program for Modeling Well Stirred Plasma and Thermal Reactors with Gas and Surface Reactions, No. SAND--96-8218, 206570 (1996).
[5] Pavan C. A. *et al*, Tutorial: Electrical measurements in nanosecond pulsed plasma reactors, *J. Phys. D: Appl. Phys*. (2024).

# Enhanced UVC surface decontamination by mercury-free excimer lamp-phosphor systems

A. Baraze[1,2], C. Muja[1], I. Courti[1], F. P. Sainct[1], S. Allix[2], P. Guillot[1] and T. Maho[1]*

[1]*DPHE laboratory, Toulouse University, INU Champollion, Place de Verdun, Albi, France*
[2]*Lab'Science, Boulevard de l'industrie, 37530 Nazelles-Negron*

Microbial contamination of surfaces is a major problem in many sectors, as it facilitates pathogen transmission and threatens public health. UVC radiation has gained popularity as a decontamination method, especially after the COVID-19 pandemic. However, concerns over the environmental impact and user safety of mercury-based UVC devices remain. Despite its proven efficacy against various microorganisms, UVC radiations can be blocked by organic matter, biofilms, or surface irregularities. This study introduces a novel approach combining a KrCl excimer lamp with a UVC phosphor. Using optical emission spectroscopy, imaging, and irradiance measurements, we characterized the lamp and two lamp-phosphor combinations, demonstrating their complementary effects. This synergy was validated against *E. coli*, *S. aureus*, and HAdV5, revealing new opportunities for improved UVC-based decontamination.

## 1 Context

Surface contamination facilitates pathogen transmission, involving a public health risk. While chemical disinfectants are widely used, they generate toxic residues and contribute to antimicrobial resistance. UVC radiation offers a rapid, chemical-free solution, but its effectiveness is limited by surface irregularities and organic matter [1]. To enhance germicidal efficiency, we propose a hybrid mercury-free approach combining a KrCl excimer lamp with a phosphor, extending the emission spectrum for improved microbial inactivation.

## 2 Experimental set-up

The system associates a support material, a phosphor powder, a quartz plate, and a light source (Fig. 1). When the phosphor is excited by the light source ($R_{LAMP}$), it emits radiation ($R_{PHOSPHOR}$). Outside of this situation, the powder does not emit any light. The innovation lies in the complementary interaction between the two radiations. When both are emitted, resulting in $R_{COMBINED}$, microorganisms present on the glass surface are sandwiched between two UVC rays, creating a biocidal synergy.

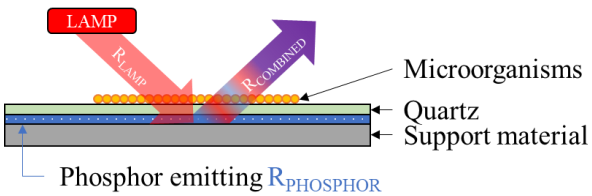



Fig. 1. Schematic of the experimental setup.

## 3 Plasma characterization

Irradiance was measured using a calibrated UVC radiometer (RM-12, Optysec Dr. Gröbel), detecting 200–280 nm wavelengths with 0.01 mW/cm² resolution. Emission from the KrCl lamp and phosphors was analyzed using a SpectraPro PI-HRS-750 monochromator coupled a Pi-Max-4 ICCD camera. Plasma streamer distribution was observed with a Pi-Max-1 ICCD camera.

## 4 Microbiological tests

*Escherichia coli* ATCC 47076 and *Staphylococcus aureus* ATCC 6538 were used in this study as model microorganisms for Gram negative and Gram positive bacteria. The effect of UV treatment on the bacterial morphology was studied by scanning electron microscopy. The virucidal efficacy was investigated by focus-forming assay using human adenovirus HAdV-5 ANCHOR™ as model virus.

## 5 Conclusion

Phosphors enhance excimer lamp efficiency and broaden the available wavelength range, enabling wider applications. These advantages position excimer lamps as viable mercury-free alternatives for rapid and effective disinfection. Future studies could further optimize their performance by exploring operating parameters and host matrix effects.

**References**

[1] Wladyslaw Kowalski. Ultraviolet Germicidal Irradiation Handbook, Springer, (2009).

# Quantitative evaluation of the thrust efficiency in a parallel-plate pulsed plasma thruster

M. Watanabe[1] and D. Matsuzaki[2]

[1] *Institute of Quantum Science, Nihon University, Tokyo 101-8308, Japan*
[2] *Graduate School of Quantum Science and Technology, Nihon University, Tokyo, Japan*

The thrust efficiency of a pulsed plasma thruster is quantitatively evaluated based on two measured specific impulses. The mass consumption of solid propellant is generally used to calculate the specific impulse. However, sublimation from the Teflon propellant surface continues even after the pulse discharge ends, and the gas generated after that is not accelerated and does not contribute to the thrust. The amount of such solid propellant that melts after the discharge is currently unknown. In this research, the thrust efficiency is estimated by the specific impulse based on the velocity of plasma jet. As a result of the experiment, the plasma velocity was estimated to be about 35 km/s. It was found that even if the input energy was changed, about 50 % of the propellant was not accelerated, resulting in a decrease in thrust efficiency.

## 1 Pulsed Plasma Thruster

We are conducting research and development of a pulse plasma thrusters (PPT), which are electric propulsion devices suitable for small satellites [1]. The parallel plate typed PPT is also one of electric thruster that uses a solid (Teflon) as a propellant. The solid propellant is ionized by discharge, and thrust is generated by plasma being launched using electro-magnetic force.

## 2 Research objective

Sublimation from the propellant surface of PPT continues even after the discharge has ended and a large amount of the generated propellant mass does not undergo acceleration [2]. The amount of the solid propellant that melts after a discharge end is currently unknown. This phenomenon prevents improvements of the thrust efficiency of PPTs. The objective of this research is to calculate such thrust loss rate based on the specific impulse.

## 3 Experimental results and discussion

In our experiment, the input energy $W_0$ was adjusted by changing the capacitor voltage to 700, 1000, and 1500 V. The discharge current was 7 to 10 kA, and the half-cycle was about 200 μs.

Specific impulse $I_{\mathrm{sp}}$ [s], which is an index of propellant efficiency, is given by,

$$I_{\mathrm{sp}} = I_{\mathrm{bit}}/(\Delta m \cdot g) \qquad (1)$$

here $I_{\mathrm{bit}}$ [Ns] is impulse bit, which is the time integral of the thrust and $g$ is the acceleration due to gravity. The $\Delta m$ [kg] is the propellant mass consumption per discharge, which also includes non-accelerated propellant mass. The specific impulse, which is estimated by the $\Delta m$, was about 200 to 1000 seconds.

The specific impulse can be also estimated by using a velocity of plasma jet,

$$I_{\mathrm{sp}} = v_p/g = I_{\mathrm{bit}}/(\Delta m_T \cdot g) \qquad (2)$$

here $v_p$ [m/s] is the plasma jet velocity, which was measured by two probes measurement. The $\Delta m_T$ [kg] is propellant mass which is contributes to thrust. The $v_p$ was almost constant of 35km/s as the input energy increased. To estimate the loss of thrust efficiency due to the propellant mass which is not contribute to thrust, we define the quantity shown by

$$\text{Trust Loss Ratio} = (\Delta m - \Delta m_T)/\Delta m \qquad (3)$$

Figure shows the dependence of thrust loss ratio on input energy.

## 4 Conclusions

The solid propellant melted by the discharge contains two masses: one is ionized and accelerated by the Lorentz force, and the other remains unaccelerated at the electrode. It was found that even if the input energy changed, almost 50% of the propellant was not accelerated, resulting in a decrease in thrust efficiency.

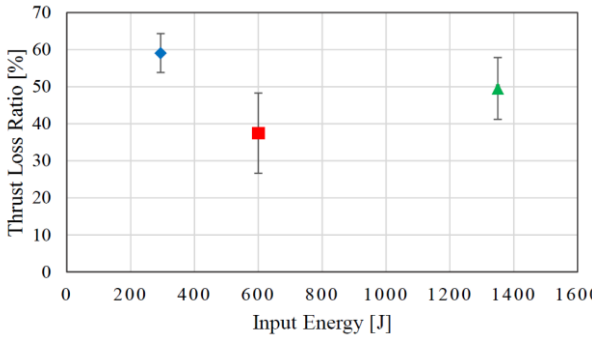



Figure Dependence of thrust loss ratio on input power

## References

[1] R. L. Burton, *et al.*, Journal of Propulsion and Power, Vol. 14, No. 5, pp. 716–735, 1998.
[2] G. G. Spanjers, *et al.* Journal of Propulsion and Power, Vol. 14, No. 4, pp. 554–559, 1998.

# Electron beam divergence and instability in ionospheric plasmas

K. Mori[1] and K. Sakakibara[1]

[1]*Osaka Metropolitan University, Gakuen, Naka, Sakai, Osaka, Japan*

Electron beam divergence and the instability in ionospheric plasma is studied systematically through the Particle-In-Cell simulation. On the basis of the present study, novel methods will be proposed to suppress the expansion of the turbulent electron beam.

## 1 Introduction

A possible method alternative to the Active Debris Removal (ADR) by laser [1] is the ablative propulsion by a remotely transmitted electron beam (e-beam). However, transmitting an e-beam efficiently through the ionosphere plasma over a long distance (10m – 100km) and focusing it to enhance its intensity above the ablation threshold of debris materials are new challenges. In the present study, as a preliminary study of the relevant challenges, the divergence and instabilities of an e-beam in an ionospheric atmosphere are identified quantitatively.

A number of the spacecraft experiments have been performed to probe the space plasma emitting an e-beam from a spacecraft to the ionosphere and/or the magnetosphere since 1960s [2]. It is presumed that an e-beam might be perturbed in the space plasma due to several micro- [3] and/or macro-instabilities [4]. In spite of the early Particle-In-Cell (PIC) simulation studies since 1980s [5], detailed phenomena in realistic conditions are not clear until today. Here, the e-beam density is set slightly different from the density of ionospheric plasma in the range from $10^{10}$ to $10^{12}$ $m^{-3}$. The e-beam velocity is changed from $10^6$ to $10^8$ m/s, in a non-relativistic range.

## 2 Methods

Extensive PIC Open Collaboration (EPOCH) [6] is used. Maxwell equations are solved using the Yee staggered 2nd order Finite-Difference Time Domain scheme. The particle motion is solved in the Buneman-Boris method. The Villasenor and Buneman scheme is used for the electric current deposition. Because the mean-free path of electron in the ionospheric plasma is around $10^2$ m, while the spatial domain is smaller than 15 m, the background plasma is assumed a fully ionized collision-less plasma. The background plasma density ($n_e$ = $n_i$), the beam density $n_b$, and the beam velocity $v_b$ are varied. The background electron temperature $T_e$ is kept at 1000K, the background oxygen ion temperature $T_i$, 100K, and the beam electron temperature $T_b$, 0K. The electron beam width $D_b$ is 10 mm.

## 3 Results

The snapshot of the electron beam density contour is shown in Fig. 1. The beam electron propagates in a laminar fashion up to a certain point, signed as ‘T’ that means ‘Transition’, and then becomes turbulent. In the laminar region, the lateral expansion of the electron beam is suppressed as compared with the case in vacuum. In the turbulent region downstream of the point ‘T’, the beam electron expands abruptly in the lateral direction. In the turbulent region, intermittent wavy structures are made.

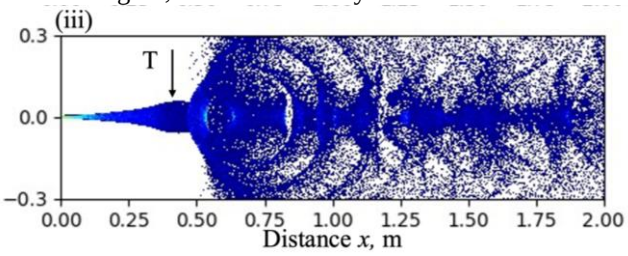



Fig. 1 Density contour for $n_b = 10^{11}$ $m^{-3}$, $v_b = 10^6$ m/s, $n_{i,e} = 10^{11}$ $m^{-3}$.

## 4 Summary

As a result of the present systematic PIC studies, empirical laws for the divergence and the instability length scale have been successfully formulated. In the presentation, we are going to propose a novel artificial method to suppress the beam expansion due to instability.

**References**

[1] Ebisuzaki, T., et al., Demonstration designs for the remediation of space debris from the International Space Station. *Acta Astronautica* **112**, pp. 102-113 (2015).

[2] Winckler, J.R., The application artificial electron beams to magnetosphere, *Reviews of Geophysics* **18**, pp. 659-682 (1980).

[3] Gary, S.P., Theory of Space Plasma Microinstabilities, Cambridge University Press, pp. 34-36,67-85 (1993).

[4] Buneman, O., Dissipation of Currents in Ionized Media, *Physical Review* **115**, pp. 503-517 (1959).

[5] Matsumoto, H., KOMORI, N., Ashour-Abdalla, M., Donatelli, D. Computer Experiments of an Electron Beam Injection into Space Plasma, *Journal of geomagnetism and geoelectricity* **40**, pp.269-292 (1988).

[6] Arber, T. D., et al., Contemporary particle-in-cell approach to laser-plasma modeling, *Plasma Physics & Controlled Fusion* **57**, No. 11 (2015).

# $CH_4$ plasma in water to produce $H_2$ and hydrophilic carbon solids

A. Saito[1], Y. Hayashi[1], T. Miyazaki[2], Y. Inagaki[2], K. Sasaki[2]

[1] *Innovative Technology Laboratories, AGC Inc., Yokohama, Japan*
[2] *Division of Quantum Science and Engineering, Hokkaido University, Sapporo, Japan*

$CH_4$ was decomposed in water using plasma, and the products and energy efficiency were compared with those of gas-phase reactions. Plasma was generated using a pulsed power source. The products were evaluated using a secondary electron microscope (SEM), an X-ray photoelectron spectroscopy (XPS), and a quadrupole mass spectrometer (QMS). The state of the plasma was measured using optical emission spectrometry (OES). $CH_4$ decomposition in water using plasma produces hydrophilic carbon solids, unlike gas-phase reactions.

## 1 Introduction

$CH_4$ decomposition using thermal plasma to produce $H_2$ and solid carbon, such as carbon black is considered a hydrogen production process with low $CO_2$ emissions [1]. Non-thermal equilibrium plasma has also been used to produce different carbon products, such as graphene, and to improve energy efficiency [2]. Most existing studies focused on gas-phase reaction fields. We considered the generation of plasma and decomposing of $CH_4$ in water. Because it is plasma in water, the reaction field is formed in bubbles; therefore, a high density of reactive species is expected. Additionally, we investigated its effects on carbon products and $H_2$ generation.

## 2 Experimental methods

Plasma was generated by applying a pulsed voltage to a pair of 5 mm diameter tungsten electrodes placed in pure water. The frequency was variable from 50 to 300 kHz, and the pulse width was 1.5 μs. The electrode distance was adjusted to 5 mm. Ar/$CH_4$ gas was introduced near the electrodes. For comparison, a setup without water was used for the gas-phase decomposition. The generated decomposition gas was measured using QMS, and the carbon solid content was evaluated using SEM and XPS. The state of the plasma was measured using OES, and its relationship with energy efficiency was examined.

## 3 Results and discussion

Figure 1 shows the OES, SEM images of the generated carbon solid and its dispersion state in water. Fig. 1 (a), (c), and (e) show the results of $CH_4$ decomposition in water, while Fig. 1 (b), (d), and (f) show the results of decomposition in the gas phase for comparison. The emission spectrum of the plasma is shown in (a) and (b). In the decomposition of $CH_4$ in water, in addition to CH, $C_2$, and $H_\alpha$, which appear in the spectrum in gas-phase decomposition, OH and O radicals are also seen, indicating that $H_2O$ interacts with the $CH_4$ plasma. The SEM images of solid carbon (Fig. 1(c) and (d)) show that particulate carbon solids are produced during gas-phase decomposition; however, in water, characteristic flaky carbon solids are also produced. The flaky carbon is a result of growth influenced by etching by the H radicals generated by the plasma.

Fig. 1 (e) and (f) show the dispersion state of the generated solid carbon in water, and solid carbon generated in water is dispersed in water. However, the solid carbon generated in the gas phase does not disperse in water and floats on the water surface; this is related to the presence or absence of OH groups on the surface of the carbon solid.

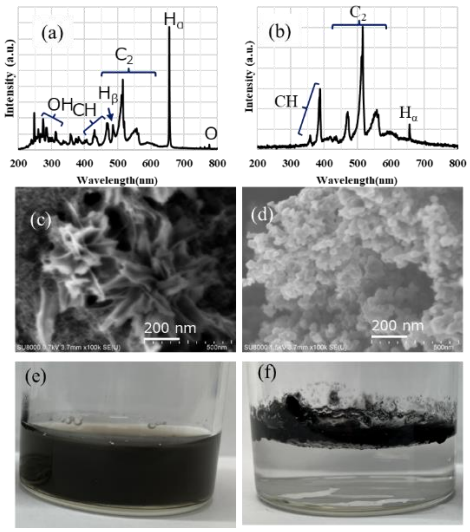



Fig. 1. Comparison of plasma emission and produced solid carbon. (a) and (b) show the results of the plasma emission spectrum. (c) and (d) show SEM images of solid carbon. (e) and (f) are photos showing hydrophilicity.

## References

[1] Laurent Fulcheri et al., International journal of hydrogen energy. 48. 2920. (2023)
[2] Rosemary Johnson et al., FlatChem. 50. 100812 . (2025)

# Development of a Low-Pressure Hydrogen Dielectric Barrier Discharge

J.A.C.R.M. Salij[1], and A. Sobota[1]

[1] *Eindhoven University of Technology, Eindhoven, The Netherlands*

A project is presented to develop a hydrogen dielectric barrier discharge (DBD) at pressures below 100 Pa. To aid in plasma ignition, a meshed electrode will be installed on both sides of a gas gap a local pressure increase obtained from the source geometry will be used to sustain a plasma.

Dielectric Barrier Discharge (DBD) plasma sources are typically developed for use at atmospheric pressure but the versatility in source geometry make it interesting for low-pressure applications as well [1]. This work focuses on designing a DBD source to function as a low-pressure source of both atomic hydrogen and hydrogen ions.

## 1 Designing a Low-Pressure Source Geometry

While DBD sources at atmospheric pressure have historically been the focus of DBD research, the reduced quenching expected in low-pressure plasmas are of interest in the generation of highly energetic plasma species at low temperatures. Published research on low-pressure DBDs is limited to pressures down to approximately 400 Pa [2] which is higher than pressures typically used in plasma processing [3]. To aid in plasma ignition, a converging nozzle inspired geometry is designed to compress a hydrogen flow to achieve locally increased pressures.

The minimum dimensions of a plasma source are determined by the electron mean free path ($\lambda_e$). A source inlet width is chosen at $4\lambda_e$ to create a narrow flow channel as illustrated in Figure 1. The gas gap geometry is characterised by a smooth transition from an inlet width of $4\lambda_e$ to a $\lambda_e$ wide outlet between 10 mm from each opening.

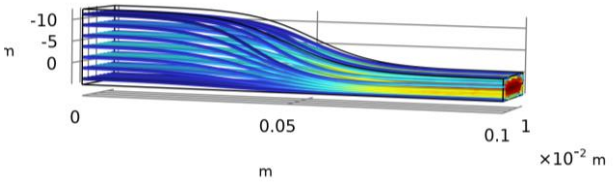



Figure 1: Hydrogen flow streamlines in a converging nozzle geometry at low-pressure.

## 2 A DBD Hydrogen Plasma

No known DBD research exists for hydrogen but the feasibility of a hydrogen plasma at pressures below 100 Pa has been shown in other source types [3]. Evaluation of Paschen's curve for hydrogen shows that a discharge is attainable at low pressures over mm-scale distances with an applied voltage below 1 kV in static conditions [4].

Plasma ignition is aided by local electric field enhancement obtained with a meshed electrode on at least one side of the gas gap [5]. The narrowing nature of the source geometry means that an applied constant potential results in an increase in electric field along the gas flow direction. If the electric field increases faster than the pressure decreases along the gas gap, the reduced electric field increases enabling plasma ignition.

## 3 Conclusion

This poster will present the design process and initial conditions for a low-pressure DBD source. An outlook will be provided on the key unknowns in the project.

**References**

[1] Rahman, M.M. Mechanisms and Signaling Associated with LPDBD Plasma Mediated Growth Improvement in Wheat. *Sci Rep* **8**, 10498 (2018).

[2] Wagenaars, E. Experimental and modelling investigations of a dielectric barrier discharge in low-pressure argon. *J. Phys. D: Appl. Phys.* **39** 700 (2006)

[3] Remes, Z. Optical emission spectroscopy of radio frequency inductively coupled plasma for cold hydrogenation of nanoparticles *IOP Conf. Ser.: Mater. Sci. Eng.* **1050** 012012 (2021)

[4] Lieberman, M.A. and Lichtenberg, A.J. (2005) Principles of Plasma Discharges and Materials Processing. Wiley-Interscience, Hoboken.

[5] Ye, Y. Uniformity of dielectric barrier discharges using mesh electrodes *Plasma Sources Sci. Technol.* **21** 065008 (2012)

# Atomic nitrogen versus vibrational excited molecular nitrogen in ammonia synthesis using low-pressure nitrogen-hydrogen plasma

Koichi Sasaki and Shogo Uebayashi

*Division of Applied Quantum Science and Engineering, Hokkaido University, Sapporo 060-8628, Japan*

We compared the synthesis rate of ammonia in low-pressure nitrogen-hydrogen plasma with the fluxes of atomic nitrogen, vibrational excited molecular nitrogen, and atomic hydrogen. As a result, it was found that the synthesis rate was governed by the flux of atomic nitrogen.

## 1 Introduction

Since nonequilibrium plasmas are useful for producing radicals with high sticking probabilities, it is reasonable to expect their contributions in the catalytic synthesis of useful gases. On the other hand, it has been reported that the dissociative adsorption probabilities of molecular species are enhanced by vibrational excitation [1]. Since nonequilibrium plasmas are efficient for the production of vibrational excites states, the contribution of vibrational excited states is discussed in the plasma-assisted catalytic synthesis. In this work, we compared the contributions of atomic nitrogen and vibrational excited molecular nitrogen in the synthesis of ammonia using a low-pressure nitrogen-hydrogen mixture plasma [2].

## 2 Experiment

We employed a miniature ECR plasma source with a permanent magnet. The total gas pressures were 1.5 − 10 Pa with the mixture ratios $P_{\mathrm{N2}}/P_{\mathrm{H2}}$ between 3/1 and 1/3. No specific catalysts were employed in this experiment, and we expected the synthesis of ammonia via reactions on the surface of the stainless-steel vacuum chamber. The densities of atomic nitrogen and atomic hydrogen were measured by vacuum ultraviolet absorption spectroscopy, while the density of vibrational excited molecular nitrogen was estimated by threshold ionization mass spectrometry. The fluxes of the three active species were evaluated based on their densities, and they were compared with the synthesis rate of ammonia.

## 3 Results and discussion

Figure 1 shows the correlations between the synthesis rate and the integrated flux of atomic nitrogen. The integrated flux means the product of the thermal flux and the effective area of the chamber surface. The dotted line represents the relationship that the synthesis rate and the integrated flux of atomic nitrogen are equal. According to the fact that the majority of the plot points coincide with the dotted line, almost all nitrogen atoms transported to the surface of the stainless-steel tube are used for the synthesis of ammonia. On the other hand, the relationship between the synthesis rate of ammonia and the integrated flux of vibrational excited molecular nitrogen did not show clear correlation. These results are different from those in our previous paper [3], where we observed a positive correlation between the synthesis rate of ammonia and the flux of vibrational excited molecular nitrogen. We believe that the different results are attributable to the difference in the flux ratios of atomic nitrogen and vibrational excited molecular nitrogen in the low-pressure and atmospheric-pressure plasmas.

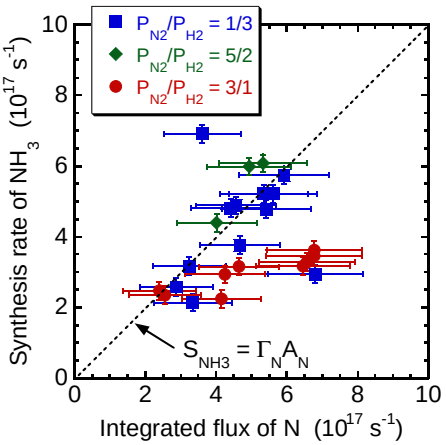



Figure 1: Correlation between the synthesis rate of ammonia and the integrated flux of atomic nitrogen.

## References

[1] Diekhöner, L., *et al.*, *J. Chem. Phys*, **115**, 9028 (2001).

[2] Uebayashi, S. and Sasaki K., *Jpn. J. Appl. Phys.*, in press (2025).

[3] Miyake, A., Shirai, N., and Sasaki, K., *J. Appl. Phys.*, **135**, 213301 (2024).

# Modeling electron beam-induced evaporation of macroparticles in vacuum arc plasma

I. Litovko[1,2], M. Rudolph[1], A. Anders[1,3] and A. Goncharov[4]

[1]*Leibniz Institute of Surface Engineering (IOM), Leipzig, Germany*
[2]*Institute for Nuclear Research NAS of Ukraine, Kyiv, Ukraine*
[3]*Felix Bloch Institute of Solid State Physics, Leipzig University, Leipzig, Germany*
[4]*Institute of Physics, NAS of Ukraine, Kyiv, Ukraine*

The study analytically explores the possibility of evaporating macroparticles in an arc plasma by injecting energetic electrons into the plasma. Modeling shows that macroparticles ≤ 1 μm in diameter can be completely evaporated over time scales typical for their transit from the cathode spot to the substrate (~ 1 ms). It is shown that small microdroplets evaporate at a higher rate. The lower limit working points in terms of plasma electron density, and the electron energy and density of the injected energetic electrons required for droplet evaporation are found.

Erosive plasma sources (vacuum-arc discharges, laser ablation) are very productive tools for synthesizing various functional coatings due to the energy provided by ions and, in the case of DC arcs, their high deposition rate. A significant limitation, however, is the presence of macroparticles in the plasma flow, which prevents the use for demanding applications in e.g. microelectronics. An approach to remove the macroparticles is the use of macroparticle filters. However, their use leads to significant losses (often more than 75%) of material in the plasma flow, which significantly reduces the productivity of deposition processes using such sources. A promising alternative to the use of filters could be the evaporation of macroparticles directly in the plasma flow, if feasible. This may be achieved by providing additional energy, e.g. by injecting energetic electrons into the plasma. The present analysis is considering this approach. It is based on an analytical zero-dimensional model. A system of equations is formulated based on energy and mass balance including electron and ion currents to and from the macroparticle.

For the example of copper macroparticles, we find minimum conditions necessary for complete evaporation of those on time scales typical for the transit between the cathode spot and the substrate deposition. By solving the system of equations, it has been shown that under the action of an electron beam, droplets reach an equilibrium temperature, which does not depend on the droplet size, but smaller droplets reach it faster. The temperature depends significantly on the energy and density of the electron beam, as well as on the plasma density. a lower limit on the plasma density ($n_e \geq 10^{11}$ cm$^{-3}$) and beam density ($n_b \geq 0.001\ n_e$). The higher the beam density, the less energetic beams can be used to pump energy into the plasma flow for droplet evaporation. Figure 1 shows the time required for complete evaporation of macroparticles of different sizes in a plasma with a density of $n_e = 10^{12}$ cm$^{-3}$ by an electron beam with a density of $n_b = 10^{11}$ cm$^{-3}$, depending on its energy.

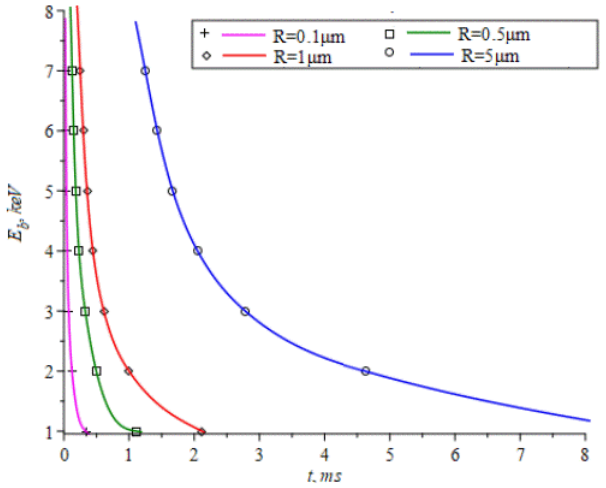



Fig. 1 Dependence time evaporation on electron beam energy for different initial droplet radius ($n_e = 10^{12}$ cm$^{-3}$, $n_b = 0.1\ n_e$)

Typical transit times for macroparticles between their emission at the cathode spot and their deposition onto the substrate lie around 1 ms. Fig. 1 shows that, under the studied plasma conditions, macroparticles with radii ≤ 0.5 μm can be completely evaporated using an electron beam injected into the plasma flow with an energy of 1 keV. For macroparticles with a radius of ~ 1 μm, a beam energy of ≥ 2 keV is required.

This work is supported partly by a grant DFG # 525228371

# Neutralization of Ion Beams at Low Background Gas Pressures

J. Carlsson[1] and M. Hopkins[2]

[1] *Avalanche Energy, Tukwila, Washington, USA*
[2] *Sandia National Laboratories, Albuquerque, New Mexico, USA*

Ion beam neutralization is simulated with the Aleph PIC-DSMC code. Results are compared with Gabovich theory in the parameter range where it is valid (at relatively high beam energies and background gas pressures). At low background gas pressures, electrons from impact ionization are supplemented by injection from a thermionic emitter. Theory and simulation results are compared and discussed.

## 1 Description

Ion beams are used in a wide variety of applications, including impacting a target with ions of controlled energy, or loading fuel ions into a fusion device, such as the Orbitron [1]. The work here is motivated by the latter, where good loading efficiency at high beam currents requires ion beam neutralization by electrons. At high background gas pressure ion impact ionization can provide sufficient electrons to neutralize the beam, as described by the theory of Gabovich [2]. However, in the parameter regime of interest, some approximations made to derive the results of Ref. [2] become questionable. Also, at lower background pressures the electrons created by impact ionization become insufficient for beam neutralization and must be complemented by electrons from an alternative source.

To model scenarios not well described by Gabovich theory, including low beam energies and background pressures, as well as with additional electrons injected from a thermionic emitter, we employ PIC-DSMC simulation using Sandia National Labs' Aleph code. Analytical and numerical results will be compared and discussed.

## 2 Acknowledgements

Sandia National Laboratories is a multimission laboratory managed and operated by National Technology & Engineering Solutions of Sandia, LLC, a wholly owned subsidiary of Honeywell International Inc., for the U.S. Department of Energy's National Nuclear Security Administration under contract DE-NA0003525. This material is supported by the U.S. Department of Energy, Office of Science, Office of Fusion Energy Sciences.

**References**

[1] M. Affolter, et al., *AIP Advances* **14** 8 (2024)
[2] M. D. Gabovich, *Sov. Phys. Usp.* **20** 134 (1977)

# Study of rotating structures in E×B plasmas and their implications on charged particle transport

J. Stevens[1], F. Gaboriau[1], L. Garrigues[1], and G. Fubiani[1]

[1] *LAPLACE, Université de Toulouse, CNRS, INPT, UPS, Toulouse, France*

This presentation covers the early stages of an experimental and computational study on rotating structures and their impact on charged particle transport in a Penning discharge. A Penning discharge is an E×B plasma, where magnetic field lines run axially in a cylindrical chamber and electric field lines point mainly in the radial direction. Charged particles experience an azimuthal or closed drift while remaining confined along magnetic field lines, enabling efficient electron confinement and sustaining ionization. This closed-drift setup is common in low temperature partially magnetized plasma applications (Hall thrusters, magnetrons, Penning gauges, etc.). However, azimuthal plasma rotation can trigger instabilities that enhance radial particle transport, reducing electron confinement. These effects remain poorly understood, making it crucial to investigate their origins and role in charged particle transport.

A Penning discharge is created in a long cylindrical chamber with magnetic field lines running parallel to its central axis. The plasma created inside said chamber is partially magnetized, meaning that the electrons are strongly affected by the magnetic field while the ions remain unperturbed due to their large Larmor radius. The plasma is generated by an electron beam[1], most often an emissive $LaB_6$ cathode or an RF antenna source, that injects seed electrons with a given energy at one end of the cylinder that interact with the plasma bulk, releasing their energy through ionising collisions (see Fig. 1) The velocity difference between the electrons and the ions can lead to the formation of rotating plasma instabilities in the plane perpendicular to the B field. These instabilities, or drift waves, can present different properties depending on the radial electric field and density gradient in the plasma, both of which can be controlled by modulating the magnetic field strength and the voltage of the end plate of the cylinder opposite to the electron source, which in turn modifies the charged particle confinement. These drift waves appear as rotating structures, resembling spokes when observed from an end plate of the cylinder, that exhibit a rigid azimuthal rotation around the central axis of the plasma column, all while driving charged particles onto the lateral wall of the cylinder, across the magnetic field lines. Two cases of gradient drift instabilities (GDIs) with notably different profiles and behaviours have been observed numerically depending on the respective orientation of the radial electric field and density gradient[2]. In the case when the radial electric field and density gradient are collinear, a rotating structure presenting a low mode number (m = 1 or 2) and a rotational frequency of a few tens of kHz is observed. This instability is called the Collisionless Simon-Hoh Instability (CSHI)[2]. In the case where $E_r$ and $\partial n/\partial_r$ are in opposite directions, a different GDI forms with a much larger mode number ($m \geq 8$) and a rotational frequency around 1 MHz. However, little experimental work has been published on these particular GDIs in a Penning discharge and that is therefore the main focus of the work presented here. As part of the IRENE project, an adaptable and transportable Penning-type plasma chamber has been built from scratch at the Laplace laboratory, Toulouse. At this conference, preliminary plasma properties such as electron temperature and density will be shown.

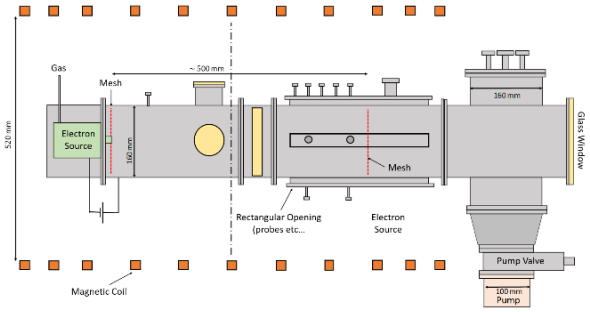



Figure 1 : Schematic of the IRENE plasma chamber

**Acknowledgments**

J. S. benefits from a PhD funding from the French Ministry of Research. This work is supported by the French Research Group on low temperature plasmas (GdR EMILI) and the INSIS CNRS Institute. We would like to thank A. Escarguel for the generous donation of the magnetic coils for the chamber.

**References**

[1] E. Rodríguez *et al.*, "Boundary-induced effect on the spoke-like activity in *E* × *B* plasma," Phys. Plasmas **26**, 053503 (2019).

[2] M. Tyushev *et al.*, "Mode transitions and spoke structures in E×B Penning discharge," Phys. Plasmas **32**, 013511 (2025).

# Dynamics of CCRF argon plasma with aerosol pulsed injection

L. A. Valdovinos Aguilar[1,2], M. Bradley[1], L. Couëdel[1,3], R. Clergereaux[2]

[1] *University of Saskatchewan, Saskatoon, SK, Canada*
[2] *Laboratoire Plasma et Conversion d'Energie, Université de Toulouse – CNRS, Toulouse, France*
[3] *Aix-Marseille Université, CNRS, PIIM UMR 7345, Marseille, France*

This study investigates the impact of pulsed aerosol injections on Capacitively-Coupled Radio-Frequency (CCRF) argon plasma, examining evolution of pressure, self-bias voltage ($V_{DC}$), electron density, RF voltage ($V_{RF}$) and RF current ($I_{RF}$) amplitudes. These variations are influenced by plasma-droplet interactions.

## 1 Introduction

Plasma has been used in material processing, etching, thin film deposition, and surface treatment. In contrast, from classical vapour assisted plasma process, injection of liquid aerosols enables formation of various innovative coatings including nanocomposite thin films [1]. Nevertheless, it introduces new plasma physics. Here, we discuss the effects of pulsed-aerosol injection in a CCRF argon plasma.

## 2 Material and Methods

CCRF argon plasma reactor consists of stainless steel of 30 cm in diameter and separated by 6 cm. The shower top electrode enables gas injection and the RF powered electrode at the bottom is used as substrate holder. A continuous argon flow was injected for constant pressure stability at $5 \times 10^{-2}$ mbar. A Pentane aerosol with argon was injected using a Direct Liquid Injection system. Plasma was ignited prior to the first aerosol injection with a forward RF power set at 75 W (on the power supply), the matching box being in manual mode [2]. During the pulsed-aerosol injection, the working pressure is recorded with a Baratron gauge. The electron density was measured with a microwave interferometer, self-bias voltage was measured directly from the power supply and $V_{RF}$ and $I_{RF}$ amplitudes from a RF probe at the powered electrode.

## 3 Argon-Pentane injection

Figure 1 shows a typical evolution of the gas discharge parameters during a pulsed aerosol injection. Pressure rapidly increases up to a maximal, reaching equilibrium after 1.2 s. This injection also affects the plasma parameters. For example, $V_{DC}$, $V_{RF}$ and $I_{RF}$ amplitudes exhibit two stages: an initial drop is observed on the first 200 ms after the pulse, when $n_e$ and pressure are at their maximum. However, $n_e$ shows a small decrease before returning to its pre-pulsed value.

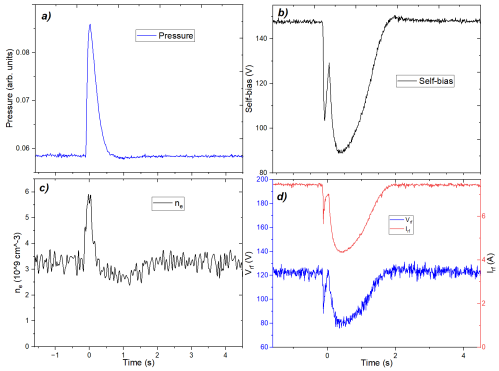



Figure 1: Time-resolved for CCRF argon plasma with pulsed aerosol injection: a) pressure, b) $V_{DC}$, c) $n_e$, and d) $V_{RF}$ and $I_{RF}$ amplitudes at the powered electrode.

## 4 Conclusion

Pulsed-aerosol injection alters plasma parameters, $V_{DC}$, $V_{RF}$ and $I_{RF}$ amplitudes due to plasma-droplet interaction. Understanding these effects will help at the optimization of thin film deposition processes.

## Acknowledgements

Authors want to thank Réseau Plasmas Froids du CNRS for microwave interferometry equipment loan and Mitacs for the funding Global Link Research Award.

## References

[1] Carnide, G. *et al. Coatings*, **13**, pp.630 (2023)
[2] Carnide, G. *et al. Plasma Chemistry and Plasma Processing*, **44**, pp.1343-1356 (2024).

# Optical actinometry in $CF_4$-containing plasmas

M. Ribeiro[1], N. Britun[2], V. Guerra[1] and T. Silva[1]

[1]*Instituto de Plasmas e Fusão Nuclear, Instituto Superior Técnico, Universidade de Lisboa, 1049-001 Lisboa, Portugal*
[2]*Center for Low-Temperature Plasma Sciences (CLPS), Nagoya University, 464-8603 Nagoya, Japan*

This study introduces an actinometry-based framework that combines emission spectra obtained in low-pressure RF discharges, sustained in $CF_4$-containing mixtures, with the LoKI simulation tool to assess the concentration of Fluorine (F) atoms. The work is complemented by a dedicated swarm analysis in $CF_4$, while systematically analysing different cross-section data relevant to actinometry measurements.

## 1 Introduction

The concentration of atomic plasma species formed as a result of molecular decomposition is crucial for fundamental research and material processing. While absorption diagnostic-based methods can be used to determine the concentration of plasma species, their applicability is often limited by the need for bulky and expensive equipment. Optical actinometry, which relies on measuring spontaneous emission, is often preferred due to its simplicity, cost-effectiveness, and versatility across a wide range of plasma conditions. Despite its simplicity, the proper use of actinometry depends on an accurate knowledge of electron-impact cross sections and access to a reliable electron energy distribution function (EEDF). In response to these challenges, many recent efforts have focused on validating actinometry methods against experimental data obatained with more advanced methods such as VUV absorption spectroscopy (see e.g. [1]). The present work builds upon these efforts and introduces an actinometry-based framework that combines emission spectra, obtained in low pressure (1-100 Pa) RF discharges, with the LisbOn KInetics Boltzmann solver, using a two-term approximation (LoKI-B) [2] and a Monte Carlo technique (LoKI-MC) [3]. This framework is used to obtain the EEDF, swarm data (see section 2) and rate coefficients relevant to actinometry measurements targeted at determining the concentration of Fluorine (F) in $CF_4$ discharges.

## 2 Results

Systematic analyses of various cross-sections were performed to derive excitation rates coefficients and electron transport coefficients in $CF_4$-containing discharges. Figure 1 illustrates this analysis, showing the characteristic energy for $CF_4$, calculated with LoKI-B and LoKI-MC, using the cross-section set from Kurihara et al. [4]. Consistent with the literature [5], these results demonstrate not only the importance of these modeling techniques to reproduce measured electron transport data in $CF_4$, but also differences between the outcomes obtained from Boltzmann and Monte Carlo solvers. The impact of these techniques and cross-section data on the determination of atomic species in $CF_4$ discharges via actinometry will be discussed in the presentation of this work.

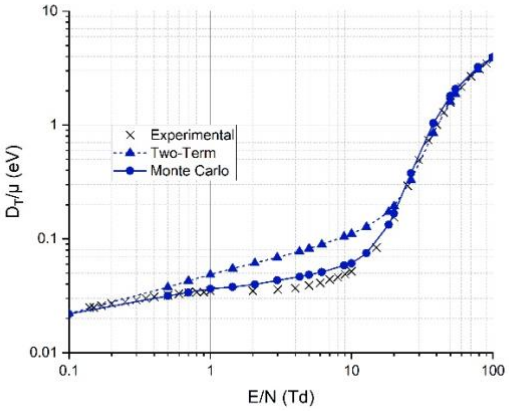



Figure 1 Characteristic energy of $CF_4$ as function of E/N. The lines are calculation results obtained with LoKI-B (triangles) and LoKI-MC (circles). The cross sections used for these calculations and the experimental data (crosses) can be found in Kurihara et al. [4]

## References

[1] J-P. Booth et al *Plasma Sources Sci. Technol.* ***29*** (2020) 115009.
[2] A. Tejero-del-Caz et al *Plasma Sources Sci. Technol.* **28** (2019) 043001.
[3] T. C. Dias et al *Computer Physics Communications* **282** (2023) 108554.
[4] M. Kurihara et al *J. Phys. D: Appl. Phys* **33** (2000) 2146–2153.
[5] S. Dujko et al *Facta Universitatis* **6** (2008) 57-69, DOI: 10.2298/FUPCT0801057D.

## Funding acknowledgments

IPFN activities we supported by the Portuguese FCT-Fundação para a Ciência e a Tecnologia, under funding to IPFN (DOI: 10.54499/LA/P/0061/2020, 10.54499/UIDB/50010/2020,10.54499/UIDP/50010/2020, and 10.54499/PTDC/FIS-PLA/1616/2021).

# Automated Processing of High-Frequency Electrodeless-Lamp Spectra

N. Zorina[1], G. Revalde[1], A. Skudra[1]

[1]*Institute of Atomic Physics and Spectroscopy, Faculty of Exact Sciences and Technology, University of Latvia, Jelgavas str. 3, LV–1004, Riga, Latvia*

Spectrum element recognition is crucial in various scientific and industrial applications, such as plasma diagnostics, material characterization, and astrophysics. This paper presents a Python-based application for spectral peak detection and element identification in spectra emitted from high-frequency electrodeless lamps. The proposed application serves as spectrum analyzer for rapid element detection. Both simulated and experimental spectra identification examples are presented, including emission spectra containing elements such as Hg, Cd, Ar, Kr, and As.

.

## 1 Introduction

High-frequency electrodeless lamps (HFEDLs) are known for producing intense and narrow spectral lines, with a full width at half maximum (FWHM) of about 0.03–0.12 $cm^{-1}$. Elemental recognition in HFEDL spectra is critical for applications that require well-defined emission line profiles of specific elements for optimal performance [1]. However, HFEDL spectra typically contain a large number of data points, each corresponding to a different wavelength, making manual analysis challenging and time-consuming.

This work presents a Python-based application for spectral peak detection and element identification. The following Python libraries were used: PyQt6 for the graphical user interface, which allows users to load spectral data, adjust peak detection parameters, view detected peaks, and export results as a graphic or in tabular form; SciPy for peak detection; and Pandas for data processing.

## 2 Results and discussion

The algorithm incorporates adaptive thresholding for peak classification, comparison with reference spectral lines from the National Institute of Standards and Technology (NIST) database [2] or a user-provided reference dataset, and automatic FWHM estimation for precise peak validation. The application provides an efficient solution for spectral data analysis, significantly reducing the need for manual interpretation.

The application was tested on multiple spectral datasets. To evaluate its accuracy, multiple spectral datasets were simulated using Gaussian functions. Various experimental conditions, such as temperature and different levels of noise, were also simulated. Additionally, experimental spectral lines emitted from HFEDL lamps filled with different element mixtures—such as mercury, argon, krypton, and arsenic—were analyzed. The experimental emission spectra were measured using a Yvon 1000M high-resolution spectrometer. The adaptive thresholding method effectively filtered out noise, and the peak matching algorithm accurately identified elements. However, further refinements in tolerance optimization could enhance precision.

## 3 Conclusion

This work introduces a Python-based application for automated spectral peak detection and element identification. By integrating adaptive thresholding, peak classification, and graphical visualization, the system provides an efficient tool for spectral analysis. Future improvements may include machine learning-based classification models to enhance element identification accuracy.

**Acknowledgements**

The work was supported by 1.1.1.9 Research application No 1.1.1.9/LZP/1/24/023 of the Activity "Post-doctoral Research" " Developing an artificial neural network model to analyze emission spectra of high-frequency electrodeless lamps "

**References**

[1] Zorina N. et al., Comparison of As, Hg and Tl high-frequency electrodeless lamps for detection of environmental pollution, ETR, vol. 1, 275–280, (2021)

[2] Sansonettia J. E et al., Handbook of Basic Atomic Spectroscopic Data, *J. Phys. Chem. Ref. Data* 34, 1559–2259 (2005)

# Quantification of ammonia production in a surfaguide discharge over a wide pressure range

V. Wolf[1], R. Friedl[1] and U. Fantz[1,2]

[1] *AG Experimentelle Plasmaphysik, Universität Augsburg, 86135 Augsburg, Germany*
[2] *Max-Planck-Institut für Plasmaphysik, Boltzmannstraße 2, 85748 Garching, Germany*

A microwave surfaguide discharge is used to study $NH_3$ formation in a low to mid pressure plasma as possible small scale, intermittent use alternative to conventional thermal synthesis (Haber-Bosch). Generator power, pressure, input gas composition and presence of a Ru catalyst in the downstream of the discharge are varied while mass spectrometry and optical emission spectroscopy in optical and vacuum-UV range are used to correlate changes in the $NH_3$ output to plasma parameters. The pressure is identified to be of major influence, where lower pressure leads to higher $NH_3$ concentration.

## 1 Experimental Setup

A $H_2$ - $N_2$ gas flow is introduced into a quartz glass tube with the length of $1\,\mathrm{m}$ and an inner diameter of $17\,\mathrm{mm}$. Using a waveguide-based launcher (surfaguide), a plasma column is generated in the quartz tube by microwave surface wave propagation. Downstream of the plasma, a movable package made of stainless steel mesh containing a commercial Ruthenium catalyst ($2\,\mathrm{wt}\%$ Ru on $\gamma$-$Al_2O_3$ pellets) can be introduced.
For detecting the composition of the output gas mixture, a residual gas analyzer is located on the downstream side of the experiment. Using a line-of-sight (LOS) perpendicular to the quartz tube, optical emission spectroscopy is used to correlate the $NH_3$ output and plasma parameters, where the vibrational population and atomic density of nitrogen are seen as the most relevant ones. While the former is obtained from the second positive system (SPS) together with $T_{\mathrm{gas}}$, the latter can be monitored by VUV spectroscopy. The vacuum UV (VUV) spectrometer (Resonance VS-7550), capable of recording spectra in the range of $112$ - $400\,\mathrm{nm}$, is attached to an axial LOS through the plasma. This provides access to a set of atomic and molecular components of both nitrogen and hydrogen.

## 2 Measurements

In this study the effects of pressure between circa $20\,\mathrm{Pa}$ and $10000\,\mathrm{Pa}$, the hydrogen-nitrogen gas composition from $10\,\%$ to $90\,\%$ $N_2$, the variation of flow between $9\,\mathrm{sccm}$ and $72\,\mathrm{sccm}$, the power output of the generator in the range of $150$ - $1200\,\mathrm{W}$, and the presence and position of the Ru-$Al_2O_3$ catalyst on $NH_3$ production are investigated.

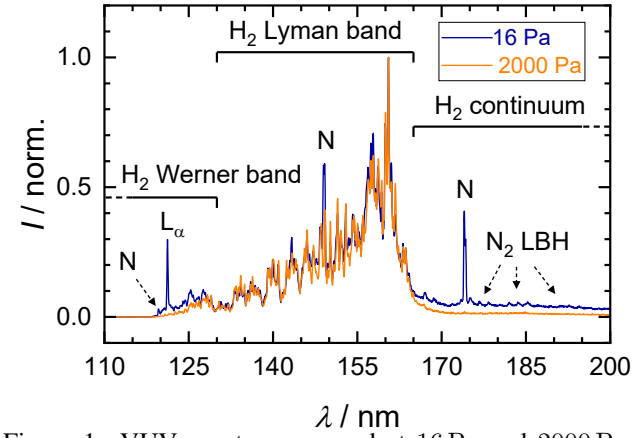



Figure 1: VUV spectra measured at $16\,\mathrm{Pa}$ and $2000\,\mathrm{Pa}$, each normalized to the most intense part of the $H_2$ Lyman band. A $H_2$-$N_2$ mixture of 1:1 is used at a generator power of $600\,\mathrm{W}$ (no catalyst present).

In Figure 1, a comparison of two VUV spectra (normalized) taken at $16\,\mathrm{Pa}$ and $2000\,\mathrm{Pa}$ is shown. While at $16\,\mathrm{Pa}$ several atomic nitrogen and hydrogen lines can be observed, these vanish compared to the Lyman band at $2000\,\mathrm{Pa}$. From $16\,\mathrm{Pa}$ to $2000\,\mathrm{Pa}$, the ratio of atomic nitrogen to the molecular SPS drops by a factor of $12.7$, indicating a reduced dissociation degree for nitrogen with increased pressure. In a similar trend, the $NH_3$ concentration decreases from $24.5$ ‰ at $16\,\mathrm{Pa}$ to $1.9$ ‰ at $2000\,\mathrm{Pa}$ (no catalyst present), which equals a drop by a factor of $12.9$.
Considering that the dissociation of nitrogen, which is also recognized as rate limiting step for $NH_3$ generation, is mainly driven by electron collisions, a decrease in the atom-to-molecule ratio hints at a diminution of electron driven processes. This indicates an overall change of the plasma regime with pressure towards heavy-particle processes. This is corroborated by the gradual equilibration of $T_{\mathrm{rot,X}}$ and $T_{\mathrm{vib,X}}$ observed during pressure increase.

# Mass spectrometry of plasma reactive species produced by a surface DBD source

N. Škoro[1], N. Selaković[1] and N. Puač[1]

[1] *Institute of Physics, University of Belgrade, Pregrevica 118, 11080 Belgrade, Serbia*

In this study a Molecular Beam Mass Spectrometer was used to investigate production of reactive species by a DBD source. The source was operated at different powers and frequencies, in air and gas mixtures and measurements were conducted at different distances from the electrode. The analysis revealed dependence of concentrations of reactive species on operating parameters of the discharge.

## 1 Introduction

As non-thermal plasmas at atmospheric pressure can be generated in ambient air or gas mixture, they have been studied extensively for different applications, including recently established applications in agrifood field [1]. Dielectric barrier discharge (DBD) sources are particularly convenient, with respect to other atmospheric pressure sources, as they can create large effective surfaces of active plasma region. So, plasma treatments with DBD source can be utilized for effective decontamination of molds, mycotoxins and other pathogens from food products [2]. In these processes ratio between concentrations of reactive short-lived and long-lived species plays a key role. Formation of reactive species depends on several parameters, e.g. input power, driving signal frequency, gas mixture etc. Mass spectrometry is a plasma diagnostic technique that can provide immediate information on created neutral and ionic species in the interaction volume which presents a crucial input parameter for studying interaction processes and revealing plasma mechanisms in plasma treatment [3].

## 2 Experimental setup

In this study mass spectrometry was used to investigate production of reactive species by a DBD source. The source was operated at different powers and frequencies, in air and gas mixtures and measurements were conducted at different distances from the electrode. The analysis of reactive species was performed using HIDEN Molecular Beam Mass Spectrometer (MBMS) HPR60 device.

For detection of neutral reactive species, the Residual Gas Analyzer (RGA) mode of the MBMS was employed in two operational ways. In the MID scan mode, a real-time monitoring of radical evolution under both active and inactive discharge conditions was performed. A shutter in the inner side of the sampling orifice (SL) allowed to measure the sum of foreground and backgound (SL open) and the background signal (SL closed).

## 3 Results and conclusion

In Fig.1 we show measurement of $O_3$ concentration at 2 distances from the source. There is a significant peak at the moment of plasma inception (6 minutes after start of the recording) when there was a gradual increase in input voltage from 0 V to 200 V.

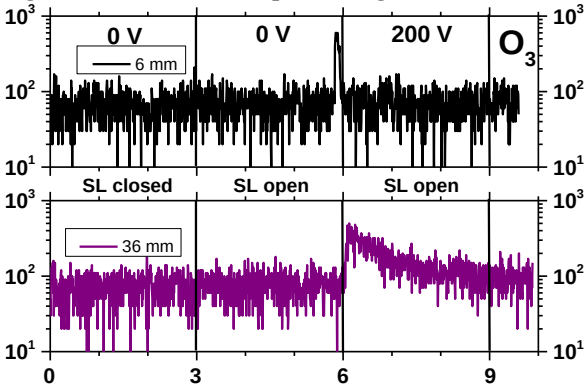



**Figure 1.** O3 time evolution in case of plasma off (0 V) and on (200 V) conditions for different distances (6 mm and 36 mm) from the plasma source to the mass spectrometer sampling orifice.

This behaviour suggests that ozone formation is initially enhanced at lower plasma power, while increasing voltage up to 200 V leads to a stabilization effect.

***Acknowledgments:*** *This work was supported by the MSTDI Republic of Serbia grant no. 451-03-66/2024-03/200024.*

**References**

[1] Bilea, F. et al. Non-Thermal Plasma as Environmentally-Friendly Technology for Agriculture: A Review and Roadmap. *Critical Reviews in Plant Sciences* **43**, 428–486 (2024).

[2] Janić Hajnal, E. et al. Effect of Atmospheric Cold Plasma Treatments on Reduction of Alternaria Toxins Content in Wheat Flour. *Toxins* **11**, 704 (2019).

[3] Maletić, D. et al. Detection of atomic oxygen and nitrogen created in a radio-frequency-driven micro-scale atmospheric pressure plasma jet using mass spectrometry. *Plasma Phys. Control. Fusion* **54**, 124046 (2012).

# Influence of axial magnetic field on the ion flux uniformity in a VHF CCP

D. Eremin[1], Yu. Sharova[1], L. Xu[2] and R.-P. Brinkmann[1]

[1] *Institute of Theoretical Electrotechnics, Ruhr University Bochum, Universitätsstraße 150, 44801 Bochum, Germany*
[2] *Department of Physical Science and Technology, Soochow University, 215006, Suzhou, China*

Capacitively coupled plasma (CCP) discharges are one of the most used tools for plasma processing technologies owing to its simplicity in terms of technical implementation and its ability to sustain plasmas in a wide range of operating parameters. For etching or deposition technologies it is often desirable to have a relatively low pressure of the working gas, which leads to a decreased power absorption efficiency. A common way to counter this issue and to increase the power absorbed by electrons from the electric field is to use a very high frequency (VHF) harmonic in the driving voltage resulting in an increase of the plasma density and ion flux to electrodes, the latter parameter being of immediate relevance for the plasma processing applications. However, the fundamental high frequency harmonic and its higher harmonics in the discharge current, which arise due to nonlinearities in the sheath motion, tend to excite surface modes propagating in the radial direction between the electrodes, electron-depleted plasma sheaths, and plasma bulk leading to undesirable nonuniformities of the plasma density and ion flux in the radial direction [1,2]. It is interesting to investigate the influence of an axial magnetic field on the excitation of such surface modes, since it is known to shift in the presence of a magnetic field to higher frequencies. For instance, the plasma series resonance frequency, which is related to excitation of such a mode, becomes the upper hybrid frequency [3].

The present contribution investigates excitation of surface modes and the related radial nonuniformities in a model CCP reactor operated at low pressures and very high driving frequencies [4] using the fully electromagnetic implicit charge- and energy-conserving PIC/MCC code ECCOPIC2M [4,5] enhanced by a constant axial magnetic field. It is shown that such a magnetic field indeed favourably affects the radial uniformity of ion fluxes to electrodes.

**References**

[1] M.A. Lieberman, J.P. Booth, P. Chabert, J.M. Rax, and M.M. Turner, Plasma Sources Sci. Technol., 11, 283 (2002)
[2] L. Sansonnens, A.A. Howling, and Ch. Hollenstein, Plasma Sources Sci. Technol., 15, 302 (2006)
[3] D. Eremin, D. Engel, D. Krüger, S. Wilczek, B. Berger, M. Oberberg, C. Wölfel, A. Smolyakov, J. Lunze, P. Awakowicz, J. Schulze, R.P. Brinkmann, Plasma Sources Sci. Technol. 32, 045007 (2023)
[4] D. Eremin, E. Kemaneci, M. Matsukuma, T. Mussenbrock, and R.P. Brinkmann, Plasma Sources Sci. Technol., 32, 044007 (2023)
[5] D. Eremin, Yu. Sharova, L. Heijmans, A.M. Yakunin, M. van de Kerkhof, R.-P. Brinkmann, E. Kemaneci, "Electromagnetic particle-in-cell modeling of an electron cyclotron resonance plasma discharge in hydrogen", submitted to Plasma Sources Sci. Technol. (2025)

# Disinfection of Bacteria- and Fungi-Contaminated Tap Water Using a Gliding Arc in Air with $CO_2$ Bubbling

M. Mobasher, M. Ahmed, A. ElSebaei, A. Zaki, M. Awad, M. El Shaer

*Plasma & Energy Applications Research Laboratory, Department of Engineering Physics and Mathematics, Faculty of Engineering, Zagazig University, 44519, Zagazig, Egypt*

Gliding arc air plasma, generated using knife-shaped electrodes, is applied to a water sample with $CO_2$ bubbling for disinfection. Air plasma produces reactive species ($O_3$, •OH, $NO_x$, $H_2O_2$) that disrupt microbial metabolism, while $CO_2$ bubbling lowers the water's pH, increases oxidative stress, and enhances microbial inactivation. Microbial tests on *Escherichia coli*, *Staphylococcus aureus*, and *Aspergillus flavus* showed D-value reductions of 30%, 36%, and 40%, respectively, when air plasma was combined with $CO_2$ bubbling, compared to air plasma alone. These results confirm that $CO_2$ bubbling enhances plasma disinfection efficiency, significantly reducing the time required for microbial inactivation.

## 1 Materials and methods

The gliding arc plasma (GAP) setup, shown in Fig. 1, consists of two knife-shaped stainless-steel electrodes, each 80 mm long and 20 mm wide at its broadest point, with a 2 mm gap at the narrowest section. A neon-sign transformer supplying 9 kV and up to 30 mA ensures arc ignition. Compressed air, used as the working gas, is injected at a flow rate of 12 SLM through a 2 mm nozzle positioned between the electrodes. A 100 mL water sample is treated in a 250 mL beaker, which has a small opening at the bottom for $CO_2$ injection. The distance between the lower tips of the electrodes and the water surface is fixed at 4 cm. To minimize contamination, the entire system is enclosed within a UV sterilization cabinet.

## 2 Results

GAP combined with $CO_2$ bubbling in water is a promising method for pathogen disinfection [1, 2]. Plasma in air generates reactive species such as ozone ($O_3$), hydroxyl radicals (•OH), nitric oxides ($NO_x$), and hydrogen peroxide ($H_2O_2$), which penetrate the water and disrupt microbial metabolism. Additionally, $CO_2$ bubbling lowers the water's pH, increasing oxidative stress and accelerating microbial inactivation.

We treated *Escherichia coli* (E. coli), a gram-negative bacterium; *Staphylococcus aureus* (S. aureus), a gram-positive bacterium; and *Aspergillus flavus* (A. flavus), a fungus, using plasma and $CO_2$ injected into the water. For a treatment duration of 20 minutes, we recorded that D-value percentage reductions for bacteria and fungi were enhanced when using air plasma with $CO_2$ bubbling compared to air plasma alone—by 30% for *E. coli*, 36% for *S. aureus*, and 40% for *A. flavus*.

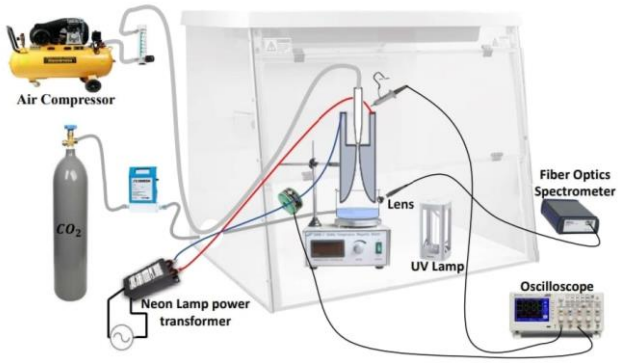



Fig. 1 GAD enclosed in a UV sterilization cabinet

## 3 Conclusion

The percentage change in D-values confirms that $CO_2$ enhances plasma disinfection efficiency, accelerating microbial inactivation. E. coli is less resistant, yet $CO_2$ still improves its inactivation by increasing acidity and oxidative stress. S. aureus is more resistant; however, $CO_2$ significantly enhances disinfection by breaking down its protective barriers. A. flavus is highly resistant, but the largest percentage reduction in D-value suggests that $CO_2$ has a strong effect when combined with plasma.

**Acknowledgements:** Authors acknowledge the support during this work of the Science, Technology & Innovation Funding Authority (STDF), Egypt, under grant number: Applied Science Grant- 45970.

**References**

[1] Kim H.S., Cho Y.I., Hwang I.H., Lee D.H., Cho D.J., Rabinovich A., Fridman A. Use of plasma gliding arc discharges on the inactivation of E. Coli in water. Sep. Purif. Technol. 120, 423-428 (2013).
[2] Garrido Sanchis A., Pashley R., Ninham B. Virus and bacteria inactivation by $CO_2$ bubbles in solution. npj Clean Water. 2, 5 (2019)

# Comparison of three plasma reactors in contact with water: application to micro-pollutant degradation

C. Ben Othmen[1*], M. Wartel[1], S. Rudz[1], S. Iséni[1] and S. Pellerin[1]

[1]*GREMI, UMR 7344 CNRS/University of Orléans, 45000 Orléans/ 18000 Bourges, France*
**cyrine.ben-othmen@univ-orleans.fr*

In the context of water treatment by plasma, this study presents a comparison of three non-thermal atmospheric pressure plasma reactor technologies developed in our lab: Gliding Arc Discharge, Dielectric Barrier Discharge (DBD), and Plasma Jet in contact with water. We evaluated their energy efficiency and their capacity to generate key reactive species—such as hydrogen peroxide and nitrogen-derived acids/bases—in Plasma Activated Distilled Water (PADW), using spectrophotometry and colorimetric analysis. The most efficient reactor is selected for degrading a specific micro-pollutant.

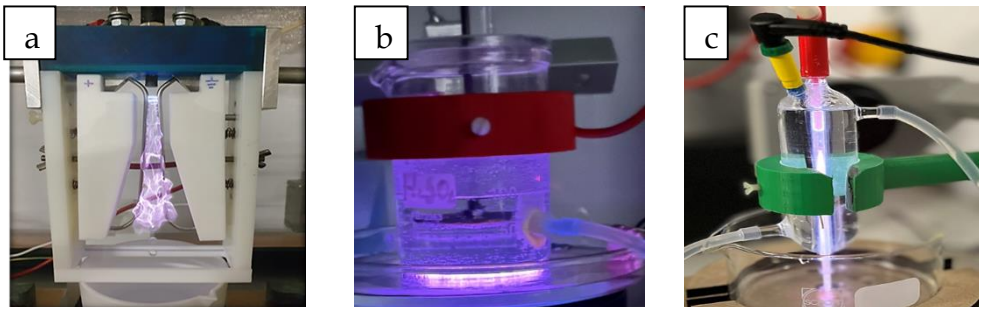



Figure 1: Non-thermal atmospheric pressure plasma reactors: (a) Gliding Arc, (b) DBD, and (c) plasma Jet

Water pollution is an increasing global issue, as micro-pollutants from industrial, agricultural, and domestic activities significantly impact water quality, human health, and the environment. To address this issue, plasma-based advanced oxidation processes are emerging as a highly effective solution, offering superior degradation and mineralization of micro-pollutants in water compared to conventional methods [1,2].

In this regard, the main objective of this study is to identify an effective non-thermal atmospheric-pressure plasma reactor for the degradation of micro-pollutants in water such as pesticide or medicine by-products.

To achieve this goal, we conducted a comparative analysis of three atmospheric-pressure plasma reactors[3]: Gliding Arc Discharge, DBD, and Plasma Jet, based on several parameters (such as solution volume, treatment time, type of plasma-forming gas, injected flow rate, etc.) to evaluate the efficiency of generating key reactive species, mainly hydrogen peroxide and nitrogen-derived acids/bases, in Plasma Activated Distilled Water (PADW) by spectrophotometry and colorimetric analysis alongside measurements of global parameters like pH and conductivity.

The second step, we combined this chemical analysis on PADW with an evaluation of power consuming by each reactor through electrical measurements to explore the role of oxygen in the feeding gas mixture (Air + x $\%O_2$ and Ar + x $\%O_2$) for the production of reactive species in water.

Finally, the most efficient reactor for generating reactive species in water, with optimized energy consumption, is used to degrade a targeted micro-pollutant by varying its concentration in water and calculating the degradation rate.

[1] Sarangapani, C., Misra, N.N., Vladimir, M., Paula, B., Finbarr, O., & Cullen, P. J. Pesticide degradation in water using atmospheric air cold plasma. *Journal of Hazardous Materials* **9**, 225-232 (2016).
[2] Nandy, N., Pasupathi, A., Subramaniam, Y. Degradation of 4-nitrophenol using Ar/air thermal plasma in submerged conditions: plasma characteristics, degradation chemical kinetics and degradation pathways, *Journal of Physics D: Applied Physics* **58**, 115202 (2025).
[3] Becker, K.H., Kogelschatz, U., Schoenbach, K. H., and Barker, R. J. Non-equilibrium air plasmas at atmospheric pressure, *Institute of Physics*, isbn:978-0-7503-0962-2 (2005).

# Modeling approach for an atmospheric pressure, compressed air inductively coupled plasma torch with arbitrary geometry

A.M.H. van Gils[1], H.C.J. Mulders[1], S. Nijdam[1] and J. van Dijk[1]

[1] *Eindhoven University of Technology, Eindhoven, The Netherlands*

The Finite Element Method (FEM), well-suited for arbitrary geometries, is employed to model electromagnetic, temperature and plasma components of a high power, atmospheric pressure, compressed air inductively coupled plasma torch.

## 1 Introduction

Applications that require a high level of purity are well served by an Inductively Coupled Plasma (ICP) torch (Fig. 1). For quartz glass welding, a high power ICP is operated at atmospheric pressure, using compressed air. An in-depth physical model of this system is sought to gain insight into the role of geometrical properties of the system on the efficiency of heat deposition. To this end, plasma modeling software PLASIMO [2, 3] is extended with FEM-based C++ library MFEM [4]. Given the relatively high pressure and power density of the plasma, Local Thermal Equilibrium (LTE) is assumed in a plasma fluid model, including an electromagnetic and a temperature component. All components are interchained and require an iterative solution procedure. This approach is intended to precede a full treatment of radiation transport and a two-temperature non-LTE description on a FEM basis in PLASIMO, currently only available in the finite-volume form. In the future, this model will be used in conjunction with experimental validation.

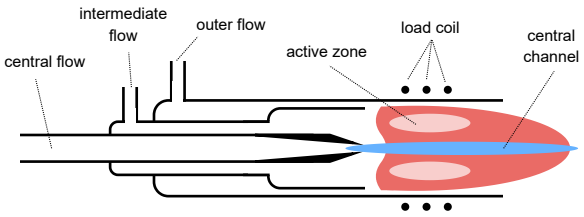



Figure 1: Schematic cross section view of an ICP setup (adapted from [1])

## 2 Model components

### 2.1 Power coupling and EM fields

The EM-field is solved in terms of the magnetic vector potential:

$$\nabla \times \nabla \times \mathbf{A} = \mu_0 \mathbf{J}, \tag{1}$$

where $\mathbf{J}$ can either be applied as a system constraint, like for a coil wire, or arise from conduction. Solving for $\mathbf{A}$ provides fields $\mathbf{E}$ and $\mathbf{B}$ through the definition of $\mathbf{A}$.

### 2.2 Fluid description

Velocity and pressure fields are calculated using the Navier-Stokes equation, modeling the plasma bulk as a fluid, combined with the mass continuity equation and the energy conservation equation. Under the assumption of LTE, the plasma composition follows from the local pressure, temperature and elemental mass fractions; the latter are fixed in the present study. From this composition, the required parameters for the temperature and EM model components are derived.

### 2.3 Temperature

The energy conservation equation is defined in terms of, and solved for, the temperature. In the LTE description, the internal energy and its transport are taken into account in the form of reactive contributions to the specific heats and the thermal conductivity, as usual.

## References

[1] Benoy, D.A. Modelling of Thermal Argon Plasmas. PhD Thesis. Technische Universiteit Eindhoven. (1993).

[2] van Dijk, J. et al. The plasma modelling toolkit Plasimo *J. Phys. D: Appl. Phys.*, **42** 194012 (2009)

[3] PLASIMO `https://plasma-matters.nl` visited: 24-3-2025

[4] Anderson, R. et al. MFEM: A Modular Finite Element Methods Library *Computers & Mathematics with Applications*, **81**, 72-74 (2021)

# Quenching of a magnetically stabilized arc discharge at different pressures for $CO_2$ conversion

V. Vasilev, S. Lazarova, Ts. Paunska and St. Kolev

*Sofia University "St. Kliment Ohridski", Faculty of Physics, James Bourchier blvd 5, Sofia, Bulgaria*

In this study, we present an experimental investigation of a magnetically stabilized arc discharge in carbon dioxide ($CO_2$) at pressures ranging from 200 to 700 mbar. The arc is stabilized by the Lorentz force $\mathbf{J}\times\mathbf{B}$, acting opposite to the gas flow. The force arises from the interaction between the arc's current and an external magnetic field generated by permanent magnets. A downstream actively cooled "quenching region" is incorporated to lower the gas temperature after it passes through the arc, thus enhancing the dissociation rate and energy efficiency by preventing the undesirable recombination reaction $CO + O \longrightarrow CO_2$.

The objective of this study is to examine the influence of the quenching region on the dissociation rate and energy efficiency at various pressures. Additionally, we investigate the effects of gas flow and discharge current.

## 1 General

Plasma conversion of carbon dioxide ($CO_2$) into value-added chemicals is a extensively studied area, driven by its application in carbon capture, utilization, and storage for mitigating climate change on Earth [1,2]. More recently, this technology has also been investigated for in-situ oxygen production on Mars [3], where the atmosphere is composed of approximately 96% $CO_2$.

Here we present a magnetically stabilized arc discharge (fig. 1) with an added actively cooled region. This type of discharge utilizes pin-to-pin electrodes, providing easy scalability by controlling the distance between the electrodes. The addition of quenching can improve dissociation rate and energy efficiency by lowering the temperature of the gas after it passes through the arc column thus reducing the rate coefficient for the recombination reaction.

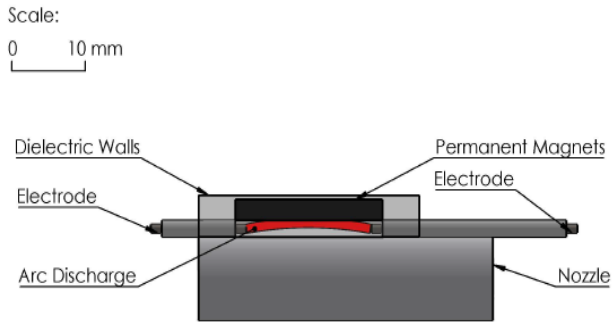



Figure 1: Schematic diagram of the magnetically stabilized arc discharge without the additional quenching region

We investigate operation at varying pressures, focusing on applications for Mars, where the primary objective is to extract oxygen from the gas mixture. This extraction process requires additional equipment, such as solid oxide electrolysis cells (SOECs), mixed ionic-electronic conducting (MIEC) materials, or various membranes, all of which can operate at different pressures, each with its own optimal value. The goal of this study is to identify the optimal discharge parameters, which will enable future integration with the extraction unit, allowing both systems to operate synergistically at their respective optimal pressures.

## References

[1] R. Snoeckx and A. Bogaerts, "Plasma technology–a novel solution for $CO_2$ conversion?" *Chemical Society Reviews*, vol. 46, no. 19, pp. 5805–5863, 2017.

[2] V. Ivanov, T. Paunska, S. Lazarova, A. Bogaerts, and S. Kolev, "Gliding arc/glow discharge for co2 conversion: Comparing the performance of different discharge configurations," *Journal of CO2 Utilization*, vol. 67, p. 102300, 2023.

[3] V. Guerra *et al.*, "Plasmas for in situ resource utilization on mars: Fuels, life support, and agriculture," *Journal of Applied Physics*, vol. 132, no. 7, 2022.

# Modelling of diffusion and viscosity of carbon nanoparticles in low-temperature plasma

A.I. Kenzhebekova[1,2], N. Kh. Bastykova[1,2], S. K. Kodanova[1,2], Junissov A.T.[1,2]

[1]*Institute of Applied Sciences and IT, Almaty, Kazakhstan*
[2]*IETP, Al-Farabi Kazakh National University, Almaty, Kazakhstan*

The method for modelling the transport properties of nanoparticles used in this study accounts for charge fluctuations in low-temperature plasma, which are comparable to the mean nanoparticle charge and have characteristic timescales similar to the collision time of plasma particles with a nanoparticle.

In recent decades, research on nanoparticle systems has gained significant importance due to their unique physicochemical properties. These systems have found widespread applications in various fields of science and technology, including next-generation materials, biomedicine, electronics, energy, and environmental protection [1–3]. Studying nanoparticle systems provides deeper insight into quantum mechanical effects, interparticle interactions, and the self-organization of nanostructures, which is crucial for advancing modern physical theories.

One of the most promising methods for synthesizing nanoparticles with tailored characteristics is low-temperature plasma synthesis [4]. By adjusting the parameters of the plasma environment, it is possible to control the size, luminescence, composition, and morphology of nanoparticles, there by optimizing their formation processes. In plasma, nanoparticles acquire charge, which affects the plasma properties, and this effect becomes more pronounced as the particles grow. Studies show that nanoparticles smaller than 1 nm can have either a negative or positive charge. Such particles often undergo charge fluctuations occurring on time scales comparable to the collision time of particles with plasma ions and electrons. Nanoparticles with sizes in the range of $1 < d < 10$ nm acquire a negative charge. Moreover, in low-temperature plasma, the nanoparticle concentration can reach values comparable to the ion density, making the study of its transport and structural properties particularly important.

The calculation of transport coefficients of nanoparticles, taking into account charge fluctuations, is carried out using a combination of molecular dynamics and Monte Carlo methods. These methods allow for the consideration of nanoparticle interactions with plasma, the probabilistic charge distribution, and the influence of charge fluctuations on particle dynamics. In this work, the transport properties of carbon nanoparticles, such as the diffusion coefficient and viscosity, are calculated, taking into account their charge fluctuations for different parameters of low-temperature plasma. [5–6].

This research is funded by the Science Committee of the Ministry of Science and Higher Education of the Republic of Kazakhstan (Grant AP23488907).

**References**

[1] Orazbayev, S. A., Utegenov, A. U., Zhunisbekov, A. T., Slamyiya, M., Dosbolayev, M. K., & Ramazanov, T. S. *Contributions to Plasma Physics* **58**(10), 961 (2018).

[2] Hino, T., Yoshida, H., Yamauchi, Y., Hirohata, Y., Nakamura, K. and Akiba, M. *Fusion Eng. Des*. **61–62**, 605 (2002).

[3] Minami, K., Yamanishi, Y., Kojima, C., Shindo, M. and Ishihara, O. *IEEE Trans. Plasma Sci.* **31**, 429 (2003).

[4] Lanham, S. J., Polito, J, Shi, X., Elvati, P., Violi, A., Kushner, M.J. *J. Appl. Phys.* **130**, 163302 (2021).

[5] Djienbekov, N. E., Bastykova, N. Kh., Bekbussyn, A. M., Ramazanov, T. S. and Kodanova, S. K. *Phys. Rev. E* **106**, 065203 (2022).

[6] Bastykova, N. Kh., Djienbekov N.E., Ramazanov, T.S., Kodanova, S.K. *Results in Physics* **69**, 108136 (2025)

# Control of average ion energy and ion flux through incorporation of helium in inductively coupled and capacitively coupled low pressure hydrogen plasmas

Max Kellermann-Stunt[1], Timo Gans[2], Kari Niemi[1], Andrew Gibson[1], James Dedrick[1]

[1] *University of York, York Plasma Institute ,School of Physics, Engineering and Technology, York, UK,YO10 5DD*
[2] *Dublin City University, National Centre for Plasma Science and Technology School of Physical Sciences, Faculty of Science and Health, Dublin, Ireland, D09 V209*

**Abstract:** In this contribution, ion energy distributions of hydrogen and hydrogen-helium plasmas were measured for inductively coupled and capacitively coupled configurations. A retarding field energy analyser was used to measure the distributions for pressures of 15 Pa to 30 Pa. From this the total ion flux and the average ion energy can be measured. The results suggest that using helium mixtures can help control the ion flux for plasma processing applications.

## 1 Introduction

Hydrogen plasmas are useful for plasma etching in semiconductor processing as they are lightweight and can lead to less structural damage [1]. One challenge identified in plasma processing is increasing the processing rate of high precision structures without damaging the surface[2]. To do this, the ion flux needs to be increased. However in conventional plasma setups that are driven by single-frequency radio-frequency (rf) power sources, the ion flux and ion energy are intrinsically linked[3]. If the ion energy is too large, this can lead to substrate defects and damage. In this work we investigate the mixture of helium into a hydrogen plasma for the purposes of controlling ion flux and energy, as helium has a similar mass to hydrogen ions but a distinct ionisation potential.

## 2 Method

This study uses a modified gaseous electronics conference (GEC) reference cell that can be used to generate both inductively coupled plasmas (ICPs) at 100W and capacitively coupled plasmas (CCPs) at 400V, for pressures between 15Pa and 30Pa. For the mixed gas experiments, the partial pressure of hydrogen was kept constant. In the ICP setup, the coils above the upper electrode are powered and the lower electrode is grounded. In the CCP setup, the coils are grounded and the lower electrode is powered. A retarding field energy analyser (RFEA) was placed on the lower electrode to measure the ion energy distribution functions (IEDFs). The measured IEDFs are used to determine average ion energy and total ion flux density incident on the lower electrode.

## 3 Results and discussion

Figure 1 shows that increasing pressure and helium addition decreased average ion energy with minimal ion flux change in the ICP configuration.

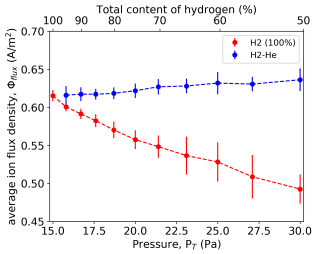



**Fig1:** Flux measurements for hydrogen and hydrogen helium ICPs at 100W, 15-30Pa.

This demonstrates the potential to reduce the ion energy while maintaining and increasing ion flux in low-pressure hydrogen ICPs.

In CCP configuration, distinct behaviour was observed, the average ion energy also decreased with increasing pressure and helium addition but increased the total ion flux.

## 3 Conclusion

The IEDFs of hydrogen and hydrogen-helium plasmas were measured for both CCP and ICP regimes. As shown on figure 1, helium admixtures can be used to maintain a constant ion flux whilst reducing the average ion energy. The results indicate that helium can optimize plasma processing techniques, especially in applications requiring precise control over ion flux.

**Acknowledgements**

The financial support of the EPSRC Centre for Doctoral Training in fusion energy is gratefully acknowledged under Financial Code EP/S022430/1.

**References**

[1] RPH Chang, CC Chang, and S Darack. “Hydrogen plasma etching of semiconductors and their oxides”. In: Journal of Vacuum Science and Technology 20.1 (1982), pp. 45–50.

[2] I. Adamovich et al. “The 2022 Plasma Roadmap: low temperature plasma science and tech- 232nology”. In: Journal of Physics D: Applied Physics 55.37 (2022), p. 373001.

[3] A. Perret, P. Chabert, J. Jolly, J.-P. Booth; Ion energy uniformity in high-frequency capacitive discharges. *Appl. Phys. Lett.* 10 January 2005; 86 (2): 02150

# Subcellular Visualization of Cold Atmospheric Plasma Effects on Living Cell Surfaces Using Scanning Ion Conductance Microscopy

Han Gia Nguyen[1], Linhao Sun[2], Shinya Kumagai[3] and Shinji Watanabe[2]

[1] *Kanazawa University, Kanazawa, Ishikawa, Japan*
[2] *WPI – NanoLSI, Kanazawa University, Kanazawa, Ishikawa, Japan*
[3] *Meijo Unversity, Nagoya, Aichi, Japan*

Cold atmospheric plasma (CAP) has been extensively applied in biology and medicine, showing potential in wound healing, selective cancer cell elimination [1], and gene transfection [2]. Despite its broad applicability, the mechanisms underlying CAP's effects remain incompletely understood.

Numerous studies have investigated the role of CAP-induced factors in enhancing transfection efficiency [3], inducing DNA damage [4], and modulating carcinoma cell responses [5]. While these studies primarily focus on post-exposure effects, little is known about the immediate changes occurring at the cell surface following CAP exposure.

To address this gap, we employed a nanopipette-based probe (Fig. 1a) to deliver localized CAP exposure to individual cells and to image the cell surface immediately after exposure using scanning ion conductance microscopy (SICM) [6]. Figure 1b illustrates the capability of this CAP nanopipette probe to selectively stimulate single cells in a physiological environment, with living cells stained by a green-fluorescent dye (Calcein AM). CAP exposure near the probe induces membrane rupture, visualized by red-fluorescent dye uptake (Propidium Iodide or PI).

When CAP exposure was carefully controlled, the cell membrane remained intact without rupture. Under these conditions, SICM imaging revealed that CAP exposure increases surface roughness while decreasing the elastic modulus (Fig. 1c) under physiological conditions. We further examined how variations in applied voltage, exposure duration, and probe-to-cell distance affected cell surface nanostructure and mechanical properties. The dependence of these parameters on the modulation of cell surface characteristics will be discussed in detail.

## References

[1] Boeckmann, L. et al. Appl. Sci. 2020, 10, 6898.
[2] Jinno M., et al. J. Photopolym. Sci. Technol., Vol. 27, No. 3, 2014.
[3] S. Sasaki et al. Jpn. J. Appl. Phys. 55, 07LG04 (2016).
[4] NGaur et al. J. Phys. D: Appl. Phys. 54 (2021) 035203.
[5] Kim, S., Chung, T. Sci Rep 6, 20332 (2016).
[6] N. G. Han et al., The 85th JSAP Autumn Meeting 2024, 20a-P03-16, (2024).

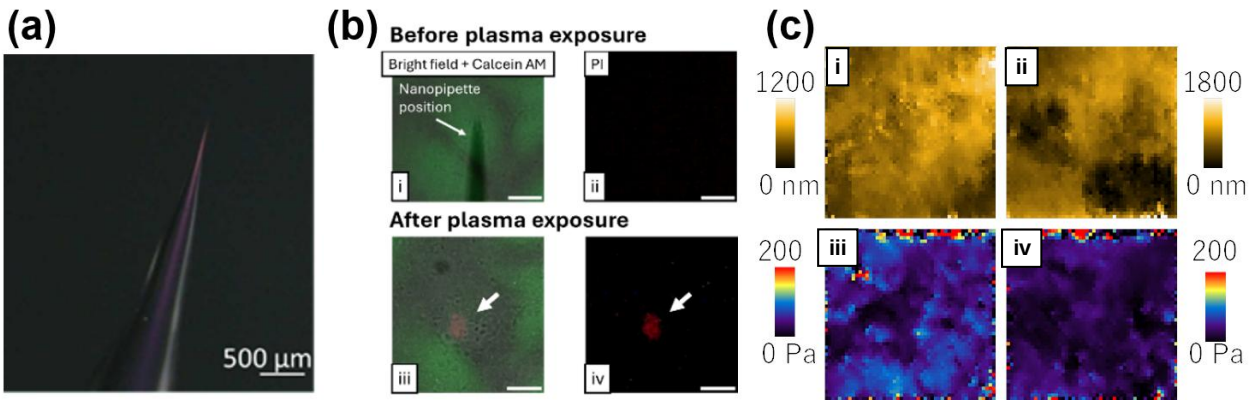



**Fig 1**. (a) Nanopipette as CAP probe and the plasma generation inside probe. (b) Fluorescent images of cell before (i and ii) and after (iii and iv) CAP exposure. (c) SICM images of cell surface topography and elasticity before (i, iii) and after (ii, iv) CAP exposure. Scan range: 5 µm x 5 µm

# An introduction to a series of linear plasma devices within CRAFT project in China

Xin Yang[1], Hai-Shan Zhou[1], Guang-Nan Luo[1]

[1] *Institute of Plasma Physics, Chinese Academy of Sciences, Hefei 230031, China*

Comprehensive Research Facility for Fusion Technology (CRAFT) is one of national large science and technology infrastructures of China, which aims to explore and master the key technologies, standards and methods for the construction and operation of future fusion reactors (especially for the China Fusion Engineering Test Reactor, CFETR). CRAFT project is divided into two research systems (for the superconducting magnet and the divertor, respectively) and includes 20 test facilities or prototypes totally. Linear Plasma Devices (LPDs) are designed to test divertor plasma-facing materials under fusion reactor relevant conditions. Hence, the research on LPDs technology is included in the CRAFT project.

Within CRAFT site, a series of LPDs have been built to address some key R&D issues of plasma-facing materials and components. Meanwhile, extended application of LPDs in space propulsion have been investigated, too.

One of the most important facilites is the Superconducting plasma Wall interactiOn lineaR Device (SWORD). It is designed to obtain a steady-state plasma with particle flux > $1\times10^{24}$ $m^{-2}s^{-1}$. Its first milestone was achieved last year —a continuous helium plasma discharge with a flux greater than $10^{24}$ $m^{-2}s^{-1}$ and a duration exceeding 1000 seconds.

To test the high flux, long term operation of the cascaded arc source for SWORD, a prototype linear device called Steady-state Plasma Apparatus foR Research of Wall materials (SPARROW) has been developed and operational. the device can deliver continuous > $1\times0^{24}$ $m^{-2}s^{-1}$ plasma flux for more than 24 hours. Currently, SPARROW is opened to users for the study of plasma surface interactions.

Expect for the DC discharge facility, a linear plasma device based on electron cyclotron resonance discharge named Permeation and Retention Evaluation FACility for fusion Experiments (PREFACE) was developed for plasma driven-permeation experiments. It is equipped with a 6kW@2.45Ghz ECR source. It is within the frame of the Hydrogen Permeation Coordination Research Program in IAEA.

Since LPDs has been applied in the field of plasma propulsion system such as helicon plasma thruster and VASIMR systems. Two LPDs named as Superconducting Tunable Acceleration Rocket (STAR) and the Linear plasma Device with Helicon source and ICRH (LDHI) have been developed. Both of them are based on helicon plasma source plus ion cyclotron resonance heating systems. In STAR, the primary investigation of the thrust performance show that at a maximum input power of 50 kW, a thrust up to 1.19 N could be achieved.

Moreover, an Advanced Research Thruster (ART) platform designed for radio frequency micro plasma thruster investigation have also been developed.




Figure 1 Representative Composition of the CRAFT LPDs facilities.

# Electron properties and non-thermal equilibrium in an 80 kV nanosecond discharge studied by incoherent Thomson scattering

P. Tardiveau[1], A. Brisset[2], P. Jeanney[1], L. Magne[1]

[1] *LPGP, CNRS, Université Paris-Saclay, Orsay, France*
[2] *EM2C, CNRS, Centrale-Supélec, Université Paris-Saclay, Gif-sur-Yvette, France*

The temperature, the density and the energy distribution of electrons are determined in an 80 kV nanosecond discharge with incoherent Thomson scattering technic. The discharge is generated by a 10 ns voltage pulse run at 10 Hz, in $N_2/O_2$ mixtures with different oxygen contents. A focus is made on the electron properties very close to the sharp anode, where the densities reach values as high as $10^{17}$ $cm^{-3}$ after breakdown and where the energy distribution function may depart from a Maxwellian profile. The gas temperature is also considered with the analysis of the Raman signals at the limit of the high voltage electrode surface. Its initial value at the start of the voltage pulse is of interest since it is an important parameter for discharge modelling. The non-thermal equilibrium of this specific high voltage discharge is discussed.

## 1 Introduction

Non-thermal and largely diffuse discharges can be obtained and stabilized in centimetre atmospheric air gaps with high overvoltage pulses [1]. They are quite new and different kinds of discharges compared to the well-known streamer regime obtained at moderate overvoltage, and the physical understanding of their dynamics still remains challenging [2]. Recent experimental work has been done on the determination of the electron density in such discharges and it shows that after breakdown the discharge is structured in two different zones with very high densities close to the pin [3]. This preliminary study has to be continued with deeper characterization of the electron population and its energy distribution. When compared to the gas temperature, the electron temperature brings some information of how far the discharge is from the thermal equilibrium and how fast it can reach it.

Incoherent Thomson scattering is used for this study as a non-invasive, time and space resolved diagnostic. The broad and low intensity scattering signal is spectrally confined next to the laser wavelength which is used, and it is highly disturbed by the Rayleigh emission and the rotational Raman lines emitted from molecular gases such as $N_2/O_2$ mixtures. The challenge is then to effectively suppress the Rayleigh component and to optimize the Raman signal quality in order to fit it as closely as possible and to finally remove it. Since the $N_2/O_2$ ratio is known as a parameter which can change the discharge behaviour and its stability, the measurements are made with different oxygen contents.

## 2 Experimental set up

The discharge is generated in a pin-to-plane configuration with a pin radius of 100 $\mu$m radius. The high voltage ns pulse is generated by a FID FPG 50–1NMX3A15 power generator. It peaks at 80 kV with a rise time of 2 ns and a FWHM of 5 ns. The repetition rate is 10 Hz. The discharge is run in $N_2/O_2$ mixtures with oxygen content between 0 and 20% with a 1 $l.mn^{-1}$ flow. A 5 ns pulsed gaussian Laser beam is generated at 532 nm by a Q-smart 850 laser and focused by a 1 m focal lens in the plane of symmetry of the discharge. The signal is collected perpendicularly to the laser beam through parabolic mirrors imaging the laser spot in the object focal plane of a lens (f = 3 cm). A high-quality Notch filter removes the Rayleigh component from the parallel beam, then focused on the entrance slit of a 75 cm ACTON spectrometer. A 1200 $l.mm^{-1}$ grating blazed at 300 nm is used. A 4-PICOS Stanford camera is used to collect the light with a time resolution lower than 1 ns.

**References**

[1] Tardiveau, P et al. Sub-nanosecond time resolved light emission study for diffuse discharges in air under steep high voltage pulses. *Plasma Sources Sci. Technol* **25,** 054005 (2016).
[2] Zhu, Y. et al. Simulation of ionization-wave discharges: a direct comparison between the fluid model and E-FISH measurements. *Plasma Sources Sci. Technol.* **30**, 075025 (2021).
[3] Brisset, A. et al. Electron density and temperature in a diffuse nanosecond pulse discharge in air at atmospheric pressure. *Plasma Sources Sci. Technol.* **32,** 065014 (2023).

# Effects of ion irradiation on the structure of a-C:H films deposited using cumene plasma CVD

Manato Eri[1], Shinjiro Ono[1], Shumpei Ohara[1], Takamasa Okumura[1], Kunihiro Kamataki[1], Haruki Kiyama[1], Naho Itagaki[1], Kazunori Koga[1], and Masaharu Shiratani[1]

[1] *Kyushu University, 744 Motooka, Nishi-ku, Fukuoka 819-0395, Japan*

We studied the effects of ion bombardment on the structure of hydrogenated amorphous carbon (a-C:H) films during their deposition via cumene plasma chemical vapor deposition (CVD). To control ion energy independently of radical generation, we applied a 400 kHz RF voltage to the substrate. As the substrate bias increased, the deposition rate rose while compressive stress decreased, with the film density remaining constant. These results suggest that the crystallinity of $sp^2$ bonds increases with increasing voltage, while the $sp^3/(sp^2 + sp^3)$ ratio remains unchanged.

Hydrogenated amorphous carbon (a-C:H) films are widely used as protective coatings in dry etching processes. Achieving high film density and deposition rates while maintaining low stress remains a significant challenge. The mechanical properties of a-C:H films are governed by the composition of $sp^2$ bonds, $sp^3$ bonds, and hydrogen atoms. During a-C:H film deposition, the energy of ions bombarding the film surface plays a critical role in determining the resulting film structure. Cumene ($C_9H_{12}$), with its high carbon content and low hydrogen content per molecule, is expected to enable both high deposition rates and high mass density. To discuss the structural changes induced by ion irradiation in cumene-based plasma CVD, we measured the dependence of film deposition characteristics on substrate bias voltage.

The films were deposited using a parallel-plate capacitively coupled plasma CVD system [1]. A Si (100) substrate was placed on the lower electrode. Cumene and Ar were introduced into the system at flow rates of 5 sccm and 45 sccm, respectively. The total gas pressure *P* was set to 10 or 50 mTorr. Plasma was generated by applying a 28 MHz RF voltage (270 Vpp) to the upper electrode. To control the substrate bias voltage |Vdc|, a 400 kHz RF voltage was applied to the substrate holder, resulting in |Vdc| values ranging from 680 to 1120 V.

We measured the deposition rate, film density, and compressive stress as functions of |Vdc|. At *P* = 10 mTorr, the deposition rate increased slightly with |Vdc|, while at *P*= 50 mTorr, the deposition rate increased significantly with |Vdc|. Optical emission spectroscopy revealed a similar trend in plasma emission intensity at 431 nm, attributed to CH radical generation, suggesting that precursor dissociation increases with |Vdc|. For both *P*= 10 and 50 mTorr, the film density remained constant while compressive stress decreased with increasing |Vdc|. To reveal the mechanism underlying this stress relaxation, we analyzed the film structure using XPS and Raman spectroscopy. Figure 1 shows typical spectra of (a) XPS and (b) Raman of the film deposited at *P*= 50 mTorr as a parameter of |Vdc|. The XPS spectra of films deposited at *P*= 50 mTorr showed no significant changes with increasing |Vdc|. However, the Raman spectra indicated that, with increasing |Vdc|, the G peak position shifted to higher wavenumbers, and the G peak FWHM decreased. These results suggest that increasing |Vdc| enhances the crystallinity of $sp^2$ bonds, reducing compressive stress while maintaining the $sp^3/(sp^2 + sp^3)$ ratio [2].

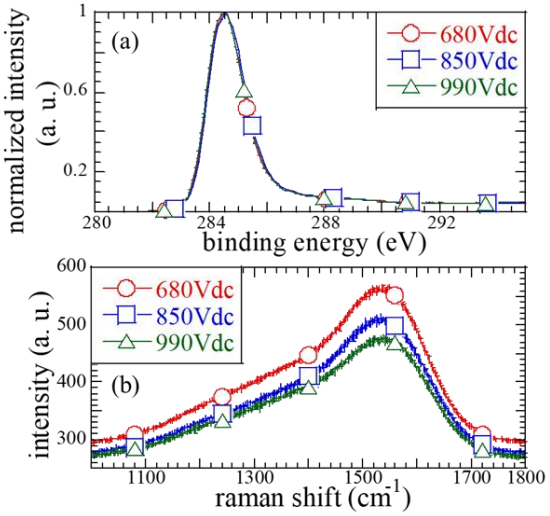



Fig.1 (a)XPS and (b)raman spectra of the a-C:H films as a parameter of |Vdc| for P= 50 mTorr

**References**

[1] Sung-Hwa Hwang et al., Thin Solid Films 729, 138701 (2021)

[2] A. C. Ferrari and J. Robertson, Phys. Rev. B 61, 14095 (2000)

# Temporal evolution of NO density after nanosecond pulses in plasma-assisted combustion

Renaud Gablier[1] and Christophe O. Laux[1]

[1] *Université Paris-Saclay, CNRS, CentraleSupélec, Laboratoire EM2C, 91190 Gif-sur-Yvette, France*

In this work we propose to use NO Laser-Induced Fluorescence (LIF) in a plasma-assisted burner to measure the temporal evolution of nitric oxide (NO) density produced by Nanosecond Repetitively Pulsed (NRP) discharges. These measurements will enable us to assess chemical kinetic models of NO formation in Plasma-Assisted Combustion (PAC).

## 1 General

Plasma-Assisted Combustion (PAC) using Nanosecond Repetitively Pulsed (NRP) discharges is a promising candidate for reducing pollutant emissions in combustion facilities [1]. The method consists in burning lean premixed flames, which allows for more complete combustion and reduced nitric oxide (NOx) emissions. However, lean flames tend to be unstable and are prone to abrupt extinction. Non-equilibrium plasmas locally create radicals that improve the combustion propagation and branching mechanisms, stabilizing the whole flame. PAC has demonstrated the ability to reduce combustion instabilities and extend the flammability domain. For these reasons, PAC affords flexibility in the operability of combustion chambers, which is of particular interest for sudden transient regimes.

However, some studies report increased nitrogen oxide ($NO_X$) emissions when applying plasmas in a flame [2,3]. The $NO_X$ penalty caused by the plasma has a double origin. First, the local extra heat released by the successive discharges will favor the thermal Zeldovich mechanism already present in non-assisted flames. Second, the production of radicals and excited electronic species will create NO through Zeldovich-like quenching reactions with low activation energy.

A recent study showed that it is possible to use the hydrodynamic properties of the NRP discharges to enhance the cooling between pulses [4], thus considerably reducing the plasma-related thermal Zeldovich NO formation pathway. Regarding the second plasma-related NO formation pathway via the quenching reactions, several mechanisms have been suggested in the literature [5–7]. However, experimental validation is lacking to fully understand NO formation in PAC.

In this study, temporally resolved NO Laser-Induced Fluorescence will be used in a lab-scale PAC burner to take advantage of the various chemical times (ns up to µs) involved in the different suggested mechanisms of NO formation. We will compare the NO density profile to computations using literature mechanisms to identify the relative intensity of NO production for each pathway, as a function of the plasma conditions in the flame. Collected data will help validate the kinetic mechanisms of NOx formation proposed in the literature.

**Acknowledgments:**
This work has received funding from the European Research Council (ERC) under the GreenBlue project (Grant Agreement No.101021538) supported by the European Union's Horizon 2020 research and innovation program. The authors thank Jérôme Bonnety, Erika Jean-Bart, Yannick Le Teno, and Koro Sokhona for their technical support on the Mini-PAC burner.

**References**

[1] Blanchard, V. P., "Thermochemical Effects of Nanosecond Plasma Discharges on Lean Flame Stabilization," Paris-Saclay, 2023.

[2] Kim, G. T., Seo, B. H., Lee, W. J., Park, J., Kim, M. K., and Lee, S. M., "Effects of Applying Non-Thermal Plasma on Combustion Stability and Emissions of NOx and CO in a Model Gas Turbine Combustor," *Fuel*, Vol. 194, 2017, pp. 321–328. https://doi.org/10.1016/j.fuel.2017.01.033

[3] Xiong, Y., Schulz, O., Bourquard, C., Weilenmann, M., and Noiray, N., "Plasma Enhanced Auto-Ignition in a Sequential Combustor," *Proceedings of the Combustion Institute*, Vol. 37, No. 4, 2019, pp. 5587–5594. https://doi.org/10.1016/j.proci.2018.08.031

[4] Gablier, R., and Laux, C. O., "Hydrodynamic Recirculation Induced by Nanosecond Discharges: A Strategy to Mitigate Cumulative Heating," presented at the AIAA SciTech 2025 Forum, Orlando, Florida, USA, 2025.

[5] Shkurenkov, I., Burnette, D., Lempert, W. R., and Adamovich, I. V., "Kinetics of Excited States and Radicals in a Nanosecond Pulse Discharge and Afterglow in Nitrogen and Air," *Plasma Sources Science and Technology*, Vol. 23, No. 6, 2014, p. 065003. https://doi.org/10.1088/0963-0252/23/6/065003

[6] Malé, Q., Barléon, N., Shcherbanev, S., Dharmaputra, B., and Noiray, N., "Numerical Study of Nitrogen Oxides Chemistry during Plasma Assisted Combustion in a Sequential Combustor," 2024. https://doi.org/10.1016/j.combustflame.2023.113206

[7] Uddi, M., Jiang, N., Adamovich, I. V., and Lempert, W. R., "Nitric Oxide Density Measurements in Air and Air/Fuel Nanosecond Pulse Discharges by Laser Induced Fluorescence," *Journal of Physics D: Applied Physics*, Vol. 42, No. 7, 2009, p. 075205. https://doi.org/10.1088/0022-3727/42/7/075205

# Study of a surface wave plasma under the influence of pulsed gas injections by rapid imaging

J. Brochier[1,2], R. Dorlé[2,1], V. Orlandi[2,3], R. Clergereaux[2] and L. Stafford[1]

[1] *Département de Physique, Université de Montréal, Montréal*
[2] *Laboratoire Plasma et Conversion d'Energie, Laplace, Université Paul Sabatier, Toulouse*
[3] *Spaceship FR, CNES, Toulouse*

Pulsed gas injection is of interest for the development of aerosol assisted plasma processes. Indeed, it enables recovering a steady state between two pulses a method to well-control the discharge. Here, we will discuss the impacts of pulsed argon injections on a sustained surface wave plasma. Indeed, the behaviour of this discharge is not only controlled by the pressure. Rapid imaging shows that instabilities are produced at the pulse injection.

## 1 Introduction

Pulsed gas injections can be used for plasma process, especially for thin film deposition of various materials. For example, it enables to inject liquid aerosols to form innovative coatings in low-pressure [1,2] or atmospheric pressure plasmas [3,4]. The advantage of a pulsed injection compared to a continue injection is that it allows the plasma to return to a steady state. However, it has been shown that it involves many temporal mechanisms that must be carefully studied [1,5]. Here, these mechanisms are discussed in a sustained wave plasma at low pressure.

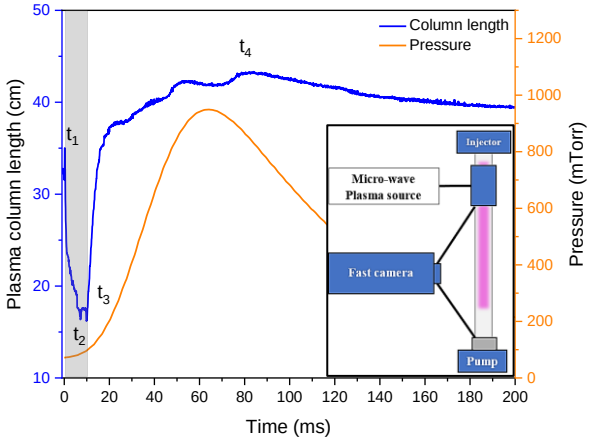
## 2 Results

The system consists in a surface-wave plasma column produced in a fused silica discharge tube. The wave frequency is set at 915 MHz and the plasma gas is argon. For steady state gas injection, the plasma column length can be controlled by the operating pressure and microwave power. For pulsed gas injections, rapid optical imaging reveals that the stationarity of the plasma is disrupted. More specifically, as shown in Fig. 1.a, for 10 ms gas injection, the plasma column is highly reduced between $t_1$ and $t_2$, and then progressively returns to its steady-state value beyond $t_4$. Between 0 and about 60 ms, the pressure recorded downstream of the microwave plasma increases from 50 mTorr up to 900 mTorr and then decreases back to 50 mTorr beyond 60 ms. Rapid imaging analysis presented in Fig. 1.b further highlight that instabilities are formed at $t_3$. These variations seem related with the gas velocity and/or the rapid pressure variations.

## 3 Conclusion

The response of a sustained surface wave plasma to pulsed gas injection was studied. The rapid variation of gas feeding induces non-linear evolutions of the plasma column length with the formation of instabilities. A key role of the gas velocity is discussed.

a)




b)




*Figure 1:* a) *Time evolution of the plasma column length and the pressure for an injection of 10ms. The set-up is reported inset. b) Time series of the plasma column obtained by rapid imaging. The injection starts in $t_2$ and stop between just after $t_3$.*

**References**

[1] Carnide, G. et al. Plasma Chem. Plasma Process. 44(3), 1343-1356 (2024)
[2] Carnide, G. et al. Adv. Sci., 10(5), 2204929 (2023)
[3] Cacot, L. et al. Plasma Process. Polym. 20(3), 2200165 (2023).
[4] Carnide G. et al. Coatings, 13(3), 630 (2023).
[5] Cacot, L. et al. J. Phys. D, 55(47), 475202 (2022).

# Experimental study and modelling of high temperature $N_2/CH_4$ plasma

C. Merhaben(*)[1], C. O. Laux[1], S. McGuire[1]

[1] *Université Paris-Saclay, CNRS, CentraleSupélec, Laboratoire EM2C, 91190, Gif-sur-Yvette, France*
(*) cyrine.merhaben@centralesupelec.fr

**Experimental measurements and model predictions of a recombining high-temperature $N_2/CH_4$ plasma are presented. A plasma torch is used to generate a $N_2/CH_4$/Ar plasma near local thermodynamic equilibrium (LTE) at atmospheric pressure and temperature of 7000 K. The LTE plasma is then forced to cool by passing at high speed through a water-cooled tube. The rapid cooling initiates chemical recombination. The evolution of the thermochemical properties of the plasma is studied experimentally as it flows through the water-cooled tube. Optical Emission Spectroscopy (OES) measurements between 320 and 880 provide direct measurements of the CN excited states densities and the rotational and vibrational temperatures of the gas. Absorption spectroscopy measurements performed between 350 and 400 nm provide density measurements of CN(X) ground state. Our experimental dataset is finally compared to the predictions of a $N_2/CH_4$ kinetic model.**

## 1 General

This work studies high temperature emission from a mixture composed of 98% $N_2$ and 2% $CH_4$ (by volume) and representative of Titan's atmosphere. During entry into the Titan atmosphere, the CN molecule forms in the shock layer and generates a substantial radiative heat flux. Previous studies have shown that excited electronic states of CN are overpopulated and do not follow a Boltzmann distribution [1–3]. This has important ramifications for the radiative heat flux to the vehicle surface. Additionally, the radiative heat loads on the surface of the vehicle are estimated to constitute 40% and 80% of the total heat load, on the forebody and the afterbody respectively. This radiative emission is primarily due to CN red ($A^2\Pi - X^2\Sigma^+$) and violet ($B^2\Sigma^+ - X^2\Sigma^+$) electronic bands [4,5]. Moreover, as the plasma flows past the forebody into the afterbody of the vehicle, it undergoes a rapid cooling, which leads to a rapid recombination and a departure from equilibrium. Therefore, a precise evaluation of the densities of CN electronic states is essential to accurately estimate the radiative heat flux. To achieve this, a chemical kinetic model is required to assess the density of the non-equilibrium CN states.

This work is comprised of three main parts. First, the emission spectroscopy measurements and associated spectral analysis are presented at different positions of the water-cooled tube. Second, absorption spectroscopy measurements of the CN violet system are used to determine the CN ground state density at the different studied positions. This combined dataset will enable us to determine the gas temperature and the densities of the CN $X$, $A$, and $B$ states. Third, the measured evolution of the temperature and the electronic distribution of CN will be used to test and validate models available in the literature describing the $N_2/CH_4$ plasma recombination kinetics.

**References**

[1] T.E. Magin, L. Caillault, A. Bourdon, C.O. Laux, Nonequilibrium radiative heat flux modeling for the Huygens entry probe, J. Geophys. Res. 111 (2006) E07S12. https://doi.org/10.1029/2005JE002616.

[2] J. Olejniczak, D. Prabhu, M. Wright, N. Takashima, B. Hollis, K. Sutton, E. Zoby, An Analysis of the Radiative Heating Environment for Aerocapture at Titan, in: 39th AIAA/ASME/SAE/ASEE Joint Propulsion Conference and Exhibit, American Institute of Aeronautics and Astronautics, Huntsville, Alabama, 2003. https://doi.org/10.2514/6.2003-4953.

[3] D. Bose, M.J. Wright, D.W. Bogdanoff, G.A. Raiche, G.A. Allen, Modeling and Experimental Assessment of CN Radiation Behind a Strong Shock Wave, Journal of Thermophysics and Heat Transfer 20 (2006) 220–230. https://doi.org/10.2514/1.16869.

[4] A.M. Brandis, R.G. Morgan, C.O. Laux, T. Magin, T. McIntyre, P.A. Jacobs, Nonequilibrium radiation measurements and modelling relevant to Titan entry, (n.d.).

[5] M. Wright, The Dragonfly Entry and Descent System, (n.d.).

# Evaluation of rice seed coat penetration characteristics of plasma-generated reactive oxygen species using the KI-starch

H. Shi[1], T. Okumura[1], P. Attri[1], K. Koga[1], M. Shiratani[1] and T. Kawasaki[2]

[1] *Kyushu University, Fukuoka, Japan*
[2] *Nishinippon Institute of Technology, Fukuoka, Japan*

The mechanism behind the growth promotion induced by plasma irradiation to seeds is a key research topic in plasma agriculture. Reactive oxygen species (ROS) generated by plasma are believed to penetrate seeds and trigger plant responses; however, the quantification of ROS introduced into seeds remains insufficiently understood. In this study, we evaluated the penetration of plasma-generated ROS through rice seed hulls using the KI-starch method, which allows easy assessment of ROS dose based on a color reaction. The coloration intensity, increase in optical density (OD), and ROS permeation through the hulls were assessed semi-quantitatively. Furthermore, scanning electron microscopy (SEM) confirmed that ROS penetrated the seed coat without causing any visible structural damage. These findings provide insights into the transport of ROS during plasma treatment and its potential role in enhancing seed germination and growth.

## 1 Introduction

Plasma treatment of seeds is recognized for triggering plant responses, such as enhancing germination [1-4]. Gaining insight into the underlying mechanisms necessitates developing techniques to quantify reactive species introduced into seeds by plasma. To examine whether plasma-generated reactive species indeed pass through seed coats, we assessed penetration of plasma-generated reactive oxygen species ROS through rice seed hulls using the KI-starch method [5].

## 2 Experimental

For KI-starch method, a reagent detects reactive oxygen species (ROS) through a color change triggered by oxidation reactions. Plasma was generated using a scalable dielectric barrier discharge (SDBD) electrode, which has been employed to enhance seed growth [6]. The discharge voltage and frequency were set at 13 $kV_{pp}$ and 9.6 kHz, respectively, with a discharge duration of 5 minutes. The resulting color changes on the KI-starch gel surface were recorded and analyzed using ImageJ software to determine the optical density (OD), which correlates with the relative concentration of ROS.

## 3 Results and discussion

Figure 1 shows the color reaction outcomes following plasma exposure for both conditions: without seed coat and with a seed coat. Visually, the reaction exhibits a circular shape in both cases. However, the color is more intense in the absence of the seed coat compared to when the seed coat is present. This suggests that plasma-generated reactive species reach the gel and trigger a reaction in both conditions, regardless of the seed coat. The OD value analysis from point A to point B allowed us to create an OD profile. It was observed that the maximum OD value at the center of the hole and reached 0.73 in the absence of the seed coat, while it was 0.5 when the seed coat was present. Though the results are currently semi-quantitative, they provide clear evidence of the transport of reactive species through the seed coat.

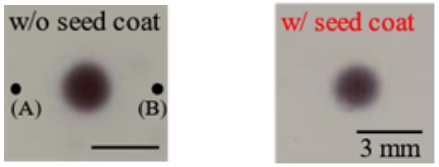



Fig. 1. Color reaction after plasma irradiation w/o and w/ seed coat.

**References**

[1] P. Attri, et. al., Agronomy, 12, 482 (2022).
[2] T. Kaneko et al., Jpn. J. Appl. Phys. 61, (2022).
[3] P. Ranieri et al., Plasma Process. Polym. 18m (2021).
[4] T. Okumura et al., Sci. Rep. 12, 12525 (2022).
[5] T. Kawasaki et al., IEEE Trans. Plasma Sci. 44, 3223, (2016).
[6] K. Koga et al., Appl. Phys. Express 9, 016201 (2016).

# Numerical and theoretical investigation of the ECRIPAC accelerator concept

A. Cernuschi[1], T. Thuillier[1] and L. Garrigues[2]

[1] *Université Grenoble Alpes, CNRS, Grenoble INP, LPSC-IN2P3, 38000 Grenoble, France*
[2] *LAPLACE, Université de Toulouse, CNRS, INPT, UPS, 31077 Toulouse, France*

This work proposes an in-depth study regarding the ECRIPAC accelerator concept, an idea developed in the nineties for an accelerator able to produce high energy pulsed ion beams. First, the physical theory of ECRIPAC is reviewed and corrected. A detailed theoretical analysis of the ion acceleration stability condition is conducted, revealing stricter limitations than previously anticipated and investigating the effects of various physical parameters on the accelerator's design. Following this study, a compact machine design capable of accelerating $He^{2+}$ ions to 9.5 MeV per nucleon in a 1.8 meter long cavity is proposed. Finally, a Monte Carlo particle-tracking code is used to investigate the electron population within the proposed accelerator design, exploring the impact of various physical parameters on the electron dynamics during the accelerator operation.

## 1 Introduction

The Electron Cyclotron Resonance Ion Plasma ACcelerator (ECRIPAC) [1] is a novel concept for an accelerator capable of generating high energy pulsed ion beams, making it suitable for many applications. The physical mechanism behind ECRIPAC consists in the combination of two experimentally verified physical principles: gyromagnetic autoresonance (GYRAC) [2] and ion entrainments inside magnetic field gradients (PLEIADE) [3]. The device is composed by an injector and two main sections (GYRAC and PLEIADE), exploiting simple and well mastered technologies such as magnetic fields and a microwave injector. The first stage of the device is used to increase the energy of the electrons through gyromagnetic autoresonance, which are used in the second stage to accelerate the ions through ion entrainment.
This work reviews and corrects the current theory behind ECRIPAC, and further expands it with novel theoretical and numerical investigations.

## 2 Accelerator stability analysis

A theoretical investigation based on the current ECRIPAC theory has been developed, further investigating the stability conditions for the ion acceleration. The required electron energy in the PLEIADE stage has been discovered to be higher than previously anticipated. Moreover, the length of the accelerating cavity has been noted to play a crucial role in the overall accelerator stability, which was not addressed in previous publications. Finally, the effects on the accelerator stability due to several physical parameters has been extensively investigated, providing a summary of attainable external fields and plasma properties. This investigation has led to the proposal of $He^{2+}$ accelerator compact design, able to accelerate the ions up to almost 10 MeV/nucleon over a length of 1.8 m.

## 3 Monte Carlo simulation

The electron population inside ECRIPAC has been simulated by means of an existing Monte Carlo particle-tracking code, already validated on ECR ion sources. The simulations validated the theoretical treatment of ECRIPAC and examined how various physical parameters influence the electron behavior during the accelerator operation.

## References

[1] Geller, R., Golovanivsky, K. S., and Melin G. ECRIPAC: A new concept for the production and acceleration to very high energies of multiply charged ions using an ECR plasma. *Proceedings of the 10th international workshop on ECR ion sources*, 449–451 (1991).
[2] Golovanivsky, K. S. The Gyromagnetic Autoresonance. *IEEE Transactions on Plasma Science*, **11**, 28–35 (1983).
[3] Bardet, R., Consoli, T., Geller, R. Mecanisme physique de l'entrainment des ions par la charge d'espace des electrons dans l'acceleration par le gradients de champs magnetique statique et electromagnetique. *Nuclear Fusion*, **5**, 7–16 (1965).

# Electron density measurements in a $H_2$/Ar microwave microplasma

Joel Jeevan, Michael Redolfi, Khaled Hassouni, Swaminathan Prasanna

*LSPM-CNRS, UPR 3407, Universite Sorbonne Paris Nord, 99 avenue J.B. Clement, 93430, Villetaneuse, France*

In this work, we report the measurement of electron density ($n_e$) using the stark broadening of the $H_2$ balmer series in Ar-$H_2$ microwave microplasma (MWMP) torch operating at moderate pressures. We also discuss the stark splitting of $H_\beta$, resulting in a dip in the profiles observed. The dip in the central structure of $H_\beta$ was found to decrease with increase in Ar concentration.

## 1 Introduction

In our earlier, work we have produced nanodiamonds in the range of 5-20 nm using an in-house developed MWMP torch of high H-atom density ($n_H$) [1]. As part of optimisation of the process, this work focusses on electrical characterisation of the MWMP torch using optical emission spectroscopy, particularly $n_e$ using the Balmer lines $H_\beta$ and $H_\gamma$ (n= 5→2) of H-atom.

Details of the experimental setup are discussed elsewhere [1]. Emission spectra were recorded using a THR 1000 spectrometer having a focal length of 1m. In this work, the $H_2$ flowrate was fixed at 100 sccm and Ar flowrate was varied between 10 and 300 sccm.

### 1.1 Result and discusssion

Stark widths of $H_\beta$ and $H_\gamma$ can be used for measurement of electron densities $n_e > 10^{12}$ $cm^{-3}$. It has been estimated from deconvolution of the respective spectra with a Voigt profile after eliminating the contributions from different broadenings. The instrumental broadening, estimated using a He-Ne laser, was found to be 15pm. The gas temperature inferred from rotational temperature of the $G^1\Sigma_g^+ \rightarrow B^1\Sigma_u^+(0, 0)$ transition of $H_2$ molecule was ≈ 1000 K and was used to estimate Doppler and Van der Waals broadening.

$H_\beta$ profile displayed two asymmetric peaks at 486.099 nm and 486.142 nm, labelled as blue and red, respectively (Figure 1a). The $H_\alpha$ and $H_\gamma$ did not have such anomalies. The wavelength corresponding to the blue and red peaks remains unchanged across all the experimental conditions. The red peak could arise due to potential contaminants such as Fe, Cu, Mn and Cr. However, no evidence of these elements was found in other spectral regions. Moreover, the red peak also disappeared in pure Ar or $N_2$ plasmas. This is indicative that the spectra are inherent feature of the hydrogen plasma and is associated with $H_\beta$.

$H_\beta$ profile with a dip could be explained by Stark effects arising from very high $n_e$, ion dynamics effect, plasma inhomogeneities and quadratic or quadrupolar effects [2]. The $n_e$ in our system measured by stark broadening of both $H_\beta$ and $H_\gamma$ were found to be ≈ $10^{12}$ - $10^{13}$ $cm^{-3}$ and is too low to cause stark splitting.

A factor δ, the difference of intensity of blue and red peak normalized to intensity of blue peak has been used to study the effect of gas composition on the $H_\beta$ profile. Figure 1b shows the variation of $n_e$ measured using $H_\gamma$ and δ as a function of Ar flow rate at 45 W power and 100 mbar pressure. The concentration of Ar and δ exhibits an inverse correlation, and at a high concentration of Ar; $I_{red} \approx 0$. This could be possibly due to difference in emitter - perturber pair when the system undergoes a transition from a $H_2$-rich, consisting mostly of lighter $H^+$ and $H_3^+$ ions towards heavier $Ar^+$ ion in Ar-rich condition; thus resulting in reduced perturbation due to ion dynamics. Further investigations are being conducted to find out the plasma phenomena leading to such $H_\beta$ profiles in a low $n_e$, high $n_H$ MWMP.

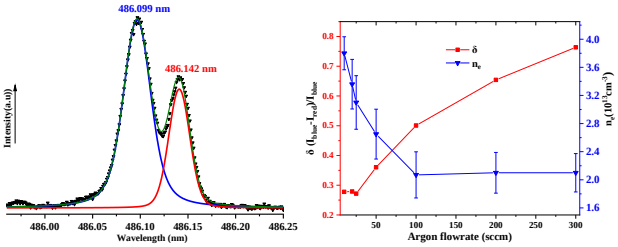



Figure 1: (a) H-β profile (left), and (b) δ and $n_e$ v/s argon flow rate (right) at 100 mbar and 45 W of MW power

### References

[1] Siby, A. Nucleation of nanodiamonds in H-atom rich microplasma. *Diamond and Related Materials* **152**, 111933 (2025).

[2] Bruggeman, P., et al. Plasma Sources Sci. Technol. **18**, 025017 (2009).

# Study of the physical properties of different µm-scale He plasma jets

Y. Agha[1], K. Giotis[1,2], D. Stefas[1], L. Invernizzi[1], H. Höft[3], P. Svarnas[2], G. Lombardi[1], and K. Gazeli[1]

[1] *Laboratoire des Sciences des Procédés et des Matériaux (LSPM), CNRS, Université Sorbonne Paris Nord, UPR 3407, F–93430 Villetaneuse, France*
[2]*University of Patras, Electrical & Computer Engineering Dept., High Voltage Lab., Rion, Patras, Greece*
[3]*Leibniz Institute for Plasma Science and Technology (INP), Felix-Hausdorff-Str. 2, Greifswald, Germany*

Atmospheric pressure plasma jets (APPJs) are widely-investigated for emerging applications, e.g., in analytical chemistry, where µm scale APPJs (µm-APPJs) are of particular interest. Due to their small dimensions and fast dynamics, these discharges are a challenge for diagnostics. This work presents investigations of the physical properties of three different µm-APPJ configurations with emphasis on the temporal and axial variation of electric field strength, gas temperature and electron density.

The study of APPJs for emerging applications is still a challenging task, requiring high accuracy of experimental methods and/or models applied [1,2]. Particularly, pulsed-driven µm-APPJs generate fast ionization waves (10s–100s km/s) with steep spatial/temporal gradients of gas temperature ($T_{Gas}$), electric field ($E_{Field}$) strength, and densities of reactive species and electrons ($N_e$). A detailed mapping of these quantities in different µm-APPJs may enable a better understanding of their complex behavior and control of their distributions. This is particularly beneficial for their implementation in analytical chemistry [2]. Advanced optical diagnostics (e.g., OES, ICCD, laser-based) may allow access to these quantities and the discharge dynamics with sufficient spatial and temporal resolution [3].

In this work, the spatial and temporal variations of ionization wave speed ($v_i$), $T_{Gas}$, $E_{Field}$, and $N_e$ are studied in three geometrically different µm-APPJs in the same configuration. All microjets use single hollow electrodes (Ø180 µm) with different lengths (5 or 27 mm). These are driven by a positive pulsed high voltage with fixed characteristics ($V_P$=10 kV, $f$=10 kHz, 160 ns pulse width, 60 ns rise time) and are installed in miniature quartz tubes of dissimilar inner diameters (400 or 600 µm). The operating gas is helium with a fixed flow rate (0.3 slm). Space- and time-resolved OES measurements are performed with two spectrometers (0.5 and 1 m focal lengths) backed with different ICCD cameras to favor either temporal (3 ns gate width) of spectral resolution (20 pm). For spatially-resolved OES measurements, µm-APPJs are installed on a translational stage and are imaged on the slit of the spectrometers using a UV lens system.

Various radiative transitions are generated along the jet axis which are useful for accessing the plasma parameters. These allow performing the following measurements for the three µm-APPJs: ionization front speed with the ICCD, $T_{Gas}$ *via* the rotational temperature of probe molecules (e.g., OH(A)) and the resonance broadening of a He I line at 667.8 nm, $E_{Field}$ based on the Stark splitting of a He I line at 492.19 nm (Fig.1), and $N_e$ through the Stark broadening of $H_\beta$ at 486.13 nm. Preliminary results obtained reveal $v_i$ of ~0.1 mm/ns, $T_{Gas}$≈330 K, axial $E_{Field}$ strength of ~10 kV/cm and $N_e$ of ~$10^{14}$ cm$^{-3}$. Slight variations of $v_i$, $T_{Gas}$, $E_{Field}$ strength, and $N_e$ are revealed along the jet axis inside the tube, independent of the jet geometry. These results help in better understanding of µm-APPJs for targeted applications.

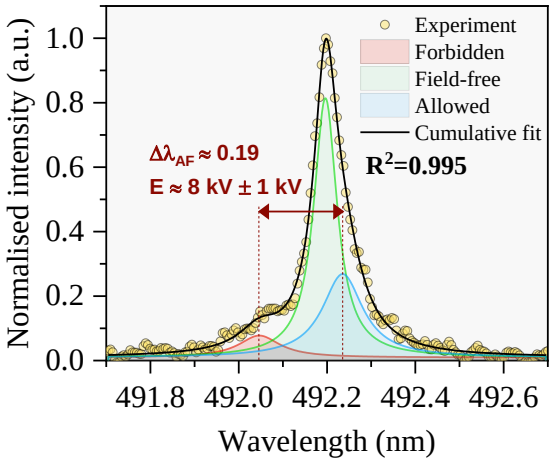



Fig.1: Indicative π–polarized He I line at 492.19 nm. The $E_{Field}$ strength is determined from the distance $\Delta\lambda_{AF}$, as detailed in [4] (µm-APPJ: 27 mm electrode, 600 µm quartz tube). The He I line is recorded at the exit nozzle.

## Acknowledgements

ANR ULTRAMAP (ANR-22-CE51-0027),
DFG d3DBD (project number 535827833).

## References

[1] C. Tian *et al., Spectrochim. Acta Part B At. Spectrosc.* **181**, 106222 (2021).
[2] P. Viegas *et al., Plasma Sources Sci. Technol.* **31**, 053001 (2022).
[3] G. Niu *et al., Anal. Chim. Acta* **1147**, 211 (2021).
[4] M. Mirzaee *et al., Phys. Plasmas* **27**, 123505 (2020).

# Real-time tracking of emissive species and gas temperature in a pulsed MHCD during the deposition of h-BN on a Si substrate

B. Menacer, N. Chazapis, K. Gazeli, C. Lazzaroni, V. Mille

*Université Sorbonne Paris Nord, CNRS, LSPM UPR 3407, Villetaneuse, France*

The optimization of Micro Hollow Cathode Discharges (MHCD) for hexagonal boron nitride (h-BN) synthesis requires real time diagnostics of various plasma parameters. This work performs spatial and temporal mappings of emissive species ($N_2$(SPS), $N_2$(FPS), Ar I) and gas temperature ($T_{Gas}$) generated by a pulsed MHCD during h-BN synthesis. All plasma parameters are measured in the MHCD hole and the deposition chamber. The rotational temperature, $T_{Rot}$, of $N_2$(C) sets an upper limit for the $T_{Gas}$, remaining below 700 K. Strong $N_2$(FPS) and Ar I emissions are measured in the deposition chamber indicating a role of $N_2$(A) and Ar($1s_5$) metastables in $N_2$ dissociation process. This MHCD achieves h-BN deposition on large-surface (Ø5 cm diameter) Si wafers. The deposition of h-BN films and their features are evidenced and assessed using Raman, SEM and AFM.

## 1 Introduction

h-BN is a wide bandgap insulator with excellent thermal conductivity, making it suitable for novel applications [1]. In this work we use a pulsed MHCD ($V_p$=-1 kV, f=10 kHz, 500 ns pulse width) to deposit h-BN on a Si substrate (Ø5 cm). This MHCD is suitable for nitride deposition since it can effectively dissociate $N_2$ [2]. The plasma source is positioned between a high-pressure (30 mbar) and a low-pressure (1 mbar) chamber, while it operates in a $N_2$/Ar gas mixture containing a $BBr_3$ precursor and $H_2$ [2]. The substrate holder is heated (800 K) and biased (200 V DC) to assist the plasma expansion towards the substrate. Optical emission spectroscopy (OES) and ICCD imaging allow measuring space- and time-resolved species intensities, $T_{Gas}$ (estimated via the $T_{Rot}$ of $N_2$(C)), and total plasma emission.

## 2 Results

The temporal evolution within the discharge current of the *(i)* emission intensities of $N_2$(SPS) around 337 nm and Ar I around 811 nm, and *(ii)* $T_{Rot}$ of $N_2$(C), in the low-pressure chamber and in real time during the deposition process, are shown in Fig.1(a). Both species intensities follow the discharge current, implying a role of electrons in the generation of their excited states. $T_{Rot}$ approximates $T_{gas}$, remaining below 700 K, i.e., lower than that of the substrate, ensuring a good energy efficiency and stability. Fig.1(b) shows a single shot ICCD image of the total plasma emission in the low-pressure chamber, revealing its morphology which affects the film properties (Fig.1(c)). This also allows studying the impact of $BBr_3$ and $H_2$ on plasma dynamics. The variation of the $N_2$(FPS) emission around 587 nm is also studied. Along with the Ar I emission, it is enhanced in the low-pressure chamber. These transitions populate $N_2$(A) and Ar($1s_5$) metastables, respectively, affecting the $N_2$ dissociation.

The h-BN films synthesized are characterized *ex-situ* with Raman spectroscopy, SEM and AFM imaging. The signature of h-BN at 1366 $cm^{-1}$ is verified in Raman spectra, while the morphology of the films is assessed with SEM (Fig.1(c)) and AFM.

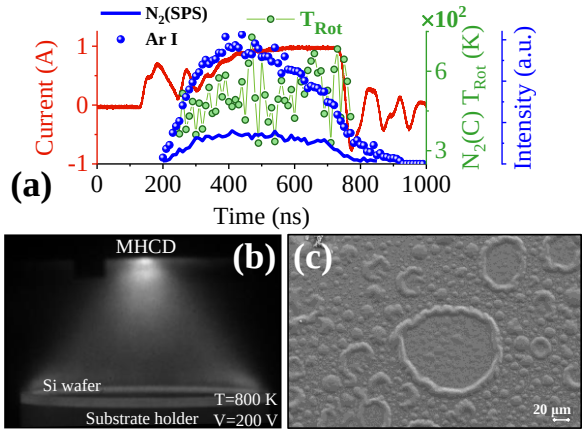



Fig. 1: (a) temporal variation of the $T_{Rot}$ of $N_2$(C) and the emission intensities of $N_2$(SPS) and Ar I within the discharge current (red); (b) single shot ICCD image (100 µs gate) of the discharge expansion in the deposition chamber; (c) SEM image of a h-BN film deposited on a Si substrate (Ø5 cm) revealing its texture/morphology.

**Acknowledgements**

ANR SPECTRON (ANR-23-CE51-0004-01), ANR PlasBoNG (ANR-20-CE09-0003-01), Labex SEAM (ANR-10-LABX-0096; ANR-18-IDEX-0001).

**References**

[1] S. J. Liang, et al Advanced Materials 32, page 1903800, 2019

[2] Jacquemin *et al*, MRS Communications **14** 63 (2024)

# Plasma irradiation to cytokines and immune cell in culture medium using a porous membrane plasma source

H. Nakamura [1], Y. Yagyu [1], N. Hayashi [1]

[1] *Interdisciplinary Graduate School of Engineering Sciences, Kyushu University, Fukuoka 816-8580, Japan*

Using an oxygen plasma source that can supply active species directly into water using a porous membrane, the activity of cytokines and immune cells were attempted to be controlled. The cell number of macrophage was increased with the plasma treatment period of 10-30 sec with the dissolved active oxygen concentration of 2 mg/L. The phagocytosis of the macrophage decreases.

## 1 Introduction

Exposure of cells to the oxygen plasma has been able to promote cell proliferation and activity. In a previous study, suppressing osteoclast proliferation has been observed by controlling the amount of the intracellular secretion, RANKL, produced by osteoblasts [1]. Also, oxygen plasma is used to control the activity of cytokines used in intercellular communication during immune cell proliferation and activation. The effect of plasma-treated cytokines on immune cell proliferation and activation has been observed. In this study, the IFN-γ as the cytokine and investigated the changes in macrophage proliferation characteristics and phagocytosis as cell activity, when a plasma-exposed IFN-γ solution was dispensed into macrophages.

## 2 Experimental setup and Results

Figure 1 shows a schematic of the plasma irradiation device. A porous PTFE membrane was used to cover the open end of a torch-type barrier discharge device, creating an atmospheric pressure plasma generator in which the discharge electrode does not contact with liquid when discharging in liquid. The surface tension generated by micro pores prevents the liquid from seeping out to the electrode. Active species generated by the plasma dissolve into the liquid phase from the gas-liquid interface in the micro pores. By applying the porous membrane oxygen plasma to the cytokine IFN-γ and providing the IFN-γ after plasma irradiation to macrophages, the changes in IFN-γ activity can be clarified from their proliferation. The plasma source was placed in IFN-γ dissolved solution at a concentration of 0.001 ppm dispensed in 500 μL portions into a 24-well plate, and plasma irradiation was performed by changing the exposure time. Macrophages were adjusted to an initial cell count of $1.0\times10^5$ cells/ml in a 96-well plate, and IFN-γ solution was dispensed in 100 μL portions and cultured again for 24 hours to measure cell count and evaluate activity.

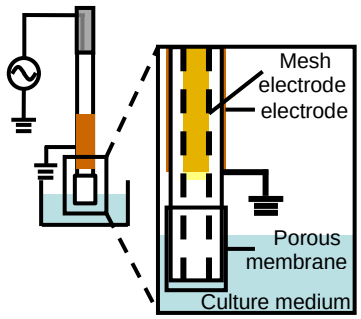



Fig. 1 Schematic of porous membrane plasma source

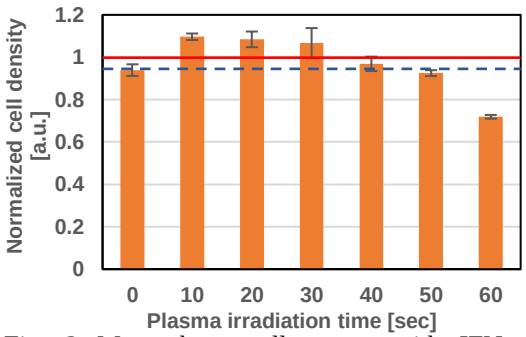



Fig. 2 Macrophage cell counts with IFN-γ at different plasma irradiation time.

The effect of plasma on cytokines was evaluated from the changes in cell number and phagocytosis when IFN-γ was added for different plasma irradiation times. Figure 2 shows the change in the number of macrophage cells when IFN-γ dissolved culture medium was exposed to liquid plasma and then added to macrophages. When IFN-γ without the plasma was added to macrophages, cell numbers were lower than in macrophages not given IFN-γ. When IFN-γ was exposed to plasma for a short period of time (10-30 seconds), the number of macrophages was about 1.2 times that of the untreated group. In addition, it was found that phagocytosis was lower than that of the unexposed IFN-γ group. It is thought that the decomposition of IFN-γ by active oxygen species in the plasma suppressed the macrophage activation and reduced phagocytosis (cell activity).

[1] Hayashi, N., Inoue, Y., Kyumoto , Y., & Kukita , T. (2020). JJAP, 59(SJ), SJJF02.

# Application of non-conformal triangular meshes in fluid modelling of low-temperature plasma discharges.

I. L. Semenov

*Leibniz Institute for Plasma Science and Technology, Felix-Hausdorff-Str. 2, 17489 Greifswald, Germany*

A novel solver for elliptic partial differential equations on non-conformal triangular meshes is introduced, with a focus on its application to fluid modelling of low-temperature plasmas. The solver is applied to model streamer discharges and a capacitively coupled radio-frequency plasma reactor. The advantages of using non-conformal triangulations in low-temperature plasma models are discussed.

One of the challenges in fluid modelling of low-temperature discharges is resolving boundary layers near plasma-facing surfaces and capturing ionization waves propagating through the plasma bulk. At atmospheric pressures, this challenge becomes even more pronounced, leading to a complex computational problem that is inherently multiscale. Using space-adaptive numerical methods in such cases is essential for maintaining reasonable computational times [1, 2]. Overall, transitioning to space-adaptive numerical frameworks is crucial for addressing the current challenges in low-temperature plasma modelling.

Currently, the use of space-adaptive numerical methods in plasma modelling remains somewhat limited. Existing examples primarily focus on problems in open spaces and typically involve structured computational meshes. To address more realistic problems, transitioning to space-adaptive methods on triangular meshes would be beneficial. These methods can be constructed based on non-conformal triangulations, as illustrated in Figure 1. In general, partial differential equations (PDEs) on these meshes can be solved using standard finite-element (Galerkin-type) methods (FEM). However, FEM methods cannot be expressed in the form of local conservation laws. This limits the adoption of these methods within the experimental community and hinders the development of conservative reinterpolation schemes on adaptively changing meshes.

Nevertheless, for linear elements, it is possible to construct a conservative control-volume scheme for both conformal and non-conformal triangular meshes. This scheme has recently been implemented in the new package *triellipt* [3] for solving elliptic PDEs. The proposed scheme is equivalent to conventional FEM on conformal meshes but allows for a conservative description of non-conformal contacts between triangles. Moreover, it supports reinterpolation between triangular meshes in a way that conserves integral quantities, such as total mass and charge.

In this work, we demonstrate how the *triellipt* package can be applied to fluid modelling of low-temperature plasma discharges. We consider simulations of streamer discharges, both in open space and in pin-to-pin and pin-to-plate configurations. Additionally, we address the standard benchmark problem: the simulation of the Gaseous Electronics Conference (GEC) capacitively coupled plasma reactor in argon. The benefits of using non-conformal triangular meshes in fluid discharge models are discussed.

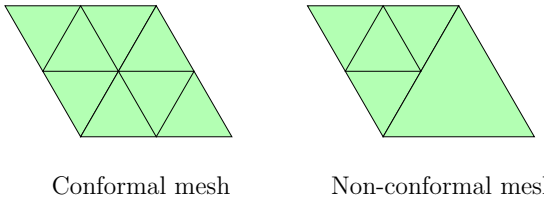



Figure 1: Example of conformal (left) and non-conformal (right) triangulations.

## Acknowledgement

This work was funded by the Deutsche Forschungsgemeinschaft (DFG, German Research Foundation) – project number 515939493.

## References

[1] Bagheri, B., et. al. *Plasma Sources Science and Technology*, **27**(9), 095002 (2018).

[2] Semenov, I. L., Weltmann K.-D. *Journal of Computational Physics*, **465**, 111378 (2022).

[3] Semenov I. L. (2025). *triellipt*, GitHub. Available: github.com/igsemenov/triellipt

# Optical Emission Spectroscopy of $Ar/CO_2/H_2O$ plasmas generated in a modified surfatron device

A. Rodero [1], F.J. Romero-Salguero[2] and M.C. García[3]
[1] *Dpto. de Física, Campus de Rabanales, Univ. de Córdoba, 14071 Córdoba, Spain*
[2] *Dpto. Química Orgánica, Campus de Rabanales, Univ. de Córdoba, 14071 Córdoba, Spain*
[3] *Dpto. de Física Aplicada, Rad. y Medicina Física, Campus de Rabanales, Univ. de Córdoba, 14071 Córdoba, Spain*

A modified surfatron design allowing non-filamented argon microwave (2.45 GHz) plasmas to be sustained under atmospheric pressure conditions and low power, was utilized to create $Ar/CO_2/H_2O$ plasmas. Optical Emission Spectroscopy techniques were conducted to identify the excited species generated in the different discharges and diagnose them. This design, which has previously proven to be useful for the production of OH species using $Ar/H_2O$ mixtures [1], will be investigated for its applicability in $CO_2$ valorization. The introduction of small amounts of water into the mixture will also be studied.

## 1 Plasma reactor

A surfatron was used to couple energy coming from a 2.45 GHz power supply to generate argon plasmas within a quartz tube using powers from 50 W. For this purpose, the electromagnetic field configuration created by the surfatron was altered by introducing in the tube a small rectangular-shaped Si(100) wafer (4 mm × 20 mm × 300 μm) (see **Fig. 1**). Thus, a strong electric field was established at the edges of the silicon strip and a plasma column was formed. Unlike usual surfatron experiments, neither plasma was observed inside the surfatron nor plasma filamentation took place. The reactor also allowed stable maintenance of plasmas with moderate fractions of $CO_2$ and water, at relatively low power.

In this work, we have studied the generation of excited species in this reactor when different amounts of $CO_2/H_2O$ were dragged through the main gas. The power was set at 190 W and, in a primary gas line, the argon flow rate was adjusted from 0 to 1250 sccm. A secondary feeding argon line bubbling through water was also used with argon flow rates set from 0 to 1250 sccm. Finaly, a third line was used to introduce 20 sccm of $CO_2$.

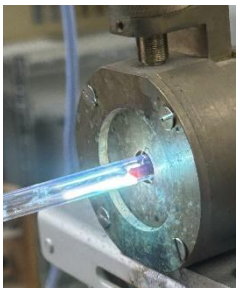


**Fig. 1.** Plasma Column

## 2 Plasma diagnosis

OES techniques were used for plasma diagnosis. A Czerny-Turner type spectrometer of 1 m focal length (with a 1200 grooves/mm holographic grating and a photomultiplier as a detector) was used for the analysis of the plasma emission.

### 2.1. Plasma excited species

The main emission from plasmas with small fractions of water corresponded to Ar I and O I lines, CN and $C_2$ bands. For larger water contents, OH bands emission dominated (**Fig. 2**).

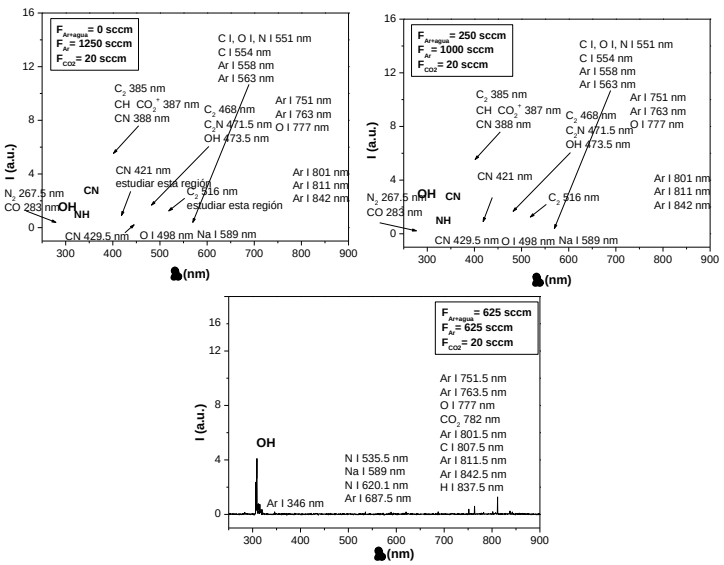



**Fig. 2.** Excited species evolution.

### 2.2. Gas temperature

The gas temperature was estimated using the fitting of the vibro-rotational bands of CN and OH radicals to simulated spectra by LIFBASE software. The temperatures obtained in this study ranged from 2500 K to 5000 K, depending on the amount of $H_2O$ present in the plasma.

**Acknowledgements**

Authors thank the project TED2021-130124A-I00 by AEI/10.13039/501100011033/Unión Europea Next Generation EU/PRTR and the University of Córdoba Plan Propio (PP-RCOPIVIPSKILLS) for support.

**References**

[1] J. Amaro-Gahete, J., Romero-Salguero, F.J., Garcia M.C., Chemosphere 349 (2024) 140820.

# Active species in the afterglow of MW $N_2$ plasma

S.A.Starostine[1] , T.C. van Eeden[1] and M.C.M. van de Sanden[1,2]

[1] *Dutch Institute for Fundamental Energy Research (DIFFER), De Zaale 20, 5612 AJ, Eindhoven, the Netherlands*
[2] *Department of Applied Physics, Eindhoven University of Technology, 5600 MB, Eindhoven, the Netherlands*

In this contribution, we report measurements of atomic nitrogen [N] and molecular metastable [$N_2(A^3\Sigma_u^+)$] concentrations in the downstream region of a microwave-driven plasma reactor operating at mid- and near-atmospheric pressure, by optical emission spectroscopy.

## 1 Introduction

Nitrogen plasma afterglow has a long history of experimental and theoretical investigation. This interest is induced by a significant practical value in different fields of plasma technologies related to gas conversion, surface modifications, agricultural and biomedical applications. While the majority of early studies were carried out at low pressure, for nowadays applications it is of special importance to determine the number densities of active species such as atomic nitrogen radicals, electronically and vibrationally excited nitrogen molecules, produced by a plasma source operating at (near-) atmospheric gas pressure.

## 2 Experimental approach

The 1 kW microwave plasma is ignited in a quartz tube (i.d. 27 mm), inserted in the microwave cavity with tangentially injected $N_2$ to create a vortex flow at rate of 10 slm in the pressure range of 300 - 900 mbar (see Fig. 1). After passing through the plasma, the gas flow is mixed and cooled through a quenching nozzle and enters the downstream region. In this region, OES measurements at multiple axial positions are performed through which temperatures, and active species densities and their spatial distribution can be deduced. The employed quantification method for atomic nitrogen concentration [N], is based on the time decay of the $N_2(1+)$ system emission as it was described in [1].

Moreover, using an approach described in [2], quantitative estimates were given to the concentration of the electronically excited metastable nitrogen molecule $N_2(A^3\Sigma_u^+)$.

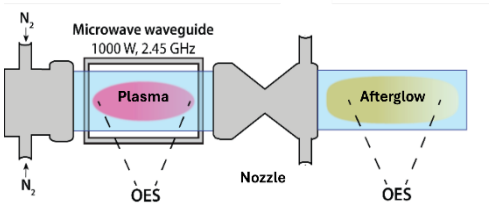



Fig. 1. Microwave plasma reactor.

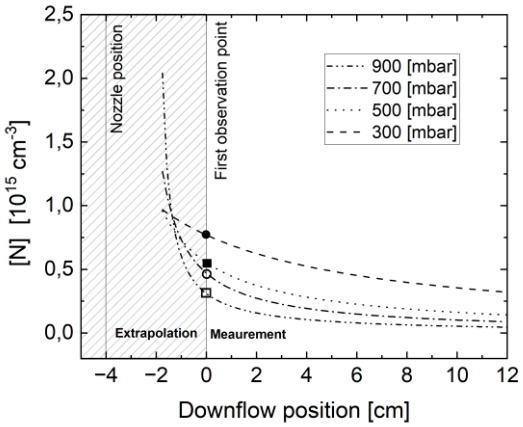



Fig. 2. Atomic nitrogen densities for different gas pressures. Extrapolation to upstream region is also shown.

## 3 Results and Discussion

The results for the [N] concentration for the gas pressure range of 300 – 900 mBar are shown in Fig. 2. This graph also presents an upstream extrapolation according [1] towards the early afterglow region, which was not accessible for OES in present experimental arrangement. A considerable density of atomic nitrogen, in the order of ~$10^{15}$ $cm^{-3}$, can be expected at high pressure just after the nozzle, while the afterglow extends as the pressure decreases. An estimate according to [2] for the $N_2(A^3\Sigma_u^+)$ concentration gives a value in the order of ~$10^{11}$ $cm^{-3}$ for (500 mBar, 10 slm, 4 cm downstream nozzle), indicating what atomic nitrogen remains the main active radical in the mid-pressure late afterglow.

**References**

[1] Peeters, F. J. J. et al *Plasma Sources Sci. Technol.* **24**, 045006 (2015).
[2] Ricard, A. et al *Plasma Sources Sci. Technol.* **22**, 035009 (2013).

# Streamer-to-spark transition: time-resolved imaging and time evolution of $n_e$ and $T_p$

A. Dorval[1], C. Latreille[1], L. Stafford[1], A. Hamdan[1]

[1] *Département de physique des plasmas, Université de Montréal, Montréal, Canada*

Nanosecond discharge is ignited at water-heptane interface and propagated in water. Here, we study discharge characteristics using time-resolved OES. Emission spectra are acquired during streamer ignition, propagation, and transition to spark. The data allowed estimation of electron density and plasma temperature from ignition to extinction. The findings provide new insights into the involved mechanisms such as the balance between ionization and recombination.

## 1 Introduction

Discharge in liquid is a fast transient and stochastic plasma and lead to the formation of streamer that may transit to spark if the experimental conditions (voltage amplitude and duration, gap distance) allow. Both discharge modes, streamer and spark, exhibit interesting properties that made them attractive for applications such as liquid processing and nanomaterial synthesis [1,2].

Recently, our group demonstrated that adding a liquid layer, that has low dielectric permittivity, at the top of another one, that has high dielectric permittivity, significantly enhances the discharge volume as well as its probability of occurrence [3]. This enhancement is due to the amplification of the electric field magnitude induced by the difference of the dielectric permittivity at the interface. The consideration of this property offers the opportunity to produce and characterize in-liquid discharges with time- and space-resolved techniques.

## 2 Experiments and Results

The discharges are ignited at heptane-water using puled high voltage: amplitude of 20 kV, duration of 500 ns, and repetition rate of 1 Hz. The anode tip, made of copper, is placed at the interface, while the ground plate electrode (made of copper) is placed in distilled water at a distance that can be adjusted (2-8 mm). Exposure time of the spectrometer's ICCD was 3 ns. The delay between the discharge and ICCD camera is controlled using a delay generator to reconstruct the temporal behavior. The OES spectra are analyzed using a Bayesian fitting procedure to determine $n_e$ (from Stark broadening and shift of the Hα and Oxygen (777 nm) lines) and $T_p$ from the continuum radiation (assumed to be dominated by Planck's radiation).

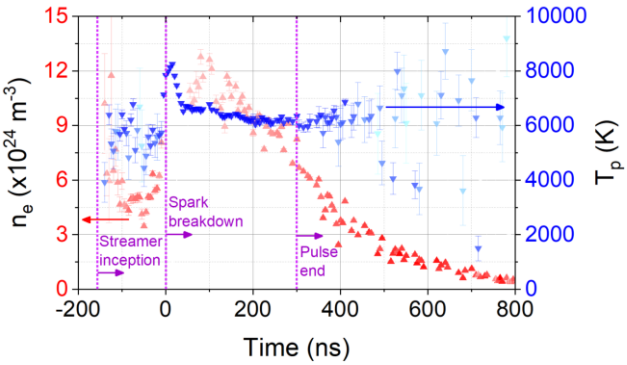



**Fig. 1**. Evolution of electron density ($n_e$, red) and the plasma temperature ($T_p$, blue) from ignition until extinction.

Figure 1 shows the evolution of ne and Tp for a gap of 4 mm. At the streamer's inception, ne is high (~$10^{25}$ $m^{-3}$) near the anode and decreases to (~5 $10^{24}$ $m^{-3}$) during propagation. During this stage, $T_p$ is ~5000 ± 1000 K; the high uncertainty is due to the low intensity of the blackbody continuum. At the breakdown, i.e. streamer-to-spark transition, the power peaks to a few of 100s kW), which results in a rapid rise of ne to a value that is unknown due to the only continuum radiation (no Hα line is detected). During this moment, Tp increases to 8000 ± 100 K. Beyond breakdown, ne gradually decreases, while Tp rapidly (within 40 ns) drops by 1500 K before reaching a plateau at ~6000 K until extinction. The evolution of the spectral features suggests a strong energy transfer by radiative processes, including recombination [4]. This aspect will be further discussed.

**References**

[1] Belmonte et al., J.Phys.D **47** 224016 (2014).
[2] Vanraes et al., Appl. Phys. Rev. **5**, 031103 (2018)
[3] Hamdan et al., PSST **30** 055021 (2021).
[4] De. Giacomo et. al., Spectrochimica Acta Part B **65** 385-394 (2010).

# Measurement of the electric field distribution in streamer discharges

Y. Guo[1], A. Limburg[1], J. Laarman[1], J. Teunissen[2] and S. Nijdam[2]

[1] *Eindhoven University of Technology, 5600 MB Eindhoven, The Netherlands*
[2] *Centrum Wiskunde & Informatica (CWI), 1090 GB Amsterdam, The Netherlands*

For the first time, we have performed detailed direction-resolved measurements of the electric field distribution in single-channel streamers in air by using E-FISH. To restore the local electric field from the E-FISH signals, we have developed a deconvolution method considering the phase variations and interference effects. The acquired field distribution agrees well with the simulation results under the same conditions in direction, magnitude, and shape. This enables a better understanding of streamers and empowers future use of E-FISH.

## 1 Introduction

Streamer discharges are fast-propagating ionization fronts that appear as the precursor to lightning leaders and as sprites in nature. The electric field is the driving force behind streamers and determines their energy transfer and chemical activity. Recently, a new technique called electric field induced second harmonic generation (E-FISH) has been introduced to the plasma community to measure the electric field of various kinds of plasmas. Superficially, the signal of E-FISH is considered easy to interpret: its intensity scales directly with the square of the electric field strength. However, it is found that the measured signals are strongly related to the properties of the laser beam and the profile of the electric field to be measured [1].

In this work, we used E-FISH to experimentally obtain for the first time a detailed direction-resolved spatio-temporal distribution of the electric field in a single-channel streamer.

## 2 Results and discussions

We used an experimental setup to generate streamers and measure E-FISH signals as described in [2]. To restore the local electric field from the E-FISH signals, we have developed a deconvolution method considering the phase variations and interference effects. A calibration measurement on a known field distribution is performed to obtain absolute electric fields.

As shown in figure 1, the space charge layer with the crescent shape of the streamer head is clearly visible. The electric field is most intense around the head of the streamer and is mostly pointing downward. Inside the streamer channel, the electric field almost vanishes, as the highly conductive streamer channel shields the electric field very efficiently. Furthermore, light emission always lags behind the electric field, as can be expected. The magnitude, shape, and direction of the field and its position relative to the light emission agree with the simulations.

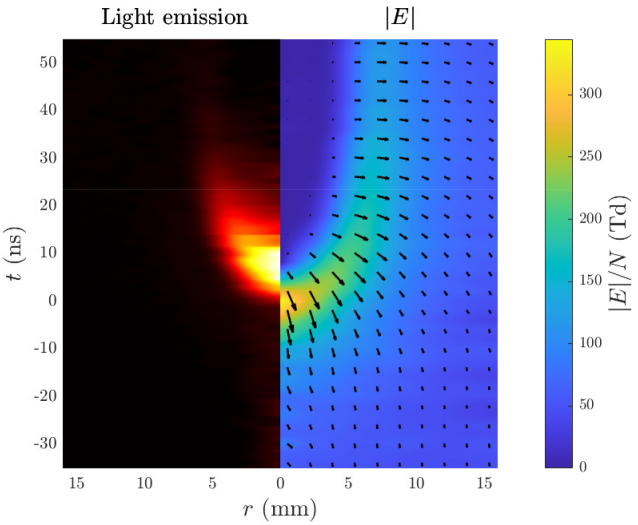



Figure 1: Experimental results of the local normalized light emission intensity and the reduced electric field amplitude, distribution, and orientation obtained with E-FISH. Image published before in [2].

## References

[1] Chng, T. L., *et al.* Electric field measurements in plasmas: how focusing strongly distorts the E-FISH signal. *Plasma Sources Science and Technology*, **29**, 125002 (2020).

[2] Guo, Y., *et al.* Measurement of the electric field distribution in streamer discharges. *Physical Review Research*, **7**, 013051 (2025).

# The McWhirter criterion revisited for laser-induced plasmas

A. Bultel, V. Morel and A. Favre

*Université de Rouen-Normandie, CNRS, CORIA UMR 6614, Saint-Étienne du Rouvray, France*

Collisional-radiative models are elaborated, for which expansion and self-absorption effects are included to evaluate the departure from equilibrium of laser-induced plasmas. The well-known McWhirter criterion can then be reestimated.

Many criteria have been established around the years 1960-1990 to rapidly discuss the departure from Local Thermodynamic Equilibrium (LTE) of a plasma. Among the proposals of Wilson [1], Griem [2], McWhirter [3], Drawin [4], Hey [5] and Fujimoto and McWhirter [6], the criterion due to McWhirter alone has been widely used. Nowadays, this criterion is used systematically within the framework of the study of laser-induced plasmas with the electron density $n_e$ and the electron temperature $T_e$. This criterion is based on the main idea that the departure from LTE results from the too strong influence of radiation in the case where the collisional coupling is due to electrons. It gives the minimum electron density value to obtain a ratio of ~ 10 between the electron-induced inelastic collision frequency and the spontaneous emission frequency. Given in 1965 and using assumptions of the hydrogenlike type, this criterion states that LTE is satisfied if

$$n_e > A\sqrt{k_B\,T_e}(\Delta\varepsilon_{ki})^3$$

where $A = 1.6 \times 10^{18}\ m^{-3}\ eV^{-7/2}$, $k_B$ is the Boltzmann constant and $\Delta\varepsilon_{ki}$ is the maximum value of the energy difference between the levels $k$ and $i$ connected by an optically allowed transition.

Laser-induced plasmas exhibit very specific characteristics. They expand into the background gas at very high, initially hypersonic, speeds. In many configurations, they also exhibit low gradients. Furthermore, they are characterized by high density. Therefore, the influence of expansion and self-absorption of radiation can lead to a change in the relative role of radiation and collisions: the McWhirter criterion must then be reestimated.

The state-to-state approach is particularly suited to the study of the temporal evolution of plasmas up to excitation and ionization equilibria. Using this approach, the development of collisional-radiative (CR) models allows for an in-depth study of the behavior of the number density of excited states and to determine the time required to reach equilibrium if this state is possible [7-8]. They can be used to estimate an LTE criterion.

We have therefore developed the relevant CR models for different elements to test the influence of $\Delta\varepsilon_{ki}$ for different temporal evolution conditions for $n_e$ and $T_e$. The self-absorption of the lines dependent on the plasma radius at time $t$ is taken into account. Figure 1 shows an example of a Boltzmann plot on neutral and ionic Aluminum, highlighting the influence of self-absorption of radiation. From such plots, the McWhirter criterion is reestimated.

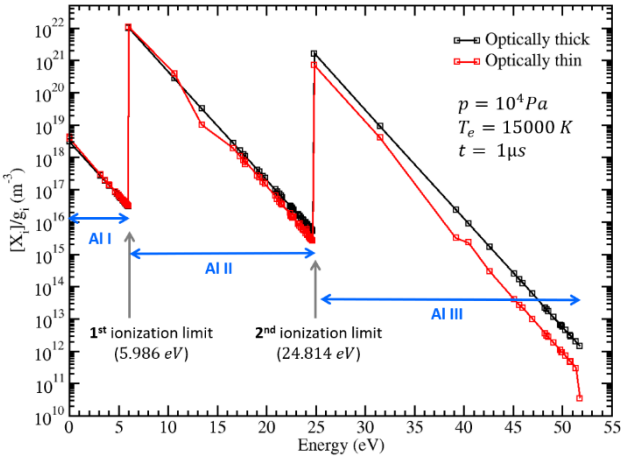



**Figure 1**. Boltzmann plot for an optically thin or thick laser-induced Aluminum plasma.

**References**

[1] R. Wilson, J. Quant. Spectrosc. Radiat. Transf. 2 (1962) 477-490.
[2] H.R. Griem, Phys. Rev. 131 (1963) 1170-1176.
[3] R.W.P. McWhirter, in: R.H. Huddlestone, S.L. Leonard (Eds.), Plasma diagnostic techniques, Academic Press, New York, 1965, pp. 201–264.
[4] H.W. Drawin, Z. Phys. 228 (1969) 99-119.
[5] J.D. Hey, J. Quant. Spectrosc. Radiat. Transf. 16 (1976) 69-75.
[6] T. Fujimoto, R.W.P. McWhirter, Phys. Rev. A 42 (1990) 6588-6601.
[7] V. Morel, A. Bultel et al., Spectrochim. Acta Part B 103-104 (2015) 112-123.
[8] V. Morel, A. Bultel et al., Spectrochim. Acta Part B 127 (2017) 7-19

# Production of durable superhydrophobic coatings using atmospheric pressure plasma

B. A. Kyrykbay[1,2], S. S. Ussenkhan[2], Ye. Yerlanuly[2], A.U. Utegenov[1,2], S.A. Orazbayev[1,2] and T.S. Ramazanov[1]

[1] *Al-Farabi Kazakh National University, Almaty, Kazakhstan*.
[2] *Institute of Applied Science and Information Technologies, Almaty, Kazakhstan*

This study explores the durability of superhydrophobic coatings synthesized via plasma polymerization, using argon (Ar) as the plasma-forming gas and hexamethyldisiloxane (HMDSO) as the precursor. The stability of these coatings was evaluated under various environmental conditions, including fogging, ice formation, and temperature fluctuations. Superhydrophobic performance was assessed by measuring water contact angles and surface roughness. The results demonstrate that the coatings exhibit strong water repellency and retain their properties over extended periods.

The development of hydrophobic surfaces through atmospheric-pressure plasma treatment has garnered significant attention due to its effectiveness in various technological applications, including self-cleaning coatings, anti-icing systems, and optical devices [1,2]. Superhydrophobic coatings, defined by their ability to repel water, act as protective layers that enhance surface durability and functionality.

This study investigates the influence of plasma deposition parameters on the structural and wetting properties of these coatings. By systematically varying key process conditions-such as discharge power, precursor concentration, and deposition time-the research aims to identify optimal settings for achieving stable superhydrophobic surfaces with improved performance characteristics [3].

Experimental results indicate that increasing the discharge power from 100 W to 200 W significantly enhances surface hydrophobicity, as evidenced by an increase in the water contact angle from 140° to 165°. This improvement suggests that higher discharge power promotes the formation of a more hydrophobic surface, likely due to modifications in the film's morphology and chemical composition.

The number of deposition cycles was found to affect coating thickness, reducing transparency without altering hydrophobic properties.

Durability tests confirmed the coatings' resistance to UV radiation, high temperatures, fogging, icing, and chemical exposure.

These obtaining results demonstrate that plasma-synthesized superhydrophobic films exhibit high stability and can effectively protect various surfaces under real-world climatic conditions.

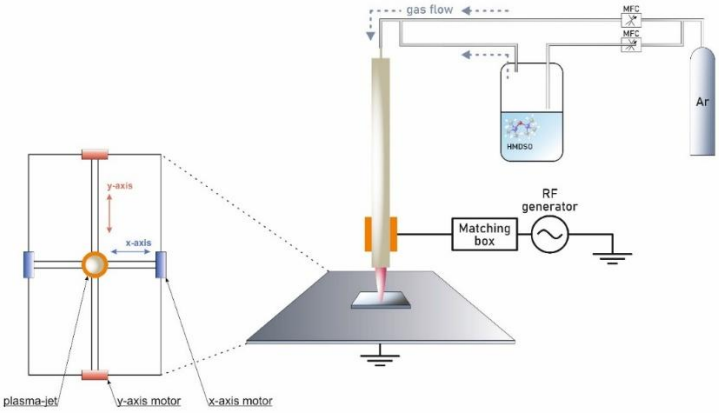



Figure 1. Schematic of an experimental setup for superhydrophobic film deposition by atmospheric pressure plasma polymerization

**References**

[1] Chattopadhyay S, Huang YF, Jen YJ, et al. Anti-reflect- ing and photonic nanostructures. Materials Science and Engineering: R: Reports **69**, 1-35 (2010).
[2] Orazbayev S, Zhumadilov R, Zhunisbekov A, Gabdullin M, Yerlanuly Y, Utegenov A and Ramazanov T. Applied Surface Science **515**, 146050 (2020).
[3] Ussenkhan S.S., Kyrykbay B.A., Yerlanuly Y., Zhunisbekov A.T., Gabdullin M.T., Ramazanov T.S., Orazbayev S.A., Utegenov A.U. Fabricating durable and stable superhydrophobic coatings by the atmospheric pressure plasma polymerisation of hexamethyldisiloxane Heliyon, **10(1)**, e23844(2024).

XXXVI ICPIG, July 20-25, 2025, Aix-en-Provence, France Topic number 9

# Temperature measurements in methane NRP discharges

S. Delahaie[1,2], PA Goutier[1,2], S. McGuire[1], N. Q. Minesi[1], E. Pannier[2], and C. O. Laux[1,2]

[1] *Université Paris-Saclay, CNRS, CentraleSupélec, Laboratoire EM2C, 91190, Gif-sur-Yvette, France*
[2] *Spark Cleantech, 91190, Gif-sur-Yvette, France*

This work compares the rotational temperatures of electronic excited states in a methane plasma generated with Nanosecond Repetitive Pulsed (NRP) discharges. Using traces of nitrogen in the plasma, we measured the rotational temperature of the $N_2$ second positive system and the $C_2$ Swan system. This poster shows that, in the case of NRP discharges, the rotational temperature of $C_2$ Swan cannot be employed as a proxy for the translational temperature measurement.

## 1 Introduction

NRP discharges in methane have been studied as a means of producing $H_2$ and solid carbon $C_{(s)}$ [1]. The gas temperature evolution plays an important role in both the discharge chemical kinetics and – because the plasma resistivity depends strongly on temperature – the power coupled into the discharge. As part of a broader effort to evaluate the performance of these discharges and their ability to convert methane to $H_2$, we pursue measurements of gas temperature. Optical emission spectroscopy (OES) can be used to measure the translational temperature, but one has to ensure that the rotational temperature of the electronic excited species is equal or close to the bulk gas temperature [2].

Gas temperature measurements with OES in methane plasmas have been tested in the literature using different proxies: $C_2$ Swan ($d^3\Pi_g - a^3\Pi_u$) in microwave plasma [3,4], $H_2$-Fulcher ($d^3\Pi_u \rightarrow a^3\Sigma_g^+$) in a DC discharge [5], and $C_2$ Mulliken ($D^1\Sigma_u^+ - X^1\Sigma_g^+$)[6]. In this work, we will compare the rotational temperature of $C_2$ Swan with the $N_2$ second positive system which is often used as a proxy for gas temperature [2].

## 2 Methodology

The plasma geometry is a pin-to-pin reactor with a gap distance of 1.6 mm. The plasma source is a nanosecond pulse generator with a voltage of about 10 kV, a repetition rate of 10 kHz, and a pulse duration of approximately 20 ns. Optical emission spectroscopy is used to measure the rotational temperature of $C_2$ Swan and $N_2$ second positive system using a Princeton Instrument Spectrometer, connected to a PI-MAX 4 camera, triggered with a BNC delay generator, that is also connected to the NRP discharges pulser.

## 3 Results

The evolution of the rotational temperature of $C_2$ Swan and the second positive system of $N_2$ is measured and compared. The $C_2$ Swan rotational temperature is significantly higher than the translational temperature. Thus, it cannot be employed as a good proxy for translational temperature measurements in NRP discharges. The experimental results will serve as valdiation data for the predictions of a spark discharge model based on the measured electronic density, discharge diameter, and applied voltage.

**References**

[1] Lotfalipour R, Ghorbanzadeh A M and Mahdian A 2014 Methane conversion by repetitive nanosecond pulsed plasma *J. Phys. D: Appl. Phys.* **47** 365201

[2] Tibère-Inglesse A C, McGuire S D and Laux C O 2023 Inferring gas temperature from $N_2$ emission via rotational distribution of the $N_2$ B $^3\Pi_g$ and C $^3\Pi_u$ states *Plasma Sources Sci. Technol.* **32** 075018

[3] Carbone E, D'Isa F, Hecimovic A and Fantz U 2020 Analysis of the C2 Swan bands as a thermometric probe in CO2 microwave plasmas *Plasma Sources Sci. Technol.* **29** 055003

[4] Kreuznacht S, Böke M and von Keudell A 2025 Space-resolved gas temperature of a microwave plasma torch used for hydrogen production via methane pyrolysis *Plasma Processes and Polymers* **22** 2400089

[5] Goyette A N, Jameson W B, Anderson L W and Lawler J E 1996 An experimental comparison of rotational temperature and gas kinetic temperature in a discharge *J. Phys. D: Appl. Phys.* **29** 1197

[6] Lombardi G, Bénédic F, Mohasseb F, Hassouni K and Gicquel A 2004 Determination of gas temperature and C2 absolute density in Ar/H2/CH4 microwave discharges used for nanocrystalline diamond deposition from the C2 Mulliken system *Plasma Sources Sci. Technol.* **13** 375

# Effects of He addition to Ar/$C_2H_2$ PECVD on a-C:H film properties

K. Nagamine[1], S. W. Fitriani[1], D. Wakita[2] , D.Yamashita[2], K. Kamataki[2], M. Shiratani[2]

[1] *Joint Graduate School of Mathematics for Innovationg, Kyushu University, Japan*
[2] *Graduate School and Faculty of Information Science and Electrical Engineering, Kyushu University, Japan*

We investigated effects of He mixing on properties of a-C:H films deposited by plasma CVD using $C_2$ $H_2$ /Ar at 5,10,40 mTorr. With increasing the mixing ratio , the film stress decreases from 5.0 GPa to 3.2 GPa at 5 mTorr, from 6.5GPa to 4.4 GPa at 10mTorr and from 4.2 GPa to 1.2 GPa at 40mTorr. The mass density remains constant (~2.1 g/cm$^3$) at 5, 10 mTor, while the mass density decreases from 2.1 g/cm$^3$ to 1.2 g/cm$^3$ as the He mix ratio increases at 40mTorr.

## 1. Introduction

For many years, the manufacturing of memory devices such as 3D NAND and DRAM has been advancing in miniaturization and high aspect structures. In recent years, thin photomask for fine lithography brings about insufficient etching resistance of photomask. As a solution to this, hard mask is being used[1]. a-C:H film is often used as hard mask owing to its film properties such as high hardness, and chemical inertness[2]. Previous research demonstrated that harder a-C:H film can be achieved by adding Ne, He to the Ar magnetron sputtering plasma[3]. However, little is known about effects of He mixing on the qualities of a-C:H films deposited by $C_2H_2$ based plasma-enhanced chemical vapor deposition (PECVD). In this study, we investigated effects of He addition on properties of a-C:H films deposited by $C_2H_2$/Ar/He PECVD.

## 2. Experimental

Experiment were performed using a capacity coupled plasma (CCP) reactor [4]. To generate plasma, we supplied an RF voltage at 13.56 MHz. The self-bias voltage was -220 V. We set the total flow rate 6 sccm with 1 sccm of $C_2H_2$ and 5 sccm of Ar+He fixed. The He mixing ratio (He/He+Ar) was varied from 0% to 80%. The pressure was 5, 10, 40 mTorr. Optical emission spectroscopy was used as a plasma diagnostic. The film properties were evaluated by Ellipsometry, X-ray reflectometry and Raman spectroscopy.

## 3. Results

Figure 1 shows effects of He mixing ratio on the film stress. With increasing the He mix ratio, the film stress decreases from 5.0 GPa to 3.2 GPa at 5 mTorr, from 6.5GPa to 4.4 GPa at 10mTorr and from 4.2 GPa to 1.2 GPa at 40mTorr. Figure 2 shows effects of He mixing ratio on the mass density. The mass density remains constant (~2.1 g/cm$^3$) at 5, 10 mTorr. The mass density decreases from 2.1 g/cm$^3$ to 1.2 g/cm$^3$ with increasing the He mixing ratio at 40mTorr.

Further details, including results from Raman spectroscopy and OES analysis, and discussion will be presented at the conference.

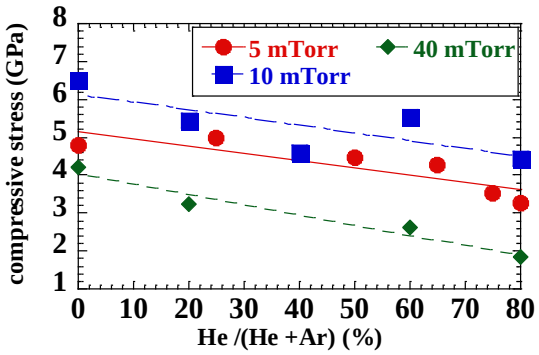



Fig. 1. He mixing ratio dependence of film stress.

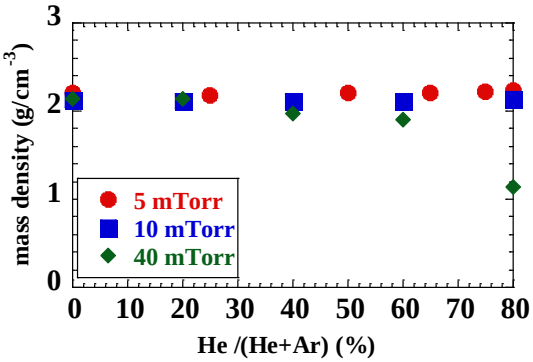



Fig. 2. He mixing ratio dependence of mass density.

**References**

[1] K.Babich *et al*, Proceedings of SPIE, (2003) 5039.
[2] M.M.Ahon *et al*, Thin Solid Films, **814** (2025) 140635.
[3] B.Akhavan *et al*, Surface & Coatings Technology, 427 (2021) 127785
[4] M. Otaka, *et al.*, Jpn. J. Appl. Phys., **63** (2024) 076001.

# Bridging structure and magnetism of diluted magnetic semiconductor films using nitrogen-mediated crystallization

Masaharu Shiratani[1], Marlis N. Agusutrisno[2], Naho Itagaki[1], and Naoto Yamashita[1]

[1] *Kyushu University, Motooka 744, Fukuoka 819-0395, Japan*
[2] *Sultan Ageng Tirtayasa University, Banten 42435, Indonesia*

We investigated the impact of nanoscale inhomogeneity on the magnetic properties of ZnO:CoN films fabricated via nitrogen-mediated crystallization. Prolonged post-annealing intensifies nanoscale inhomogeneity, significantly enhancing both coercivity and blocking temperature while preserving the films' wurtzite structure and chemical composition. This suggests that post-annealing primarily governs the spatial distribution of Co atoms, making nanoscale inhomogeneity the crucial factor driving these property enhancements.

## 1 Introduction

Diluted magnetic semiconductors (DMS) have garnered significant attention due to their potential applications in spintronics. However, the origins of magnetism in DMS remain a subject of debate, largely due to the challenge of controlling nanoscale inhomogeneity in their structures. In this study, we propose a novel approach to precisely manipulate the film structure of DMS by combining nitrogen-mediated crystallization with post-deposition annealing [1-5].

## 2 Results and Discussion

We synthesized ZnO:CoN films using a reactive sputtering technique in a nitrogen atmosphere, followed by post-annealing under controlled conditions. This method allows for the fine-tuning of crystallization dynamics, thereby regulating the spatial distribution of Co atoms within the wurtzite ZnO matrix. Our findings reveal that prolonged annealing leads to an increase in nanoscale inhomogeneity, significantly enhancing both the coercivity and blocking temperature of the films. Importantly, these magnetic property enhancements occur without altering the overall chemical composition or crystalline phase of the materials.

Our results indicate that the key factor governing the magnetic behavior of ZnO:CoN films is the degree of nanoscale inhomogeneity, which is dictated by post-annealing conditions. The controlled introduction of nitrogen during sputtering plays a crucial role in mediating the crystallization process, enabling a tuneable and reproducible approach to modifying DMS properties. This work provides new insights into the interplay between structure and magnetism in DMS and demonstrates a pathway for engineering their functional properties for future spintronic applications.

**Acknowledgement**

This work was supported by JICA, JSPS KAKENHI Grant Numbers JP21H01372, JP21K18731, JP22H05000, JP20H00142, JP22K14292, Core-to-Core program Grant Number JSPSCCA2019002, Early-career Scientists Grant Number 22K14292, Murata Science Foundation, and Iketani Science and Technology Foundation. NY applicate Mr. Tomoya Watanabe for his support.

**References**

[1] Suhariadi I., et al., Improved nanoscale Al-doped ZnO with a ZnO buffer layer fabricated by nitrogen-mediated crystallization for flexible optoelectronic devices. *ACS Appl. Nano Mater.* **3**, 2480 (2020).

[2] Kamataki K., et al., Prediction by a hybrid machine learning model for high-mobility amorphous In2O3: Sn films fabricated by RF plasma sputtering deposition using a nitrogen-mediated amorphization. *J. Appl. Phys.* **134**, 163301 (2023).

[3] Agusutrisno, M. N., et al., Control of magnetic transition of ZnO:Co grown by RF-sputter using post-annealing. *2022 International Conference on Informatics Electrical and Electronics (ICIEE)*, Yogyakarta, Indonesia (2022), pp. 1–4. https://doi.org/10.1109/ICIEE55596.2022.10010108

[4] Agusutrisno, M. N., et al., Control of inhomogeneity and magnetic properties of ZnO:Co films grown by magnetron sputtering using nitrogen. *Mater. Sci. Semicond. Process.* **162**, 107503 (2023).

[5] Agusutrisno, M. N., et al., Effect of nanoscale inhomogeneity on blocking temperature of ZnO:Co films fabricated by using nitrogen-mediated crystallization. *MRS Adv.* **9**, 1234-1239 (2024).

# 2D spatial mapping of the fundamental properties of a microwave argon plasma jet in contact with surfaces

F. Khazem[1], A. Durocher-Jean[1], A. Hamdan[1], and L. Stafford[1]

[1] *Département de physique, Université de Montréal, Montréal, Canada*

Hyperspectral imaging of Ar 4p-4s line emission intensities was combined with a collisional-radiative model (describing Ar 4p state populations) and a fluid model (describing electron energy balance) to extract 2D spatial mappings of electron temperature, electron and molecular ion densities, and electric field intensity in both a free-expanding jet and a jet in contact with surfaces. This approach provides high diagnostic precision and unprecedented spatial resolution, making it a powerful tool for advancing understanding and optimizing microwave plasma systems used for different applications.

## 1. Introduction

Microwave atmospheric-pressure plasmas are increasingly used in diverse fields of application such as nanomaterials synthesis, surface modification, plasma conversion, and environmental remediation. Fundamental plasma parameters such as the electron temperature, $T_e$, the number density of electrons, $n_e$, and of molecular ions, $n_{Ar_2^+}$, and electric field intensity,$|E_z|$, govern plasma's behavior and the resulting plasma chemistry. This study presents a detailed characterization of these parameters in both a free-expanding plasma jet and a jet interacting with dielectric and conductive surfaces, highlighting the impact of surface properties on plasma structure, energy distribution, and 2D spatial gradients.

## 2. Methods

A microwave argon plasma jet was generated using a surfatron connected to a 2.45 GHz solid-state microwave generator operating in continuous mode. The plasma was sustained in pure argon (1 L/min) flowing through a fused silica discharge tube with a 2 mm inner diameter, with the outlet positioned 5.6 mm from the surfatron. To investigate the effect of surface interactions, a dielectric or conductive surface was introduced below the jet. A recently developed hyperspectral imaging system (HSI) [1] was used to record optical emission spectra from the plasma with high spatial resolution, where each pixel captured a spectrum corresponding to a 13.9 µm × 13.9 µm region over a 16.68 × 16.68 mm² area. Post-processing of the hyperspectral data ensured that no spectral information was lost [1].

## 3. Results

$T_e$ was determined by comparing the measured HSI-recorded 2D mapping of the Ar 4p-4s line emission intensities with those predicted by a collisional radiative model in optically thick conditions [2]. The minimum relative standard error obtained at each spot in the HSI data provides the most likely value of $T_e$ (Figure 1a). As for $n_e$, it was first calculated in relative units from the line emission intensity of a selected Ar 4p state (and the corresponding particle balance equation) and then converted to absolute values from a known plasma condition (Figure 1b). $n_{Ar_2^+}$ was calculated by solving the electron particle balance equation, considering the electron gain and loss reactions, and evaluating the diffusion term. These plasma parameters, along with others, were then used in the electron energy balance equation to determine the 2D mapping of the electric field intensity (Figure 1c). The obtained high-resolution 2D mappings of plasma parameters are consistent with theoretical and experimental studies of microwave plasmas. These mappings also show a clear difference between the properties of the free jet and the jet in contact with surfaces, especially their $T_e$ and $|E_z|$.

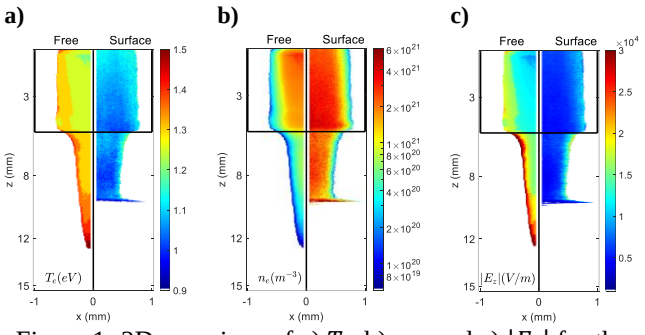



Figure 1- 2D mappings of a) $T_e$, b) $n_e$, and c) $|E_z|$ for the free jet and the jet in contact with a dielectric surface.

## Acknowledgements

This research was supported by the National Science and Engineering Research Council and Fondation Courtois.

## References

[1] F Khazem et al., *Rev Sci Instrum*, 2024.
[2] A. Durocher-Jean et al., *Phys Plasmas*, 2019.

# The 2025 status report on the LXCat project

E. Carbone[1], D. Boer[2], J. van Dijk[2], W. Graef[3], G. Hagelaar[4] and L. Pitchford[4], on behalf of the LXCat Team*

[1] *Institut National de la Recherche Scientifique, Centre Énergie Matériaux Télécommunications, 1650 Blvd Lionel Boulet,* J3X 1P7 Varennes, QC, Canada
[2] *Dept. Applied Physics, Eindhoven Eindhoven University of Technology, The Netherlands*
[3] *Plasma Matters B.V., Eindhoven, The Netherlands*
[4] *CNRS & Univ. of Toulouse, Toulouse, France*

* Contact email: info@lxcat.net

An essential ingredient for the simulation of low temperature plasmas (LTPs) is accurate data describing electron and ion collisions with neutrals and their transport. LXCat is an open-access, on-line platform providing such data, as well as services for selecting, plotting, and comparing that data. Details and recent developments of the project are presented, while the LXCat team also aims to contact members of the LTP community for future contributions and participation.

LXCat [1] is an online platform for the curation of data needed for modeling the electron and ion components of Low Temperature Plasmas (LTPs). LXCat (`https://lxcat.net`) is open-access and no sign-up is required. The platform is organized in databases which are named and maintained by individual contributors. More than 60 people from around the world participate in this project, either by contributing data or by volunteering time to work on other aspects of the project. The data types available now are electron-neutral or ion-neutral scattering cross sections (also differential), oscillator strengths, and transport parameters (e.g., mobility, diffusion coefficients) and rate coefficients. The LXCat team does not recommend data and hence data for the same process can appear in one or more of the databases. On-line tools are available that allow visitors to search for specific data, plot and compare data from different databases, download data, or use the available complete sets of electron-neutral scattering cross sections in an on-line version of the Boltzmann solver BOLSIG+ [2] to calculate transport and rate coefficients in pure gases or gas mixtures. At the last Gaseous Electronics conference 2024 in San Diego, the first presentation of the complete redesign of the platform [3] to better cater to community needs was presented [4]. Any person interested can test the new infrastructure by logging into `https://demo.lxcat.net`. While the current focus of the project is to complete the translation of existing data into the new format, the latter was conceived to allow hosting various new data types in the future. A specific attention is also given for the storage and accessibility of any metadata associated to datasets. These informations are essential for the traceability of the data but also for understanding the purpose for which any data (cross section, transport coefficient, or dataset made of any of these) were measured, calculated or assembled. The LXCat team is interested in discussing with members of the LTP community about data needs, data formats, and about how people can volunteer to participate in this project.

## References

[1] Carbone, E., Graef, W., Boer, D., Hopkins, M.M., Stephens, J.C., Yee, B.T., Pancheshnyi, S. & Pitchford, L. Data needs for modeling low-temperature non-equilibrium plasmas: The LXCat project, history, perspectives and a tutorial. *Atoms* **9** (2021), 16. `https://www.mdpi.com/2218-2004/9/1/16`.

[2] Hagelaar, G. J. M. & Pitchford, L. C. Solving the boltzmann equation to obtain electron transport coefficients and rate coefficients for fluid models. *Plasma Sources Science and Technology* **14**, 722 (2005). `https://dx.doi.org/10.1088/0963-0252/14/4/011`.

[3] Verhoeven, S., Boer, D., Ali, S., Graef, W. & van Dijk, J. LXCat (2022). `https://doi.org/10.5281/zenodo.7381574`.

[4] Boer, D.J., Graef, W.A.A.D. & van Dijk, J. An introduction to version 3 of the LXCat plasma input data platform. *Gaseous Electronics Conference* (2024), San Diego, USA.

# Ionization Region Model (IRM) for Helium High Power Impulse Magnetron Sputtering (HiPIMS) with Mo target

Z. BELKAID[1], T.MINEA[1],Jon Tomas Gudmundsson[2,3], A.REVEL[1], E.MOREL[1]

[1] Laboratoire de Physique des Gaz et Plasmas - LPGP, UMR 8578 CNRS,
Université Paris–Saclay, 91405 Orsay Cedex, France

[2] Science Institute, University of Iceland, Dunhaga 3, IS-107 Reykjavik, Iceland

[3] Division of Space and Plasma Physics, School of Electrical Engineering and Computer Science,
KTH Royal Institute of Technology, SE-10044 Stockholm, Sweden

The use of helium as a working gas in HiPIMS is considered an alternative to heavier gases like argon. Helium HiPIMS features significantly higher current densities ( 6 $\mathrm{A\,cm^{-2}}$) than conventional pulses ( 2 $\mathrm{A\,cm^{-2}}$). Using a molybdenum target, the peak discharge current increases with pulse voltage, exhibiting a rapid rise time (<5 $\mu$s). The ionization region model (IRM) has been applied to helium HiPIMS to analyze current waveforms and plasma composition, revealing a transition from a helium-dominated to a metal-dominated discharge.

## 1 Introduction

Experiment with helium in HiPIMS showed distinct plasma properties, notably higher operating current densities as compared to argon, for the same pulse voltages [1, 2]. With a molybdenum target is used, the peak discharge current increases with pulse voltage, with a very fast rise time (<5 $\mu$s).

To understand this current behavior, the ionization region model (IRM) is applied to helium HiPIMS, using voltage and current measurements as inputs [3]. IRM provides the time evolution of plasma species and electron temperature, averaging physical quantities over the ionization region volume.

## 2 Results and Discussion

IRM results show that, initially, the peak current is mainly carried by helium ions. Due to helium's inefficient sputtering of molybdenum, metal ion contribution remains low, at least in the rise-up phase of the current. . Ionization is dominated by secondary electrons before the current rise and until the current reaches the peak value. which ionize helium ground-state atoms (24.58 eV). Over time, helium metastables (19.6 eV) enable a more efficient two-step ionization process, lowering the required energy to 4.76 eV and 3.96 eV (Fig. 2).

After the peak current the, molybdenum self-sputtering becomes significant, increasing metal atom density in the plasma. The lower ionization threshold of these metal species facilitates electron cooling, reducing electron temperature and the production of $Mo^{++}$. This transition leads to a metal-dominated discharge, where metal ions sustain the plasma (Fig. 1).

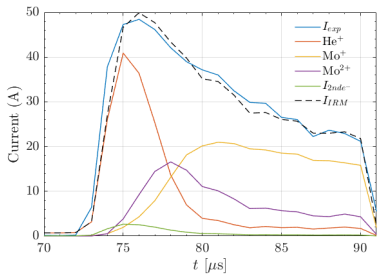



Figure 1: Current composition obtained from IRM for a 650V pulse.

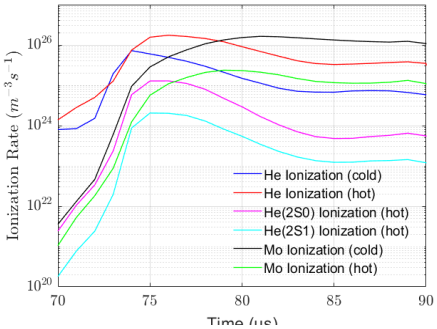



Figure 2: IRM ionization rates for a 650V HiPIMS pulse.

## 3 Conclusion

IRM analysis of helium HiPIMS reveals a transition from helium-ion-dominated to metal-ion-dominated discharge, governed by metastable-enhanced ionization and self-sputtering effects.

## References

[1] E. Morel et al., Plasma Sources Sci. Technol. 30(12), 125001 (2021). doi:10.1088/1361-6595/ac3341

[2] E. Morel et al., J. Appl. Phys. 133, 2023. doi:10.1063/5.0145547

[3] J. T. Gudmundsson et al., Plasma Sources Sci. Technol. 25, 065004 (2016). doi:10.1088/0963-0252/25/6/065004

# A hybrid FTIR system for process characterisation and in-situ plasma diagnostics for gas conversion reactors

F. Franco[1], A. Meindl[1], R. Antunes[1], A. Hecimovic[1], A. A. Ben Yaala[1] and U. Fantz[1,2]

[1] *Max Planck Institute for Plasma Physics, Boltzmannstr. 2, D-85748 Garching b. München*
[2] *University of Augsburg, Universitätsstr. 1, D-86159 Augsburg*

Low-temperature plasmas are finding promising application in the gas conversion sector. In view of process optimisation and more complete physical characterisation, a new Fourier Transform InfraRed (FTIR) spectrometer has been implemented, allowing to characterise the composition of the cold gas outflow and the energy distribution of ground-state molecules in the plasma for a wide range of conditions (e.g.: pressure, power and flow). In this contribution, the implementation of the mobile FTIR system is presented with an overview of its current diagnostic capabilities, ranging from gas sampling, for the analysis of species produced in the plasma process, to in-situ probing of volatile compounds in the plasma phase.

## 1 Motivation

Fourier Transform InfraRed (FTIR) spectroscopy is a robust, versatile and fast diagnostic for characterisation of several plasma parameters. The unique fingerprint of each molecular population is quantified in an infrared absorption spectrum, where each rovibrational band depends on the concentration and energy distribution of each infrared-active species [1]. Here, FTIR is applied in the field of non-equilibrium plasmas for gas conversion, where gaseous chemical species are converted into useful compounds for the market using renewable energy [2] (e.g.: $CO_2$ conversion into CO or $N_2$ and $H_2$ conversion into $NH_3$). Outflow composition can be derived via cold gas analysis and provides quantitative information on the conversion products and efficiency. In-plasma species can be characterised in composition and rovibrational temperature via in-situ spectroscopy. The accurate estimation of these parameters contributes to the fundamental understanding of the non-equilibrium plasma environment for a wide variety of conditions, such as gas flow, delivered power and reactor pressure. In this contribution, the development of a hybrid FTIR system is presented, demonstrating its cold gas sampling capabilities – for process output analysis – and the possibility for in-situ energy distribution characterisation (i.e.: rotational and vibrational energies) of radicals and ground-state molecules in the plasma. Key features are presented, including mobility of the setup (to move and adapt to several reactor designs), beamline fine adjustments and stabilisation (with dedicated optics and atmospheric control) and custom-made plasma cells or reactors for in-situ measurements.

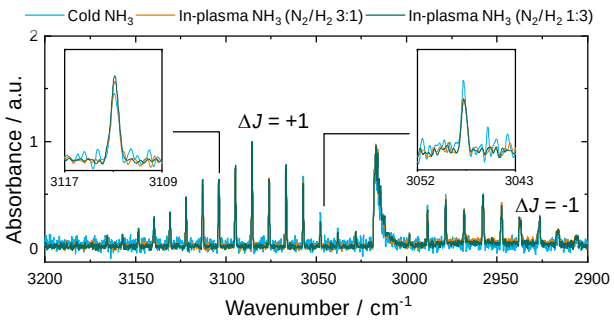



**Figure 1:** in-situ spectrum of the $NH_3(3\nu_2 / \nu_2 + \nu_4)$ band in a $N_2/H_2$ cold gas mixture and in a pDBD plasma.

## 2 Experiment

The setup consists of a commercial FTIR device equipped with a nitrogen-cooled external MCT detector. For gas sampling, the infrared beam can be directed through a gas cell and into the MCT detector inside a controlled-atmosphere enclosure. For in-situ spectroscopy, the setup can be moved to the experiment and gold mirrors allow to steer the beam outside of the assembly, through the plasma reactor and to the detector. The moisture control system can easily be extended to enable purging of the entire beamline, if required. The in-situ capability has been successfully demonstrated in a custom-designed planar Dielectric Barrier Discharge (pDBD) reactor with a $N_2/H_2$ mix for $NH_3$ synthesis, showing effects of the plasma phase on the rotational transitions of $NH_3$ and opening the way to further refinements in the measurement setup.

**References**

[1] P. R. Griffiths, J. A. De Haseth, *Fourier Transform Infrared Spectrometry*, Wiley-Interscience (2007).
[2] Y. Yin et al., *Physical Chemistry Chemical Physics*. **23**, 7974–7987 (2021).

# Elucidation of the Nitrogen Blue Afterglow in Atmospheric Pressure Helium Plasma Jet

Jun Enomoto[1], Wataru Kikuchi[1], Tomoya Taguchi[1], Nezu Atsushi[1] and Hiroshi Akatsuka[1]

[1] *Institute of Science Tokyo, Tokyo, Japan*

For atmospheric pressure plasma jet, which is expected to have applications in medicine and other fields, atomic and molecular processes have been shown to determine the electron temperature and density using optical emission spectroscopy. Blue light, which was not observed in previous studies, was detected in the plasma plume. This phenomenon will be called “blue afterglow.” The continuum spectrum of atmospheric pressure plasma was previously thought to be be due to electron-neutral atom bremsstrahlung. However, the blue afterglow was considered to be origineated from excited states or ions of molecular nitrogen generated by Penning effect. It can be concluded that the blue afterglow is a plasma with a lower electron temperature than the helium plasma.

## 1 Introduction

The atmospheric pressure helium plasma jet is expected to be a low-temperature plasma source with potential applications in medical treatments. In this study, the continuum spectrum of a helium plasma jet was analyzed using optical emission spectroscopy to investigate the reaction processes occurring within the plasma.

## 2 Results and Discussion

The plasma jet spectrum was measured using the apparatus shown in Figure 1. The spectrum is shown in Figure 2. Blue light, which is not observed between the electrodes, can be seen in the plume. This light is named the ”blue afterglow”. Between the electrodes, reactions 1 and 2 are occurring, while in the plume, reaction 3 is considered to take place[1]. The blue afterglow is light emitted due to the excited states or ions of molecular nitrogen generated by Penning effect. This can be explained by considering the energy equation of radiation and the potential energy diagram of nitrogen. It indicates that the blue afterglow is a plasma with a lower electron temperature than the helium plasma.

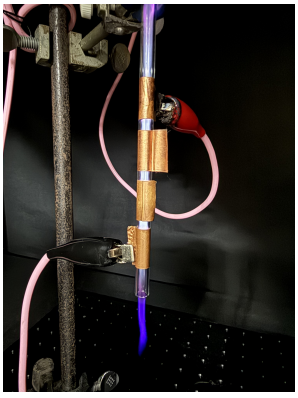


Figure 1: The Appearance of a Plasma Jet

$$\mathrm{He} \longrightarrow \mathrm{He^+} + \mathrm{e^-} \quad (1)$$

$$\mathrm{e^-} + \mathrm{He} \longrightarrow \mathrm{He^*} + \mathrm{e^-} \quad (2)$$

$$\mathrm{He^*} + \mathrm{N_2} \longrightarrow \mathrm{N_2^+(B)} + \mathrm{He} + \mathrm{e^-} \quad (3)$$

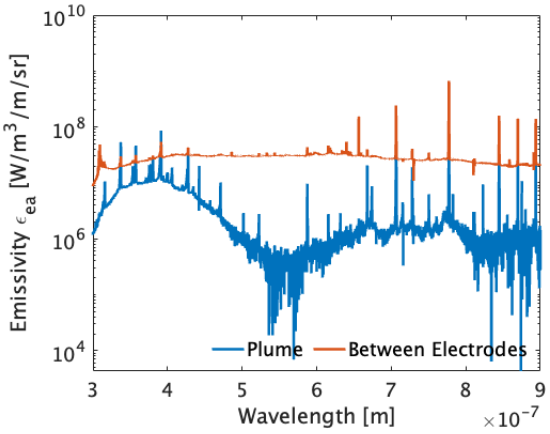



Figure 2: Plasma Spectrum Using a Jet Device

## References

[1] I Radu and R Bartnikas and M R Wertheimer Dielectric barrier discharges in atmospheric pressure helium in cylinder-plane geometry: experiments and model *Journal of Physics D: Applied Physics*, **37**, 449 (2004).

# Influence of air admixture in an Ar pin-jet on water treatment

O. Jovanović[1], N. Puač[1] and N. Škoro[1]

[1]*Institute of Physics, University of Belgrade, Pregrevica 118, 11080 Belgrade, Serbia*

In this work, we have characterized an atmospheric-pressure plasma jet (APPJ) with a pin electrode configuration, powered by a 350 kHz continuous sinusoidal signal and operating in contact with water. The effects on the electrical (discharge current-voltage characteristics, power) and optical emission spectrum characteristics of the streamer discharge after adding synthetic air to argon were analyzed. The influence of gas-phase discharge parameters and treatment duration on plasma-activated water (PAW) properties and deposited reactive oxygen and nitrogen species (RONS) concentrations was investigated.

## 1 Introduction

Atmospheric pressure plasma jets (APPJs) generate reactive oxygen and nitrogen species (RONS), which are key agents in advanced oxidation processes. Their ability to produce RONS in both gas and liquid phases makes them highly relevant for wastewater treatment applications [1]. In our previous studies, we successfully applied a pin-electrode APPJ for the degradation of organic pollutants in water, demonstrating its potential for removing persistent contaminants [2,3]. This study explores the effects of air admixture on plasma properties and RONS production in plasma-activated water (PAW), aiming to tailor its reactivity and optimize treatment conditions.

## 2 Experimental setup

In this study, an APPJ with a pin electrode configuration was employed in direct contact with distilled water. The streamer discharge was generated above the liquid surface [2]. As the working gas pure argon (Ar) and argon mixtures with synthetic air (1% and 3%), with a total gas flow of 1 slm were used. Electrical characterization provided information on the discharge power while optical emission spectroscopy monitored the emission of important excited species at the plasma-liquid interface. PAW was produced by varying discharge parameters: treatment time, gas mixture, and power. Obtained PAW physico-chemical properties and concentrations of $NO_3^-$, $NO_2^-$, and $H_2O_2$ species were compared.

## 3 Results and conclusions

Figure 1 shows the relative radiation intensities of the most intense lines and bands of detected excited species for different gas compositions.

With the addition of 1% Air into Ar flow total emission intensities of OH, $N_2$ SPS, and $N_2^+$ FNS molecular bands increased, while atomic oxygen lines slightly decreased. With 3% synthetic air, the total emission intensity increased by approximately 30% compared to the case without synthetic air.

Adding synthetic air to the gas admixture increased the $NO_3^-$ concentration in PAW, compared to discharge in pure argon, but it had no significant effect on the $H_2O_2$ concentration.

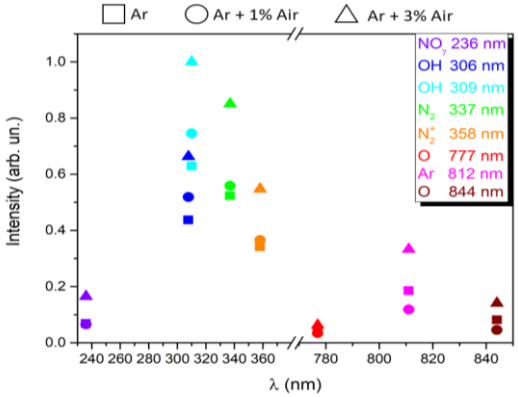



**Figure 1.** Relative radiation intensities of excited species from discharge in Ar, Ar+1%Air, and Ar+3%Air. Intensities were normalized to the emission of the most intense OH(A-X) band line at 309 nm.

**Acknowledgment**

This work was supported by MSTDI Republic of Serbia grant number 451-03-68/2025-14/200024.

**References**

[1] Brisset, J.-L., & Pawlat, J. Chemical Effects of Air Plasma Species on Aqueous Solutes in Direct and Delayed Exposure Modes: Discharge, Post-discharge and Plasma Activated Water. *Plasma Chemistry and Plasma Processing* **36**, 355–381 (2016).

[2] Kumar, A. et al. Degradation of diclofenac and 4-chlorobenzoic acid in aqueous solution by cold atmospheric plasma source. *Science of the Total Environment*, **864**, 161194.

[3] Topolovec, B. et al. Plasma water treatment for PFAS: Study of degradation of perfluorinated substances and their byproducts by using cold atmospheric pressure plasma jet. *Journal of Environmental Chemical Engineering*, **12(3)**, 112979 (2024).

# Controlling Pulsed Dielectric Barrier Discharges Using Shaped High-Voltage Waveforms

Jeroen J. van Oorschot[1], H. Höft[2], T. Huiskamp[1], Markus M. Becker[2]

[1] *Eindhoven University of Technology, Department of Electrical Engineering, EES, Eindhoven, Netherlands*
[2] *Leibniz Institute for Plasma Science and Technology (INP), Greifswald, Germany*

For a single-filament dielectric barrier discharge arrangement in a $N_2$-$O_2$ gas mixture, it was shown that precisely shaped high-voltage pulses from a custom-built Marx generator can modulate discharge inception jitter and discharge characteristics. Synchronised diagnostics confirm that waveform shaping influences the Townsend pre-phase and discharge structure, underscoring the synergy of pulsed power engineering and plasma diagnostics.

In this work, the influence of precisely tailored high-voltage (HV) pulse waveforms on the breakdown and subsequent evolution of single-filament dielectric barrier discharges (DBDs) was investigated in a 1 mm gas gap at atmospheric pressure using 0.1 vol% $O_2$ in $N_2$. Two pin stainless-steel electrodes, each covered by a hemispherical dielectric ($Al_2O_3$), serve as the single-filament DBD configuration [1]. The voltage waveforms—shaped to exhibit distinct rise times, steps, and plateaus—are generated using a custom-built, solid-state, impedance-matched Marx generator [2,3]. In figure 1, three used HV pulse shapes are exemplarily displayed.

Synchronised electrical and optical diagnostics are performed to characterise the discharge. Electrical measurements quantify discharge current, transferred charge, and energy/power. Furthermore, a combined iCCD–streak camera system with sub-nanosecond and sub-millimetre resolution captures the streamer propagation and temporal evolution of the discharge, similar to the system used in [1]. An example of the discharge emission structure is presented in figure 2. It shows the DBD emission during the rising and falling slope of a stepped HV pulse ($t_S$ = 1 µs, blue waveform in figure 1). Both discharges feature a distinct constricted channel in the volume, which widens in front of the anode and continues as surface discharges on both anode and cathode. These structures in the volume and on the surface depend on the chosen step height and length, as well as partly on the streamer propagation itself. It was found that the waveform shaping modulates the discharge inception jitter and the discharge initiation, e.g. the Townsend pre-phase and subsequent streamer development. This work demonstrates the synergistic potential of advanced electrical engineering approaches and comprehensive plasma diagnostics to precisely control non-thermal plasma formation at atmospheric pressure.

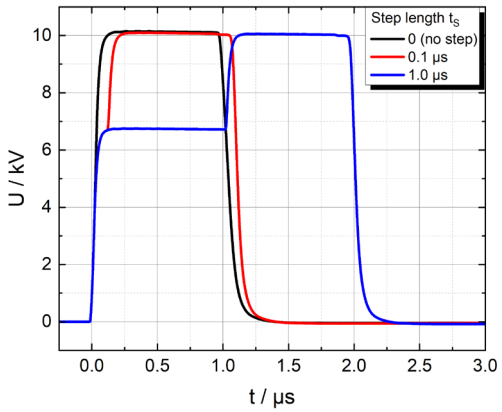



**Fig. 1** Three examples of the HV pulse shape manipulation used in this work with a fixed maximum voltage of 10 kV.

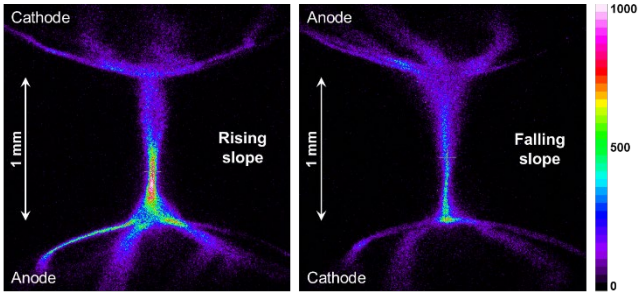



**Fig. 2** Discharge emission of individual discharge events at the rising and falling slope of a $t_S$ = 1 µs HV pulse (see Fig. 1) recorded by an iCCD camera (250 ns gate width, MCP gain 200, intensity in counts in pseudo-colour).

This work is supported by the German Research Foundation (DFG) - project number 535827833 and by the Dutch growth fund "Nxtgen hightech plasma4agrifood".

## References

[1] H. Höft, M. Kettlitz, M.M. Becker, T. Hoder, D. Loffhagen, R. Brandenburg, K.-D. Weltmann: J. Phys. D: Appl. Phys. 47 465206 (2014)
[2] T. Huiskamp, C. Ton, M. Azizi, J.J. van Oorschot, H. Höft: J. Phys. D: Appl. Phys. 55 024001 (2022)
[3] J. J. van Oorschot, T. Huiskamp: IEEE Trans. Plasma Sci. 51 pp.560-571 (2023)

# Particle-In-Cell Study of Laser Wakefield Acceleration in a Gas Cell for GeV-Scale High-Quality Electron Beams

S. Maity[1], F. Massimo[2], P. Sasorov[1] and A. Molodozhentsev[1]

[1] *The Extreme Light Infrastructure ERIC, ELI Beamlines Facility, Za Radnicí 835, 25241 Dolní Břežany, Czech Republic*
[2] *LPGP, CNRS, Université Paris-Saclay, 91405 Orsay, France*

Laser wakefield acceleration (LWFA) [1] is a promising technique for generating high-quality, GeV-scale electron beams. This scheme relies on the injection, trapping, and acceleration of electrons within a laser-driven plasma wakefield. A key challenge in LWFA is achieving precise control over the injection mechanism to enhance beam quality. Recent research [2, 3, 4] indicates that ionization-induced injection is a promising approach for producing intense electron bunches with high mean energy and low divergence. This technique exploits the high ionization threshold of inner-shell electrons in high-$Z$ gases (e.g., nitrogen, argon) mixed with low-$Z$ gases (e.g., hydrogen, helium) to facilitate controlled electron injection. However, continuous injection along the laser propagation path often leads to a large energy spread in the resultant accelerated electron beams.

In this study, we use Particle-In-Cell simulations [5, 6] to investigate laser wakefield acceleration (LWFA) in a capillary gas cell containing a nitrogen-helium mixture. A terawatt-class laser ionizes the gases and drives wakefields within a 15–20 mm capillary. We conduct a detailed parametric study to optimize the quality of accelerated electron beams and explore strategies for minimizing energy spread. Specifically, we examine the effects of beam loading on beam quality and analyze how smooth density variations at the plasma exit can be used to manipulate and control electron beam properties. Our simulations demonstrate the generation of electron beams with mean energies between 1.0 and 1.5 GeV, an energy spread below $5\%$ (FWHM), a divergence under five milliradians (FWHM), and beam charges ranging from 25 to 100 pC.

## References

[1] Tajima, T., and Dawson, J. M. Laser electron accelerator. *Physical review letters*, **43(4)**, 267 (1979).

[2] Irman, A., Couperus, J., Debus, A., Köhler, A., Krämer, J., Pausch, R., Zarini, O., and Schramm, U. Improved performance of laser wakefield acceleration by tailored self-truncated ionization injection. *Plasma Physics and Controlled Fusion*, **60(4)**, 044015 (2018).

[3] Kirchen, M., Jalas, S., Messner, P., Winkler, P., Eichner, T., Hübner, L., Hülsenbusch, T., Jeppe, L., Parikh, T., Schnepp, M., et al. Optimal beam loading in a laser-plasma accelerator. *Physical review letters* , **126(17)**, 174801 (2021).

[4] Maity, S., Mondal, A., Vishnyakov, E., and Molodozhentsev, A. Parametric analysis of electron beam quality in laser wakefield acceleration based on the truncated ionization injection mechanism. *Plasma Physics and Controlled Fusion*, **66(3)**, 035012 (2024).

[5] Derouillat, J., Beck, A., Pérez, F., Vinci, T., Chiaramello, M., Grassi, A., Flé, M., Bouchard, G., Plotnikov, I., Aunai, N., et al. Smilei: A collaborative, open-source, multi-purpose particle-in-cell code for plasma simulation. *Computer Physics Communications*, **222**, 351–373 (2018).

[6] Massimo, F., Beck, A., Dérouillat, J., Zemzemi, I., and Specka, A. Numerical modeling of laser tunneling ionization in particle-in-cell codes with a laser envelope model. *Physical Review E*, **102(3)**, 033204 (2020).

# Time and space dependence of iodine atomic density produced by laser photodissociation

C. Drag[1], C. Blondel[1], B. Esteves[2] and J.L. Raimbault[1]

[1] *Laboratoire de Physique des plasmas, CNRS, Sorbonne Univ., Univ. Paris-Saclay, École polytechnique, Palaiseau, France*
[2] *Safran Spacecraft Propulsion, Vernon, France*

This work investigates the evolution of the density of iodine atoms generated by laser photodissociation in a molecular vapor, both experimentally and theoretically. This study enabled to determine the diffusion coefficient $D$ and demonstrates a variation in the wall-recombination coefficient $\gamma$, ranging from 0.25 to 0.05 for pressures between 3 and 30 Pa in a quartz cell.

We investigate the recombination of I atoms in a cylindrical quartz cell containing $I_2$ molecular gas. The pressure of molecular iodine vapor is regulated by the temperature of a grain of solid iodine. The atoms are generated by photodissociation with a CW laser at 488 nm. The evolution of the atomic density, after the laser is switched on and off, is then monitored, using the two-photon absorption laser-induced fluorescence (TALIF) technique, around 300 nm [1]. Figure 1 shows the relative evolution of atomic density after 30 ms of photodissociation, for different positions of the TALIF detection laser.

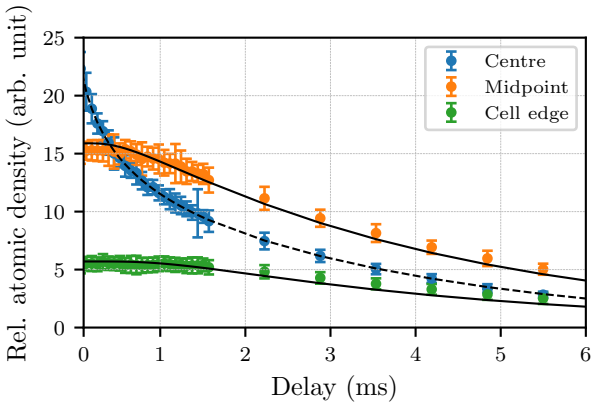



Figure 1: Decay after 30 ms of photodissociation for three different positions of the TALIF laser detection for a pressure of 24.2 Pa. The theoretical calculations are represented by the black lines, for values of radial distance $r = 0$, $R/2$, and $R - 2w_{\mathrm{TALIF}}$, where $R$ is the radius of the cell and $w_{\mathrm{TALIF}}$ the waist of the TALIF laser. The dotted curve is the decay at the center, obtained with parameters $D = 0.02\ \mathrm{m^2\ s^{-1}}$ and $\gamma = 0.072$.

The mathematical formulation of the problem, in the absence of volume recombination, reduces to a diffusion problem with a boundary condition of the mixed Dirichlet-Neumann type. This formulation depends on two parameters, namely the diffusion coefficient $D$ and the wall-recombination coefficient $\gamma$. The problem is solved analytically, which brings forward particular spatio-temporal density profiles, which are also discussed in the steady-state limit. This model allows us to fit the time decay measurements obtained at a given pressure and to determine independently a pair of values for $D$ and $\gamma(p)$, assuming that the diffusion coefficient is independent of pressure. As shown in Fig. 1, the model also reproduces spatio-temporal variations in density.

This procedure is repeated for several pressures between 3 and 30 Pa. A notable feature is that the density adjustment to the theoretical solution obliges the variation of $\gamma$ with pressure to be a decreasing one. This dependency escapes the usual approximation proposed by Chantry [2]. Moreover, the obtained results differ from those obtained in iodine fifty-three years ago by Brewer and Tellinghuisen, who had neglected the variations of $\gamma$ with pressure [3].

## References

[1] Esteves, B. and Blondel, C. and Chabert, P. and Drag, C. Two-photon absorption laser induced fluorescence (TALIF) detection of atomic iodine in low-temperature plasmas and a revision of the energy levels of II. *Journal of Physics B: Atomic, Molecular and Optical Physics*, **56**, 055002 (2023).

[2] Chantry, P. J. A simple formula for diffusion calculations involving wall reflection and low density. *Journal of Applied Physics*, **62**, 1141–1148 (1987).

[3] Brewer, L. and Tellinghuisen, J.B. Detection of Iodine atoms by an atomic fluorescence technique: application to study of diffusion and wall recombination. *The Journal of Chemical Physics*, **54**, 5133–5138 (1971).

# Measurement of $N_2(C)$ and $N_2(B)$ quenching rate constants

J.-L. du Garreau de la Méchenie[1], J.-B. Perrin-Terrin[1] and C. O. Laux[1]

[1] *Université Paris-Saclay, CentraleSupélec, CNRS, Gif-sur-Yvette, France*

This work presents the measurement of collisional deexcitation rate constants of $N_2(C^3\Pi_u)$ and $N_2(B^3\Pi_g)$ vibrational levels by $O_2$, $N_2$, $H_2$, $CO_2$, $CH_4$ and $NH_3$ at room temperature. Excited states of nitrogen are produced using nanosecond repetitively pulsed discharges. The temporal evolution of the number densities of the vibrational levels are measured using optical emission spectroscopy of the $N_2$(C→B, Δv=0) and $N_2(B \rightarrow A, \Delta v = 0 - 5)$ vibrational bands. Quenching rate constants for each vibrational level are inferred from the measured lifetimes. The comparison to the available literature validates the measurement methods. New values are provided for the missing rate constants.

## 1 Introduction

Quenching reactions play an important role in various plasma applications such as Plasma-Assisted Combustion (PAC) [1–3] or atmospheric re-entry. These reactions are key for fast gas heating and the creation of radicals. Quenching rate constants of the excited states of nitrogen have been extensively measured for the lower vibrational levels of $N_2$(C) and $N_2$(B) by $N_2$, $O_2$ and $H_2$, however quenching of higher vibrational levels have not been measured in all cases or differ significantly between various authors. In addition, there is a need to extend these measurements to additional quenching species of interest.

## 2 Measurement method

NRP discharges are applied between two electrodes placed in a vacuum cell called “quenching reactor” as shown in Fig 1. The gas pressure in the quenching reactor is measured by a capacitance manometer and controlled by a pump and a valve. The composition of the gas can be controlled with two mass flow controllers. The light emitted by the plasma is focused by two parabolic mirrors onto the entrance slit of a spectrometer equipped with three gratings placed on a rotating turret. A gated ICCD camera is mounted on the exit of the spectrometer to measure emission spectra with 2-ns gates.

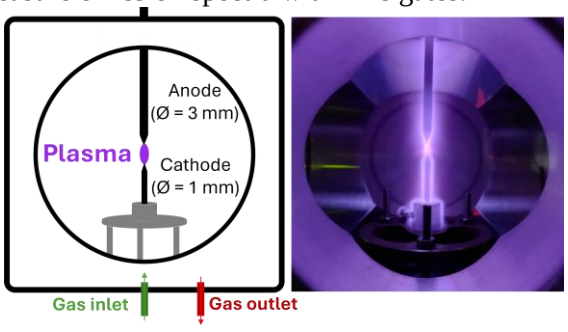



Fig. 1 Schematic (left) and photograph (right) of the quenching reactor

Numerical fitting of the emission spectra is done using Specair. The lifetimes calculated are used to measure the quenching rate constants. The measured quenching rate constants of $N_2$(C) by $O_2$ are displayed in Fig. 2 and compared to the literature.

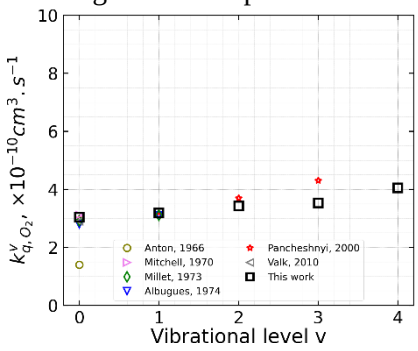



Fig. 2 Comparison of the quenching rate constants of N2(C, v=0-4) by O2.

**Acknowledgements**

This work has received funding from the European Research Council (ERC) under the European Union’s Horizon 2020 research and innovation program (grant agreement No. 101021538). The authors thank E. Jean-Bart, Y. Le Teno and M. Ramires Garcia for their help in the design and construction of the setup.

**References**

[1] Castela, M. *et al.*, Modelling the Impact of Non-Equilibrium Discharges on Reactive Mixtures for Simulations of Plasma-Assisted Ignition in Turbulent Flows, *Combustion and Flame*, **166**, (2016).

[2] Barleon, N., Detailed modeling and simulations of Nanosecond Repetitively Pulsed Discharges for Plasma-Assisted Combustion. Fluid Dynamics [physics.flu-dyn]. Institut National Polytechnique de Toulouse - INPT, 2022.

[3] Blanchard, V., «Thermochemical Effects of Nanosecond Plasma Discharges on Lean Flame Stabilization» Ph.D. Thesis, CentraleSupélec, University Paris Saclay, 2023.

# Synergestic effect of coupling Non thermal plasmas with perovskite-type membranes for oxygen permeation

D. Sadi[1], O. Guaitella[1]

[1] *Laboratoire de Physique des Plasmas (LPP), CNRS, Sorbonne Université, Université Paris Saclay, École Polytechnique, Institut Polytechnique de Paris, 91128 Palaiseau, France*

Recycling $CO_2$ is crucial for sustainable energy storage and utilization. A promising approach involves its dissociation into CO and $O_2$, with non-thermal plasmas offering an efficient alternative by selectively exciting molecular vibrations. However, reverse reactions can reform $CO_2$. Ionic membranes offer an innovative solution by continuously extracting oxygen via permeation, driven by temperature, pressure gradients, and, in some cases, an electric field. Perovskite-type BSFC membranes are mixed ionic-electronic conductors (MIEC) that transport $O^{2-}$ ions and electrons under an oxygen partial pressure gradient at 700–1000°C. Coupling these membranes with plasma introduces interactions involving surface and gas chemistry, heating, and ionic bombardment. This study examines the coupling of a hollow fiber BSFC membrane with $O_2$ and $CO_2$ plasmas, revealing that plasma significantly enhances oxygen flux compared to pure $O_2$ gas. Deconvolution experiments suggest atomic oxygen plays a key role in improving permeation performan

## 1. Oxygen Permeation in BSFC Membranes

Oxygen permeation in BSFC membranes is driven by an oxygen partial pressure gradient. The process involves surface adsorption, dissociation, charge transfer to $O^{2-}$, bulk diffusion (coupled with electron transport in the opposite direction), and desorption. These steps require activation energy, defining a threshold temperature. Before analyzing the benefit of coupling the membrane with the plasma, it is necessary to determine the permeation capability of the material used when the permeation is driven solely by heating.

A **hollow fiber BSFC membrane** (2 mm diameter) is placed in a quartz tube filled with $O_2$ at **2–5 Torr**, while the membrane volume is pumped to **0.1 Torr**. The system is heated to **1000°C**, and oxygen flux is quantified using **mass spectrometry** and **time-resolved pressure measurements**. Permeation flux increases with temperature, confirming the thermal activation process and allowing to determine the permeation fluw at a gicen gas temeprature The oxygen permeation observed can then be compared to the one obtained when the membrane is placed in close post-discharge of the plasma for the same gas temperature.

## 2. Plasma-Membrane Synergy

Plasma exposure introduces ions and atomic oxygen, reducing the activation energy for surface reactions (e.g., bypassing the dissociation step). Additionally, plasma-induced heating lowers the required oven temperature. When a **DC glow discharge ($O_2$ or $CO_2$ plasma)** is ignited in direct contact with the membrane, **oxygen flux measurements confirm enhanced permeation** under plasma conditions. However the presence of the Perovskite perturbs significantly the plasma and therefore the parameters of the gas phase (gas temperature, O atoms density, electric field) are not well controlled.

To isolate plasma effects, the membrane is placed in the **afterglow region**, where electric fields and direct heating are negligible, but atomic oxygen generated in the plasma reach it still. The fig 1 shows an example of results obtained with a pure O2 plasma and the membrane places about 2 cm downstream the plasma. Results show a **strong correlation between atomic oxygen concentration and permeation enhancement**,increasing with the power of the plasma. Axial profile of gas temperature along the plasma suggest that extra heating of the gas induced by the plasma is not sufficient to explain the large increase of permeation. The atomic oxygen fluw reaching the surface of the membrane could explain the enhancement of permeation. .

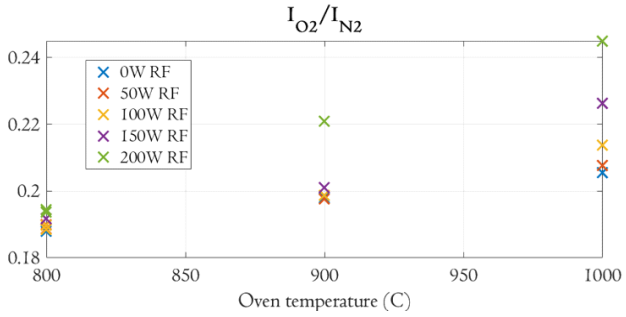



Fig 1 : Oxygen quantity inside of the membrane volumes when situated in post-dicharge as a function of the oven temperature

Differences between $O_2$ and $CO_2$ plasma exposure are investigated, revealing variations in oxygen flux and possible chemical interactions. **Membrane stability under prolonged plasma exposure remains a key research question**, with potential implications for **$CO_2$ splitting efficiciency.**

## References

[1] Understanding and identifying the oxygen transport mechanisms through a mixed-conductor membrane, P.M Geffroy

[2] A novel plasma-assisted hollow fiber membrane concept for efficiently separating oxygen from CO in a CO2 plasma G. Chen, F. Buck

# Ion acceleration in a diverging magnetic nozzle : Laser Induced Fluorescence measurements and expansion model.

R. Pioch[1,2], V. Désanlges[2], F. Boni[2] and P. Chabert[1]

[1] *LPP, Sorbonne Université, CNRS UMR 7648, Palaiseau, France*
[2] *ONERA DPHY FPA, Palaiseau, France*

The longitudinal and transversal components of the ion velocity field of a plasma in expansion in the diverging magnetic nozzle of an ECR thruster are measured with the diagnostic of Laser Induced Fluorescence. Results show that the acceleration profile of the ions depends of the operating condition of the thruster in mass flow rate and power. These measurements are compared with an isotropic and isothermal model of plasma expansion in a diverging magnetic field, showing a good agreement.

**Context and motivation**

The Electron Cyclotron Resonance thruster (ECRT) is an electric propulsion device which uses a diverging field, called magnetic nozzle (MN), to accelerate a plasma and produce a thrust force. Understanding the acceleration of a plasma in a MN is then crucial to improve the performance of this device, and more generally of MN thrusters. This work presents the measurements of ion acceleration profiles performed with the Laser Induced Fluorescence (LIF) diagnostic in the plume of the ECRT for several operating conditions and their comparison with a theoretical model of plasma expansion in a diverging magnetic field.

**Laser Induced Fluorescence measurements**

The transition from the $5d^2F_{7/2}$ excited state to the $6p^2D_{5/2}$ was excited with a laser at 834.955 nm and the fluorescence signal from the upper state to the $6s^2P_{3/2}$ state at 541.915 nm was collected. Two LIF signals were measured, one in the plasma plume of the ECRT and one in a reference cell filled with a Xenon plasma with a null velocity. The comparison of these two signals allowed us to measure the ion velocity projected in the direction of the excitation laser, the first signal being shifted from the second because of the Doppler effect.

Measurements were performed in the source of the ECRT and along the axis of the thruster for several operating conditions (figure 1) and in the whole plume region for one condition and two magnetic topologies.

**Fluid model of plasma expansion**

The experimental data hence gathered was compared with the analytical solution of an isotropic and isothermal fluid model of plasma expansion in a diverging magnetic nozzle. For all the thruster operating conditions tested, this model performs well at describing the acceleration of the ions in the axis of the thruster, as shown in figure 1. The good comparison of these theoretical models with experimental data illustrates that, in the source region, the ion acceleration is driven by the electron temperature and the shape of the magnetic field. It is found that the electron temperature increases with the microwave power and decreases with the mass flow rate, while being poorly dependent on the magnetic nozzle topology.

## References

[1] Pioch, R. Ion dynamics in the magnetic nozzle of an Electron Cyclotron Resonance thruster. *PhD dissertation, Institut Polytechnique de Paris*, (2024).

[2] Little, J. M. and Choueiri, E. Y. Thrust and efficiency model for electron-driven magnetic nozzles. *Physics of Plasmas*, **20**, 103501 (2013).

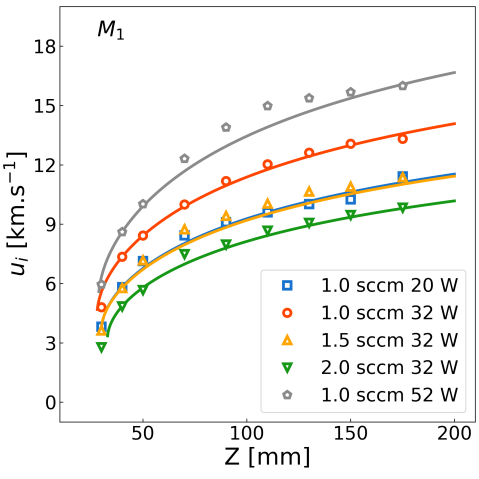



Figure 1: Ion acceleration profiles measured by LIF (scattered symbols) compared with an isotropic and isothermal fluid model (solid line).

# Particle-in-Cell Modeling of EUV-Induced Plasma Dynamics in Lithography Exposure Chamber

Y. Sharova[1,2], R. P. Brinkmann[1], E. Kemaneci[2], D. Eremin[1]

[1] *Institute of Theoretical Electrical Engineering, Ruhr University Bochum, Universitätsstrasse 150, D-44801 Bochum, Germany*
[2] *ASML Netherlands B.V., De Run 6501, 5504 DR Veldhoven, The Netherlands*

In modern extreme ultraviolet (EUV) lithography, plasma–surface interactions significantly influence the lifetime and performance of optical components such as multilayer mirrors and photomasks.

The 13.5 nm EUV beam-line 2 nanolithography research machine [1], designed to provide accelerated tests for next generation lithography, is used to investigate EUV-induced plasma phenomena. Typical operating conditions include $H_2$ gas at pressures ranging from 5 to 20 Pa , 3 kHz repetition rate of EUV pulses, 150 ns–EUV pulse duration. This exposure generates a transient plasma, whose temporal and spatial evolution is characterized using a movable retarding field energy analyzer (RFEA).

We present a numerical investigation of extreme ultraviolet (EUV) induced plasma formation in a lithography exposure chamber environment [1] using a GPU-accelerated Particle-in-Cell (PIC) approach. The simulation captures essential physics within the exposure chamber geometry, including photoionization events, electron impact ionization, and plasma-surface interactions, with particular attention to plasma behavior around the sample holder. Initial results demonstrate the spatiotemporal evolution of the EUV-induced plasma. The simulation provides detailed insights into electron density distributions, ion fluxes, and plasma potential development near the sample holder and other critical surfaces within the chamber geometry. These findings are particularly relevant for the understanding of plasma-induced effects in experimental analysis of the sample in the exposure chamber.

Ultimately, the work provides valuable insights to plasma-related phenomena affecting next-generation semiconductor manufacturing.

**References**

[1] J. van Veldhoven, C.-C. Wu, A. J. Storm, M. van Putten, J. R. Meijlink, A. G. Ushakov; Measurements of ion fluxes in extreme ultraviolet-induced plasma of new EUV-beam-line 2 nanolithography research machine and their applications for optical component tests. *J. Vac. Sci. Technol. B* 1 January 2023; 41 (1): 012603. https://doi.org/10.1116/6.0002132

[2] D. Astakhov, (2016). Numerical study of extreme-ultra-violet generated plasmas in hydrogen. PhD Thesis, University of Twente. https://doi.org/10.3990/1.9789036541114

[3] M. H. L. van der Velden, (2008). Radiation generated plasmas: a challenge in modern lithography. Phd Thesis, Technische Universiteit Eindhoven. https://doi.org/10.6100/IR634669

# About the sensitivity of atomic hydrogen surface loss coefficients with respect to Si contamination

A. Remigy[1], S.-J. Klose[1,2], A.S.C Nave[1,3], F. Hempel[1], N. Lang[1] and J.H. van Helden[1,4]

[1] *Leibniz Institute for Plasma Science and Technology (INP), Felix-Hausdroff-Str. 2, 17489 Greifswald*
[2] *Research Department Plasmas with Complex Interaction, Ruhr University Bochum, Universitätsstr. 150, 44780 Bochum, Germany*
[3] *Silicon Austria Labs GmbH, Europastraße 12, 9524 Villach, Austria*
[4] *Experimental Physics V, Spectroscopy of Atoms and Molecules by Laser Methods, Faculty of Physics and Astronomy, Ruhr University Bochum, Universitätsstr. 150, 44780 Bochum, Germany*

Surface loss coefficients of hydrogen atoms (H) are of great importance, in particular for numerical simulations of industrial plasma processes. In this work, we use two-photon laser induced fluorescence to measure the surface loss coefficient of H atoms on stainless steel and tungsten as a function of the plasma treatment time. In parallel, the surface element composition of the sample is monitored using in-situ x-ray photo-electron spectroscopy (XPS). Cross-comparison between the two techniques reveals the influence of small silicon (Si) contamination of the reactor on the measured surface loss coefficient. This work demonstrates the need for a characterization of the vacuum quality when measuring surface loss coefficients to be taken as reference values for further work, even with brand new reactors, as commercial plasma sources can introduce significant contamination. It also highlights the necessity for a solid characterization of the surface to enable comparisons between different experimental setups.

Hydrogen-containing low pressure and low temperature plasmas interacting with surfaces are ubiquitous in many applications. In order to reliably simulate the complex plasma configurations used for these applications, a deeper understanding of the prevailing plasma-surface interactions is required. An important parameter here is the surface loss coefficient, which is known inadequately for hydrogen atoms (H) for many materials.

In this work, we study the interaction of H atoms with stainless steel (SST) and tungsten (W) surfaces in an electron cyclotron resonance (ECR) plasma in a pure hydrogen atmosphere at low pressure [1]. The surface loss coefficients are derived from the density distribution of H atoms in the vicinity to the investigated surfaces. Two-photon absorption laser-induced fluorescence (TALIF) spectroscopy was employed to determine the spatial distributions of the H atoms near the surface. In parallel, the surface element composition was monitored using x-ray photo-electron spectroscopy (XPS).

The surface loss coefficient was measured on SST and W as a function of plasma treatment time. On both surfaces, the surface loss coefficient decreases exponentially as a function of plasma treatment time, with a decay time of 850 ± 20 min. The XPS analysis shows a steady increase of the amount of Si atoms on the surface for both target materials, which may be the reason for the temporal evolution of the surface loss coefficient.

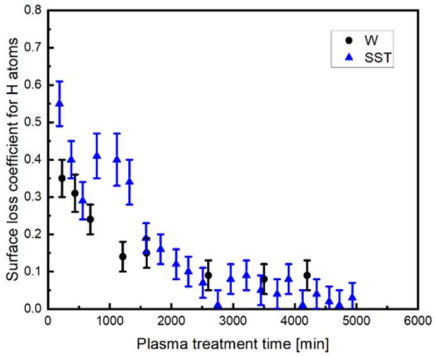



Figure 1: Surface loss coefficient of H atoms on SST and W as a function of plasma treatment time in Si-contaminated chamber.

To get rid of the Si contamination, a new reactor is built, with a protected plasma source to avoid contamination from it. A baking-out and condition procedure is followed, monitoring contamination using Ru probes. New surface loss coefficient measurements are then made in this new chamber on SST and W, which display a constant value of 0.34 ± 0.02 and 0.33 ± 0.02 respectively.

This study demonstrates the necessity for better vacuum and surface characterization when measuring surface loss coefficients, which would allow for more conclusive data and easier comparison between different experimental setups.

## References

[1] F. Sigeneger *et al.* Plasma Sources Sci. Technol. 31, 105011 (13pp) (2022).

# Log-normal density scaling of species embedded in chemical network topology in low-temperature silane plasma

K. Hamano[1], I. Yonemoto[1], T. Itoh[2], T. Murakami[3] and O. Sakai[1]

[1] *Department of Electronic Systems Engineering, The University of Shiga Prefecture, Hikone, Shiga 522-8533, Japan*
[2] *Graduate School of Frontier Science, The University of Tokyo, Kashiwa, Chiba 277-8561, Japan*
[3] *Faculty of Science and Technology, Seikei University, Musashino, Tokyo 180-8633, Japan*

A plasma chemical reaction system in molecular gases is complex, which is numerically analysed in most cases. To visualize and characterize its complexity, network topology offers a framework for describing its interwoven system. In this study, we connect the network topology to the statistics found in species-density distribution. In $SiH_4$ plasma, a log-normal density distribution is found among species calculated in our numerical model. This result indicates that various species of radicals and polymers branch from pure silane molecules, with increasing number of species, while the corresponding system yields a new species that is likely to react with major species in each reaction network preferentially, leading to a scale-free network.

## 1 Introduction

Low-temperature molecular plasma is in a non-thermal and non-equilibrium state with high-energy electrons and low-energy neutral gases. Inelastic collisions by electrons induce various chemical reactions like dissociation/polymerization originating from mother molecular gases. Eventual species dispersity is very complex with several tens of species existing in a quasi-steady state [1]. So far details of plasma chemical processes have been investigated by numerical models based on rate constants [2] or elementary collision cross sections, which are rather specific and seem to lack universality.

Even if quantities of reaction rates are specific, when we consider them *statistically*, some underlying processes with ubiquitous principles may be common to molecular plasma processes. Here, we consider scale-free properties in reaction network topology [1] and log-normal distributions in species dispersity [2]. Performing numerical calculations of rate-constant equations, we analyse datasets of time-evolving densities over tens of species in $SiH_4$ plasma.

## 2 Methods and results

Our theoretical model is based on a classical zero-dimensional rate-equation solution of $SiH_4$ plasma chemistry [2]. We fixed $SiH_4$ and electron densities, and 254 chemical reactions are explicitly solved in finite difference formulation. In our previous study [1], the derived web-like reaction network has a scale-free property, which ensures system robustness.

Densities of the total 54 species calculated numerically form a time-varying dataset of species dispersity. When we count number of species on each log-density span, we found that the spectra of the density count fit a log-normal function (a straight line in Fig. 1). Such log-normal distributions are frequently observed in which quantities in a dataset are fractions of one initial unit. That is, in low-temperature plasma, seed species generated by initial decomposition (i.e., $SiH_x$ with $x$ = 1-3) can trigger preferential attachment of other species, leading to scale-free network, while, in another aspect, the mother gas is converted into small fractions of species, leading to a log-normal distribution.

**References**

[1] Sakai, O., Kawaguchi, S., Murakami, T. Complexity visualization, dataset acquisition, and machine learning perspectives for low-temperature plasma: a review. *Japanese Journal of Applied Physics* **61**, 070101 (2022).
[2] Hamano, K., Miyagi, S., Murakami, T., Ito, T., Sakai, O. Statistical measure of dispersity in complex weighted networks of low temperature plasma chemistry. *Journal of Physics: Complexity* **6** (2025) (in press).

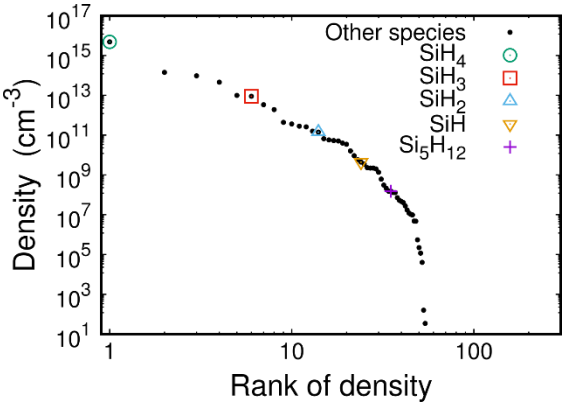



Fig. 1. Rank-size plot of species density in $SiH_4$ plasma after 10-ms discharge.

# Evidence for sputtering of D and O adsorbed on W(110) by a $D_2^+$ ion beam

Matthieu Latournerie[1], Thierry Angot[1], Éric Salomon[1], Marco Minissale[1], Régis Bisson[1]

[1] *Aix-Marseille Université, CNRS, PIIM, Marseille, France*

The investigation of interactions between a W target and a $D_2$ ion beam at 500 eV finds an interest in the fusion reactors operation. Indeed, the recycling of the fuel (D, T) through the vessel walls is one the main problem concerning this technology. This work presents the results obtained following a study of a clean W(110) sample under various fluences of $D_2^+$. These results are obtained through TPD studies performed in Ultra-High Vacuum conditions. Although experimental limitations prevent us to quantify this effect precisely, this work brings evidences concerning a sputtering of adsorbed atoms on the W surface sample by the ions impinging the surface.

## 1 General

The divertor and first wall of ITER will be made of tungsten (W) thus a detailed understanding of their interaction with fusion fuel is needed. In particular, characterizing the release kinetics of hydrogen isotopes from W materials is important to model fuel recycling [1], which could be influenced by impurities such as oxygen (O) [2]. Recently, an Auger Electron Spectrometer (AES) has been added to the Temperature Programmed Desorption (TPD)-ion implantation apparatus AMU-PSI to quantify thin films of O in the sub-monolayer (sub-ML) regime, and determine their influence on deuterium (D) release kinetics from W. In this contribution, we present, first, how D ion implantation affects D release kinetics at various D coverage suggesting self-sputtering and, second, how D ion implantation sputters sub-ML O on W.

Starting with a clean W(110) sample, we realize various D exposures either by thermal neutral $D_2$ exposure (surface loading) or by 500 eV $D_2^+$ ion (bulk loading). Surface loading with a D coverage of 0.25 ML gives a desorption temperature of 540 K. Increasing the D surface coverage to 1.00 ML, decreases the desorption temperature down to 455 K. These results agree with Whitten and Gomer [3]. Bulk loading with $D_2^+$ ion implantation in the $10^{19\text{-}20}$ $D^+.m^{-2}$ range gives desorption temperature that are systematically lower than surface loading. One could interpret it as an increased of the surface coverage with D atoms due to diffusion from the bulk to the surface. However, modifications in the line shape of the TPD peak suggests that self-sputtering of D adsorbed at the surface by D ions occurs simultaneously with bulk loading.

Then, we deposited 0.5 ML of O at the surface of W(110) and exposed it to the $D_2^+$ ion beam to evaluate the corresponding poorly-known sputtering yield. To this purpose, we use AES to quantify the evolution of O coverage with increasing D ions fluence. We show that for D ions at 250 eV/D and at normal incidence, the sputtering yield for O adsorbed on W is $4\times10^{-3}$. This sputtering yield is smaller than the one for a massive C target, consistent with the higher mass of O. Finally, using a Low–Energy Electron Diffractometer, we measure a loss of periodicity of the initial O surface lattice, supporting the observation of D-ion-induced depletion of O observed by AES.

**References**

[1] Smirnov et al., Physics of Plasmas 27 (2020) 032503

[2] Dunand et al., Nuclear Fusion 62 (2022) 054002

[3] Whitten and Gomer, Surface Science (1998) 409

# ps-TALIF and streak camera system for measuring sub-ns decay times and densities of reactive atoms in collisional microplasmas

L. Invernizzi, D. Stefas, S. Prasanna, G. Lombardi, and K. Gazeli

*Laboratoire des Sciences des Procédés et des Matériaux (LSPM), CNRS, Université Sorbonne Paris Nord, UPR 3407, F–93430 Villetaneuse, France*

The usefulness of ps-TALIF and streak camera diagnostics for the accurate measurement of decay times and absolute densities of key atomic species in collisional microplasmas is shown. Exemplary measurements are presented for H– and N–atoms generated in a He microjet and an air microdischarge, respectively. The present diagnostic platform allows directly measuring sub-ns decay times of the laser-excited states of H- and N-atoms as well as their absolute densities (~$10^{14}$ $cm^{-3}$ and ~$10^{15}$ $cm^{-3}$, respectively).

## 1 Introduction and methodologies

Nanosecond (ns) Two Photon Absorption Laser Induced Fluorescence (TALIF) has been a standard method for measuring atomic densities in plasmas, the most representative cases referring to O–, N– and H–atoms [1]. An essential quantity to be determined for achieving precise measurements of species densities ($N$) with TALIF is the effective decay time ($\tau_{eff}$) of the laser-excited states, as follows:

$$N = f(\tau_{eff})$$

In collisional environments such as atmospheric pressure plasmas, strong quenching of excited states of reactive atoms may happen and their decay times can become even smaller than 1 ns depending on the quencher type and density [2]. In this case, ns-TALIF can no more directly resolve these decay times because the pulse duration of ns lasers (typically few ns) becomes comparable or largely exceeds the $\tau_{eff}$. Thus, a solution to effectively resolve reactive species lifetimes is the use of picosecond (ps) TALIF.

However, the combination of ps-TALIF with conventional ns-timescale detectors (photomultiplier tubes, ICCD cameras) may also limit the precision of the diagnostic. As a matter of fact, directly capturing sub-ns decay times requires employing detectors with exceptional temporal resolution (ps timescale). A streak camera is a representative ultrafast detector, reaching temporal resolution as low as few ps or even lower (e.g., model C16910, Hamamatsu Photonics). Therefore, backing ps-TALIF with a streak camera is a perfect choice for measuring sub-ns decay times of fluorescing atoms in collisional plasmas.

However, the reliable use of ps-TALIF and streak camera requires careful consideration of the laser and detector peculiarities. For instance, a streak camera must be used with caution when capturing ultrafast TALIF signals since its instrumental function distorts the TALIF shape [2].

In this work we address some key requirements for the application of ps-TALIF and streak camera on the measurement of decay times and absolute densities of reactive atoms in atmospheric pressure plasmas. TALIF signals of H– and N–atoms are captured in a helium microplasma jet (APPJ) and a pin–dielectric–electrode (PDE) air discharge, respectively. The duration of the laser pulse is ~6 ps at 205 nm, which is measured with the streak camera (highest temporal resolution of ~1 ps). Both atomic densities were calibrated by applying ps-TALIF in krypton gas in a sealed gas cell (2 mbar).

## 2 Results

The present system allows measuring $\tau_{eff}$ as low as ~100 ps for both species depending on the operating conditions and position of the measurement. These are used for the determination of the absolute density of H–atoms (~$10^{14}$ $cm^{-3}$) and N–atoms (~$10^{15}$ $cm^{-3}$). These densities drastically change along the plasma propagation axes and depend on the parameters of each plasma source such as voltage pulse properties (amplitude, width, burst mode or not) and gas flow rate (APPJ only).

### Acknowledgments

ULTRAMAP (ANR-22-CE51-0027), SPECTRON (ANR–23–CE51–0004–01), Labex SEAM (ANR–10–LABX–0096; ANR–18–IDEX–0001).

### References

[1] K. Gazeli, G. Lombardi, X. Aubert, C. Duluard, S. Prasanna, K. Hassouni, *Plasma* **4**, 1 145 (2021).
[2] L. Invernizzi, C. Duluard, H. Höft, K. Hassouni, G. Lombardi, K. Gazeli, S. Prasanna, *Meas. Sci. Technol.* **34**, 095203 (2023).

# Effects of material properties on Surface Semiconducting Barrier Discharges

Ayah S. Taihi[1] and David. Z. Pai[1]

[1]*Laboratoire de Physique des Plasmas, CNRS, Sorbonne Université, Ecole Polytechnique, Institut Polytechnique de Paris, 91120 Palaiseau, France*

Semiconducting Barrier Discharges exhibit robust homogeneity and potential high energy density in air at atmospheric pressure. A suspected plasma-semiconductor interaction motivated a parametric study to explore how material properties - such as $SiO_2$ and Si layer thicknesses, as well as Si doping - affect plasma behaviour. Fast imaging, optical emission spectroscopy, and current-voltage measurements revealed trends linked to electron-hole dynamics, and competing effects of surface charging and electric field coupling.

## 1. Introduction

Surface Semiconducting Barrier Discharges (SeBD) [1] are gaining interest in atmospheric-pressure plasma research due to their homogeneity and potential high energy density, key advantages for applications like aerodynamic flow generation [2]. In contrast, surface dielectric barrier discharges, widely used in these applications, often exhibit inhomogeneity and limited energy density, affecting their performance.

A key factor in SeBD behaviour is a suspected plasma-semiconductor photoelectric interaction [3]. To investigate this, we conducted a parametric study on material properties, aiming to deepen our understanding of SeBD physics and optimize material selection for improved plasma efficiency.

## 2. Experimental methods

The plasma was ignited by applying a 2 kV, 100 Hz nanosecond high-voltage pulse through a 100 µm diameter pin electrode. The electrode was placed on a substrate consisting of 1 µm thick $SiO_2$ on p-doped Si (1-10 Ω·cm resistivity, 525 µm thickness). The $SiO_2$-Si wafer sits on a 1 mm thick glass plate and a copper ground plane. We analyzed properties such as plasma propagation, energy, and electric field using ICCD imaging, current-voltage measurements, and optical emission spectroscopy (OES), while varying mainly the $SiO_2$ thickness, Si doping and thickness.

## 3. Main results

The parametric study revealed several key trends. In particular, intermediate doping level for both n- and p-type Si improved plasma propagation while reducing current amplitude (Figure 1). This suggests a possible balance between sufficient free carriers in Si to couple with the plasma while preventing excessive charge loss. Also, increasing the $SiO_2$ thickness generally enhanced propagation, but in a few cases had no effect or even reduced propagation, indicating the existence of an optimal $SiO_2$ thickness. This reveals a possible competition between plasma-Si electric field coupling and $SiO_2$ surface charging.

This study highlights the potential of optimizing semiconductor barriers to improve plasma performance for future applications.

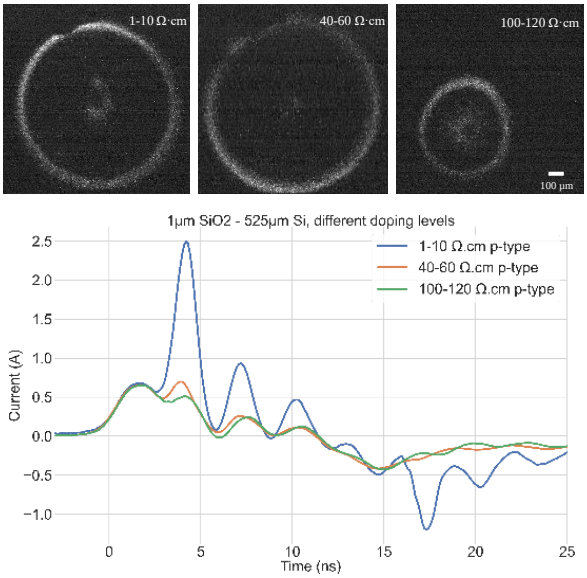



Figure 1: For different resistivities of Si, *(Top)* ICCD Images of plasma at 10.8 ns after ignition. *(Bottom)* Corresponding current measurements.

## References

[1] Darny, T., et al. Plasma Sources Science and Technology 29, 065012 (2020).
[2] Leonov, S. B., et al. Plasma Sources Science and Technology 25, 063001 (2016).
[3] Taihi, A., & Pai, D. Bulletin of the American Physical Society (2024). Presented at the 77th Gaseous Electronics Conference, September 30 - October 4, 2024; San Diego, California.

# Electrohydrodynamic flows induced by DC and AC needle-to-liquid discharges

E. Moreau[1], L. Alomari[1,2], F. Dyson[1], T. Orriere[1] and B. Teychene[2]

[1]*Université de Poitiers, PPRIME Institute, UPR CNRS 3346, Poitiers, France*
[2]*Université de Poitiers, IC2MP, UMR CNRS 7285, Poitiers, France*

When an electrical discharge is established above the surface of a liquid, various physical phenomena generate flows within the liquid. In this presentation, we will discuss the different discharge regimes and provide a detailed characterization of these induced flows as a function of a wide range of input parameters.

## 1 Introduction

The interactions between a plasma discharge and a liquid are very complex, but very important to study due to various applications, such as water treatment [1]. Indeed, when a plasma interacts with water, it produces reactive species that can be useful in chemistry and biology applications. Moreover, due to different physical phenomena, several mechanical effects can occur: a gas flow induced by the discharge (ionic wind), a deformation of the liquid surface, and a liquid flow, all these electrohydrodynamic (EHD) phenomena being currently investigated by our research team. In these experiments, our first objective is to investigate how the flows generated by the plasma in the liquid influence the chemistry, by controlling the convection of reactive species from the plasma–liquid interface into the rest of the liquid. Second, we aim at better characterizing the physical phenomena at the origin of the liquid flows.

In this context, we developed a simple device that consists in applying a high voltage at a needle placed a few millimeters above the surface of the liquid to be treated, in order to ignite a discharge between the needle tip and the water surface. Two geometrical designs have been used. In the first design (case 1), the grounded electrode is placed inside the liquid and we apply a DC voltage at the needle. In the second one (case 2), the grounded electrode is located below the glass vessel that contains the liquid, and the application of an AC sine high voltage at the needle results in the formation of a dielectric barrier discharge above the water surface (Fig. 1a).

## 2 Experimental results

In the case 1, when the voltage is increased, two discharges regimes have been observed: a corona regime (current of a few dozens of µA) and a normal glow one with current up to 10 mA (see photos of Fig. 1b). In the case 2, two distinct discharge regimes have also been observed, depending on the magnitude and the frequency of the applied voltage.

Then, we investigated the EHD flows induced inside the liquid with the help of a particle image velocimetry (PIV) system. Several input parameters have been investigated, including the geometrical design used to produce the discharge, the discharge regime, its polarity, the AC voltage frequency, the gap between the needle tip and the water surface, the liquid conductivity, and the liquid surface tension.

This in-depth investigation allowed us to better understand the phenomena at the origin of the liquid flows. In this oral presentation, we propose to present all our results and to discuss the underlying physics.

Fig. 2 presents an example of the liquid flow in the case of a negative DC corona discharge impacting the water surface.

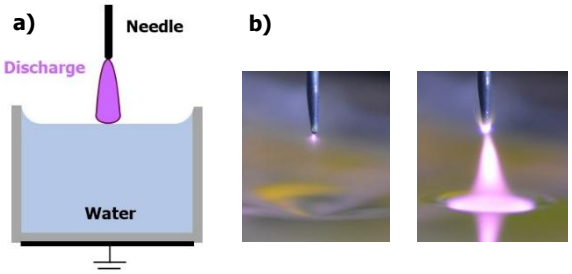



Fig. 1. Discharge experimental setup (a) and pictures of the corona and glow discharges (b).

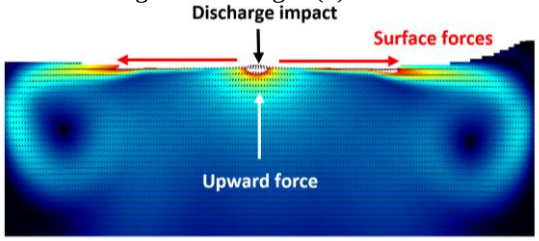



Fig. 2. EHD flow under the surface of the liquid resulting from a DC negative corona discharge.

**References**

[1] Bruggman P. et al. Plasma–liquid interactions: a review and roadmap. *Plasma Sources Sci Technol* **25** (2016).

# Similarities between formation of low-current self-sustained discharge and breakdown in industrial gas insulation

R. Almeida[1,2], P. Almeida[1,2], H. Kaufmann[3] and M. Benilov[1,2]

[1] *Departamento de Física, FCEE, Universidade da Madeira, Largo do Município, 9000 Funchal, Portugal*
[2] *Instituto de Plasmas e Fusão Nuclear, Instituto Superior Técnico, Univ. de Lisboa, 1041 Lisboa, Portugal*
[3] *Siemens Energy, 10553 Berlin, Germany*

In this work, a setup of interest for high-voltage circuit breakers is studied. In this setup the self-sustainment and breakdown voltages are known to be close. An analysis was performed of the temporal evolutions starting from conditions of no-discharge, to either the self-sustained discharge, or to breakdown. Special attention was given to physical similarities that could help understand the closeness of self-sustainment and breakdown voltages in stated conditions.

## 1 Introduction

For industrial applications where breakdown is an unwanted phenomenon, much effort goes into the design of electrical devices able to withstand ever higher breakdown voltages. In another contribution to this conference entitled 'Hold-Off Voltage Computation in Industrial Gas Insulation' the inception voltage was found to be very close to the breakdown voltage in vacuum interrupters in high-voltage circuit breakers enclosed in a pressurized container with air.

It is of interest to understand the physical reasons for the closeness between the self-sustainment voltage and the breakdown voltage in these conditions.

## 2 Model and conditions

The numerical model employed in this work was detailed in [1] and was supplemented with a charge accumulation condition on dielectric surfaces. The simulated setup is that of a 4 mm high dielectric disk close-stacked between two 2 mm high disk electrodes in air at 1 atm. All disks have 7.5 mm radius and 0.2mm roundings. A dielectric constant of 1 was used. Two types of breakdown were studied; 'first breakdown', where there is no surface charge on the dielectric and 'repetitive breakdown', where a certain amount of surface charge is initially present over the dielectric surface.

## 3 Results and discussion

With a given external circuit the setup evolved from a no-discharge state to the self-sustained state, as shown in Fig. 1. Two timescales can be identified in these conditions: one for the volume discharge formation, which is of the order of fractions of millisecond, and one for the surface charge deposition, which is of the order of a few milliseconds.

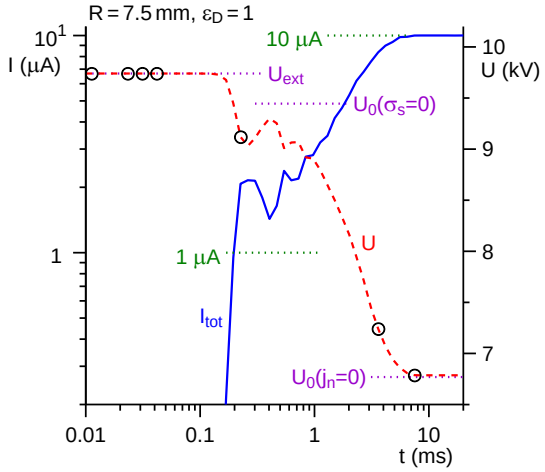



Figure 1. Response of the setup when in series with a voltage source of 9.74kV and a ballast resistor of 295MΩ.

Other results show that during the evolution towards first (repetitive) breakdown, a volume discharge is established very similar to the stationary volume discharge associated with the self-sustainment discharge without (with) surface charge on the dielectric. The development of this volume discharge within fractions of a millisecond, constitutes the physical reason for the similarity between self-sustainment and breakdown voltages. At the given breakdown voltage, and with no limitation on current, the volume discharge evolves rapidly to breakdown.

## 4. Acknowledgments

This work was supported by FCT of Portugal under Project Nr. IPFN/UID/50010/2025, and by Siemens Energy Global GmbH & Co. KG.

## References

[1] M. Benilov, P. Almeida, N. Ferreira, R. Almeida, and G. Naidis, *J. Appl. Phys.* **130**, 121101 (2021).

# Phenomenological description and numerical modelling of vacuum breakdown

C. Cró[1,2], H. Kaufmnann[3], N. Almeida[1,2], P. Almeida[1,2] and M. Benilov[1,2]

[1] *Departamento de Física, FCEE, Universidade da Madeira, Funchal, Portugal*
[2] *Instituto de Plasmas e Fusão Nuclear, Instituto Superior Técnico, Univ. de Lisboa, Lisboa, Portugal*
[3] *SE GT PRM D AIS VI, Siemens Energy Global GmbH & Co. KG, Berlin, Germany*

Numerical simulations of vacuum breakdown were conducted based on a phenomenological description of the mechanism of enhanced field emission. It is shown that field emission can initiate breakdown in a nanosecond timescale, for reasonably sized field emitters, and produce currents that are comparable to those in experiments. A full model including the effects of hydrodynamics and crater formation is being developed.

## 1 Introduction

Vacuum breakdown plays a critical role in many technical devices, such as high voltage circuit breakers and particle accelerators. Field emission is necessary for the initiation of breakdown. The currents produced by field emission are insufficient to lead to breakdown — enhancement of the electric field by a factor of $10^2$ is needed. In previous works in which a phenomenological approach was used, e.g. [1, 2], the field enhancement factor β was kept constant in time. However, measurements of the current during a breakdown [3] suggest there is a characteristic activation time of the field emission centres, of around 10ns, during which β gradually increases. Using these experimental measurements of current and voltage, the time dependence of β was determined.

## 2 The model

Simulations were done for a 2D, axially symmetrical copper cathode using COMSOL Multiphysics, using a numerical model based on the work presented in [4]. The electric field on the surface of the cathode is given by $E = \beta E_{app} + E_{sheath}$. $E_{app}$ is the macroscopic electric field that is applied to the cathode. $E_{sheath}$ is the sheath electric field.

Figure 1 shows the evolution of breakdown for a field emission centre with radius of 1μm. Initially, a 200 MV/m electric field is applied to the cathode's surface. As the field enhancement factor grows over time, so does the field emission current, and consequently, the cathode is heated. A maximum current of around 25A is reached after 10ns. The cathode surface temperature reaches 3500K, and the bulk of the cathode reaches a maximum temperature of more than 4000K. Comparing these results with the experimental data, the onset of breakdown is in good agreement in terms of the values of current that are measured and the time it takes for breakdown to develop. More results, including similar calculations considering the effects of hydrodynamics and surface deformation will be presented at the conference.

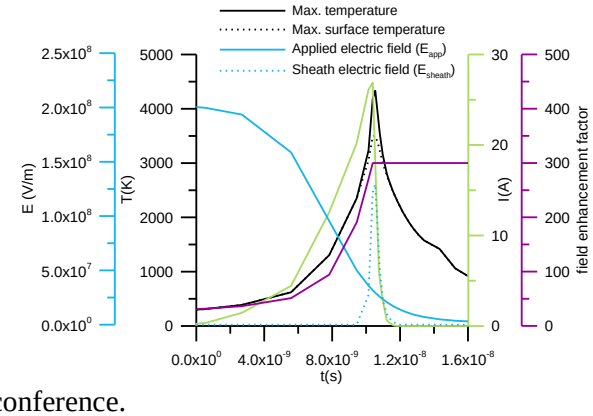



**Figure 1:** Cathode temperature, current, electric field and field enhancement factor for a field emitter with radius of 1μm and $\boldsymbol{E_{app,0}}$ =200 MV/m.

### References

[1] C. Cro, H. Kaufmann, N. Almeida, P. Almeida, and M. Benilov, 'Phenomenological description of vacuum breakdown and detailed modelling of cathode spots', in ESCAMPIG XXVI, 2024.
[2] N. A. Almeida, H. T. C. Kaufmann, and M. S. Benilov, 'Phenomenological Description of Vacuum Breakdown', in MeVArc 2022, 2022.
[3] W. Wuensch, 'Advances in the Understanding of the Physical Processes of Vacuum Breakdown', in *High Gradient Accelerating Structure*, Tsinghua University, China: WORLD SCIENTIFIC, 2013.
[4] H. T. C. Kaufmann, M. D. Cunha, M. S. Benilov, W. Hartmann, and N. Wenzel, 'Detailed numerical simulation of cathode spots in vacuum arcs: Interplay of different mechanisms and ejection of droplets', *J. Appl. Phys*, 2017.

### Acknowledgements

This work at UMa was supported by FCT of Portugal under Project Nr. IPFN/UID/50010/2025, and by Siemens Energy Global GmbH & Co. KG.

# Program of Poster Session #2

| # | In Competition | Title | Speakers | Topic |
|---|---|---|---|---|
| Tu-1 | NO to be considered for a student award | Synchronization phenomenon of plasma generation between plasmas with slightly different driving frequencies | Iwanaga Nano | Collective and nonlinear phenomena |
| Tu-2 | NO | The study on the distribution of dust particles in Capacitively Coupled Radio Frequency (CCRF) discharges | Zhang Yingying | Complex and dusty plasmas, ion-ion plasmas, mixed phase plasmas |
| Tu-3 | NO to be considered for a student award | Electric field measurements of single and multijet systems | Sidharth Sidharth | Elementary processes and fundamental data, Medical, biological, environmental and aeronautical applications, Plasma diagnostics methods |
| Tu-4 | NO | Kinetic mechanisms and species densities in Ar/N2, He/N2 and H2/N2 reduced pressure afterglows | Sarrette Jean-Philippe | Elementary processes and fundamental data, Plasma diagnostics methods |
| Tu-5 | NO to be considered for a student award | Investigation of Electric Field Dynamics and Backward Discharge in Atmospheric-Pressure Nano-Pulsed DBD | Wang Yuhui | High frequency and pulsed discharges |
| Tu-6 | YES | Characterization of a plasma generated by nanosecond repetitively pulsed discharges in a swirled stabilized combustor | Perrin-Terrin Jean-Baptiste | High frequency and pulsed discharges |
| Tu-7 | NO | Temporal evolution of the Sn concentration in pulsed MHz DBD atomizer | Pazderka Michal | High frequency and pulsed discharges |
| Tu-8 | NO | Discharge Plasma Source for Laser Plasma Accelerator at ELI ERIC | Whitehead Alex | High frequency and pulsed discharges |
| Tu-9 | YES | Plasma-assisted combustion in a premixed H2/air flame | Perrin-Terrin Jean-Baptiste | High frequency and pulsed discharges |

| # | In Competition | Title | Speakers | Topic |
|---|---|---|---|---|
| Tu-10 | YES | Analytical Modelling of the Interaction Between an Intense Electromagnetic Pulse and a Spherical Plasma Discharge | Juste Maëva | High frequency and pulsed discharges |
| Tu-11 | NO | The Impact of Electrode Contact with Water on Plasma Bubbles in Plasma-Water Treatments | Petkovic Jovana | High frequency and pulsed discharges, Plasma wall interactions, electrode and surface effects, Plasma in/with liquids |
| Tu-12 | YES | Preheating Temperature Study in a Graphite Electrode Based Plasma Gasification Chamber for Waste Processing | Rana Tejashwi | High pressure and thermal plasma processing |
| Tu-13 | YES | A Feasible Tomographic Reconstruction Strategy for Optical Diagnostics in Capacitively Coupled Plasma | Lee Hyunseung | Low pressure plasmas |
| Tu-14 | YES | A minimally invasive surgical platform for pancreatic and biliary tract cancers using cold atmospheric plasma: The EIC project "IgnitePLASMA" | Giotis Konstantinos | Medical, biological, environmental and aeronautical applications |
| Tu-15 | YES | Cold Plasma-Driven Pectin Extraction from Dragon Fruit Peels: A Sustainable Approach for Stronger Biodegradable Films | Mishra Ritesh | Medical, biological, environmental and aeronautical applications |
| Tu-16 | NO | Enhancing CO2 Plasma Conversion with In-Situ Oxygen Removal Using SOECs | Chen Xingyu | Medical, biological, environmental and aeronautical applications |
| Tu-17 | YES | Evaluating the efficacy of clove extract activated by cold plasma as a novel approach for caviar processing | Jamshidi Alashti Fatemeh | Medical, biological, environmental and aeronautical applications |
| Tu-18 | NO | Influence of current intensity on combustion in scramjet | Rocamora Ancelin | Medical, biological, environmental and aeronautical applications |

| # | In Competition | Title | Speakers | Topic |
|---|---|---|---|---|
| Tu-19 | NO | Spatiotemporal Colorimetric Response of KI-Starch on Reactive Oxygen Species | Kazunori Koga | Medical, biological, environmental and aeronautical applications |
| Tu-20 | NO | Impairment and recovery of immune cell function induced by oxygen plasma irradiation | Yonesu Hinako | Medical, biological, environmental and aeronautical applications |
| Tu-21 | NO | Liquid purification from bacteria and viruses by surface dielectric barrier discharge | Lavrikova Aleksandra | Medical, biological, environmental and aeronautical applications |
| Tu-22 | NO | Temperature and electron density investigation of micro structured pin-to-pin discharge for Hydrogen production | Garcia Soto Carolina Alejandra | Medical, biological, environmental and aeronautical applications |
| Tu-23 | YES | Modelling of positive and negative streamers interaction in dry air with imposed density gradient | Paredes Joaquin | Medical, biological, environmental and aeronautical applications |
| Tu-24 | NO | Direct $H_2O_2$ Delivery and Initial Cellular Responses in Marchantia polymorpha upon Cold Plasma Irradiation | Tsuboyama Shoko | Medical, biological, environmental and aeronautical applications |
| Tu-25 | NO | Simulation of an ionization wave propagating along a silicon-based surface | Herrmann Antoine | Modelling and simulation techniques |
| Tu-26 | NO | Influence of photo-ionization on propagation of streamer discharges at atmospheric pressure | Nikic Dejan | Modelling and simulation techniques |
| Tu-27 | NO | Simulation of He APPJ - dielectric surface action process under external electric field | Wang Lijun | Modelling and simulation techniques |
| Tu-28 | NO | Towards a spatial dust fluid model | Janssen Jesper | Modelling and simulation techniques |
| Tu-29 | NO | Progress report on the LoKI-B+C simulation tool | Pereira P. | Modelling and simulation techniques |
| Tu-30 | NO | Recent developments on LoKI-MC: Coulomb collisions and efficient null-collision method | Dias Tiago | Modelling and simulation techniques |

| # | In Competition | Title | Speakers | Topic |
|---|---|---|---|---|
| Tu-31 | NO | Two-way coupling of plasma-fluid interactions for ionic wind modelling | Dias Coelho Marques Jose Maria | Modelling and simulation techniques |
| Tu-32 | NO | Axisymmetric fluid streamer model with curvilinear electrodes in the AMReX environment | Simonovic Ilija | Modelling and simulation techniques |
| Tu-33 | NO | Comparison of PIC and Experimental Pin-to-Plane Breakdown | Moore Chris | Modelling and simulation techniques |
| Tu-34 | NO | Argon metastable densities in CO2/N2/Ar DC glow discharges at Mars atmospheric pressures | Ben Slimane Tarek | Modelling and simulation techniques |
| Tu-35 | NO | Optimizing Ammonia Decomposition for Enhanced Hydrogen Production: A Comparative Study of Carrier Gases | Garcia Maria C | Non-equilibrium plasmas and microplasmas at high pressure |
| Tu-36 | NO | Numerical investigation of stability of pin-to-plane negative corona in air | Pedro Jorge Gomes Camacho Almeida | Non-equilibrium plasmas and microplasmas at high pressure |
| Tu-37 | NO | Optimisation study of a DBD for CO2 conversion using in-depth electrical analysis | Buddhadasa Madhuwanthi | Non-equilibrium plasmas and microplasmas at high pressure |
| Tu-38 | NO | Synergistic control of radical generation in a radio frequency atmospheric pressure plasma jet via voltage waveform tailoring and structured electrodes | Vass Mate | Non-equilibrium plasmas and microplasmas at high pressure |
| Tu-39 | YES | Self-organized luminous pattern formation in a pin-to-plate DC glow discharge generated in helium | Miyazaki Toshiaki | Non-equilibrium plasmas and microplasmas at high pressure |
| Tu-40 | NO | Parametric study of NO reduction in a confined RF plasma in atmospheric pressure helium | Sigeneger Florian | Non-equilibrium plasmas and microplasmas at high pressure |
| Tu-41 | NO | RF Magnetron Plasma nitriding of quartz | Muhl Stephen | Other applications such as low temperature plasma applications for magnetically confined fusion |

| # | In Competition | Title | Speakers | Topic |
|---|---|---|---|---|
| Tu-42 | NO | Mass separation using rotating electric and magnetic fields | Fruchtman Amnon | Other applications such as low temperature plasma applications for magnetically confined fusion |
| Tu-43 | NO | Combining Infrared transmission and Raman scattering for the fundamental study of CO2 plasma – surface interaction : in situ probing of CeO2 surface and bulk properties | Sadi Dihya | Plasma diagnostics methods |
| Tu-44 | YES | Time-resolved spectroscopic investigation of N2/H2 low-temperature plasmas | Maestri Luca | Plasma diagnostics methods |
| Tu-45 | NO | Multi-diagnostic of dust growth in a capacitive Ar/C2H2 plasma | Herrero Víctor J. | Plasma diagnostics methods |
| Tu-46 | NO | Laser Induced Breakdown Spectroscopy from fs to ns laser pulses for the detection of deuterium in fusion plasma walls | Hussain Arshad | Plasma diagnostics methods |
| Tu-47 | NO | High-sensitivity E-FISH measurement on low-pressure streamer discharge | Wang Jianan | Plasma diagnostics methods |
| Tu-48 | YES | Femtosecond laser-induced fluorescence for atmospheric plasma diagnostics: Stark detuning and power saturation effects | Pascual Fort Carmen | Plasma diagnostics methods |
| Tu-49 | YES | Influence of ambient air humidity on discharge modes for a pin-to-pin discharge with a water droplet | Riazantceva Valentina | Plasma in/with liquids |
| Tu-50 | NO | Simulating H2O2 and OH-driven chemical reaction kinetics and diffusive mass transport in a He/H2O-plasma treated water | Wright Matthew | Plasma in/with liquids |
| Tu-51 | NO | Bubble formation and droplet ejection from liquid metals interacting with inductively coupled hydrogen plasma | Sasaki Koichi | Plasma in/with liquids |

| # | In Competition | Title | Speakers | Topic |
|---|---|---|---|---|
| Tu-52 | NO | Space- and Time-Resolved Studies in Liquid Water Discharges: Insights into Emission Continua and Atomic Line Profiles during Primary and Reflected Pulses | Arora Garima | Plasma in/with liquids |
| Tu-53 | NO | Controlling plasma produced fluxes to liquid surfaces by acoustic structuring: applications to plasma driven solution electrochemistry | Doyle Scott | Plasma in/with liquids |
| Tu-54 | NO | Investigation of reactive species formation in surface dielectric barrier discharge with liquid electrodes | Galmiz Oleksandr | Plasma in/with liquids |
| Tu-55 | YES | Characterization and optimisation of a plasma source for the biological decontamination of wastewater in volume. | Saba Maria | Plasma in/with liquids |
| Tu-56 | YES | Plasma-based Nanoarchitectonics for Dual Gate Graphene Field Effect Transistor (GFET) Device: Effect of Plasma Parameters on Transistor Properties | Verma Monika | Plasma processing of surfaces and particles |
| Tu-57 | YES | Sputter epitaxy of atomically flat Zn1-xMgxO films on sapphire using wurtzite MgO buffer layer fabricated in Ar/O2 discharges | Otsuyama Hiroki | Plasma processing of surfaces and particles |
| Tu-58 | YES | A poly diagnostic study of an atomic oxygen plasma source: Application in cultural heritage | Poupouzas Michail | Plasma processing of surfaces and particles |
| Tu-59 | YES | Magnetron sputtering deposition of strained epitaxial SrTiO3 thin films on MgO vicinal surfaces | Familsatarian Elnaz | Plasma processing of surfaces and particles |
| Tu-60 | NO | Production of durable superhydrophobic coatings using atmospheric pressure plasma | Kyrykbay Baglan | Plasma processing of surfaces and particles |

| # | In Competition | Title | Speakers | Topic |
|---|---|---|---|---|
| Tu-61 | NO | Influence of Gas Pressure On Quartz and Silicon Etching in a Dual-Frequency Capacitively Coupled NF3/Ar/O2 Plasma | Mei Xianxiu | Plasma processing of surfaces and particles |
| Tu-62 | NO | Surface Modification of Polyethylene by Atmospheric Pressure Plasma Jet | Wangkanai Jidchanok | Plasma processing of surfaces and particles |
| Tu-63 | NO | Sulphur-containing organic films grown by $SH_2/CH_4$/He plasmas | Peláez Ramón | Plasma processing of surfaces and particles |
| Tu-64 | NO | Enhancement of Cu and Ti catalysts with nanostructuring by laser irradiation and simultaneous chemical modification by plasma treatment | Schicke Alexander | Plasma processing of surfaces and particles |
| Tu-65 | NO | COMSOL simulation for dual frequency inductively coupled plasma | Alemu Biruk | Plasma processing of surfaces and particles |
| Tu-66 | NO | Insights into the Role of Plasma Jet Reactive Species for the Formation of Gold-based Nanocatalysts Confined in Nanoreactors | Boitel-Aullen Gabriel | Plasma processing of surfaces and particles |
| Tu-67 | NO | Study of ozone production by surface processes | Mazankova Vera | Plasma wall interactions, electrode and surface effects |
| Tu-68 | NO | Microscopic and macroscopic investigation of He bubbles formation on tungsten via in situ spectroscopic ellipsometry | Pappalardo Federica | Plasma wall interactions, electrode and surface effects |
| Tu-69 | NO | High-pressure inductively coupled plasmas with bidirectional vortex gas injection | Corr Cormac | Thermal plasmas |
| Tu-70 | YES | Voltage evolution in low pressure free electric arcs in air | Pietri Carla | Thermal plasmas |
| Tu-71 | NO | Study of stopping processes and transport properties of heated dense plasmas based on the density functional theory | Uderbayeva Akbota | Thermodynamics and transport phenomena |

# Presenter Index


- **Alemu Biruk**: Tu-65
- **Arora Garima**: Tu-52
- **Ben Slimane Tarek**: Tu-34
- **Boitel-Aullen Gabriel**: Tu-66
- **Buddhadasa Madhuwanthi**: Tu-37
- **Chen Xingyu**: Tu-16
- **Corr Cormac**: Tu-69
- **Dias Coelho Marques Jose Maria**: Tu-31
- **Dias Tiago**: Tu-30
- **Doyle Scott**: Tu-53
- **Familsatarian Elnaz**: Tu-59
- **Fruchtman Amnon**: Tu-42
- **Galmiz Oleksandr**: Tu-54
- **Garcia Maria C**: Tu-35
- **Garcia Soto Carolina Alejandra**: Tu-22
- **Giotis Konstantinos**: Tu-14
- **Herrero Víctor J.**: Tu-45
- **Herrmann Antoine**: Tu-25
- **Hussain Arshad**: Tu-46
- **Iwanaga Nano**: Tu-1
- **Jamshidi Alashti Fatemeh**: Tu-17
- **Janssen Jesper**: Tu-28
- **Juste Maëva**: Tu-10
- **Kazunori Koga**: Tu-19
- **Kyrykbay Baglan**: Tu-60
- **Lavrikova Aleksandra**: Tu-21
- **Lee Hyunseung**: Tu-13
- **Maestri Luca**: Tu-44
- **Mazankova Vera**: Tu-67
- **Mei Xianxiu**: Tu-61
- **Mishra Ritesh**: Tu-15

- **Miyazaki Toshiaki**: Tu-39
- **Moore Chris**: Tu-33
- **Muhl Stephen**: Tu-41
- **Nikic Dejan**: Tu-26
- **Otsuyama Hiroki**: Tu-57
- **Pappalardo Federica**: Tu-68
- **Paredes Joaquin**: Tu-23
- **Pascual Fort Carmen**: Tu-48
- **Pazderka Michal**: Tu-7
- **Pedro Jorge Gomes Camacho Almeida**: Tu-36
- **Peláez Ramón**: Tu-63
- **Pereira P.**: Tu-29
- **Perrin-Terrin Jean-Baptiste**: Tu-6, Tu-9
- **Petkovic Jovana**: Tu-11
- **Pietri Carla**: Tu-70
- **Poupouzas Michail**: Tu-58
- **Rana Tejashwi**: Tu-12
- **Riazantceva Valentina**: Tu-49
- **Rocamora Ancelin**: Tu-18
- **Saba Maria**: Tu-55
- **Sadi Dihya**: Tu-43
- **Sarrette Jean-Philippe**: Tu-4
- **Sasaki Koichi**: Tu-51
- **Schicke Alexander**: Tu-64
- **Sidharth Sidharth**: Tu-3
- **Sigeneger Florian**: Tu-40
- **Simonovic Ilija**: Tu-32
- **Tsuboyama Shoko**: Tu-24
- **Uderbayeva Akbota**: Tu-71
- **Vass Mate**: Tu-38
- **Verma Monika**: Tu-56
- **Wang Jianan**: Tu-47
- **Wang Lijun**: Tu-27

- **Wang Yuhui**: Tu-5
- **Wangkanai Jidchanok**: Tu-62
- **Whitehead Alex**: Tu-8
- **Wright Matthew**: Tu-50
- **Yonesu Hinako**: Tu-20
- **Zhang Yingying**: Tu-2

# Synchronization phenomenon of plasma generation between plasmas with slightly different driving frequencies

N. Iwanaga[1], T. Fukuyama[2], and N. Hayashi[1]

[1] *Interdisciplinary Graduate School of Engineering Sciences, Kyushu University, Fukuoka 816-8580, Japan*
[2] *Faculty of Education, Nagasaki University, 1-14 Bunkyo-machi, Nagasaki, 852-8521, Japan*

Synchronization of two helium plasma jets at atmospheric pressure by a dielectric barrier discharge were studied. The flicker of luminescence produced in the plasma jets was observed as a discharge current value. It was found that as the distance between the two plasma jets was increased, a transition from a synchronized state to an asynchronized state was observed caused by the mutual induction of the pulsed voltage.

## 1 Background

When a plasma jet generated at atmospheric pressure is observed by a high-speed camera, the flickering of the luminescence is observed in accordance with the frequency of the power supply used to generate the plasma. A study focusing on the flickering rhythm is carried out. We consider the flickering rhythm of the plasma jet observed in this experiment as an object of non-linear science. The aim of this study is to obtain knowledge on the synchronization of the flickering rhythm due to the interaction between plasma jets by measuring helium plasma jets generated at atmospheric pressure using a current probe.

## 2 Experimental setup and results

As shown in Fig. 1, two plasma jets were placed vertically parallel to each other, and the flickering rhythm was measured as the current value. The synchronization was investigated by varying the distance $L$ between the plasma jets, and it was found that there is a transition from a synchronized state to an asynchronized state. Regarding the time evolution of the phase difference, among the states including synchronization and desynchronization, the structure of a devil's staircase was observed in the case with plasma $L$ = 110 mm, repeating a flat part and a jump with a phase difference of 2π, as shown in Fig. 2.

For the two plasma jets, the fundamental frequency was measured while varying the distance $L$. As shown in Figs. 3 and 4, the two plasma jets with and without plasma separated at a threshold of $L$ = 100 mm and transitioned to an asynchronized state as the distance was increased from synchronized state. The process of transition to the asynchronized state differed depending on the presence or absence of plasma. In the presence of plasma, the transition process was slower. In addition, the fundamental frequency of the power supply increased with the presence of plasma.

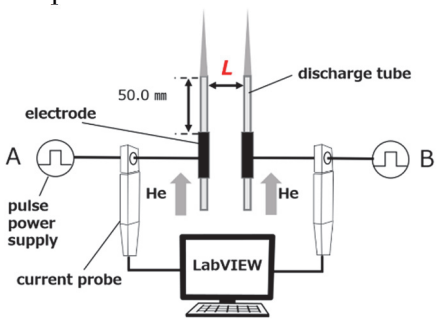



Fig. 1 Schematic configuration of the experiment

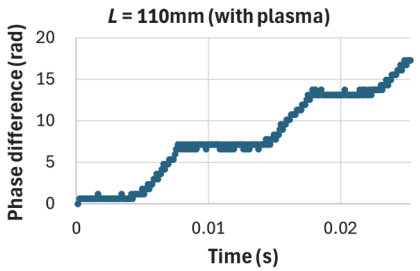



Fig. 2 Structure of a devil's staircase

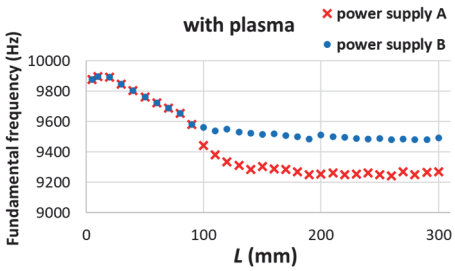



Fig. 3 Fundamental frequency with plasma

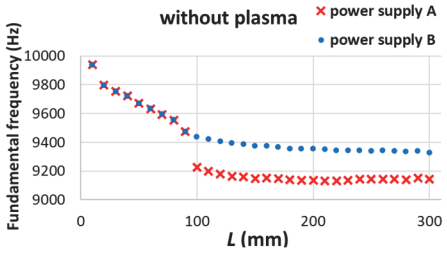



Fig. 4 Fundamental frequency without plasma

# The study on the distribution of dust particles in Capacitively Coupled Radio Frequency (CCRF) discharges

Ying-Ying Zhang, Rui Deng, Yu-Feng Huang, Yuan-Hong Song

*School of Physics, Dalian University of Technology, Dalian, China*

In the research of dusty plasmas, the spatial distribution of dust particles is relevant for research and applications. The work is about the micrometer-sized dust particle moving observation in dusty plasmas, which were sprinkled into a Capacitively Coupled Radio Frequency(CCRF) discharge chamber. A three-dimensional fluid simulation study was also performed. In the experimental study, dust lattice, dust stratification and dust instability in the sheath of argon gas CCRF discharge were observed.

## 1 Introduction

The technology of plasma is widely used in many fields such as energy, chemical industry and aerospace. The capacitive coupled plasma (CCP) is often used as a source of dust plasma, as which has the simple structure, and can produce large areas of homogeneous plasma.

Initially, the study of dust plasma is focused on the space plasma field. With the development of the microelectronics industry, the dust particles produced under ground-based laboratory conditions are gradually attracted attention[1]. Because the lab-produced plasma has a higher plasma density, the dust particles are more likely to exhibit collective behaviour, for example, dust lattice, dust cavity, dust vortex and so on.

Under ground experimental conditions, in order to limit the concentration of dust particles in the middle of the lower plate, a ring is usually placed on the lower plate. The inner diameter of the ring is generally much larger than its thickness (generally 1mm), to avoid the influence of the ring on the dust particles distribution.

With the development of semiconductor manufacturing industry, multiple cylindrical hollow grooves[2] on the lower plate are designed, in order to meet the industrial demand for higher density uniform plasma. The groove inner diameter varies from a few milli-meters to centi-meters, which are almost equal to its depth. With the small inner diameter, the groove will lead to unequal voltage drop in the sheath area, which will affect the distribution of dust particles in the sheath, making it show unusual collective behaviour.

## 2 Model

The RF-CCP discharge device is shown in Figure 1. In the experiment, dust particles (melamine resin) with a diameter of 6.1μm were sprinkled in.

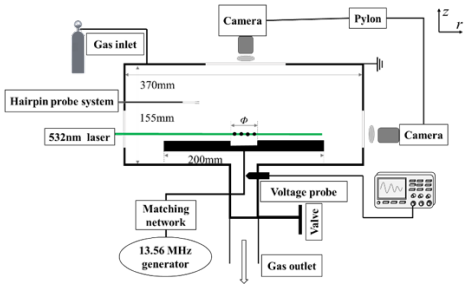



Figure 1 Schematic diagram of the discharge device

## 3 Results

It found that the dust particles were distributed in multiple layers, like a "bowl". When the pressure is fixed at 5pa and the RF power increases from 2w to 10w, the dust particles move upward as a whole, but the dust cloud volume is compressed. When the fixed RF power is 2w, the dust particles move overall downward as the air pressure increases, but the dust cloud volume changes less.

The dust cavity first appears in the lower layer of dust particles, and as the pressure or power increases, the upper layer gradually appears again. When the inner diameter of the groove on the lower plate is small(2mm), the diameter of the dust cavity increases rapidly with the increase of the pressure. After reaching the maximum value, the diameter of the dust cavity gradually decreases as the pressure continues to increase until the dust cavity disappears.

About the reasons of the above experimental phenomenon, an explanation is given in terms of dust particles force, based on the three-dimensional fluid simulation[3].

**References**

[1] Iwashita S., Uchida G., Schulze J., et al. *Plasma Sources Sci. Technol.* **21**, 032001(2012).

[2] Wang L., Hartmann P., Donko Z., et al *J. Vac. Sci. Technol.* **39**, 063004(2021).

[3] Duan M. Y., Jia W. Z., Zhang Y. Y., Zhang Y. F., Song Y. H. *Acta Phys. Sin.* **72**, 165202(2023).

# Electric field measurements of single and multijet systems

S.Sidharth[1], A.Sobota[1]

[1] *Department of Applied Physics and Science Education, Eindhoven University of Technology, Eindhoven, The Netherlands*

In this project, a comparative study will be conducted between a single plasma jet and a multi-jet system. The study will begin with electrical measurements to analyse the voltage and current characteristics, followed by power calculations. Subsequently, ICCD imaging will be performed for both the single and double jet configurations to capture plasma dynamics, including velocity measurements. These measurements will help assess how jet velocity varies with different applied voltages and gas flow rates. For the double jet setup, imaging will also be used to determine whether both jets are synchronized and simultaneously reach the target. This will provide insight into possible interactions or mutual influences between the jets. Finally, electric field measurements for the single jet will be presented using the Stark spectroscopy method.

Actinic keratosis (AK) manifests as small, rough, scaly lesions on the skin, typically caused by prolonged exposure to sunlight. If left untreated, these lesions may progress into squamous cell carcinoma, a form of skin cancer [1]. Cold plasma, a cutting-edge advancement in plasma medicine, has emerged as a promising solution for AK treatment. Its optimal therapeutic temperature, combined with the unique generation of reactive oxygen species (ROS) and reactive nitrogen species (RNS), holds significant potential in addressing this dermatological concern.

An additional benefit of plasma treatment is *plasma poration*, where the electric field of the plasma increases the permeability of cell membranes [2]. This enhanced permeability allows reactive substances to pass through more easily, thereby improving the effectiveness of plasma therapy.

These findings emphasize the need for a deeper understanding of the plasma and the measurement of its electric field near the skin. The main focus of the project is the characterization of a non-thermal atmospheric pressure plasma jet with particular attention to gas-phase electric fields and their interaction with substrates. This will include basic electrical diagnostics, fast imaging and electric field measurements using Stark shift, for both single-jet and double-jet systems. The study also aims to compare single-jet and multi-jet configurations under different target conditions.

**References**

[1] E Wu.; et al., Free Radic Biol Med 2023 Mar:198:109-117

[2] Mariachiara Arisi.; et al., Dermatol Ther (Heidelb) (2021) 11:855–866

# Kinetic mechanisms and species densities in Ar/$N_2$, He/$N_2$ and $H_2$/$N_2$ reduced pressure afterglows

J.P. Gardou[1], F. Marchal[1], A. Ricard[1] and J.P. Sarrette[1]

[1] *LAPLACE, Université de Toulouse, CNRS, INPT, UPS, 118 route de Narbonne, 31062 Toulouse, France*

Emission spectra of nitrogen and of mixtures of nitrogen with argon, helium and hydrogen were studied by Optical Emission Spectroscopy (OES) in the afterglows of flowing microwave discharges. Absolute concentrations of N, $N_2(X, v'=12\text{-}13)$, $N_2(A)$ and $N_2^+$ were determined in the mixtures at different distances from the discharge from band intensity ratios and from NO titration. In Ar/$N_2$ and He/$N_2$ mixtures, absolute N atom densities were compared with Two-photon Absorption Laser-Induced Fluorescence (TALIF) measurements. As all bands originating from the $v'$ = 0-12 levels of the $N_2(B)$ state were observed, it was possible to obtain rate coefficients for the N-atom 3-body recombination towards every $N_2(B,v')$ levels in each studied mixture. In $H_2$/$N_2$ mixtures, absolute H-atoms densities were also measured with the TALIF technique and a kinetic model was built, demonstrating how H and NH densities can be derived from the observed NH *A-X* (0-0) band intensity at 336 nm.

At reduced pressure (2-20 Torr), two distinct regions can be considered in the afterglows of $N_2$ and of M = (1-x)%R/x%$N_2$ mixtures (R = Ar, He, $H_2$), characterized by different population mechanisms of the $N_2(B,v')$ levels. In the pink afterglow, the $N_2(B,v')$ population is no longer due to direct electron excitation of ground $N_2(X)$ molecules as in the discharge but from:

- excitation transfer mechanisms involving the $N_2(A)$ metastable state and vibrationally excited $N_2(X,v')$ molecules [1]:

$N_2(A,v=0,1) + N_2(X,4\leq v<14) \rightarrow N_2(B,0\leq v'\leq 12) + N_2(X,w)$, (a)

- radiative de-excitation of the $N_2(C)$ state through the nitrogen second positive system (2+):

$N_2(C,v) \rightarrow N_2(B,v') + h\nu$, (b)

- and from 3-body recombination of the ground state nitrogen atoms $N(^4S)$:

$N(^4S) + N(^4S) + M \rightarrow N_2(B,v') + M$, associated with the rate coefficient $k_c^M(v')$. (c)

In the considered pressure range, for afterglow times higher than 5 ms (late afterglow region), $N_2(A)$ and $N_2(C)$ densities have decreased enough to make the 3-body recombination reaction the main channel for the formation of the $N_2(B)$ state. The $N_2$ first positive system (1+) is then dominated in pure $N_2$ by the intense (11-7) band head peak at 580 nm, which is not always the case in M mixtures (Fig. 1), due to the dependence of the $k_c^M(v')$ rate coefficients on the considered M mixtures.

In the present work, $k_c^M(v')$ rates were obtained from the $N_2$ 1+ intensities $I_{v'-v''}^{N_2 1+}$ observed in pure $N_2$ and in the M mixtures, considering the overall recombination rate $k_c^{N_2} = \sum_{v'=0-12} k_c^{N_2}(v')$ = 6.5 $10^{-33}$ $cm^3$ $s^{-1}$. [2]

N and H atoms absolute densities were also measured by TALIF and compared with the atomic densities obtained using band intensities ratios, in different mixtures and at several distances from the discharge.

From these data, a simplified kinetic model was established, allowing obtaining the H and NH densities in the afterglow region from the measurement of the NH *A-X* (0-0) band intensity at 336 nm. [3]

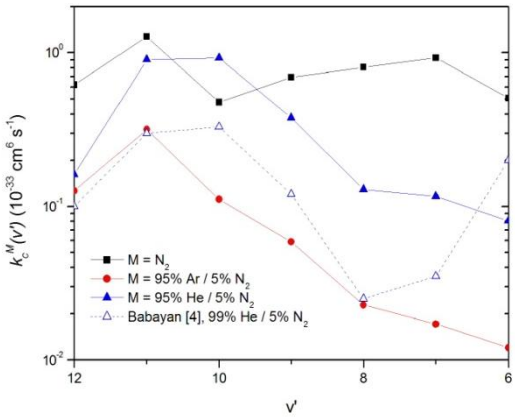



Fig. 1. Rate coefficients for 3-body recombination of N-atoms $k_c^M(v')$ in the M mixtures

**References**

[1] Loureiro J. *et al. J. Phys. D: Appl. Phys.* 34, 1769–1778 (2001).
[2] Ferrer V. *et al. Eur. Phys. J. D* 76:191 (2022).
[3] Ferrer V. *et al. Chem. Phys. Lett.* 838, 141079 (2024).
[4] Babayan S.E. *et al. Plasma Chem. Plasma Process.* 21, 505-521 (2001).

# Investigation of Electric Field Dynamics and Backward Discharge in Atmospheric-Pressure Nano-Pulsed DBD

Y.WANG[1] , A.Rousseau[1]

[1] *LPP, Ecole Polytechnique, IP-Paris, CNRS, Palaiseau, France*

In this study, nanosecond pulsed dielectric barrier discharges (DBD) were investigated by the current, voltage, electric field measurements and iCCD imaging. Different geometries and electrode configurations have been studied. Typical homogeneous discharges were observed; however, an additional backward negative discharge occurred during the positive high-voltage pulse plateau following the forward positive discharge.

## 1 General

Nanosecond pulse DBDs may generate uniform plasmas at atmospheric pressure due to strong overvoltage. Typically, each pulse induces two discharges: a forward discharge on the rising edge of the pulse and a backward discharge on the falling edge [1,2]. Notably, discharges generated by nanosecond pulses exhibit greater uniformity than those produced by microsecond pulses, regardless of the target surface [3]. Under specific conditions, our experiments have revealed that an atypical backward discharge can occur almost immediately—within tens of nanoseconds—after the forward discharge during the high voltage pulse plateau. This study presents measurements of this abnormal discharge and discusses the possible mechanisms contributing to its formation.

### 1.1 Experimental Set up

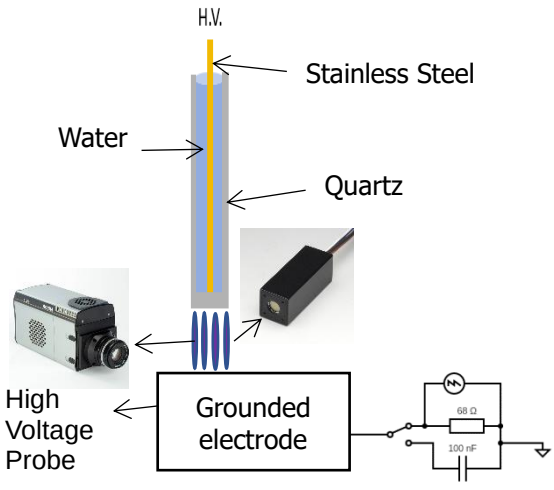



Figure 1. Experiment set up schematic diagram.

Figure 1 shows the schematic diagram of the DBD setup and its measurement system. The high-voltage electrode consists of a stainless-steel wire immersed in water and housed within a cylindrical or hemispheric glass tube. The grounded electrode is configured as either a metallic plate, a glass plate, or an electric field probe. DC nanosecond pulses at a frequency of 2 kHz, with voltages ranging from 2 kV to 16 kV, were applied to the high-voltage electrode; Figure 2 displays the 14 kV waveform as a blue solid line. The current was measured using a 68 Ω resistor, and the potential at the grounded electrode was recorded with a high-voltage probe. Additionally, an iCCD camera and a PMT were positioned laterally to capture the discharges.

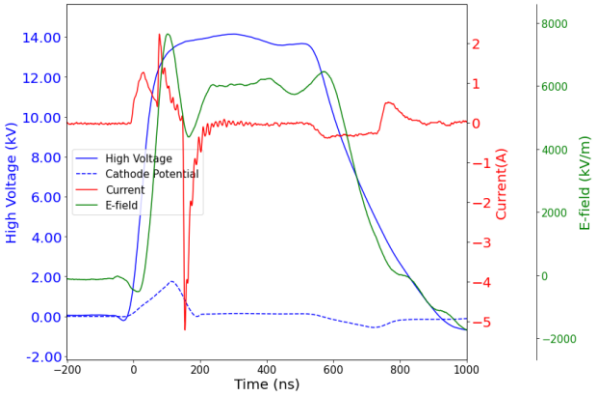



Figure 2. Voltage, current waveforms and E-field of Figure 1. Applied voltage 14 kV, voltage rising time is 50ns and falling time is 400 ns, pulse duration is 500 ns.

**References**

[1] Liu, F. et al. *Uniform and stable plasma reactivity: Effects of nanosecond pulses and oxygen addition in atmospheric-pressure dielectric barrier discharges.* Journal of Applied Physics 129, 033302 (2021).

[2] Yang, X. et al. *Experimental study of transient surface charging during dielectric barrier discharges in air gap in needle-to-plane geometry.* J. Phys. D: Appl. Phys. 56, 465202 (2023).

[3]. Ayan, H. et al. *Nanosecond-Pulsed Uniform Dielectric-Barrier Discharge.* IEEE Trans. Plasma Sci. 36, 504–508 (2008).

# Characterization of a plasma generated by nanosecond repetitively pulsed discharges in a swirled stabilized combustor

J.-B. Perrin-Terrin[1], H. Veran[1,2], P. Scouflaire[1], S. Ducruix[1] and C. O. Laux[1]

[1] *Université Paris-Saclay, CNRS, CentraleSupélec, Laboratoire EM2C, France*
[2] *Safran Aircraft Engines, Réau, 77550 Moissy-Cramayel, France*

This work investigates the properties of NRP discharges in a swirled-stabilized $CH_4$/air flame. NRP discharges are applied directly in the swirled reactive flow in a pin-to-ring configuration. Using fast imaging, a periodic elongation of the discharge following the swirled flow is observed and the arc dynamics are quantitatively determined. In addition, optical emission spectroscopy is performed to measure the rotational temperature of $N_2(C)$, the electron number density and the reduced electric field to infer the plasma regime. Finally, influence of the flow velocity and pulse repetition frequency are assessed.

## 1 Introduction

Plasma-assisted combustion (PAC) is a novel and promising technique for flame stabilization [1]. In recent years, great progresses in PAC using Nanosecond Repetitively Pulsed (NRP) were made and the ignition and flame stabilizing mechanisms are now well understood [2]. However, flame stabilization mechanism was studied and validated in a bluff-body stabilized burner, with low flow velocity. In industrial combustion systems, velocities are larger, and flows are usually swirled which might change stabilization processes. Because of the strong turbulence, characterizing a plasma formed in a swirled flow is challenging and only a few studies with detailed plasma characterization are available in the literature.

## 2 Objectives

This work is performed on BIMER-PAC facility, in which previous studies have revealed that NRP discharges can greatly enhance the flame stability [3]. Figure 1 shows the two-stage injector of BIMER-PAC. The plasma is generated by NRP discharges with a pulse duration of 10 ns and a peak voltage of 13 kV between the edge of the inner divergent nozzle of the pilot injector and the high-voltage electrode. In this pin-to-torus configuration, the plasma is formed within a strong swirling flow of $CH_4$ and air. This configuration affects the dynamics of the repetitive discharges by creating a *sliding* arc: each pulse is formed in the hot and ionized gas of the previous discharge that has been convected by the flow, thus the plasma is sliding along the flow. The plasma is elongated by this mechanism until the gap becomes so large that the breakdown field is lower in the smallest interelectrode gap than in the pre-heated and pre-ionized channel of the previous pulse.

The objective of this work is to characterize the properties and dynamics of these *sliding* arcs and to understand the effect of the flow velocity, the pulse repetition frequency (PRF) and the applied voltage. The characterization of the arc dynamic is done with fast imaging synchronized to the PRF. Optical emission spectroscopy is performed to obtain the plasma composition, measure the rotational temperature of $N_2(C)$, the electron number density and the reduced electric field.

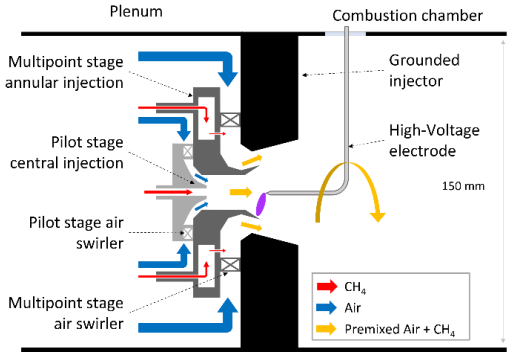



Figure 1: Schematic of the BIMER-PAC injector and the high-voltage pin electrode. Swirlers are represented

**Acknowledgment**

This work has received funding from the European Research Council (ERC) under the European Union's Horizon 2020 research and innovation program (ERC GreenBlue grant agreement No.101021538). The authors thank E. Jean-Bart, Y. Le Teno, H. Jubeau, and K. Sokhona for technical assistance.

**References**

[1] Starikovskiy, A. *et al.*, Plasma-Assisted Ignition and Combustion, *Progress in Energy and Combustion Science*, **39**, No. 1, (2013).
[2] Laux, C., Applications of Plasma Discharges to Combustion, 日本燃焼学会誌, **64**, No. 209, (2022).
[3] Blanchard, V. P. *et al.*, Combustion Performance of Plasma-Stabilized Lean Flames in a Gas Turbine Model Combustor, *Applications in Energy and Combustion Science*, **15**, (2023).

# Temporal evolution of the Sn concentration in pulsed MHz DBD atomizer

M. Pazderka[1], M. Mrkvickova[1], T. Medek[1], and P. Dvorak[1]

[1] *Department of Plasma Physics and Technology, Masaryk University, Brno, Czechia*

Atomizers play an important role in detection of trace amounts of various elements. However, some elements are challenging to be properly atomized in common DBD atomizers, e.g. atoms of Sn seems to be localized only in close vicinity of gas inlet for standard continuous DBD. Therefore we used novel MHz power supply to ignite MHz DBD plasma in atomizer in two modes: continuous and pulsed MHz discharge. Although the continuous MHz discharge showed the same behaviour of Sn atoms, pulsed MHz discharge lead to significant spread of Sn atoms over the full atomizer, which is advantageous for their detection by absorption methods. Furthermore, due to precise discharge triggering we were able to detect highly nontrivial temporal evolution of Sn concentration in first few ms of discharge.

Atomizers are highly useful tool s for detecting low concentrations of various species [1]. Although carrier molecules (typically hydrides) of some elements are easy to atomized in DBD atmomizers (e.g. Te), carrier molecules of some elements are more difficult to atomize, e.g. Sn, as LIF signal from Sn atoms is located only in close vicinity of the gas inlet and not in the full volume of the atomizer when the T-shaped atomizer is used ( the gas inlet is in the middle of 5 cm long rectangular quartz glass atomizer).

We used recently developed high voltage MHz power supplies to show that there is a positive effect of the MHz power supply frequencies on the concentration of H radicals in the discharge, which are assumed to be a key element in atomisation of hydrides [2]. Although the usage of MHz frequencies lead to Sn concentration increase compared to 30 kHz power supply frequency, the main issue remained: signal from SN atoms remained in the close vicinity of the gas inlet.

A significant progress has been done using power signal with not continuous MHz output but bursts of sinusoidal MHz signal. Using bursts with repetition frequency around 1 Hz lead to spread of the Sn signal over the whole atomizer. Furthermore, low duty cycle bursts can be used a powerful diagnostic tool. Scanning the time evolution Sn signal reviled non-trivial temporal evolution, see Figure 1. The integrated signal (proportional to the concentration) exhibits a strong maximum after approx. 2 ms followed by slow decay. This imply that usage of properly tuned bursts of MHz HV signal has a strong potential to significantly increase effectivity of atomizers for Sn and potentially other elements.

This research has been supported by the Czech Science Foundation under contract 23-05974K and by the Project LM2023039 founded by the Ministry of Education, Youth and Sports of the Czech Republic.

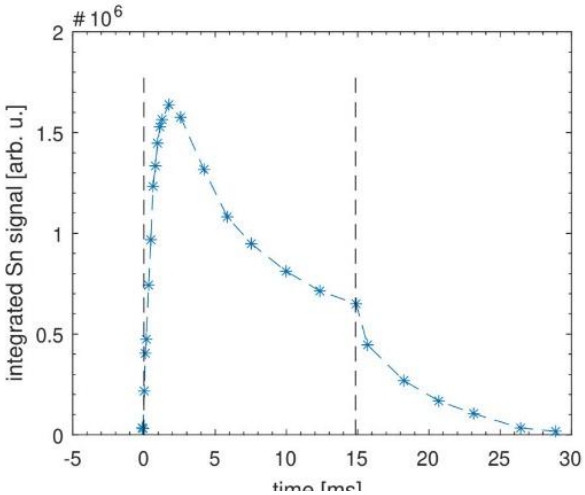



Figure 1: Temporal evolution of Sn LIF signal over 15 ms long burst of MHz discharge (2,28 MHz frequency, burst repletion period 297 ms).

**References**

[1] Dědina, J. Atomization of volatile compounds for atomic absorption and atomic fluorescence spectrometry: On the way towards the ideal atomizer. *Spectrochim Acta Part B* 62(9):846–872 (2007).

[2] Dvořák P., Talába M., Obrusník A., Kratzer J., Dědina J. Concentration of atomic hydrogen in a dielectric barrier discharge measured by two-photon absorption fluorescence, *Plasma Sources Sci. Technol.* 26, 085002, (2017).

# Discharge Plasma Source for Laser Plasma Accelerator at ELI ERIC

A. Whitehead[1,2], M. Miceski[1,2], R. Demitra[3,4], P. Zimmermann[1], S. Niekrasz[1], A. Jancarek[1,2], S. Maity[1], P. Sasorov[1], J. T. Green[1] and A. Molodozhentsev[1]

[1] *ELI Beamlines Facility, The Extreme Light Infrastructure ERIC, Za Radnicí 835, 25241 Dolní Břežany, Czech Republic*
[2] *Czech Technical University in Prague, Faculty of Nuclear Sciences and Physical Engineering, Břehová 7, 115 19 Prague 1, Czech Republic*
[3] *INFN-LNF, Via Enrico Fermi 40, 00044 Frascati, Rome, Italy*
[4] *Sapienza University of Rome, 00161 Rome, Italy*

Laser-plasma accelerators have demonstrated the ability to accelerate high-energy electrons but require improved beam stability and repeatability for practical applications [1]. Pre-formed plasma channels enhance the stability in Laser-Wakefield Accelerators by overcoming diffraction effects and maintaining laser focus over longer distances, increasing energy transfer efficiency. The characteristics of such channels are highly dependent on capillary geometry, gas parameters, discharge setup, and repetition rate. This study investigates the electron density profiles in plasma from gas-filled capillary discharges. Using Stark broadening [2], we measured profiles under varying conditions, achieving densities of (2-3)×10ˆ18 cmˆ-3. In this presentation, we showcase the stability and uniformity of the plasma, and the necessity to use long capillaries with limited apertures to preserve beam quality in high-energy, high-repetition-rate applications. This type of plasma source is a crucial technology for the 100 Hz plasma accelerator based Free Electron Laser developed at ELI-ERIC [3] as well as for the EuPRAXIA project.

**References**

[1] Malka, V., Faure, J., Gauduel, Y. A., Lefebvre, E., Rousse, A., and Phuoc, K. T. Principles and applications of compact laser–plasma accelerators. *Nature physics* **4**, 447-453 (2008).
[2] Ashkenazy, J., Kipper, R., and Caner, M. Spectroscopic measurements of electron density of capillary plasma based on Stark broadening of hydrogen lines. *Physical Review A* **43**, 10 (1991).
[3] Molodozhentsev, A. Y. and Kruchinin, K. O. Compact LWFA-Based Extreme Ultraviolet Free Electron Laser: Design Constraints. *Instruments* **6**, 4 (2022).

# Plasma-assisted combustion in a premixed $H_2$/air flame

J.-B. Perrin-Terrin[1], R. Gablier[1], T. Popa[1] and C. O. Laux[1]

[1] *Université Paris-Saclay, CNRS, CentraleSupélec, Laboratoire EM2C, 91190 Gif-sur-Yvette, France*

This work presents an experimental study of plasma/flame interactions in a premixed $H_2$/air flame stabilized by Nanosecond Repetitively Pulsed discharges. This work is performed on the bluff-body stabilized burner Mini-PAC, already extensively studied with methane/air plasma-assisted flames. The stability map of the burner with and without plasma is experimentally determined. The effect of the plasma on lean blow-off and flashback is quantified. Optical Emission Spectroscopy is performed to determine the NRP discharge regime and validate a phenomenological plasma-assisted combustion model.

## 1 Introduction

New carbon-free fuels such as $H_2$ are now considered as a major lever for decarbonation of combustion. Several challenges arise with this new fuel, notably the higher flame temperature at stoichiometry, which requires combustion systems to be operated with excess of air, *i.e.* in the lean-regime. However, lean flames are prone to instabilities [1]. Plasma-assisted combustion (PAC) help regain flame stability and operate safely in the lean-regime.

PAC with Nanosecond Repetitively Pulsed (NRP) discharges has been shown to successfully enhance combustion in different burner types with flame thermal powers up to 150 kW [2]. These were obtained mostly with fossil fuels, and only few references with $H_2$ can be found in the literature. In addition to experimental demonstrations, funda-mental studies have improved the under-standing of NRP discharges, their plasma regimes, and their effect on the gas [2]. These findings laid the theoretical bases of a phenomenological model of PAC [3]. This model enables the incorporation of the plasma effects into Large Eddy Simulation (LES) at affordable computing cost. However, these findings have only been validated against $CH_4$/air flames [4]. Recent work extended the model of [3] to new fuels [5], notably $H_2$, but still requires validation.

## 2 Objectives

In this work, we propose to (i) measure the effects of NRP discharges in a premixed $H_2$/air flame stabilized by bluff-body (see Figure 1) and to (ii) validate the model proposed in [5]. For (i), stability maps of the burner with and without plasma will be determined, with a special focus on the lean blow-off and flashback limits. Additionally, flame imaging with OH chemiluminescence will be performed. For (ii), optical emission spectroscopy will be performed to determine the rotational temperature of $N_2(C)$ by fitting the second positive system and the electron number density by fitting the Balmer $H_\beta$ line.

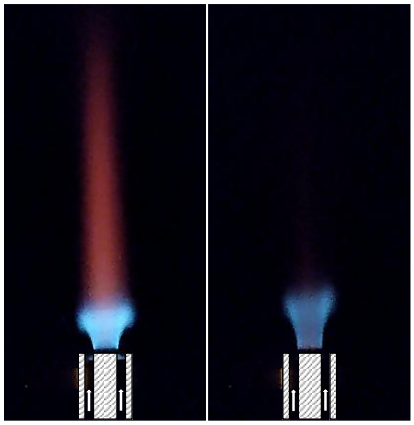


Figure 1: Pictures of premixed $H_2$/air flame at stoichiometry (left) and in lean condition (right) in the mini-PAC burner.

**Acknowledgment**

This work has received funding from the European Research Council (ERC) under the European Union's Horizon 2020 research and innovation program (ERC GreenBlue grant agreement No.101021538). The authors would like to thank E. Jean-Bart, J. Beaunier, J. Bonnety, Y. Le Teno, H. Jubeau, and K. Sokhona for technical assistance.

## References

[1] Huang, Y. *et al.*, Dynamics and Stability of Lean-Premixed Swirl-Stabilized Combustion, *Prog. Energy Combust. Sci.*, **35**, No. 4, (2009).

[2] Laux, C., Applications of Plasma Discharges to Combustion, *J. Combust. Soc. Jpn*, **64**, (2022).

[3] Castela, M. *et al.*, Modelling the Impact of Non-Equilibrium Discharges on Reactive Mixtures for Simulations of Plasma-Assisted Ignition in Turbulent Flows, *Combust.Flame*, **166**, (2016).

[4] Blanchard, V. P. *et al.*, Experimental Characte-rization and 3D Simulations of Turbulent Flames Assisted by Nanosecond Plasma Discharges, *Combust. Flame*, **270**, (2024).

[5] Blanchard, V., Thermochemical Effects of Nanosecond Plasma Discharges on Lean Flame Stabilization, thesis. (2023).

# Analytical Modelling of the Interaction Between an Intense Electromagnetic Pulse and a Spherical Plasma Discharge

M. Juste[1,2,3], G. Hagelaar[2], R. Pascaud[3], T. Callegari[2], R. Maisonny[1], S. Vauchamp[1], C. Pouant[1]

[1] *CEA, DAM, Gramat, France*
[2] *LAPLACE UMR 5213, Université de Toulouse, CNRS, INPT, UPS, Toulouse, France*
[3] *ISAE-SUPAERO, Université de Toulouse, Toulouse, France*

This study presents an analytical model describing the interaction between an intense electromagnetic pulse (EMP) and a spherical plasma discharge. The objective is to characterize the nonlinear response of a plasma-based antenna when subjected to EMP during experiments. The model underscores the crucial role of energy absorption by individual electrons from the EMP and highlights the significance of radiation, particularly within the electron density range of the antenna. Ultimately, this approach provides valuable insights into the physical mechanisms governing the interaction.

The role of radio-frequency (RF) and microwave (MW) antennas is to efficiently transmit and receive useful signals for wireless communication systems. They are thus directly coupled through the front door during electromagnetic (EM) attacks in the context of EM warfare. For example, a major source of vulnerability is intense EM pulses (EMP). EM hardening, which involves reducing EM stresses, is a solution to protect radio frequency (RF) communication systems. Of late, a new type of electrically small plasma-based antenna with self-limiting power capabilities has been developed [1]. It couples a coaxial probe with a sub-wavelength hemisphere of plasma as suggested in [2, 3]. This antenna radiates with the resonance of the free electrons in the plasma, called localized surface plasmon resonance (LSPR) [4]. In recent years, experiments have shown a nonlinear response of the antenna when exposed to an increasingly intense EMP. The voltage collected by a receiving antenna increases before saturating [5]. This suggests potential EM hardening of the systems. This study aims at enhancing the understanding of this physical phenomena. We present here a simple analytical physical model describing the interaction of an EMP and a spherical plasma discharge.

The spherical plasma discharge is modeled as a homogeneous, quasi-neutral, unmagnetized plasma sphere. Its radius being much smaller than the operating wavelength, the system can be considered as electrostatic. Ions, considering the superior relative mass to electrons, are assumed immobile. When exposed to an external EM field, electrons are displaced from the ions. The system is governed by a motion equation incorporating three main forces affecting the electrons : the unmagnetized Lorentz force, including the incident field and the inherent plasma field, friction due to electron-particle collisions and momentum losses due to EM radiation. The external EM field is an EMP modeled as a double exponential pulse, with a time scale of about 150 $ns$ and a maximum field of several dozen $kV/m$ reached after a few $ns$. The general system, when solved with this incident EM field, provides analytical expressions for all variables as functions of time. The input parameters are the electron density, the plasma sphere radius, the peak EMP value, the inverse of the EMP decay time at half maximum and the inverse of the EMP rise time. The study was carried out with a fixed radius and collision frequency for a pressure of a few mTorr.

The results show that the plasma electrons absorb significant energy from the EMP, reaching several hundreds of $eV$ for a single electron. This energy absorption is highly dependent on electron density, with densities above $10^{15}\ m^{-3}$ favoring radiation over dissipation. EMP rise time plays a crucial role with shorter rise times leading to higher energy absorption. The absorbed energy may contribute to increase plasma ionization, leading to nonlinear antenna responses.

This preliminary study provides insights into the fundamental physical processes governing EMP-plasma interactions. Future work will integrate Monte Carlo simulations to model detailed non-equilibrium collision and ionization dynamics, further refining the understanding of these nonlinear plasma responses.

This work was supported by the French defense procurement agency (DGA).

[1] V. Laquerbe et al., *Phys. Plasmas*, **26**, 033509 (2019).
[2] H. R. Stuart et al., *IEEE Trans. Antennas Propag.*, **54** (6), 1644-1653 (2006).
[3] R. W. Ziolkowski et al., *IEEE Trans. Antennas Propag.*, **54** (7), 2113-2130 (2006).
[4] A. Laffont et al., *Phys. Plasmas*, **28**, 033503, (2021).
[5] A. Laffont et al., *16th EuCAP* (2022)

# The Impact of Electrode Contact with Water on Plasma Bubbles in Plasma-Water Treatments

J. Petković[1], A. Sobota[1]

[1] *Eindhoven University of Technology, Eindhoven, The Netherlands*

Plasma bubbles are highly effective in increasing the interaction area between plasma and water, enhancing the transfer of chemical species. This study explores both the effects of plasma bubbles on water and how changes in water characteristics influence the discharges within the bubbles. Plasma treatment leads to increased water conductivity, impacting plasma generation, resulting in water heating, power losses, and reduced plasma emission. Understanding these processes is crucial for optimizing reactor design and treatment efficiency.

## 1 Plasma-water treatments

With the rising number of applications for plasma-treated water (PTW), it is essential to understand the physical processes behind its generation. This understanding is crucial for effectively adapting the water chemistry for specific uses [1]. Plasma water treatment is known for its ability to produce reactive chemical species that help break down contaminants and disinfect water.

Plasma can be applied to the water surface, as a direct discharge into the water or formed in gas bubbles dispersed throughout the water.

### 1.1 Plasma bubbles

Discharges generated in bubbles enhance the interaction area between plasma and water, leading to improved mass transfer of species produced during plasma treatment [2]. As bubbles can move freely in water, pulse waveforms are used to ensure the capacitive character of the discharge. In order to create plasma in the bubbles both the powered electrode and the ground electrode are in direct contact with the water.

The dynamic movement of the bubbles helps spread the species and induces mixing [3]. Combining these processes can lead to a more efficient system in PTW production.

### 1.2 Sustaining plasma in complex systems

As treatment time increases, the conductivity of the water rises, which alters the character of the plasma discharge. Both the plasma's impact on the water and the water's effect on the plasma are crucial for generating and sustaining plasma in these complex systems. In the case of plasma bubble reactors where both powered and ground electrode are in direct contact with water the reactor itself the obtained chemistry of plasma-treated water is due to synergy of plasma treatment and electrolysis, as these two processes exist simultaneously [4].

## 2 The impact of electrode configuration on plasma generation

This study examines the effect of plasma on the water sample during the evolving water conditions as well as basic plasma properties. The appearance of electrolysis will be shows as a function of time as well as its effect on spectra collected from the discharges inside the bubbles. The generated species will be discussed. Finally, the measurements showing bubble dynamics will help understand the conditions under which plasma forms in the bubbles.

**References**

[1] P. J. Bruggeman et al., *Plasma Sources Sci. Technol.* **25** 053002, (2016).
[2] Y. Liu et al., *Chemical Engineering Journal* **8**, 345:679–687, (2018).
[3] P. Khan, *Water Supply*. **20** (6): 2021–2035 (2020).
[4] M. Albornoz et al., *Sensors* **23**(8), 3820. (2023).

# Preheating Temperature Study in a Graphite Electrode Based Plasma Gasification Chamber for Waste Processing

Tejashwi Rana and Satyananda Kar

*Plasma Applications Laboratory, Department of Energy Science and Engineering, Indian Institute of Technology Delhi, Hauz Khas, New Delhi-110016, India*

Given the increasing challenges in waste management and the limitations of existing conventional technologies, this study focuses on optimizing operational parameters to achieve a preheating temperature of 850°C, which is essential for effective waste treatment while preventing toxic emissions like dioxins and furans. The experiments were carried out for several carrier gases at varied power inputs. A detailed graphite electrodes' erosion rate analysis was conducted considering dependent factors such as the surrounding environment, carrier gas fed, power input, and electrode tip geometry. An economic feasibility analysis for the experiments was also performed to determine the technology's applicability.

## 1 Introduction

Plasma gasification represents an innovative and environmentally sustainable approach to waste management, transforming waste materials into valuable byproducts while minimizing environmental impact. This technology surpasses conventional methods by offering high destruction efficiency, reduced $CO_2$ emissions, and eco-friendly operational processes. It facilitates the simultaneous conversion of combustible waste fractions into syngas for energy production and non-combustible fractions into vitrified slag, positioning it as a promising solution for waste management [1]. In conventional (non-transferred) thermal plasma torches, tungsten is typically favoured due to its exceptionally high melting point (>3400 °C). However, the necessity for continuous water cooling to prolong the material's lifespan leads to significant energy losses (30-50%) attributable to waste heat dissipation [2]. Consequently, alternative configurations utilizing graphite electrodes have been explored and implemented alongside traditional plasma torches for arc plasma generation in waste processing applications. This study aims to analyze temperature profiles within the chamber over an hour to optimize energy efficiency and minimize power consumption for economical waste processing.

## 2 Experimental setup

A lab-scale plasma gasification chamber with an operating capacity of 5 kg/h, which resembles a fixed bed updraft, has been designed and developed for municipal solid waste treatment applications. The system incorporates graphite electrodes connected to a DC power supply (400A, 75V) for thermal arc plasma generation. Experimental investigations used various carrier gases, including argon, nitrogen, air, and mixtures.

## 3 Results and discussion

Experiments were conducted at current inputs of 250 A and 300 A to evaluate the most suitable carrier gas for optimizing power consumption. Optimized conditions were identified as follows: argon plasma (15 LPM, 300 A) achieved 850 °C in 16 minutes, consuming 1.95 kW; air plasma (15 LPM, 300 A) took 20 minutes, consuming 2.33 kW; and argon-air plasma (10 LPM argon and 5 LPM air, 300 A) achieved the same in 20 minutes with a power consumption of 2.23 kW. Additionally, an electrode consumption study was conducted to assess long-term operational feasibility. The lowest electrode consumption was observed with argon-nitrogen plasma (9 g/h), while air plasma exhibited the highest consumption rates (66 g/h). A cost analysis study was performed to evaluate the economic viability of the technology, revealing a trade-off between energy consumption, electrode consumption, and carrier gas costs. The findings contribute to advancing plasma-assisted waste treatment technologies by improving energy efficiency, extending electrode lifespan, and ensuring economic feasibility. The insights derived from this study can support the development of more sustainable and cost-effective waste management systems, promoting environmentally friendly and efficient waste treatment solutions.

**References**

[1] Rana T., and Kar S., “Assessment of energy consumption and environmental safety measures in a plasma pyrolysis plant for eco-friendly waste treatment,” J. Energy Inst., vol. 114, p. 101617 (2024)

[2] Aikas M., Gimžauskaitė D., Tamošiūnas A., Uscila R., and Snapkauskienė V., “Thermal arc air plasma application for biomass (wood pellets) gasification,” Clean Technol. Environ. Policy, vol. 1, 31–43 (2024)

# A Feasible Tomographic Reconstruction Strategy for Optical Diagnostics in Capacitively Coupled Plasma

Hyunseng Lee, Jiwon Choi, Jeonghun Ko, Daehee Wi, and Sanghoo Park

*Korea Advanced Institute of Science and Technology (KAIST), Daejeon, Republic of Korea*

We developed a tomographic reconstruction method that corrects erroneous line-of-sights (LoS) in low-temperature processing plasma. Experimental validation demonstrated a 78% reduction in the error of validation camera, significantly improving real-time plasma uniformity monitoring. This technique has strong potential to be implemented in active plasma control during industrial processes.

## 1 Introduction

Ensuring spatial uniformity in plasma processing has become increasingly crucial as both the number and complexity of semiconductor manufacturing steps continue to rise. Real-time, in-situ visualizing of such plasma has long been desired to monitor spatial parameters and to preemptively mitigate unexpected issues inside chambers. Although optical diagnostics in conjunction with tomographic reconstruction has been investigated [1,2], practical challenges inherent to real-world environments have limited its widespread application. Here, we propose an advanced tomographic reconstruction incorporating a line-of-sight (LoS) correction technique to enable robust and reliable plasma monitoring.

## 2 Materials and Methods

A capacitively coupled plasma (CCP) chamber, consisting of two parallel cylindrical electrodes with a diameter of 200 mm, was employed to validate our measurement methodology. The operating pressure was varied in the range of 100−500 mTorr with a constant argon flow rate of 15 sccm. Plasmas were generated by a 250-W sinusoidal power at 13.56 MHz. Line-integrated plasma emission was measured using six detector units, each equipped with a pinhole and a line-scanning camera (Fig. 1).

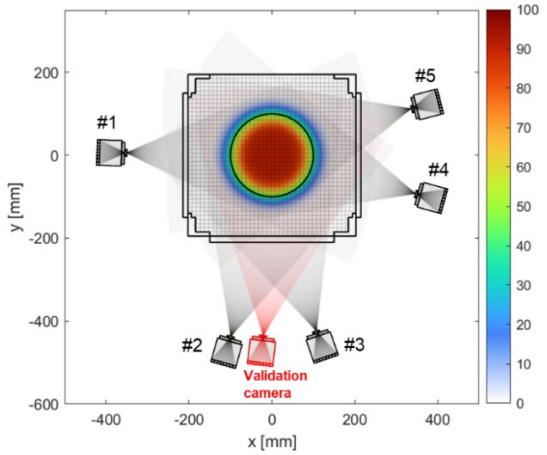



Fig. 1 Top view of the chamber with LoSs of cameras.

Among the practical issues, we here focused on LoS distortions induced by refraction and reflection at the chamber's viewport and inner walls. Using COMSOL Multiphysics, the accurate LoS was simulated precisely accounting for the actual chamber geometry. The corresponding weight matrix was then derived for Philips-Tikhonov regularization [1,2] to reconstruct plasma emission profiles. Reconstruction was conducted using data from five cameras (see Fig. 1), while an extra camera was reserved for validation to assess the reconstruction accuracy.

## 3 Results and Discussion

Figure 2 presents the emission profiles reconstructed from the measured line-integrated emission data with and without the LoS correction. By accounting for LoS distortions, the mean-squared error of validation camera decreased from 448 to 99.8, achieving a 78% reduction and thus significantly improving reconstruction accuracy. These advancements in tomographic reconstruction can be applied for active control of industrial plasma processes as well as for real-time plasma monitoring. Future work will integrate this technique with the collisional-radiation model to determine the spatial distribution of plasma parameters such as electron temperature and density.

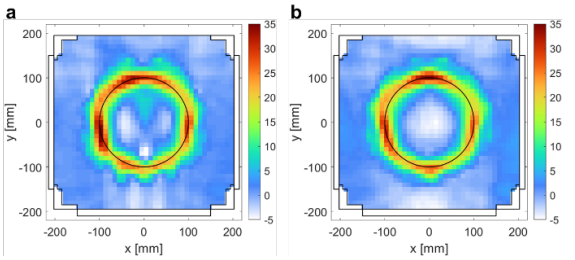



Fig. 2 Reconstructed plasma emission (a) without and (b) with the LoS correction.

### References

[1] Jang, J. et al. *Review of Scientific Instruments.* **89**, 10E111 (2018).
[2] Park, S. et al. *Plasma Sources Science and Technology.* **28**, 035012 (2019).

# A minimally invasive surgical platform for pancreatic and biliary tract cancers using cold atmospheric plasma: The EIC project "IgnitePLASMA"

P. Svarnas[1], K. Giotis[1], I. Anastasopoulos[1], A. Panourgias[1], G. Diamantis[1], K. Petrou[1], G. Dimitrakakis[1], L. Fouassier[2], T. Dufour[3], I. Kambili[4], G. Kapetanakis[4], E. Papageorgiou[5], C. Anastasiou[6], V. Vavourakis[6,7]

[1] *University of Patras, Electrical & Computer Eng. Dept., High Voltage Lab., 26504 Rion, Patras, Greece*
[2] *Sorbonne Université, Inserm, Centre de Recherche Saint-Antoine, CRSA, F-75012 Paris, France*
[3] *LPP, Sorbonne Université, CNRS, Ecole Polytechnique, F-75005 Paris, France*
[4] *Synnous Ltd, United Kingdom*
[5] *Bank of Cyprus Oncology Centre, Clinical Trials Unit, 2300 Nicosia, Cyprus*
[6] *University of Cyprus, Mechanical & Manufacturing Engineering Dept., 1678 Nicosia, Cyprus*
[7] *University College London, Medical Physics & Biomedical Engineering Dept., WC1E 6BT London, UK*

The project "IgnitePLASMA" spans across the field of plasma biomedicine, and it has been recently (2024) awarded by the EIC. The consortium encompasses members from the academia and industry across four different countries. In the present short report, the concept of the project is outlined, with a special focus on the development of a closed-loop, computer-trainable platform for the generation of cold atmospheric pressure plasma, which concerns a key technological objective of the project.

## 1. Introduction

Pancreatic cancer and biliary tract cancer are classified as rare gastrointestinal adenocarcinomas with an increasing incidence particularly among elderly and women in an ageing European population. Cold atmospheric plasmas (CAPs) have shown potential in regressing neoplasia. Despite the great promise of this concept, there is no medical device available based on CAP to treat carcinomas.

The EIC-funded "IgnitePLASMA" project (https://igniteplasma.eu) proposes to develop a novel solution using cutting-edge plasma technology. It integrates an advanced platform that ensures stabilized plasma parameters, guided by *in silico* modelling. The model combines plasma fluid dynamics with solid tumour biophysics simulations, while it takes inputs from pre-surgery diagnostics for model initialisation and plasma operational window determination. During surgery, real-time diagnostics will feed optimisation algorithms for the adaptation and delivery of CAP dose. In this project, the technology will be demonstrated through *in vitro* and *in vivo* biological experiments.

## 2. Experimental Setup

The platform comprises: (i) the cold plasma reactor; (ii) the pneumatic gas mixture feeding system; (iii) the sinusoidal high voltage power supply; (iv) the ns-pulsed high voltage power supply; (v) the plasma probing sensors; (vi) the micro-positioning stage; (vii) the *in silico* model, and (viii) a closed-loop control system which schedules the entire operation.

## 3. Discussion

Fig. 1 illustrates the front panel of the main part of the plasma platform, depicting the user interface touch screens and the plasma parameter (electrical, spectroscopic, thermal, *etc.*) monitoring display. A closed-loop design ensures different operational modes, like "constant power", "constant species density", "constant temperature", among others.




Figure 1. The main part of the implemented prototype of the closed loop, computer-trainable cold plasma platform.

*"IgnitePLASMA" has received funding from the Horizon-EIC-2023 Pathfinder Open (Agreement No. 101129853) and UKRI (Grant No. 10106237).*

# Cold Plasma-Driven Pectin Extraction from Dragon Fruit Peels: A Sustainable Approach for Stronger Biodegradable Films

Ritesh Mishra[1], Meenu Chhabra[1,3], and Ram Prakash[1,2]
[1]*Inter-Disciplinary Research Division- Smart Healthcare, Indian Institute of Technology Jodhpur, Rajasthan -342037, India*
[2]*Department of Physics, Indian Institute of Technology Jodhpur, Rajasthan -342037, India*
[3]*Department of Bioscience and Bioengineering, Indian Institute of Technology Jodhpur, Rajasthan -342037, India*
E-mail : mishra.15@iitj.ac.in

## Abstract

In recent years, dragon fruit (Hylocereus spp.) has gained significant attention due to its unique flavour and rich nutritional and medicinal properties(Zitha et al., 2022). The peel of dragon fruit, often considered agricultural waste, contains a high concentration of pectin, a valuable polysaccharide widely used in the food industry(Jiang et al., 2022). Traditional sources of pectin, such as citrus and apple residues, are limited in supply, necessitating the exploration of alternative sources. This study investigates the potential of cold plasma-assisted extraction as an innovative, eco-friendly method for pectin extraction from dragon fruit peel, comparing its efficiency and the functional properties of the extracted pectin with those obtained through conventional methods.The primary objective of this study was to evaluate the impact of cold plasma treatment on the chemical properties of pectin extracted from dragon fruit peel and to explore its application in the development of biodegradable films. Cold plasma treatment, known for generating reactive oxygen and nitrogen species (RONS), was employed to enhance pectin extraction efficiency and improve its functional properties. The results demonstrated a significant increase in pectin yield, reaching up to 35%, compared to untreated peels. The extracted pectin exhibited a higher degree of esterification, indicating superior gelling capabilities, which are essential for film formation. Furthermore, cold plasma treatment enhanced the antioxidant activity of the pectin, attributed to the generation of bioactive compounds during the extraction process. The treated peels also showed improved colour stability and a more vibrant red hue, making them suitable as natural colorants in food applications.

Physicochemical analysis revealed that the pectin yield ranged from 6.0% to 35.0%, with significant differences observed between extraction methods ($p < 0.05$). Fourier-transform infrared spectroscopy (FTIR) confirmed that the structural integrity of the pectin remained intact, regardless of the extraction technique. The study also explored the application of dragon fruit peel pectin in biodegradable films. Then prepared films were treated with cold plasma and comparison were made with untreated pectin films. The cold plasma-extracted pectin demonstrated excellent film-forming ability, with enhanced mechanical and barrier properties, making it a promising alternative for sustainable packaging materials. Cold plasma treatment not only enhanced the extraction efficiency and functional properties of pectin but also significantly improved the barrier properties of the resulting biodegradable films. The reactive species generated during cold plasma treatment, such as hydroxyl radicals ($OH\cdot$) and ozone ($O_3$ ), modified the surface properties of the pectin, leading to a more compact and homogeneous film structure.

This study highlights the potential of cold plasma treatment as a green and efficient method for pectin extraction from dragon fruit peel, offering a sustainable solution for valorising agricultural waste. The findings suggest that cold plasma-extracted pectin can be utilized as a functional ingredient in the food industry, serving as a natural colorant, gelling agent, and biodegradable film material. By transforming dragon fruit peel into valuable functional constituents, this approach contributes to reducing food waste and promoting a circular economy in the food sector.

**References**

[1] E. Z. M. Zitha, et al.Sci Hortic, vol. 291, p. 110611, Jan. 10.1016/j.scienta.2021.110611.

[2] H. Jiang, et al. *Food Packag Shelf Life* vol. 34, p. 100 2022, doi: 10.1016/j.fpsl.2022.100952

# Enhancing $CO_2$ Plasma Conversion with In-Situ Oxygen Removal Using SOECs

X.Chen[1,2,3], A. Pikalev[1], G. J. Zhang[3] and M.C.M. van de Sanden[1,2]

[1] *Dutch Institute of Fundemental Energy Research, Eindhoven, The Netherlands*
[2] *Eindhoven Institute of Renewable Energy Systems, Eindhoven Univ. Techn., The Netherlands*
[3] *School of Electrical Engineering, Xi'an Jiaotong University, Xi'an, China*

In this contribution, we investigate key factors affecting oxygen production in a plasma-assisted SOEC with $CO_2$ feed gas, focusing on reducing operating temperatures of the SOEC. Using a symmetric LSM | YSZ | LSM SOEC, experiments show that a He-$CO_2$ glow discharge reaches up to 90% conversion. Under oxygen pumping conditions, the plasma-SOEC system achieves a higher $CO_2$ conversion rate than plasma-only processes, demonstrating a true synergistic effect. Plasma improves the surface-limiting step of $CO_2$ electrolysis, i.e., shifting from dissociative adsorption of $CO_2$ towards oxygen surface adsorption reactions, enhancing energy efficiency. Additionally, oxygen removal via SOEC shifts $CO_2$ plasma splitting equilibrium, increasing gas conversion rates, while $CO_2$ plasma inhibits CO oxidation on the LSM electrode, further boosting SOEC oxygen pumping performance.

$CO_2$ is an abundant resource on both Earth and Mars that can be converted into carbon monoxide and oxygen, with distinct applications on each planet. On Earth, $CO_2$ utilization turns a greenhouse gas into valuable CO, which serves as a building block for syngas production. On Mars, $CO_2$ conversion produces vital oxygen for life support and rocket propellants. Hybrid plasma-solid oxide electrolysis cell (SOEC) systems have shown promise in this $CO_2$ splitting processes [1,2]. In this contribution, we investigate how plasma parameters, SOEC working temperatures, and bias affect catalytic processes to achieve higher oxygen production at lower operating temperatures.

Oxygen pumping experiments using a LSM | YSZ | LSM SOEC demonstrated that He (80%)-$CO_2$ (20%) glow discharge can enhance oxygen production with low SOEC working temperatures (500 - 700 °C). At 692 °C with -0.5 V bias, the enhancement factor increased forty-fold compared to conventional $CO_2$ electrolysis. Notably, this substantial improvement in $O_2$ production performance was achieved with an additional plasma power input (135 W) comparable to the SOEC heating power (261 W).

The integrated system's $CO_2$ conversion rate (χ) exceeded the combined individual rates of plasma (α) and electrochemical (β) conversion, as shown in Figure 1, confirming a true synergistic effect. This improved performance stems from plasma's ability to enhance the rate-limiting surface step of $CO_2$ electrolysis, shifting the mechanism from slow $CO_2$ reduction kinetics to faster $O_2$ pumping kinetics. Ex-situ experiments revealed an optimal temperature balance between oxygen pumping efficiency and competing reactions (CO oxidation and reverse Boudouard reaction). This temperature optimization strategy offers additional avenues for enhancing the overall performance and energy efficiency of plasma-SOEC hybrid systems.

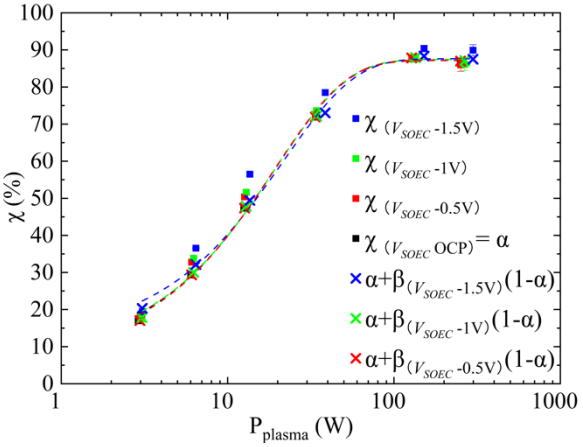



Figure 1 $CO_2$ synergistic conversion rate, SOEC temperature 692 °C.

These results validate the feasibility of in situ $O_2$ removal using a SOEC from plasma-based $CO_2$ conversion and provide a very promising aspect for both optimization of carbon capture and utilization (CCU) and further portable design in the Martian scenario to reduce dependence on high operating temperatures.

## References

[1] S. Mori et al, Synergistic $CO_2$ conversion by hybridization of dielectric barrier discharge and solid oxide electrolyser cell, *Plasma Process. Polym.* 14, 1600153 (2017).

[2] G. Chen et al., A novel plasma-assisted hollow fiber membrane concept for efficiently separating oxygen from CO in a $CO_2$ plasma, *Chem. Eng. J.* 392, 123699 (2020).

# Evaluating the efficacy of clove extract activated by cold plasma as a novel approach for caviar processing

F.Jamshidi Alashti[1,2], F.Sohbatzadeh[1,2]

[1] *Department of Atomic and Molecular Physics, Faculty of Science, University of Mazandaran, Babolsar, 4741695447, Iran*

[2] *Plasma Technology Research Core, Faculty of Science, University of Mazandaran, Babolsar, 4741695447, Iran*

The present work provides new insights into the utilized activated clove extract for inactivating microbial contaminants in caviar. For this purpose, clove aquas extract 1% (w/v) treated by the surface dielectric barrier discharge (SDBD) for 20 min. Then, the caviars were inoculated with E. coli, S. and immersed in activated clove extract (ACE) up to 7 min. Next, the inactivation rate of microorganisms was measured. The results revealed that the ACE completely inactivated microorganisms. Also, there were no significant changes between the brightness of control groups and groups treated with ACE.

## Introduction

Air plasma is generated using an SDBD[1].This system consists of aluminum adhesive tapes (2 cm × 18 cm), which are edge to edge on the top and below the surface a 4 mm thick glass dielectric. The applied AC voltage was 16 kV. The 10 mL of clove aquas extract 1% (w/v) was placed in a dish and activated by SDBD for 20 min. The caviar was inoculated with E. coli and immersed in activated clove extract (ACE) for 7 min.

## Result and discussion

The inactivation efficacies of clove extract untreated and treated by SDBD device on the reduction rate of bacteria is shown in Fig.2. Treatment of caviar with untreated clove extract for 7 min showed a reduction rate of 1.63 logs for *E.coli*. While treatment of caviar with ACE for 7 min resulted in a decrease of 4.03 logs in the population of *E.coli*.

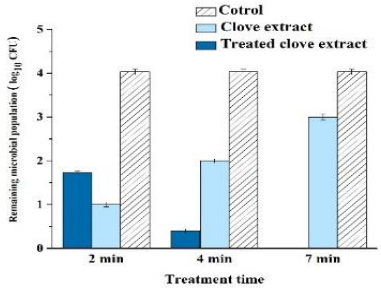



Fig.1 Effect of plasma treatment on microbial load caviar inoculated with E. coli.

The mechanism for inactivation involves the impact of plasma-induced species on the cell membrane, resulting in oxidative stress, DNA damage, destruction, and ultimately, cell death [2].

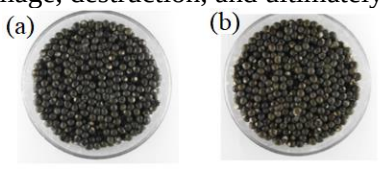



Fig.2 Images of the caviar eggs of control groups (a) and groups treated with activated clove extract (b).

The color of caviar plays a significant role in influencing consumers' willingness to accept it. Fig.2 shows the effect of PAS treatment on caviar color. There were no significant changes between the brightness of control groups and groups treated with ACE. Also, a significant difference in protein percentage was observed for control and treated sample. The highest protein content belonged to the control sample (31.03%) and ACE sample was 29.57 %. The pH value of caviar eggs treated decreased significantly from 7.02 to 3.07 ($p < 0.05$) compared to the control group. Moreover, the pH value of caviar eggs treated decreased significantly from 7.02 to 6.46 compared to the control group. The presented results prove plasma's synergistic and antimicrobial properties in pasteurization when combined with a solution with antimicrobial properties. Consequently, the proper plasma activated solution (PAS) is a flexible approach that could be employed for caviar sterilizing, extending shelf life, and preserving its physicochemical properties.

## References

[1] Alashti, F.J., F. Sohbatzadeh, S. Ahmadian, and E. Nazifi, Enhancing the biological activities and altering the chemical structure of clove aqueous extract prepared with plasma-activated water as a novel technique. LWT, 2024. **207**: p. 116687.

[2] Pourbagher, R., M.H. Abbaspour-Fard, F. Sohbatzadeh, and A. Rohani, In vivo antibacterial effect of non-thermal atmospheric plasma on pseudomonas tolaasii, a causative agent of Agaricus bisporus blotch disease. Food Control, 2021. **130**: p. 108319.

# Influence of current intensity on combustion in scramjet

A. Rocamora[1], J. Labaune[1], F. Tholin[1] and C. O. Laux[2]

[1] *ONERA, Université Paris Saclay, 91120, Palaiseau, France*
[2] *Laboratoire EM2C CNRS-CentraleSupélec, Université Paris Saclay, Gif-sur-Yvette, France*

This work presents an investigation of plasma-assisted combustion (PAC) in a supersonic hydrogen-air flow by means of a DC gliding arc discharge. The goal of this investigation is to determine the minimum current intensity threshold required to successfully ignite combustion. Furthermore, a 0D chemical model is developed to investigate the kinetics of combustion when the supersonic flow interacts with the arc.

## 1 Introduction

A crucial aspect of hypersonic flight engine design is ensuring supersonic combustion stability. Among the explored approaches, the application of an electric arc to generate plasma close to the injector has shown promise. This plasma serves a dual purpose. First, it produces a high temperature volume of gas. Second, it promotes reaction kinetics via radical production. Both effects promote ignition and flame sustainment.

Building on the Plasma Injector Module (PIM) concept of Leonov et al. [1], which utilizes a Quasi-DC gliding arc and was extensively studied in a series of experiments, this study undertakes a numerical simulation of the implementation of PIM in the LAPCAT-II facility of LAERTE (ONERA) at Mach 2 conditions. We simulate the test rig, with generator temperatures below sufficient level for autoignition in the presence of the DC gliding arc discharge with a current level ranging from 0 to 5 A.

## 2 Study

The Navier-Stokes equations with species transport are solved with the CEDRE CFD solver, with a Delayed Detached Eddy Simulation (DDES) approach. The electric field is determined by the quasi-neutral plasma solver TARANIS. The codes are coupled each time-step with the CWIPI library as described in [2]. The kinetic mechanism used for the $H_2$-air combustion is adapted from the one described by Jachimowski [3], neglecting $N_2$ dissociation.

## 3 Results and Discussion

A comprehensive study was conducted for six current cases (0, 1, 2, 3, 4 and 5 A) to elucidate the relationship between electric current and combustion stability. The simulations began from a stabilized state characterized by stable combustion at 5 A. A stable combustion is observed at current levels of 5 to 3 A. The transition to instability is detected for the 2 A case which corresponds to a highly unstable combustion regime. Finaly the combustion is extinguished at current levels of 1 & 0 A, according to the experimentally observed phenomena.

A limitation of the experimental studies is the difficulty to understand the impact of the high temperature arc on the chemical composition of the flow. Indeed, the temperature can reach 10,000 K in the arc. By using the Lagrangian approach for fluid particles, we obtain the residence time in the arc. This information is useful to assess radicals' production and its influence on combustion.

## 4 Conclusion

3D numerical simulations of a PIM in a scramjet have been successfully performed. A parametric study on the current level made it possible to determine the current threshold for ignition, with good qualitative agreement with experiments. A statistical study on the residence time of the gas molecules in the plasma is performed to feed a 0D model used to determine the plasma composition.

**Acknowledgments**
The authors thank the French Defense Innovation Agency (DGA), the French Procurement Agency (AID) and the ONERA's scientific direction for funding and supporting the present work.

**References**

[1] Savelkin K. V., et al. Ignition and flameholding in a supersonic combustor by an electrical discharge combined with a fuel injector. Combust Flame, 162-3, 825–835 (2015).
[2] Bourlet A., et al. Numerical model of restrikes in DC gliding arc discharges AIAA SCITECH (2022).
[3] Jachimowski, C. J. An analysis of combustion studies in shock expansion tunnels and reflected shock tunnels NASA-TP-3224 (1992).

# Spatiotemporal Colorimetric Response of KI-Starch on Reactive Oxygen Species

Kazunori Koga[1], Heping Shi[1], Daiki Ura[2], Takamasa Okumura[1], Masaharu Shiratani[1], Ryo Ono[2], and Toshiyuki Kawasaki[3]

[1] *Kyushu University, Fukuoka, Japan*
*2 The University of Tokyo, Tokyo, Japan*
[3] *Nishinippon Institute of Technology, Fukuoka, Japan*

In this study, we examined the colorimetric response of KI-starch gel to selective ROS irradiation using vacuum ultra violet lamp system. The KI-starch gel was employed to analyze two-dimensional profile of ROS dose as OD-value. After a 450 s irradiation of 1.72 ppm H2O2 gas irradiation, the OD profile widened and increased in maximum value with settling time after irradiation. The findings provide insight into the oxidation mechanisms for each ROS and contribute to a better understanding of its applications in material processing and biological treatments such as agriculture.

In recent years, atmospheric pressure plasma-induced oxidation and reactive species generation have gained attention in agricultural applications [1-5]. Optimizing these processes requires quantitative analysis of reactive oxygen species (ROS) generated by plasma irradiation. The KI-starch reagent offers a simple method for evaluating ROS dosage based on color intensity [6-8]. However, it is generally believed that the KI-starch method responds uniformly to molecules with oxidation potentials above 0.54 V, limiting its ability to distinguish between ROS types. In this study, we examined the KI-starch reaction for individual ROS. Using vacuum ultraviolet (VUV) light, we selectively generated O, OH, and $H_2O_2$, then analyzed their spatiotemporal color distribution patterns to assess their distinct reactivity.

As shown in Fig.1, the ROS-selective irradiation system used in the experiment introduces material gas molecules into a quartz tube, where VUV photons decompose the gas to generate specific ROS [9]. In the experiment, the distance between the quartz tube outlet and the KI-starch gel reagent surface was set to 1 mm. The color change was recorded using a scanner both 1 minute after plasma irradiation and 15 minutes after resting. The captured images were analyzed with ImageJ to obtain the optical density (OD) values.

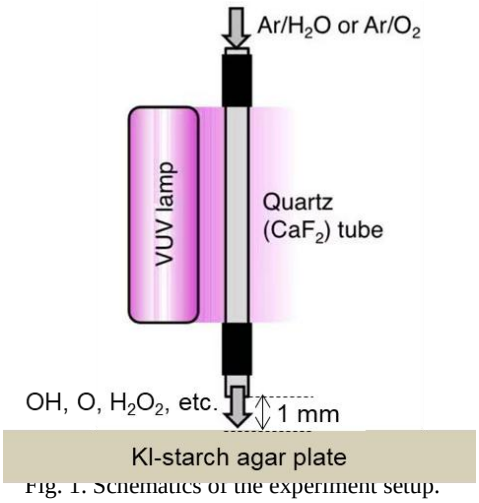



Fig. 1. Schematics of the experiment setup.

First, the coloration of the KI reagent was examined after irradiating 1.72 ppm $H_2O_2$ for 450 seconds. The coloration observed 15 minutes after irradiation was darker and covered a larger area compared to that observed 1 minute after irradiation. To quantify the coloration, we analyzed the spatial distribution of OD values. The maximum OD values were 0.1 after 1 minute and 0.25 after 15 minutes, revealing that both the OD value and coloration area increased over time. These results suggest that $H_2O_2$ not only reacts immediately but continues to engage in further reactions with the reagent over time.

The results of the spatiotemporal analysis of coloration induced by each reactive oxygen species will be presented in the lecture.

**References**

[1] P. Attri, et. al., Agronomy, 12, 482 (2022).
[2] T. Kaneko et al., Jpn. J. Appl. Phys. 61, (2022).
[3] P. Ranieri et al., Plasma Process. Polym. 18m (2021).
[4] T. Okumura et al., Sci. Rep. 12, 12525 (2022).
[5] H. Du et al., Appl. Sur. Sci. 648, 159086 (2024)
[6] T. Kawasaki et al., IEEE Trans. Plasma Sci. 44, 3223, (2016).
[7] T. Kawasaki et al., Jpn. J. Appl. Phys. 59, SHHF02 (2020).
[8] H. Shi et al., Int. J. Plasma Environ. Sci. Technol. 17, e01003 (2023) .
[9] R. Ono et al., J. Phys. D, 47, 445203 (2014).

# Impairment and recovery of immune cell function induced by oxygen plasma irradiation

H. Yonesu[1], H. Nakamura[1], S. Kodaka[1], and N. Hayashi[1]

[1] *Interdisciplinary Graduate School of Engineering Sciences, Kyushu University, Fukuoka 816-8580, Japan*

Recovery of weakened immune cells is attempted by using electrical discharge plasma. When cytokines (IFN-γ) produced by plasma-exposed T lymphocytes were added to plasma-exposed macrophages, phagocytosis was found to be improved and gene expression for cell division, cytokine production, cell differentiation, etc. was enhanced, indicating the possibility of recovery from functional decline.

## 1 Introduction

Compared to other cells, immune cells are more vulnerable to external stimuli. For example, when macrophages are exposed to plasma or radiation as an external stimulus, their immune function, phagocytosis, tends to decrease. At this time, genes for DNA repair and other functions are expressed, suggesting that the genes are affected or damaged by the high energy particles. It has been shown that adding cytokines from T cells to macrophages improves their functional activity, and this is particularly significant when the cytokines are exposed to plasma. Therefore, the purpose of this study is to investigate the change in macrophage activity when macrophages with reduced immune function due to stimuli are exposed to plasma and T cell-derived Interferon-gamma (IFN-γ) is added.

## 2 Experimental setup and Results

Figure 1 shows a torch-shaped atmospheric pressure DVD plasma source. Ozone generated from pure oxygen gas irradiates the culture medium in a 96-well plate, and OH radicals or atomic oxygen generated from ozone are applied to monocyte-like macrophages in the culture medium. Figure 2 shows the immune function (phagocytosis) of macrophages exposed to the oxygen plasma when cytokines produced by plasma-stimulated T cells were added with various parameters. The phagocytosis of macrophages was evaluated by measuring the amount of fluorescent nanoparticles taken up into the cells using a fluorescent microscope. The horizontal axis of the figure shows the plasma exposure conditions (ozone concentration) for T cells. Control is the phagocytosis of macrophages not exposed to plasma. No add indicates the phagocytosis of macrophages exposed to plasma for 40 s at an ozone concentration of 10 ppm, and the phagocytosis was reduced by about 25% due to active species in the plasma. No plasma means that macrophages were not exposed to plasma but were given IFN-γ derived from T cells.

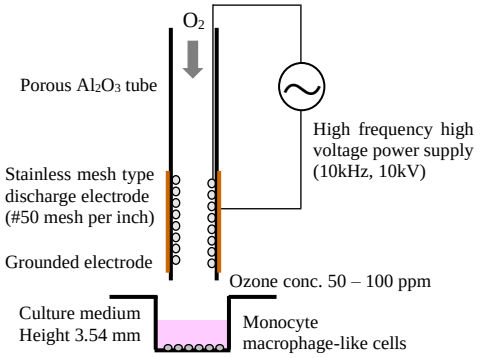



Fig. 1 Schematic of experimental apparatus.

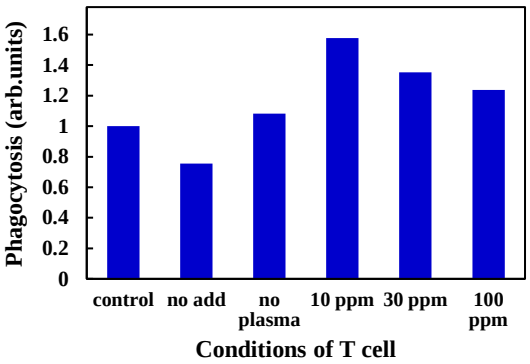



Fig. 2 Macrophage phagocytosis in each condition.

IFN-γ increased the cell number by about 10% compared to the control group.

IFN-γ produced by plasma exposed T cells at 10 ppm ozone was added to macrophages exposed to plasma at 10 ppm ozone. They phagocytosed 2.1 times as many fluorescent beads as in the no add group. In the case of plasma at 100 ppm ozone, the amount of fluorescent beads phagocytosed was 1.6 times that of the no add group. This suggests that the high concentration of reactive species tend to inactivate the cells. These results show that it is possible to restore or improve the function of immune cells whose functional activity has been reduced by external stimuli by applying cytokines produced by plasma exposed T cells.

# Liquid purification from bacteria and viruses by surface dielectric barrier discharge

A. Lavrikova, F. Avino, R. Agus, Y. Asnis, I. Furno

*Swiss plasma center (SPC), École Polytechnique Fédérale de Lausanne (EPFL), Lausanne, Switzerland*

Antimicrobial and antiviral effects of the air surface dielectric barrier discharge are studied for liquid purification. The energy consumption as well as the log reduction are measured as a function of various experimental parameters. The kinetics of the reactive oxygen and nitrogen species are measured in plasma-activated water and plasma-activated media. The presence of organic matter in a liquid negatively affects bacteria and virus inactivation by plasma. Yet, post-treatment incubation reveals a high potential of cold atmospheric plasmas for organic wastewater treatment.

## 1 Introduction

Cold atmospheric plasmas are one of the most promising bio-decontamination techniques in clinical, food processing, and environmental practices [1]. Yet, current solutions remain unsatisfactory for organic wastewater purification (e.g., [2, 3]). The presence of organic matter in a liquid, such as proteins and sugars, causes a reduction of the microbial inactivation. Along with target microbial cells, plasma–generated reactive oxygen and nitrogen species (RONS) interact with biomolecules thus shielding microbial cells [4].

The physicochemical properties of plasma-activated Luria-Bertani broth (PALB) and plasma activated water (PAW) are compared to explore the shielding effect of plasma activated medium reactivity. The analysis of bacterial membrane potential by flow cytometry reveals different bacteria responses to plasma when treated in PALB and PAW. Moreover, the plasma energy consumption for the treatment of densely contaminated LB broth is estimated. The results of this study provide a potential practical solution to organic wastewater decontamination by cold atmospheric plasmas.

## 2 Experimental

Surface dielectric barrier discharge (SDBD) (Fig. 1) [5] is used for direct treatment of a liquid sample. Antimicrobial effects are studied on *Micrococcus luteus* and *Escherichia coli* through bacterial survival, cell membrane permeabilization, and membrane potential. Antiviral effects are studied on adeno-associated virus (AAV) by digital PCR and transduction assay. RONS in PAW and PALB are measured by vis-spectrophotometry and high-performance liquid chromatography.

The SDBD treatment induced rapid total inactivation of *M. luteus* and *E. coli* in DI water within 3 min and 10 min treatment, respectively. Bacteria inactivation is enhanced during post-plasma treatment time. To achieve a total bacteria inactivation of $10^7$–$10^8$ CFU/ml in the presence of the LB broth, 24-h post-plasma treatment in PALB is required. Similarly, total AAV inactivation is achieved only without organic matter in a treated liquid.

**References**

[1] A. Bajrasteh et al., *Appl. Sci.*, **11**, 3372 (2021).
[2] A. Patange et al., *Sci. of the Total Environment.* **631–632**, 298-307 (2018).
[3] X. Liao et al., *Environmental Technology*, **42**(1), 58–71 (2021).
[4] Y-M. Zhao et al., Compr. *Rev. Food Sci. Food Saf.*, **19** (6), 1–29 (2020).
[5] R. Agus et al., *Chemical Engineering Journal*, **486**, 149915 (2024).

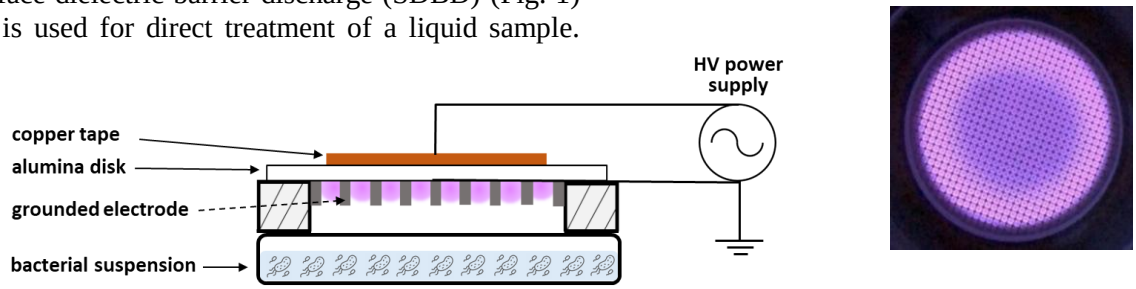



**Figure 1.** Schematic of the experimental setup of the SDBD applying on bacterial suspension in a Petri dish and the photo of the SDBD-generated plasma.

# Temperature and electron density investigation of micro structured pin-to-pin discharge for Hydrogen production

C.A. Garcia-Soto[1], M. Jacquart[1,2], F. Boni[1], M-E. Galvez[2,3], P-Q. Elias[1]

[1]*DPHY, ONERA, Université Paris-Saclay, 91120, Palaiseau, France*
[2]*Sorbonne Université, Institut Jean le Rond d'Alembert, CNRS UMR 7190, 78210, St-Cyr l'Ecole, France*
[3]*Instituto de Nanociencia y Materiales de Aragon (INMA), CSIC-Universidad de Zaragoza, 50009, Zaragoza, Spain*

$H_2$ production from natural gas via non-thermal plasma offers a low-temperature, $CO_2$-free alternative to conventional methods. A microstructured pin-to-pin discharge inside a 1 mm diameter capillary is used to study key physical parameters. $CH_4$ mixed with 1% $N_2$ was used at 10 sccm flowrate under 0.5–1 bar, ignited at 13–20 kV. Optical emission spectroscopy and electrical diagnostics revealed electron densities on the order of $10^{17}$–$10^{18}$ $cm^{-3}$ and gas temperatures around 500 K. Plasma processes were observed to occur within ~300 ns at 0.5 bar, doubling at 1 bar and 15 kV.

## 1 Introduction

$H_2$ production from natural gas is traditionally achieved through methods such as steam reforming or partial oxidation, but these processes have the major drawback of generating large amounts of $CO_2$ [1]. Conventional techniques typically operate at high temperatures and often require active catalysts to achieve optimal $H_2$ yields [2]. An appealing alternative for efficient and environmentally friendly $H_2$ production is the direct decomposition of methane by non-thermal plasma technology, which results in hydrogen and solid carbon. A pin-to-pin discharge offers a reactive environment with high electron density ($n_e$) at relatively low gas temperatures ($T_{gas}$) [3]. An innovative approach is the utilization of a microstructured pin-to-pin discharge enabling the confinement and miniaturization of the discharge that reduces dead volume and enhances residence time, thereby improving heat and mass transfer efficiency. Here, we study a pulsed micro structured pin-to-pin discharge inside a long capillary of 1 mm diameter. The combination of time resolved optical emission spectroscopy, imaging and electrical measurements provide crucial information for describing the plasma.

## 2 Experimental setup

A borosilicate glass capillary with 1 mm outer diameter, 0.58 mm inner diameter and 150 mm length is used as miniaturized plasma reactor. Two wires are inserted inside the capillary that serve as HV and ground electrodes. The ground electrode is connected to a resistor to limit the current. $CH_4$ gas was used with 1% $N_2$ as tracer molecule. Total gas flow was set to 10 sccm at 0.5-1 bar. The plasma was ignited at 13-20 kV using a custom-made bipolar HV pulse generator. A Rogowski coil was used to extract information on the current. Time-resolved optical emission spectra were taken with a spectrometer SpectraPro 2750 from PI. The gate width and delay were set to 0.02-1 µs for spectrum and imaging analysis. $T_{vib}$ and $T_{rot}$ were obtained by fitting the spectra with SPECAIR software [4]. The $n_e$ was obtained by fitting of the $H_\alpha$ Balmer line.

## 3 Results

$T_{gas}$ is around 500 K while $T_e$ was not >10 000 K. $C_2$ Swan system, CH bands and $H_\alpha$ line dominate the spectrum. The $n_e$ is around $10^{17}$-$10^{18}$ $cm^{-3}$. The pulse lasts around 50 µs but the $H_\alpha$ emission suggests that the plasma is short lived within ~300 ns at 0.5 bar but it doubles at 1 bar (fig. 1) at 15 kV.

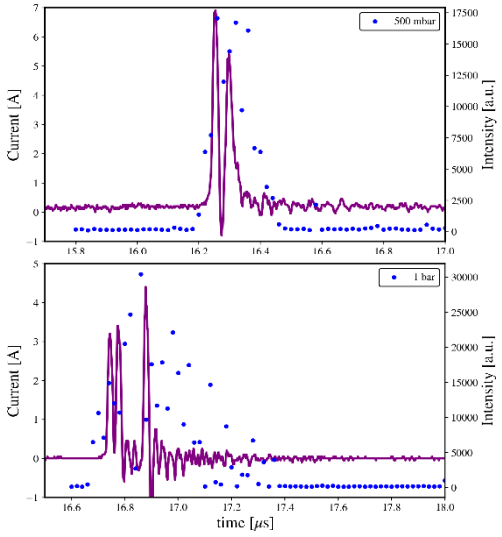



Fig. 1. $H_\alpha$ Balmer line emission (dotted) and current (line) as a function of time at 0.5 bar (top) and 1 bar (bottom).

The results will be compared to our previous surface DBD configuration.

**References**

[1] R. Kumar, R. Singh and S. Dutta, 2024 *Energy & Fuels* **38** pp 2601.

[2] M. Msheik, S. Rodat, and S. Abanades, S. 2021 *Energies*, **14** pp 3107.

[3] Yao Li et al., 2024 *J. Phys. D: Appl. Phys.* **57** 225201

[4] SPECAIR, Software Ver. 3.0 *SpectralFit S.A.S.*

# Modelling of positive and negative streamers interaction in dry air with imposed density gradient

J. Paredes, N. Barléon, and O. Dounia

*CERFACS, 42 Avenue Gaspard Coriolis, 31057 Toulouse, Cedex 1, France*

This study models the interaction of positive and negative streamers in dry air with a density gradient using a 2D axi-symmetrical fluid model. A pin-to-pin electrode configuration simulates a single pulse of Nanosecond Repetitively Pulsed Discharges (NRPD). The impact of different density ratios, representing a flame front, is analyzed, along with variations in gradient width. Energy deposition in high- and low-density regions is studied, as well as the effect of polarity, which can enhance or extinguish the discharge. Results provide first insights into streamer behavior in realistic conditions relevant for burner applications.

Streamers are fast ionization waves associated to plasma discharges eventually leading to glow, corona or spark regimes. This first stage of the discharge, strongly depends on the reduced electric field $E/N$ which can be notably influenced by potential spatial inhomogeneities in the flow. In combustion environments, a inhomogeneous background density can be studied as a first step towards a detailed model representative of a flame. Recent studies have shown how a density gradient can block a positive streamer when it goes from a low to a high density region ( [1], [2]).

Depending on the geometry of the electrodes, voltage polarity, and ionization of the gas before the discharge, a positive or a negative streamer can start. This work will focus on the development and interaction of two streamers (positive and negative) in dry air when a gradient of density is imposed between the two electrodes. Numerical simulations of a canonical pin to pin electrodes configuration are performed using a single pulse of NRPD.

For the simulations a 2D axi-symmetrical domain is used and a fluid model with the Poisson equation is solved to compute the transport of electrons and ions. A minimal cell size of 2.5 micrometer is used following mesh convergence verification. The chemistry of the discharge is defined by transport coefficients in the local electric field approximation defined by [3]. The model of [4] is used for photoionization.

First, this study examines the impact of different background density ratios $N_1/N_2$ (see figure 1), where $N_1$ in the density near the cathode and $N_2$ corresponds to the density near the anode. $N_1$ and $N_2$ represent the densities which could be found on both sides of a flame front (unbunrt and burnt gases.) The transition from $N_1$ to $N_2$ is imposed and located at the center of the electrode gap. Its width, $\delta_L$ is set equal to the thermal thickness of a H2/air flame at stoichiometry. The electrical energy deposition in the different density regions will be analyzed.

After studying the range of densities ratios, the electrodes polarity is inverted to see the effects of the density inhomogeneities in the inverted streamers. It was found that, for some density ratios the inverted polarity can either improve or extinguish the electrical discharge.

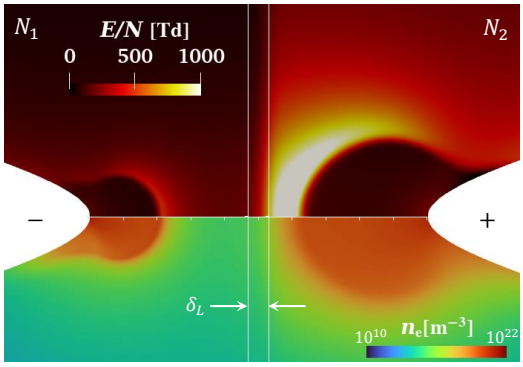



Figure 1: Reduced electric (top) field and electron density (bottom) at 0.9 ns of the pulse. The case corresponds to $N_1/N_2 = 0.25$

## References

[1] Guo, B., Ebert, U., Teunissen, J. 3D modeling of positive streamers in inhomogeneous air. *Plasma Sources Sci. Technol*, **32**(9), 095015 (2023).

[2] Kosarev, I. N., Starikovskiy, A. Y., Aleksandrov, N. L. Development of high-voltage nanosecond discharge in non-uniform gas. *Plasma Sources Sci. Technol*, **28**(1), 015005 (2019).

[3] Morrow, R., Lowke, J. J. Streamer propagation in air. *J. Phys. D: Appl. Phys*, **30**(4), 614–627 (1997).

[4] Bourdon, A., Pasko, V. P., Liu, N. Y., Célestin, S., Ségur, P., Marode, E. Efficient photoionization models for non-thermal discharges in air. *Plasma Sources Sci. Technol*, **16**(3), 656–678 (2007).

# Direct $H_2O_2$ Delivery and Initial Cellular Responses in *Marchantia polymorpha* upon Cold Plasma Irradiation

S. Tsuboyama[1], T. Okumura[2], K. Koga[2], M. Shiratani[2] and K. Kuchitsu[1]

[1]*Tokyo University of Science, Chiba, Japan*
[2]*Kyushu University, Fukuoka, Japan*

Cold atmospheric pressure plasma (CAPP) irradiation has emerged as a promising technique for enhancing seed germination and plant growth. However, the molecular mechanisms mediating these effects remain largely unexplored. To facilitate the practical application of CAPP technology in agriculture, we are investigating the plant responses to CAPP irradiation at the cellular and molecular levels using *Marchantia polymorpha* as a model system, capitalizing on its amenability to genetic, cellular, and molecular analyses. Recently, we had recently developed model experimental systems to investigate the initial cellular responses triggered by pen-shaped dielectric barrier discharge (PDBD) plasma irradiation using *M. polymorpha*. By integrating detailed characterization of plasma sources with genetic and cell biological approaches, we aim to elucidate the molecular pathways underlying CAPP-induced plant responses and identify key regulatory factors.

## 1. Introduction

Cold atmospheric pressure plasma (CAPP) generators, capable of operating under ambient conditions, have been increasingly utilized in biological applications. While CAPP irradiation has been reported to modulate plant germination and growth, the underlying molecular mechanisms and immediate cellular responses remain largely unexplored. To elucidate these mechanisms, we have established novel experimental systems utilizing the model liverwort *Marchantia polymorpha*.

*Marchantia polymorpha*, with its relatively simple genetic composition and organizational system conserved across many terrestrial plants, serves as an excellent experimental model in molecular plant physiology. Our previous findings have demonstrated that scalable dielectric barrier discharge (SDBD) irradiation can both positively and negatively regulate the growth of its gemmae [1], highlighting its suitability for investigating the effects of plasma irradiation.

## 2. Results and discussion

In this study, we focused on the initial cellular responses to CAPP irradiation using *M. polymorpha*. To precisely monitor these responses, we developed a custom-designed CAPP device compatible with live fluorescence microscopy. This integrated system enabled real-time tracking of intracellular $H_2O_2$ and $Ca^{2+}$ dynamics, key early signaling events. We observed that CAPP irradiation rapidly and transiently increased cytosolic $H_2O_2$ and $Ca^{2+}$ levels in *M. polymorpha* gemmalings. Pharmacological analyses indicated that exogenous $H_2O_2$ generated by the CAPP device directly entered plant cells. Furthermore, competitive inhibitors of $Ca^{2+}$ channels abolished the $Ca^{2+}$ influx, suggesting that CAPP irradiation rapidly activates plasma membrane $Ca^{2+}$ channels [2].

Currently, we are integrating detailed characterization of plasma sources with genetic and cell biological approaches to comprehensively elucidate the molecular pathways underlying CAPP-induced plant responses and identify key regulatory factors involved in these signaling cascades.

## 3. Acknowledgments

This work was supported by Tokyo University of Science, the Plasma-Bio Consortium project, Center for Low-temperature Plasma Sciences, Nagoya University, JSPS KAKENHI JP22H04734, JP22H01212, JP22K19160, JP22K03586, JP24H02246, JP24H02250, JP24A206, JST COI-NEXT JPMJPF2302, and JST PARKS JPMJSF2317.

## 4. References

[1] S. Tsuboyama†, T. Okumura†, P. Attri, K. Koga*, M. Shiratani and K. Kuchitsu*, *Sci. Rep.,* 14: 3172, (2024) †equally contributed

[2] S. Tsuboyama, T. Okumura, K. Watanabe, K. Koga*, M. Shiratani and K. Kuchitsu*, *Plant Physiol. Biochem.*, 216:109172-109172, (2024)

# Simulation of an ionization wave propagating along a silicon-based surface

A. Herrmann[1], A.S. Taihi[1], F. Plouraboué[2] and D. Z. Pai[1]

[1]*Laboratoire de Physique des Plasmas (LPP), CNRS, Sorbonne Université, École Polytechnique, Institut Polytechnique de Paris, 91120 Palaiseau, France*
[2]*Institut de Mécanique des Fluides de Toulouse (IMFT), Université de Toulouse, CNRS, Toulouse, France*

We have developed a numerical model to simulate a surface ionization wave (SIW) generated in atmospheric-pressure air in contact with p-doped silicon covered by $SiO_2$. Following a validation of the model using experimental results, we will demonstrate how an increase in the doping of the silicon affects the initiation and propagation of the SIW in air.

## 1 Introduction

Positive SIW propagating over dielectric materials have been extensively studied. Recently, a silicon-based barrier was used instead of a dielectric, which allowed for uniform propagation of the SIW without filament (streamer) formation [1]. The impact of silicon can come from several parameters: the mobility of electrons and holes in silicon is of the same order of magnitude as that of electrons in air, enabling electrostatic coupling between the two media. Additionally, photons generated by the SIW in air can generate electron-hole pairs upon penetrating silicon, further enhancing the coupling between the two media.

## 2 Numerical model and results

Simulations are performed using a 2D axisymmetric fluid model on a non-uniform grid, part of which is shown in Figure 1a. A nanosecond pulse of 2-kV amplitude is applied to a pin electrode, and drift-diffusion equations are solved for a typical SIW as in Herrmann et al. [2]. In the silicon, depending on the doping, two types of charges are considered: mobile and fixed charges [3]. Thus, the mobile charges in the silicon follow a drift-diffusion model as in Ward et al. [3], with an additional gain term from photons generated by the SIW in the air that are absorbed by the silicon. The fixed charges, on the other hand, are only involved in solving Poisson's equation. The model then captures the propagation of the SIW in the air, as illustrated in Figure 1b with the electric field generated by the SIW at t = 6 ns, while resolving the formation and propagation of charges in the silicon, as illustrated in Figure 1c with the charge density in the silicon (intrinsic case) propagating in volume. The model has been validated using experimental data. We will show that increased charge caused by an increase in silicon doping allows for faster initiation of the SIW because the reorganization of charge in the silicon impacts the field generated in the air. Regarding surface propagation, two modes will be identified depending on the resistivity (ρ) of the silicon. For ρ > 40 Ω.cm, a decrease in ρ allows for greater surface propagation, whereas for ρ < 40 Ω.cm the opposite is true. We will explain these two trends through the competition between charges from doping and those photo-generated in silicon.

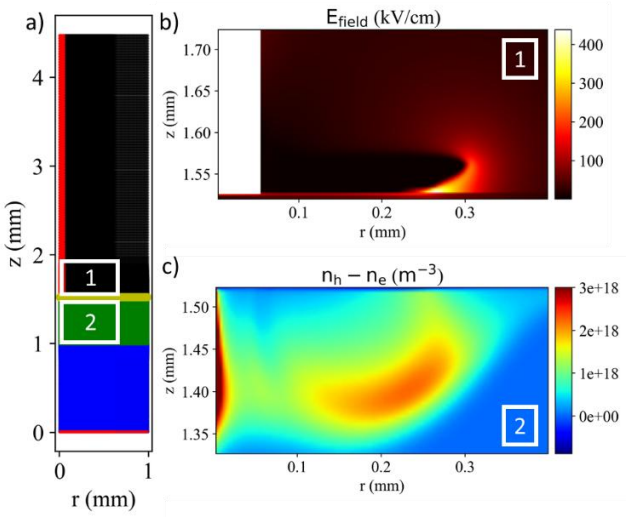



**Figure 1**: a) Simulation domain with air (black), $SiO_2$ (yellow), silicon (green), glass (blue) and electrodes (red), b) the electric field generated by the SIW in air, and c) the charge density in the silicon at t = 6 ns.

**Acknowledgements**

This research has received funding from the European Union's Horizon Europe Research and Innovation Programme's project EIC Pathfinder: IPROP.

**References**

[1] T. Darny et al 2020 Plasma Sources Sci. Technol. 29 065012
[2] A. Herrmann et al 2024 Plasma Sources Sci. Technol. 33 025022
[3] A. Ward et al 1968 IEEE Transactions on Electron Devices, 15(11), 847-851

# Influence of photo-ionization on propagation of streamer discharges at atmospheric pressure

D. Nikic[1], A. Fierro[2], J. Lehr[1], and C. H. Moore[3]

[1] *University of New Mexico, Albuquerque, NM USA*
[2] *New Mexico Tech, Socorro, NM USA*
[3] *Sandia National Laboratoires, Albuquerque, NM USA*

Photoionization plays an important part in propagation of positive streamer discharges. The influence of this process is investigated by comparing particle-in-cell (PIC) simulations of streamer discharges in which only the photoionization cross section is varied. All simulations are performed using Empire [1], a Sandia National Laboratories (SNL) PIC code which utilizes the Direct Simulation Monte Carlo (DSMC) method. Furthermore, relation between photoionization and level of background ionization is presented to determine when photoionization becomes a dominant propagation process. Finally, a study of the numerical heating is presented to justify the choice of mesh grid size and number of particles used in the simulations [2].

## 1 Introduction

Streamer discharges require a source of electrons to propagate across an electrode gap. Negative streamers (propagating from cathode to anode) are aided by existence of available free charge in the gas which propagates in the same direction as the streamer and thus aids streamer growth. Positive streamers require an additional source of electrons since available free charge propagates against the streamer direction. For some gases these electrons may come from photo-ionization. The set of interactions shown below demonstrates a photo-ionization pathway in gas A with a quantity of gas B present:

$$\begin{aligned} e^- + A &\rightarrow e^- + A^* \\ A^* &\rightarrow A + \gamma \\ \gamma + B &\rightarrow B^+ + e^- \end{aligned} \qquad (1)$$

Excitation of gas A leads to creation of an excited state, $A^*$, that spontaneously emits a photon which can ionize gas B. This process requires an excited state of gas A to have energy greater than B's ionization energy. For example, $N_2^*$ can emit a photon that can ionize $O_2$, thus making photoionization an important process in air and air-like mixtures.

## 2 Simulations

Streamer simulations are performed using the Empire PIC plasma code. Two-dimensional simulations of a 1 cm gap discharge simulation domain was comprised of 1M cells and over 100M computational particles. Electrostatic formulation is used for all calculations. A simple cylindrical electrode with rounded tip is used as an anode with planar cathode placed 1 cm away.

## 3 Results

The photoionization mean free path has been shown to significantly increase the propagation speed of the streamer and change the overall nature of the streamer discharge. Namely, short range photons provide a more uniform ionization front and less branching of the streamer, while a long range photon drives formation of additional streamer channels.

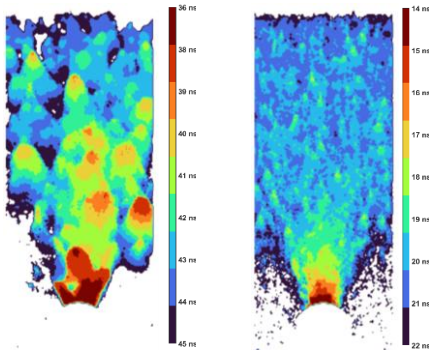


*Figure 1: Example of long range photoionization (left) versus short range photoionization (right). Color represents time when electron density exceeds $10^{17}$ $m^{-3}$.*

**References**

[1] Bettencourt et. al., EMPIRE-PIC: A performance portable unstructured particle-in-cell code, *Comm in Comp Phys*, **30**, no. 4, 2021.

[2] Nikic, D., Moore, C., Lehr, J., and Fierro, A. Numerical-heating effects in atmospheric pressure streamer discharges simulated with a PIC code. *Physics of Plasmas, under review*.

**Acknowledgement**

This work was supported in part by the U.S. Department of Energy under award No. DE-SC0022201, and in part by Sandia National Laboratories. Sandia National Laboratories is a multi-mission laboratory managed and operated by National Technology and Engineering Solutions of Sandia, LLC., a wholly owned subsidiary of Honeywell International, Inc., for the U.S. Department of Energy's National Nuclear Security Administration under Contract No. DE-NA0003525.

# Simulation of He APPJ - dielectric surface action process under external electric field

H. Zhao[1], L. Wang[1] and Z. Han[1]

[1] *Xi'an Jiaotong University, State Key Laboratory of Electrical Insulation and Power Equipment, Xi'an, China*

A two-dimensional fluid model is established to study the effect of external electric field and its amplitude on He APPJ - dielectric surface action process. The self-established electric field $E_1$ between the charge at the jet head and the external electrode causes the change of propagation speed and intensity of APPJ. The radial component is generated when the jet develops down the axis, which results in the change of the jet width. The electric field intensity on the external positive and negative voltage side is weakened and strengthened respectively to inhibit and promote ionization respectively. Under the external asymmetric voltage, the jet center deviates from the central axis. $E_1$ and the radial electric field $E_3$ generated by the accumulated surface charge guide the radial propagation of the jet. Higher ionization rate, radial mean propagation velocity and wider radial development range can be obtained under external negative voltage. What's more, excessive external voltage amplitude may lead to the generation of parasitic ionization waves.

## 1 General

Atmospheric pressure plasma jet (APPJ) have the following advantages: The discharge is generated in an open atmospheric environment, and the jet length can reach centimeter level, APPJ's temperature is close to room temperature and it is rich in high-energy reactive species. Therefore, APPJ has been widely used in materials science[1], biomedicine[2] and other fields. However, the current research still faces the following challenges: The existing researches mainly focus on the optimization of passive parameters, lack of researches on controlling the propagation process of APPJ through external field intervention. The mechanism of the influence of external electric field on the APPJ - dielectric surface interaction is still not clear.

In this paper, a two-dimensional fluid model is established to simulate the interaction between the APPJ and the dielectric surface under the external electrode, as shown in FIG.1.

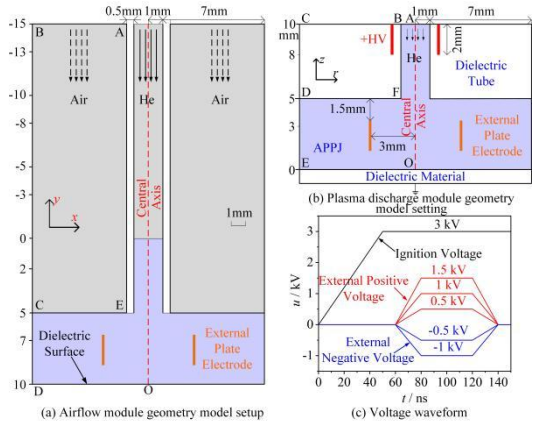



FIG. 1. Geometric model settings and voltage waveform.

The whole simulation process includes the solution of the neutral gas flow module and the plasma discharge module, which is independently solved by COMSOL Multiphysics. He with a flow rate of 1 standard liter per minute is used as the working gas. The voltage waveform is shown in FIG. 1(c). The ignition voltage is applied to the high-voltage electrode, and the remaining voltage is applied to external electrodes, including symmetric pulse voltage and asymmetric pulse voltage.

The conclusion of this paper is as follows: The radial component of the external electric field changes the jet width. The field intensity on the external positive and negative voltage side decreases and increases respectively to inhibit and promote ionization respectively. With asymmetric voltage applied, the jet center deviates from the central axis. The self-built electric field between the jet head and the external electrode and the radial electric field generated by the surface accumulated charge guide the radial propagation of the jet, and the surface development range is larger under negative voltage. When the applied positive voltage is increased, the ionization wave is derived between the bottom of the positive voltage electrode and the surface. When the negative voltage is increased, an ionization wave is generated between the bottom end of the negative voltage electrode and the jet head.

### References

[1] Booth J P, Mozetič M, Nikiforov A, et al. Foundations of plasma surface functionalization of polymers for industrial and biological applications. *Plasma Sources Science and Technology* **31**, 103001 (2022).

[2] Zheng L, Gao J, Cao Y, et al. Two case reports of inverse psoriasis treated with cold atmospheric plasma. *Dermatol Ther* **33**, e14257 (2020).

# Towards a spatial dust fluid model

J. Janssen[1], K. van 't Veer[1], W. Graef[1], D. Mihailova[1], R. Budé[1] and J. van Dijk[2]

[1] *Plasma Matters B.V., Eindhoven, The Netherlands*
[2] *Eindhoven University of Technology, Eindhoven, The Netherlands*

A dust growth and transport model is developed and self-consistently coupled to the existing drift-diffusion models in PLASIMO. Three different methods for accounting the charging of the dust particles are investigated and compared. The first method accounts for each charge state with a separate continuity equation. The second method uses an extra balance for the average charge of the dust particle. The third method always assumes the equilibrium charge based on OML theory.

## 1 Introduction

Dust control is a major challenge for the hightech industry. For that reason understanding dust formation and the transport of dust is crucial. In this work a self-consistent model is discussed that can account for the dust transport and growth in a plasma environment. This makes the model an ideal tool for studying and understanding dust related phenomena. The model is integrated in the PLASIMO framework [1]. The specific topic of this work is the comparison of three options for handling the charge distribution of the dust particles.

## 2 Dust model

The model is based on a standard drift-diffusion approach [2]. A continuity equation is set up for the ions, electrons and dust particles. The electron and ion fluxes contain drift and diffusion contributions. For the dust particles an additional term is included that accounts for the ion induced drag. The components included in the ion drag are based on OML theory.

### 2.1 Charge distribution

The chemical term in the continuity equation is handled in three different ways.

The first method uses a charge state resolved approach. Every charge state of a dust particle is considered to be a separate species and thus a separate continuity equation is set up. The exact source terms are based on the OML fluxes of the ions and the electrons.

The second method considered simplifies the charge balance and assumes only one charge state per included dust mass. The charge is calculated by solving a time dependent equation for the average charge of the dust particles.

The third method introduces an additional simplification. The charge on the dust particle is always assumed to be the equilibrium charge based on the OML fluxes.

A comparison of the three models shows that resolving the charge state distribution with separate continuity equations is not always necessary. In many cases solving for the average charge distribution or even assuming the equilibrium charge at all times is accurate enough. The results are validated with literature data.

## References

[1] van Dijk, J. The plasma modelling toolkit Plasimo *Journal of Physics D: Applied Physics*, **42**, 194012 (2009).

[2] Warthesen, S.J. and Girshick, S.L. Numerical simulation of the spatiotemporal evolution of a nanoparticle–plasma system *Plasma Chem Plasma Process*, **27**, 292-310 (2007).

# Progress report on the LoKI-B+C simulation tool

P. Pereira[1], A. Tejero-del-Caz[2], A. Gonçalves[1], N. Pinhão[1], J. van Dijk[3], D Boer[3] and L.L. Alves[1]

[1] *Instituto de Plasmas e Fusão Nuclear, Instituto Superior Técnico, Universidade de Lisboa, Portugal*
[2] *Departamento de Física, Facultad de Ciencias, Universidad de Córdoba, Campus de Rabanales, Spain*
[3] *Department of Applied Physics and Science Education, Eindhoven University of Technology, The Netherlands*

The LisbOn KInetics LoKI-B+C [1] is a simulation tool for plasma chemistry that couples two main calculation blocks: a Boltzmann solver (LoKI-B) [2,3] and a Chemical solver (LoKI-C), developed / consolidated resorting to the well-grounded scientific foundations of the Portuguese group N-PRiME. This contribution presents a progress report on the development of LoKI-B+C and is intended to also receive comments and suggestions from the low-temperature plasmas community, in preparation of its release as open-source code.

LoKI-B (released as open-source code [4] licensed under the GNU GPL v3.0) solves the space independent form of the two-term electron Boltzmann equation for non-magnetised non-equilibrium low-temperature plasmas, excited by DC/HF electric fields or time-dependent (non-oscillatory) electric fields from different gases or gas mixtures.

LoKI-C [5] solves the system of zero-dimensional (volume average) rate balance equations for the most relevant charged and neutral species in the plasma, receiving as input the kinetic schemes for the gas/plasma system under study.

LoKI-B+C has been originally developed with flexible and upgradable object-oriented programming under MATLAB, adopting an ontology that privileges the separation between tool and data.

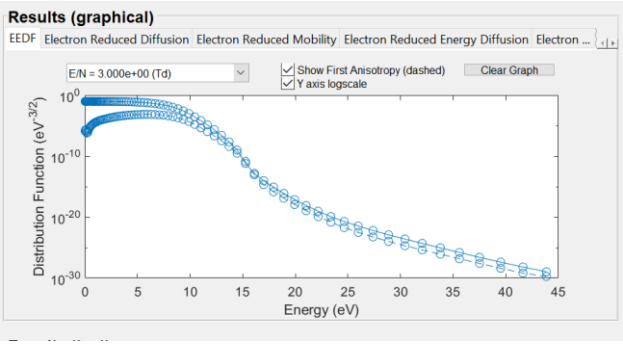



Figure 1: Plot of the electron energy distribution function (upper solid curve) and of the first anisotropy (lower dashed curve), for a solution of the electron Boltzmann equation in argon, on a variable energy grid using LoKI-B. The plot appears embedded in the GUI of the code. The location of the points shows the evolution in the energy steps, for different electron kinetic energies.

Presently, evolutions of LoKI-B+C comprise mostly: (i) the development of LoKI-B++, the C++ mirror version of LoKI-B MATLAB, in a collaboration with TU/e; (ii) the implementation of electron energy distribution function (EEDF) calculations on a variable energy grid in LoKI-B (see Fig.1); (iii) the inclusion of an additional heating operator in LoKI-B, describing the combined ohmic-stochastic interaction of electrons with the applied electric field [6]; (iv) the packaging of LoKI-B+C as MATLAB toolbox [7], allowing resorting to an online-help feature; (v) the integration of input files in JSON format, compliant with the new LXCat 3.0 [8,9]; (vi) the implementation of time-dependent calculations, coupling LoKI-B and LoKI-C under different approximations; (vii) the design and development of a regression test suite; (viii) the optimization of the iterative calculation cycles.

**Acknowledgements**
This work was funded by Fundação para a Ciência e a Tecnologia under projects UIDB/50010/2020, UIDP/50010/2020, LA/P/0061/2020 and 2022.04128.PTDC.

**References**

[1] nprime.tecnico.ulisboa.pt/loki/
[2] Tejero-Del-Caz, A. *et al.*, *Plasma Sources Sci. Technol.* **28**, 043001 (2019).
[3] Tejero-del-Caz, A. *et al.*, *Plasma Sources Sci. Technol.* **30**, 065008 (2021).
[4] github.com/IST-Lisbon/LoKI/
[5] Guerra, V. *et al.*, *Plasma Sources Sci. Technol.* **28**, 073001 (2019).
[6] Czarnetzki, U. and Alves, L.L., *Rev. Mod. Plasma Phys.* **6**, 31 (2022).
[7]https://www.mathworks.com/help/matlab/creating-help.html
[8] https://demo.lxcat.net/
[9] https://github.com/LXCat-project/LXCat

# Recent developments on LoKI-MC: Coulomb collisions and efficient null-collision method

G. A. Cardoso[1], V. Guerra[1], D. Valverde[1] and T. C. Dias[2]

[1] *Instituto de Plasmas e Fusão Nuclear, Instituto Superior Técnico, Universidade de Lisboa, Portugal*

[2] *Engineering and Computer Science Department, University of Michigan, Ann Arbor, USA*

This work presents two developments on the electron kinetics solver LoKI-MC: (i) the inclusion of electron-electron (e-e) and electron-ion (e-i) collision effects, and (ii) the implementation of an efficient null-collision method. The impact of Coulomb collisions is analyzed across a wide range of conditions. With the recent improvements in computational efficiency, LoKI-MC can often provide statistically precise solutions within tens of seconds, offering a feasible and more accurate alternative to two-term solvers.

The electron kinetics in gas discharges can be described by the electron Boltzmann equation (EBE) or by Monte Carlo (MC) simulations. Very often, the former approach is adopted using the two-term approximation for the electron velocity distribution function, which is valid under sufficiently low anisotropies in velocity space. Various two-term EBE solvers are openly available to the community, such as Bolsig+ [1] and the LisbOn KInetics Boltzmann (LoKI-B) [2]. More recently, the Monte Carlo solver LoKI-MC has been released as open source, offering an alternative means of describing the electron kinetics when the two-term solution is not sufficiently accurate [3]. LoKI-MC efficiently solves the electron kinetics under time-dependent (AC or pulsed) electric fields combined with DC magnetic fields, and includes a general user-friendly interface. LoKI-MC is under continuous development. Here, we present its two most recent features: (i) the inclusion of e-e and e-i collisions, and (ii) the implementation of an efficient null-collision method.

The importance of Coulomb collisions in electron kinetics is closely linked to the ionization degree. Figure 1 presents LoKI-MC simulations of the electron energy distribution functions (EEDFs) in argon, for a reduced electric field (*E/N*) of 10 Td and various ionization degrees $n_e/N$, taking into account the effect of e-e collisions. In general, e-e collisions increase diffusion in energy space, contributing to the Maxwellization of the EEDF and increasing the population of high-energy electrons. At lower values of *E/N*, e-i collisions act in the opposite direction, driving the EEDF towards a Maxwellian distribution at the temperature of the colder background ions.

LoKI-MC employs a null-collision method to compute electron kinetics. However, this method can be inefficient due to the high frequency of null collisions, where no real interaction occurs. To overcome this limitation, we have implemented a modified version of the method proposed by Brennan [4]. An example of the computational advantage of this approach compared to the standard method is shown in figure 2, demonstrating speed-ups of up to 8-fold. With these recent developments, LoKI-MC can often deliver statistically precise solutions within tens of seconds.

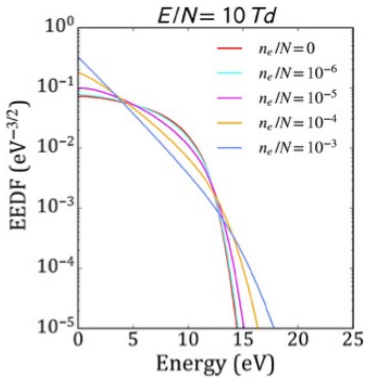



**Figure 1:** EEDFs in argon, for *E/N* =10 Td and various ionization degrees $n_e/N$.

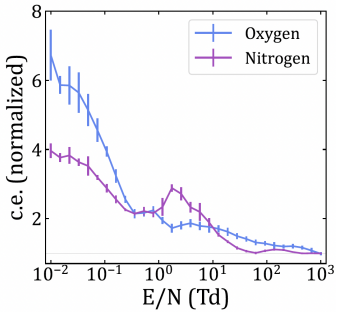



**Figure 2:** Computational efficiency gains (c.e.) of the efficient null-collision method face to the standard method.

**Acknowledgments:** IPFN activities were supported by the Portuguese FCT – Fundação para a Ciência e Tecnologia, under funding to Instituto de Plasmas e Fusão Nuclear (https://doi.org/10.54499/LA/P/0061/2020, https://doi.org/10.54499/UIDB/50010/2020 , https://doi.org/10.54499/UIDP/50010/2020 , and https://doi.org/10.54499/PTDC/FIS-PLA/1616/2021).

**References**

[1] G. J. M. Hagelaar and L. C. Pitchford *Plasma Sources Sci. Technol.* **14**, 722 (2005).

[2] A. Tejero-del-Caz *et al. Plasma Sources Sci. Technol.* **28**, 043001 (2019).

[3] T. C. Dias *et al. Plasma Sources Sci. Technol.* **32**, 095003 (2023).

[4] M. J. Brennan *IEEE Trans. Plasma Sci.* **19** 256 (1991).

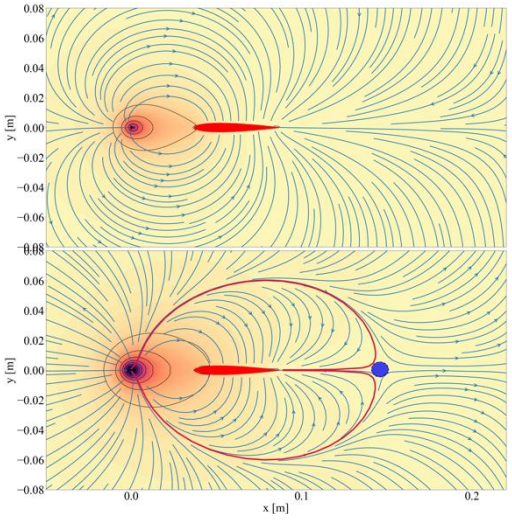
# Two-way coupling of plasma-fluid interactions for ionic wind modelling

José Maria Dias Coelho Marques[1], David Fabre[1] and Franck Plouraboué[1]

[1] *Université de Toulouse, CNRS, INPT, UPS, Allée du Pr. Camille Soula, 31400 Toulouse, France*

This contribution is interested in the modelling of ionic wind generated by a stationary corona discharge within a steady imposed external flow. Since, the macroscopic electro-drift velocity of charges in air is generally of a few hundred meter per second, whereas ionic wind flow velocity is of the order of a few meter per second, the influence of fluid advection is generally neglected resulting in a one-way coupling of the charges onto the flow. Nevertheless, when considering an adverse fluid velocity larger than ten meter per second, a one way coupling approximation falls short and a two-way coupling arises between charges drift and fluid flow. This contribution develops a perturbative two-way coupling over a multi-scaled two-domain approach based upon a non-dimensional number Mc being the ratio between the external velocity flow to the drift velocity of charges.

Electro-Aero-Dynamic (EAD) low-plasma gas flows are of interest in many applications such as particles cleaning with electro precipitators, electronic cooling, flame ignition control, plane safety against storms, plasma torches, and more recently atmospheric propulsion. In the context of plane safety against storms, Chapman [1] and Guerra-Garcia et al [2] performed wind tunnel experiments for various electrode configurations and measured the influence of a high velocity external flow, up to 200m/s on the current-voltage characteristic, both finding current's linear variation with the imposed external velocity. This finding has recently been confirmed by Grosse et al [3] at lower velocities. These observations however cannot be predicted with one-way coupling models (such as [4]), because in this framework the electrical charge transport problem producing the current is decoupled from the fluid flow. This approximation is no longer valid when the fluid velocity reaches the order of magnitude of the macroscopic electro-drift velocity of charges in air. In this contribution we propose a new two-way perturbative approach of isothermic plasma/gas flow EAD. Considering the two-domain corona-discharge region of [5], this contribution elaborates a perturbative solution for the complete EAD problem over the small parameter being the ratio of the macroscopic ionic wind velocity over the microscopic ion velocity being, in every context cited above, a small parameter that we denote Mc. This small parameter permits to build a perturbative sequence which can be solved numerically at each order, so as to obtain the electric charge density distribution, current flux, electric field, ionic wind, and propulsive features. This approach recovers the linear relation between the electric current and the flow field, as well as a very satisfactory estimation of the predicted slope, matching various experimental configurations without any adjusted parameter, given the air plasma parameters used in the literature, as in [5]. These findings support the proposed two-way EAD perturbative formulation so as to permit reliable quantitative predictions for air-plasma interactions at high speed. Furthermore, how the electric field lines are deformed by the external flow, is illustrated, in the figure below, leading to a shrinkage of charge collection zones with increasing external velocity.




**References**

[1] S. Chapman. Corona point current in wind, *J. of Geophysical Research*, 75(12), **1970**, pp :2165–2169

[2] C. Guerra-Garcia, et al. *J. of Geophysical Research*, 125, 16, **2020**, pp1-14.

[3] S. Grosse, N. Benard, E. Moreau, *J. Electrostatic*, 130, **2024**, pp103950

[4] F. Picella, D. Fabre, & F. Plouraboué, *AIAA. J.*, Vol. 62, No. 7, **2024**, pp. 2562–2573

[5] N. Monrolin & F. Plouraboué. *J. Comp. Phys.* 443:110517, **2021**

# Axisymmetric fluid streamer model with curvilinear electrodes in the AMReX environment

I. Simonović[1], D. Bošnjaković[1] and S. Dujko[1]

[1] *Institute of Physics Belgrade, University of Belgrade, Pregrevica 118, 11080 Belgrade, Serbia*

We have extended our axisymmetric fluid streamer model, that is implemented in the AMReX library, to include curvilinear electrodes by employing the AMReX inbuilt embedded boundary functionality. We have investigated the dynamics of both positive and negative streamers in the pin-to-plane electrode configuration. The verification of our code is performed by comparing its results to those of the Afivo-streamer open-source code.

Streamers are precursors of lightning leaders and arcs in nature and technology [1]. Streamers are used for purification of polluted gases and liquids, surface processing, and plasma medicine. Further optimization of these applications requires both experimental investigation and theoretical modelling of streamer dynamics.

We have developed an axisymmetric streamer model in the AMReX library [2]. AMReX is an open-source library for massively parallel scientific computing applications with block-structured adaptive mesh refinement [3]. AMReX supports both MPI and OpenMP parallelization on central processing units as well as parallelization on graphic processing units. Although AMReX is implemented in C++ it has both Fortran and Python interfaces.

Our model is based on the first-order fluid model with local field approximation. The time evolution of the number density of electrons is described by the advection-diffusion-reaction equation, while the time evolution of the number densities of positive and negative ions is described by the reaction equations. We employ the finite volume method for the spatial discretization of our model. Time integration is performed by using the second-order Runge-Kutta method.

In this work, we have extended our code to enable for the inclusion of curvilinear electrodes by using the AMReX inbuilt embedded boundary functionality. In this approach, the electrode is included as a curvilinear embedded boundary that conceptually cuts through a rectangular mesh. Thus, various electrode shapes can be generated by combining the basic shapes that are implemented in the classes which already exist in AMReX. For instance, a rod electrode can be generated as a union of a semisphere and a cylinder.

The resulting electric field is determined from the gradient of the resulting electrostatic potential, which is obtained by solving the Poisson equation. This equation is solved by employing the geometric multigrid method. We use Dirichlet boundary condition for the electrostatic potential at boundaries that are perpendicular to the applied electric field, and zero Neumann boundary condition at other boundaries.

It is important to note that the AMReX inbuilt linear operator, that is used for solving the Poisson equation and the Helmholtz equation when embedded boundaries are present, is defined only for Cartesian coordinates. For this reason, the coefficients of this linear operator must be explicitly set by the user to be equal to the metric terms for cylindrical coordinates in order to obtain the correct solution of these equations for the axisymmetric model.

Verification of our model is performed by comparing its results with the results of the open-source Afivo-streamer code [1] for both positive and negative streamers in the pin-to-plane electrode configuration.

**Acknowledgments**: This work is supported by the Science Fund of the Republic of Serbia, Grant No. 7749560, Exploring ultra-low global warming potential gases for insulation in high-voltage technology: Experiments and modelling EGWIn.

## References

[1] Teunissen, J. and Ebert, U. Simulating streamer discharges in 3D with the parallel adaptive Afivo framework. *Journal of Physics D: Applied Physics*, **50**, 474001 (2017).

[2] Simonović, I. *et al.* Axisymmetric fluid streamer model in the AMReX library. *Plasma Sources Sci. Technol.*, **33**, 085012 (2024).

[3] Zhang, W. *et al.* AMReX: a framework for block-structured adaptive mesh refinement. *Journal of Open Source Software*, **4**, 1370 (2019).

# Comparison of PIC and Experimental Pin-to-Plane Breakdown

C.H. Moore[1], L.P. Beving[1], A.K. Jindal[1], M.M. Hopkins[1], L.B. Biedermann[1], J.J. James[1], E. Bussmann[1], J.N. Tilles[1], D. Bosomtwi[1], R.J. Martinez[1] and A.S. Padgett[1]

[1] *Sandia National Laboratories, Albuquerque, NM USA*

In devices where high voltages are present, thin (≪1mm) dielectric epoxy coatings are often used to increase the standoff voltage of the air-filled gap since discharge can damage the device and/or prevent proper operation. In prior work [1] 2D electrostatic Particle-In-Cell (PIC) simulations for a 1 mm gap with various dielectric coating thicknesses found breakdown voltages that were ~3× smaller than the experimentally measured voltages. Here we will present new experimental and simulation results in order to better understand the discrepancy between the modelled and measured breakdown voltages. In particular, we will examine the sensitivity of the air gap streamer evolution to dielectric surface charging due to partial discharge as the voltage ramps up from below the breakdown voltage at 1 kV/μs.

## 1 General

In order to better aid design of devices that must holdoff high voltages, we desire a predictive modelling capability. Given that operating scales (and pressures) of devices might be small enough to be field emission driven and highly non-equilibrium, we compare the PIC code Empire to experiments in order to establish the model's credibility. The initial results in air at atmospheric pressure [1] found large (~3×) discrepancies between the simulated and measured breakdown voltages.

The Empire plasma chemistry model includes the standard streamer electron-neutral collisions, excited states, spontaneous emission, and photoionization. The simulated streamers initiate at ~30-35 kV/cm, require a sustaining field of ~6 kV/cm, and travel at ~$10^6$ m/s. All of these are in line with expected values for atmospheric pressure air and yet the experimental breakdown voltages are ~12kV compared to ~3.5kV for the simulations.

Fig. 1(a) shows a surface flashover breakdown observed at ~12 kV. The detachment of the streamer off the surface close to the tip might indicate charging of the dielectric prior to the breakdown arc. Fig. 1(b) shows the simulated streamer 1.5 ns after setting the anode to 4 kV. Fig. 1(c) shows that the dielectric surface charges during flashover; however, the simulated streamer does not detach from the surface before reaching the cathode at ~3 ns.

We will present simulations with the voltage ramped like the experiments and include cosmic ray source ionization in the gap. Thus as the voltage slowly increases, the cosmic ray source electrons will avalanche and result in surface charging of the dielectric. We will present the effect this has on the simulated streamer dynamics and breakdown voltage.

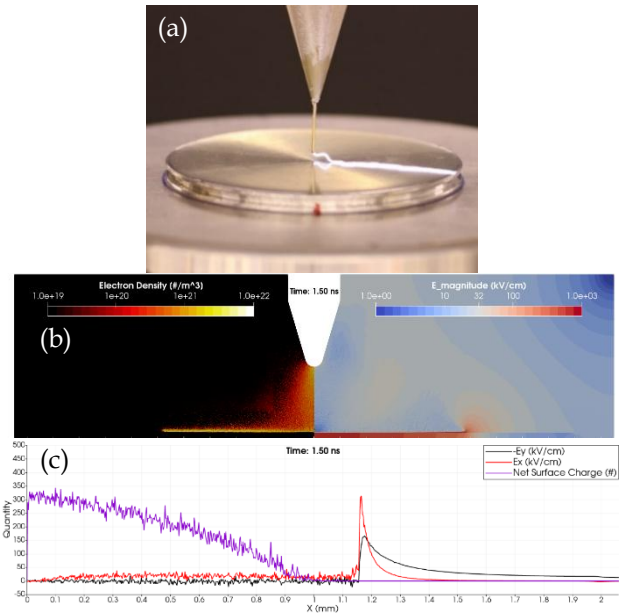



Figure 1: (a) ~12kV experimental surface flashover with thin dielectric coating, (b) Simulation showing the streamer $e^-$ density (left) and |E| (right) 1.5ns after instantaneously applying 4kV to the anode tip with an initial seed plasma present, (c) Simulated streamer E-field and net surface charge of the dielectric radially from pin.

### References

[1] C.H. Moore, A.K. Jindal, R.J. Martinez, A.S Padgett, Comparison of 2D and 3D PIC-DSMC Simulations of Pin-to-Plane Breakdown Through a Thin-Film Dielectric Coated Electrode, ESCAMPIG XXVI, Brno, 2024

### Acknowledgement

This work was supported in part by the U.S. Department of Energy under award No. DE-SC0022201, and in part by Sandia National Laboratories. Sandia National Laboratories is a multi-mission laboratory managed and operated by National Technology and Engineering Solutions of Sandia, LLC., a wholly owned subsidiary of Honeywell International, Inc., for the U.S. Department of Energy's National Nuclear Security Administration under Contract No. DE-NA0003525.

# Argon metastable densities in $CO_2/N_2/Ar$ DC glow discharges at Mars atmospheric pressures

T. Ben Slimane[1], M. Budde[2], T. Silva[1], O. Guaitella[2], V. Guerra[1]

[1] *Instituto de Plasmas e Fusao Nuclear, Instituto Superior Técnico, Universidade de Lisboa, 1049-001 Lisboa, Portugal*
[2] *Laboratoire de Physique des Plasmas (LPP), Ecole Polytechnique, CNRS, Palaiseau, France*

Laser absorption spectroscopy is applied to study the plasma chemistry in a DC glow discharge under conditions relevant to the Martian atmosphere. In this work, tunable diode laser absorption is used to measure argon metastable densities and gas temperatures in gas mixtures of $CO_2$ , $N_2$ , and Ar. Simulations using the Lisbon Kinetic (LoKI) tool are performed in parallel to validate the chemical kinetics at pressures ranging from 1 to 8 Torr allowing the extrapolation to lower argon content where the metastable measurements using absorption fails. The influence of pressure and argon content on the metastable population and kinetics is examined, bringing us one step closer to a consistent kinetic model for plasma-$CO_2$ dissociation relevant for in-situ resource utilization in future Mars missions.

## 1 Introduction

The development of sustainable in-situ resource utilization strategies is essential for permanent Mars settlement, with oxygen production being a central requirement for life support systems and return trip ascent propulsion. Given that the Martian atmosphere is composed of approximately 96% $CO_2$ , plasma-based $CO_2$ dissociation emerges as a promising alternative to conventional electrochemical processes such as MOXIE, which rely on solid oxide electrolysis cells (SOEC) [1,2]. Plasma systems present potential advantages, including a lower sensitivity to inlet gas purity, modularity, operation at low pressures without the need for gas compression, and compatibility with intermittent renewable energy sources.

In the present work, we focus on the systematic study of DC glow discharge plasmas in gas mixtures relevant to the Martian atmosphere $CO_2$/Ar, $N_2$/Ar, and $CO_2/N_2$/Ar. This study aims to improve our understanding of the plasma kinetics at pressures relevant to Mars from previous work of P. Ogloblina [3] by investigating how different mixture compositions affect the density of metastable species and the bulk gas temperature ($T_{gas}$).

## 2 Methods

The experimental campaign is carried out using a DC glow discharge plasma reactor operating at pressures between 1 and 8 Torr, representative of conditions on the Martian surface. Gas mixtures consisting of $CO_2$ , $N_2$ , and varying concentrations of Ar (from 0% to 100%) are injected into the reactor.

Tunable Diode Laser Absorption Spectroscopy (TDLAS) is used to quantify argon metastable densities (1s5 and 1s3) and measure $T_{gas}$. The reduced electric field (E/N) is measured experimentally and compared with numerical results obtained using the LoKI (Low-temperature Kinetics) simulation tool.

## 3 Results

Preliminary results demonstrate that the addition of Ar significantly influences the plasma characteristics. Higher Ar content lead to systematically lower gas temperatures. The addition of molecular gases highly reduces the Ar metastable densities and increases $T_{gas}$ in the plasma bulk. These effects are more prominent with $CO_2$ compared to $N_2$ as one would expect. The effect of the operating pressure is also examined. The experimental E/N shows a systematic decrease with the operating pressure indicating a shift in the electron energy distribution towards lower electron energies.

Comparison with simulations is underway, with preliminary results showing a good agreement between the trends in the experiments and LoKI simulation results.

**Funding acknowledgments:** The authors would like to acknowledge the support by the Portuguese FCT-Fundação para a Ciência e a Tecnologia, under funding to IPFN (DOI: 10.54499/LA/P/0061/2020, 10.54499/UIDB/50010/2020,10.54499/UIDP/50010/2020, and 10.54499/PTDC/FIS-PLA/1616/2021).

**References**

[1] Guerra. V *et al.*, J. Appl. Phys. 132, 070902 (2022); https://doi.org/10.1063/5.0098011

[2] Sanders *et al.*, AIAA 2015-4458 *AIAA SPACE* 2015 Conference and Exposition, (2015); https://doi.org/10.2514/6.2015-4458

[3] P Ogloblina *et al.*, Plasma Sources Sci. Technol. **30** 065005 (2021).

# Optimizing Ammonia Decomposition for Enhanced Hydrogen Production: A Comparative Study of Carrier Gases

S. Marin-Meana[1,2], A. Megías-Sánchez[1,2], M. Ruiz-Martin[1,2], J. Cotrino[1,2], A. González-Elipe[1], M. Oliva-Ramírez[1,2], M.C. García[3] A. Gómez-Ramírez[1,2]

[1] *Instituto de Ciencia de Materiales de Sevilla (CSIC-U. Sevilla), Av. Américo Vespucio 49, 41092 Sevilla, Spain*
[2] *Dpto Física Atómica, Molecular y Nuclear, Fac. Física, U. Sevilla, Av. Reina Mercedes s/n, 41012 Sevilla, Spain*
[3] *Dpto. de Física Aplicada, Rad. y Medicina Física, Campus de Rabanales, Univ. de Córdoba, 14071 Córdoba, Spain*

This study investigates ammonia ($NH_3$) as a sustainable hydrogen carrier using a Rotating Gliding Arc reactor for its decomposition. Results show that using nitrogen as the carrier gas improves decomposition rates over argon, with optimal hydrogen production at specific ammonia flow rates. The findings underscore ammonia's potential in hydrogen energy systems and offer insights for optimizing reactor conditions, contributing to clean energy advancements and hydrogen transport solutions.

## 1 Introduction

The increasing demand for clean energy has heightened interest in hydrogen as a sustainable fuel, necessitating efficient carriers. This study investigates ammonia ($NH_3$) as a viable hydrogen carrier due to its energy density and established infrastructure. Using a Rotating Gliding Arc reactor, the research herein focuses on ammonia decomposition into hydrogen and nitrogen, examining the effects of carrier gases ($N_2$ and Ar) on efficiency. By assessing ammonia flow rates, power consumption, and hydrogen yield, the study aims to optimize conditions for enhanced hydrogen production.

## 2 Methods

Experiments used a Rotating Gliding Arc reactor with a semi-ellipsoidal electrode for ammonia ($NH_3$) decomposition, with $NH_3$ at 0.75 L/min and carrier gases ($N_2$ and Ar) at 9.25 L/min. Mass flow controllers regulated gas flows, and power consumption and decomposition rates were measured. Ammonia flow rates varied from 0.25 L/min to 2.25 L/min to assess their impact on hydrogen yield and energy efficiency. Optical emission spectroscopy and mass spectrometry analyzed reaction dynamics to optimize conditions for enhanced hydrogen production.

## 3 Results and Conclusion

Figure 1 indicates that ammonia concentration impacts hydrogen production and energy efficiency. Hydrogen yield peaked at 1 L/min for nitrogen ($N_2$) and increased linearly for argon (Ar) up to 2.25 L/min. The percentage of ammonia decomposed decreased from 40% to 14% in the $N_2$ system, while the Ar system remained stable. Power consumption was constant for $N_2$ but rose with ammonia flow in the Ar system, emphasizing the need to optimize ammonia concentration for better hydrogen output and efficiency.

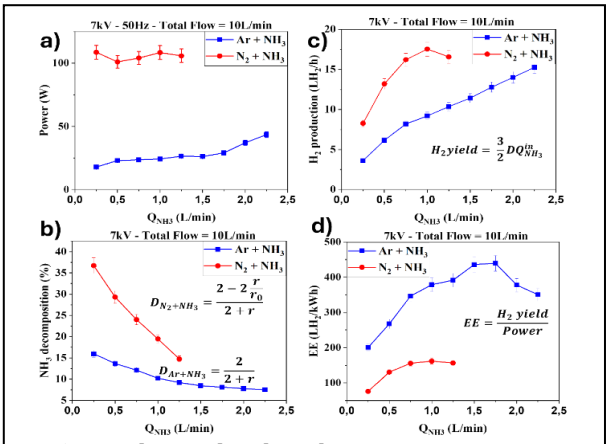



**Fig. 1**. Electrical and production parameters as a function of the input ammonia flow a) Power , b) $NH_3$ decomposition rate, c) $H_2$ yield, d)

Thus, ammonia ($NH_3$) is an effective hydrogen carrier, with nitrogen ($N_2$) providing higher decomposition rates and hydrogen yields than argon (Ar). While increasing ammonia flow rates improved hydrogen output, efficiency plateaued at higher levels. The Ar + $NH_3$ system showed lower power consumption, indicating better energy efficiency.

**Acknowledgements**

The authors acknowledge projects PID2020-114270RA-I00, PID2023-147916NA-I00, and PID2020-112620GB-I00 by MCIN/AEI/10.13039/501100011033, project TED2021-130124A-I00 by AEI/10.13039/501100011033/Unión Europea Next Generation EU/PRTR. M. M. Oliva-Ramírez received support from Grant IJC2020-045087-I, and S. Marín Meana from Grant PRE2021-100465, both funded by MCIN/AEI and the European Union NextGeneration EU.

**References**

[1] Młotek, M., et al. Chem. Process Eng., 2024, 45(3), e67.

# Numerical investigation of stability of pin-to-plane negative corona in air

N. G. C. Ferreira[1,2], P. G. C. Almeida[1,2], A. Eivazpour Taher[3], G. V. Naidis[4], and M. S. Benilov[1,2]

[1] *Departamento de Física, Faculdade de Ciências Exatas e da Engenharia, Universidade da Madeira, 9000 Funchal, Portugal*
[2] *Instituto de Plasmas e Fusão Nuclear, Instituto Superior Técnico, Universidade de Lisboa, 1041 Lisboa, Portugal*
[3] *University of Antwerp, Belgium*
[4] *Joint Institute for High Temperatures, Russian Academy of Sciences, Moscow 125412, Russia*

This work reports a numerical investigation of low-current negative corona, in a point-to-plane discharge configuration at atmospheric-pressure air, with emphasis on thresholds for appearance of Trichel and stochastic pulses. Obtained results are in good agreement with a classic experiment.

## 1 Summary

The ignition of DC corona discharges has been studied significantly and is still a hot topic today. In negative DC coronas, it is commonly assumed that Trichel pulses appear immediately upon the inception of the discharge, or alternatively, that a few large stochastic current pulses are seen in the current waveform. Some works reported the observation of an initial pulseless mode at inception of DC coronas. The ignition of DC corona discharges was theoretically investigated recently, and the stability of DC discharges at inception has been studied numerically for a negative corona between concentric cylinders in air: the theory, the linear stability analysis, and the time-dependent modelling all show that the negative corona is stable, i.e., pulseless, immediately after the ignition [1]. The present work studies the width of the stability range for the pin-to-plane geometry, which can be useful before performing experiments that aim to study different regimes of the negative corona. It also provides insight about stochastic Trichel pulses. After the negative corona loses stability, the current evolution shows, after a small region of harmonic oscillations, pulses. These can be of small amplitude or regular Trichel pulses. In certain conditions, an ionization wave may develop at the vicinity of the cathode and propagates towards it. Modelling results have been compared with a classic experiment [2] and are in good agreement with experimental data, both for the ignition voltage and the voltage stability limit of the negative corona discharge, as shown in Figure 1. Full results will be given at the conference.

## 2 The model

The model comprises equations of conservation and transport of charged particles and the Poisson equation. Also included in the model are equations governing the photoionization source term in the framework of the three-exponential model. The system of equations is supplemented by standard boundary conditions. Results reported in this work were obtained with the use of commercial software COMSOL Multiphysics®.

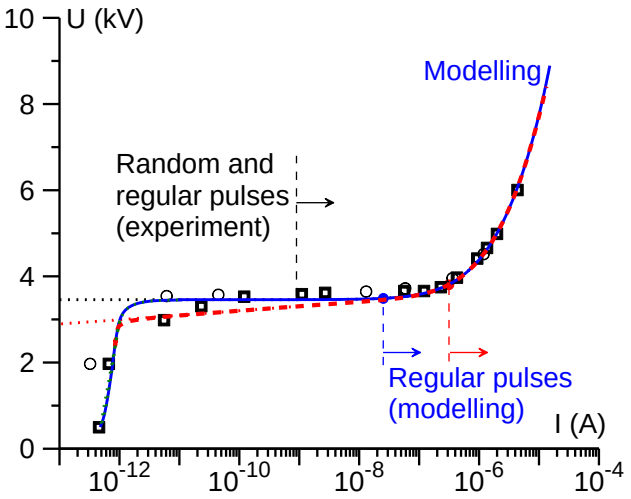



Figure 1: Experimental (points) [2] and calculated (lines) CVC for negative rod-to-plane geometry in atmospheric pressure dried air. Simulations with (dashed) and without (solid) field emission.

## 3 Acknowledgements

The work at UMa was supported by FCT of Portugal under Project Nr. IPFN/UID/50010/2025.

**References**

[1] P G C Almeida, G V Naidis and M S Benilov, *Phys. Rev. E* **110**, 045201 (2024).
[2] H. W. Bandel, *Phys. Rev.* **84**, 92 (1951)

# Optimisation study of a DBD for $CO_2$ conversion using in-depth electrical analysis

M. Buddhadasa[1]

[1]*Max Planck Institute for Plasma Physics, Boltzmannstrasse 2, Garching, Germany*

Electrical properties of a cylindrical dielectric barrier discharge reactor operated under pure $CO_2$ are investigated via an in-depth analysis of Lissajous figures and I-V profiles in order to systematically optimise process conversions and energy efficiencies. Influence of various operating parameters including pressure, discharge power, gas flow rate and reactor configurations defined by discharge gap and length are explored. Conversions up to 25 % and energy yields up to 15 $g_{co}$/kWh are discussed.

## 1 Motivation

While the many interrelated operating parameters that can be readily modified in a DBD can render a vast array of discharge conditions and potentially, discharge chemistries, making the analysis complicated, it gives a significant opportunity to tune reactor performance following careful investigation. $CO_2$ conversion in DBDs is considered to occur via electron impact processes, the dominant mechanism being electron impact dissociation, which are characteristic of the high E/N typically observed in these reactors. The efficiency of the process relies upon how well the energy is transferred to the dominant mechanisms avoiding losses in gas heating as well as minimising reverse reactions leading to reformation of $CO_2$. Electrical characterisation studies can potentially help understand the efficiency via the analysis of discharge voltage, charge transferred, discharging fraction and so on [1, 2].

This work aims to optimise reactor performance by correlation with electrical properties of a pure $CO_2$ DBD, primarily, through rigorous analysis of Lissajous figures and I-V profiles over several operating conditions, such as, power, flow rate, pressure, temperature, discharge gap and length.

## 2 Experiment

The cylindrical DBD setup consists of a stainless steel (SS) mesh, as the high voltage electrode, tightly wrapped around a quartz tube. Parasitic discharges are minimised by the choice of a very fine cloth-like mesh, tight wrapping and the application of a silicone paste at the mesh edges. The ground electrode is a SS rod centred within the tube. Parasitic capacitance of the setup is accounted for in the analysis of Lissajous figures. $CO_2$ conversion is measured downstream in real-time using mass spectrometry.

Figure 1a shows the influence of pressure and flow rate on $CO_2$ conversion and energy yield for a discharge gap of 1 mm and length 23 mm, at a discharge power of 30 W. For a constant standard volumetric flow rate (273 K, 1 atm) and thus, constant energy available per molecule (SEI), similar conversions and therefore, energy yields are observed at both the low and high pressures, despite the higher E/N and charge transferred per half cycle ($\Delta q_{dis}$) at the low pressure (Fig. 1b). However, at similar residence times ($\tau$), higher conversions are observed at 200 mbar, where SEI is also greater, albeit the lower energy yield. While this indicates a dependence on SEI, the significantly lower E/N and $\Delta q_{dis}$ at the high pressure suggest possible differences in reaction pathways between the two regimes. Additionally, current profiles (not shown) reveal a significant reduction in current peak intensities and longer discharging times at 200 mbar, corresponding to a more diffused discharge, as also observed visually. These findings highlight the importance of correlating discharge electrical properties with conversion efficiencies in optimising the process.

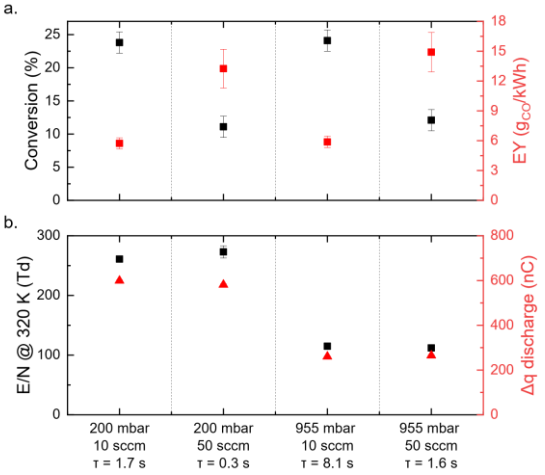



Figure 1: $CO_2$ conversion and energy yield (a) and time-space averaged reduced E-field (E/N) and charge transferred per half cycle ($\Delta q_{dis}$) (b). SEI 43 and 8.6 eV/molecule at 10 and 50 sccm, respectively.

### References

[1] Rad, R. H. et al. Chemical Engineering Journal, 456, 141072 (2023).
[2] Ozkan, A. et al. J. Phys. D: Appl. Phys., 50, 084004 (2017).

# Synergistic control of radical generation in a radio frequency atmospheric pressure plasma jet via voltage waveform tailoring and structured electrodes

M. Vass[1,2], X. Wang[1], I. Korolov[1], T. Mussenbrock[1] and J. Schulze[1]

[1] *Chair of Applied Electrodynamics and Plasma Technology, Ruhr-University Bochum, 44780 Bochum, Germany*
[2] *Institute for Solid State Physics and Optics, HUN-REN Wigner Research Centre for Physics, 1121 Budapest, Hungary*

The spatio-temporal dynamics of electron power absorption and radical species densities are studied in an RF-driven atmospheric pressure microplasma jet with a structured electrode configuration, operated in helium with a 0.1% admixture of oxygen and driven by tailored "peaks-" and "valleys-" waveforms synthesized from four harmonics (with a base frequency of $f_\mathrm{b} = 13.56$ MHz) at 1 W (500 $V_\mathrm{pp}$). Using (i) two-dimensional fluid simulations and (ii) experimental diagnostics (Phase-Resolved Optical Emission and Tunable Diode Laser Absorption Spectroscopy), we demonstrate that voltage waveform tailoring enables precise control of plasma penetration into trenches, allowing spatially selective radical generation.

Radiofrequency (RF)-driven micro-atmospheric pressure plasma jets are widely utilized in applications such as surface processing, sterilization, and plasma medicine due to their ability to efficiently generate reactive species [1]. Optimizing these processes requires precise control over radical generation. In this work, we investigate the COST reference microplasma jet [2], which operates in a helium-oxygen mixture (99.9%/0.1%) and features a structured electrode design with multiple trenches on both the top and bottom electrodes. Previous studies [3] have shown that under single-frequency excitation, this configuration enhances radical production near and inside the trenches due to the current focusing effect, which locally increases electron power absorption. Additionally, [4] reported that in a non-structured plane-parallel electrode configuration, voltage waveform tailoring (VWT) alone can enhance radical generation efficiency.

Building upon these findings, this work explores the synergy between voltage waveform tailoring and structured electrodes in controlling plasma dynamics. Using "peaks-" and "valleys-" waveforms synthesized from four harmonics (with a base frequency of $f_\mathrm{b} = 13.56$ MHz), we analyze plasma penetration into trenches and the spatial localization of radical generation. The plasma is driven at 500 V peak-to-peak (1 W). Simulations, conducted with the 2D fluid code nonPDPSIM [5], solve continuity equations for neutral and charged species (using the local mean energy approximation for electrons) and the compressible Navier-Stokes equations for the gas flow. The discharge model follows [3], including 7 charged and 8 neutral species with 19 electron impact and 91 chemical reactions. Experimentally, Phase-Resolved Optical Emission Spectroscopy (PROES) measures the excitation rate of the He-I $(3s)^3S_1$ level to the ground state, while Tunable Diode Laser Absorption Spectroscopy (TDLAS) determines the density of He-I $2\,^3S_1$.

The results demonstrate that waveform tailoring precisely controls plasma penetration into electrode trenches, with the plasma entering either the top or bottom trench during the voltage peak. This enhances local electron power absorption, facilitating the efficient generation of high-energy threshold species like helium metastables, as confirmed by PROES and TDLAS data. In contrast, lower-energy threshold radicals such as atomic oxygen are predominantly produced near the opposing electrode, where the sheath persists longer. This synergy enables precise plasma localization, offering new possibilities for targeted plasma treatment.

## References

[1] Sushil Kumar KC *et al. J. Phys. D: Appl. Phys.*, **58**, 143006 (2025).
[2] Golda, J. *et al. J. Phys. D: Appl. Phys.*, **49**(8), 084003 (2016).
[3] Liu, Y. *et al. Plasma Sources Sci. Technol.*, **32**(2), 025012 (2023).
[4] Vass, M. *et al. Plasma Sources Sci. Technol.*, **33**(11), 11LT01 (2024).
[5] Norberg, S. A. *et al. Plasma Sources Sci. Technol.*, **24**(3), 035026 (2015).

# Self-organized luminous pattern formation in a pin-to-plate DC glow discharge generated in helium

T. Miyazaki, K. Sasaki and N. Shirai

*Division of Applied Quantum Science and Engineering, Hokkaido University, Sapporo, Japan*

In this work, we generated a pin-to-plate DC glow discharge in helium and investigated experimental conditions where self-organized luminous patterns are formed above the anode. The patterns tended to form at a higher pressure and a longer distance between the electrodes. The same trend was observed when $N_2$ and Ne were admixed into helium. It was found that the *pd* product with *p* and *d* being the pressure and the electrode distance was a key parameter for the luminous pattern formation.

## 1 Introduction

Self-organized luminous pattern formation is observed above the anode of atmospheric-pressure DC glow discharge under certain conditions. However, the detailed pattern formation mechanism has not been understood well. To understand the mechanism, it is necessary to figure out what the key parameter is. Recently, we reported the gas density or temperature may be an important parameter in the discharge generated in ambient air [1]. In many studies, liquid is used as the anode, but it is not clear whether the liquid plays an important role in the pattern formation. There are some reports on the pattern formation in noble gases although the discharge configurations are different from ours [2,3]. Therefore, we expected that the pattern could form in helium also in our pin-to-plate electrode configuration. In this work, we report the results observed in helium DC glow discharges and consider what the key parameter is based on the results.

## 2 Experimental procedures

A DC glow discharge was generated in a chamber filled with helium by applying a DC high voltage between a brass cathode (pointed like a pencil tip) and a metal plate anode. The gas inside the chamber was first evacuated below a few Torr using a diaphragm pump, and then helium gas was introduced to set the pressure inside the chamber. The pressure inside the chamber (*p*: 0.1-1.0 atm), the discharge current (*I*: 1-80 mA), and the distance between the electrodes (*d*: 1-12 mm) were varied to investigate experimental conditions for the pattern formation. In addition, the same experiment was repeated in He-$N_2$ and He-Ne mixtures when the partial pressure of $N_2$ and Ne were a few percents.

## 3 Results and discussion

Figure 1 shows example pictures of the discharges with the pattern formation in helium (Fig. 1(a)), in He-$N_2$ mixture (Fig. 1(b)), and in He-Ne mixture (Fig. 1(c)). To the best of our knowledge, this is the first observation of the luminous pattern formation in pure helium at pressures of 0.1-1 atm. The pattern tended to form at a higher pressure and a longer distance between the electrodes. Figure 2 shows the relationship between the *pd* product and the discharge voltage in the helium discharge at various discharge currents. The plots were obtained at pressure of 0.2, 0.6 and 1.0 atm and various electrode distances between 1 and 12 mm. The pattern formation was observed at *pd* larger than approximately $10^2$ Pa · m. At *pd* products larger than the threshold, we observed the increase in the discharge voltage when keeping the discharge current. It was found that the *pd* product is a key parameter for the luminous pattern formation.




Fig. 1 Pictures of luminous patterns in (a) He, (b) He + 1 % $N_2$ and (c) He + 1 % Ne discharges.

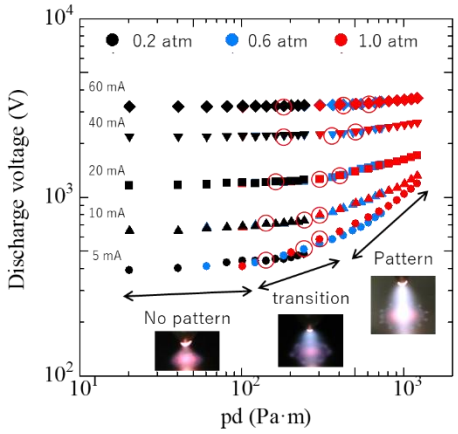



Fig. 2 Relationship between the discharge voltage and the *pd* product in helium discharge. Luminous pattern formations were observed at *pd* products larger than the thresholds indicated by red circles.

## References

[1] T. Miyazaki, *et al*., Plasma Sources Sci. Technol. 33, 115007 (2024)
[2] K. Schoenbach, *et al*., Plasma Sources Sci. Technol. 13, 177 (2004).
[3] W Zhu, *et al.*, Plasma Sources Sci. Technol. 23, 054012 (2014),

# Parametric study of NO reduction in a confined RF plasma in atmospheric pressure helium

T. Zhu[1], M. Baeva[1], F. Sigeneger[1], S. Dongawar[2], P. Bruggeman[2]
[1]*Leibniz Institute for Plasma Science and Technology (INP), Greifswald, Germany*
[2]*University of Minnesota, Minneapolis, USA*

The reduction of NO in a helium plasma jet at atmospheric pressure is studied by a plug flow model and by experiments. The plasma is sustained by an RF voltage which is supplied to cylindrical electrodes. Some short-lived species are generated in the plasma region. As such, metastable helium atoms and excimers predominantly cause the reduction of NO and the generation of long-lived species $N_2$, $O_2$, $N_2O$ and $NO_2$. The dependences of this conversion on power, flow rate and gas composition are investigated.

## 1. Introduction

Non-thermal plasmas operated at atmospheric pressure can be used to efficiently remove unwanted compounds from exhaust gases, as most of the supplied energy is transferred to energetic electrons, while the heating of the gas remains low. The reduction of NO by an RF helium plasma jet in a confined cylindrical geometry is investigated here using a plug flow model and LIF measurements.

## 2. Methods

The helium plasma jet is operated in a capillary at atmospheric pressure. The RF power of a few watts is supplied to ring-shaped electrodes with a gap of 5 mm. The power is approximated by an axial profile in the active region. LIF measurements deliver axial profiles of the NO density along the central region of the capillary. A plug flow model was developed to describe the plasma chemistry using rate equations for relevant species similarly to those in [1-3], the electron energy balance, and the gas heating. The model comprises 33 species which are involved in 305 volume and 23 surface reactions. The computed temporal evolution is converted into spatial profiles in terms of the plug-flow concept.

## 3. Results and discussion

Investigations have been performed for varying power P, gas flow rate Q, and initial gas composition. Fig. 1a shows the reduction of NO for a mixture of 20 ppm NO and 2.25 slm He. The active region is marked in grey color. Reasonable agreement between experimental and modelling result was obtained. The observed deviations can be explained by limitations of the plug flow model, e.g., the experimentally observed drop and the subsequent recovery are caused by radial inward diffusion which cannot be resolved by the plug flow model. Fig. 1b shows profiles of some short-lived species which cause the production of the long-lived species $O_2$, $N_2$, $N_2O$, and $NO_2$. The degradation of NO is mainly due to collision with $He^*$ and $He_2^*$ as well as dissociating electron collisions. The neutralization of $NO^+$ at the wall represents a competing gain process.

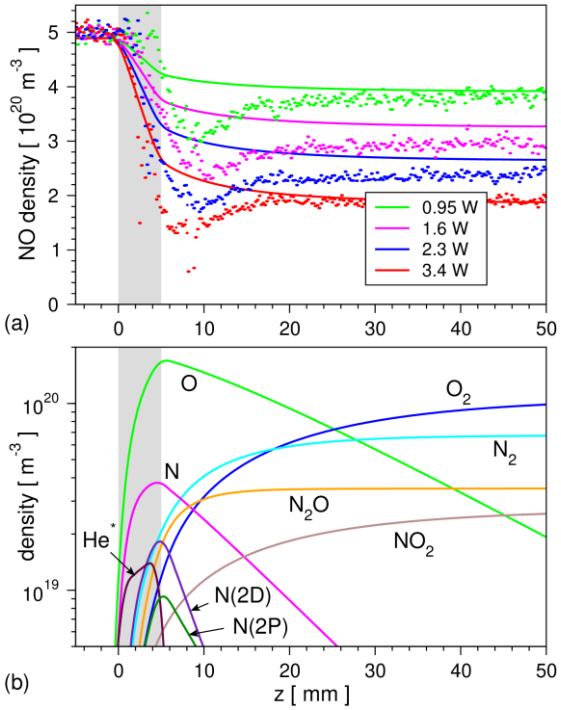



**Fig. 1**. Results for a mixture of 20 ppm NO and 2.25 slm He: (a) Reduction of NO obtained by the model and LIF for various power input, (b) Predicted densities of dominant neutral species for a power P = 3.4 W.

**References**

[1] D. X. Liu et al., *Plasma Sources Sci. Technol.*, **19**, 025018 (2010).
[2] B. Sun et al., *Plasma Sources Sci. Technol.*, **28**, 035006 (2018).
[3] Y. F. He et al., *Plasma Sources Sci. Technol.*, **30**, 105017 (2021).

# RF Magnetron Plasma nitriding of quartz

Stephen Muhl[1], Julio Cruz[1], Enrique Camps[2]

[1] *Depto. de Materiales de Baja Dimensionalidad, Instituto de Investigaciones en Materiales, Universidad Nacional Autónoma de México, CDMX, México*
[2] *Depto. de Física, Instituto Nacional de Investigaciones Nucleares, Carret. Mex-Tol. s/n, La Marquesa, Ocoyoacac, Edo. México C.P 52750, Mexico*

**1** Plasma nitriding is a widely studied and well-established technique for modifying the surface of metals to improve their mechanical and tribological properties, such as hardness and wear resistance. Normally, plasma nitriding involves the use of a low-pressure glow discharge of nitrogen or a mixture of nitrogen and hydrogen, where the metal component to be treated is the cathode and the chamber wall is the anode. The low-pressure plasma (15–1500 Pa) is produced by the application of a DC potential (0.3–1.0 kV) and contains nitrogen ions, which are accelerated towards the cathode and implanted in the surface of the metal. The treatment time, surface concentration of nitrogen, and temperature of the metal component determines the depth and gradient of the nitride layer, but tens of microns are often produced. The same process cannot directly be used to nitride insulators since such materials cannot be used as a cathode in a DC plasma.

We have developed a variant of the normal plasma nitriding scheme where the discharge is produced by applying an RF potential and the piece to be nitrided is mounted on a magnetron cathode. This is the same as a RF magnetron sputtering system. Previous studies have shown that the DC voltage bias generated on the surface of an insulting target used in a RF magnetron sputtering cathode depends on the many factors: the relative areas of the anode and cathode, the applied RF power, the gas pressure and composition, and the degree of matching of the impedance of the electrical supply to the impedance of the plasma. We have measured the DC bias potential and the rate of sputtering of a quartz target mounted on a 2” MAK magnetron cathode in a pure nitrogen gas discharge as a function of the area of the anode, the gas pressure, the applied power, and the degree of matching indicated by the ratio $RF_R$ (Reflected Power) / $RF_F$ (Forward Power). Using conditions which produced a minimum etching of the target, we generated samples nitrided for 40, 80 and 120 min, and also under different conditions of mismatch of the matching network. We present the dimensions and composition of the nitride layer measured using XPS and RBS, and the hardness and wear resistance of these layers.

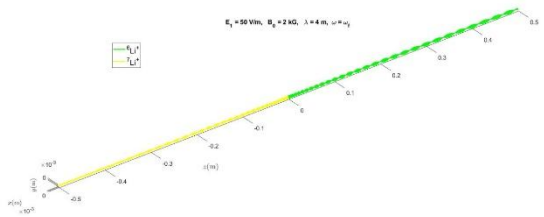
# Mass separation using rotating electric and magnetic fields

A. Fruchtman[1] and G. Makrinich[1]

[1] *Department of Physics, Holon Institute of Technology, Holon 58102, Israel*

Rotating electric and magnetic fields, parallel to each other and both perpendicular to a steady magnetic field, generate a ponderomotive force on ions along the magnetic field. The direction of the force along the magnetic field depends on whether the ion cyclotron frequency is larger or smaller than the fields rotation frequency. Thus, by tuning either the rotation frequency or the intensity of the steady magnetic field, ions of different mass could be pushed in opposite directions. This process could be used for mass separation. Two ways are described for realizing this process. One way is to excite a planar standing electromagnetic wave. A second way is to generate the desired rotating fields by a set of current-carrying coils and a set of biased electrodes. The generated rotating fields and the ion trajectories will be described.

Mass separation is an important process for a variety of societal needs [1]. For example, $Li^6$, crucial for generating tritium for fusion, has to be separated from $Li^7$, the majority isotope. Such mass separation occurs when rotating electric and magnetic fields, parallel to each other and both perpendicular to a steady magnetic field, generate a ponderomotive force on ions along a uniform steady magnetic field. The direction of the force along the magnetic field depends on whether the ion cyclotron frequency is larger or smaller than the fields rotation frequency. Thus, by tuning either the rotation frequency or the intensity of the steady magnetic field, ions of different mass could be pushed in opposite directions [2]. In a planar standing electromagnetic wave, the electric and magnetic fields are parallel to each other (in difference from travelling wave). Therefore, such standing waves of an appropriate frequency exert the desirable ponderomotive force of a varying direction. Indeed, we have recently studied the trajectory of an ion under the forces by such waves [3]. Figure 1, taken from Ref. [3], shows how the two-lithium isotope-ions are pushed in opposite directions.



However, exciting such standing waves in a plasma (like the shear Alfven wave) is difficult, and the wave magnetic field is weak, leading to a weak ponderomotive force. We examine a second way for generating the electric and magnetic field. We design sets of biased electrodes and current-carrying coils that generate vacuum electric and magnetic fields. Two pairs of coils and two pairs of electrodes generate rotating electric and magnetic field at a central point between the two pairs. However, away from that central point, the fields vary and are not uniform. Such gradients in the electric and magnetic fields could generate undesirable drifts. We show an ideal configuration that generates rotating electric and magnetic fields that are **uniform** across a cylinder cross section. We then seek a realistic configuration of coils and electrodes that approximates the ideal configuration. The vacuum fields may not penetrate a dense plasma. In order for the fields to penetrate, the plasma density should be low enough. The yield can be increased though by increasing the electric and magnetic fields introduced by the external coils and electrodes.

In the talk, we will describe particle trajectories in the specified fields and examine the effect of field gradients on the separation mechanism.

**References**

[1] S. Zweben, R. Gueroult, and N. J. Fisch, Plasma mass separation, *Phys. Plasmas* **25**, 090901 (2018).

[2] S. Weibel, Separation of isotopes, *Phys. Rev. Lett.* **44,** 377 (1980).

[3] A. Fruchtman and G. Makrinich, Ion dynamics in standing electromagnetic wave, *Phys. Plasmas* **31**, 043502 (2024).

XXXVI ICPIG, July 20–25, 2025, Aix-en-Provence, France Topic number 6,8

# Combining Infrared transmission and Raman scattering for the fundamental study of $CO_2$ plasma – surface interaction : *in situ* probing of $CeO_2$ surface and bulk properties

D. Sadi[1], K. Polprasarn[1], O. Guaitella[1], and D. Pai[1]

[1] *Laboratoire de Physique des Plasmas (LPP), CNRS, Sorbonne Université, Université Paris Saclay, École Polytechnique, Institut Polytechnique de Paris, 91128 Palaiseau, France*

The combination of non-thermal plasmas with catalytic materials enhances the efficiency and selectivity of gas conversion processes. Cerium oxide, known for its redox properties, oxygen mobility, and storage capacity, plays a key role in catalysis. However, its interaction with NTPs is complex and not well understood. While $CeO_2$ has been studied using XRD, TEM, and Raman spectroscopy, investigations under plasma exposure—especially with simultaneous gas-phase characterization—are rare. Here, we employ a well-characterized DC glow discharge to perform an *in situ* study of both gas-phase and surface interactions using FTIR, OES, and Raman spectroscopy. Time-resolved IR studies indicate that carbonate formation on $CeO_2$ is more complex than expected from thermal effects alone. Complementary Raman spectroscopy, which provides insight into lattice expansion and oxidation states, reveals that atomic oxygen species significantly impact surface defects, influencing carbonate adsorption and desorption.

## 1. Raman Scattering

The Raman spectra of $CeO_2$ exhibit a primary phonon mode at ~460 $cm^{-1}$ (Ce-O wagging) and a smaller peak around 1189 $cm^{-1}$, attributed to the convolution of a second-order mode of Ce-O and O-O bonds in superoxides formed on the surface, as seen on Fig 1. Stokes and anti-Stokes peaks provide insights into lattice structure via intensity ratio, peak position, and broadening [2]. Upon oxygen plasma exposure, an additional lattice expansion beyond thermal effects is observed, indicating the formation of oxygen vacancies. This vacancy formation strongly correlates with the absolute flux of atomic oxygen at the surface [3].

## 2. *In Situ* IR Transmission

$CO_2$ gas and $CO_2$ plasma exposure induce surface modification including carbonate species formation, monitored via *in situ* infrared (IR) transmission spectroscopy [1] as seen on Fig. 2. Time-resolved measurements allows the study of the key parameters governing carbonate adsorption/desorption kinetics and equilibrium surface coverage.

## 3. Combined Interpretation

The combined Raman and IR analyses highlight the critical role of atomic oxygen in generating oxygen vacancies and surface oxygen species. Pre-existing vacancies seems to promote carbonate formation upon $CO_2$ exposure. Under $CO_2$ or $O_2$ plasma, carbonate kinetics and coverage strongly depend on atomic oxygen, suggesting plasma-assisted desorption is primarily chemically driven rather than controlled by ionic bombardment or thermal effects.

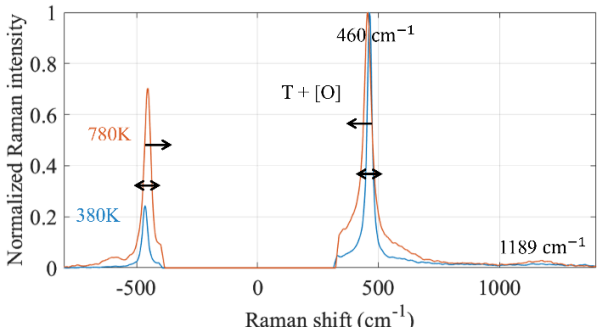



Fig 1 : Raman scattering spectra deformation of $CeO_2$ under controlled heating, using in situ spectrometer developed by Polprasarn [4]

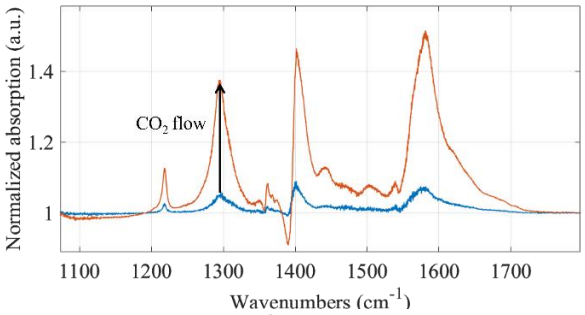



Fig 2 : *In situ* IR spectra of carbonate bands appearing on the $CeO_2$ surface under $CO_2$ gas exposure

## References

[1] C Garcia-Soto et al. *Plasma Chemistry and Plasma Processing, 2024.*

[2] Stéphane Loridant, *Catalysis Today*, 373:98–111, 2021.

[3] Vladimir V Pushkarev, et al. *The Journal of Physical Chemistry B*, 108(17):5341–5348, 2004.

[4] Polprasarn, K. et al, XXXVI ICPIG, July 20-25, 2025, Aix-en-Provence, France

# Time-resolved spectroscopic investigation of $N_2/H_2$ low-temperature plasmas

L. Maestri[1], R. Engeln[2,3] and L. M. Martini[1]

[1]*University of Trento, Department of Physics, Trento, Italy*
[2]*ASML Holding N.V., Veldhoven, The Netherlands*
[3]*Eindhoven University of Technology, Eindhoven, The Netherlands*

This work explores the dynamics of transient plasmas in $N_2/H_2$ mixtures relevant to EUV lithography. Using time-resolved optical emission spectroscopy (TR-OES), we analyse the evolution of excited states and gas temperature following nanosecond pulsed discharges. The findings provide insight into the formation of stable species, such as ammonia, and the role of reactive intermediates, with potential applications in both lithography and sustainable ammonia production.

## 1 Introduction

In extreme ultra-violet (EUV) lithography machines, a pulsed EUV-induced non-equilibrium plasma is generated in nitrogen-hydrogen mixtures. In highly transient environments, reactive species (e.g. molecular and atomic excited states and radicals) may form and lead to stable products. Understanding the process of converting $N_2$ and $H_2$ into stable species, such as ammonia, is crucial for several advanced technological processes relevant for EUV lithography machines. In addition, understanding the complex chemistry/physics of $H_2/N_2$ plasma and the mechanisms of $NH_3$ formation can promote the development of new technologies that convert $N_2$ into ammonia for renewable electricity storage. The study of transient non-thermal plasmas requires using non-invasive diagnostic techniques, such as time-resolved optical emission spectroscopy (TR-OES) [1, 2]. In this contribution, we will present the results of the spectroscopic investigation of plasmas generated by applying a nanosecond voltage pulse in $N_2$ and $H_2/N_2$ mixtures.

## 2 Experimental methods

TR-OES measurements were performed in a pin-to-plate configuration at pressures ranging from a few to hundreds of millibars. Emission spectra were measured using an intensified CCD camera at the exit of a 300 mm spectrograph with a minimum exposure time of 2.5 ns. The population distribution of the $C^3\Pi_u$ state of N2 and the translational temperature after a discharge pulse were determined from the emission of the second positive system (SPS, $C^3\Pi_u \rightarrow B^3\Pi_g$ transition). The emission from the hydrogen's Balmer series has been collected and analysed in the case of $H_2/N_2$ plasma. The experimental emission spectra for molecular species have been fitted to infer the emitting states' rotational and vibrational population distributions.

## 3 Results

An example of experimental and fitted SPS emission of $N_2$ for the vibrational transitions with $\Delta\nu = \nu' - \nu'' = -2$ and $\Delta\nu = -3$, and first negative system of $N_2^+$ with $\Delta\nu = 0$ are presented in Fig. 1.

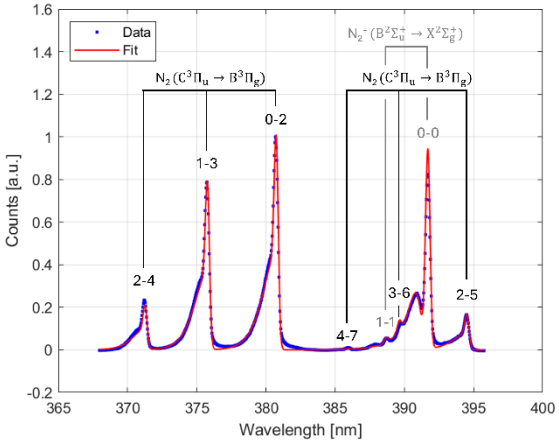



Fig. 1: OES data and relative fit for the $N_2$ second positive system and $N_2^+$ first negative system bands.

Results will be presented on the time evolution of the vibrational population distribution of $N_2$'s $C^3\Pi_u$ state, as well as the gas temperature in relation to the discharge energy and repetition rate. The potential impact of reactive species on the formation of stable molecules will be discussed.

**References**

[1] Richard Engeln et al 2020 Plasma Sources Sci. Technol. 29 063001.
[2] M Ceppelli et al 2021 Plasma Sources Sci. Technol. 30 115010.



Public

# Multi-diagnostic of dust growth in a capacitive $Ar/C_2H_2$ plasma

R. J. Peláez[1], V. J. Herrero[1], M. Jiménez-Redondo[2], B. Maté[1], I. Tanarro[1]

[1] *Instituto de Estructura de la Materia, IEM-CSIC, Serrano 123, 28006 Madrid, Spain.*
[2]*Max-Planck Institut für Extraterrestrische Physik, Gißenbachstraße 1, Garching, 85748, Germany*

The production of nanoparticles in acetylene reactive plasmas is a subject of current interest due to their potential application in functional materials and to the likely similitude of these particles with carbonaceous cosmic dust grains. In this work, capacitively coupled $Ar/C_2H_2$ RF discharges have been studied using a variety of complementary diagnostic tools including light scattering, emission spectroscopy, and mass spectrometry of the plasma, as well as ex-situ electron microscopy and infrared spectroscopy of the nanoparticles. The combination of data from the various techniques provides a comprehensive picture of the process of particle growth and of the chemical composition of both the gas and solid phases.

## 1 Introduction

Reactive plasmas, characterized by extensive polymerization and particle formation [1], find widespread application both in basic research and in technology where they are used for thin film deposition, and in the manufacturing of electronic devices. Moreover, hydrocarbon dust produced in acetylenic plasmas is currently taken as a laboratory analogue of interstellar carbonaceous dust [2]. In this work [3] we have carried out an extensive study of the growth of nanoparticles (NPs) in $Ar/C_2H_2$ RF discharges using a panoply of experimental techniques. The combination of multiple diagnostics tools provides a global picture relating plasma properties and particle formation.

## 2. Results

The plasma reactor is described in [3]. Dusty plasmas are produced between the electrodes of a capacitively coupled $Ar/C_2H_2$ RF discharge (13.56 MHz, 15W). The lower electrode is grounded. A mixture of $C_2H_2$ (2 sccm) and Ar (5 sccm) giving a 0.22 chamber pressure is used as fuel gas. The behaviour of the plasma is monitored with different on/off intervals.

Polarized-sensitive laser light scattering (PSLLS) is employed in combination with light extinction measurements to derive time-resolved bidimensional distributions of NP sizes and densities. Diameter growth rates of tens of nm/s are observed in the first seconds (t =1-3 s). This time interval, culminating with diameters of ≈ 100 nm, corresponds to the early stages of particle formation, characterized by nucleation and coagulation, as corroborated by the evolution of the self-bias and by mass spectrometric measurements showing the growth and decay of polyynes (e.g. $C_4H_2$), which carry the polymerization chain. The growth rate stays on average below 4 nm/s for t > 4s when accretion dominates. For the longest plasma lifetime studied (14 s), diameters d ≈ 130 nm and particle densities, $n_{dust} \approx 4\times10^8$ cm$^{-3}$ are reached. Ex-situ secondary electron microscopy (SEM) images corroborate the particle diameters. An intrinsic mass density of 0.85 - 1.2 g cm$^{-3}$ is estimated for the NPs by measuring the falling velocity of the particle cloud in the afterglow.

The time evolution of the electron density, $n_e$, and excitation temperature, $T_{ex}$, which is expected to be close to the electron temperature, $T_e$, are estimated from optical emission spectra in conjunction with a collisional/radiative model. A decrease in $n_e$ and a concomitant growth in $T_{ex}$ are obtained in the t= 2-4 s interval. The drop in $n_e$ is likely due to the attachment of free electrons to the surface of the growing NPs.

Ex-situ IR spectra of the deposited dust show that the particles contain H and variously hybridized C atoms. Measurements carried out for different plasma lifetimes show that the proportion of C in double and triple bonds decreases with increasing plasma lifetime and particle size and suggest that the particles consist of a core, relatively rich in sp and sp$^2$ C atoms, surrounded by a sp$^3$-rich C mantle.

## 3. Acknowledgements

This work was funded by the Spanish M. de Ciencia, Innovación y Universidades under grant PID2023-146415NB-I00 and the CSIC i-LINK project SENTINEL (ILINK23017).

## References

[1] Berndt, J. et al. Some aspects of reactive complex plasmas, *Contribut. Plasma. Phys.* **49**, 107 (2009).
[2] Herrero, V. J. et al. Structure and evolution of interstellar carbonaceous dust. Insights from the laboratory *Frontiers in Astronomy and Space Sciences* **9,** 1083288 (2022).
[3] Peláez, R. J. et al. Multi-diagnostic of dust growth in a capacitive $Ar/C_2H_2$ plasma. *Plasma Sources Sci. Tech.* 33, 105006 (2024).

# Laser Induced Breakdown Spectroscopy from fs to ns laser pulses for the detection of deuterium in fusion plasma walls

A. Hussain[1,2], D. Aceto[1], P.F. Ambrico[1] and G. Dilecce[1]

[1] *Institute for Plasma Science and Technology – CNR via Amendola 122/D 70125 Bari - Italy*
[2] *University of Padova/RFX Consortium – Via VIII Febbraio, 2, 35122 Padova – Italy*

We report on LIBS studies on W surfaces which address a comparison of laser pulse durations of 400 fs, 10 ps and 10 ns and of transverse vs. collinear detection schemes, in the frame of LIBS measurements of fuel retention in Tokamak's plasma walls.

## 1 Introduction

The problem of fuel retention in the walls in contact with the plasma in Tokamak's devices can be addressed by LIBS surface diagnostics or both in-situ and in machines dedicated to plasma-wall interaction studies.

The interest in the depth profile of fuel adsorption makes it attractive to employ a fs laser which is reported to produce geometrically regular craters with more vertical walls compared to common ns lasers. On the other hand, it is expected that the plasma plume produced by fs shots is less energetic than that of ns shots, giving rise to less rich and intense spectra of atomic lines.

The geometry of light collection is also an issue. Collinear detection is preferable for its simplicity, that better adapts to complex machines where only one optical window is available. It nevertheless suffers the overlap of a blackbody continuum radiation whose source is located on the sample surface. This overlap can limit the signal to noise ratio. On the other hand, 90 deg. observation at a distance from the target, while suppressing the continuum radiation, greatly reduces the signal strength and calls for two optical viewports on the machine. Here we report on studies addressing these issues, together with further variable conditions, like the gas pressure in the environment of the plume.

## 2 Preliminary results

We show in fig. 1 a comparison of wide spectral range spectra obtained by 400 fs and 10 ns laser shot durations, with collinear light collection. One basic difference is the slower time evolution of the plasma plume in the ns case. As an example, with fs pulse the LIBS signal at 600 ns delay is almost extinguished, while, with ns pulse it is still well measurable. Nevertheless, although it is known that with ns pulse part of the laser energy is spent in the plasma plume excitation, no significant differences are observed in the intensity of atomic lines. Rather, line ratios can be somewhat different, indicating that in the two cases, the electron temperature of the plume can be different.

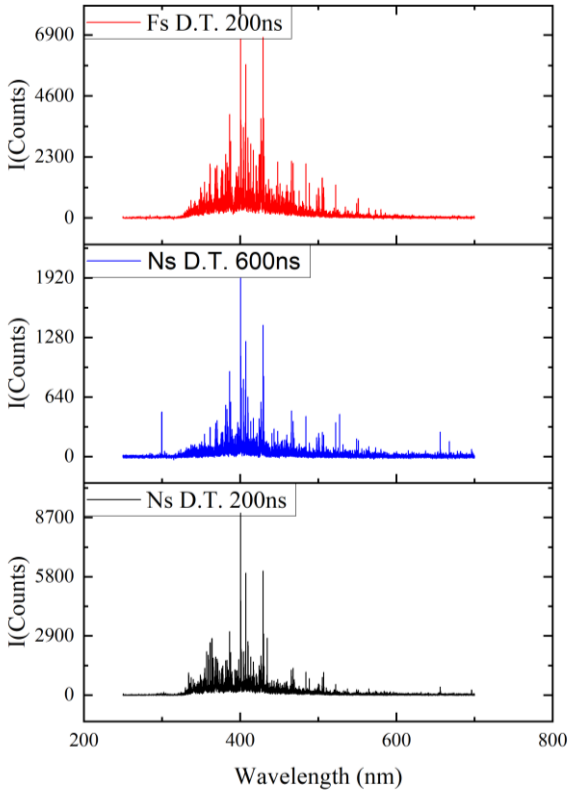



**Fig. 1** Comparison of spectra taken with fs pulse - 400 ns, 1 mJ – and ns pulse – 10 ns, 10 mJ. I.C.C.D gate= 50 ns, D.T = gate delay from the laser pulse.

We shall address these point together with strategies for reducing the background at collinear detection and to increase the emission intensity of atomic lines.

### Acknowledgements

Work carried out in the frame of project NEFERTARI – CUP B53C22003070006, funded by the European Union under the National Recovery and Resilience Plan (NRRP) – NextGenerationEU.

# High-sensitivity E-FISH measurement on low-pressure streamer discharge

Jianan Wang[1], and Sander Nijdam[1]

[1]*Eindhoven University of Technology, Eindhoven. The Netherlands*

In this work, we investigate streamer dynamics in a low-pressure plasma environment using electric-field induced second harmonic (E-FISH) generation. Plasma is generated in a low-pressure vessel filled with dry air, triggered by a pulsed power circuit applying 10 kV with a 400 ns pulse duration. A picosecond Nd: YAG laser is used for E-FISH diagnostics. The second harmonic signal induced by the electric field is separated, filtered, and detected using a silicon photomultiplier (SiPM). Optimized to reduce optical components, this setup minimizes signal loss and enhances detection sensitivity. This work offers insights into streamer propagation, particularly in the streamer head and post-discharge region.

## 1 General

Understanding streamer discharges in low-pressure environments is essential for both scientific research and engineering applications [1]. The electric field plays a key role in discharge breakdown, streamer propagation, and plasma channel formation. A non-intrusive technique for measuring the electric field is electric-field induced second harmonic (E-FISH) generation, a promising nonlinear optical method widely used in recent studies [2]. In this work, we use E-FISH to measure the electric field during and after a streamer's propagation in a pin-to-plate pulsed discharge. The setup is optimized to minimize signal losses and enhance sensitivity. This approach provides valuable insights into streamer dynamics, particularly in the streamer head and post-discharge region.

## 2 Experimental setup

Plasma is generated in a low-pressure vessel flushed with dry air continually. A pulsed power circuit triggers the plasma, applying a pulse with a 10 kV voltage amplitude and a 400 ns duration. The diagnostic setup is shown in Figure 1. It uses a picosecond Nd: YAG laser providing the probing laser beam. The beam is guided through a half-wave plate, a cube polarizer, a focal lens, and a long-pass filter. This results in a fully polarized, tunable-energy beam with a diameter of less than 1 mm and no existing second harmonic. The laser is then focused on the streamer propagation path, where it induces a second harmonic signal in the presence of an electric field. The mixed 1064 nm and 532 nm wavelengths are separated by a dichroic mirror and a prism, with a collimating lens ensuring beam parallelism. The second harmonic signal is then filtered through a pinhole and a cube polarizer to remove unpolarized 532 nm signals from surface reflections before being sent to a silicon photomultiplier (SiPM). This setup uses fewer optical components, minimizing signal loss and enhancing detection sensitivity.

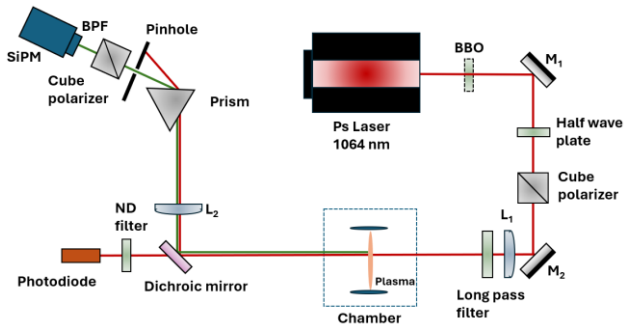



Figure 1. Experimental setup diagram

Further demonstrations will be conducted, and additional results on streamer dynamics will be presented.

**References**

[1] Nijdam, Sander, et al. Plasma Sources Science and Technology 29.10 (2020): 103001.
[2] Guo, Yihao, et al. Physical Review Research 7.1 (2025): 013051.

# Femtosecond laser-induced fluorescence for atmospheric plasma diagnostics: Stark detuning and power saturation effects

C. Pascual Fort, A. Brisset, G.D. Stancu

[1] *Laboratoire EM2C, CNRS, CentraleSupélec, Université Paris-Saclay, 3 rue Joliot Curie, 91192, Gif-sur-Yvette Cedex, France*

Atmospheric-pressure plasmas produce reactive species like atomic nitrogen, essential for energy, materials, environmental and biomedical applications. Their characterization and understanding of generation mechanisms are important for advancing applications. Two-photon absorption laser-induced fluorescence (TALIF) is a powerful diagnostic tool for measuring atomic radicals such as N($^4$S) with high spatial and temporal resolution. While traditional nanosecond TALIF faces challenges like quenching in high-pressure environments, ultrafast lasers enable quenching-free and photolytic-free measurements at high laser intensities. This work employs femtosecond (fs) TALIF to map N($^4$S) densities in a microwave (mw) plasma jet at atmospheric pressure, addressing effects such as Stark detuning and power saturation in nitrogen and krypton gases. By combining fs-TALIF with an atomic nitrogen etalon source, the present study provides accurate, spatially resolved measurements of nitrogen radical density.

## 1 Context: a quench-free technique

TALIF is a powerful *in situ* diagnostic technique for measuring key atomic radicals (e.g. N, H, O) in reactive environments with high spatial and temporal resolution. It can determine absolute densities at low laser intensities (< 1GW/cm² for typical ns lasers), where fluorescence scales quadratically with the laser energy. However, accurate measurements in atmospheric-pressure plasmas are challenging due to quenching effects.

Employing higher laser fluence mitigates quenching by making stimulated emission and photoionization the dominant decay pathways of excited states [1]. Ultrafast lasers allow even higher instantaneous intensities (up to PW/cm²). Ps- and fs-TALIF also reduce photolytic effects, enhancing measurement accuracy and enabling more reliable quenching rate measurements.

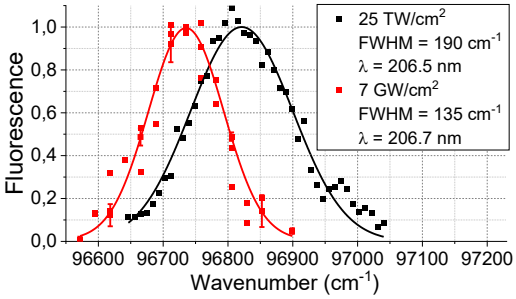



Fig. 1: N two-photon absorption spectral profile in a discharge cell at 4 mbar for two laser's intensities.

In this work, fs-TALIF is developed for spatial mapping of N($^4$S) in an atmospheric pressure MW plasma jet. Here, a 100-fs laser at a repetition rate of 1 kHz is employed. The Ti:sapphire laser system (Spectra Physics Solstice ACE) integrated with an optical parametric oscillator (TOPAS Light Conversion), allows tunable wavelengths between 204 nm and 207 nm to probe atomic nitrogen and calibrate measurements using the classical calibration with krypton gas.

## 2 Stark detuning and power saturation

At high intensities and employing mode-locked lasers, the TALIF enters the saturation regime, exhibits coherent effects such as Rabi oscillations, Stark detuning and power line broadening. Here, the laser intensity was adjusted more than 5 orders of magnitude, demonstrating quadratic and saturation regimes in nitrogen and krypton gases. In Fig. 1, the N two-photon absorption spectral profile presents a -0.2 nm Stark detuning and +55 cm$^{-1}$ power broadening at 25 TW/cm² compared to 7 GW/cm².

These phenomena challenge the validity of rate equations [1] and, consequently, the classical krypton calibration. To address this, our N($^4$S) mapping strategy incorporates a novel calibration using an atomic nitrogen etalon source as described in [2].

In the present contribution diagnostic insights and absolute spatially resolved N($^4$S) density in the MW plasma jet using calibrated fs-TALIF will be reported.

### Acknowledgments

This research was funded by ANR-ULTRAMAP project (ANR-22-CE51-0027) and IdF SESAME, project DIAGPLAS.

### References

[1] Stancu G.D. *Plasma Sources Sci. Technol.* **29** 054001 (2020)

[2] Dumitrache C. et al. *Plasma Sources Sci. Technol.* **31** 015004 (2022)

# Influence of ambient air humidity on discharge modes for a pin-to-pin discharge with a water droplet

V. Riazantceva[1], L. Sebih[2], A. Hamdan[2], E. Carbone[1]

[1] *Institut National de la Recherche Scientifique, centre Énergie, Matériaux et Télécommunications, 1650, blvd Lionel Boulet, Varennes J3X 1P7, Québec, Canada*
[2] *University of Montreal – campus MIL, 1375, Avenue Thérèse-Lavoie-Roux, H2V 0B3, Montréal (Québec), Canada*

The impact of ambient air humidity on the occurrence of different discharge modes is discussed for a discharge generated in a pin-to-pin configuration with a water droplet in the gap. The probability of various plasma regimes is strongly affected by the humidity with a much higher occurrence of spark discharges. The water droplet affects the propagation path of the streamers whereas the probability of different modes is relatively weakly changed.

## 1 Introduction

Plasma is an effective and powerful tool in various fields, including water treatment, sterilization, and material processing. Because of the possibility of producing highly reactive oxygen and nitrogen species (RONS), which affect the physico-chemical characteristics of water, the interaction between cold atmospheric plasma and water is important. Humidity is essential for controlling these interactions, impacting the production of reactive species, ionization kinetics [1] (increasing the electron density) and the chemistry between plasma and water [2]. Understanding the extent of humidity's influence is essential for optimizing plasma-based applications in environmental sciences. In this work, a pin-to-pin gap with plasma-water interaction will be discussed. Electrical measurements and iCCD imaging will be presented together with FTIR data from the ambient environment surrounding the water droplet.

## 2 Experimental set-up and Results.

Environmental factors like temperature and humidity are regulated by constructing a small cavity with two tungsten wire electrodes (W) horizontally positioned 7 mm apart over a glass substrate. The substrate is made of glass and the plasma is generated using a pulser generating 50 - 400 ns pulses at varying peak voltages 14 -18 kV and pulse repetition rates. In our research, 3 µl drop of deionised water is placed between the electrodes.

In figure 1, the probability of discharges using 16 kV pulse without a droplet for two different humidity levels, 60 % and 94 % are shown for different repetition frequencies. Four distinct modes were observed: Sp - only sparks mode, Sp-str - streamers transition into a spark discharge, Str - only streamers, and Failed - no discharges. For all frequencies, it is seen that humidity has a highly significant effect on plasma formation. The water droplet also modifies the probability of different modes. Preliminary FTIR data indicates however that the humidity around the droplet is not significantly affected. For understanding plasma-liquid water interactions, ambient air humidity needs thus to be controlled and the water droplet does not appear to have its own "atmosphere" around it that would allow to ignore environmental factors. Mass transport at the plasma/water boundary between pulses and air flow around the droplet due to convection should be further investigated in the future.

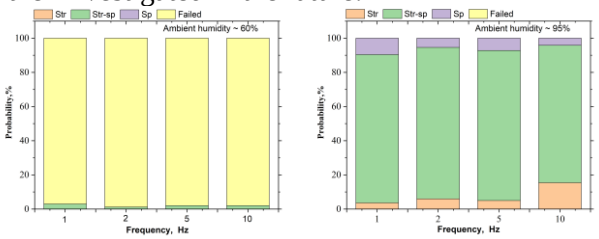



**Fig.1:** The probability of the occurrence of different discharge modes at 16 kV without a droplet vs frequency of the pulse with ambient humidity of 60 % (left); of 95% (right). See in the text for the notations.

Most recent works have focussed on the nature of the dielectric, and in the case of water, also its conductivity [3], the present results indicate that an environmental factor such as ambient air humidity must be controlled as well for describing and controlling the plasma dynamics.

**References**

[1] Yagi I. *et al*. Two-dimensional LIF measurements of humidity and OH density resulting from evaporated water from a wet surface in plasma for medical use. *Plasma Sources Sci. Technol.* **24**, 015002 (2015).

[2] Ono R. *et al*. Effect of humidity on gas temperature in the afterglow of pulsed positive corona discharge. *Plasma Sources Sci. Technol*. **19**, 015009 (2010).

[3] Sebih L. *et al.* Electrical and optical characteristics of a nanosecond pulsed electrical discharge in air in contact with a water droplet for various electrical conductivities *J. Phys. D: Appl. Phys*. **58** 045206 (2024)

# Simulating $H_2O_2$ and OH-driven chemical reaction kinetics and diffusive mass transport in a He/$H_2O$-plasma treated water

Matthew Wright[1] , Tomoyuki Murakami [2], Timo Gans [1] and Deborah O'Connell[1]

[1] *School of Physical Sciences, Dublin City University, Dublin, Ireland*
[2] *Faculty of Science and Engineering, Seikei University, Tokyo, Japan*

In this work, we report results of a coupled reaction-diffusion-electrostatics model for reactive species transport in plasma-treated water and investigate liquid composition during and after treatment with a noble gas plasma μ-APPJ with admixture of water. Results demonstrate that the production of short-lived species during treatment are dominated by OH consumption processes, while after treatment hydrogen peroxide dominates.

## Introduction

Plasma-treated water has been shown to have many applications, one of which is direct degradation of biological and persistent organic contaminants (for example PFAS). To gain a mechanistic insight into deconstruction pathways of these contaminants, the liquid composition and electrical properties during and after treatment need to be known. Benchmarked modelling can bridge this gap providing knowledge on the liquid environment. Models have previously been developed for reactive species (RS) transport, fluid flow and heat transfer [1-2], but little has been reported differentiating the effects of short-lived and long-lived species on liquid chemistry.

Here, we demonstrate a first step into developing a plasma treated liquid model for this purpose, presenting RS production and transport through a liquid water sample during plasma treatment.

## Methods

A coupled liquid-phase reaction-Poisson-Nernst Planck model in 1D was used to simulate plasma treatment of water. Parallel electrode geometry was assumed (e.g. COST μ-APPJ), with gas flow impinging normal to the liquid surface, meaning simulated plasma treatments contained only neutral species [3]. A helium plasma with admixture of water was assumed throughout, with simulated treatments consisting of $H_2O_2$ (Case 1), and $H_2O_2$ with OH (Case 2). This was considered analogous to treatments with species in the far effluent of a COST μAAPJ (Case 1 - long-lived only), and with species in the near effluent (Case 2 - long and short-lived). Other plasma-produced RS (i.e. H, $H_2$, $O_3$) are excluded due to their low solubility in comparison to those mentioned above [3-4].

## Results and Discussion

Figure 1 displays RS produced in water due to plasma treatment for Case 1 and 2 as outlined above. In Case 1 treatments, the production of $OH^-$ through $H_2O_2$'s conjugate base $HO_2^-$ leads to an increased concentration in comparison to $OH^-$ produced due to the autoionization of the $H_2O$ solvent. This can be visualised by the leftmost branch of Figure 1 (bottom). In addition, the dissociation of $H_2O_2$ temporarily forming OH, is followed by the production of $HO_2$ and $O_2^-$ in very small concentrations. In Case 2 treatments, OH is largely consumed in the first 100 nanometres and converted (through reactions with $H_2O_2$) into $HO_2$, which permeates through diffusion and leads to the production of $O_2^-/H^+$ deeper in the liquid.

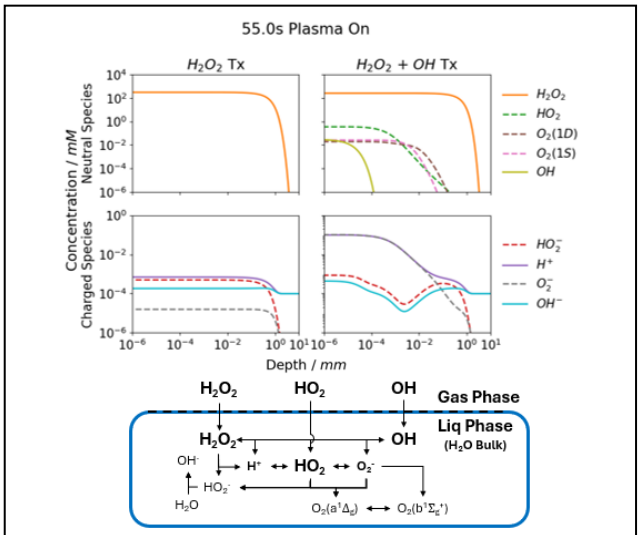



**Fig. 1**. Spatial profile of reactive neutral (top) and charged species (middle) for treatment with a noble gas plasma with admixture of water, including $H_2O_2$ only (Case 1 - left column) and $H_2O_2$ with OH (Case 2 - right column) after 55s of plasma treatment.

Further chemical reaction network analysis demonstrates that only $OH^-$ originates from hydrogen dissociated from the $H_2O$ solvent. All other species in both cases are directly produced in the liquid through plasma-delivered $H_2O_2$, OH and $HO_2$, and their products as shown in Figure 1 (bottom).

## Conclusion

For a noble gas (e.g. helium) plasma with admixtures of humidity, although $H_2O_2$ is the most abundant RS in the liquid phase due to its high solubility, highly reactive OH dominantly leads to increased short-lived RS production during treatment. OH is rapidly consumed leading to the production of $HO_2$ almost immediately upon entering the liquid phase, with $HO_2$ and its conjugate base $O_2^-$ propagating further into the liquid through diffusion. After treatment, the liquid composition is dominated by $H_2O_2$.

## References

[1] Y. Liu et al., AIP Adv., **14**, 055019 (2024).
[2] P. Heirman et al., Phys. Chem. Chem. Phys, **21,** 12881-12894 (2019).
[3] T. Murakami et al., Plasma Sources Sci. Technol., **23**, 025005 (2014).
[4] S. Schroeter et al., Phys. Chem. Chem. Phys, **20**, 24263−24286 (2018)

# Bubble formation and droplet ejection from liquid metals interacting with inductively coupled hydrogen plasma

Koichi Sasaki and Yuki Hamana

*Division of Applied Quantum Science and Engineering, Hokkaido University, Sapporo 060-8628, Japan*

We observed the formation of bubbles in liquid gallium and liquid tin interacting with inductively coupled hydrogen plasma. The ejection of droplets were observed at the burst of the bubble. The origin of the bubble formation and its burst is the forced transport of positive ions toward the liquid metal surface, which results in the supersaturated density of dissolved hydrogen in the liquid metal.

## 1 Introduction

The plasma-liquid interaction is studied widely using atmospheric-pressure plasma and water. However, atmospheric-pressure plasma has difficulty in diagnostics, in comparison with conventional low-pressure plasma. Although easier experiments are expected if we can use low-pressure plasma for the study of the plasma-liquid interaction, water is not compatible with the vacuum environment. Our idea for this issue is to use liquid metals with negligible vapor pressures [1–3]. We observed the formation of bubbles in liquid metals when they were exposed to an inductively coupled hydrogen plasma. In addition, we observed the ejection of droplets from liquid metals, which would be a serious problem in the development of a liquid metal diverter system in nuclear fusion research.

## 2 Experiment

The details of the experimental apparatus and the methods are reported in [2]. Briefly, liquid metals were stored in a quartz container which was installed in inductively coupled hydrogen plasma. The temperature of liquid metal was controlled using a heater. The positive ion flux toward the liquid metal surface was controlled by the rf power, while the ion energy was controlled by connecting liquid metal to a negatively biased dc power supply. Droplets were detected by laser Mie scattering, and we examined the frequency of the droplet ejection.

## 3 Results and discussion

We observed the formation of bubbles inside liquid metals, and the droplet ejection was synchronized with the burst of a bubble. The trajectories of droplets were close to perpendicular to the liquid metal surface, suggesting that the droplets are so called “jet drops” [4]. The ejection frequency increased with the ion flux, but it was independent of the flux of atomic nitrogen. We also observed the increase in the ejection frequency with the liquid metal temperature. The frequency of the droplet ejection from liquid tin was an order of magnitude higher than that from liquid gallium.

Considering the experimental results, we have proposed the following mechanism for the droplet ejection. The droplets are produced by the burst of a bubble formed in liquid metal. The bubble formation is owing to the supersaturated density of dissolved hydrogen. The irradiation of positive ions plays an important role for the supersaturation of the dissolved hydrogen density. This is because it is the forced transport of atomic hydrogen into liquid gallium. Note that the Henry’s law does not work against the ion irradiation. The increase in the ejection frequency with the liquid metal temperature is explained by the temperature dependence of the dissolution limit under the plasma irradiation condition [5]. The higher ejection frequency from liquid tin than liquid gallium is understood considering the deference in their surface tensions, viscosities, and dissolution limits. Only an experimental result that cannot be explained by the above mechanism is the decrease in the ejection frequency with the ion energy, which could be a hope for researchers who try to develop a liquid metal diverter system.

## References

[1] Sasaki, K. and Koyama. H., *Appl. Phys. Express*, **11**, 036201 (2018).
[2] Hamana, Y., Shirai, N., and Sasaki, K., *J. Phys. D: Appl. Phys.*, **56**, 475204 (2023).
[3] Hamana, Y. and Sasaki, K., *Jpn. J. Appl. Phys.*, **64**, 028003 (2025).
[4] Georgescu, S.-C., *et al.*, *Eur. J. Mech. B-Fluid*, **21**, 265 (2002).
[5] Ou, W., *et al.*, *Nucl. Fusion*, **60**, 026008 (2020).

# Space- and Time-Resolved Studies in Liquid Water Discharges: Insights into Emission Continua and Atomic Line Profiles during Primary and Reflected Pulses

Garima Arora[1], Petr Hoffer[1], Václav Prukner, Petr Bílek[1] and Milan Šimek[1]

[1] *Institute of Plasma Physics of Czech Academy of Sciences, U Slovanky 2525/1a, 18200Prague, Czech Republic*
e-mail: *arora@ipp.cas.cz*

## 1 Introduction

Understanding the mechanisms behind nano-second discharges in liquid water is crucial for unlocking the potential of plasma-liquid interactions [1-3]. Plasma formation involves the multiplication of free electrons through ionization processes, with energy loss leading to significant radiation emission. Emission spectroscopy appears to be an effective non-invasive method for studying nanosecond nonequilibrium discharges in liquids. Our previous studies utilized time-resolved microscopy techniques to capture the unique signatures of micro discharges in deionized water (DI). Triggered by high-voltage (HV) pulses, these discharges unfold in two phases: dark and luminous, each with distinct morphology and dynamics [4-6].

## 2 Results and Discussion

In this work, we systematically investigated the ICCD images of discharge luminosity together with imaging spectra of discharge events produced in liquid DI water under single HV pulse conditions. The discharge reactor consists of a tungsten pin and grounded stainless-steel chamber walls. The short HV pulse (FWHM~ 7ns) was delivered into the reactor through a 2.8 m long coaxial cable (unmatched load). The emission spectra were recorded for the primary pulse and its reflections. The primary pulse consists of diffuse morphology is associated with weak broad-band emission continua, while the subsequent filamentary morphology in the reflections shows much more intense spectra consisting of significantly broadened $H_\alpha$ and several $O^I$ atomic lines superimposed on continua (Fig.1). The line profiles were extracted from the modelled continuum to get the spectral line shape. Temporal and spatial electron number densities were estimated from the Stark broadening of atomic lines emission. Temporal and spatial electron number densities notably evolve with time $2.1 \times 10^{20}$ cm$^{-3}$ – $6 \times 10^{18}$ cm$^{-3}$ with only slight density variation with distance from the anode tip.

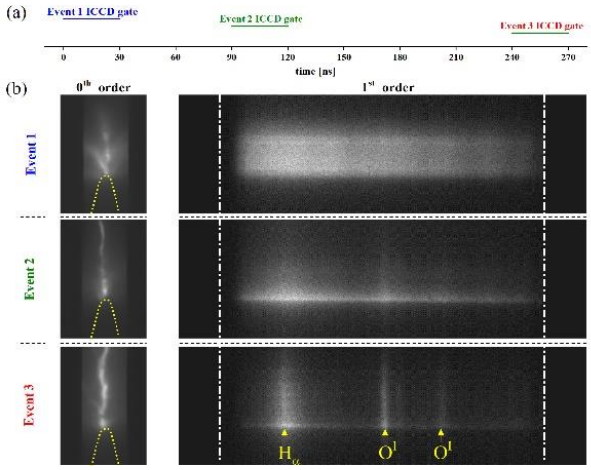



Fig.1 Selected ICCD spectrometric images acquired in 0$^{th}$ and 1$^{st}$ diffraction orders using grating 300 G/mm and fixed ICCD gate of 30 ns.

## References

[1] Šunka P. Phys. Plasmas **8** 2587–94 (2001).
[2] Sato M. Plasma Sources Sci. Technol. **17** 024021 (2008).
[3] Graham W. G. and Stalder K. R. J. Phys. D. Appl. Phys. **44** 174037 (2011).
[4] Šimek M., Hoffer P., Tungli J., Prukner V., Schmidt J., Bílek P. and Bonaventura Z. Plasma Sources Sci. Technol. **29** 064001 (2020).
[5] Šimek M., Pongrác B., Babický V., Člupek M. and Lukeš P. Plasma Sources Sci. Technol. **26** 07LT01 (2017).
[6] Šimek M, Hoffer P, Prukner V and Schmidt J Plasma Sources Sci. Technol. **29** 095001(2020).

## Acknowledgement

This study was supported by the Grant Agency of the Czech Republic (grant number: GA24-10903S).

# Controlling plasma produced fluxes to liquid surfaces by acoustic structuring: applications to plasma driven solution electrochemistry

Scott J. Doyle[1], Tiago C. Dias[2], Mackenzie Meyer[2], and Mark J. Kushner[2]

[1]*University of Aberdeen, King's College, Fraser Noble Building, Aberdeen, AB24 3FX, United Kingdom*
[2]*Electrical Engineering and Computer Science Department, University of Michigan, Ann Arbor, MI 48109-2122, USA*
*Scott.Doyle@abdn.ac.uk*

In this presentation, results are discussed from a computational investigation of pulsed atmospheric pressure plasma jets onto acoustically structured water solutions containing $AgNO_3$ as may be used in PDSE for silver nanoparticle (NP) formation. The surface of the AgNO3 solution is altered to include standing wave patterns, having wavelength and wave depth of hundreds of microns to 1 mm. The potential for structured liquid surfaces to facilitate spatially differentiated chemical selectivity and enhance NP synthesis in the context of PDSE is discussed.

Plasmas interacting with liquid surfaces produce a complex interfacial layer where the local chemistry in the liquid is driven by fluxes from the gas phase of electrons, ions, photons, and neutral radicals. Typically, the liquid surface has at best mild curvature with the fluxes of impinging plasma species and applied electric field being nominally normal to the surface. With liquids such as water having a high dielectric constant, structuring of the liquid surface by producing a wavy surface enables local electric field enhancement due to polarization of the liquid, as well as producing regions of higher and lower advective gas flow across the surface.

This structuring (or waviness) can naturally occur or can be achieved by mechanical agitation such as with acoustic transducers. Electric field enhancement at the peaks of the waves of the liquid produces local increases in sources of reactive species and incident plasma fluxes which may be advantageous for plasma driven solution electrochemistry (PDSE) applications.

This work was supported by the Army Research Office (W911NF-20-1-0105), the U.S. Department of Energy Office of Fusion Energy Sciences (DE-SC0020232), and the National Science Foundation (CBET-2032604).

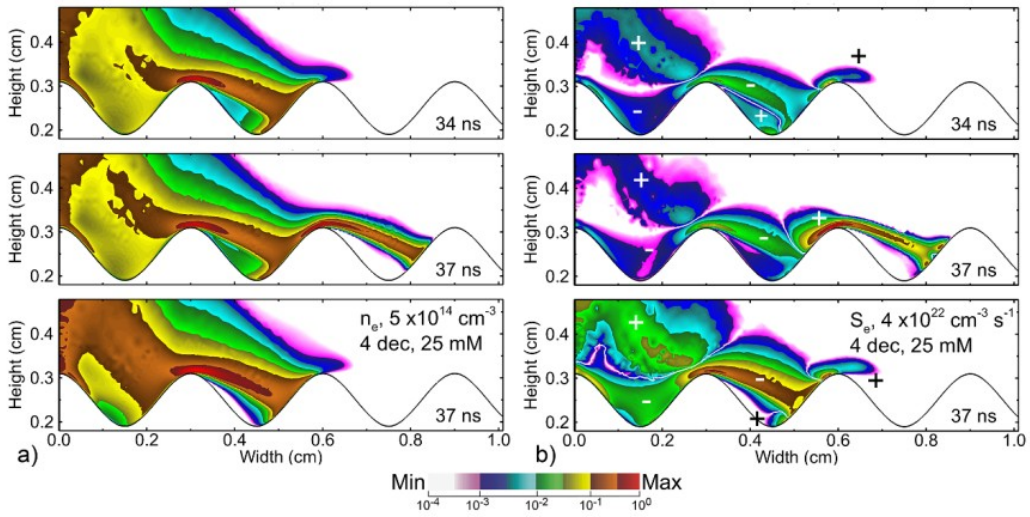



Figure 1 – Macroscopic plasma properties for the n04 structured surface for a −15 kV pulse. Values are shown for 5 mM AgNO3 solution for times of 34 ns–37 ns, and a 25 mM solution at 37 ns. (a) Electron density and (b) electron-impact ionization source, both with a 4-decade log scale. The absolute value of the electron-impact ionization source is plotted. The portions of the image labeled '+' and '−' indicate regions of net electron source and loss.

# Investigation of reactive species formation in surface dielectric barrier discharge with liquid electrodes

O. Galmiz[1], R. Cimerman[1], M. Janda[1], N. Selaković[2], N. Puač[2] and Z. Machala[1]

[1]*Division of Environmental Physics, Faculty of Mathematics, Physics and Informatics, Comenius University Bratislava, Slovakia*
[2]*Institute of Physics, University of Belgrade, Pregrevica 118, 11080 Belgrade, Serbia*

This study focuses on the characterization and quantification of reactive species produced by cold plasma generated using liquid electrodes in a surface dielectric barrier discharge system. By varying experimental conditions, the production of reactive oxygen and nitrogen species in both gas and liquid phases was systematically analysed. Several analytical techniques were employed to assess the chemical composition of the plasma-treated medium.

## 1 General

The typical surface dielectric barrier discharge (SDBD) systems, produce plasma along a thin dielectric layer and are not capable of direct interaction with liquids. This limitation restricts the formation of short-lived, highly reactive species, such as hydroxyl (·OH) and oxide (·O) radicals and their transport to liquids. To overcome this challenge, we use a liquid electrode SDBD system, where plasma is ignited directly from the liquid surface [1,2]. This approach significantly enhances plasma-liquid interactions, making the system more versatile for applications such as water activation, material surface treatment, and biomedical sterilization.

Liquids that are plasma-treated and contain a mixture of various reactive oxygen and nitrogen species (RONS) are typically referred to as plasma-activated liquids (PAL). Key reactive species such as ·OH, $O_3$ , NO, $NO_2$ , and $H_2O_2$ play crucial roles in plasma-driven surface modifications and decontamination processes [3,4]. The interaction of these species with target surfaces during plasma treatment significantly influences the reaction pathways and outcomes.

This study presents an investigation of the electrical discharge properties of a cold plasma that is created using liquid electrodes. The chemical species that are created during the discharge and subsequently transferred into the liquid are systematically characterized and quantified.

To characterize the reactive species formed in the gas phase, Fourier-transform infrared (FTIR) spectroscopy was used to quantify gas-phase species, such as NO, $NO_2$ , $N_2$ O, and $O_3$ . The concentration of nitrogen-containing species showed fluctuations with increased discharge power, peaking at approximately 50 ppm. Meanwhile, $O_3$ concentrations reached up to 150 ppm, varying based on reactor type and discharge power.

In addition, the analysis of these species, as well as the detailed composition of the plasma were studied by using mass spectroscopy. The spatial evolution of $O_3$ within the liquid phase was further analyzed using in-situ UV-VIS spectroscopy.

In parallel, absorption spectroscopy was employed to quantify key plasma-induced species in the plasma-treated liquid, with concentrations measured in the mM range.

**Acknowledgment**
This work was funded by the EU NextGenerationEU through the Recovery and Resilience Plan for Slovakia under the project No.09I03-03-V04-00094, the Marie S. Curie Action Postdoctoral Fellowship under Horizon Europe with grant agreement number 101066764, and Slovak Research and Development Agency grants APVV SK-SRB-23-0043.

**References**

[1] Galmiz, O. et al. Hydrophilization of outer and inner surfaces of Poly(vinyl chloride) tubes using surface dielectric barrier discharges generated in ambient air plasma. *Plasma Process. Polym*. **14**, 1600220 (2017).
[2] Galmiz, O. et al. Production of reactive species by using surface dielectric barrier discharge in direct contact with water. *Plasma Sources Sci. Technol.* **34** 025011 (2025).
[3] Brandenburg, R. et al. Antimicrobial Treatment of Heat Sensitive Materials by Means of Atmospheric Pressure Rf-Driven Plasma Jet. *Contrib. Plasma Phys*. **47**, 72 (2007).
[4] Machala, Z. et al. Plasma agents in bio-decontamination by dc discharges in atmospheric air. *J. Phys. D: Appl. Phys*. **43,** 222001 (2010).

# Characterization and optimisation of a plasma source for the biological decontamination of wastewater in volume.

M. Saba, T. Maho, C. Muja and P. Guillot.

*Laboratoire DPHE, Université de Toulouse, INU Champollion, Place de Verdun, 81000 Albi*

Several studies have shown that non-thermal plasma can be used for biological decontamination of wastewater due to its ability to produce reactive species with antimicrobial properties [1]. The project aims to characterize and optimize a modifiable wastewater decontamination system, conceived in our laboratory. The system operates by the generation of an immersed plasma at atmospheric pressure that should reduce the bacterial and viral load within a reasonable treatment time. Electrical and optical measurements of the plasma, along with chemical characterization of the liquid phase, were conducted to determine the optimal system configuration and plasma parameters for maximizing the system's microbicidal effect.

## 1 Experimental setup

The plasma source consists of a 50 ml glass container with a tube inserted for gas injection. The gas is introduced into the tube and released from its submerged end, forming bubbles in the water. A high-voltage electrode is inserted into the tube and connected to a pulsed power supply that generates pulses with widths of less than 3 µs. The voltage amplitude ranges from 1 to 20 kV, with a fixed repetition frequency of 20 kHz. A grounded counter-electrode is wrapped around the water container. This system can be considered a complex form of a coaxial dielectric barrier discharge (DBD) (Figure 1). Additionally, the standard tube can be replaced with tubes featuring different nozzle designs, allowing for variations in bubble in the water. The plasma source can be connected to a 500 ml container for treating larger liquid volumes. In this configuration, the water circulates in a closed loop using a peristaltic pump.

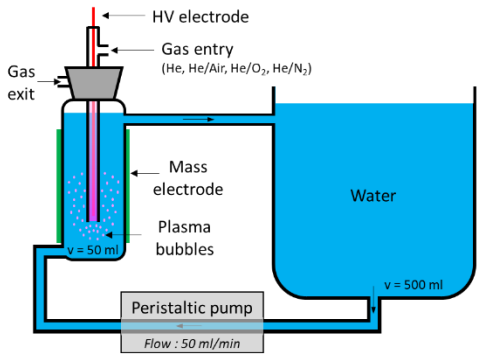



Figure 1: Schematic of the experimental setup.

## 2 Plasma characterisation

First, an equivalent electrical circuit was used to estimate the energy deposited into the plasma discharge during a single pulse. The total current was measured with a current monitor (PEARSON™), while the applied voltage was recorded using a voltage probe (Tektronix P6015A). Both waveforms were captured by a digital oscilloscope (ROHDE & SCHWARZ RTE1204). Next, optical emission spectroscopy (PI-HRS-750 coupled with a PI-MAX4) was conducted to identify the reactive species generated by the plasma for various gas mixtures. Additionally, an ICCD camera (PI-MAX1) was used to follow the plasma propagation during a single pulse. Different optical filters were applied to visualize the spatial distribution of specific species within the plasma.

## 3 Liquid-plasma interactions

The study of plasma-liquid interactions was divided into two parts. A solution of KI and starch was first used to detect the presence of reactive oxygen and nitrogen species (RONS) in the liquid phase after plasma treatment for different working gas types. This approach helped us to identify the optimal system configuration and the most efficient gas composition for RONS production. Secondly, the concentrations of $H_2O_2$, $NO_2^-$, and $NO_3^-$ in the treated water were measured to further evaluate the system's effectiveness.

## 4 Upcoming works

Decontamination efficiency will be assessed on *Escherichia coli* bacteria, first in clean water, then in dirty water containing organic matter.

**References**

[1] Murugesan, P., Moses, J. A., & Anandharamakrishnan, C. (2020). Water decontamination using non-thermal plasma: Concepts, applications, and prospects. *Journal of Environmental Chemical Engineering*, *8*(5), 104377.

# Plasma-based Nanoarchitectonics for Dual Gate Graphene Field Effect Transistor (GFET) Device: Effect of Plasma Parameters on Transistor Properties

Monika Verma[1], Suresh C. Sharma[1]

[1] *Department of Applied Physics, Delhi Technological University, Delhi, India*

A graphene layer is developed using plasma enhanced CVD process in order to form the channel of a dual gate GFET device. Numerical analysis and simulations are performed using TCAD tool to study the effect of plasma parameters on the transistor properties of the designed GFET.

## Abstract

For the past two decades, extensive research has been conducted on Carbon Nanotubes (CNTs) and Graphene to improve semiconductor devices. This study builds upon recent advancements in the development of Graphene-based Field-Effect Transistors (FETs) manufactured using the Plasma-Enhanced Chemical Vapor Deposition (PECVD) process. A similar investigation was carried out by M. Kansal et al., focusing on CNTs as the channel material in FETs and exploring the relationship between FET characteristics and the plasma parameters that influence their fabrication through PECVD.

In this research, we propose a novel device that incorporates a two-dimensional (2D) graphene sheet as the channel in a FET. Our primary objective is to examine how different plasma parameters impact the performance of this designed device. Through a systematic analysis of various properties, we aim to determine the optimal conditions for achieving superior device performance. Lower plasma parameter values play a crucial role in enhancing key performance indicators such as higher drain current, improved output conductance, and a reduced cutoff frequency. Striking the right balance in plasma parameters is essential for optimizing the device's overall efficiency.

By fine-tuning these parameters, we can significantly improve the device's functionality, making it particularly suitable for practical applications, especially in biosensing technologies. Our simulated results closely align with existing experimental findings, reinforcing the feasibility and potential of this device for real-world use.

**References**

[1] Suresh C. Sharma, Neha Gupta, Theoretical modeling of the plasma-assisted catalytic growth and field emission properties of graphene sheet. *Physics of Plasmas* **22**, 123517 (2015).

[2] M. Kansal, Suresh C. Sharma, Plasma-based nanoarchitectonics for vertically aligned dual-metal carbon nanotube field-effect transistor (VA-DMCNFET) device: effect of plasma parameters on transistor properties. *Applied Physics A*, ***128*(1)**, 1-11 (2022).

[3] Alarcon A, Nguyen V, […] Dollfus P, Pseudosaturation and negative differential conductance in graphene field-effect transistors. *IEEE Transactions on Electron Devices* **60(3)**, 985-991 (2013).

[4] Bechhofer A, Ueda A, […] Teherani J, The 2D Debye length: An analytical study of weak charge screening in 2D semiconductors. *Journal of Applied Physics* **129(2)**, (2021).

[5] R. Vishnoi and M. J. Kumar, A Pseudo-2-D-Analytical Model of Dual Material Gate All-Around Nanowire Tunneling FET. *IEEE Transactions on Electron Devices*, vol. **61**, no. 7, pp. 2264-2270, ( 2014).

[6] Simionescu O-G, Avram A, Adiaconiță B, Preda P, Pârvulescu C, Năstase F, Chiriac E, Avram M. Field-Effect Transistors Based on Single-Layer Graphene and Graphene-Derived Materials. *Micromachines*. **14**(6):1096 (2023).

[7] S.C. Sharma, & N. Gupta,"Theoretical modeling of the plasma-assisted catalytic growth and field emission properties of graphene sheet", *Physics of Plasmas*, **22**(12), 123517 (2015).

# Sputter epitaxy of atomically flat $Zn_{1-x}Mg_xO$ films on sapphire using wurtzite MgO buffer layer fabricated in $Ar/O_2$ discharges

H. Otsuyama, H. Noguchi, K. Harada, N. Yamashita, T. Okumura, K. Kamataki, K. Koga, M. Shiratani and N. Itagaki

*Graduate School of Information Science and Electrical Engineering, Kyushu Univ, Fukuoka, Japan*

Epitaxial $Zn_{0.9}Mg_{0.1}O$ films were successfully grown on 18%-lattice-mismatched sapphire substrates using wurtzite MgO buffer layers fabricated by radio-frequency magnetron sputtering. The buffer layers enabled the growth of atomically flat $Zn_{1-x}Mg_xO$ films, reducing the root-mean-square roughness from 11 nm to 0.60 nm with a 1.5 nm-thick buffer. However, increasing the buffer thickness to 6 nm induced phase separation into wurtzite $Zn_{1-x}Mg_xO$ and rock-salt MgO, likely due to the phase transition of the MgO buffer to a rock-salt structure, resulting in increased roughness of $Zn_{0.9}Mg_{0.1}O$ films. We attribute these effects to the 1.5-nm-thick MgO buffer providing lattice-relaxed nucleation centers and a small lattice mismatch with $Zn_{1-x}Mg_xO$, promoting 2D growth of the subsequent films.

## 1. Introduction

Wurtzite $Zn_{1-x}Mg_xO$, with tunable bandgaps (3.4–4.5 eV), large exciton binding energies (60–90 meV), and strong ferroelectricity, is promising for next-generation optoelectronic devices and memory applications. Recently, we successfully grew single-crystalline $Zn_{1-x}Mg_xO$ films on 18%-lattice mismatched sapphire using ZnO buffer layers [1,2]. The buffers were synthesized via $Ar/N_2$ sputtering, where the adsorption-desorption behaviours of N atoms are controlled to form strain-relaxed nanosized 3D islands. Due to their large surface-to-volume ratios, the islands effectively relieve misfit strain, providing well-aligned nucleation sites. Here, we explore MgO as an alternative buffer layer. Though typically cubic, MgO can form nanosized islands with metastable wurtzite structure [3] and a smaller lattice mismatch (1.21–1.54%) particularly under non-equilibrium processes such as magnetron sputtering. Moreover, this structure can be achieved without nitrogen, likely minimizing impurity-induced defects.

## 2. Experimental

All films were fabricated by radio-frequency magnetron sputtering in an $Ar/O_2$ atmosphere at 800°C. First, MgO buffer layers were deposited on c-plane sapphire substrates, followed by the deposition of $Zn_{0.9}Mg_{0.1}O$ films on the buffer layers.

## 3. Results and discussion

We observed that MgO buffer layers significantly improved the surface flatness of $Zn_{0.9}Mg_{0.1}O$ films. The root-mean-square (RMS) roughness decreased from 11 nm to 0.60 nm with a 1.5 nm-thick MgO buffer (Fig. 1), attributed to wurtzite-phase 3D islands that relaxed lattice strain and facilitated 2D growth of $Zn_{0.9}Mg_{0.1}O$ films. However, a 6 nm-thick MgO buffer increased RMS roughness to 8.3 nm, likely due to the phase transition of the buffer from wurtzite to rock-salt above 3 nm [3]. In fact, structural analysis confirmed phase separation in the film grown on a 6 nm-thick buffer, forming wurtzite $Zn_{0.9}Mg_{0.1}O$ and rock-salt MgO. This is attributed to the rock-salt structure of the thick buffer and is considered a key factor contributing to the increased roughness.

These findings highlight the potential of wurtzite MgO buffer layers for growing atomically-flat $Zn_{1-x}Mg_xO$ films as well as other wurtzite materials on lattice-mismatched substrates.

This work was supported by JSPS KAKENHI JP22H05000, JP23K17752, and JP24K00929, JST ASPIRE 1234505, Tokyo Electron Ltd (TEL).

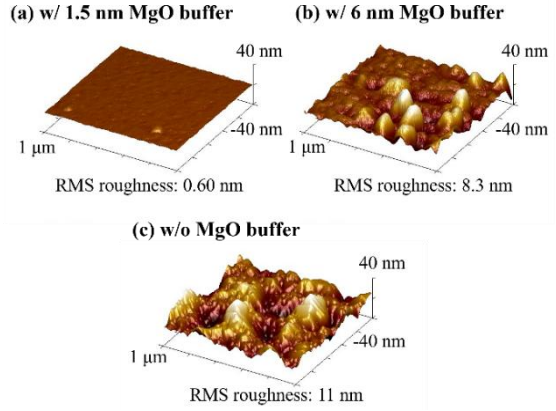



Fig. 1. AFM images of $Zn_{0.9}Mg_{0.1}O$ films with MgO buffers ((a), (b)) and without a buffer (c).

## References

[1] N. Itagaki, et al., *Sci. Rep.*, **10** (2020) 4669.
[2] D. Takahashi, et al., *MRS Adv.*, **7** (2022) 415–419.
[3] H. Kato, et al., *Appl. Phys. Lett.*, **84** (2004), 4562.

# A poly diagnostic study of an atomic oxygen plasma source: Application in cultural heritage

M. Poupouzas[1,2], N. Yang[2,3], A. Nikiforov[2], R. Morent[2] , G. Van der Snickt[3,4] and A. Sobota[1]

[1] *Department of Applied Physics, EPG, Eindhoven University of Technology, 5600 MB Eindhoven, The Netherlands*
[2] *Research Unit Plasma Technology (RUPT), Department of Applied Physics, Ghent University, Sint-Pietersnieuwstraat 41, 9000 Ghent, Belgium*
[3] *ARCHES Research Group, Faculty of Design Sciences, University of Antwerp, Mutsaardstraat 31, B-2000 Antwerp, Belgium*
[4] *AXIS Group, University of Antwerp (UA), Groenenborgerlaan 171, 2020 Antwerp, Belgium*

Atmospheric pressure plasma jets (APPJs) have a wide variety of applications including in cultural heritage. In the present study, a novel He-$O_2$ RF source surrounded by shielding gas is employed. The latter is optimized, by means of OES, with respect to the $O_2$(%), shielding gas flow and type as well as O production. Gas temperature is investigated with a temperature sensor. COMSOL modelling is employed to validate experimental results. Finally a first estimation of electron temperature and density is given at around 2.5 eV and $\sim 10^{18}$ $m^{-3}$ for powers between 1-10W.

Non-thermal radio frequency (RF) driven Atmospheric Pressure Plasma Jets (APPJs) are efficient sources of reactive oxygen and nitrogen species (RONS)[1]. Recently our team started investigating the applications of plasma technology in cultural heritage[2] for the treatment of different samples/artifacts.

Within the context of this study, a parametric investigation of emission spectra is conducted by varying the ratio of the flows of main gas and shielding gas. Emission bands and lines such as OH at 309 nm, $N_2$ at 316, 337, 357, and 379 nm, O at 777.4, 844, 926 nm and He at 706.5 nm are observed in all experimental cases.

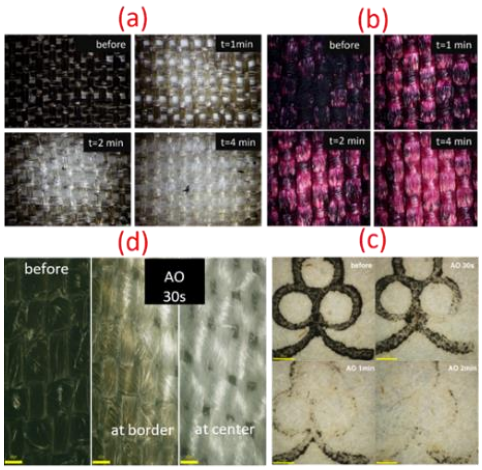



**Figure 1**: Samples: (a) Sooted silk blank, (b) Sooted silk cochineal, (c) Ink from paper, (d) Sooted linen blank.

A strong O emission (777 nm) is observed and its line intensity is optimized based on the gas flow and $O_2$(%). OH and $N_2$ lines show a decrease in the presence of shielding gas supporting its utility in the present application. Gas temperature is measured with a temperature sensor, unveiling the effect of power level and shielding gas presence on temperature. Finally the electron temperature is assessed by means of Boltzmann plot of all major O lines. A power balance equation is employed to estimate the electron density for all working conditions. The subsequent optimization of the source leads to the optimal treatment shown in Figure 1.

## References

[1] A. Schmidt-Bleker, J. Winter, S. Iseni, M. Dünnbier, K. D. Weltmann, and S. Reuter, "Reactive species output of a plasma jet with a shielding gas device - Combination of FTIR absorption spectroscopy and gas phase modelling," *J Phys D Appl Phys*, vol. 47, no. 14, Apr. 2014, doi: 10.1088/0022-3727/47/14/145201.

[2] A. Patelli *et al.*, "A customised atmospheric pressure plasma jet for conservation requirements," in *IOP Conference Series: Materials Science and Engineering*, Institute of Physics Publishing, Jun. 2018. doi: 10.1088/1757-899X/364/1/012079.

# Magnetron sputtering deposition of strained epitaxial $SrTiO_3$ thin films on MgO vicinal surfaces

Elnaz Familsatarian, Katharina Kohlmann, Andreas Ruediger, Emile Carbone

*Institut National de la Recherche Scientifique, centre Énergie, Matériaux et Télécommunications, 1650, blvd Lionel Boulet, Varennes J3X 1P7, Québec, Canada*

Epitaxial $SrTiO_3$ thin films are grown on MgO vicinal surfaces by magnetron sputtering. The impact of RF power, deposition pressure and annealing on $SrTiO_3$ thin film morphology are studied. Increasing RF power and lowering deposition pressure lead to higher surface roughness. Post-annealing induces strain relaxation, evidenced by new surface features nucleation. This study demonstrates that it is possible to control $SrTiO_3$ thin-film properties through the control of plasma parameters and via thermal post-treatment.

## 1 Introduction

Magnetron sputtering is a flexible and powerful method for depositing large area thin films on various substrates such as silicon wafer or MgO. Perovskites are a class of materials used notably for memory devices. Among perovskites, $SrTiO_3$ is of particular interest. At room temperature it is a dielectric while under strain, or with doping, it can become ferroelectric. Due to lattice mismatch between MgO and $SrTiO_3$, homo- and heterogeneous strain will be present in ultra-thin $SrTiO_3$ films. In this presentation, the morphology of epitaxial thin films of $SrTiO_3$ and its relation to the MgO vicinal surface topography will be discussed. Strain-induced effects during the deposition process as well as post-annealing steps are highlighted, and we will present correlations between plasma parameters (due to, e.g. ion bombardment) and surface morphology. Moreover, annealing temperatures strongly affect the mechanism of strain relaxation of the $SrTiO_3$ thin film.

## 2 Methodology

For epitaxial growth, a flat substrate is mandatory. Therefore, MgO substrates are annealed at 1100°C from 30 minutes up to 3 hours, resulting in atomically flat terraces with roughness in the tens of picometer range (Figure 1-a).

For the deposition of $SrTiO_3$, an on-axis RF magnetron sputtering system (SPT310, Plasmionique Inc.) is used with a $SrTiO_3$ target under $Ar/O_2$ atmosphere at pressures of 10-40 mTorr typically. A temperature-controlled substrate holder is used and a temperature of 550°C is fixed for $SrTiO_3$ deposition. The $SrTiO_3$ films are annealed after deposition at temperatures between 400-900°C with variable times between 1 and 10 h allowing for surface self-diffusion and relaxation.

Atomic Force Microscopy (AFM) is utilized for the determination of the surface morphology of MgO and $SrTiO_3$. Additionally, X-ray Diffraction, X-ray Photoelectron Spectroscopy (XPS), and Transmission Electron Microscopy (TEM) are used for substrate and film characterization. Finally, the plasma process is monitored by time resolved optical emission spectroscopy.

## 3 Results and Discussion

The surface topography of the $SrTiO_3$ films follows the pattern of the terraces of the MgO substrates, which is indicative of epitaxial growth. In Figure 1, an example of MgO substrate before and after deposition is shown.

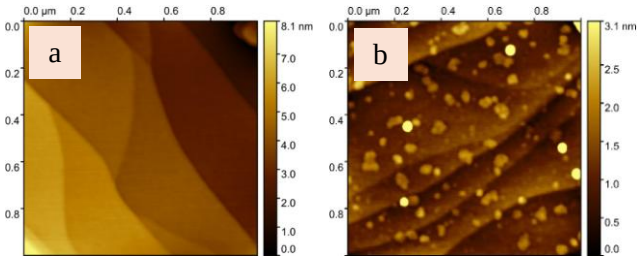



Figure 1: (a) MgO substrate annealed at 1100°C for 3 hours, (b) annealed $SrTiO_3$ thin film at 500°C for 1 hour after deposition on the same MgO substrate.

Our study indicates that the MgO single crystal miscut angle, dislocations as well as impurities diffusion from the crystal bulk influence the MgO surface morphology after annealing and thus the one of deposited $SrTiO_3$ thin films. Furthermore, XPS analysis confirms that each film exhibits the expected $SrTiO_3$ stoichiometry. Increasing the power and/or decreasing the deposition pressure leads to rougher $SrTiO_3$ films. Higher surface roughness is likely due to the bombardment of energetic particles in the plasma which increases with RF power/self-bias. Post-annealing of $SrTiO_3$ also shows an increase of roughness (i.e. number of adatoms), formation of grains and even nucleation of islands of $SrTiO_3$ depending on annealing time and temperature. The increase of roughness as well as the formation of pores or islands is enabled by higher mobility of atoms on the surface and in the bulk during annealing and leading to relaxation of the strained layer.

# Production of durable superhydrophobic coatings using atmospheric pressure plasma

B. A. Kyrykbay[1,2], S. S. Ussenkhan[2], Ye. Yerlanuly[1], A.U. Utegenov[1,2], S.A. Orazbayev[1,2] and T.S. Ramazanov[2]

[1] *Kazakh-British Technical University, Almaty, Kazakhstan*.
[2] *Institute of Applied Science and Information Technologies, Almaty, Kazakhstan*

This study explores the durability of superhydrophobic coatings synthesized via plasma polymerization, using argon (Ar) as the plasma-forming gas and hexamethyldisiloxane (HMDSO) as the precursor. The stability of these coatings was evaluated under various environmental conditions, including fogging, ice formation, and temperature fluctuations. Superhydrophobic performance was assessed by measuring water contact angles and surface roughness. The results demonstrate that the coatings exhibit strong water repellency and retain their properties over extended periods.

The development of hydrophobic surfaces through atmospheric-pressure plasma treatment has garnered significant attention due to its effectiveness in various technological applications, including self-cleaning coatings, anti-icing systems, and optical devices [1,2]. Superhydrophobic coatings, defined by their ability to repel water, act as protective layers that enhance surface durability and functionality.

This study investigates the influence of plasma deposition parameters on the structural and wetting properties of these coatings. By systematically varying key process conditions-such as discharge power, precursor concentration, and deposition time-the research aims to identify optimal settings for achieving stable superhydrophobic surfaces with improved performance characteristics [3].

Experimental results indicate that increasing the discharge power from 100 W to 200 W significantly enhances surface hydrophobicity, as evidenced by an increase in the water contact angle from 140° to 165°. This improvement suggests that higher discharge power promotes the formation of a more hydrophobic surface, likely due to modifications in the film's morphology and chemical composition.

The number of deposition cycles was found to affect coating thickness, reducing transparency without altering hydrophobic properties.

Durability tests confirmed the coatings' resistance to UV radiation, high temperatures, fogging, icing, and chemical exposure.

These obtaining results demonstrate that plasma-synthesized superhydrophobic films exhibit high stability and can effectively protect various surfaces under real-world climatic conditions.

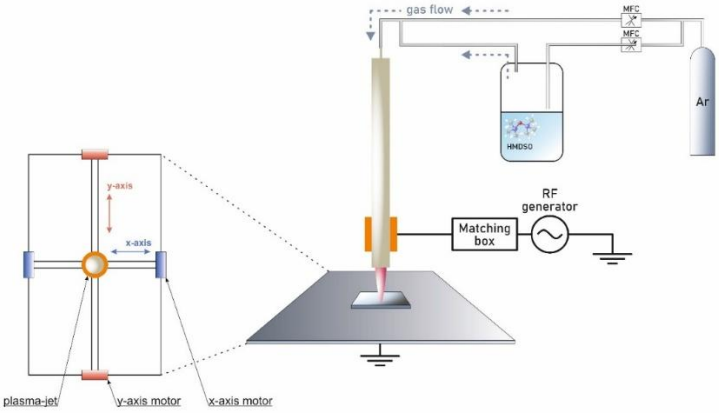



Figure 1. Schematic of an experimental setup for superhydrophobic film deposition by atmospheric pressure plasma polymerization

**References**

[1] Chattopadhyay S, Huang YF, Jen YJ, et al. Anti-reflect- ing and photonic nanostructures. Materials Science and Engineering: R: Reports **69**, 1-35 (2010).

[2] Orazbayev S, Zhumadilov R, Zhunisbekov A, Gabdullin M, Yerlanuly Y, Utegenov A and Ramazanov T. Applied Surface Science **515**, 146050 (2020).

[3] Ussenkhan S.S., Kyrykbay B.A., Yerlanuly Y., Zhunisbekov A.T., Gabdullin M.T., Ramazanov T.S., Orazbayev S.A., Utegenov A.U. Fabricating durable and stable superhydrophobic coatings by the atmospheric pressure plasma polymerisation of hexamethyldisiloxane Heliyon, **10(1)**, e23844(2024).

# Influence of Gas Pressure On Quartz and Silicon Etching in a Dual-Frequency Capacitively Coupled $NF_3/Ar/O_2$ Plasma

Chan Li, Yongxin Liu, Fei Gao and Xianxiu Mei

*Dalian University of Technology School of Physics, Dalian 116024, China*

**Abstract：** This study investigates the effect of air pressure on the etching of quartz and silicon in an $NF_3/Ar/O_2$ plasma. Higher pressure increases the F radical concentration, which enhances the fluorination reaction, increasing the etching rate and surface roughness. Rough quartz etches faster than smooth quartz due to more surface defects, forming etching pits and granular structures. In silicon, etch rates vary with surface roughness, with polycrystalline silicon showing the most significant changes. Monocrystalline and polycrystalline silicon develop irregular surface structures, while polished monocrystalline silicon remains largely unchanged. These findings help to optimise plasma etching processes and improve the etch resistance of materials.

## 1. Plasma Diagnostics & Etching Rate

Fig. 1(a) shows that the relative concentration of F atoms with increasing gas pressure in the $NF_3/Ar/O_2$ plasma. Fig. 1(b) presents that the etching rate of both rough and smooth quartz increases with gas pressure, and the etching rate of rough quartz is faster. Fig. 1(c) illustrates the surface roughness of rough and smooth quartz changes significantly with increasing air pressure. Fig.1(d) compares the etch rates of monocrystalline silicon, monocrystalline polished silicon wafers, and polycrystalline silicon at different air pressures, revealing that all three materials etched faster as air pressure increased. This indicated that higher air pressure enhanced the concentration of reactive plasma particles, particularly F radicals, which accelerated the etching reaction [1].

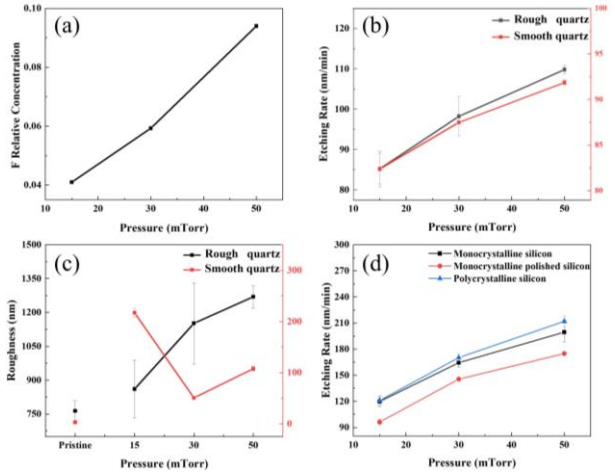



Fig. 1 $NF_3/Ar/O_2$ plasma (a) relative concentration of F atoms (b) etching rate of quartz (c) roughness of quartz (d) etching rate of silicon

## 2. Microstructure of quartz and silicon

Fig. 2($a_0$)-($a_1$) and ($b_0$)-($b_1$) display the surface morphology of rough and smooth quartz before and after etching. After etching at 15 mTorr, both quartz surfaces developed pits and small spheres. Fig. 2($c_0$)-($c_1$) and ($d_0$)-($d_1$) illustrate the surface morphology of monocrystalline silicon and monocrystalline polished silicon wafers. The polished silicon surface remained flat and mostly unchanged during etching, while monocrystalline silicon gradually formed a granular structure.

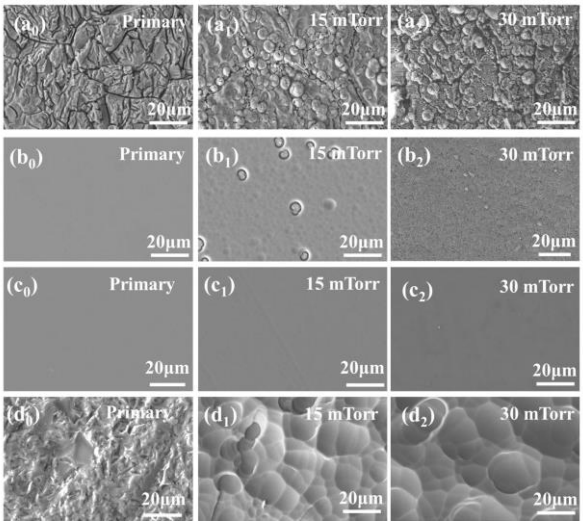



Fig. 2 Surface morphology of quartz and silicon before and after etching at different air pressures ($a_0$)- ($a_2$) rough quartz, ($b_0$)- ($b_2$) smooth quartz($c_0$)-($c_2$) monocrystalline polished silicon, ($d_0$)-($d_2$) monocrystalline silicon

**References**

[1] Kang, H., Lee, S., Jeon, M. & Chae, H. Plasma atomic layer etching of tantalum nitride with surface fluorination and Ar ion sputtering. *Journal of Vacuum Science & Technology A* **43,** 022601-1–022601-8 (2025).

# Surface Modification of Polyethylene by Atmospheric Pressure Plasma Jet

J. Wangkanai and E. Wagenaars

*York Plasma Institute, School of Physics, Engineering and Technology, University of York, York, UK*

The surface modification of polyethylene (PE) is studied by plasma treatment, focusing on investigating the underpinning mechanism of the surface interaction. The nonthermal plasmas are generated using a micro-scaled atmospheric pressure plasma jet (μAPPJ). The analyses focus on the surface structural properties using contact angle measurement and Fourier Transform Infrared Spectrometry (FTIR). Plasma-treated PE showed a rapid decrease in contact angle with treatment time, with significant reduction observed within one second. Different feed gas admixtures result in different surface modifications for short treatment times. In addition, the FTIR results showed an increase in some functional groups, including carbonyl bonds (C=O), on the PE surface. These functional groups are known to increase the surface energy of a sample, explaining the improved wettability observed.

## 1 Introduction

Reactive species inside plasmas play a crucial role in many applications including polymers such as polypropylene (PP) [1] and polyethylene (PE). The functionality of the polymer surface can be improved to be more chemically compatible. However, the mechanisms of the interaction between the plasma and the surface are complex and not well understood.

## 2 Methodology

The cold plasma is generated by a micro-scaled atmospheric pressure plasma jet (μAPPJ) as a capacitively coupled RF discharge ($1\times1\times30$ mm$^3$). The system typically flows with helium (He) containing small amounts of admixtures such as oxygen ($O_2$) 0.5% or water vapour ($H_2O$) 0.33%. The power supply is adjustable power at 13.56 MHz. The samples of PE are placed at a distance of 10 mm from the jet nozzle. The treatment time are considered from 0-900 s.

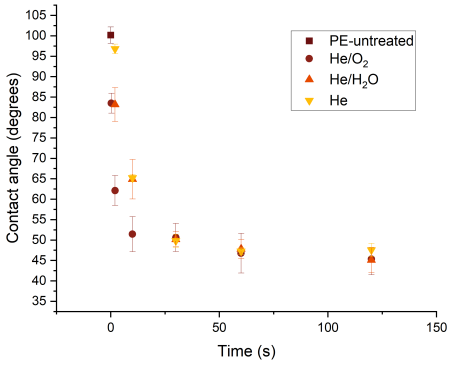



Figure 1: Contact angle of PE treated with different plasma gas admixtures.

## 3 Results

The treated PE samples were analysed for their wettability by contact angle sessile drop tests and their structural properties by Fourier Transform Infrared Spectrometry (FTIR) in Attenuated Total Reflectance (ATR) mode. PE samples were treated by different plasma gas admixtures and treatment times.

Contact angle results for PE treated by He, He/$O_2$ and He/$H_2O$ are shown in Figure 1. The FTIR results of PE treated by He/$O_2$ plasmas are shown in Figure 2. FTIR peaks at 1642 and 1717 cm$^{-1}$ are associated with the functional group carbonyl (C=O) and they can be seen to increase with increasing treatment time, indicating incorporation of O atoms on the surface, creating polar groups that enhance the surface wettability.

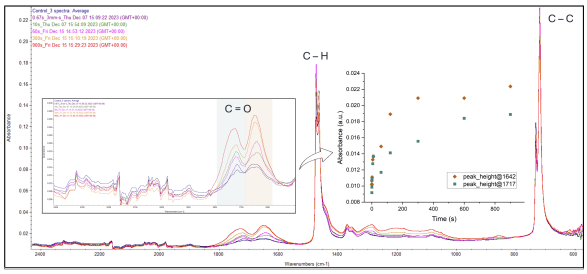



Figure 2: FTIR results of PE treated by He/$O_2$ plasmas.

## References

[1] Shaw, D., West, A., Bredin, J., & Wagenaars, E. Mechanisms behind surface modification of polypropylene film using an atmospheric-pressure plasma jet. *Plasma Sources Science and Technology*, **25(6)**, 065018 (2016).

# Sulphur-containing organic films grown by $SH_2/CH_4$/He plasmas

R. J. Peláez, I. Tanarro, B. Maté and V. J. Herrero
*Instituto de Estructura de la Materia (IEM-CSIC), Madrid, Spain*

Sulfur-containing thin films are gaining attention due to their potential applications in biomedicine and astrophysics. This study focuses on the production and characterization of such films generated by an inductively coupled RF plasma using $SH_2$ and $CH_4$ precursors. Mass spectrometry, optical emission spectroscopy, and different surface analysis techniques, are employed to analyze the film properties and growth mechanisms. The results reveal efficient film growth at specific $SH_2$ partial pressures and confirmed sulfur incorporation into the deposited material

## 1 Introduction

The production of sulfur-containing films is receiving growing interest in numerous fields. SH groups on surfaces facilitate biomolecule functionalization, making them highly useful in biomedical applications, where thiol-based coupling enables the attachment of proteins, DNA, and other biomolecules [1]. On the other hand, infrared (IR) observations of dense clouds in the interstellar medium reveal an unexpectedly low concentration of sulfur, which remains unexplained. Some models and recent observations highlight the relevance of refractory materials as a possible reservoir for this missing sulfur. Thus, the characterization of organic sulfur-containing cosmic dust analogs could be key to explain this sulfur depletion [2].

Plasma-assisted deposition of thin films using $SH_2$ has been shown as an effective single-step process for the production of these materials [3]. Herein we explore the deposition of the sulfur-organic films, focusing not only on the material properties but also on plasma characteristics and the growth process.

## 2 Experiment

The films are produced in an inductively coupled RF discharge on Al substrates at a power of 40 W. The total pressure is 0.31 mbar, with $SH_2$ and $CH_4$ partial pressures in a 2:5 ratio. Mass spectrometry (MS) and optical emission spectroscopy (OES) are used for plasma characterization. The growth process is monitored using multi-λ two-θ laser thin-film interferometry, which also determines the refractive index and film thickness (n~1.4 for λ=664 nm and d~3 μm after 2 hours). The films are characterized by Fourier transform infrared spectroscopy (FTIR), X-ray photoelectron spectroscopy (XPS) and energy-dispersive X-ray analysis (EDX).

## 3 Results and discussion

The interferometric measurements show that efficient film growth occurs at a maximum partial pressure of $SH_2$ of 0.023 mbar. This suggests that sulfur-richer gas mixtures are dominated by etching processes, which prevent the formation of films.

The precursors dissociation and the formation of $H_2$, $CS_2$, $S_2$, and $C_2H_x$ species are confirmed by MS. Additionally, strong bands of CS and $S_2$ are detected by OES. These results suggest that multiple polymerization processes involving hydrocarbons, SH and $CS_2$ might occur simultaneously. The estimated density and optical properties of the deposited material are consistent with those reported for a-C:H thin films. XPS, EDS, and FTIR spectra (see Fig. 1) confirm sulfur incorporation into the deposited film.

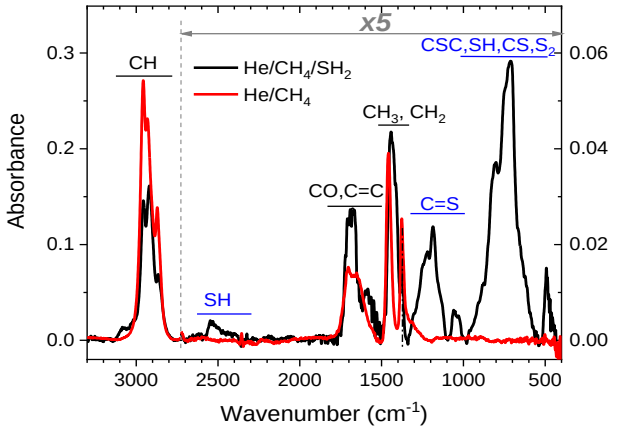



Fig 1: FTIR spectra of films grown with and without $SH_2$.

**4. Acknowledgements**

This work is funded by the Spanish M. de Ciencia, Innovación y Universidades under grant PID2023-146415NB-I00 and the CSIC i-LINK project SENTINEL (ILINK23017).

**References**

[1] Zahedifar P, *et al.* Progress in Organic Coatings, 196, 108771 (2024).

[2] M. Kama *et al.*, Astrophysical Journal 885,114 (2019).

[3] E. Kasparek *et al.*, Plasma Processes and Polymers, 15, e1800036 (2018).

# Enhancement of Cu and Ti catalysts with nanostructuring by laser irradiation and simultaneous chemical modification by plasma treatment

A. Schicke[1], S. Chur[1], J. Kaufmann[1], M. Böke[2], and J. Golda[1]

[1] *Plasma Interface Physics, Ruhr-University Bochum, Bochum, Germany*
[2] *Reactive Plasmas, Ruhr-University Bochum, Bochum, Germany*

Surfaces of copper bulk material were simultaneously altered by laser irradiation and reactive species of an atmospheric plasma jet. Structures in the nanometer regime are observed on bulk copper via Scanning Electron Microscopy. The chemical composition of copper can be changed by plasma treatment as measured by X-ray Photoelectron Spectroscopy, showing an increase in the concentration of CuO of more than 30%. This knowledge is transferred to the nitration of titanium, but the first measurements of titanium suggest, that surface structuring is more difficult.

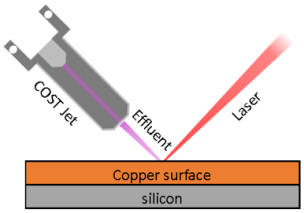



Figure 1: Schematic of the combined laser-plasma treatment.

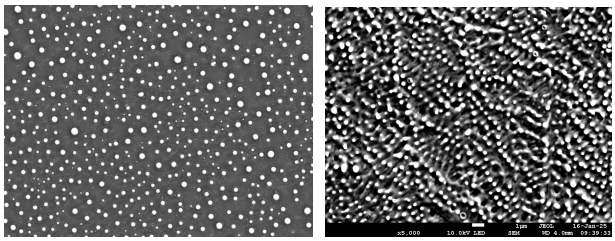


Figure 2: PLIDS on Cu layer on Si wafer (left) and LIPSS on Cu bulk material (right).

## Motivation

The surface characteristics of a catalyst have a major impact on its efficiency. The most significant changes in efficiency are caused by surface morphology, i.e. the catalyst's nanostructure, and chemical composition [1].

We investigate the simultaneous application of electric fields and energy input of pulsed laser irradiation with reactive species produced by a micro-scaled atmospheric plasma jet (see Fig. 1). These plasma-laser-surface interactions can lead to effective functionalisation of the surface, which causes higher selectivity and overall higher efficiency of the catalyst. This has been done to improve the $CO_2$ reduction rate with copper (Cu) catalysts. The goal is to transfer the successfully proven modification of Cu to titanium (Ti).

## Surface structuring by laser irradiation

The first step in increasing the catalyst's efficiency is controlling the surface morphology of the samples. Usually, these surfaces are thin layers deposited on, e.g. silicon (Si) wafers, irradiated by a frequency-doubled Nd:YAG laser (532 nm). On these Cu layers, Pulsed Laser Induced Dewetting Structures (PLIDS) are formed [2]. Additionally, we produced Laser Induced Periodic Surface Structures (LIPSS) in the nanometer regime on Cu bulk material. Both were measured via Scanning Electron Microscope (SEM), as seen in Fig. 2.

## Combined laser and plasma treatment

Secondly, the chemical composition of the samples is changed by additionally exposing the surface to the effluent of a COST Reference Microplasma Jet [3] operated with a helium-oxygen admixture in a controlled atmosphere. Measured by X-ray Photoelectron Spectroscopy (XPS), the concentration of CuO in the Cu samples is rising from 0% (in the untreated case) to more than 30% depending on treatment time.

## Acknowledgements

This work was funded by the German Research Foundation (DFG) within the CRC1316 (project B2).

## References

[1] Arán-Ais, R. M. *Nat. Energy*, **5**, 317-325, (2020)
[2] Chur, S. *ACS Omega*, **9**, 29234-29243 (2024).
[3] Golda, J. *J. Phys. D: Appl. Phy.*, **49**, 084003 (2016).

# COMSOL simulation for dual frequency inductively coupled plasma

B. Alemu[1], L. Terraz[1] and R. Kling[1]

[1] *Karlsruhe Institute of Technology, Light Technology Institute, 76131 Karlsruhe, Germany*

In this work, results from a COMSOL simulation of a dual-frequency Argon inductively coupled plasma torch at atmospheric pressure are discussed. To have optimum operating conditions, the effects of distance variations between the two coils and of the power of the high frequency coil have been evaluated.

## 1 Introduction

The conventional single frequency atmospheric-pressure inductively coupled plasma (ICP) torch has been an exciting part of investigations since it was discovered. In a typical setup, a coil surrounding the plasma confinement tube is excited with a radiofrequency current, which in turn creates a strong magnetic field. The charge carriers gain energy through the magnetic field and are then able to ionize more particles. Being electrodeless, ICPs can be used to produce contamination-free plasmas with high enthalpy. As a result, it has many industrial applications, for instance in nanoparticle synthesis, spectrochemical analysis, powder spheroidization, material testing in the aerospace industries, and the fiber optics industries [1], etc. However, working with high–frequency electronics is feasible for higher plasma power coupling but not at a desirable cost.

Figure 1 illustrates a hybrid approach, in which the high frequency (HF) coil ignites the plasma at a relatively low power, while the medium frequency (MF) coil supplies the remaining power in a cost-effective manner that can be customized. Here we study to what extent sustaining the discharge is easier with one HF coil and one MF coil rather than with only one MF coil.

## 2 Simulation Method

We use COMSOL Multiphysics® to study discharge that are sustained by induction currents. Laminar flow, heat transfer and electromagnetic fields interfaces are coupled in the numerical model. Frequency transient runs are performed with different distances between the coils and excitation powers of the HF coil. For each variation, the minimum sustaining power, its corresponding coil current and the temperature distribution are evaluated.

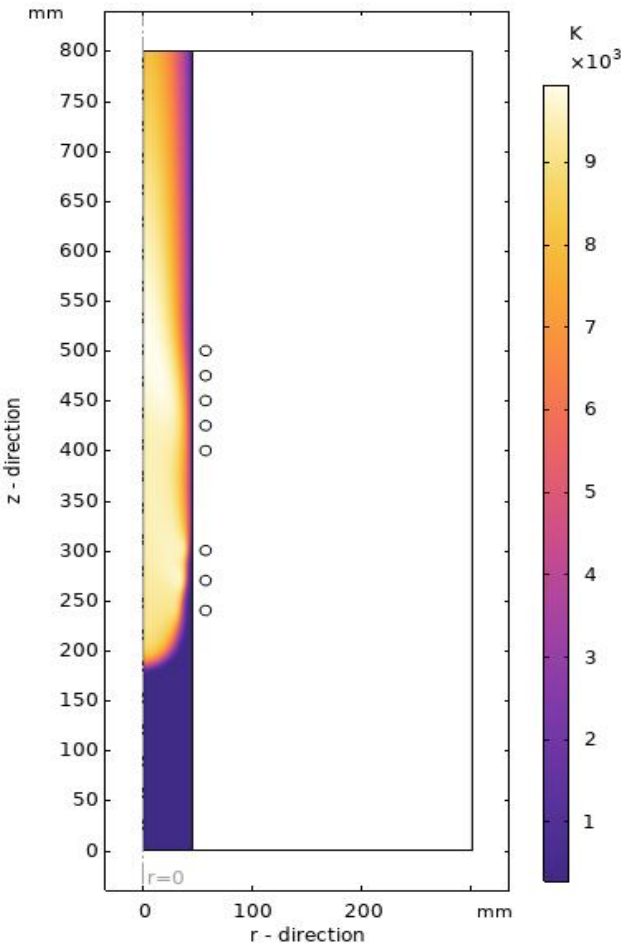



**Figure 1: Temperature profile of 2D axisymmetric model of the dual frequency ICP torch**

## References

[1] Boulos M.*et al*. RF Inductively Coupled Plasma Torches. *Handbook of Thermal Plasma.* 850 - 857

# Insights into the Role of Plasma Jet Reactive Species for the Formation of Gold-based Nanocatalysts Confined in Nanoreactors

G. Boitel-Aullen[1], L. Sicking[1], S. Schüttler[2], P. A. Kopton[1], F. Brämer[1], A. Loukovitou[1], P. Cignoni[1], C. Kaiser[1], L. Jolmes[1], J. Golda[2] and K. Tschulik[1]

[1] *Ruhr University Bochum, Research group of Electrochemistry and Nanoscale Materials, Bochum, Germany*
[2] *Ruhr University Bochum, Research group of Plasma Interface Physics, Bochum, Germany*

With the objective of developing new routes for the synthesis of nanocatalysts, we propose here a step through the understanding of the formation of gold-based nanoparticles (NPs) from metal salt precursors in solutions treated by an atmospheric pressure plasma jet (APPJ). The APPJ produces highly reactive species inducing in situ nucleation and growth of the Au NPs by reduction of the metal salt, that we investigate by imaging and electrochemical techniques. The metal precursor is either freely moving in water, in aqueous-organic mixtures or confined inside a nanoreactor composed of an aqueous phase dispersed into an organic one, for a better control of the configuration and size of the NPs. In presence of an organic phase, NPs can also be decorated on a carbon supporting material like carbon black, for further electrocatalytic applications.

## 1 Obtention of the nanocatalysts

We propose an original bottom-up synthesis route of Au and AuPd NPs, in which the metal salts are encapsulated inside reverse micelles (RMs), which consist of aqueous microemulsions dispersed in an organic phase and stabilized by molecular surfactants (SDS, AOT). Reduction of the metal salts inside the RMs has already been achieved by electrochemistry [1]. Here, we take advantage of the reactive species produced by an APPJ [2,3] to directly treat RMs in solution (**Figures 1a** and **b**). A suspension of carbon black can be added to the solution before APPJ treatment, acting as supporting material for the NPs. They are further deposited on glassy carbon (GC) for characterization by scanning electron microscopy (SEM, **Figure 1c**) and electrochemistry (**Figure 1d**). Hence, we can determine the mass of the synthesized NPs, as well as their electrocatalytic activity towards hydrogen evolution reaction or glucose oxidation. [4]

## 2 Role of the reactive species

To better understand the role of the plasma generated reactive species in the formation mechanism of the NPs, we compared the treatment of Au-containing RMs with aqueous solutions of $HAuCl_4$, in presence or not of an organic phase. $H_2O_2$ present in significant quantity in our APPJ effluent is known to proceed to the NPs growth, but $N_2$ species also present influence their nucleation and dissolution [3,4]. This is visible when comparing a plasma treatment of the RMs, which leads to the formation of AuNPs characterized by an oxidation peak on the cyclic voltammogram (CV), while a simple addition of $H_2O_2$ to the RMs does not lead to the formation of any NP (**Figure 1d**).

We are now implementing a method to follow in situ the formation of NPs from the plasma effluent by electrochemistry coupled with optical imaging.

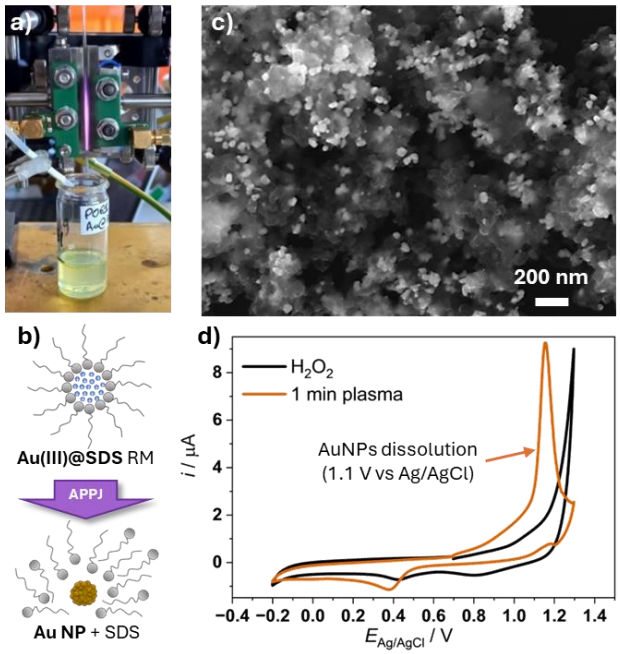



**Figure 1. a)** Photo and **b)** scheme of the APPJ treatment of Au@SDS RMs suspension; **c)** SEM image of AuNPs onto Carbon black after APPJ; **d)** Stripping CV (HCl 0.1M) of Au@SDS drop cast onto GC after APPJ or $H_2O_2$ treatment.

### References

[1] M.V. Evers, M. Bernal, B. Roldan Cuenya, K. Tschulik, *Angew. Chem.* **58** 8221-8225 (2019).
[2] T. Winzer, D. Steuer, S. Schüttler, N. Blosczyk, J. Benedikt, J. Golda, *J. Appl. Phys* **132** (2022) 183301.
[3] S. Schüttler, L. Jolmes, E. Jeß, K. Tschulik, J. Golda, *Plasma Process. Polym.* **21** (2023) e230079.
[4] G. Boitel-Aullen, L. Sicking, S. Schüttler, J. Golda, K. Tschulik, *to be submitted soon*.

# Study of ozone production by surface processes

V. Mazankova[1], D. Trunec[2] and F. Stanek[3]

[1]*Faculty of Military Technology, University of Defence in Brno, Kounicova 65, 662 10 Brno, Czech Republic*
[2]*Faculty of Science, Masaryk University, Kotlarska 2, 611 37 Brno, Czech Republic*
[3]*Faculty of Chemistry, Brno University of Technology, Purkyňova 118, 612 00 Brno, Czech Republic*

The ozone production by surface processes was studied on inner surface in a quartz cuvette. The time dependence of produced ozone concentration was measured by absorption spectroscopy in the same cuvette. The rate coefficient for ozone production on surface was determined from linear part of the measured dependencies. The measured rate constant was 2.05 $\cdot 10^{-19}$ $cm^{-2}s^{-1}$.

## 1 Introduction

Plasma surface interactions are of considerable importance for a wealth of discharge phenomena. They are especially important in the formation and destruction of ozone in the afterglow of a DC low-pressure discharge in pure $O_2$ [1] and also in a dielectric barrier discharge at atmospheric pressure [2]. Nevertheless, the rates or probabilities associated with these surface reactions remain unknow. This contribution focuses on elucidating the determination of ozone production rates on silica surfaces.

When the solid surface is into contact with oxygen discharge or ozone, the surface is quickly covered by adsorbed atomic oxygen species and also by molecular oxygen species. Then the ozone is created by surface reactions via Langmuir-Hinshelwood (LH) mechanism or via Eley-Rideal (ER) mechanism. The LH mechanism is described by reaction

$$O_{2S} + O_S \rightarrow O_3 + 2S, \quad (1)$$

where $O_S$ and $O_{2S}$ are adsorbed oxygen atoms and molecules, respectively, S is the vacant site. The ER mechanism is described by reaction

$$O_2 + O_S \rightarrow O_3 + S, \quad (2)$$

where $O_2$ is molecule arriving at the surface from gas phase.

## 2 Results

The kinetics of ozone production was studied on inner surface of the cuvette which was at the same time used for absorption measurement of ozone concentration. The inner surface of the cuvette was treated by ozone for 5 min. After that the ozone was removed from the cuvette and the cuvette was filled by the mixture of oxygen and argon with different ratio. The time dependence of originated by surface reaction was measured using absorption spectroscopy. The results are shown in Fig.1. For short reaction time the ozone concentration increases linearly, when the ozone concentration increases above $2 \cdot 10^{15}$ $cm^{-3}$ also the destruction processes of ozone occur. When the cuvette is filled by argon only, the ozone originated by LH processes only. If the oxygen is added to the argon, the ozone is created also by ER mechanism and the increase of ozone concentration is faster and the final ozone concentration is also higher, see Fig.1.

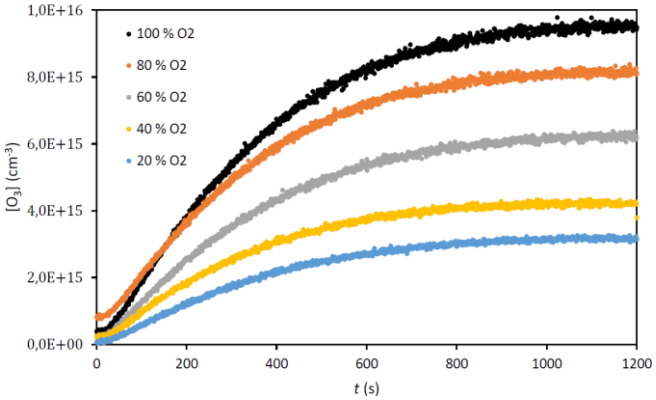



Fig.1 The dependence of ozone concentration on reaction time.

The rate coefficient for surface ozone production was determined from the slope of linear part of dependencies.

We assumed that the surface concentration of active sites is $10^{16}$ $cm^{-2}$ and one half of these sites is occupied by atomic oxygen and second half is occupied by molecule oxygen. Under this assumption the rate coefficient derived from these slopes is 2.05 $\cdot 10^{-19}$ $cm^{-2}s^{-1}$ for LH mechanism.

**Acknowledgement**

This research work was supported by the Project for the Development of the Organization "DZRO Military autonomous and robotic systems" under Ministry of Defence and Armed Forces of Czech Republic.

**References**

[1] Booth, J. P. et al, *Plasma Sources Sci. Technol*. **32** (2023) 095016.

[2] Meyer, M., Foster, J. and Kushner, M. J. *Plasma Sources Sci. Technol.* **32** (2023) 085001.

# Microscopic and macroscopic investigation of He bubbles formation on tungsten via *in situ* spectroscopic ellipsometry

F. Pappalardo[1,*], M. Alfaazza[3], G. Cartry[1], C. Martin[1], A. Campos[2], J. Mougenot[4], T. Angot[1], R. Bisson[1] and M. Minissale[1]

[1]*Aix-Marseille Université, CNRS, PIIM, Marseille, France*
[2]*Aix-Marseille University, CNRS, Centrale Marseille, CP2M, Marseille, France*
[3] *CNRS, Université d'Orléans, CEMHTI UPR 3079, Orléans, France*
[4]*Université Sorbonne Paris Nord, LSPM, CNRS, Villetaneuse, France*

In the experimental fusion reactor ITER, the divertor and first wall components will be realized in tungsten (W) and will experience under operational regime both high heat fluxes and ion fluxes, mostly hydrogen isotopes and helium (He) ions. The interaction of such charged particles with W can induce material modifications [1-3], from microscopic lattice defects to mesoscopic damages such as near-surface (<50 nm) bubbles, already observed on W exposed to low energy (<100 eV) He ions at high temperatures (<1273 K) [4]. The formation of these near-surface structures can lead to a modification of the optical properties of W, for example by an increase of surface roughness.

In this work, we investigate the evolution of surface morphology and optical properties of W exposed to He plasma via *in-situ* spectroscopic ellipsometry. This technique uses a polychromatic source of polarized light (400-1000 nm) impinging on a sample and measures the change in its polarization upon reflection from the surface. The experimental setup is composed by a RF plasma chamber in which *in situ* spectroscopic ellipsometry measurement is realized during He plasma exposure of W samples. The He ion energy is around 80 eV, the He ion flux is $2x10^{19}$ $m^{-2}s^{-1}$ and after about 8 hours of plasma exposure the total fluence is $5x10^{23}$ $m^{-2}$. We perform different plasma exposures varying multiple parameters (sample temperature, ion flux and initial W surface state), with a double purpose. First, we use ex-situ imaging techniques (SEM, AFM) to characterize microscopically the size and density of He bubbles as a function of temperature and grain orientation after the 8 hours of plasma exposure. Secondly, we couple these microscopy results with the *in situ* time resolved ellipsometry data to reconstruct the temporal evolution of porosity and surface roughness during the 8 hours of plasma exposure, with an appropriate effective-medium layer that takes into account the volume fraction of He bubbles (porosity) in W sub-surface,. Eventually, we validate our results using a model implemented in FEniCS code [5], which describes He bubbles growth and transport.

**References :**

[1] A. Mahnard *et al*, Nucl. Fusion **57**, 126012 (2017)
[2] L. Gao *et al.*, Nucl. Fusion **54**, 122003 (2014)
[3] D. Nishijima *et al.*, Nucl. Fusion **45**, 669-674 (2005)
[4] R. Kolasinski *et al.*, J. Appl. Phys. **131**, 063303 (2022)
[5] R. Delaporte-Mathurin *et al.*, Sc. Reports 11:146681 (2021)

# High-pressure inductively coupled plasmas with bidirectional vortex gas injection

Cormac Corr[1], Trevor Lafleur[2], Ash Pascale[1], Thomas Hort[1], Murray Jobbins[1], Josh Wei[1], Yani Ait Ammar[3]

[1] *Research School of Physics, Australian National University, Canberra, Australia*
[2] *School of Engineering and Technology, University of New South Wales, Canberra, Australia*
[3] *Ecole Polytechnique, F-91128, Palaiseau, France*

This work examines high-pressure inductively coupled plasmas (ICPs) in near-thermal equilibrium operating with both argon and nitrogen as feed gas. The plasma system uses the inductive fields of a radio-frequency (rf) antenna surrounding a dielectric tube to generate and sustain a plasma, which superheats the feed gas to temperatures up to 10,000 K. The heated gas then exits the plasma production zone through either subsonic or supersonic nozzles. We introduce the fundamental operation of the newly developed ICP technology that employs bidirectional vortex gas injection, significantly reducing heat losses while enhancing thermal plasma efficiency. The plasma properties are analysed using optical emission spectroscopy, calorimetry, and electrical circuit measurements. This adaptable technology has broad potential applications, such as propulsion systems, materials processing, gas conversion, and aerothermodynamics testing.

Thermal plasmas are defined by the nearly uniform equilibrium of temperatures among electrons, ions, and neutrals. These plasmas are typically observed under conditions of high pressures or high densities, where frequent collisions between particles promote thermal equilibrium. In this study, we focus on high-pressure inductively coupled plasmas (ICPs), which operate in a state of near thermal equilibrium, as reported in prior research [1-3]. These plasmas are generated and maintained through inductive coupling, where a radio-frequency (rf) antenna surrounds a dielectric tube containing the feed gas. The resulting plasma achieves extremely high temperatures, capable of superheating the feed gas to values as high as 10,000 K. This heated gas is subsequently expelled through nozzles – either subsonic or supersonic – positioned at the downstream end of the plasma production region.

In this work, we study the operation of a newly developed ICP technology, which incorporates bidirectional vortex gas injection. This approach to gas flow management is demonstrated to significantly mitigate thermal losses by promoting enhanced energy retention within the plasma. Consequently, this feature substantially improves the overall efficiency, making the plasma system viable for a broad spectrum of applications. The performance of the plasma is characterized through optical emission spectroscopy, calorimetric analysis, and electrical circuit measurements.

Furthermore, we highlight the versatility of this ICP technology, emphasizing its potential across diverse fields of application including its use in advanced propulsion systems, enabling efficient and high-performance thrust generation; materials processing, particularly for cutting-edge manufacturing; gas conversion for energy storage or chemical synthesis; and aerothermodynamics testing to simulate extreme thermal and aerodynamic environments.

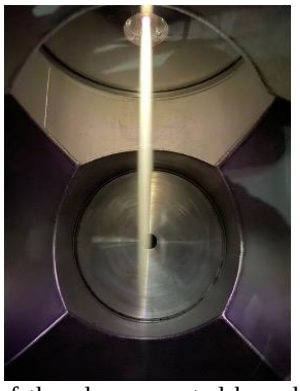


Figure 1. Photo of the plume created by a high-pressure inductively coupled nitrogen plasma with a supersonic nozzle.

## References

[1] Lafleur T and Corr C. Characterization of a radio-frequency inductively coupled electrothermal plasma thruster. *J. Appl. Phys.* ***130*** *043304* (2021).
[2] Pascale A, Lafleur T, Corr CS. Bidirectional vortex stabilization of a supersonic inductively coupled plasma torch. *J. Phys. D: Appl. Phys.* ***56*** *105202* (2023).
[3] Pascale A, Lafleur T, Corr CS. Parametric study of a vortex-enhanced supersonic inductive plasma torch. *J. Phys. D: Appl. Phys.* ***57*** *435206* (2024).

# Voltage evolution in low pressure free electric arcs in air

C. Pietri[1], Y. Aïchoun[1], R. Landfried[1], T. Leblanc[1] and Ph. Testé[1]

[1]*Université Paris-Saclay, CentraleSupélec, CNRS, Laboratoire de Génie Electrique et Electronique de Paris, 91192, Gif-sur-Yvette, France.*
[1]*Sorbonne Université, Université Paris-Saclay, CNRS, CentraleSupélec, Laboratoire Génie électrique et électronique de Paris, GeePs, F-91192 Gif-sur-Yvette, France*

In this paper we will discuss some phenomena occurring in free electric arcs in air, in pressure ranging from 25 hPa to 200 hPa, for this we will use arc voltage and high-speed films to try and compare the information.

## 1 General

Arc voltage evolution during the contact opening phase has been studied over the past few decades to characterise electric signals in an electric arc. Most studies are conducted at atmospheric pressure [1], or using vacuum switching device [2]. However, to our knowledge, some of the phenomena occurring in the pressure ranging from 25 hPa to 200 hPa with copper electrodes have not yet been addressed. In this work some original behaviours observed in the arc voltage evolution are presented. Interpretations of these are proposed, according to physical phenomena likely to contribute to them.

## 2 Experimental setup

The setup described in figure 1 is composed of an electric contact opening system in which the arc current and voltage, length and opening speed are controlled. Two high-speed cameras are used to record the arc, at 10 000 fps; they are triggered so that they start recording at the same time. One is equipped with a filter centered on 515 nm, which enables us to evaluate when excited copper first appears in the arc.

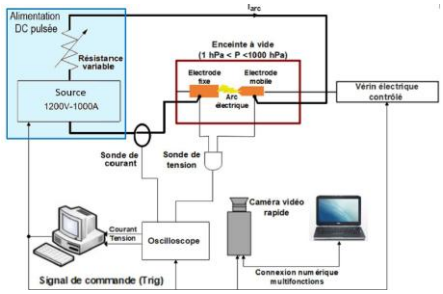



Fig 1. Experimental setup

Arcs were made with $U_{supply} = 540\ V$ and $I_{arc} = 50$ A.

## 3 Observations

For each pressure condition, at least five tests were performed to estimate repeatability. Some distinct behaviours still occurred : voltage instabilities, as shown in figure 2 with P = 40 hPa and P = 75 hPa, that seem to become a change in the slope of voltage and to happen earlier as pressure increases. These could be linked to the motion of arc roots, especially at the cathode. At pressures below 200 hPa, a voltage surge appearing a few ms after arc initiation, highlighted in figure 2 for 40 hPa and 75 hPa was observed inconsistently, at the same pressure. Below 200 hPa, a voltage leap ΔU is also observed. It could be linked to the first appearance of copper in the arc.

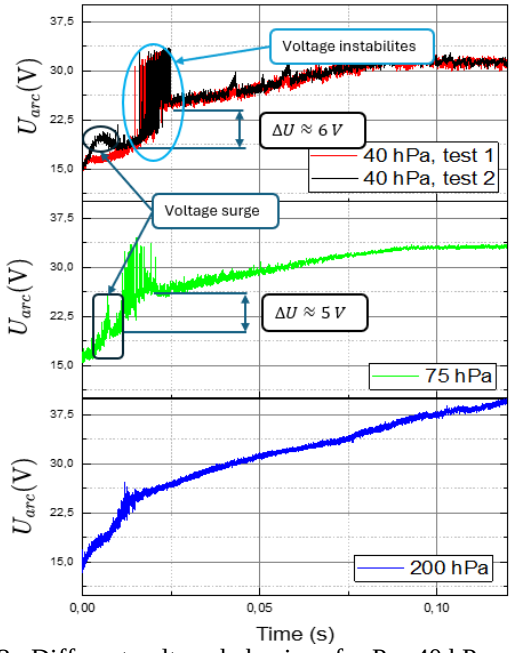



Fig 2. Different voltage behaviour for P = 40 hPa, P = 75 hPa and P = 200 hPa.

## 4 References

[1] L. Féchant, Le Contact Électrique : Phénomènes physiques et matériaux. 1996, 678 pages, ISBN 978-2-86601-554-1.
[2] P. G. Slade, The Vacuum Interrupter. CRC Press, 2020. doi : 10.1201/9780429298912

# Study of stopping processes and transport properties of heated dense plasmas based on the density functional theory

A. Uderbayeva[1,2], M. Issanova[1,2], N. Turekul[1,2] and N. Djienbekov[1,2]

[1] *Institute of Applied Sciences and Information Technology, Almaty, Kazakhstan*
[2] *Al-Farabi Kazakh National University, Almaty, Kazakhstan*

This study investigates stopping processes and transport properties in heated dense plasmas using density functional theory (DFT). By accurately simulation electron-ion interactions and screening effects, DFT provides a detailed description of energy loss mechanisms for charged projectiles traversing plasma under extreme conditions. In this work also investigated transport coefficients of beryllium, aluminium and silicon dioxide. The results are analyzed and compared with existing experimental data and theoretical models.

## 1 General

Warm dense matter is being intensively studied all over the world both experimentally and theoretically. At high temperatures and pressures, the existing theoretical models of liquid, gas, solid and plasma are inapplicable to the extreme state of matter. The main obstacle to the application of these models is the strong nonideality of the medium, that is, the significant role played by the interaction of particles and quantum effects.

The dynamical and transport properties of materials in a wide range of densities and temperatures, in particular, for substances under extreme conditions, are important in various fields. Some systems of interest include the interiors of giant planets, white dwarfs, and heated dense matter generated by laser heating and shock compression in experiments. In addition, heated dense matter is actively studied in connection with the development of inertial thermonuclear fusion facilities [1-2]. Due to the difficulties of diagnostics under extreme conditions in experiments, quantum molecular dynamics (QMD) modeling based on the density functional theory has become an integral part of modern studies of heated dense matter. Knowledge of the ranges and profiles of energy losses, transfer coefficients, and optical properties of heated dense beryllium, aluminium, and silicon dioxide will make it possible to more accurately calculate the design and production technology of a thermonuclear target.

## 2 Results and discussion

In presented work stopping processes and transport properties of heated dense beryllium, aluminum and silicon dioxide based on the density functional theory (DFT) in a wide range of temperatures and densities are considered. This approach allows for an accurate description of electronic structure effects in strongly coupled and partially degenerate plasma conditions. The study focuses on the energy loss mechanisms of charged particles moving through a heated dense plasma, considering the influence of electron-ion interactions and screening effects. By leveraging DFT calculations, key transport properties and stopping power are analyzed, providing insights into how plasma heating impacts energy dissipation and particle dynamics. We also have computed diffusion and viscosity coefficients based on DFT simulation for various values of parameters of heated dense beryllium, aluminium and silicon dioxide. Figure 1 shows the dependence of the diffusion coefficient on temperature calculated by the mean-square displacement (MSD) and velocity autocorrelation function (VACF) methods, as well as the data obtained using the Coulomb logarithm. It can be seen that the diffusion coefficients calculated using different techniques show good agreement, which confirms the validity of the values obtained.

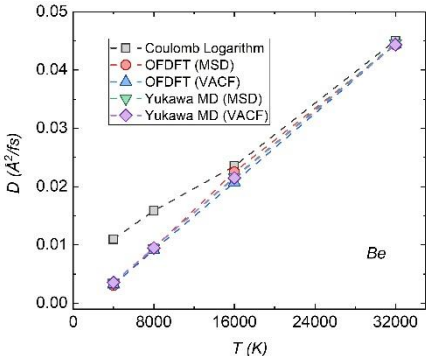



Figure 1. Diffusion coefficient as a function of temperature.

**References**

[1] Drake R.P., *Phys. Today*, **63(6)**, 28 (2010).
[2] Shao X., Jiang K., Mi W., Genova A., Pavanello M. *WIREs Comput Mol Sci.*, **e1482** (2020).

# Program of Poster Session #3

| # | In Competition | Title | Speakers | Topic |
|---|---|---|---|---|
| Th-1 | NO | Insights into nucleation of nanodiamonds in microplasma | Prasanna Swaminathan | Complex and dusty plasmas, ion-ion plasmas, mixed phase plasmas |
| Th-2 | NO | Photoionization process in a nonextensive plasma | Lee Myoung-Jae | Elementary processes and fundamental data |
| Th-3 | NO | Inelastic momentum transfer cross-sections for electron-impact excitation in Helium: scaling rules for n≥4 states | Carman Robert | Elementary processes and fundamental data |
| Th-4 | YES | Variable-pulse streamer discharges using an Impedance-matched Marx Generator | Meekes Wouter | Elementary processes and fundamental data, High frequency and pulsed discharges |
| Th-5 | NO | Recent advances in reproducible plasma simulation: LXCat 3.0 and LoKI-B++ | Boer Daan | Elementary processes and fundamental data, Modelling and simulation techniques |
| Th-6 | NO | Application of field electron emission model to pulsed discharge | Takahashi Kazuhiro | High frequency and pulsed discharges |
| Th-7 | NO | Modified plasma pencil for use in chemical trace element detection | Medek Tomas | High frequency and pulsed discharges |
| Th-8 | NO | Preventing the formation of vortexes in an atmospheric ICP | Terraz Loann | High frequency and pulsed discharges, Thermodynamics and transport phenomena, High pressure and thermal plasma processing |
| Th-9 | NO | Carbon-Enhanced Plasma-Based $CO_2$ Conversion: From Fixed Beds to Direct Microparticle Injections | Eivazpour Taher Ataollah | High pressure and thermal plasma processing |

| # | In Competition | Title | Speakers | Topic |
|---|---|---|---|---|
| Th-10 | NO | Spectral characteristics of indium-argon inductively coupled plasma | Abola Anda | Low pressure plasmas |
| Th-11 | NO | Experimental characterisation of the electrode-to-wall area ratio's influence on the plasma and electrode potential for large cathode size | Hiret Paul | Low pressure plasmas |
| Th-12 | NO | Detection of reactive species in plasma-treated water using Electrochemical Impedance Spectroscopy | Saeedeh Saeedeh | Low pressure plasmas, Plasma in/with liquids |
| Th-13 | NO | Evaluation of growth characteristics of sugarcane in response to plasma-activated leafmold application | Okumura Takamasa | Medical, biological, environmental and aeronautical applications |
| Th-14 | YES | Design and Evaluation of a Low-Cost Air Ionic Wind Thruster | Polanšek Juš | Medical, biological, environmental and aeronautical applications |
| Th-15 | NO | Numerical Modeling of Ionic Wind and Ozone Production in a DC Corona Discharge under Humid Air Conditions | Khattara Toufik | Medical, biological, environmental and aeronautical applications |
| Th-16 | NO | Surface-enhanced NOx formation in microwave-driven atmospheric pressure air plasma with downstream catalyst | Gans Jonas | Medical, biological, environmental and aeronautical applications |
| Th-17 | YES | Transient phase of the flow field induced by an AC-driven SDBD | Giotis Konstantinos | Medical, biological, environmental and aeronautical applications |
| Th-18 | NO | Improved efficiency in micro-structured plasma reactor for Hydrogen production using a pin to pin spark configuration | Jacquart Maxime | Medical, biological, environmental and aeronautical applications |
| Th-19 | YES | Zero-Dimensional Simulation of Nitrogen NRP Discharges and Dissociation Efficiency | Roger Edouard | Modelling and simulation techniques |
| Th-20 | NO | Modeling of N2-H2 DC discharges for ammonia production | Alves Luís | Modelling and simulation techniques |

| # | In Competition | Title | Speakers | Topic |
|---|---|---|---|---|
| Th-21 | NO | Boosting the NOx production in microwave air plasma: A synergy of chemistry and vibrational kinetics | Shen Qinghao | Modelling and simulation techniques |
| Th-22 | NO | Magnetic moment based on gyrocoordinates in partially magnetized plasmas in an axisymmetric magnetic field | Vogelhuber Lukas | Modelling and simulation techniques |
| Th-23 | NO | PICCOLO: a PIC code suite for low-temperature plasmas | Taccogna Francesco | Modelling and simulation techniques |
| Th-24 | NO | Data-driven reduced modeling of streamer discharges in air | Teunissen Jannis | Modelling and simulation techniques |
| Th-25 | NO | Self-consistent PLASIMO global model for dust growth and plasma chemistry | Van 't Veer Kevin | Modelling and simulation techniques, Complex and dusty plasmas, ion-ion plasmas, mixed phase plasmas |
| Th-26 | NO | Electric Field and Chemical Kinetics in a Nanosecond-Pulsed DBD in Humid Air | Popoli Arturo | Modelling and simulation techniques, High frequency and pulsed discharges, Non-equilibrium plasmas and microplasmas at high pressure |
| Th-27 | NO | Spatiotemporal distribution of surface potential on barrier during atmospheric pressure Townsend discharge in air and N2 | Osawa Naoki | Non-equilibrium plasmas and microplasmas at high pressure |
| Th-28 | YES | Impact of different dielectric materials on the performance and optical features of a Micro-Hollow Cathode Discharge | Chazapis Nikolaos | Non-equilibrium plasmas and microplasmas at high pressure |
| Th-29 | NO | Numerical thermalization in 3D PIC plasma simulations | Park Ryan | Non-equilibrium plasmas and microplasmas at high pressure |

| # | In Competition | Title | Speakers | Topic |
|---|---|---|---|---|
| Th-30 | NO | Hybrid mode of DBD at atmospheric pressure in Ar-HMDS mixtures: modelling and experimental studies | Marjan Stankov | Non-equilibrium plasmas and microplasmas at high pressure |
| Th-31 | NO | Gradient nanosecond pulsed plasmas for enhanced deflagration to detonation transition: measurements of atomic oxygen density production and reduced electric field | Lafaurie Victor | Non-equilibrium plasmas and microplasmas at high pressure |
| Th-32 | NO | Computational study of a pulsed atmospheric pressure dielectric barrier discharge (DBD) in humid air | Van Hove Sarah | Non-equilibrium plasmas and microplasmas at high pressure |
| Th-33 | NO | Design and safety assessment of a low-temperature plasma device for the treatment of large and medium wounds | Liao Jiunn-Der | Non-equilibrium plasmas and microplasmas at high pressure |
| Th-34 | NO | Systematic experimental investigation of N2/H2 plasmas for NH3 synthesis in a dielectric barrier discharge | Meindl Arne | Non-equilibrium plasmas and microplasmas at high pressure |
| Th-35 | YES | Fluid Dynamics and Surface Interactions of Helical Plasma Plumes in a Radiofrequency Atmospheric Pressure Plasma Jet | T. P. Radhika | Non-equilibrium plasmas and microplasmas at high pressure |
| Th-36 | NO | Diffuse Dielectric Barrier Discharge in air: role of Ozone? | Naude Nicolas | Non-equilibrium plasmas and microplasmas at high pressure |
| Th-37 | YES | Atmospheric re-entry plasma characterization | Brault Adrien | Non-equilibrium plasmas and microplasmas at high pressure, Plasma wall interactions, electrode and surface effects, Plasma diagnostics methods |

| # | In Competition | Title | Speakers | Topic |
|---|---|---|---|---|
| Th-38 | NO | Experimental comparison of detached vibrationally-resolved D2 SOLPS-ITER simulations on MAST-Upgrade | Bryant Joseph | Other applications such as low temperature plasma applications for magnetically confined fusion |
| Th-39 | NO | First measurements of the WEST Thomson scattering system | Schiesko Loïc | Other applications such as low temperature plasma applications for magnetically confined fusion |
| Th-40 | YES | LIBS for fusion : tungsten and boron spectral characterization | Gosse Léo | Plasma created by laser and EUV radiations |
| Th-41 | NO | Fiber PROES: High-Speed, Low-Cost Plasma Monitoring | Korolov Ihor | Plasma diagnostics methods |
| Th-42 | YES | Comparison of PMT and iCCD detectors for resolving low SNR TALIF signals in hydrogen plasmas | Hörsch Julian | Plasma diagnostics methods |
| Th-43 | NO | On the gas temperature variations in a DC Ar/N2 MHCD | Stefas Dimitrios | Plasma diagnostics methods |
| Th-44 | NO | The Applicability of a Microwave Resonant Probe to the Plasma Processing of Silicon Oxide | Ellis James | Plasma diagnostics methods |
| Th-45 | YES | Development of a miniaturized hollow-core fiber plasma spectroscopy technique | Radu Vlad-Ștefănuț | Plasma diagnostics methods |
| Th-46 | NO | Measurement and simulation of time-resolved N2(A,v) densities in a sub-microsecond pulsed near-atmospheric pressure discharge | Kuhfeld Jan | Plasma diagnostics methods |
| Th-47 | YES | Cross-Validated Electron Diagnostics in Atmospheric-Pressure RF Plasmas | Choi Jiwon | Plasma diagnostics methods |
| Th-48 | YES | Comparison of Electrical Diagnostic Techniques for Capacitively Coupled Radio Frequency (CCRF) Plasma | Sunil Varsha | Plasma diagnostics methods |

| # | In Competition | Title | Speakers | Topic |
|---|---|---|---|---|
| Th-49 | NO | Comparative Study on Microwave Diagnostics: Cutoff Probe, Hairpin Probe, and Microwave Interferometer | Kim Sijun | Plasma diagnostics methods |
| Th-50 | NO | Nanosecond point-to-plane high-pressure discharge: PIC modelling and comparison with experiments | Dilecce Giorgio | Plasma diagnostics methods |
| Th-51 | NO | Electrical characteristics of low-pressure radio frequency capacitively coupled discharges used for plasma polymer deposition | Polaskova Katerina | Plasma diagnostics methods, Low pressure plasmas |
| Th-52 | YES | On Transient Nature of Polarized Emission from Laser Produced Plasma | B R Geethika | Plasma diagnostics methods, Plasma created by laser and EUV radiations |
| Th-53 | NO | Stability of reactive species produced in plasma-activated water by various atmospheric air discharges and their antimicrobial properties combined with UV-A irradiation | Machala Zdenko | Plasma in/with liquids |
| Th-54 | NO | Tuning properties of activated liquids produced by an atmospheric pressure plasma jet for application in plasma medicine | Markovic Andjelija | Plasma in/with liquids |
| Th-55 | NO | Influence of Pulsed Plasmas in Liquids on Copper Surfaces | Pottkämper Pia-Victoria | Plasma in/with liquids |
| Th-56 | NO | Penning mixture experiments in an inductively driven lamp | Anantharaman Raghuraman | Plasma power and pulsed power technology, particle and radiation sources |
| Th-57 | NO | Iron ore reduction in hydrogen-containing low-pressure plasma | Mayer Marimel | Plasma processing of surfaces and particles |
| Th-58 | YES | Sputter epitaxy of ZnO films on lattice mismatched sapphire substrates using MgO buffer layers fabricated in Ar/O2 discharges | Harada Katsuyuki | Plasma processing of surfaces and particles |

| # | In Competition | Title | Speakers | Topic |
|---|---|---|---|---|
| Th-59 | NO | Synthesis of Chondrule-like Particles Based on Si-Fe in RF Discharge Conditions | Akdaulet Baikaliyev | Plasma processing of surfaces and particles |
| Th-60 | NO | Correlation between work function and H-/D- production on C12A7 electride surface | Sasao Mamiko | Plasma wall interactions, electrode and surface effects |
| Th-61 | NO | Electron surface scattering kernel in the few-eV energy range for plasma-facing dielectric solids | Bronold Franz Xaver | Plasma wall interactions, electrode and surface effects |
| Th-62 | NO | Influence of oxygen on arsenic containing inductively coupled plasma | Abola Anda | Plasma wall interactions, electrode and surface effects |
| Th-63 | NO | Is the use of the Sagdeev potential a legitimate way of deriving collisional Bohm criteria? | Benilov Mikhail | Plasma wall interactions, electrode and surface effects |
| Th-64 | NO | Investigation of H- surface-production in low-pressure plasma using a magnetized RFEA and in-situ photoemission | Cartry Gilles | Plasma wall interactions, electrode and surface effects |
| Th-65 | NO | Space Charge Structures on a Gridded Spherical Hollow Electrode | Ionita Codrina | Plasma wall interactions, electrode and surface effects |
| Th-66 | NO | Space Charge Structures on Smooth Spherical Hollow Electrodes | Schrittwieser Roman | Plasma wall interactions, electrode and surface effects |
| Th-67 | NO | Comparison of Calculated Oxygen Thermodynamic Transport Properties with Literature | Dycke Jan | Thermal plasmas |
| Th-68 | NO | Diagnostic of DC arc plasmas in aeronautic conditions: application to detection | Hellé Arthur | Thermal plasmas |
| Th-69 | NO | Calculation of the Radiative Properties of a Thermal Plasma $H_2O$-Air | Bendida Imane | Thermal plasmas |
| Th-70 | NO | Evaluation of Plasma Fluctuation Using Stochastic Model Based on Relative Entropy | Akatsuka Hiroshi | Thermodynamics and transport phenomena |

| # | In Competition | Title | Speakers | Topic |
|---|---|---|---|---|
| Th-71 | NO | Two-temperature modelling of ignition of high-current arc discharges on cold cathodes in atmospheric-pressure argon | Santos Diego | Thermal plasmas |

# Presenter Index


- **Abola Anda**: Th-10, Th-62
- **Akatsuka Hiroshi**: Th-70
- **Akdaulet Baikaliyev**: Th-59
- **Alves Luís**: Th-20
- **Anantharaman Raghuraman**: Th-56
- **B R Geethika**: Th-52
- **Bendida Imane**: Th-69
- **Benilov Mikhail**: Th-63
- **Boer Daan**: Th-5
- **Brault Adrien**: Th-37
- **Bronold Franz Xaver**: Th-61
- **Bryant Joseph**: Th-38
- **Carman Robert**: Th-3
- **Cartry Gilles**: Th-64
- **Chazapis Nikolaos**: Th-28
- **Choi Jiwon**: Th-47
- **Dilecce Giorgio**: Th-50
- **Dycke Jan**: Th-67
- **Eivazpour Taher Ataollah**: Th-9
- **Ellis James**: Th-44
- **Gans Jonas**: Th-16
- **Giotis Konstantinos**: Th-17
- **Gosse Léo**: Th-40
- **Harada Katsuyuki**: Th-58
- **Hellé Arthur**: Th-68
- **Hiret Paul**: Th-11
- **Hörsch Julian**: Th-42
- **Ionita Codrina**: Th-65
- **Jacquart Maxime**: Th-18
- **Khattara Toufik**: Th-15
- **Kim Sijun**: Th-49

- **Korolov Ihor**: Th-41
- **Kuhfeld Jan**: Th-46
- **Lafaurie Victor**: Th-31
- **Lee Myoung-Jae**: Th-2
- **Liao Jiunn-Der**: Th-33
- **Machala Zdenko**: Th-53
- **Marjan Stankov**: Th-30
- **Markovic Andjelija**: Th-54
- **Mayer Marimel**: Th-57
- **Medek Tomas**: Th-7
- **Meekes Wouter**: Th-4
- **Meindl Arne**: Th-34
- **Naude Nicolas**: Th-36
- **Okumura Takamasa**: Th-13
- **Osawa Naoki**: Th-27
- **Park Ryan**: Th-29
- **Polanšek Juš**: Th-14
- **Polaskova Katerina**: Th-51
- **Popoli Arturo**: Th-26
- **Pottkämper Pia-Victoria**: Th-55
- **Prasanna Swaminathan**: Th-1
- **Radu Vlad-Ștefănuț**: Th-45
- **Roger Edouard**: Th-19
- **Saeedeh Saeedeh**: Th-12
- **Santos Diego**: Th-71
- **Sasao Mamiko**: Th-60
- **Schiesko Loïc**: Th-39
- **Schrittwieser Roman**: Th-66
- **Shen Qinghao**: Th-21
- **Stefas Dimitrios**: Th-43
- **Sunil Varsha**: Th-48
- **T. P. Radhika**: Th-35
- **Taccogna Francesco**: Th-23

- **Takahashi Kazuhiro**: Th-6
- **Terraz Loann**: Th-8
- **Teunissen Jannis**: Th-24
- **Van 't Veer Kevin**: Th-25
- **Van Hove Sarah**: Th-32
- **Vogelhuber Lukas**: Th-22

# Insights into nucleation of nanodiamonds in microplasma

S. Prasanna[1], J. Jeevan[1], A. Siby[1], A. Michau[1], M. Redolfi[1] and K. Hassouni[1]

[1] *LSPM UPR 3407 CNRS, Université Sorbonne Paris Nord, Villetaneuse, France*

In this study we discuss the plasma chemistry leading to the nucleation of nanodiamonds in a microplasma.

## 1 General

Through the work of Siby et al1, we have demonstrated the feasibility of producing diamond nanoparticles or nanodiamonds (NDs) of size < 10 nm in gas phase using a microwave assisted microplasma torch when using hydrogen and methane as precursor gases. We had showed that substantial concentrations of hydrogen atom are critical to support the nucleation of diamond nanoparticles in the gas phase.

In this work, we provide insights into the chemistry of the formation of the different carbon nanostructures phase in a MW micro-plasma torch with hydrogen-methane-Argon gas mixtures by combining plasma diagnostics, material characterization and 0D-plasma simulations. The micro-plasma was characterized using optical emission spectroscopy (OES) for gas temperature, electron density and ps-TALIF for H-atom density.While the gas temperatures varied in the range 1000-1400 K, the electron density was nearly constant for the different conditions studied (about 2.1013 cm -3). Similarly, the concentration of H-atom measured using ps-TALIF was estimated to be nearly constant $10^{16}$ cm-3, indicating dissociation of hydrogen through electron impact processes. The high atomic hydrogen produced plays an essential role in stabilizing the diamond phase by saturating the dangling bonds of the carbon atoms on the surface and ensuring the etching of the non-diamond phases likely to co-deposit ($sp^2$ carbon); this ensures a $sp^3$ bond for the carbon (diamond).

However, little changes in H-atom concentration for the studied conditions indicate that the hydrocarbon chemistry leading to the formation of carbon nanostructures is strongly influenced by the gas temperature and concentration of carbon radicals such as $C_2$ and $CH_3$. The phase of the carbon collected are estimated using Raman spectroscopy and give insights into the chemistry prevailing in the plasma and its downstream. Figure 1a shows the variation of $\%sp^3$ phase (inferred from Raman spectra) with Argon and methane flow rates at 100 mbar pressure, $H_2$ flow rate fixed at 100 sccm and power of 90 W. The optimum condition where $sp^3$ molecular growth and nucleation of NDs takes place is at 4% methane and 20 sccm of Ar. Interestingly, the emission intensities of $C_2$ (Figure 1b) and CH are also the maximum at these conditions. This is indicative that the abundance of these radicals is key for nucleation of nanodiamonds. On the other hand, simulations indicate that presence of acetylene favor formation of amorphous carbon.

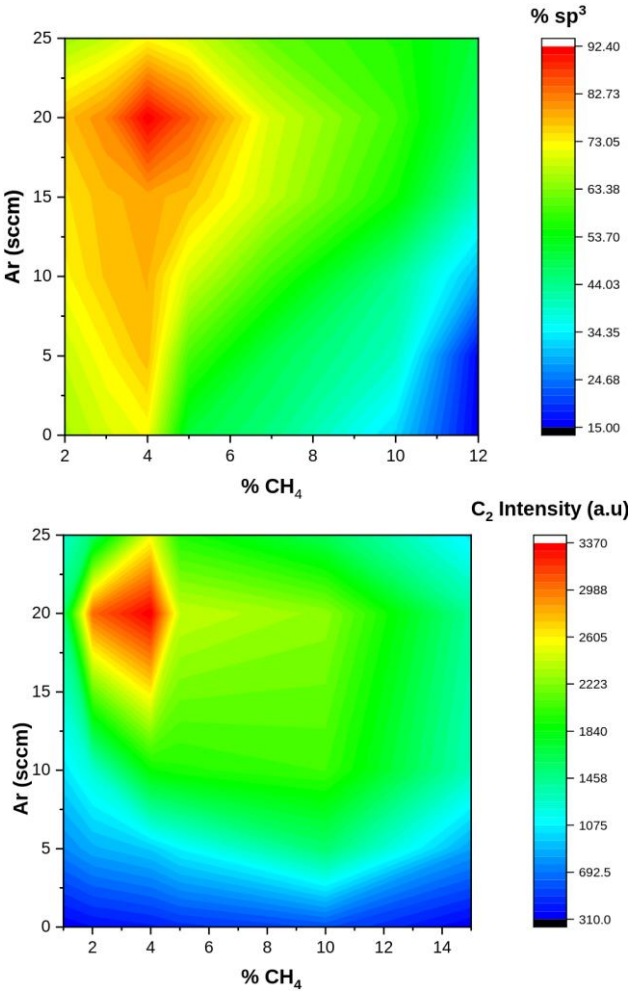



Fig. 1: Contour plots depicting a) abundance of sp3 fraction in carbon nanostructures b) intensities of $C_2$ Swann band as a function of Ar and $CH_4$ concentration at 100 mbar pressure and 90 W operations.

**References**

[1] Siby, Abdoulaye, et al. Diamond and Related Materials **152** (2025): 111933

# Photoionization process in a nonextensive plasma

Myoung-Jae Lee[1] and Young-Dae Jung[2]

[1]*Department of Physics, Hanyang University, Seoul 04763, South Korea*
[2]*Department of Applied Physics, Hanyang University ERICA Campus, Ansan, Kyunggi-Do 15588, South Korea*

The influence of Tsallis $q$-entropy is investigated on the photoionization process in a nonextensive plasma. The eigen functions and energy eigenvalues for the ground of the target ion in a non-extensive plasma are obtained by the Ritz variation method. It is shown that the influence of Tsallis $q$-entropy suppresses the photoionization cross section. In addition, the $q$-entropy effect on the photoionization cross section is found to be decreased with an increase of the photon energy.

## 1 Computation

Photoionization process is a subject of a special attention in many areas of physics, such as atomic and plasma physics since it is extremely sensitive to the details of atomic structure and the correlation effects between atomic electrons. Recently, photoionization process in plasmas is of great interest since this process can be used for plasma diagnostics.

The photoionization process in a nonextensive plasma have not been investigated yet. Hence, we have investigated the influence of Tsallis $q$-entropy on the K-shell photoionization of hydrogenic ions in non-extensive plasmas.

The eigen functions and energy eigenvalues for the ground of the target ion in a nonextensive plasma are obtained by the Ritz variation method. The differential cross section for the photo ejection is obtained by the dipole acceleration formula including the retardation correction, Coulomb correction, and plasma screening effects.

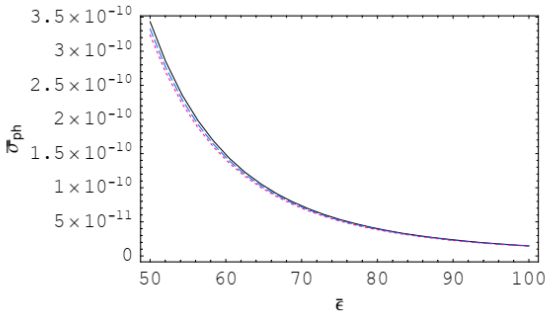



FIG1. Photoionization cross section as a function of the photon energy

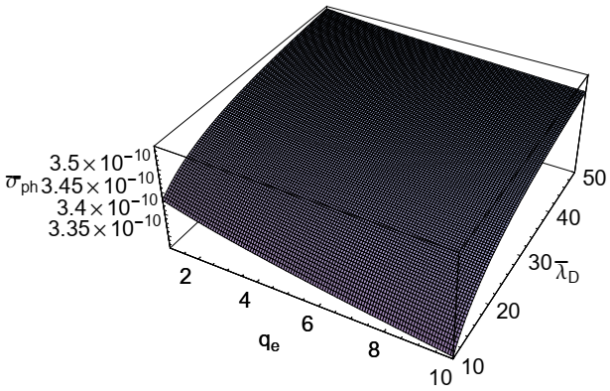



FIG2. Surface plot of the photoionization cross section as a function of the $q$-entropy and the Debye length.

## 2 Results

It is shown that the influence of Tsallis $q$-entropy suppresses the photoionization cross section. In addition, the $q$-entropy effect on the photoionization cross section is found to be decreased with an increase of the photon energy.

**References**

[1] Tucker, W. H., Radiation Processes in Astrophysics (MIT Press, Cambridge, 1975).
[2] Joachain, C. J., Quantum Collision Theory, 3rd ed. (North-Holland, Amsterdam, 1983).
[3] McGuire, J. H. Electron Correlation Dynamics in Atomic Collisions (Cambridge University Press, Cambridge, 1997).

# Inelastic momentum transfer cross-sections for electron-impact excitation in Helium: scaling rules for n≥4 states

R.J. Carman[1], J.R. Machacek[2] and R.P. McEachran[2]

[1] *Dept. of Physics and Astronomy, Macquarie University, Sydney, NSW 2109, Australia*
[2] *Research School of Physics, Australian National University, Canberra, ACT 2601, Australia*

A comprehensive set of state-specific inelastic momentum transfer cross-sections associated with electron-impact excitation in helium will be reported. These cross-sections have been evaluated from the underlying differential cross-sections for excitation which have been calculated using the relativistic distorted wave (RDW) method over a broad range of incident electron energies up to E=5keV. A key result demonstrates that simple scaling rules may be applied to determine these cross-sections for the higher-lying n≥4 excited states.

The inelastic momentum transfer (IMT) cross-sections associated with electron-impact excitation and ionisation of helium have not been fully determined to date, although they are expected to play an important role in modelling electron transport in helium plasmas with improved accuracy [1]. These cross-sections are particularly important for characterising the behaviour of energetic or "runaway" electrons (E~10eV to 10keV) generated in fast transient pulsed discharges, in electron-beam plasmas [2] or in fusion reactors such as the ITER project (e.g. relating to helium "ash") [3].

For plasma modelling, the IMT cross-section $Q_{mj}(E)$ is required to be defined as a smooth, continuous function of the incident electron energy starting at the excitation/ionisation thresholds (e.g. $E_{ex}$ for excitation). In the case of excitation, this task is dependent on the availability of the differential cross-sections (DCS) $\sigma_j(E,\theta)$ (in $cm^2/sr$) between $\theta$= 0-180$^o$. The IMT cross-section for electron excitation collisions is given by [4]:

$$Q_{mj}(E) = \int_0^{\pi}\left(1-(1-E_{ex}/E)^{1/2}\cos\theta\right)\sin\theta\,\sigma_j(E,\theta)d\theta.$$

In this work, the differential cross-sections for excitation have been calculated using the relativistic distorted wave (RDW) method which was originally developed in [5] and then applied to the excitation of the $6s\left[\frac{1}{2}\right]_1^o$ and $6s\left[\frac{3}{2}\right]_1^o$ states of Xenon between 30-80eV. The method was subsequently used to treat excitation processes in Argon, Krypton and Xenon up to 500eV [6].

Although the original version of the RDW method required that the ground and excited state wavefunctions be determined in a single multi-configuration Dirac-Fock (MCDF) calculation, a modified version of the RDW method has been used here which allows for the ground and excited state wavefunctions to be determined in separate MCDF calculations, thereby giving a more accurate representation of both atomic states.

In this paper, a set of state-specific IMT cross-sections for helium (10 excited states - $n^{1,3}S$, $n^{1,3}P$, $3^{1,3}D$, with n=2,3) covering a broad range of electron energies (E~$E_{ex}$ to 5keV) will be presented. Our results are compared to other theoretical IMT cross-sections (evaluated from the corresponding DCS's [3][7]) and IMT's derived from experimental DCS's, where they available from the literature. Based on the results for the $n^{1,3}P$ states with n=2,3,4,8,9, a key result from this study demonstrates that simple scaling rules may be applied to estimate IMT cross-sections for the higher-lying helium excited states with n≥4, where existing data is particularly scant.

**References**

[1] T. Makabe, R. White, *J. Phys. D: Appl. Phys*. **48** 485205 (2015)
[2] Special issue on Fast Pulse Discharges, *Plasma Sources Sci. Tech.* **26**, 020201 (2017)
[3] M. Hoshino, H. Kato, H. Tanaka, I. Bray, D.V. Fursa, S.J. Buckman, O. Ingolfsson and M.J. Brunger, *J. Phys. B: At. Mol. Opt. Phys.* **42** 145202 (2009)
[4] N.T. Padial, G.D. Meneses, F.J. Paixao, and Gy. Csanak, *Phys. Rev A* **23** 5, 2194-2212 (1981)
[5] T. Zuo, R.P. McEachran, A.D. Stauffer, *J. Phys. B*, **24** 2853 (1991)
[6] T. Zuo, R.P. McEachran, A.D. Stauffer, *J. Phys. B*, **25** 3393 (1992)
[7] D.V. Fursa and I. Bray, *Phys Rev A*, **52**(2), 1279-1297 (1995) and *J. Phys. B: At. Mol. Opt. Phys.* **30** 757 (1997).

XXXVI ICPIG, July 20-25, 2025, Aix-en-Provence, France Topic number 9

# Variable-pulse streamer discharges using an Impedance-matched Marx Generator

W. Meekes[1], S. Nijdam[1]

[1] *Eindhoven University of Technology, Eindhoven, the Netherlands*

To strengthen the link between experiments and simulations in the field of plasma physics, an Impedance-matched Marx Generator will be used to create streamers with highly variable voltage pulse shapes with amplitudes up to 20 kV. This allows the creation of a dataset with many more variables, which can be used to verify simulations. Voltage pulse rise times and widths will be varied, and the overall shape of the voltage pulse can be changed, such as square, triangular, or stepped. The voltage and current characteristics of the plasma will be measured, and high-speed images of the optical emission of the plasma will be taken.

## 1 General

An important aspect of scientific research is the link between experiments and simulations. Simulations provide much more control over experimental parameters and enable the analysis of parameters that are unreachable to experimenters. At the same time, a simulation cannot exist without experimental verification.

Streamer discharges are present in nature as the early stages of lightning. In the high-voltage industry, understanding streamer discharges is critical for spark protection and the design of high-voltage switchgear.

To gain more fundamental understanding of the physics underpinning streamer discharges, it is possible to set up increasingly advanced diagnostics. Alternatively, the already existing diagnostic methods can be applied to a greater variation of discharges. This way, the physics in both a theoretical and numerical models can be held up to greater scrutiny, by investigating how the model compares to experiments in different situations.

In this work, streamer discharges will be made using an Impedance-matched Marx Generator (IMG)[1], which allows great flexibility in the voltage pulse used to produce the plasma.

## 2 Variable-pulse streamer

The IMG is a solid-state Marx generator. It consists of 25 stages that can be charged up to 800 V and discharged independently to produce many different voltage pulse shapes.

This way, the IMG has the capability to influence the rise and fall times of pulses and modify their shapes to, for example, square or triangular. It can generate high-frequency voltage bursts as well as stepped pulses. By utilizing these variable pulses to create streamer discharges, a variety of similar yet distinct discharges can be produced and compared to models.

## 3 Measurement methods

For the different plasma pulses, the current and voltage characteristics of the streamers will be measured, and using ICCD imaging the time-resolved optical emission can be recorded with high accuracy, providing valuable insights into the dynamics of the streamers during the plasma pulses.

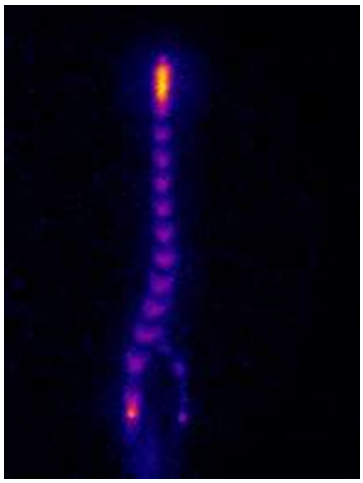


**Figure 1: Stroboscopic image of a streamer discharge in air**

**References**

[1] van Oorschot, J. J., & Huiskamp, T. Fast and flexible, arbitrary waveform, 20-kV, solid-state, impedance-matched Marx generator. *IEEE Transactions on Plasma Science*, ***51*(2)**, 560-571 (2023).

# Recent advances in reproducible plasma simulation: LXCat 3.0 and LoKI-B++

D. Boer[1], P. Pereira[2], W. Graef[3], A. Tejero-del-Caz[4], L.L. Alves[3] and J. van Dijk[1]

[1] *Elementary Processes in Gas Discharges, Eindhoven University of Technology, Eindhoven, The Netherlands*
[2] *Instituto de Plasmas e Fusão Nuclear, Instituto Superior Técnico, Universidade de Lisboa, Portugal*
[3] *Plasma Matters BV, Campus Eindhoven University of Technology, The Netherlands*
[4] *Departamento de Física, Facultad de Ciencias, Universidad de Córdoba, Campus de Rabanales, Spain*

Reproducing plasma simulation studies is notoriously difficult. There are two contributing aspects, input data and simulation tools. This work presents recent advances in both areas. The main contribution comprises LoKI-B++, a new, open-source, C++ implementation of the LoKI-B Matlab Boltzmann solver, which introduces a nonuniform energy discretization and provides a full-featured web interface. In conjunction with recent developments in LXCat 3.0, LoKI-B++ facilitates perfectly reproducible electron Boltzmann simulations.

LXCat 3.0 is the next generation of the LXCat data platform for electron and ion collisional data [1, 2]. It significantly improves data management through the introduction of a comprehensive plasma input data schema, improves reproducibility through proper versioning of data, and increases transparency by improving traceability of the data and its sources. The development of LXCat 3.0 is in the final stages before its release. Recent progress includes porting and annotating a large amount of cross section data from the current generation of LXCat, and the development of peripheral tooling. A live demo deployment is available that can be used to check on the progress [3].

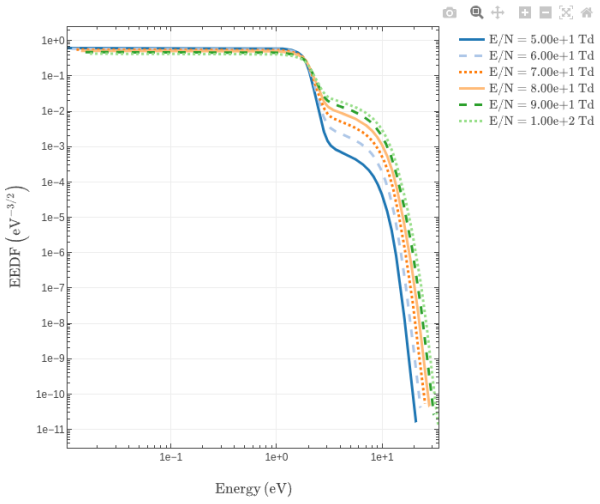



Figure 1: A screenshot of the plotting area of the LoKI-B++ web interface. The results show computed electron energy distribution functions in a $N_2$ plasma. The cross section data is obtained directly from the LXCat 3.0 API.

LoKI-B++ is developed in conjunction with the recent advances in plasma data management. It solves the two-term expanded Boltzmann equation for electrons and provides a fast, interoperable, and truly open-source alternative to the existing offer. The first goal is to mirror the functionality and leverage the solid scientific foundation of the original LoKI-B Matlab code [4, 5]. This led to the development of a rigid testing harness, including a comprehensive suite of unit tests, regression tests, the development of analytical solutions in the presence of inelastic collisions, and testing against LoKI-B Matlab and BOLSIG+ [6].

Furthermore, a non-uniform energy discretization is being developed, which allows to solve the Boltzmann equation on arbitrary, unstructured grids. Special attention is paid to the conservation of mass and energy in the presence of inelastic processes. In addition, a grid placement algorithm is in development that automatically arranges grid cells based on the given input data. Moreover, LoKI-B++ runs natively in the browser as a full-featured web application by compilation into WebAssembly. The web deployment of LoKI-B++ can automatically retrieve cross section data from the LXCat 3 API. The combination of LXCat 3 and the LoKI-B++ web deployment allows for perfectly reproducible studies of the electron Boltzmann equation. Full studies can be reproduced exactly by simply sharing a uniquely generated URL, paving the way for fully reproducible plasma simulation studies.

## References

[1] E. Carbone *et al.*, *Atoms*, vol. 9, no. 1, p. 16, Feb. 2021. DOI: 10.3390/atoms9010016.
[2] https://github.com/lxcat-project/lxcat.
[3] https://demo.lxcat.net.
[4] A. Tejero-Del-Caz *et al.*, *PSST*, vol. 28, no. 4, 2019. DOI: 10.1088/1361-6595/ab0537.
[5] https://github.com/IST-Lisbon/LoKI.
[6] G. J. Hagelaar *et al.*, *PSST*, vol. 14, no. 4, pp. 722–733, 2005. DOI: 10.1088/0963-0252/14/4/011.

**Acknowledgements**: This work is supported in part by the PPS-Contribution Research and Innovation of the Ministry of Economic Affairs and Climate Policy (The Netherlands), by ASML, and by FCT under project 2022.04128.PTDC.

# Application of field electron emission model to pulsed discharge

K. Takahashi[1], I. Timoshkin[2], and S. J. MacGregor[2]

[1] *Muroran Institute of Technology, Muroran, Hokkaido, Japan*
[2] *University of Strathclyde, Glasgow, UK*

Pulsed discharge experiments were conducted to investigate the role of field electron emission in atmospheric-pressure breakdown. The standard Fowler-Nordheim equation for the emission current was used to estimate electron emission, and field enhancement factor was estimated. It was found that the field enhancement factor increases with the inter-electrode gap distance, while the local enhancement factor attributed to the electrode surface decreases, likely due to electrode surface erosion caused by repeated discharges.

## 1. Introduction

Pulsed discharge under atmospheric pressure is widely used in various applications. Understanding the fundamental mechanism governing its initiation is critical for optimizing these applications. In particular, accurate modelling of the breakdown process requires a thorough understanding of the initial electron supply mechanism. Among the possible mechanisms, the field electron emission, governed by the Fowler-Nordheim tunnelling effect, is considered a primary candidate for electron supply under high electric field conditions.

In this study, we investigate the role of field electron emission in pulsed discharge at atmospheric pressure by applying an electron emission model to the obtained experimental data. The number of electrons emitted from the electrode surface is estimated using the Fowler-Nordheim tunnelling effect, and field enhancement factor is estimated.

## 2. Experimental setup and analysing model

Spark discharge experiments were conducted to determine the formative time $t_f$ and the statistical time $t_s$ from a Laue plot. A steel needle electrode with a tip radius of 80 μm was used as the high-voltage electrode, while a stainless-steel sphere with a half-inch diameter served as the ground electrode. The gap distance was varied in 0.5 mm increments from 0.5 to 2.0 mm. The spark discharge was generated 30 times in ambient air using a Blumlein pulse generator with the voltage rate of -2kV/ns. The values of $t_f$ and $t_s$ were determined from the resulting Laue plot.

Assuming that the initial electrons required for spark discharge generation were supplied via the Fowler-Nordheim tunnelling effect, the number of electrons injected into air by field emission was calculated from the current density according to the Fowler-Nordheim equation [1]. The current density depends on the electric field $E$, the work function $\phi$, and the field enhancement factor $\beta$. The average electric field was determined by dividing the applied voltage by the gap distance, with the voltage derived from the measured average voltage waveform. The work function was assumed to be 4.1 eV (steel). The field enhancement factor $\beta$ was adjusted so that the cumulative number of electrons reached 1000 at the determined formative time $t_f$. Furthermore, the enhancement factor $\beta$ is considered to be the product of the geometric enhancement factor $\beta_G$, which depends on the electrode shape and gap distance, and the local enhancement factor $\beta_L$, which is influenced by the electrode surface condition. $\beta_G$ is determined from the ratio of the maximum electric field to the average electric field and calculated under the assumption of a needle-to-plane electrode configuration.

## 3. Results and discussion

Table 1 shows the estimated field enhancement factors for each gap distance. As the gap distance increases, the total field enhancement factor $\beta$ also increases, while the local enhancement factor $\beta_L$ decreases. The decrease in $\beta_L$ may be attributed to electrode-surface erosion caused by the discharged in the present experiments.

Table 1. Estimated field enhancement factor

| Gap distance $d$ [mm] | $\beta$ (= $\beta_G \times \beta_L$) | $\beta_G$ | $\beta_L$ |
|---|---|---|---|
| 0.5 | 87.0 | 3.84 | 22.7 |
| 1.0 | 128.5 | 6.36 | 20.2 |
| 1.5 | 156.0 | 8.66 | 18.0 |
| 2.0 | 180.0 | 10.8 | 16.6 |

**References**

[1] Wang J. W. and Loew G. A. Loew, SLAC-PUB-7684 (1997).

# Modified plasma pencil for use in chemical trace element detection

T. Medek[1], M. Mrkvičková[1] and P. Dvořák[1]

[1] *Dept. of Plasma Physics and Technology, Masaryk University, Brno, Czech Republic*

Our aim is to develop and test a modified plasma pencil for use as an atomiser for chemical trace element detection. We propose a device with improved geometry and investigate its atomisation capability using laser-induced fluorescence measurements.

The general aim of our research in the past couple of years has been the development and evaluation of new designs of atomisers for use in trace element (Bi, Te, Se, Sn, Hg, etc.) detection in analytical chemistry. There, it is common to use atomic absorption spectroscopy, but for that the elements need to be in atomic state. One technique of the extraction of the atoms from the liquid sample is the hydride generation followed by the introduction of hydrides into an atomiser (a device used for dissociation of carrier molecules) [1]. Conventionally, an externally heated quartz tube atomiser (QTA) is used, but recently, plasma-based atomisers have also shown very promising results. [2]

This contribution focuses on the hydride atomisation in the plasma pencil [3]. Our previous experiments with plasma pencil have shown promising results in atomising $SeH_2$ and $GeH_4$ (which has been problematic in other atomisers), but we believe suboptimal geometry was limiting our sensitivity. To optimise the device for its desired use in absorption spectroscopy, we use a T-shape geometry with a pair of grounded electrodes on the horizontal optical arm, see fig. 1. The HV electrode is on the tube perpendicular to the main tube. There is also a separately connected tube for the analyte, as we aim to improve the stability of the discharge by keeping a region of pure carrier gas (argon) close to the HV electrode. The discharge is powered by an Advanced Energy Cesar 136 14.56 MHz power supply with a matching network.

For the evaluation of the atomisation ability, we plan to measure the spatial maps of analyte atoms concentrations by the laser-induced fluorescence (LIF) method. If possible, the concentration of hydrogen radicals will also be studied by TALIF, as they play a significant role in the atomisation of analytes [4]. Our recent experiments in DBD atomisers have also shown that some analytes (mainly tin) have shown a strong signal right after igniting the plasma, but then the signal quickly decreases. Thus, the temporal development of the concentration and pulsing of the discharge will be studied as well.

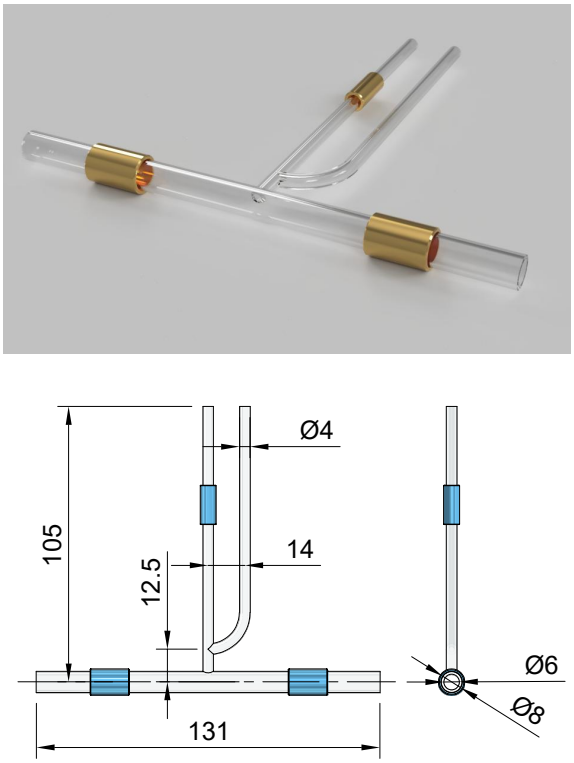



Figure 1: Modified plasma pencil

This research is supported by the Czech Science Foundation under contract 23-05974K and by the Project LM2023039 founded by the Ministry of Education, Youth and Sports of the Czech Republic.

[1] J. Dědina et al, Spectrochim Acta Part B 62(9):846–872. (2007)
[2] S. Brandt et al, Spectrochim. Acta, Part B 123 (2016) 6–32
[3] M. Klima et al, Surf. Coat. Technol. 116. 547-551. (1999)
[4] P. Dvořák et al, Plasma Sources Sci. Technol. 26 (2017), 085002.

# Preventing the formation of vortexes in an atmospheric ICP

L. Terraz[1], B. Alemu[1]

[1] *Karlsruhe Institute of Technology, Light Technology Institute, Karlsruhe, Germany*

We report the results of numerical simulations of an atmospheric inductively coupled nitrogen plasma. The focus is set on vortex formation using the Froude number as an indicator. The influences of gas flow rate, excitation current, coil and torch geometries are investigated.

## 1. Introduction

Inductively coupled plasmas (ICPs) have been investigated since the mid-20th century. They can reach high electronic and energy densities without pollution from electrodes, hence they are suitable for many applications, like heating, spheroidization, thin film deposition, etc. Typically, a copper coil surrounding a cylindrical burner is excited with a radiofrequency varying current, creating a magnetic field in the tube. During ignition, free charge careers gain enough energy from the field to further ionize the gas molecules, resulting in a plasma state. However, although ICPs offer interesting advantages in comparison with other types of plasma discharges, they are also difficult to operate and control. One of the issues is the formation of vortex. They can trap heat in non-suited locations, resulting in a drop of efficiency and possibly damaging the walls, among various drawbacks.

## 2. Method

We use the software COMSOL Multiphysics® to model a nitrogen ICP at atmospheric pressure. Under the assumption of a thermal plasma, we do not model any kinetic reaction but consider the whole gas as a conducting medium, described by magnetohydrodynamics, laminar flow and heat transfer equations [1,2].

We focus our study on the parameters which can influence vortex formation and location, such as gas flow, coil spacing, coil turns [3], inclusion of nozzle [1], etc. The simulations reproduce an experimental setup with a specific geometry, excitation frequency and power supply. We verify that Lorentz force is the main actor for vortex formation, within our operation range, and compute the Froude number [4] (ratio of gas inertia to Lorentz force) over the plasma torch. Subsequent steps are dedicated to increasing locally this Froude number, in order to avoid the formation of vortexes or move them to a different location.

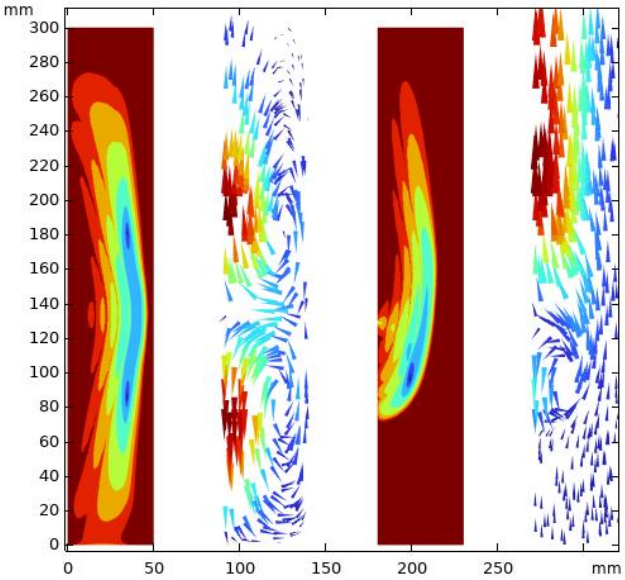



**Figure 1: representation of Froude number and the corresponding velocity field in a 2D axisymmetric argon ICP simulation. Left: gas flow rate = 2 L/min. Right: gas flow rate = 120 L/min. The lowest values of Froude number (blue spots in the filled charts) correspond to the center of the vortexes.**

## References

[1] Jiang, Q. *et al.* Calculations of flow field and heat exchange properties in high-power high-enthalpy inductively coupled plasma generator. *Physics of Plasmas*. **31** (2024).

[2] Bernardi, D. *et al.* Numerical simulation for the characterization of operating conditions of RF-RF hybrid plasma torches. *Eur. Phys. J. D* **28**, 399–422 (2004).

[3] Sangeeta B. Punjabi *et al.* The effect of various coil parameters on ICP torch simulation. J. Phys.: Conf. Ser. **208** 012048 (2010).

[4] Voronov, M. *et al.* Force-based analysis of vortexes in atmospheric pressure ICPs. *Plasma Sources Sci. Technol.* **27** 125005 (2018).

# Carbon-Enhanced Plasma-Based $CO_2$ Conversion: From Fixed Beds to Direct Microparticle Injections

A. Eivazpour Taher[1,2], I. Tsonev[1,2] and A. Bogaerts[1,2]

[1]*Research Group PLASMANT, Department of Chemistry, University of Antwerp, Antwerp, Belgium*
[2]*Electrification Institute, University of Antwerp, 2020 Antwerp, Belgium*

Plasma-based $CO_2$ conversion is an alternative approach to conventional methods by transforming $CO_2$ into valuable products like CO. Recent advancements highlight the role of carbon in enhancing conversion efficiency, particularly by using post-plasma carbon beds. In this work, we introduce a novel method by directly injecting carbon microparticles into the plasma reactor, aiming to assess their quenching and enhancement effects on the $CO_2$ dissociation process, by means of CFD modelling, including surface chemical reactions. We focus on the plasma-particle interactions, investigating the effect of particle size, injection rate and injection position on the gas flow and temperature profiles.

## 1. Introduction

Plasma-based $CO_2$ conversion utilizes electrical energy to dissociate $CO_2$ into valuable products like CO [1]. Post-plasma carbon beds have been recently proposed to overcome limitations of pure $CO_2$ splitting, demonstrating significant improvements in conversion efficiency [2,3]. Nevertheless, carbon beds face challenges such as requirement of reactor design optimization to avoid gradual carbon bed deactivation due to oxygen accumulation and for replenishment of carbon to ensure continuous and stable operations. In this study, we propose an alternative approach to overcome the limitations of a fixed carbon bed, namely the direct injection of carbon microparticles within the plasma. This method ensures a continuous and reactive carbon supply by preventing the carbon bed deactivation. In addition, the particles can interact with the altered chemical composition along the temperature gradients of the plasma potentially enhancing conversion. In this work, the injection of graphite microparticles of 5, 10, and 20 µm diameter was modelled in COMSOL Multiphysics to investigate their effect on gas flow and temperature profiles. A multi-physics approach is implemented solving a fully-coupled set of equations including: a Reynolds-Averaged Navier-Stokes (RANS) Menter's Shear Stress Transport (SST) turbulent flow model to describe gas flow behaviour, a heat balance equation to describe the conservation of energy, conservation of mass to describe transport of species, and Lagrangian formulation for particle tracing. The plasma acts as a heat source with $T_{max}$=7400 K and with 50 mm and 5 mm length and width, respectively.

## 2. Results

The simulation results show a drop in gas temperature as the particles are injected, due to enhanced heat transfer mechanisms introduced by the carbon microparticles. Figure 1 presents the trajectories of the injected particles and the temperature drop of the gas compared to the case before particle injection. This cooling effect primarily arises from the high thermal conductivity of the particles, allowing them to absorb and dissipate heat from the surrounding plasma. This cooling leads to quenching of the reverse reactions and preserving the converted $CO_2$. Further investigations will focus on enhancement of the quenching effect and explore the enhancement role of the particles in improving conversion efficiency.

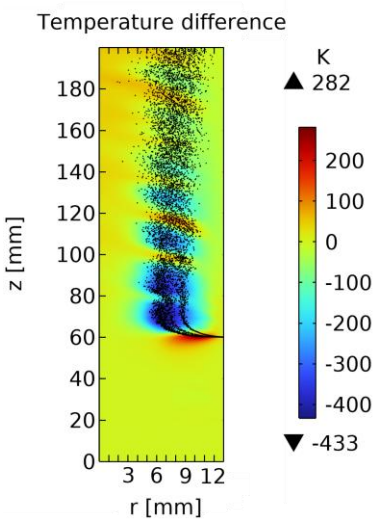



Figure 1. Gas temperature difference between the cases before and after injection of the microparticles

### References

[1] R. Snoeckx, A. Bogaerts, Plasma technology – a novel solution for CO2 conversion? Chem. Soc. Rev. 46 (2017) 5805–5863
[2] F. Girard-Sahun, O. Biondo, G. Trenchev, G. Van Rooij, A. Bogaerts. Chem. Eng. J. 442 (2022) 136268
[3] C. O'Modhrain, Y. Gorbanev, A. Bogaerts. J. Energy Chem. 104 (2025) 312–323

# Spectral characteristics of indium-argon inductively coupled plasma

A. Abola[1]

[1] *Institute of Atomic Physics and Spectroscopy, Faculty of Science and Technology, University of Latvia, Riga, Latvia*

This work focuses on indium-argon inductively coupled plasma spectral analysis. The plasma is induced in electrodeless lamps, that are often used as light sources for atomic absorption spectroscopy. The interest in indium light sources is based on the fact, that use of indium in the last decades is growing, as it is being used to manufacture many currently in-demand devices and technologies. Thus rises the need for its determination in the environment. Results of the study include analysis of relative intensity changes of several In and Ar spectral lines depending on the excitation generator voltages, as well as emission radiation stability measurements.

## 1 Introduction

Compared to such well-known environmental pollutants, as mercury, lead, and arsenic, indium is a lot less studied heavy metal. At the same time, its use in practical applications, for example, solar panels, touchscreens, and smart devices, is rising [1], meaning that the need for environmental assessment of its presence is also on demand.

Atomic absorption spectroscopy (AAS) is a trusted and sensitive method for determining the concentration of various metals in different mediums. One of the main components of the spectrometer is the light source. High-frequency electrodeless lamps (HFEDLs) are a suitable choice for use in AAS because they emit narrow, intense, and stable spectral lines.

In this work, spectral characteristics of a low-temperature inductively coupled plasma in an indium-containing HFEDL are determined, to analyse lamp's performance and possible improvements for use in AAS.

## 2 Experiment and results

### 2.1 Experimental setup

An inductively coupled plasma in an indium-argon high-frequency electrodeless lamp was induced by placing the lamp in the excitation generator coil.

The emission spectra of the lamp in the range of 200 nm to 850 nm were registered using a high-resolution spectrometer Jobin Yvon SPEX 1000 M (resolution 0.008 nm) coupled with a thermo-cooled CCD camera.

The most important spectral lines analysed included In resonance spectral lines at 303.9 nm and 410.2 nm and a few Ar spectral lines in the 600-800 nm range.

### 2.2 Results

A series of spectral measurements were performed to analyse the indium-argon plasma spectral characteristics.

Intensity stability measurements were done, showcasing the intensity fluctuations during longer time periods. After the initial warm-up, the intensity fluctuations of In 303.9 nm spectral line during 60 min period were approximately 2.5%.

Also, relative intensities were obtained for different excitation generator voltages (up to 29 V), giving information on voltage (power) influence on spectral line intensity.

## 3 Conclusions

Data on spectral characteristics of In/Ar HFEDLs are important to assess lamp performance and possible improvements for practical applications, such as for use in AAS, as well as the possibility of using them for plasma diagnostics and more fundamental understanding of plasma processes.

**Acknowledgments**

This work was supported by 1.1.1.9 Research application No 1.1.1.9/LZP/1/24/141 of the Activity "Post-doctoral Research" "Heavy metal concentration in precipitation and their impact on the environment".

**References**

[1] Mejias O. et al. Indium in ore deposits and mine waste environments: Geochemistry, mineralogy and opportunities for recovery. *Journal of Geochemical Exploration*, **255**, 107312 (2023). https://doi.org/10.1016/j.gexplo.2023.107312

# Experimental characterisation of the electrode-to-wall area ratio's influence on the plasma and electrode potential for large cathode size

P. Hiret[1], F. Bottarlini[1], A. Dmitriev[1], L. Marot[1] and E. Meyer[1]

[1] *Department of Physics, University of Basel, Klingelbergstrasse 82, 4056 Basel, Switzerland*

Understanding how electrode asymmetry affects self-bias in radio-frequency (RF) capacitively coupled plasma (CCP) is crucial for plasma sputtering in semiconductor fabrication. These discharges are driven using a blocking capacitor, which isolates the driven electrode and affects the voltage drop across the plasma sheath by leading to the formation of a strong self-bias. Although many studies have explored these parameters' dependencies on the area ratio between the electrode and grounded wall, measurements for large cathode configurations are limited. This contribution presents experimental results on plasma potential and self-bias across various area ratios and experimentally validates the analytical models from Köhler and Lieberman.

Understanding the influence of electrode asymmetry on self-bias in radio-frequency (RF) glow discharges is of significant interest in various applications such as plasma sputtering for semiconductor fabrication or first mirror cleaning in the next generation of fusion devices. Such discharges are commonly driven by an electrode isolated from the ground via a blocking capacitor, which charges up negatively in asymmetric discharges, forming a self-bias on the substrate. Self-bias voltage influences the energy distribution of the ions on surfaces, contributing to voltage drop into the driven sheath. In such asymmetric plasma discharges, the plasma potential ($V_p$) and the self-bias ($V_{bias}$) are then the main parameters to control the plasma-wall interactions. Knowing these two parameters allows for controlling the ion energy distribution on the electrode surface. $V_p$ and $V_{bias}$ depend strongly on the area ratio between the driven electrode and the grounded wall in such discharges. $V_p$ and $V_{bias}$ dependency on the electrode-wall area ratio in CCP has been extensively studied theoretically through different models and experimental characterisation, however, there is a lack of measurements in the case of large cathode configurations. This contribution discusses and compares the experimental characterisation of the plasma potential and self-bias of capacitive discharges for a wide range of area ratios to analytical models. The impact of pressure, gas composition, and radio frequency (RF) voltage amplitude on the dependency of plasma characteristics is also discussed.

A Langmuir probe and a retarding field energy analyser (RFEA) were used in a vessel made of removable parts which could be either grounded, floated or driven to measure the plasma potential and other parameters such as electron temperature and density while changing the electrode wall ratio. The plasma potential was measured using a Langmuir probe and RFEA, both allowing the measurements of the bulk average potential. The electrode potential was measured directly on the electrode using a peak-to-peak sensor for different area ratios and RF voltage amplitude. The measured potentials were close to the Köhler model [1] for the entire range of area ratios. The Lieberman model [2], which considers more phenomena, was comparable to the experimental results and exhibited the presence of local ionisation near the electrode in the vessel. That was experimentally validated by RFEA measurements on the powered area.

## References

[1] Köhler, K. *et al.* Plasma potentials of 13.56-MHz rf argon glow discharges in a planar system. *Journal of Applied Physics*, **57**, 59--66 (1985).

[2] Lieberman, M. A. and Lichtenberg A.J. Principles of Plasma Discharges and Materials Processing. 2nd ed. *Wiley* (2005).

# Detection of reactive species in plasma-treated water using Electrochemical Impedance Spectroscopy

S. Khosravi[1], G. Zarate Segura[1,2], L. Zampieri[1], C. Riccardi[1] and E. Martines[1]

[1] *Department of Physics "Giuseppe Occhialini", University of Milano-Bicocca, 20126 Milano, Italy*
[2] *Physics Section, Pontificia Universidad Católica del Perú, 15088 Lima, Perú*

Measuring reactive species produced in water by the action of cold atmospheric plasmas with selective and non-invasive techniques is a problem of interest for the design and characterization of plasma sources in biomedical and agricultural applications. Here we propose a novel approach based on electrochemical impedance spectroscopy. After demonstrating that this technique can be used to characterize saline solutions, both regarding salt concentration and salt type, we show its application to water treated with different cold plasma sources and discuss the reliability and effectiveness of the technique.

## 1 Introduction

Cold atmospheric plasma (CAP) treatments of water generate complex mixtures of reactive oxygen and nitrogen species (RONS), playing important roles in emerging applications across biomedicine and agriculture [1]. The characterization of these species presents an analytical challenge due to their varying concentrations. Most of the techniques nowadays used require the use of reagents, and therefore the loss of the sample.

Electrochemical impedance spectroscopy (EIS) is a powerful analytical technique for characterizing the electrical properties of solutions and interfaces [2]. By applying a sinusoidal voltage perturbation across a range of frequencies and measuring the current response, EIS provides information about ion concentrations, charge transfer processes, diffusion phenomena, and interfacial properties. As a fast and non-destructive method, EIS is an innovative candidate for real-time characterization of plasma-treated water (PAW) samples, offering distinct advantages for probing multi-ion systems without perturbing the original chemical environment.

## 2 Materials and methods

EIS measurements were performed using a digital impedance analyser (MFIA, Zurich Instruments). The instrument was configured to measure impedance in the frequency range of 10 Hz to 100 kHz, with a test voltage of 300 mV. A custom measurement cell was designed. In a non-conductive container, holding the liquid samples, two parallel stainless steel cylindrical electrodes with a diameter of 2 mm were positioned at 22 mm distance.

Saline solutions of varying concentrations were prepared using three different salts. The impedance was measured, and the results were summarized as a point in the plane defined by amplitude and position of the peak of the imaginary part of the admittance [3]. The measurements were then repeated using ultrapure water treated with different plasma sources, varying the treatment time.

## 3 Results

The points in the plane cited above were found to be aligned along a straight line for different salt concentrations. Furthermore, different lines were found for different salts, showing the potential of species detection. The data obtained from the plasma-treated water were also plotted in this plane, showing a tendency to align according to the reached concentration of reactive species, quantified by the treatment time. An attempt of calibration against nitrite and nitrate ion concentrations was made. While further studies are still required to develop a calibration method and optimize the salt discrimination in multi-ion solutions, the preliminary results show the potential of this technique.

**References**

[1] P. J. Bruggemann *et al.*, J. Appl. Phys. **130**, 200401 (2021).
[2] B-Y Chang et al., Annu. Rev. Anal. Chem. **3**, 207–229 (2010).
[3] M. Grossi *et al.*, Eng. Sci. Technol. Int. J. **22**, 102-108 (2019).

This work was funded by the National Plan for NRRP Complementary Investments (PNC, established with the decree-law 6 May 2021, n. 59, converted by law n. 101 of 2021) in the call for the funding of research initiatives for technologies and innovative trajectories in the health and care sectors (Directorial Decree n. 931 of 06-06-2022) - project n. PNC0000003 - AdvaNced Technologies for Human-centrEd Medicine (project acronym: ANTHEM). This work reflects only the authors' views and opinions, neither the Ministry for University and Research nor the European Commission can be considered responsible for them.

# Evaluation of growth characteristics of sugarcane in response to plasma-activated leafmold application

T. Okumura[1,2], T. Nakao[1], G. Ono[1], H. Otobe[1], N. Hidaka, S. Takamine[1], P. Attri[1], K. Kamataki[1,2], N. Itagaki[1,2], M. Shiratani[1,2], Y. Mizuno[3], and K. Koga[1,2]

[1] *Kyushu University, Fukuoka, Japan,*
[2] *Center of Plasma Nano-interface Engineering, Kyushu University, Fukuoka, Japan,*
[3] *Mizukamo Farm, Okinawa, Japan,*

The growing food consumption due to population increase is a major challenge. Fertilizers are essential for crop yield increases, but the Haber–Bosch process used for nitrogen fertilizers is energy-intensive and emits significant $CO_2$. This study examines the phenotypic response of sugarcane to plasma-irradiated leafmold. The results showed no significant growth differences in the first 150 days. After 150 days, the plasma-irradiated group showed an 8.5% increase in growth compared to the control ($p$ = 0.008). These findings highlight the potential of plasma-irradiated fertilizers for sustainable, nitrogen fixation.

## 1 Introduction

The Food and Agriculture Organization of the United Nations (FAO) projects that the global population will reach 9.1 billion by 2050, requiring a approximately 70% increase in total food production between 2005/07 and 2050 to meet the growing demand [1]. A conventional method for increasing crop yields is fertilizer application. Currently, ammonia, the primary component of nitrogen fertilizers, is mainly synthesized via the Haber–Bosch (H-B) process. The H-B process accounts for 1–2% of global energy consumption, with an estimated $CO_2$ emission of 500 million tons, which constitutes approximately 1% of total global $CO_2$ emissions [2,3]. Therefore, the development of fertilizer production methods independent of fossil fuels is a crucial issue. This study analyzed the phenotypic response of plants to leafmolds in which nitrogen was directly fixed using plasma irradiation, aiming to develop a low-environmental-impact nitrogen fixation method without fossil fuel use.

## 2 Experimental

Field trials were conducted in Yaeyama District, Okinawa, to examine sugarcane's response to plasma-irradiated leafmold. The field had rows 30.6 m long with 1.4 m spacing. Fertilization was applied to three rows per condition, and the middle row was analyzed to minimize external influences. Fertilization took place from October 2021 to June 2022, with aboveground plant length measured from December 2021 to March 2023.

## 3 Results and discussion

The time course of aboveground length is shown in Fig. 1, where day 0 (0d) indicates the planting date. Up to approximately 150 days after planting, no significant differences in growth were observed.

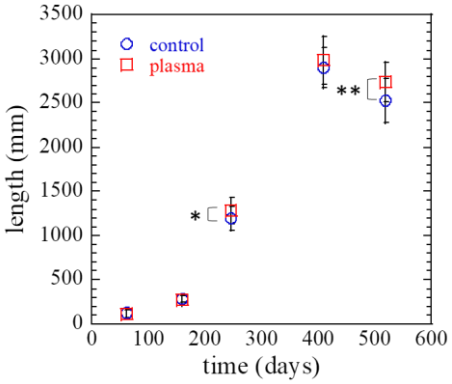



Fig. 1. Length of the sugarcane cultivated in the field with leafmold with and without plasma irradiation as a function of the time of cultivation (n = 20, *: $p$ < 0.05, **: $p$ < 0.01).

However, as cultivation progressed, the effects of plasma irradiation became more pronounced. By March 2023 (519d), the aboveground length of sugarcane in the plasma-irradiated leafmold group (plasma) was 2742 ± 221 mm, whereas the non-irradiated leafmold group (control) measured 2527 ± 251 mm ($p$-value = 0.008), representing an 8.5% increase in plasma compared to control. These results indicate that nitrogen-fixing leafmold produced via plasma irradiation promotes sugarcane growth.

**Acknowledgements**

This work was supported by JSPS KAKENHI JP22H04734, JP22H01212, JP20K05812, JP22K19160, JP22K03586, JP24H02246, JP24H02250, JST COI-NEXT JPMJPF2302, JST PARKS JPMJSF2317.

**References**

[1] FAO. 2024. World Food and Agriculture – Statistical Yearbook 2024. Rome.
[2] R. R. Schrock Proc. Natl. Acad. Sci. 103, 17087 (2006).
[3] S. Woods et al., IEA Bioenergy Task 38 (2004).

# Design and Evaluation of a Low-Cost Air Ionic Wind Thruster

J. Polanšek[1,2], L. Cvelbar[1]

[1]*Department of Gaseous Electronics (F6), Jožef Stefan Institute, Ljubljana, Slovenia*
[2]*Jožef Stefan International Postgraduate School, Ljubljana, Slovenia*

We present a cost- effective air ionic wind plasma thruster for atmospheric- pressure operation, assembled from 3D- printed supports and copper- tape electrodes. A small, off- the- shelf high- voltage transformer ionizes ambient air, generating electrohydrodynamic thrust without moving parts. Measurements show a near- linear decrease in wind speed with distance from the thruster exit, with negative- polarity operation yielding approximately 10% higher wind speeds. A two- stage electrode configuration increases thrust by around 20%. The setup, which includes a protective acrylic tube for safety, can be built easily with minimal materials cost, making it an ideal educational tool for exploring plasma physics and electrohydrodynamics.

## 1 Introduction

This work details a practical method for constructing and characterizing an air ionic wind plasma thruster operating at atmospheric pressure (Figure 1a). The device generates thrust by applying high voltage to ambient air to form a plasma (Figure 1b), where the electric field accelerates ions and produces an electric wind. Its simple design—utilizing copper tape electrodes and 3D-printed supports—offers a cost-effective platform for both small-scale propulsion and undergraduate education in plasma physics and high-voltage engineering.

## 2 Experimental Setup and Methodology

The thruster is assembled by optimally spacing the emitter and collector electrodes to avoid electrical breakdown while maintaining a sufficiently strong electric field. Measurements of the generated wind speed were performed with an anemometer placed at various distances from the thruster outlet. Two operational modes were observed depending on the polarity of the emitter electrode: a bright, louder plasma when using positive polarity, and a quieter discharge with negative polarity, the latter yielding roughly 10% higher wind speeds. A “two- stage” configuration, consisting of two sets of emitter and collector electrodes placed in series, was also tested to increase thrust. All primary experiments employed a small, low- cost HV transformer, although additional tests at broader power levels were performed using a Trek 20/20HS amplifier.

## 3 Results and Conclusions

Wind speed measurements show a near- linear decrease with distance from the thruster exit, with maximum velocity achieved at smaller electrode gaps and negative polarity on the emitter. The two- stage setup increased wind speed by approximately 20% compared to a single- stage arrangement. A protective tube around the electrodes reduced performance slightly (by about 15%) but greatly enhanced safety, making this design suitable for instructional demonstrations. Under prolonged operation, the small HV transformer exhibited thermal overload, causing a drop in output power and wind speed—an issue mitigated by using a more robust HV source. Overall, the results confirm that this low- cost thruster configuration provides a versatile platform for studying atmospheric- pressure plasma and electrohydrodynamic propulsion principles, while offering room for optimization through improved electrode geometry and power delivery.

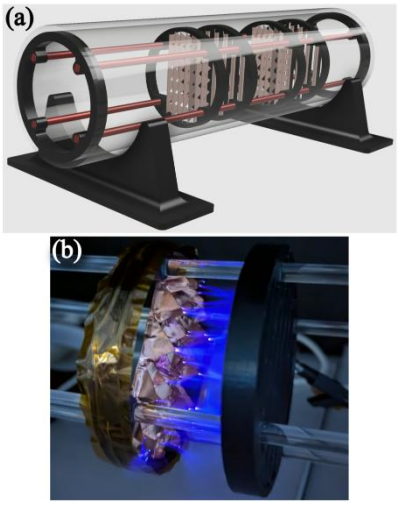



Figure 1. Thruster design: (a) 3D render of the assembled thruster; (b) plasma discharge between electrodes.

# Numerical Modeling of Ionic Wind and Ozone Production in a DC Corona Discharge under Humid Air Conditions

T. Khattara[1,2], J. -M. Orlac'h[3], P. Guitton[1] and C O. Laux[2]

[1] *Teqoya, Villandraut, 33730, France*
[2] *Laboratoire EM2C, CNRS, CentraleSupelec, Université Paris Saclay, 91192 Gif-sur-Yvette, France*
[3] *DAAA, ONERA, Institut Polytechnique de Paris, 92320 Châtillon, France*

This study presents a two-dimensional steady-state simulation of ionic wind and ozone generation in a DC corona discharge between two parallel wires in ambient humid air at atmospheric pressure. The developed kinetic model incorporates a detailed humid air chemistry mechanism to simulate the spatial distribution of ozone and charged species, as well as the velocity of the ionic wind in both dry and humid conditions. Simulation results are validated against experimental measurements, revealing that in humid air, $H_3O^+(H_2O)_n$ ions dominate, whereas $O_4^+$ ions prevail in dry air. The findings indicate that increasing the relative humidity from 0 to 100% leads to a roughly 50% increase in the corona discharge current, which in turn enhances the ionic wind velocity. Additionally, a significant decrease in the ozone production rate is observed at constant current as the humidity rises.

## 1. Introduction

Corona discharge, essential in air flow control [1] and electrostatic precipitation, is influenced by factors such as voltage, electrode configuration, and air humidity [2]. An important limitation for air purification is that the corona may also generate harmful ozone if the discharge conditions are not carefully controlled. This study investigates the impact of relative humidity on electrical properties, ionic wind, and ozone production, using a 2D drift-diffusion model validated against experiments.

## 2. Experimental Setup and Numerical Model

The experimental setup, shown in Fig. 1. features two parallel wires with a 9 mm gap, a high-voltage DC power supply, an anemometer for velocity measurement, and a UV ozone analyzer, all within a controlled atmosphere chamber.

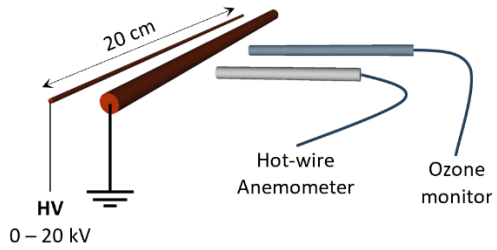



**Fig. 1. Schematic of the experimental setup**

The numerical model solves Poisson's equation, drift-diffusion equations for charged species, and the continuity equation for neutrals in a 10×6 cm² domain. The kinetic model includes 35 species (19 charged, 14 neutral) and 152 reactions, accounting for clustering and declustering processes.

## 3 Results

The two-dimensional profile of ionic wind velocity is plotted in Fig. 2. The profile is calculated under ambient conditions (HR = 50% and T = 25 °C) at 9 kV. Our numerical simulations of DC corona discharges in humid air accurately predict the discharge current, showing good agreement with experiments. The ozone production decreases significantly with increasing humidity at constant current. Additional results on ozone and current behaviour are currently being validated to further refine the model's accuracy.

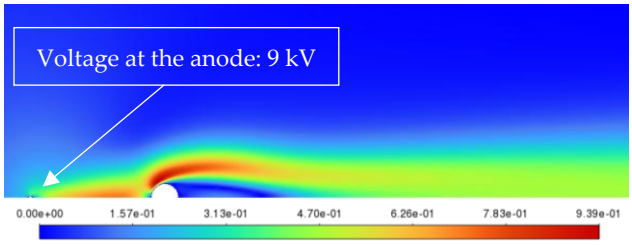



**Fig. 2. 2D Profile of ionic wind velocity, RH = 50%**

### References

[1] E. Moreau, "Airflow control by non-thermal plasma actuators," *J. Phys. D: Appl. Phys.*, vol. 40, no. 3, p. 605, Jan. 2007, doi: 10.1088/0022-3727/40/3/S01.

[2] M. Khalifa and S. El-Debeiky, "Analysis of the effect of humidity on d.c. corona power losses," *Proc. Inst. Electr. Eng. UK*, vol. 118, no. 5, p. 714, 1971, doi: 10.1049/piee.1971.0131.

# Surface-enhanced $NO_x$ formation in microwave-driven atmospheric pressure air plasma with downstream catalyst

J. Gans[1], Q. Shen[1], W.A. Bongers[1], K.R. Ehrhardt[2], I. Jevtovikj[3], S. Schunk[2,3], A.C. Hurtado Rivera[2], S. Titlbach[2], M.C.M. van de Sanden[1,4]

[1]*Dutch Institute for Fundamental Energy Research, Eindhoven, Netherlands*
[2]*BASF SE, Ludwigshafen am Rhein, Germany*
[3]*HTE GmbH, Heidelberg, Germany*
[4]*Eindhoven University of Technology, Eindhoven, Netherlands*

Measurements of $NO_x$ concentrations and energy costs of a microwave-driven atmospheric pressure plasma and down-stream catalyst are reported in this contribution. FTIR spectroscopy was used to investigate possible reaction mechanisms of plasma assisted $NO_x$ formation on the catalyst surface. Findings suggest that surface-mediated reactions involving plasma activated nitrogen and oxygen are responsible for additional $NO_x$ formation.

## 1. Introduction

The synergistic enhancement of $NO_x$ formation through plasma-catalyst coupling has been well-documented in low-temperature plasma systems [1]. Previous studies suggest that surface-adsorbed N and O species, generated from plasma-activated nitrogen and oxygen, are the primary contributors to this synergy [2, 3, 4]. In this study, we demonstrate that synergistic effects can be achieved in microwave plasma systems, possibly through comparable pathways.

## 2. Methods

Experiments were conducted using a microwave-driven atmospheric pressure air plasma coupled with a downstream packed-bed of $Al_2O_3$ spheres (1.6 mm diameter). FTIR spectroscopy was employed to analyse gas sampled after the packed bed. To evaluate synergistic effects, we systematically varied the catalyst fill volume and plasma-catalyst distance while monitoring temperature gradients throughout the pellet bed using K-type thermocouples (Fig. 1).

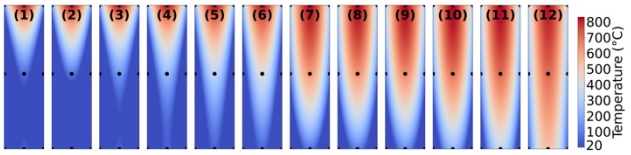



Fig. 1: Heat profile of the downstream catalyst bed for the twelve measurements taken in a total of 30 minutes.

## 3. Results and Discussion

Our findings, presented in Figure 2, illustrate the relationships between energy cost, $NO_x$ concentration, and $NO_2/NO$ ratio as functions of time (indicating the heating-up of the catalyst bed by the plasma exhaust). The results demonstrate clear correlations between $NO_x$ formation and catalyst quantity, plasma-catalyst separation distance, and catalyst temperature. Time-integrated $NO_x$ concentration measurements reveal enhanced total production, which we attribute to interactions between the (excited) plasma exhaust and surface-adsorbed N and O species on the $Al_2O_3$ substrate.

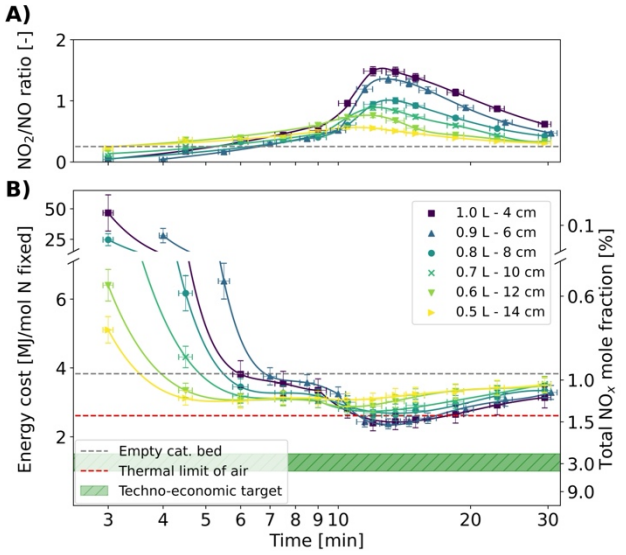



Fig. 2: A) $NO_2/NO$ ratio and B) Energy cost and $NO_x$ concentration with respect to the reference temperature for different $Al_2O_3$ fill volumes.

## 5. Conclusion

The downstream placement of $Al_2O_3$ pellets increases total $NO_x$ formation, indicating microwave plasma-catalyst synergy. Three key parameters are identified: catalyst quantity, plasma-catalyst distance, and catalyst temperature.

## Acknowledgement

The authors of this paper would like to thank BASF SE, NWO, and ARC CBBC for financial support of this research.

## References

[1] Pei et al., Plasma Processes and Polymers, **21**, 1, 2300135 (2024).
[2] Guaitella et al., Contributions to Plasma Physics, **51**, 2-3, 176–181 (2011).
[3] Guerra et al., Journal of Physics D: Applied Physics, **47**, 22, 224012 (2014).
[4] Gamallo et al., Physical Chemistry Chemical Physics, **9**, 37, 5112–5120 (2007).

# Transient phase of the flow field induced by an AC-driven SDBD

K. Giotis[1,2], G. Makrypodi[1], G. Vafakos[3,4], P. Papadopoulos[3],
G. Lombardi[2], K. Gazeli[2], P. Svarnas[1]

[1] *Univ. of Patras, Electrical & Computer Eng. Dept., High Voltage Lab., 26504 Rion, Patras, Greece*
[2] *Univ. Sorbonne Paris Nord, LSPM, CNRS, 8 UPR 3407, F-93430 Villetaneuse, France*
[3] *Univ. of Patras, Mechanical Eng. & Aeronautics Dept., 26504 Rion, Patras, Greece*
[4] *Univ. of Cyprus, Mechanical & Manufacturing Eng. Dept., 2109 Aglantzia, Nicosia, Cyprus*

Surface dielectric barrier discharges comprise a widely used and promising type of plasmas for various applications in atmospheric air, notably for plasma actuators, due to the development of appealing flow fields. In this report, time-resolved schlieren imaging is carried out to study such a field during its transition from quiescence to steady state. The discharge is sustained by means of AC high voltage (kHz), and the induced flow dynamics are recorded and illustrated over various periods.

## 1 Introduction

Surface dielectric barrier discharges (SDBDs) are utilised in flow field control as active actuators avoiding moving parts; see, SDBD plasma actuators. When they are driven by AC high voltage, adequate control may be achieved in subsonic airflows. The underlying physical mechanisms have been widely studied in planar configurations and refer to momentum transfer between ions and neutrals, due to electro-hydrodynamic (EHD) forces [1]. In the present work, the temporal evolution of the flow field induced by a cylindrical AC SDBD is investigated. The results provide insights on the complex fluid-plasma interaction, starting from the initial quiescent state and reaching to the steady state airflow.

## 2 Experimental Setup

The SDBD reactor has been described elaborately in [2]. Briefly, it comprises a cylindrical arrangement of two stainless-steel electrodes. The outer (driven) one is shaped as a hollow truncated cone and the inner (grounded) one forms a cylindrical tube. These electrodes are separated by a quartz dielectric tube, filled with transformer oil, while the vertical gap between their edges is set to zero.

A high voltage AC sinusoidal power supply (PlasmaHTec®) drives the SDBD reactor. Variable voltage amplitude (up to 25 $kV_{pp}$) and fixed frequency (10 kHz) are here applied. To visualise the airflow in a temporally resolved and non-invasive manner, a "Z-type" schlieren imaging system has been developed. It consists of two spherical mirrors (Ø152.4 mm; $f$=1524 mm), a high-power green led, a Foucault knife, and a high-speed camera (Chronos 2.1-HD).

## 3 Results and Conclusions

Starting from a zero-flow field before the voltage application, Fig. 1 unveils the transition to a localised air disturbance close to the driven electrode edge (Fig. 1a) and, eventually, to a distinguished propagation of an air jet downstream of this electrode (Fig. 1b–1e).

A pattern consisting of both laminar and turbulent profiles is demonstrated. It has been found that different amplitudes of the driving voltage led to similar patterns (16–24 $kV_{pp}$). Regarding the jet propagation speed, it increases versus the time in a diminishing way. Finally, it has been observed that higher voltage amplitudes tend to increase this speed.

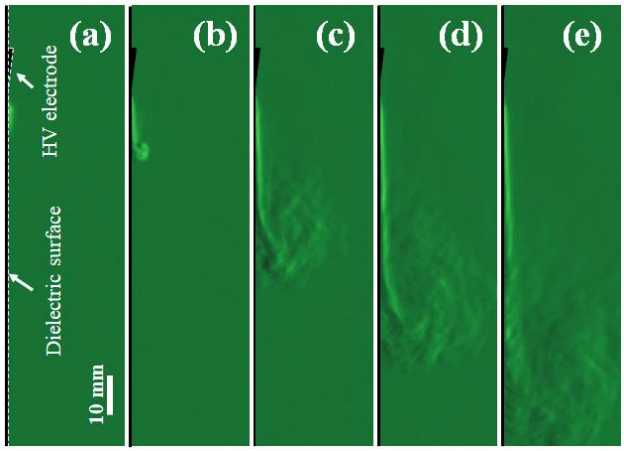



Figure 1. Transient flow downstream of the vertically oriented SDBD reactor. Images (100 μs exposure time) are recorded over the (a) 5th, (b) 45th, (c) 220th, (d) 405th, and (e) 605th cycle of the AC driving voltage.

It is assumed that the present results may be interpreted on the base of the interplay between the formed ions (both positive and negative) and the air molecules due to the induced EHD forces.

**References**

[1] Leonov, B. S. *et al*. *Plasma Sources Sci. Technol.* **25**, 063001 (2016).
[2] Stefas, D. *et al*. *J. Phys. D: Appl. Phys.* **57**, 455206 (2024).

# Improved efficiency in micro-structured plasma reactor for Hydrogen production using a pin to pin spark configuration

M. Jacquart[1,2], C. Garcia-Soto[1], F. Boni[1], M-E. Galvez[2,3], P-Q. Elias[1]
[1] *DPHY, ONERA, Université Paris-Saclay, 91120, Palaiseau, France*
[2]*Sorbonne Université, Institut Jean le Rond d'Alembert, CNRS UMR 7190, 2 place de la gare de Ceinture, 78210 St-Cyr l'Ecole, France*
[3]*Instituto de Nanociencia y Materiales de Aragon (INMA), CSIC-Universidad de Zaragoza, C/ Pedro Cerbuna 12, 50009 Zaragoza, Spain*

To produce carbon-free hydrogen, methane cracking presents an energetically efficient alternative. The micro-structured plasma reactor is a compact design based on glass capillaries, aimed at maximizing the energetic efficiency of the reaction. When used in dielectric barrier discharge configuration, A maximum methane conversion rate of 1.8% and an energy efficiency of 1.9% have been achieved when using the reactor in a dielectric barrier discharge configuration, which is significantly below state-of-the-art performance. When operated in direct discharge configuration, with a ballast resistor to limit the discharge current, the reactor reached a maximum conversion of 9.1% and a maximum efficiency of 14.5% at low repetition frequencies. While these values are slightly below those of state-of-the-art reactors, this configuration offers advantages compared to large-scale reactors.

## 1 Context

The demand for Hydrogen as a clean fuel has greatly increased over the past decade. However, the most common production methods, steam reforming [1] and water electrolysis, are either carbon intensive or energetically costly. An alternative approach is methane dissociation using plasma discharges.

Plasma assisted pyrolysis is already a proven method, and while it does have a very high yield (~99%), the current reactors do not exceed 20% efficiency and are constrained by large-scale structural and thermal limitations [2]. To maximize the efficiency, we investigate an out of equilibrium plasma reactor design with a fast cooling rate and a minimal dead volume. This reactor is based on a micro-structured configuration, using small cross section capillaries to confine the discharge and optimize performance.

## 2 Experiment

The micro-structured reactor consists of one or more glass capillaries, with two gas plenums at the inlet and outlet. These plenums serve as macro to micro transition to direct gas flow through the capillary while also providing electrical connection to the electrodes. The reactor can be operated in two configurations: indirect surface discharges (DBD) and direct pin to pin spark discharge [3]. In both configurations, a grounded copper wire is wound around the capillary to facilitate the discharge propagation. In the indirect configuration, only one electrode is inserted in the capillary. In the direct configuration(fig.1), an additional wire electrode is placed inside the other end of the capillary and is connected to ground through a resistor. In both cases, the high-voltage pulses are applied through a 150 µm diameter tungsten wire in the capillary.

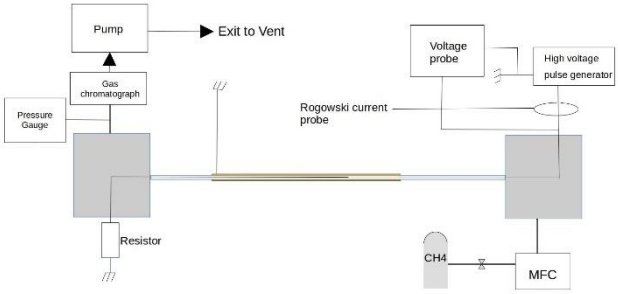



Fig.1: Schematics of the micro-structured reactor in the direct configuration

## 3 Results

In the indirect discharge configuration, the reactor yielded a maximum 1.8% methane conversion with an energy efficiency of 1.9%. In contrast, the direct pin to pin configuration resulted in maximum methane conversion of 9.1% and a maximum efficiency of 14.5%. These results were obtained with a gas flowrate of 10 sccm, 20 mm gap, high-voltage pulsed discharges at 19 kV with a repetition frequency of 12 Hz, and a 100 kΩ ballast resistor.

**References**

[1] Zhang, Sun, et Hu, « Steam reforming of methane » *Renewable and Sustainable Energy Reviews*, 2021
[2] L.Fulcheri et al, An energy-efficient plasma methane pyrolysis process for high yields of carbon black and hydrogen, *International Journal of Hydrogen Energies*, 2023
[3] Salem Achat, Étude d'un plasma de décharge pour le déclenchement des réactions de combustion dans un mélange air-propane, *Thesis, University Paris 6*, 1992

# Zero-Dimensional Simulation of Nitrogen NRP Discharges and Dissociation Efficiency

E. Roger[1], P. Mariotto[1] and C. O. Laux[1]

[1] *Laboratoire EM2C, CNRS, Université Paris-Saclay, Centralesupélec, 3 rue Joliot-Curie, 91190 Gif-sur-Yvette, France*

This study investigates the efficiency of nitrogen dissociation in nanosecond discharges at different pressures, ranging from 3 mbar to 10 bar. First, we examine the effect of the discharge parameters, such as the reduced electric field and the ambient conditions, on the nitrogen dissociation efficiency. In particular, we compare the dissociation efficiency in the non-thermal and thermal discharge regimes. Second, we investigate the kinetic and hydrodynamics phenomena impacting the density of N during the post-discharge phase. The various simulations were performed using a 0D kinetic model coupled to the electron Boltzmann equation and a two-temperature thermodynamic model. The solver is coupled to an electric circuit model and a hydrodynamic model, accounting for the effect of the blast wave expansion and heat diffusion.

## 1 Introduction

Nitrogen atoms are crucial in various industries, including metal nitriding, biomedical treatments, semiconductor doping, and the production of fertilizers and explosives. Consequently, the energy-efficient and decarbonized production of nitrogen atoms is important in these fields. Plasma discharges, such as nanosecond repetitively pulsed discharges (NRPD), are promising technologies for efficiently dissociating nitrogen molecules at near-atmospheric pressure using electrical energy. However, the optimal NRPD parameters—such as applied voltage, pulse frequency, interelectrode gap, and ambient pressure—are still unknown. NRPDs involve a range of physical phenomena, including plasma kinetics (state-to-state kinetics and non-Maxwellian electron velocity distribution) and flow dynamics (blast wave expansion and heat diffusion). One way to optimize dissociation efficiency is to employ a multiphysics model, such as the one presented in this work.

## 2 Results and Future Work

We developed a multiphysics simulation tool capable of handling all physical phenomena that occur during both the pulse and inter-pulse phases. This tool features a 0D state-to-state plasma kinetic solver including two temperature equations. The kinetic model includes the electronic-specific mechanism developed in Ref. [1] for $N_2$, N, $N^+$, and $N_2^+$. It accounts for the stepwise ionization of nitrogen molecules and atoms and can handle transitions from the non-thermal spark to the thermal spark regime.

During the discharge pulse, the kinetic solver is coupled with the Bolos electron Boltzmann equation solver [2,3] and a circuit model accounting for the fractional reflection of the voltage signal within the plasma. During the post-discharge, the kinetic solver is coupled with a hydrodynamic model to capture gas expansion and cooling due to diffusive heat losses.

We performed many simulations of pulses for which the initial temperature, electron density, and reduced electric field were fixed to 300 K, $10^{11}$ $cm^{-3}$, and 204 Td. The pressure was set to: 3, 30, 300 mbar, 1 atm, and 10 bar. We identified the discharge configurations with the greatest ability to dissociate $N_2$ during the pulse phase. In the cases at 1 atm and 10 bar, we observed a transition to the thermal spark regime with a sharp increase in gas temperature up to ~10,000 K and a full nitrogen dissociation. The energy efficiency of nitrogen atom production increases in these configurations (~10 atom / 100 eV). We observed the same trends when the reduced electric fields are 163 and 266 Td.

We plan to use the strategy to simulate the experiment from Ref. [4] up to tens of microseconds after the pulse and compare the results with the experimental data.

**Acknowledgments**

This work has received funding from the European Research Council (ERC) under the European Union's Horizon 2020 research and innovation program (grant agreement No. 101021538).

**References**

[1] Minesi, N., Thermal Spark Formation and Plasma-Assisted Combustion by Nanosecond Repetitive Discharges, PhD thesis. (2020).

[2] Hagelaar, G. J. M. *et al.*, Solving the Boltzmann Equation to Obtain Electron Transport Coefficients and Rate Coefficients for Fluid Models, *Plasma Sources Science and Technology*, **14**, No. 4, (2005).

[3] Luque, A., Bolos, (2018).

[4] Gallant, A., Kinetic of Atomic Nitrogen Production by NRP Discharges, PhD thesis. (2024).

# Modeling of $N_2$-$H_2$ DC discharges for ammonia production

L.L. Alves[1], P. Pereira[1], S.S. Baghel[1], A. Gonçalves[1], M. Budde[2], J.P. Booth[2], O. Guaitella[2], N. Pinhão[1], C.D. Pintassilgo[1,4], L. Marques[3]

[1] *Instituto de Plasmas e Fusão Nuclear, Instituto Superior Técnico, Universidade de Lisboa, Portugal*
[2] *LPP, Ecole Polytechnique, Sorbonne Université, Institut Polytechnique de Paris, CNRS, France*
[3] *Centro de Física das Universidades do Minho e do Porto, Braga, Portugal*
[4] *Faculdade de Engenharia, Universidade do Porto, Portugal*

In this work we present the on-going validation of a kinetic model for nitrogen-hydrogen plasmas, highlighting the significance of plasma-surface interactions in ammonia production.

We present the on-going validation of a kinetic model for nitrogen-hydrogen plasmas, leveraging complementary modeling and diagnostic analyses. We model cylindrical DC glow discharges (10's cm long and $\sim 1$ cm inner radius), produced in $N_2$-$H_2$ gas mixtures ($0-100\%$ $H_2$ concentrations), at $0-600$ sccm flows, $p = 10-700$ Pa pressures and $I_{dc} = 5-100$ mA discharge currents [1]-[6].

Simulations use the LisbOn KInetics (LoKI-B+C) simulation tool [7, 8], comprising an electron Boltzmann equation solver (LoKI-B) and a Chemical solver (LoKI-C), adopting an updated version of the kinetic scheme for volume mechanisms in [9], complemented by a mesoscopic kinetic model for plasma-surface interactions inspired in [6]. Diagnostics use electric measurements, mass spectrometry, OES and FTIR spectroscopy.

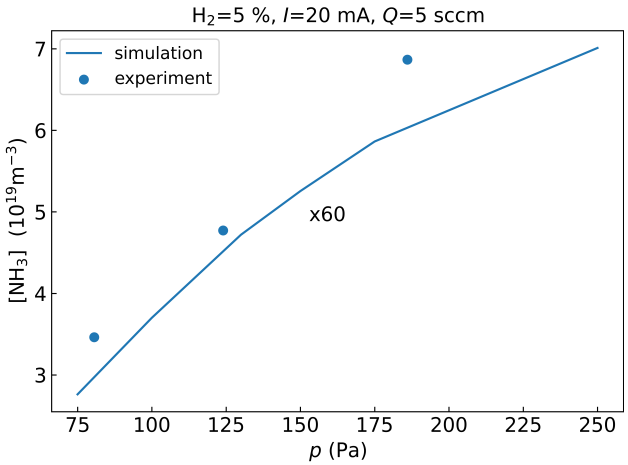



Figure 1: Density of $NH_3$ as a function of pressure, obtained from numerical simulations (line, multiplied by $60\times$) and from experimental measurements (points) at $5\%H_2$ + $95\%N_2$ and $I_{dc} = 20$ mA.

Simulation results confirm that the main production mechanisms of $NH_3$ occur at the surfaces (Langmuir-Hinshelwood and Eley-Rideal recombinations), while the main destruction mechanism is due to collisions with the $N_2$(A) metastable. Figure 1 shows current results for the $NH_3$ density as a function of pressure, at $5\%$ $H_2$ and $I_{dc} = 20$ mA. One observes good qualitative agreement between simulations and measurements, although the model still predicts $NH_3$ densities $\sim 50\times$ below the experiment. This discrepancy is likely due to the high rate of the destruction reaction, which may result from an overestimation of the corresponding rate coefficient or the $N_2$(A) population.

The validation effort will continue, focusing on improving the agreement between model results and experimental measurements for the discharge characteristics, the populations of $N_2$(A,C), $N_2^+$(B), N($^4$S,$^2$D,$^2$P) and H($^1$S).

## Acknowledgments

This work was funded by FCT - Fundação para a Ciência e Tecnologia under projects UIDB/50010/2020, UIDP/50010/2020, LA/P/0061/2020, 2022.04128.PTDC and PTDC/FIS-PLA/1616/2021.

## References

[1] Chatain, A. *et al.*, *Plasma Sources Sci. Technol.* **32**, 035002 (2023).
[2] Brovikova, I. N. and Galiaskarov, E. G. *High Temperature*, **39**, 809–814 (2001).
[3] Cernogora, G. *et al*, *J. Phys. B: Atom. Mol. Phys.* **14**, 2977 (1981).
[4] Popa, S. *et al*, *Journal de Physique III* **7**, 1331-1337 (1997).
[5] Amorim, J. *et al*, *J. Phys. D: Appl. Phys.* **68**, 1915-1917 (1996).
[6] Gordiets, B. *et al.*, *Plasma Sources Sci. Technol.* **7**, 379–88 (1998).
[7] Tejero-del-Caz, A. *et al.*, *Plasma Sources Sci. Technol.* **28**, 043001 (2019).
[8] https://github.com/IST-Lisbon/LoKI
[9] Jiménez-Redondo, M. *et al.*, *Plasma Sources Sci. Technol.* **29**, 085023 (2020).

# Boosting the $NO_x$ production in microwave air plasma: A synergy of chemistry and vibrational kinetics

Q. Shen[1], A. Pikalev[1], J. Gans[1], A. Hughes[1,2], V. Guerra[3], M. C. M. van de Sanden[1,4]

*1, Dutch Institute for Fundamental Energy Research, Eindhoven, The Netherlands*

*2, Department of Electrical Engineering and Electronics, The University of Liverpool, Liverpool, United Kingdom*

*3. Instituto de Plasmas e Fusão Nuclear, Instituto Superior Técnico, Universidade de Lisboa, Portugal*

*4, Department of Applied Physics, Eindhoven Institute of Renewable Energy Systems, Eindhoven University of Technology, Eindhoven, The Netherlands*

This study employs a quasi-1.5D multi-temperature model to investigate the mechanisms governing $NO_x$ production in microwave plasma reactors at 80 mbar, focusing on the interplay of vibrational excitation, chemical and electron kinetics, thermodynamics, and transport processes across the discharge and afterglow. A pronounced non-thermal state is predicted in the plasma region, which enhances $NO_x$ production. However, the non-thermal state is found to diminish rapidly within the afterglow. The simulation results show good agreement with experimental data for both the temperature profile and energy cost.

## 1. Introduction

Recently, plasma-based nitrogen fixation has garnered increasing attention, offering the potential to replace the Haber-Bosch process and enable carbon-free fertilizer production. However, limited studies have focused on simulation of the plasma region for intermediate pressures of 10-100 mbar.

## 2. Methods

The quasi-1.5D model of a tubular chemical reactor is represented by a network of five connected plug flow reactor (PFR) models (for the central region and 4 outer layers) and simulates both the discharge and the afterglow incorporating the radial diffusion. By coupling LoKI-B Boltzmann solver [1] with Cantera [2], the model calculates the time-resolved evolution of species concentrations and different temperatures. The calculations were performed for an airflow of 10 SLM and a power of 800 W.

## 3. Results and Discussion

Based on the calculation, 71% of the electron energy is utilized for vibrational excitation of $N_2$ in the discharge-plasma region. As a result, the peak vibrational temperature of $N_2$ significantly exceeds the gas temperature (see Fig. 1), leading to an NO mole fraction close to 10% in the discharge-plasma region. As a comparison, the maximum of NO molar fraction under the thermal model at 80 mbar is 7.2%. Due to radial concentration gradients, a part of NO generated in the central region can diffuse outward, where the lower gas temperature inhibits NO destruction via reverse Zeldovich reactions, thereby increasing overall NO production. A stronger turbulent effect facilitates NO diffusion into cooler regions while simultaneously enhancing the cooling rate, both of which contribute to the prevention of NO destruction. Overall, the total energy cost predicted by the non-thermal model is 3.42 MJ/mol, aligning with the experimental results of 3.43±0.1 MJ/mol. In comparison, the total energy cost of the pure thermal model is 4.49 MJ/mol, highlighting the impact of non-thermal behaviour on the $NO_x$ production at 80 mbar.

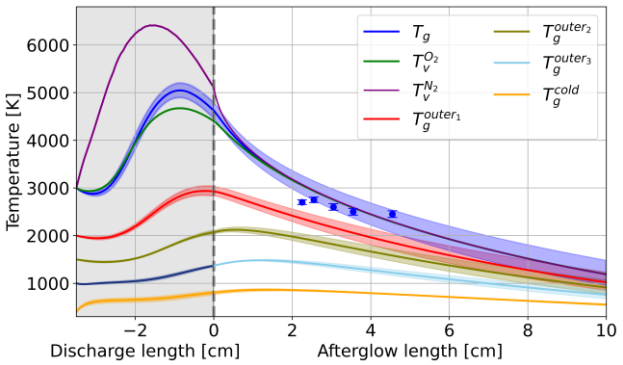



Figure 1: The evolution of various temperatures throughout the entire process (including discharge and afterglow). The shaded areas across different solid lines represent different temperature variations as the peak turbulent viscosity is varied by 30%. $T_g$, $T_v^{O_2}$ and $T_v^{N_2}$ represent the gas temperature and vibrational temperatures of $O_2$ and $N_2$ in the central region. The blue dots indicate the experimental temperature profile measured by rotational Raman scattering spectroscopy at the tube axis.

## 4. Acknowledgement

This work is financially supported by the China Scholarship Council Grant No. CSC202106240037. IPFN activities we supported by the Portuguese FCT-Fundação para a Ciência e a Tecnologia, under funding to IPFN (DOI: 10.54499/LA/P/0061/2020, 10.54499/UIDB/50010/2020,10.54499/UIDP/50010/2020, and 10.54499/PTDC/FIS-PLA/1616/2021).

## References

[1] A. Tejero-del-Caz *et al.*, PSST., **28**, 043001, (2019).

[2] See https://cantera.org.

# Magnetic moment based on gyrocoordinates in partially magnetized plasmas in an axisymmetric magnetic field

L. Vogelhuber[1], K. Köhn[1], L. Xu[2], Y. Sharova[1], D. Krüger[1], J. Kallähn[1], D. Eremin[1] and R. B. Brinkmann[1]

[1] *Institute of Theoretical Electrical Engineering, Ruhr University Bochum, Universitätsstrasse 150, D-44801 Bochum, Germany*

[2] *Department of Physical Science and Technology, Soochow University, Suzhou 215006, China*

In this work, we investigate the dynamics of the magnetic moment of electrons in axisymmetric magnetic field configurations, similar to those in magnetron discharges of partially magnetized plasmas. The magnetic moment is expressed as a power series in the small parameter $\eta$, defined as the ratio of the gyroradius $r_\mathrm{L}$ to the system dimension $L$. The magnetic moment is formulated as a power series in this small parameter, which calculates the magnetic moment up to third-order correction.

## 1 Introduction

Partially magnetized plasma discharges in $E \times B$ configurations are versatile, with applications ranging from Hall-effect thrusters for space propulsion to high-power impulse magnetron sputtering (HiPIMS) for thin-film deposition. Their magnetic fields are typically described in cylindrical coordinates $(r, \theta, z)$, with field lines lying in the $r$–$z$ plane [1]. Electrons confined in the race-track region are considered magnetized, with their magnetic moment serving as an indicator of the degree of confinement; if the magnetic moment is conserved along the trajectory, the electron remains magnetized. However, various processes can disrupt this conservation, including collisions, electric field interactions, and resonant particle motion [2, 3].

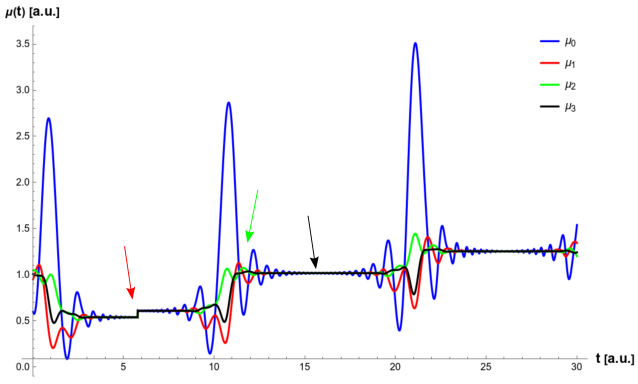



Figure 1: Magnetic moment: Leading order (blue); first order correction (red); second order correction (green); third order correction (black).

## 2 Objective

This work explores the dynamics of the electron magnetic moment $\mu$ in these configurations with an axisymmetric magnetic field. To describe electron behavior in such discharges, a coordinate transformation is performed from cylindrical phase space coordinates $(r, \theta, z, v_r, v_\theta, v_z)$ to gyrocoordinates $(\psi, \theta, s, v, \chi, \phi)$. This transformation is based on the smallness of the gyroradius $r_\mathrm{L}$ relative to a characteristic system dimension $L$, introducing the small parameter $\eta = \frac{r_\mathrm{L}}{L}$ [4]. To calculate $\mu$ it is formulated as a series expansion in the form

$$\mu = \mu_0 + \eta^1 \mu_1 + \eta^2 \mu_2 + \eta^3 \mu_3,$$

accurate up to third-order corrections.

## 3 Outlook

The magnetic moment is shown in figure 1. Magnetic mirror effects are visible in regions where $\mu$ shows little to no oscillations in all its orders (black arrow). Sharp jumps (red arrow) in $\mu$ are due to collisions, in this case, with a wall. Oscillations observed when crossing magnetic field strength minima (green arrow) are pronounced at lower orders but are effectively suppressed at higher orders of accuracy. The jumps of $\mu$ in this region can be attributed to resonances in particle motion; these jumps persist even when higher-order corrections are included.

## References

[1] R. P. Brinkmann et al. 2020 Phys. Plasmas; 27 (5): 053504.
[2] R. J. Hastie et al. 1969 IAEA pp. p. 389–401
[3] C. D. Stephens et al. 2017 Phys. Plasmas; 24 (10): 102517.
[4] K. Köhn et al. 2023 Plasma Sources Sci. Technol; 32 055012

# PICCOLO: a PIC code suite for low-temperature plasmas

F. Taccogna[1], P. Minelli[1] and F. Cichocki[2]

[1] *Institute for Plasma Science and Technology (ISTP), CNR, via Amendola 122/D 70126, Bari, Italy*
[2] *Nuclear Department (NUC), ENEA, C.R. Frascati, via Fermi 45, 00044 Frascati, Italy*

A new Particle-in-Cell suite, named PICCOLO, designed to simulate partially ionized low temperature plasmas in multi-dimensional scenarios, is presented. Its versatility is demonstrated by selecting a few applications in low- and high-pressure regimes.

## 1 General

This paper presents the results obtained with the code PICCOLO [1] (PIC COde for LOw temperature plasmas), a versatile suite implementing the Particle-in-Cell (PIC) technique, specifically designed to simulate low temperature plasma scenarios. The numerical code supports Cartesian and cylindrical coordinate systems in 1D, 2D and 3D geometries. PICCOLO considers charged species (electron, positive, and negative ions) represented by macro-particles and a fixed neutral fluid background. A set of Python scripts was also developed to plot and analyze simulation data. PICCOLO has been parallelized with a hybrid Open MP-MPI approach.

## 2 Applications

### 2.1 The negative ion source SPIDER

Fig. 1 reports the negative ion density $H^-$ in the plane perpendicular to the magnetic filter direction inside the negative ion source SPIDER by neglecting the surface production on the plasma grid, assuming uniformity along the direction of the magnetic filter and a uniform absorbed power $P = 100$ kW inside each driver. A vibrational distribution corresponding to a temperature $T_\nu = 3000$ K has been considered for the molecular hydrogen $H_2$ background. A scaled value of the vacuum permittivity $\epsilon_0' = 2.25 \times 10^4 \epsilon_0$ has been assumed to speed up the execution of the code.

### 2.2 The hollow cathode discharge

Fig. 2 shows the 2D$(r, z)$ axisymmetric map of the electron density inside a particular configuration of Kr gas hollow cathode and in the plume region, for a $LaB_6$ disk emitter (at $z = 0$) heated at a temperature $T$ = 1820 K. In this case, a scaling factor of the vacuum permittivity $\epsilon_0' = 1 \times 10^3 \epsilon_0$ has been used.

**Acknowledgements** - Work carried out in the frame of project NEFERTARI – CUP B53C22003070006, funded by the European Union under the National Recovery and Resilience Plan (NRRP) – NextGenerationEU.

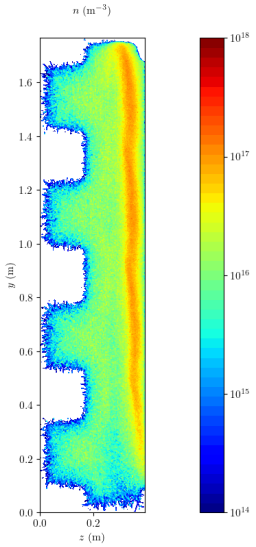



Figure 1: $H^-$ ion (volumetric production) density map in the plane perpendicular to the magnetic filter in Spider source.

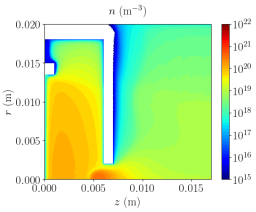



Figure 2: Electron density in the 2D$(r, z)$ axial-symmetric geometry inside the hollow cathode and plume region.

## References

[1] Cichocki, F., et al., PIC modeling challenges in diverse low temperature plasma scenarios. Invited talk at 26th ESCAMPIG conference, Brno, Czech Republic, July 9–13 (2024).

# Data-driven reduced modeling of streamer discharges in air

J. Teunissen[1], A. Malagón-Romero[2,1]

[1] *Centrum Wiskunde & Informatica (CWI), Amsterdam, The Netherlands*
[2] *Instituto de Astrofísica de Andalucía (IAA), CSIC, Granada, Spain*

Numerical simulations of streamer discharges are typically computationally expensive, since small spatial and temporal scales have to be resolved. We present a new reduced model for simulating filamentary electric discharges, in which time steps and the spatial resolution can be orders of magnitude larger than in conventional models. Discharge channels are represented as conducting cylindrical segments. The growth of these channels is described by fit formulas obtained from a large dataset of axisymmetric positive streamer simulations in air.

## 1 Description

On this poster, we introduce a reduced model for streamer discharges that we are currently developing [1]. The model can be split in three components, which are briefly described below.

### 1.1 Framework for conducting cylinders

We introduce a framework for simulating the growth of imperfectly conducting channels. As input, a model is required that predicts the next position, radius and conductivity of each channel. The conductivity is mapped onto a numerical mesh, and by solving a modified Poisson equation on this mesh, the electric potential at the next time step is self-consistently determined. We use the `afivo` library, which provides a field solver with adaptive mesh refinement and electrode support. The growth model can be written purely in Python, enabling easy experimentation with various data-driven or physics-based approaches.

### 1.2 Simulation dataset and fits

We have compiled a dataset of 1000 axisymmetric positive streamer simulations in air at 1 bar and 300 K. The simulations were performed with a standard fluid model, and the applied voltage and the electrode geometry were varied. From this dataset, we derive simple fit expressions to predict the streamer radius, velocity and conductivity, taking as input a length scale of the high-field region around the streamer head.

### 1.3 Reduced model

By combining the framework, the fit expressions, and a heuristic description of streamer branching, we construct a reduced simulation model for positive streamers in air. With this model, the grid spacing and time step can be orders of magnitude larger than with a standard fluid model. We compare the reduced model against standard axisymmetric simulations and we show 3D results.

## References

[1] Teunissen, J. & Malagón-Romero, A. Data-driven reduced modeling of streamer discharges in air (2025). URL `https://arxiv.org/abs/2501.06093`. `2501.06093`.

# Self-consistent PLASIMO global model for dust growth and plasma chemistry

K. van 't Veer[1], W. Graef[1], J. Janssen[1], D. Mihailova[1], R. Budé[1] and J. van Dijk[2]

[1] *Plasma Matters B.V., Eindhoven, The Netherlands*
[2] *Eindhoven University of Technology, Eindhoven, The Netherlands*

A particle growth model has been developed in PLASIMO that can describe the growth of dust due to nucleation, coagulation, charging and surface growth. This model is self consitently coupled to a global model that can describe complete plasma chemistries. Electrons, ions and neutral plasma species can be taken into account in the dust formation, growth and charging.

## 1 Introduction

A particle growth model has been developed within the PLASIMO framework [1, 2] to describe the time evolution of dust particles. Starting from nucleation species, the coagulation, charging, and surface growth of dust particles is described.

This model is self consistently coupled to a global model to describe the plasma chemistry. Multiple plasma species can be specified as nucleation species to start the dust growth, including electrons, (positive) ions and neutrals. The composition of the dust particles can then also be calculated.

In this work we compare our model results with experiments in which the interaction of plasma species and the formed dust is studied in afterglow conditions [3].

Furthermore, we explore the composition of the dust particles according to the model, and the effect the ion energy has on it.

## 2 Methods

In the particle growth model we solve the discrete Smoluchowski equation, ensuring mass and charge conservation over a fixed mass and charge grid [4]. Surface growth is assumed to take place via ion collisions. This surface growth and the ion charging effects are coupled. The electron and ion collision frequencies are based on the Orbital Motion Limited theory [5].

The composition of dust particles is calculated by solving the nucleation species number density balance (for each dust particle) rather than only the dust particle number density.

**Acknowledgements**

This work is supported by the Chips Joint Undertaking and its members, including the top-up funding by RVO.

**References**

[1] https://plasma-matters.nl/
[2] van Dijk, J., Peerenboom, K.S.C., Jimenez-Diaz, M., Mihailova, D.B., and van der Mullen, J.J.A.M. Journal of Physics D: Applied Physics, 42(19), 194012-1/14 (2009)
[3] Hasani, M., Donders, T. J. M., and Beckers, J., J. Phys. D: Appl. Phys. 56 365204 (2023)
[4] Prakash, A., Bapat, A. P., and Zachariah, M. R. Aerosol Science & Technology, 37:11, 892-898 (2003)
[5] Kortshagen, U. and Bhandarkar. U., Phys. Rev. E 60, 887 (1999)

# Electric Field and Chemical Kinetics in a Nanosecond-Pulsed DBD in Humid Air

L. Ibba[1], G. Pierotti[2], A. Popoli[2], A. Cristofolini[2], D. Aceto[3], P.F. Ambrico[3], and I. Furno[1]

[1] *Swiss Plasma Center (SPC), Ecole Polytechnique Federale de Lausanne (EPFL), CH-1015, Lausanne, Switzerland*
[2] *Department of Electrical, Electronic, and Information Engineering "Guglielmo Marconi", University of Bologna, Viale Risorgimento 2, Bologna 40136, Italy*
[3] *CNR, Istituto per la Scienza e Tecnologia dei Plasmi, Sede di Bari, Via Amendola 122/D, Bari, Italy*

A nanosecond-pulsed DBD in humid air was investigated through experiments and numerical simulations. Electric field measurements were performed using the EFISH technique with picosecond laser resolution at three positions within the plasma volume. A zero-dimensional kinetic model was developed, incorporating measured electric field data. The model showed good agreement with experimental measurements of NO and OH concentrations obtained via laser-induced fluorescence (LIF). Key chemical pathways for NO and OH formation and destruction were identified, highlighting the dynamics governing the main ion species over long- and short-time scales.

This study investigates the dynamics of a nanosecond-pulsed dielectric barrier discharge (DBD) in atmospheric-pressure humid air through a combination of experimental diagnostics and computational modeling. The experimental setup involved measuring the electric field within the plasma using the electric field-induced second harmonic generation (EFISH) technique [1], employing a picosecond laser. Time-resolved measurements were conducted at three distinct positions within the plasma gap: near the high-voltage electrode, the ground electrode, and the center. Additionally, laser-induced fluorescence (LIF) was used to measure absolute NO concentrations and relative OH densities over multiple pulses.

The computational model was implemented within the MERLINO global model framework, a zero-dimensional (0D) kinetic model developed at the University of Bologna. The model incorporated 126 species and nearly 5000 reactions, from [2]. The considered species include vibrationally excited nitrogen, as well as reactive species like NO and OH. The model used the measured (reduced) electric field data as input. Rate coefficients for electron impact reactions were obtained by solving the electron Boltzmann equation using the LoKI-B solver.

The simulation results showed good agreement with experimental measurements for both NO and OH. Also, different key reaction pathways for studied radicals were identified: NO primarily forms via $O_2$ + N($^2$D), but only when the applied field is strong, while OH is predominantly created through reactions involving excited atomic species (O($^1$D) and N($^2$D)) with water vapor.

The study also analyzed long-lived ionic species, identifying $NO^+$ (shown in Fig. 1) and $NO_3^-$ as dominant ions between discharge pulses. These insights into both short- and long-lived species highlight the complex interplay of plasma chemistry in humid air environments.

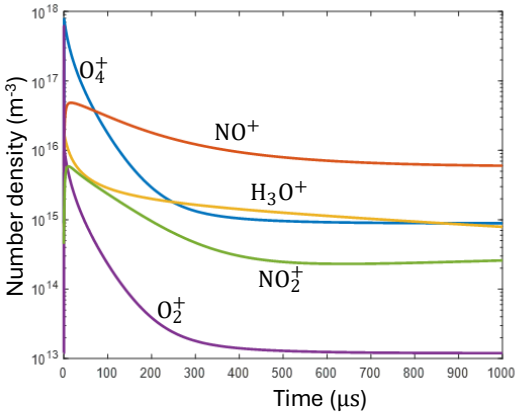



Figure 1: Computed number densities of positive ions over 1 ms.

**References**

[1] Ambrico, P. F., Aceto, D., Ibba, L., Yang, X., Dilecce, G., Ambrico, M., Furno, I., & Adamovich, I. V. Breakdown development in a nanosecond pulsed dielectric barrier discharge in humid air in plane-to-plane geometry. *Plasma Sources Science and Technology* , 32(9), 095008 (2023).

[2] Pierotti, G., Popoli, A., Pintassilgo, C. D., & Cristofolini, A. Modeling Study of Chemical Kinetics and Vibrational Excitation in a Volumetric DBD in Humid Air at Atmospheric Pressure. *Plasma Chemistry and Plasma Processing* , 1–20 (2024).

# Spatiotemporal distribution of surface potential on barrier during atmospheric pressure Townsend discharge in air and $N_2$

N. Osawa[1] and S. Hori[1]

[1] *Kanazawa Institute of Technology, Nonoichi, Ishikawa, Japan*

Atmospheric Pressure Townsend Discharge (APTD) is a type of homogeneous dielectric barrier discharge. While we have successfully generated APTD in air and nitrogen using appropriate dielectric materials, the spatiotemporal distribution of surface charge on the barrier during APTD generation in nitrogen has not been investigated. In this study, we investigate the spatiotemporal distribution of surface charge density during APTD in $N_2$ and compare it with that observed in air.

## 1 Introduction

Atmospheric pressure Townsend discharge (APTD) is a promising plasma processing technology for homogeneous surface treatment and other applications. In 2011, we achieved stable APTD generation in air, oxygen, nitrogen ($N_2$) and helium using a dielectric barrier discharge (DBD) device with an appropriate alumina barrier [1]. We hypothesized that the surface charge density on the alumina barrier prior to APTD initiation is important for stable APTD in air. To investigate this, we developed a method for observing the spatiotemporal distribution of surface charge density during APTD using a non-contacting electrostatic voltmeter [2].

In this study, we investigated the spatiotemporal distribution of surface potential on the barrier during APTD in $N_2$ and air, aiming to understand the influence of gas composition on APTD generation.

## 2 Method

The DBD setup employed in this study consisted of a hemispherical rod electrode (diameter: 10 mm) and an alumina dielectric coated plane electrode. The gap length and the applied voltage frequency were 3 mm and 50 Hz, respectively. Spatiotemporal distribution of surface potential on the barrier was observed by a surface potential analysis system [2].

## 3 Results

Fig. 1 shows waveforms of voltage, measured current ($i$), displacement current ($i_d$), and discharge current ($i_{dis}$) in $N_2$. In Period A, the observation of continuous currents confirms the generation of APTD. On the other hand, in Period C, the generation of a single pulse current indicates the occurrence of a single streamer discharge.

Fig. 2 shows the spatiotemporal distribution of the surface potential on the barrier. During Period A, the surface potential in $N_2$ increased from -8.7 kV to -0.2 kV. In contrast, the surface potential in air increased from -3.0 kV to 1.1 kV under the same conditions.

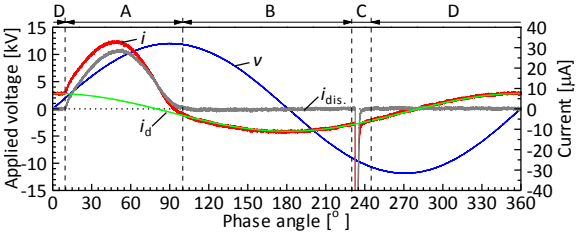



Fig. 1 Waveforms of measured current, displacement current, and discharge current in $N_2$.

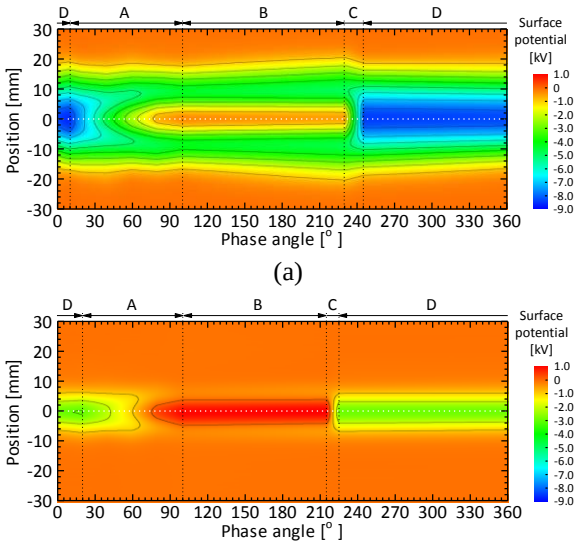



Fig. 2 Spatiotemporal distribution of surface potential on barrier in $N_2$ (a) and in air (b).

This work was supported by JSPS KAKENHI Grant Number JP23K03824.

**References**

[1] N. Osawa, Y. Yoshioka, *IEEE Trans. Plasma Sci.*, **40**, 2-8 (2011).
[2] K. Watanabe, N. Osawa, *J. Inst. Electrostat. Jpn.*, **48**, 143-148 (2024).

# Impact of different dielectric materials on the performance and optical features of a Micro-Hollow Cathode Discharge

N. Chazapis, B. Menacer, D. Stefas, G. Lombardi, C. Lazzaroni, and K. Gazeli

*Laboratoire des Sciences des Procédés et des Matériaux (LSPM), CNRS, Université Sorbonne Paris Nord, UPR 3407, F–93430 Villetaneuse, France*

Micro Hollow Cathode Discharges (MHCDs) are promising microplasma sources for the deposition of large band gap nitrides such as hexagonal boron nitride (h-BN). Particularly, MHCDs can dissociate the molecular nitrogen, which is an attractive feature for the synthesis of h-BN. Their efficiency in producing N-atoms depends on the endurance of their structural materials, which also affect their performance. This work investigates the influence of the type of the dielectric material on the performance and optical properties of a DC MHCD in Ar/$N_2$ mixtures.

The optimization of MHCDs for the growth of high-quality h-BN films over large surfaces of different substrates remains a challenge, requiring a deeper understanding of their physical properties [1]. Furthermore, ensuring their reliable performance in the long-term is a prerequisite to enhance their energy efficiency, better control the N-atom production and improve h-BN film properties. h-BN synthesis on a 5 cm diameter $SiO_2$/Si substrate has been achieved using a pulsed-driven MHCD using an alumina ($Al_2O_3$) dielectric [2]. However, this may be a source of trace amounts of oxygen which was found in the film lowering its quality, while source aging has been also evidenced limiting its reliable operation.

In this work, we study a representative case of drastic MHCD operation, i.e., MHCD driven by a DC voltage (~kV), where the components (dielectric and electrodes) are constantly exposed to the plasma. The influence of different dielectric materials ($Al_2O_3$, aluminium nitride (AlN), sapphire, Macor) on the durability of the MHCD and its optical features (morphology and area of the cathodic expansion, emissive species in the hole, etc.) are studied. The MHCD operates in various $N_2$/Ar gas mixtures and discharge currents applied. The pressure is kept the same in two MHCD chambers (20 – 100 mbar).

The choice of the dielectric material not only affects the cathodic sheath formation but also modifies the discharge reactivity, determining the efficiency of $N_2$ dissociation. Preliminary results indicate significant differences in the form and area (S) of the cathodic expansion in the DC MHCD using $Al_2O_3$ (Fig. 1). Both features also depend on the gas mixture type and the applied electric current.

These differences are further studied using optical emission spectroscopy (not shown) and image processing techniques (such as in Fig.1) to analyse spatial emission profiles of the discharge.

These studies help in better understanding the MHCD peculiarities under and validating relevant analytical models of the cathodic region. By refining the MHCD parameters (constructive materials, gas composition, current), an improved control of h-BN growth may be achieved, enhancing film properties.

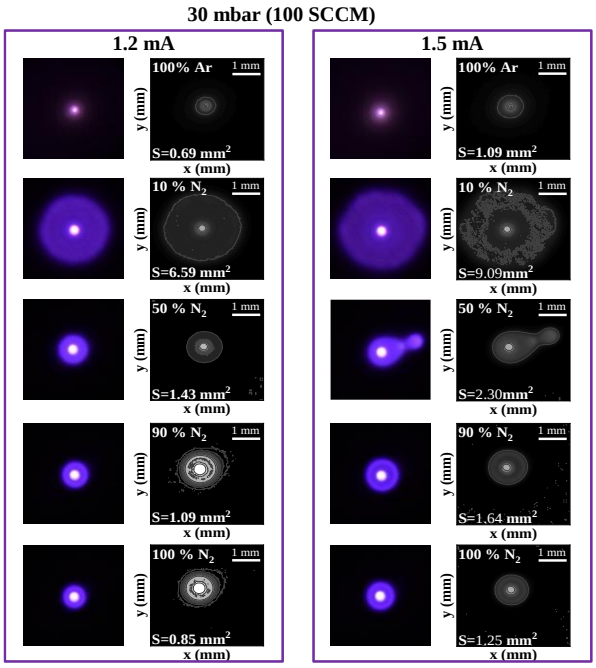



Fig. 1. Actual photos (left columns) and corresponding contour plots (right columns) showing the discharge expansion on the cathode for different Ar/$N_2$ mixtures and currents applied.

**Acknowledgements**

ANR SPECTRON (ANR-23-CE51-0004-01).

**References**

[1] Schoenbach, K. H. et al., *Applied Physics Letters* **68**, 13 (1996).

[2] Kabbara, H. et al., *Applied Physics Letters* **116**, 171902 (2020).

# Numerical thermalization in 3D PIC plasma simulations

R. M. Park[1], C. Moore[2], and S. D. Baalrud[1]

[1] *University of Michigan Department of Nuclear Engineering, Ann Arbor, MI, 48109*
[2] *Sandia National Laboratories, Albuquerque, NM 87185, USA*

The particle-based approach to simulating macroscopic plasmas traditionally suffers from artificially high collision rates due to the underresolution of particle number. The degree to which collisional shape effects can compensate for large macroparticle weight is presented. It is determined that reaching the physical collision rate in 3D PIC simulations may be intractable for simulations that resolve the Debye length. The previously established [1] kinetic equation for finite-sized particles is found to accurately predict the plasma collision time resulting from velocity autocorrelation data of 3D PIC simulations with various grid spacings and plasma conditions.

The kinetic behavior of momentum conserving explicit PIC methods has been studied extensively, including finite particle [1], aliasing, and finite field [2] effects. In simulations which avoid aliasing effects, the primary contribution to collision time reduction is the characteristic width of the particle, rather than the order or filtering applied to the particle. Recent interest in numerical thermalization [3] has emphasized the necessity for maintaining order and separation of physical timescales. With the present scaling, specific particle size and weight requirements are established to achieve this timescale separation in 3D. Ultimately, the simulator must sacrifice the Debye-scale resolution of the particle interactions or face rapid thermalization of the distribution.

## References

[1] Langdon, A. B. & Birdsall, C. K. Theory of plasma simulation using finite-size particles. *The Physics of Fluids* **13**, 2115–2122 (1970).

[2] Birdsall, C. K. & Langdon, A. B. *Plasma physics via computer simulation* (CRC press, 2018).

[3] Jubin, S. *et al.* Numerical thermalization in 2d pic simulations: Practical estimates for low-temperature plasma simulations. *Physics of Plasmas* **31** (2024).

[4] Hockney, R. W. & Eastwood, J. W. *Computer simulation using particles* (crc Press, 2021).

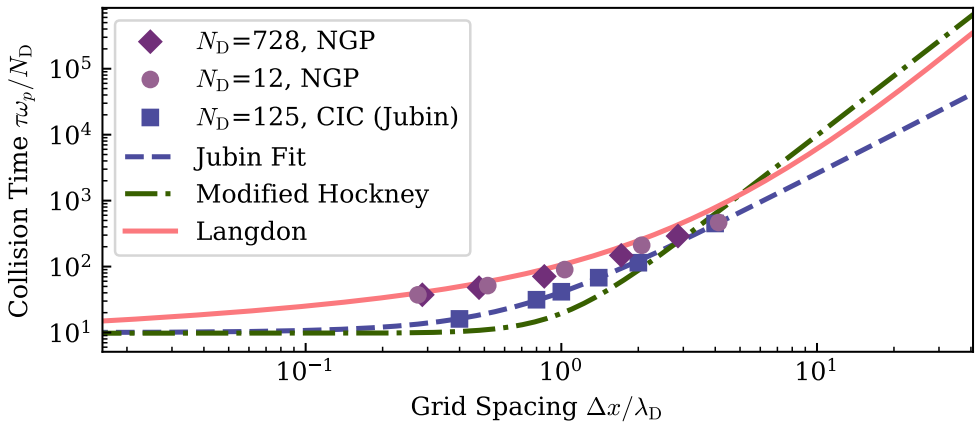



Figure 1: The collision time versus grid spacing in a 3D PIC plasma using NGP (zero-order spline) and CIC (first-order spline) particle shapes. Symbols are from simulation of slowing down time in a homogeneous plasma. The lines are: Langdon's kinetic theory of isotropic shapes [1], Hockney's empirical scaling with particles per grid element [4] adapted to 3D, and Jubin's empirical fit. The squares and fit were obtained from Jubin's OLTP Seminar [#s1875, 14 Jan 2025]. Here, $N_D = n\lambda_D^3$.

This work was supported in part by the U.S. Department of Energy under award No. DE-SC0022201, and in part by Sandia National Laboratories. Sandia National Laboratories is a multi-mission laboratory managed and operated by National Technology and Engineering Solutions of Sandia, LLC., a wholly owned subsidiary of Honeywell International, Inc., for the U.S. Department of Energy's National Nuclear Security Administration under Contract No. DE-NA0003525.

# Hybrid mode of DBD at atmospheric pressure in Ar-HMDS mixtures: modelling and experimental studies

Marjan Stankov[1], Lars Bröcker[2], Claus-Peter Klages[2], Markus M. Becker[1], Detlef Loffhagen[1]

[1] *Leibniz Institute for Plasma Science and Technology (INP), 17489 Greifswald, Germany*
[2] *Institute for Surface Technology (IOT), Technische Universität Braunschweig, 38108 Braunschweig, Germany*

This study reports on a hybrid discharge mode found in a pin-to-plate atmospheric pressure dielectric-barrier discharge (DBD) with pin-backed glass dielectric using argon with 100 ppm hexamethyldisilane (HMDS). A unique discharge appearance, characterized by a diffuse plasma region from which short filaments propagate towards the surface, is observed in the experiment and obtained by fluid modelling. Surface analysis of the deposited films shows a high density of hillocks, likely associated with the appearance of the hybrid discharge.

Atmospheric pressure DBDs can operate in diffuse, filamentary, and various hybrid modes. A unique hybrid discharge mode has been found in a pin-to-plate DBD with pin-backed glass dielectric in argon with small fractions of organosilicon monomers and short deposition times $t_d$. The observed discharge is characterised by a diffuse region, from which short filaments propagate towards the surface. To investigate its properties, modelling and experimental studies have been conducted.

The plasma source has a powered pin electrode attached to 1.1 mm thick borosilicate glass and a grounded electrode covered with a Si wafer, separated by a gap of 2.5 mm [1]. For this study, the plasma was operated in a mixture of Ar and 100 ppm HMDS by a sinusoidal voltage with an amplitude of 1.75 kV and a frequency of 19 kHz. The discharge appearance was recorded with a commercial camera (Canon EOS 7D Mark II) and surface analysis of the deposit was made by laser-scanning microscopy (LSM).

A time-dependent, spatially two-dimensional fluid-Poisson model was employed to simulate the plasma evolution from $t = 0$ until the first breakdown event. The model considers a reaction kinetic scheme with 13 species involved in about 60 collisional and radiative processes [2].

The photo of the discharge taken for $t_d < 1$ s presented in Figure 1a) clearly shows a unique structure with a diffuse part in the top 2 mm of the discharge gap and a single filament in front of the Si wafer. The spatial distribution of the electron number density $n_e$ obtained from the modelling (Figure 1b)) reproduces the discharge pattern observed in the experiment. The modelling studies reveal that Penning ionization leads to the ignition of a diffuse discharge that spreads towards the cathode. An increased electron density and electric field in the remainder of the gap initiate streamer inception and formation of a thin discharge channel between the diffuse region and the momentary cathode. LSM analysis of the film deposited during the hybrid discharge (Figure 1c)) reveals a unique topography of dense ($10^7$–$10^8$ cm$^{-2}$) flat growth hillocks. This indicates an influence of the observed hybrid discharge on the deposit properties, offering new insights for PECVD enhancements.

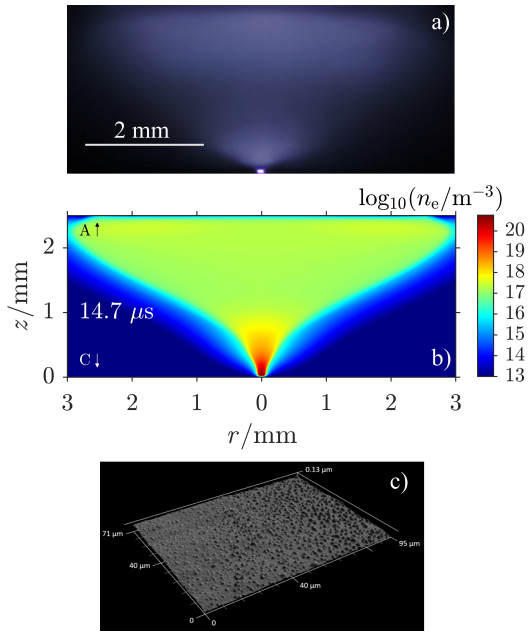



**Figure 1** a) Photo of discharge for 100 ppm HMDS in Ar ($t_d < 1$ s), b) modelled spatial profile of $n_e$ ($t$ =14.7 μs) and c) topography measurement of deposit for 50 ppm HMDS.

**Acknowledgement**
The work has been funded by the Deutsche Forschungsgemeinschaft (DFG, German Research Foundation) – project number 504701852.

**References**

[1] Bröcker, L. *et al.*, *Plasma Process. Polym.* **17**, 2000129 (2020)
[2] Loffhagen, D. *et al.*, *Plasma Chem. Plasma Process.* **41**, 289 (2021)

# Gradient nanosecond pulsed plasmas for enhanced deflagration to detonation transition: measurements of atomic oxygen density production and reduced electric field

V. Lafaurie[1], Z. Shu[1] M. Sadauskaite[1], J. B. Billeau [1], P. Vidal[2], S. M. Starikovskaia[1]

[1] *Laboratoire de Physique des Plasmas (LPP), UMR 7648 CNRS, Sorbonne Université, Université Paris-Saclay, École Polytechnique, Institut Polytechnique de Paris,Route de Saclay, Palaiseau, France*

[2] *Institut Pprime, UPR 3346 CNRS, ENSMA, Chasseneuil-du-Poitou, France*

This work aims at producing a gradient of atomic oxygen on a scale of centimetres in a plane-to-plane nanosecond discharge in 150 mbar of air. Measurement of atomic oxygen along the discharge span at varying heights between high-voltage and grounded electrode is done with O-TALIF. Measurements of the reduced electric field are performed with OES band ratio, E-FISH and back-current shunts and show propagation of the discharge as a FIW (500 Td) and, upon closing of the gap, values in the range of 60 to 220 Td.

## 1 Introduction

Climate change has become an undeniable reality in everyday life, and with it the role of combustion in our societies is coming under review. Sustainable combustion practices are required to ease the green transition but also as long-term sources for many applications currently taken for granted. One such technology is propulsion. While electrification of the aerospace industry is actively on-going, it is unlikely to completely erase combustion. One possible alternative to constant-pressure combustion used in most modern engines is the detonation wave. Pressure-gain combustion has been found to allow theoretical improvements in efficiency up to 30% [1]. Although extensive research has been performed on this method, application of non-equilibrium plasma to detonation waves is still a topic of active research. One possible problem is the reliable, "at-will", energy-efficient ignition of a detonation wave. This work studies a nanosecond discharge which aims to produce a gradient of atomic oxygen over a scale of centimetres.

## 2 Experimental setup and results

An 80 by 25 mm$^2$ high-voltage electrode is placed above a rounded triangular grounded electrode, producing a varying gap size between 28 and 48 mm. Plasma is formed by application of a single pulse of negative polarity high-voltage (-22.5 kV in the cable, 25 ns FWHM), depositing a total energy of 190 mJ.

O-TALIF measurements are performed 4.7 $\mu$s after the discharge to record density of atomic oxygen on a time-scale relevant to combustion. Initial results

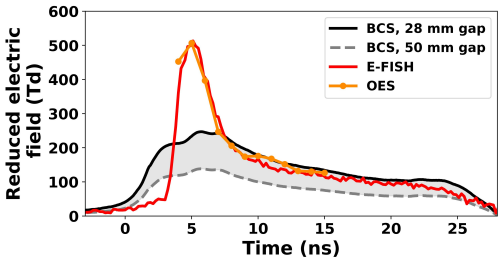



Figure 1: Variations of the reduced electric field with time measured by E-FISH, OES molecular band ratio and back-current shut

at 100 mbar [2] showed a decreasing distribution of atomic oxygen with gap size. This trend is confirmed at 150 mbar, this time looking at various distance from the high-voltage electrode. Measurements of reduced electric field using E-FISH, OES molecular band ratio and back-current shunts are presented in Figure 1. They show good agreement, with initial propagation of the discharge in the form of a fast ionisation wave (FIW) reaching 500 Td. After closing of the gap, values are recorded in the range of 60 to 220 Td by all three diagnostics.

## Acknowledgments

The work was partially supported by AID/CIEDS PPRINCE (3335).

## References

[1] Wolański, P. Detonative propulsion *Proceedings of the combustion Institute*, **34.1** (2013)

[2] Lafaurie, V., Shu, Z., Vidal, P., Starikovskaia, S. M. Gradient pulsed transient plasma for initiation of detonation. *Combustion and Flame*, **261, 113311**, (2024).

# Computational study of a pulsed atmospheric pressure dielectric barrier discharge (DBD) in humid air

Sarah Van Hove[1], Ivan Tsonev[1] and Annemie Bogaerts[1]

[1]*PLASMANT, University of Antwerp, Antwerp, Belgium*

A one-dimensional model of a pulsed dielectric barrier discharge (DBD) operating in air at atmospheric pressure was constructed using the plasma module in COMSOL Multiphysics 6.2, aiming in the next step to describe its interaction with water surfaces, as performed in [1]. The DBD is operated with pulses of 27 kV amplitude with a pulse width of 2 µs, as was measured during experiments [2]. An extensive chemistry set of about 50 species and 800 reactions was constructed. We vary e.g. the pulse shape and the permittivity of the dielectric, to study their effect on the current and electron density, which in turn influences the number of reactive species formed. By tailoring the discharge parameters, we can observe how this influences the formation of reactive nitrogen species (RNS) vs. reactive oxygen species (ROS).

## 1 Introduction

An important plasma source in the field of plasma medicine is the DBD, which operates at low gas temperatures and prevents arcing due to the presence of a dielectric material on at least one of the electrodes. This makes it suitable for various applications, including wound healing and cancer treatment. ROS such as hydrogen peroxide ($H_2O_2$) have demonstrated cancer-killing properties, while RNS such as nitric oxide (NO), can influence angiogenesis (the formation of new blood vessels) [3]. Given this, we aim to investigate what the underlying mechanisms are that lead to the production of reactive oxygen and nitrogen species (RONS). In this work we constructed a 1D axial model of a microsecond-pulsed DBD in contact with a liquid. At this stage, the liquid is modelled as a dielectric medium with dielectric permittivity of 78.4, while the second electrode is covered by a dielectric. The model includes 32 charged particles and 19 neutral species representing a humid air chemistry set consisting of 800 reactions.

## 2 Results

Figure 1a shows the current pattern during the first pulse. A positive current peak is observed during the rise of the applied electric potential and a negative one during the decrease in potential. When we double the relative permittivity of the dielectric material from 4 to 8, we observe that the positive current peak doubles in value, while the negative current peak triples, as shown in Figure 1b. In addition, this leads to partial discharging after the main current peak. Furthermore, as shown in Figure 2, the higher permittivity results in NO, OH and $O_3$ densities twice as high, and the amount of $H_2O_2$ produced is even ten times greater after four pulses.

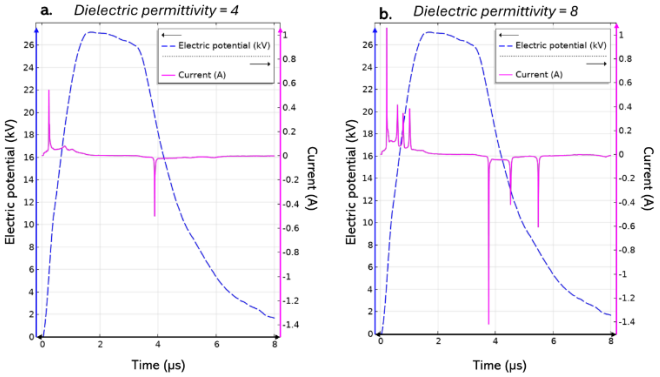



*Figure 1* – Current and applied electric potential as function of time, for a) dielectric permittivity of 4 and b) dielectric permittivity of 8.

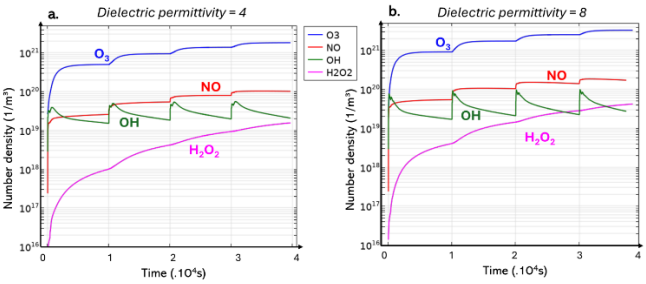



*Figure 2* – Density of RONS as function of time, for a) dielectric permittivity of 4 and b) permittivity of 8.

## References

[1] Tian, W. Atmospheric pressure dielectric barrier discharges interacting with liquid covered tissue. *Journal of Physics D: Applied Physics* **2014**, *47* (16), 165201.
[2] Lin, A. Non-thermal plasma as a unique delivery system of short-lived reactive oxygen and nitrogen species for immunogenic cell death in melanoma cells. *Advanced Science* **2019**, *6* (6), 1802062.
[3] Von Woedtke, T. Plasma medicine: A field of applied redox biology. *In vivo* **2019**, *33* (4), 1011-1026.

# Design and safety assessment of a low-temperature plasma device for the treatment of large and medium wounds

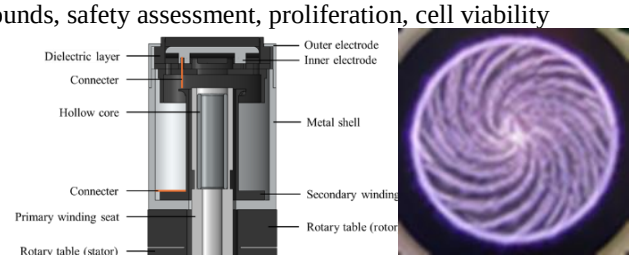
Jiunn-Der Liao[1], Chong-Yu Tai[1], Vincent Cheng[1], Shin-Chen Pan[2], Yu-Sheng Ju[1], and Han Wu[1]

[1] *Department of Materials Science and Engineering, National Cheng Kung University, Tainan, Taiwan*
[2] *Division of Plastic and Reconstructive Surgery, Department of Surgery, National Cheng Kung University Hospital, College of Medicine, National Cheng Kung University, Tainan, Taiwan*

**Abstract**
Non-thermal plasma has recently emerged as a promising technology for the treatment of chronic wounds due to its antibacterial properties, promotion of tissue repair, and anti-inflammatory effects. Most devices are designed for small wounds, making the treatments of medium to large wounds time-consuming. This study aims to develop a non-thermal plasma device optimized for the medium to large wound treatment. By modifying the nozzle and electrode design, the plasma output shifts from point-like to line-like. A separate step-up transformer is fixed to the rotor and stator of the rotating platform, which transmits energy wirelessly to the nozzle during rotation, allowing a linear plasma to cover an area of approximately 19.6 cm² without the need for frequent repositioning. Safety assessment followed DIN SPEC 91315. At a working distance of 5-10 mm, the accumulated temperature of the plasma after two min was 38.1°C (e.g., depending on gas flow and voltage), remaining below 40°C, and the UV radiation was measured at 806.33 μJ/cm², well below the daily limit of 3000 μJ/cm². Biocompatibility was assessed using mouse fibroblasts (L929) according to ISO 10993-5. Plasma treatment (30–120 s) did not show obvious cell morphological changes, and proliferation assays showed statistically significant cell growth compared to the control group. Cell viability after 48 hr remained above 90% for all treatment durations exceeding the 70% criterion. The plasma device GPSR_M3 meets medical safety standards and shows strong potential in treating medium to large wounds, supporting further clinical trials.
Key words: Non-thermal plasma, medium to large wounds, safety assessment, proliferation, cell viability

## General

Cold atmospheric plasma (CAP) has significant advantages, such as the production of various reactive oxygen and nitrogen species, high efficacy, low side effects, portability, and cost-effectiveness, showing great potential in medical applications. These properties make CAP highly suitable for infection control, tissue repair, and other clinical treatments, offering new directions in medical technology. For example, in the management of diabetic foot ulcers, wound sizes and shapes vary, with multiple studies demonstrating that wounds larger than 25 cm² are not uncommon. [1,2] To achieve effective treatment for medium and large wounds, the plasma treatment area needs to be expanded. Therefore, the plasma source was modified from a point form to a linear form by changing the nozzle and electrode design to expand the processing range, as shown in Figure 1 (a) and can generate plasma covering an area of 19.6 cm², as shown in Figure 1 (b). [3,4] It is also tested and ensured that the generated plasma complies with relevant medical device regulations, i.e., DIN SPEC 91315 guidelines and ISO 10993-5 tests. Adherence to these standards ensure the safety, efficacy, and regulatory compliance of the device, thereby supporting its further clinical use.




(a) (b)

Figure 1. (a) The plasma generation device consists of a nozzle, a metal shell, a rotary transformer, stator and rotor. The secondary winding is connected to the inner electrode and the metal shell through two spring probes (connecter). Once the metal shell is connected to the outer electrode, a high-voltage electric field is formed between the two electrodes. (b) The plasma coverage area of GPSR_M3 is approximately 19.6 cm².

## References

[1] L. Wang et al., Influence of high-voltage electrode arrangement on downstream uniformity of jet array, IEEE Transactions on Plasma Science 47,1926-1932, 2019.
[2] X. Li et al., Generation of a large-scale uniform plasma plume through the interactions between a pair of atmospheric pressure argon plasma jets, Applied Physics Letters 117, 134102, 2020.
[3] W. Chen et al., Treatment of enterococcus faecalis bacteria by a He atmospheric cold plasma brush with $O_2$ addition, Journal of Applied Physics 112, 011304, 2012.
[4] C. Buske et al., Device for generating an atmospheric plasma beam, and method for treating the surface of a workpiece, Google Patents, 2020.

# Systematic experimental investigation of $N_2/H_2$ plasmas for $NH_3$ synthesis in a dielectric barrier discharge

A. Meindl[1], R. Antunes[1] and U. Fantz[1,2]

[1] *Max Planck Institute for Plasma Physics, Boltzmannstrasse 2, 85748 Garching b. München, Germany*
[2] *AG Experimentelle Plasmaphysik, University of Augsburg, Universitätsstrasse 1, 86135 Augsburg, Germany*

$N_2/H_2$ plasmas created in a dielectric barrier discharge for the purpose of $NH_3$ synthesis are investigated experimentally. The investigation includes systematic variations in pressure, $N_2/H_2$ concentration, flow rate, as well as discharge power. In view of plasma catalytic applications, the influence of introducing a packing material into the discharge in the pressure range between 13 and 920 mbar is investigated. The experiments have been performed both for a packed bed ($SiO_2$) configuration as well as without packing. The discharges are characterized with regard to their electrical properties, the ammonia yield of the process determined via mass spectrometry, and the rotational and vibrational temperatures of excited nitrogen molecules measured via optical emission spectroscopy.

## 1 Motivation

Plasma technology is considered one possible pathway towards the goal of electrifying the $NH_3$ synthesis process. Due to the challenges associated with $NH_3$ synthesis, e.g. breaking of the nitrogen triple bond, and avoiding of undesired $NH_3$ dissociation, non-equilibrium plasma discharges are predominantly investigated for this application. They can be operated with low overall gas temperatures and thus allow for the introduction of catalytic material into the plasma phase [1]. One such type of plasma source is the dielectric barrier discharge (DBD). Figure 1 shows a cylindrical DBD operated with $N_2/H_2$ plasma at different pressures with and without packing to produce $NH_3$.

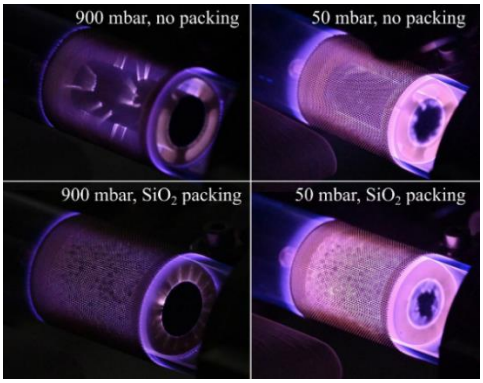



**Figure 1: $N_2/H_2$ plasmas in a DBD reactor.**

## 2 Experiment

The DBD is characterized via the electrical properties of the discharges, and emission spectra recorded with a high-resolution Echelle spectrometer with a resolution of $\Delta\lambda/\lambda = 45{,}000$ allow for the determination of rotational and vibrational temperatures of excited $N_2$ molecules, and can provide insights into the formation of NH*. The $NH_3$ yield is measured using a mass spectrometer. Systematic variations in pressure, flow rate, discharge power, and $N_2/H_2$ concentration are carried out both for a packed bed configuration ($SiO_2$ beads) as well as without packing. In particular the pressure variation is a novelty for the investigation of $NH_3$ synthesis in this type of reactor. As can be seen in Fig. 1, the introduction of the packing material as well as a decrease in operating pressure both influence the discharge in significant ways, for example leading to greater spatial uniformity, see also [2]. Figure 2 shows the $NH_3$ yields and the temperatures for varying $N_2$ concentrations. At high pressure, the introduction of packing leads to significantly reduced rotational temperatures, which could help avoid undesired $NH_3$ dissociation.

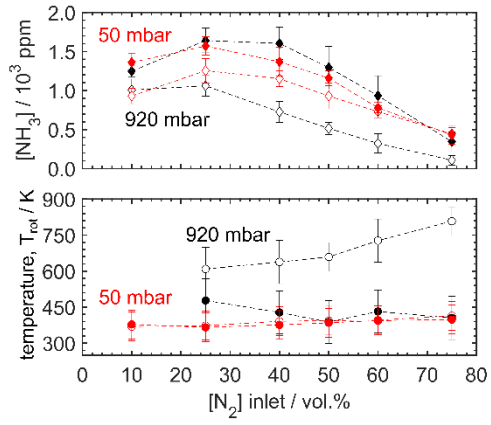



**Figure 2: $NH_3$ yields and temperatures for different $N_2/H_2$ concentrations. The filled symbols correspond to the packed bed configuration.**

### References

[1] Carreon, *J. Phys. D: Appl. Phys.* **52** 483001, 2019
[2] Patil et al., *J. Phys. D: Appl. Phys.* **53** 144003, 2020

# Fluid Dynamics and Surface Interactions of Helical Plasma Plumes in a Radiofrequency Atmospheric Pressure Plasma Jet

Radhika T. P.[1], Aishik Basu Mallick[1], Manish Kumar[2], Satyananda Kar[1]

[1] *Atmospheric Plasma Research Laboratory, Department of Energy Science and Engineering, Indian Institute of Technology Delhi, Hauz Khas, New Delhi 110016*
[2] *SeNSE, Indian Institute of Technology Delhi, Hauz Khas, New Delhi*

This study investigates the fluid dynamics of helically structured plasma plumes, demonstrating their superior turbulence causing enhanced air mixing compared to conventional conical plumes. High-speed Schlieren imaging reveals a shorter laminar region, a more dynamic turbulent front, and increased uniform surface interaction coverage in the helical geometry. These characteristics lead to improved reactive species generation, making helical plumes more effective for plasma-based surface treatments and biomedical applications.

## 1 Introduction

Atmospheric Pressure Plasma Jets (APPJs) serve as effective plasma chemical reactors, generating Reactive Oxygen and Nitrogen Species (RONS) for heat-sensitive applications [1, 2]. Compared to a conical plume, a helically structured plasma plume, controlled by pulse frequency and duty cycle, enhances plasma-chemical activity by improving air mixing within the ionized region, leading to greater RONS generation at lower temperatures [3]. This study examines fluid-dynamic instabilities, turbulence propagation, and the laminar-to-turbulent transition in helical plumes. By analyzing their surface interactions, the research provides insights into optimizing plasma treatments for heat-sensitive materials. The findings highlight the role of turbulence in enhancing reactive species transport and advancing plasma process design.

## 2. Experimental Setup

The plasma reactor consisted of a Pyrex glass tube with a pin-to-ring electrode configuration, where argon plasma was ignited using a 13.56 MHz radio-frequency power supply through a matching network. To establish a well-defined helical plume, the RF power was applied to the central electrode at a pulse frequency of 500 Hz with a 50% duty cycle, representing the minimum required conditions. High-speed Schlieren imaging was utilized to study the impact of mass flow rate (Q) and input power on the fluid dynamics of a helical plume as it moved through ambient air. Furthermore, in cases where the plasma jet interacted with a surface, the technique was applied to assess the propagation of the turbulent front across various substrate materials. Eight target conditions were tested, including grounded and floating metallic substrates, the same with a 4 mm dielectric layer, and a polystyrene Petri dish with a liquid sample, with and without a metal layer beneath.

## 3. Results and Discussion

The helical plume exhibits a more uniform distribution across the target surface, with a 20–26% increase in radius compared to the conical plume, resulting in enhanced surface interaction. Plasma ignition induces fluid-dynamic instabilities that propagate along the jet flow, influenced by the plume geometry. The helical plume also exhibits a shorter laminar region, resulting in a stronger and more dynamic turbulent front when directed onto a substrate. This increased turbulence promotes better air mixing, which enhances the formation of reactive species, improving plasma reactivity. When directed onto a substrate, a turbulent front emerges and spreads outward from the impingement point, with faster and more pronounced propagation in the helical geometry, further supporting its effectiveness in surface treatment. These findings highlight the helical plume's potential for optimizing plasma-based applications that require efficient reactive species generation and controlled surface interactions compared to the conical counterpart.

**References**

[1] Radhika T. P. & S. Kar, Effect of an additional floating electrode on radio frequency cross-field atmospheric pressure plasma jet. *Scientific Reports*, ***13***(1), 10665 (2023).
[2] Radhika T. P. & S. Kar. Glow-to-arc discharge transitions in a radio frequency atmospheric pressure plasma jet. *Physics of Fluids* **36**(8) (2024).
[3] Mahreen et. Al Excitation of helical shape argon atmospheric pressure plasma jet using RF pulse modulation. *Journal of Applied Physics*, ***130***(8), 083301 (2021).

# Diffuse Dielectric Barrier Discharge in air: role of Ozone?

J. Haton[1,2], R. Robert[2], A. Belinger[1], S. Dap[1], L. Stafford[2] and N. Naudé[1]

[1] *LAPLACE, Université de Toulouse, CNRS, INPT, UPS, Toulouse, France*
[2] *Université de Montréal, Montréal, Canada*

This contribution investigates how the production of ozone in a plane-to-plane dielectric barrier discharge operated in air affects the gas breakdown voltage. It is found that the gas breakdown voltage increases when the gas residence time increases and this seems correlated with the creation of ozone recorded by absorption spectroscopy.

## 1 Introduction

Diffuse dielectric barrier discharge (DBD) has been observed in air and studied since the last decade [1]. However, as it was observed with other gas, before to obtain the diffuse discharge, there is one to many filamentary discharges [2]. This transition from filamentary to diffuse discharge regime is due to many processes enabling the production of seed electrons. Gas breakdown voltage is a good indication of the seed electrons creation: the lower the gas breakdown voltage, the higher the source of seed electrons. Attachment on electronegative species such as ozone can consume seed electrons between successive discharges and can thus strongly modify discharge ignition. This work focuses on the study of the evolution of the gas breakdown voltage as a function of the amount of ozone created during the discharge.

## 2 Experimental details

The vessel and discharge configurations and electrical measurement details are provided in a previous publication [3]. In this study, the gas flow varies between a few sccm to 4 slm to change the ozone concentration. Electrical measurements are made using a segmented electrode, allowing spatially resolved electrical characteristics [4]. The ozone density is measured by absorption spectroscopy, using a deuterium lamp.

## 3 Results and Discussion

As shown in Figure 1, the gas breakdown voltage increases with the ozone density in the diffuse air discharge. It reveals that the ozone density has a "negative" impact on the memory effect and then on the seed electrons production. In air, the seed electron production is mainly due to surface processes and probably due to the desorption of electrons from the surface. Moreover in air, the principal electronegative specie produced during the discharge is ozone [5].

Then, the increase of the ozone density in the discharge could affect seed electron creation through attachment processes and decrease the memory effect.

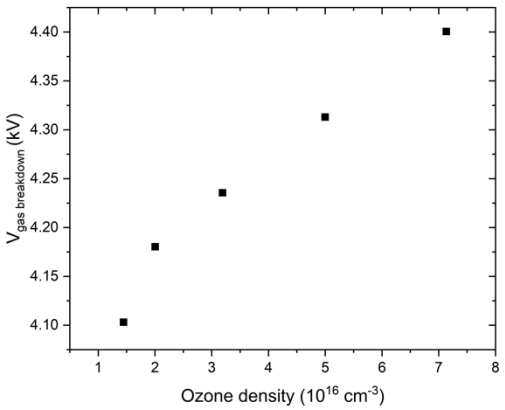



**Fig. 1**. Gas breakdown voltage versus ozone density in an Atmospheric Pressure Townsend Discharge (APTD) in air

It is thus easier to obtain an APTD in air when the ozone concentration is very low *i.e.* for the higher gas flow rate, when the gas composition is more efficiently renewed.

## Acknowledgement

This work was supported by Agence Nationale de la Recherche (ANR) in France (DECAIR project ANR-20-CE08-0014), and the National Science and Engineering Research Council (NSERC) in Canada.

## References

[1] N. Osawa and Y. Yoshioka, IEEE Trans. Plasma Sci. **40**, 2 (2012).
[2] F. Massines *et al.*, Eur. Phys. J. Appl. Phys. **47**, 22805 (2009).
[3] A. Belinger, S. Dap, and N. Naudé, J. Phys. D: Appl. Phys. **55**, 465201 (2022).
[4] C. Tyl *et al.*, J. Phys. D: Appl. Phys. **51**, 354001 (2018).
[5] A. M. Lietz and M. J. Kushner, J. Phys. D: Appl. Phys. **49**, 425204 (2016).

# Atmospheric re-entry plasma characterization

A. Brault[1], S. Jouen[2], D. Gibouin[2] and P. Boubert[1]

[1] *Université de Rouen Normandie, CNRS, CORIA UMR 6614, Saint-Etienne du Rouvray, France*
[2] *Université de Rouen Normandie, CNRS, GPM UMR 6634, Saint-Etienne du Rouvray, France*

Over the past 20 years, the amount of space debris orbiting the Earth has more than doubled, increasing the risk of collisions and making the study of atmospheric re-entry of space debris crucial. During atmospheric re-entry, debris undergoes intense heating, forming an air plasma that leads to oxidation, nitruration and ablation. For this study, the TA6V titanium alloy, commonly used in aerospace, was exposed to an inductively coupled plasma in the SOUPLIN set-up at the CORIA laboratory, allowing atmospheric re-entry conditions to be reproduced. Two plasma operating points were studied: (1400 Pa, 4.6 $MJ.kg^{-1}$) and (4500 Pa, 7.3 $MJ.kg^{-1}$), for oxidation times up to 120 s. Oxygen atomic densities of the order of $10^{22}$ $m^{-3}$ were measured in the boundary layer by the TALIF method. Surface analyses at the GPM laboratory revealed a predominance of $TiO_2$ rutile as well as the localized presence of $\alpha$-$Al_2O_3$ and $Al_2TiO_5$ at temperatures above 1150°C. TiN nitride was also detected in small proportions.

In 20 years, the number of space debris objects larger than 10 cm orbiting the Earth has more than doubled, from around 5,000 in 2004 to 12,000 in 2024 [1]. This rise in debris increases the risk of collision, potentially generating even more debris and threatening current and future space missions. In 2008, France became the first country to adopt a legal framework covering the entire life cycle of space objects, with the LOS law (Loi relatives aux Opérations Spatiales), including risk mitigation for atmospheric re-entry and debris production. In this context, the study of atmospheric re-entry of space debris is crucial.

During atmospheric re-entry, debris enters the dense layers of the atmosphere from an altitude of around 120 km at a speed of around 7 $km.s^{-1}$. The kinetic energy of the debris is converted into internal energy, leading to the formation of an air plasma that drives its oxidation, nitruration and ablation. A boundary layer forms at the wall, where the plasma is in thermodynamic non-equilibrium, making it difficult to characterize by calculation.

To study these plasmas, the CORIA laboratory operates the SOUPLIN (SOUfflerie à PLasma INductif) set-up, a wind tunnel equipped with an inductively coupled plasma torch capable of reproducing atmospheric re-entry conditions [2]. The Two-photon Absorption Laser Induced Fluorescence (TALIF) [3] is used to determine two key plasma parameters influencing oxidation: atomic oxygen density and translation temperature. This laser diagnostic technique allows for the characterization of the boundary layer in thermodynamic non-equilibrium during oxidation of a sample. Thus, by combining TALIF measurements and oxide layer analyses carried out at the GPM laboratory, plasma and material can be characterized, providing a complete understanding of plasma-material interaction.

For this study, TA6V titanium alloy, commonly used in aerospace, was exposed to an inductively coupled plasma in the SOUPLIN set-up. Two plasma operating points were studied: (1400 Pa, 4.6 $MJ.kg^{-1}$) and (4500 Pa, 7.3 $MJ.kg^{-1}$), for oxidation times up to 120 s. Using the TALIF method to probe the boundary layer, atomic oxygen densities of the order of $10^{22}$ $m^{-3}$ were measured. Surface analyses (XRD, Raman spectroscopy and SEM-EDS) revealed a predominance of $TiO_2$ rutile throughout the oxide layer, as well as the localized presence of $\alpha$-$Al_2O_3$ and $Al_2TiO_5$ at temperatures above 1150°C. TiN nitride was also detected in small proportions. These results highlighted that for similar oxidation times, a higher atomic oxygen density implied a more severe oxidation and the more rapid appearance of oxides.

**References**

[1] Liou, J-C and al. Orbital Debris and the NASA Orbital Debris Program Office. In *Trilateral Safety & Mission Assurance Conference (TRISMAC 2024)*.
[2] Brémare, N., Jouen, S., and Boubert, P. Non-equilibrium radiation during SiC–$CO_2$ plasma interaction. *Journal of Physics D: Applied Physics*, *49*(16), 165201 (2016).
[3] Niemi, K., Schulz-Von Der Gathen, V., & Döbele, H. F. Absolute atomic oxygen density measurements by two-photon absorption laser-induced fluorescence spectroscopy in an RF-excited atmospheric pressure plasma jet. *Plasma Sources Science and Technology*, *14*(2), 375 (2005).

# Experimental comparison of detached vibrationally-resolved $D_2$ SOLPS-ITER simulations on MAST-Upgrade

J. Bryant[1], K. McKay[1], J.R. Harrison[2], D. Moulton[2], K. Verhaegh[3],
R. Bergmayr[4], U. Fantz[4], D. Wünderlich[4]
MAST Upgrade Team[2], and EUROfusion Tokamak Exploitation Team[5]

[1] *Department of Electrical Engineering and Electronics, University of Liverpool, Liverpool L69 3GJ, UK*
[2] *UKAEA, Culham Campus, Abingdon OX14 3DB, UK*
[3] *Eindhoven University of Technology, 5612 AZ Eindhoven, Netherlands*
[4] *Max Planck Institute for Plasma Physics, 85748 Garching bei München, Germany*
[5] *EUROfusion, 85748 Garching bei München, Germany*

Plasma-molecular interactions such as MAR and MAD, have been experimentally determined to provide critical ion power, particle and momentum sinks, resulting in an earlier onset of detachment on extended divertor legs. These sinks are strongest in divertors with low $n_e$ and $T_e$ in addition to high neutral baffling. Triggering these reactions may be essential in preventing damage to plasma-facing components in reactor-relevant devices. Current SOLPS-ITER simulations do not replicate the levels of plasma-molecular interactions MAST Upgrade. The source of these discrepancies originates from the effective molecular rate coefficients used in SOLPS-ITER. X1EXT is a molecular rate database constructed using the Yacora-$H_2(X^1, v)$ model and provides better agreement with experiment. Vibrationally-resolving these simulations provides realistic transport of $D_2(v)$ into colder regions which triggers detachment onset earlier through increased MAR, MAD, EIR and EID.

## 1 General

MAST Upgrade experimental comparison studies with SOLPS-ITER show discrepancies in MAR and MAD [1, 2]. These inaccuracies originate from the AMJUEL molecular charge exchange effective rate coefficient. Below 2 $eV$ these lead to an underprediction of $D_2^+$ in detached regimes [2]. Note that these rates are mass-rescaled from $H_2$ to $D_2$. The X1EXT molecular rate database was constructed using Yacora-$H_2(X^1, v)$ model [3, 4]. X1EXT was applied to an isolated divertor leg geometry in SOLPS-ITER with MAST Upgrade L-mode Super-X conditions. Below $T_e = 1\ eV$, X1EXT increases the levels of $D_2^+$, resulting in increased ion particle sinks (via MAR and EIR), larger neutral buffer (via MAR, MAD, and EIR), and stronger power losses due to the formation of excited $D$ (via MAR, MAD, and EIR). The trends in stronger ion target flux roll-over, and larger power dissipation during detachment are qualitatively in better agreement with trends on MAST-U [1, 2].

Applying the X1EXT effective rate coefficients to L-mode Super-X MAST-U simulations and comparing against the reference simulations and experimental analysis from Moulton (2024) we see better agreement in MAR, MAD and EIR resulting in an earlier onset of detachment [1]. Employing effective rate coefficients results in the assumption that the lifetimes of all vibrational levels are assumed to be extremely small. However, in deep detachment the mean free path of $D_2(v)$ exceeds the divertor length. Using vibrationally-resolved SOLPS-ITER simulations, we see an increased transport of vibrationally excited $D_2(v)$ from hotter regions into detached regions. This enhances electron quenching so that the levels of MAR, MAR, EIR, and EID are elevated resulting in further power dissipation and ion target flux rollover than in the effective rate simulations, providing greater agreement with experiment.

## References

[1] Moulton, D. Super-X and conventional divertor configurations in MAST-U ohmic L-mode; a comparison facilitated by interpretative modelling. *Nuclear Fusion*, **64(076049)**, (2024).

[2] Verhaegh, K. Spectroscopic investigations of detachment on the MAST Upgrade Super-X divertor. *Nuclear Fusion*, **63(016014)**, (2023).

[3] Bryant, J. Impact of Yacora evaluated molecular effective rate coefficients on detached SOLPS-ITER simulations. *Nuclear Fusion*, **65(036025)**, (2025).

[4] Wünderlich, D. Yacora on the Web: Online collisional radiative models for plasmas containing H, H2 or He. *Journal of Quantitative Spectroscopy and Radiative Transfer*, **240(106695)**, (2020).

# First measurements of the WEST Thomson scattering system

L. Schiesko, M. Carole, G. Colledani, Y. Moudden, C. Bouchand, R. Sabot, G. Moureau, S. Vives, A. Bec, L. Doceul, F. Faïsse, N. Fedorczak and the WEST team*

*CEA, IRFM, F-13108 Saint-Paul-Lez-Durance, France*
*∗see http://west.cea.fr/WESTteam*

The WEST Thomson scattering system consists in 20 line-of-sight (LoS) for the core plasma and 30 LoS for the edge. These LoS are meant to achieve a complete overview of the density and temperature of the plasma including a spacial resolution in the SOL to resolve the pedestal and improve the understanding of plasma the transport to the wall. The firsts results presented here have been obtained with ohmic, LH-heated (Lower-Hybrid) and XPR plasmas (X-Point Radiator).

The WEST Thomson scattering system [1, 2] is a critical diagnostic tool that enables the measurement of electron temperature ($T_e$) and density ($n_e$) from the plasma core to the edge in the upper part of the tokamak, where no other diagnostics are available to resolve these parameters. An Nd:YAG laser, with a wavelength of 1064 nm, a repetition rate of 30 Hz, a pulse duration of 10 ns, and an energy of 2 J per pulse, traverses the plasma vertically. Photons scattered by the electrons are collected by 50 optical fibers housed within two endoscopes. The core endoscope consists of 20 lines of sight (LoS) with a spatial resolution of 24.2 mm, while the edge endoscope contains 30 LoS with a finer spatial resolution of 6 mm to resolve the pedestal region. The first mirror of the edge endoscope, located inside the vessel, is actively cooled, and the in-vessel optics are safeguarded by a thermal shield. The acquisition system relies on Nectarines boards [2], which provide six triggered fast channels to capture the scattered pulse shape at sampling rates of 1 to 3.2 GS/s. This is achieved using three Nectar chips, ensuring precise sampling of the Thomson signal and minimizing errors. Additionally, six slower ADC channels monitor the background signal.

The electron temperature is determined using a synthetic diagnostic [3] that accurately replicates the entire Thomson scattering setup, including photon propagation along the laser path, losses at the mirrors, Thomson scattering by electrons, and the precise positioning of the optical fibers. This synthetic diagnostic generates lookup tables (abaci) that are compared with measurements, leveraging the spectral calibration curves of each polychromator that have been designed and procured by UKEA [4]. The electron density is derived through an absolute $N_2$ calibration based on Raman anti-Stokes scattering. One compute to this aim the Raman anti-Stockes wavelength shift, the associated cross-section pondered by the transmission function of each pomlychromator's channel. This enables the evaluation of $n_e$. Figure 1 illustrates the temporal evolution of $T_e$ and $n_e$ measured for shot 61603 at z = 251.4 mm, with 4 MW of lower hybrid (LH) power injected. The data demonstrate that the system achieves excellent temporal resolution for both $T_e$ and $n_e$, in particular it is straightforward to see the temperature increase during the LH ramping-up. It will be shown that the results obtained with ohmic discharges and during XPR are consistent with other diagnostics.

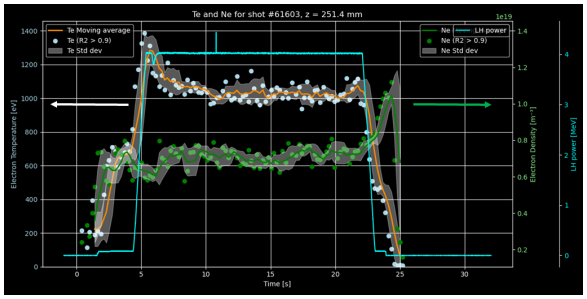



Figure 1: Variation over time of the electron temperature and density for the shot 61603 measured at z = 251.4 mm and 4 MW injected LH power.

## References

[1] Colledani G. et al, LAPD20 - 20th International Symposium on Laser-Aided Plasma Diagnostics (2023).

[2] Bouchand C. et al, IEEE Trans. Nucl. Sci., **8**, 575 (2025).

[3] Carole M., Bouchand Ch., et al. Journal of Instrumentation, Accepted.

[4] Carole M. *Development of a Thomson High Resolution Diffusion Diagnostic for Real-Time Monitoring of Particle Extraction and Power from Edge Kinetic Profiles*, PhD Thesis, https://theses.fr/s378053 (2025).

# LIBS for fusion: tungsten and boron spectral characterization

L. Gosse[1], A. Bultel[1], V. Morel[1] and A. Favre[1]

[1] *CORIA UMR 6614, Université de Rouen - Normandie, 76801 Saint-Etienne du Rouvray, France*

This communication explores the use of CF-LIBS for analyzing the inner walls of ITER. We characterize the emission spectra of boron and tungsten and highlight the acquisition conditions that enable the observation of a plasma in local thermodynamic equilibrium (LTE).

This study is set within the context of fusion by magnetic confinement and the analysis of tokamak inner walls using laser-induced breakdown spectroscopy (LIBS). During operation, tokamak reactors, such as ITER, subject their walls to stresses that lead to erosion, material displacement, and full retention. For safety reasons, regular analysis of the system walls is required.

Laser-induced breakdown spectroscopy is an analytical method based on the measurement of the radiation emitted by a plasma formed by the interaction between a laser pulse and the sample to be analysed. Traditionally, concentration measurements by LIBS are performed using calibrated reference samples. However, this approach has its limitations: in the presence of matrix effects, the concentration measurements of trace elements or minor components in the sample can be skewed. Moreover, in certain cases—such as the analysis of the internal walls of tokamak reactors—the use of reference samples is simply not feasible [1]. The in-situ diagnostics of ITER's internal walls will therefore be carried out using CF-LIBS (Calibration-Free LIBS), a quantification method based on characterizing the laser-induced plasma through its emission spectrum without the need for reference samples [2].

The application of this method requires prior knowledge of the emission spectrum associated with the constituent elements of the tokamak reactor walls, namely primarily tungsten (W) and boron (B). The difficulties in interpreting the tungsten spectrum stem from the very large number of transitions associated with this species. For boron, the challenge is linked to the lack of detailed spectroscopic studies on this element. This method also requires that the medium be in local thermodynamic equilibrium (LTE), so that the elemental composition of the emitting medium can be determined—either through the construction of Saha-Boltzmann diagrams or by calculating the emission spectrum using a radiative transfer code [3] [4].

In this communication, the preliminary results associated with measurements on tungsten carbide (WC) and boron carbide ($B_4C$) samples, performed under standard experimental conditions in a helium atmosphere at different pressure levels (10 Pa, 100 Pa, $10^5$ Pa) is presented. An Nd:YAG ns laser source was used, with a repetition rate of 10 Hz and a pulse duration of 4 ns. The energy delivered per pulse is $E_L = (106 \pm 0.5)$ mJ, with an average irradiance on the sample of $\varphi_L \sim 10^{15}$ W m$^{-2}$. The spectra were acquired between 200 nm and 800 nm using an Echelle broadband spectrometer. The first objective is to characterize the emission spectra associated with tungsten and boron. The second objective is to identify the acquisition conditions necessary to observe a laser-induced plasma in local thermodynamic equilibrium (LTE) for CF-LIBS measurements, by comparing the experimental calibrated emission spectra with those resulting from the implementation of the MERLIN code based on the resolution of the radiative transfer equation [4].

## References

[1] Hahn, D. *et al. Appl. Spectrosc.*, **64**, 335-366 (2010).
[2] Philipps, V. *et al. Nucl. Fusion*, **53**, 093002 (2013).
[3] Ciucci, A. *et al. Appl. Spectrosc.*, **53**, 960-964 (1999).
[4] Favre, A. *et al. J. Quant. Spectrosc. Radiat. Transf.*, **330**, 109222 (2025).

# Fiber PROES: High-Speed, Low-Cost Plasma Monitoring

F. Beckfeld[1], M. Ryppa[1], C. Neuroth[1], I. Korolov[1], J. Schulze[1]

[1] *Chair of Applied Electrodynamics and Plasma Technology, Ruhr University Bochum, Universitätsstr. 150, 44801 Bochum, Germany*

High-frequency low-temperature plasmas are crucial for industrial applications like semiconductor manufacturing and gas conversion, but their complex behavior is often not well understood. Phase Resolved Optical Emission Spectroscopy (PROES) is a key diagnostic tool for studying plasma dynamics, yet traditional setups using ICCD cameras are costly, slow, and impractical for commercial reactors. To address these limitations, we introduce Fiber PROES, which uses an optical fiber and a photon-counting photo-multiplier tube (PMT). This approach significantly reduces costs, increases measurement speed, and requires only a small access port while providing comparable results to classical PROES.

Plasma diagnostics, such as Phase-Resolved Optical Emission Spectroscopy (PROES), provide critical insights into electron dynamics but face limitations in industrial applications due to high costs and accessibility constraints. To overcome these challenges, we introduce Fiber PROES [1], a cost-effective and compact alternative that utilizes an optical fiber and a photomultiplier tube (PMT), enabling fast, non-intrusive plasma monitoring with results comparable to conventional ICCD-based PROES [2]. This advancement enhances the viability of PROES for industrial plasma process control, particularly in semiconductor manufacturing, where precise plasma monitoring is increasingly essential.

To demonstrate the capability of the new method, experiments using both diagnostic methods were performed in a geometrically symmetric, capacitively coupled low-pressure plasma (CCP). The CCP reactor consists of two plane-parallel electrodes with a diameter of 120 mm, and the interelectrode gap is set to 40 mm.

For the ‘classical’ PROES, an ICCD camera equipped with a telecentric lens and an interference filter is synchronized with the RF generator using a camera gate width of 1 ns. The emission at a specific wavelength is then recorded for different phases of the RF period.

In the Fiber PROES method, a photomultiplier operated in a photon-counting mode is used instead of the camera. Light is collected via an optical fiber, with an interference filter installed between the fiber and the PMT. By simultaneously recording the voltage waveform and the signal from the PMT, each arriving photon can be assigned to a specific phase of the RF period. To obtain spatially resolved data and cover the entire gap, the fiber, together with the collecting optics, is mounted on a movable stage.

The results of the measurements using both diagnostics in an Ar/Ne mixture are shown in Fig. 1, demonstrating excellent agreement.

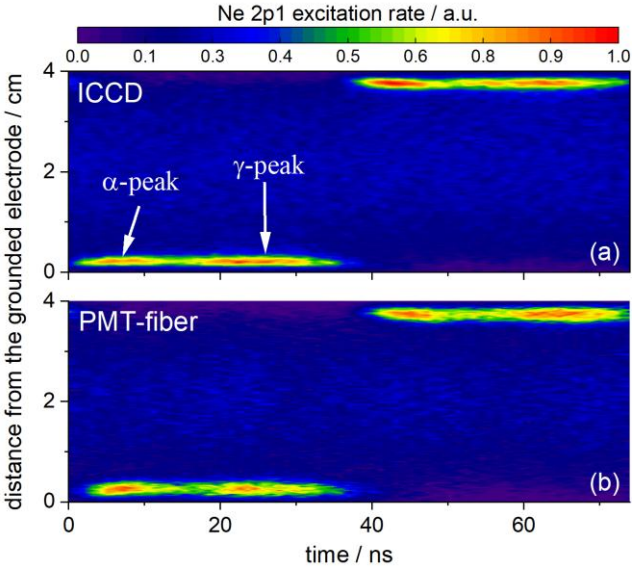



Fig.1 Spatio-temporally resolved electron-impact excitation rate from the ground state into the Ne 2p1 level measured with (a) ICCD camera and (b) Fiber PROES. $U_{pp}$ = 400 V, $p$ = 200 Pa, $f$ = 13.56MHz, Ar:Ne = 10:1 mixture.

Overall, Fiber PROES enables efficient monitoring of process drifts and mode transitions, offering significant advantages over ICCD-based PROES, including lower cost, compact integration, and faster measurement times. This technique has strong potential for plasma process development and control, particularly in semiconductor applications, where it provides direct insights into electron dynamics in molecular gas discharges.

*This work was supported by the German Research Foundation in the frame of project T09 of the CRC TR-87 (Grant No. 138690629).*

**References**

[1] F. Beckfeld et al., *Rev. Sci. Instrum.* **96**, 033507 (2025); patent application PCT/EP2023/085902
[2] T. Gans et al., *Phys. Rev. A* **67**, 012707 (2003); B. Horvath et al., *Plasma Sources Sci. Technol.* **29** 055002 (2020)

# Comparison of PMT and iCCD detectors for resolving low SNR TALIF signals in hydrogen plasmas

J. Hörsch, C. Wimmer, A. Meindl and U. Fantz

*Max Planck Institute for Plasma Physics, Boltzmannstraße 2, 85748 Garching, Germany*

Two-photon absorption laser induced fluorescence (TALIF) can be used for measurements of the density and the energy distribution function (EDF) of ground state hydrogen atoms in hydrogen plasmas. For EDF measurements the line profile needs to be measured precisely and especially in the wings of the distribution with a sufficient signal to noise ratio (SNR). As strong H alpha radiation is emitted by the plasma, weak fluorescence signals in the wings of the distribution are difficult to measure. In order to optimize the SNR of the TALIF signal, the performance of detecting the signal with a photomultiplier tube (PMT) in comparison with an intensified CCD (iCCD) camera is investigated.

## 1 Motivation

For measuring the density and the EDF of ground state hydrogen atoms in a hydrogen plasma, optical emission spectroscopy (OES) combined with collisional radiative (CR) modeling and TALIF are possible diagnostics. As OES observes the emission of excited states only, the EDF determined from OES line profiles resembles the excited state energy distribution. In case of a recombining plasma a significant amount of the excited atoms are produced via ion recombination and can have a different EDF [1]. For a recombining plasma also the density values calculated from OES data with the CR models are subject to large uncertainties and therefore TALIF as a direct diagnostic can help to overcome these issues.

In negative hydrogen ion sources the EDF of hydrogen is of particular relevance as this is the precursor species for conversion of negative ions at a caesiated surface. The respective plasma parameters ($n_e \approx 10^{17}\,m^{-3}$, $T_e \approx 2\,eV$) imply a strong H alpha background compared to the TALIF fluorescence signal, which negatively affects measurements in the wings of the EDF. However, from OES and simulations there are hints for the presence of a two temperature distribution of the atoms which would be visible in the wings of the EDF. With our TALIF setup it was not yet possible to resolve the wings with a sufficient accuracy [2] and therefore optimizations of the SNR are required.

## 2 Experiment

To optimize the SNR, the performance of detectors used for the TALIF measurement is investigated. The two different types of detectors commonly used for TALIF are PMTs and iCCD cameras. PMTs usually allow for a better time resolution than iCCDs, but do not yield any spatial information about the fluorescent cord. The spatial distinction between H alpha background and the fluorescence cord can be done by post processing the spatially resolved iCCD image, but needs to be done optically with an imaging system or a slit mask for PMT measurements beforehand. To determine the performance of both approaches in terms of the SNR, both detector setups are compared at the same experiment.

In addition to the investigations on detector performance, OES measurements are carried out with high resolution spectroscopy to resolve the EDF of the excited states of hydrogen and compare them with TALIF measurements of the ground state EDF.

## References

[1] Briefi, S. et al. Spectroscopic investigations of the ion source at BATMAN upgrade. *AIP Conference Proceedings*, **2052**, 040005, (2018).

[2] Merk, F. Implementation of TALIF on negative ion sources for the determination of the properties of atomic hydrogen. *PhD Thesis Augsburg University*, (2023).

# On the gas temperature variations in a DC Ar/$N_2$ MHCD

D. Stefas[1], G. Makrypodi[2], B. Menacer[1], P. Svarnas[2], G. Lombardi[1], C. Lazzaroni[1] and K. Gazeli[1]

[1] *LSPM & Univ. Sorbonne Paris Nord, CNRS, UPR3407, Villetaneuse, France*
[2] *High Voltage Lab., Electrical & Computer Eng. Dept., University of Patras, Rion, Greece*

Microhollow cathode discharges (MHCD) allow for the dissociation of $N_2$ and can be useful for nitride deposition on large surfaces under relatively low gas temperatures ($T_{Gas}$<1000 K). This work deals with the estimation of $T_{Gas}$ in a DC Ar/$N_2$ MHCD. This is done by fitting experimental rotational spectra of NO(A–X), OH(A–X) and $N_2$(C–B) with corresponding synthetic spectra. $T_{Gas}$ is inferred from the comparison of their different rotational temperatures ($T_{Rot}$) in the MHCD hole and the low-pressure chamber (few mbar), which is used for deposition. The impact of the MHCD pressure, electric current, and gas mixture on the $T_{Rot}$, as well as the role of different mechanisms on the excitation of probe species used for $T_{Rot}$ are studied. $T_{Rot}$ varies from 600 K to 1200 K depending on the discharge conditions, showing non-equilibrium between the molecules studied. These insights in the temperature variation are useful for MHCD optimization in frame of material synthesis and deposition.

Microhollow Cathode Discharges (MHCDs) are defined by a hole of few 100s μm diameter embedded within a flat electrode–dielectric–electrode assembly. They consume low electric power while generating large power densities (~kW/cm$^3$) as well as electron densities ($\geq 10^{14}$ cm$^{-3}$). Besides, they are out of thermal equilibrium which is highly attractive for various applications such as synthesis of hexagonal boron nitride (h-BN) [1]. Specifically for h-BN, they allow an efficient dissociation of $N_2$ and N-atoms generation by tuning different plasma parameters [2].

MHCDs can be configured to better control $N_2$ dissociation, as follows [2]:

- Generation of plasma in the MHCD hole only, spreading over the cathodic surface; here, reactive species such as N-atoms are created in the hole and simply diffuse in the low-pressure chamber.
- Formation of a plasma jet that expands into the low-pressure chamber, enhancing the transport of N-atoms onto a substrate used for h-BN deposition.
- Formation of a voluminous plasma in the low-pressure chamber by biasing the substrate holder with a positive DC voltage. This further affects plasma reactivity by generating a conductive channel between the MHCD anode and the holder.

A key advantage which defines energy efficiency for h-BN deposition, is MHCDs' ability to operate under relatively low $T_{Gas}$ (typically <1000 K [1]). However, $T_{Gas}$ is affected by MHCD operating conditions, and its precise determination is challenging. Thus, knowing the $T_{Gas}$ range in different MHCD configurations is pivotal to better understand $N_2$ dissociation efficiency.

In this work, $T_{Gas}$ is estimated in a DC Ar/$N_2$ MHCD operated in the three above-mentioned configurations. Optical emission spectroscopy (OES) is used to record high resolution rotational spectra of NO(A–X), OH(A–X) and $N_2$(C–B) (Fig.1). $T_{Gas}$ is estimated through their $T_{Rot}$, which are obtained by fitting their emissions with synthetic spectra. These, however, only consider a single temperature to perform the fitting, which is not always valid. Therefore, the Boltzmann plot method is also applied when possible, revealing dissimilar $T_{Rot}$ due to different excitation mechanisms of a probe species, and enabling a more accurate $T_{Gas}$ estimation. The influence of MHCD operating conditions (pressure, current, gas composition and substrate bias) on $T_{Rot}$ is shown, with an overall range between 600 and 1200 K. Possible mechanisms involved in the excitation of a probe species (e.g, energy transfer from argon metastables to $N_2$ creating $N_2$(C) (Fig.1)) are also discussed.

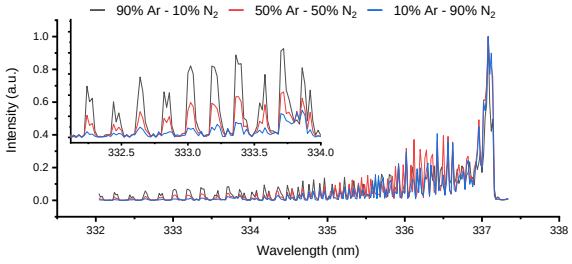



Fig. 1: Impact of Ar addition in the Ar/$N_2$ mixture on the rotational spectrum of $N_2$(C–B).

**Acknowledgements**
ANR SPECTRON (ANR-23-CE51-0004-01), Labex SEAM (ANR-10-LABX-0096; ANR-18-IDEX-0001)

**References**

[1] H. Kabbara et al., Appl. Phys. Lett. 116, 171902 (2020).
[2] A. Remigy et al., J. Phys. D 55, 105202 (2022).

# The Applicability of a Microwave Resonant Probe to the Plasma Processing of Silicon Oxide

D. White[1], G. Hassall[1] and J. Ellis[1]

[1] *Oxford Instruments Plasma Technology, Severn Beach, BS35 4GG, UK*

Plasma diagnostics are often incompatible with industrial applications due to a variety of reasons; however, microwave resonant probes are a promising example of a sensor that does not interfere with the plasma process. In this work, a curling probe was developed and investigated within a commercially relevant ICP etching reactor during a $SiO_2$ blanket etch process. It was demonstrated that the curling probe had no impact on wafer outcomes and had the sensitivity required to detect changes in the plasma processing conditions.

In-situ diagnostics for industrial scale plasma processing represents a sizeable challenge for multiple semiconductor hardware companies. Simple, robust, and inexpensive sensors are required both to understand process development challenges and for real-time monitoring of the plasma process; the advent of machine learning only enhances the importance of such sensor development.

A microwave enhanced resonance probe with a spiral-shaped slot design, also known as a curling probe[1-3], has been used to measure relative electron densities in the edge region of a Plasma Pro 100 Oxford Instruments Plasma Technology reactor as shown by Figure 1.

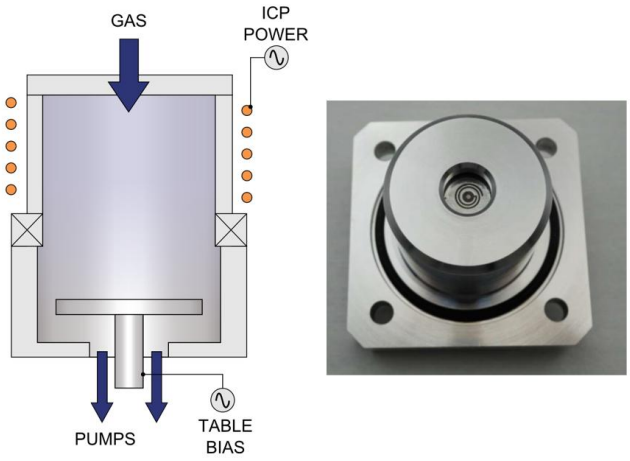



Figure 1: A schematic representation of the Plasma Pro 100 ICP reactor shown (left) alongside a picture of the curling probe that was used throughout the experimental campaign (right).

Etch tests were run across a broad range of plasmas processing parameters centred around a $CF_4/O_2$ plasma chemistry to ascertain the potential impact of the curling probe on the process. It was confirmed through both global and localised etch rate measurements that the curling probe was not observed to have any impact on the wafer outcomes. Figure 2 shows the comparison of the macroscopic etch rates both with and without the curling probe installed. The sensitivity of the curling probe enabled changes in the plasma conditions to be tracked in real time with failure modes clearly visible from the measured shift in the resonant frequency.

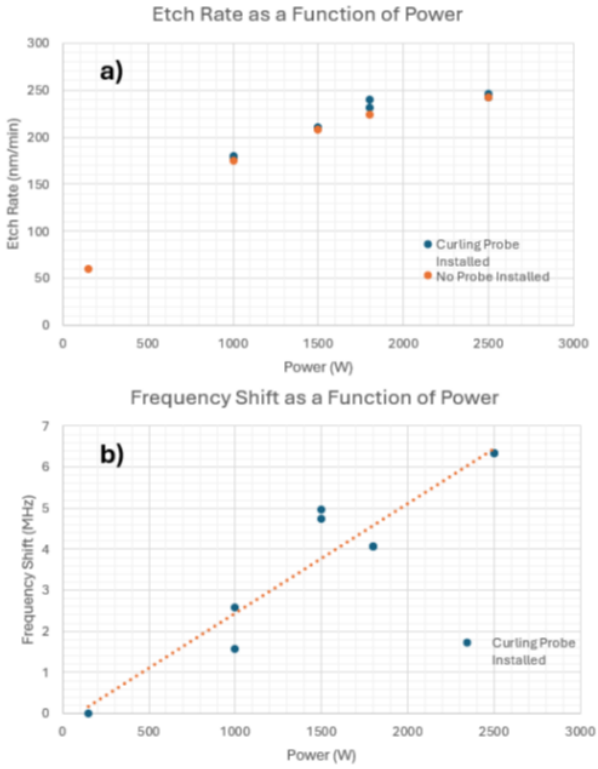



Figure 2: (a) The etch rate of $SiO_2$ is shown as a function of power with curling probe installed and without (b) The frequency shift measured by the curling probe as a function of power during the process.

## References

[1] R. L. Stenzel; *Rev. Sci. Instrum.*, ***47***, *603 (1976).*
[2] I. Liang, K. Nakamura, and H. Sugai, *Appl. Phys. Express*, **4**, 066101 (2011)
[3] F. Boni *et al.*, *Rev. Sci. Instrum.*, **92**, 033507 (2021)

# Development of a miniaturized hollow-core fiber plasma spectroscopy technique

Vlad-Ștefănuț Radu[1], Jean-Baptiste Billeau[1,2], Kasidapa Polprasarn[1], Benoit Debord[3], Ali Al Dhaybi[3], Denis V Seletskiy[4], Stephan Reuter[2], Frédéric Gérôme[3], David Z Pai[1], Fetah Benabid[3] and Svetlana Starikovskaia[1]

[1] *Laboratory of Plasma Physics (CNRS, Ecole Polytechnique, Univ. Paris-Sud, Observatoire de Paris, Sorbonne Université, l'Institut Polytechnique de Paris), Ecole Polytechnique, route de Saclay, 91128 Palaiseau, France*
[2] *PPSL Laboratory, Department of Engineering Physics, Polytechnique Montréal, Montréal, Québec H3T 1J4, Canada*
[3] *GPPMM Group, XLIM Research Institute, CNRS UMR 7252, University of Limoges, 87060 Limoges, France*
[4] *femtoQ Laboratory, Department of Engineering Physics, Polytechnique Montréal, Montréal, Québec H3T 1J4, Canada*

This work makes a proof of concept, illustrating the possibility to develop a hollow-core fiber spectroscopy technique for miniature probing of plasma-produced species. A hollow-core fiber with Kagomé lattice was integrated in a Raman spectroscopy setup, acting as a container for both light and gas molecules, thus increasing the interaction length and enhancing the Raman signal. The enhancement was proven by comparing the spectra of air with and without the hollow-core fiber.

## 1 Introduction

In plasma and combustion, robust techniques requiring minimum amounts of sample are of great interest. Hollow-core fibers (HCFs) have emerged as a transformative technology in gas-phase diagnostics, facilitating the fabrication of compact and efficient all-fiber gas cells, which provide strong gas-laser interactions [1]. The typical HCF core size is of the order of tens of microns, so this reduces significantly the amount of sample volume required, while simultaneously increasing the interaction length through light guiding. Applications of HCF-based detection techniques in combustion/plasma physics remain unexplored. This study aims to make a proof of concept, by building a working device for miniature probing of the species produced in the afterglow of an atmospheric pressure plasma jet.

## 2 Experimental method

The fiber used is a negative curvature HCF with a Kagomé lattice cladding, with a transmission window from 500 nm to 625 nm. The fiber was integrated in the Raman spectroscopy setup, which was a new version of the setup reported in [2, 3]. A 532 nm pulsed laser (30 kHz frequency, 2 ns FWHM) was coupled into the HCF using a dichroic mirror and a lens. The backscattered Raman light was collected, by blocking the Rayleigh scattered light with a notch filter and focusing the resulting beam onto the spectrometer slit with a lens. A ns pulsed atmospheric pressure helium plasma jet (5 kV amplitude, 3 ns FWHM, 715 Hz frequency, helium flow rate of 95 sccm) was used and the fiber probe end was placed in the afterglow of the plasma jet.

## 3 Results

Measurements were made inside and outside the jet. The Raman spectra of air in Figure 1 show the enhancement of the Raman lines for $O_2$ (1567 $cm^{-1}$) and $N_2$ (2341 $cm^{-1}$) when using the HCF. In the free-space configuration, the two peaks cannot be distinguished from the background. The HCF recorded spectrum has a higher background due to Raman scattering and fluorescence of the cladding silica.

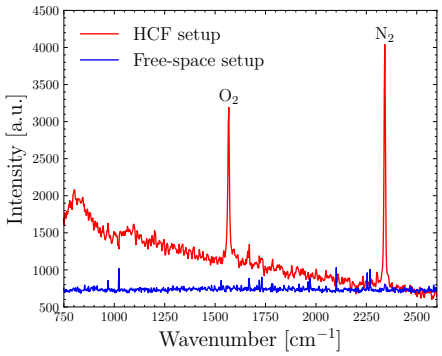



Figure 1: Raman spectra of air from the HCF setup (red) and the free space setup (blue)

## Acknowledgments

This work has been carried out at the Energy4Climate Interdisciplinary Center (E4C) of IP Paris and Ecole des Ponts ParisTech, which is in part supported by ANR-18-EUR-0006-02. The LPP authors would like to thank Prof. H. Zhao for sharing his knowledge about using HCFs as miniature probes. GPPMM thanks GLOphotonics for their collaboration in fiber fabrication.

## References

[1] Benabid, F. *et al.* Compact, stable and efficient all-fibre gas cells using hollow-core photonic crystal fibres. *Nature*, **434**, 488-491 (2005).
[2] Pai, D. Z. Plasma-liquid interfacial layer detected by in situ Raman light sheet microspectroscopy. *Journal of Physics D: Applied Physics*, **54**, 355201 (2021).
[3] Polprasarn, K. *et al.* XXXVI ICPIG, July 20-25, 2025, Aix-en-Provence, France.

# Measurement and simulation of time-resolved $N_2$(A,v) densities in a sub-microsecond pulsed near-atmospheric pressure discharge

Jan Kuhfeld and Koichi Sasaki

*Hokkaido University, Sapporo, Hokkaido, Japan*

Measurements of particle densities of the metastable $N_2$(A) in various vibrationally excited states are performed with ~10 ns time resolution by tuneable diode laser absorption spectroscopy (TDLAS). The dependence of the excited state densities on different discharge parameters, e.g., pressure, power, and flow rate are investigated, and the measurement results are compared to a reaction kinetic model of the discharge.

## 1 Discharge setup

To separate fast electron excitation processes from slower neutral particle kinetics, a pulsed sub-microsecond DC discharge is investigated in terms of particle densities of the metastable $N_2$(A) dependent on vibrational excitation. A homogeneous DC discharge is created between two plane, parallel metallic electrodes (1 mm x 20 mm surface) by applying high-voltage pulses of 200 ns duration [1].

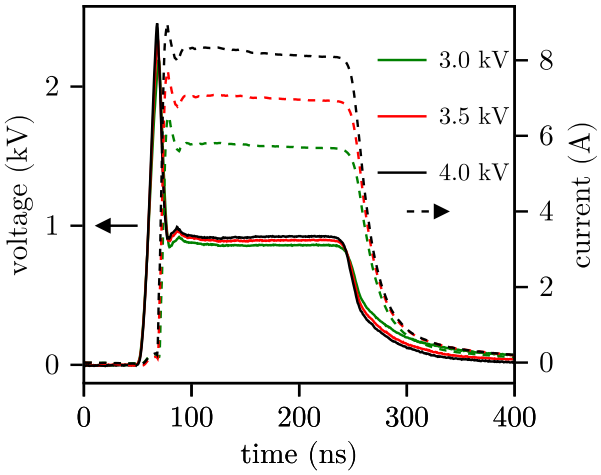



**Figure 1:** Exemplary wave forms of discharge voltage (solid) and current (dashed) for different input voltages, i.e., discharge powers.

## 2 Measurement method

The absolute number densities of the $N_2$(A,v=0,1,2,3,6,7,8) states are measured by time-resolved TDLAS [2]. An external cavity diode laser is scanned over wavelength ranges (~ 1 $cm^{-1}$) corresponding to transitions in the First Positive System of nitrogen on timescales of ~100 s. During this slow scan, for each discharge pulse the intensity of the laser is recorded by a fast oscilloscope with large buffer memory, synchronized with the applied high-voltage pulse with sampling rates in the order of ~10 ns (discharge phase) or ~100 ns (afterglow) (see Figure 2).

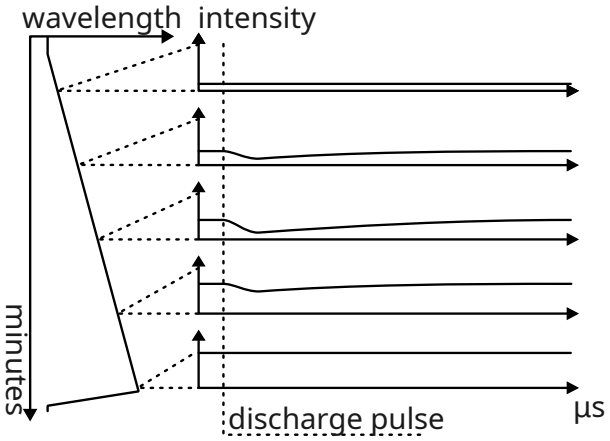



**Figure 2:** Measurement scheme (see text). From the intensity variations of the transmitted laser light on the discharge time scales (nanosecond to microsecond) together with the wavelength information (from a Fabry-Perot etalon) the time resolved absorption spectra are obtained.

## 3 Simulation method

A simple global discharge model was developed. The model incorporates the electrical characteristics of the discharge and a kinetic reaction model for nitrogen. The master equations (ordinary differential equations) for the various plasma species,

$$\frac{\partial n_\sigma}{\partial t} = \sum_\nu k_{\nu\sigma} n_\nu n_\sigma \ ,$$

are solved in conjunction with the algebraic equation connecting the (homogeneous) current density with the electric field and the charge carrier densities,

$$I/A = \sum q_i \mu_i (E/N) n_i E \ .$$

**References**

[1] Kuhfeld, J. et al. PIC/MCC simulation for a ns-pulsed glow discharge in nitrogen at sub-atmospheric pressure and analysis of its quasi-steady state physics. *Plasma Sources Sci. Technol.* **32**, 084001 (2023).

[2] Du, Y. Nanosecond resolved ro-vibrational CO2 excitation measurement. *J. Phys. D: Appl.Phys.* **54**, 34LT02 (2021).

# Cross-Validated Electron Diagnostics in Atmospheric-Pressure RF Plasmas

Jiwon Choi, Daehee Wi, and Sanghoo Park*
*Korea Adavanced Institute of Science and Technology (KAIST), Daejeon, Republic of Korea*

A multi-diagnostic strategy is introduced to ensure reliable electron temperature and density diagnostics in atmospheric RF plasmas. Continuum radiation analysis serves as the primary method, supported by cross-validation through Thomson scattering and CR modelling. The consistent results verify the diagnostic robustness under high-pressure conditions.

## 1 Introduction

Atmospheric-pressure plasma jets deliver high electron density and low electron temperature under ambient conditions without requiring vacuum systems. Despite these advantages, accurate electron diagnostics remain challenging because frequent collisions yield strong non-equilibrium conditions that make electron temperature ($T_e$) and density ($n_e$) diagnostics complicated. Here, we report a detailed comparison among promising electron diagnostics; optical methods based on continuum radiation (e-neutral bremsstrahlung), the collisional-radiative (CR) model, and laser Thomson scattering (LTS). We believe that this cross-validation approach provides robust diagnostics for identifying and mitigating experimental or theoretical biases, resulting in more consistent electron parameter measurements.

## 2 Experimental setup

We investigated 5 MHz argon plasma jets operating at atmospheric pressure (see Fig. 1) with power ranging from 20 to 60 W and an argon flow rate of 1–5 slm. Time-integrated optical emission from the plasma column was collected using a compact spectrometer (HR6, Ocean Insights) with a UV-enhanced detector, covering 170–800 nm in a single acquisition. For LTS, a frequency-doubled Nd:YAG laser (25 mJ, 100 Hz) was directed through the plasma column. Corrective optics and interference filtering suppressed Rayleigh scattering signal near 532 nm.

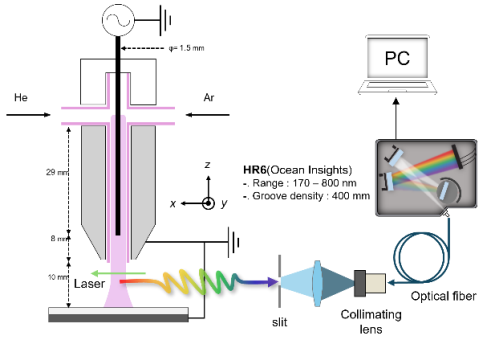



Figure 1. Schematic of the experimental setup.

## 3 Results

Electron temperature 0.9–1.4 eV and density (1.0–10.0) × $10^{12}$ $cm^{-3}$ measured by continuum radiation closely matched those from LTS and CR model. A two-dimensional spectral image centered near 532 nm was used to capture the Thomson signal; by integrating along the spatial axis, a 1D scattering profile was obtained and fitted assuming a Maxwellian distribution. At 40 W and 3 slm, we found $T_e$= 1.08 eV and $n_e$= 7.8×$10^{12}$ $cm^{-3}$ from LTS—consistent with continuum radiation and CR model results.

These results confirm the reliability of continuum radiation as a standalone diagnostic and underscore the advantages of cross-validating with Thomson scattering and CR modeling.

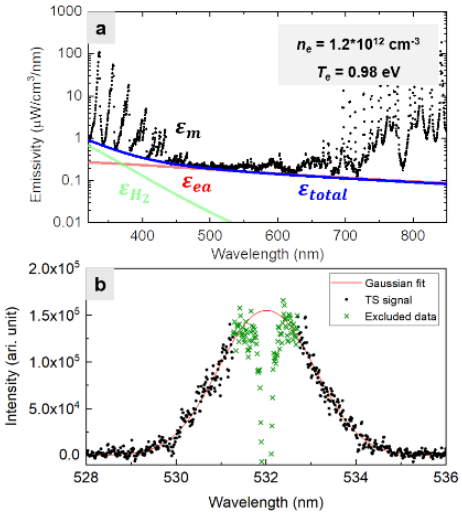



Figure 2. (a) Continuum radiation fitting results, yielding $T_e$= 0.98 eV and $n_e$= 1.2×$10^{12}$ $cm^{-3}$. (b) Measured LTS profile with a Gaussian fitting.

### References

[1] Park, S. et al. *Applied Physics Letter*. **104**, 084103 (2014).
[2] Park, S. and Yoon, S.-Y. *Plasma Sources Science and Technology*. **31**, 055011 (2022).
[3] Chai, K.-B. and Kwon, D.-H. *Journal of Quantitative Spectroscopy & Radiative Transfer*. **227**, 136-144 (2019).

# Comparison of Electrical Diagnostic Techniques for Capacitively Coupled Radio Frequency (CCRF) Plasma

Varsha S[1, 2], Prabhakar Srivastav[1], Yukti Goel[1] and Jinto Thomas[1,2]

*1Institute for Plasma Research, Gandhinagar, India*

*2 Homi Bhabha National Institute, Training School Complex, Anushaktinagar, Mumbai, 400094, India.*

Capacitively coupled radio-frequency (CCRF) plasma devices play a crucial role in the semiconductor industry, where precise control of plasma profiles, particle energy distribution, and transport dynamics is essential. This study utilizes Single and Double Langmuir probe diagnostics to investigate key plasma parameters and their spatial variations. The primary objective is to detect the presence of energetic electrons using the Single Langmuir probe and evaluate their impact on Double Langmuir probe measurements. Additionally, the study explores plasma behavior across different gas species to assess their influence on plasma characteristics. This comprehensive analysis enhances the understanding of RF plasma behavior and the effectiveness of various diagnostic techniques, contributing to the optimization of semiconductor manufacturing processes.

## Preface

Capacitively Coupled Radio-Frequency (CCRF) plasma has attracted significant research interest due to its wide range of applications and the scientific challenges it presents. It is widely used in etching, thin-film deposition, and microfabrication processes in the semiconductor industry [1]. The complex behavior of CCRF plasma, especially sheath dynamics, remains an active area of research. To better understand plasma parameters, researchers use various diagnostic techniques, with Langmuir probes being widely utilized due to their cost-effectiveness and ease of fabrication.

In this study, a CCRF plasma system powered by a 13.56 MHz RF power supply was carefully designed and built. Preliminary comparisons were made using both Single Langmuir Probe (SLP) and Double Langmuir Probe (DLP) diagnostics to analyze the plasma [2–4]. The SLP, being the simplest diagnostic tool, provides key information about plasma temperature, density, and the Electron Energy Distribution Function (EEDF), which helps identify the role of high-energy electrons. A specially designed RF-compensated SLP was used to minimize the interference of RF harmonics with the probe signal [5]. Additionally, DLP measurements were conducted, allowing for a comparison of plasma parameters such as electron temperature and density. This comparison provides deeper insights into the advantages and limitations of each diagnostic technique.

Furthermore, experiments were conducted using different gas types to study how plasma properties vary based on the gas used. This comprehensive approach enhances our understanding of CCRF plasma behavior and its dependence on operating conditions, contributing to advancements in plasma physics and its applications in the semiconductor industry.

### References

[1] Y. X. Liu, Q. Z. Zhang, K. Zhao, Y. R. Zhang, F. Gao, Y. H. Song, and Y. N. Wang, Fundamental study towards a better understanding of low pressure radio-frequency plasmas for industrial applications, *Chinese Phys.* B **31**, (2022).

[2] B. M. Annaratone, G. F. Counsell, H. Kawano, and J. E. Allen, On the use of double probes in RF discharges, Plasma Sources Sci. Technol. **1**, 232 (1992).

[3] I. D. Sudit and F. F. Chen, Rf compensated probes for high-density discharges, Plasma Sources Sci. Technol. **3**, 162 (1994).

[4] R. L. Merlino, Understanding Langmuir probe current-voltage characteristics, Am. J. Phys. **75**, 1078 (2007).

# Comparative Study on Microwave Diagnostics: Cutoff Probe, Hairpin Probe, and Microwave Interferometer

S. Kim[1], J. P. Booth[1] and G. Curley[1]

[1] *Laboratoire de Physique des Plasmas, École Polytechnique, 91128 Palaiseau, France*

We have compared three microwave diagnostic techniques for electron density measurement in a 13.56MHz ICP reactor in pure Ar: the cutoff probe, hairpin probe, and a microwave interferometer. The interferometer showed the highest density, followed by the hairpin and cutoff probes, indicating that the probe antenna surface acts as a loss channel for charged particles, leading to a reduction in electron density. Furthermore, we found that the perturbation is localized near the probe.

Microwave techniques are promising tools for electron density measurement of low-temperature plasmas and various microwave probes have been developed. In general, the microwave power used is too small to perturb the plasma since the power is much lower than the plasma generation power [1]. However, inserting probes into a plasma reduces the local electron density due to surface charged particle recombination [2]. However, an experimental comparative study between microwave probes has yet to be conducted. In this work, we compare three microwave diagnostics in an inductively coupled plasma (ICP) reactor in pure Ar: a microwave cutoff probe, a hairpin probe, and a microwave interferometer.

Measurements were conducted in the INCLINE 13.56 MHz ICP reactor, described in [3], operating in Argon gas at 5-100 mTorr. As shown in Fig. 1, the Fourier cutoff probe [4] and the floating hairpin probe are inserted into the cylindrical vacuum chamber (height 120 mm and an inner diameter 550 mm). The cutoff probe antenna, comprises two 9.5 mm long wires with a diameter of 0.52 mm, covered by glass tubes of external diameter 1.2 mm. The floating hairpin antenna, made of 0.1 mm diameter tungsten wire with a length of 30 mm, is directly exposed to the plasma, and is excited by a loop antenna enclosed by a glass tube. The hairpin probe is mounted on a linear drive, allowing the electron density profile to be measured from the centre to the wall. This is used to determine the relation between the central electron density and the line-integrated density. The commercial 26.5 GHz microwave interferometer measures the phase shift induced by the plasma and thereby measures the line-integrated electron density.

We observe that the microwave interferometer shows the highest value, followed by the hairpin probe, then the cutoff probe. As the microwave interferometer is a non-invasive method, this result indicates that the cutoff probe perturbs the plasma more than the hairpin probe. To determine whether the perturbation is localized or global, we measured the electron density using the cutoff probe while moving the hairpin probe inside the chamber. The measured electron density remains constant, showing that the probe perturbation is localized near the probe. Considering that the surface area of the quartz tubes covering the cutoff probe antenna is larger than that of the hairpin antenna, the perturbation is attributed to additional charged particle loss on the antenna side where the local electron density is measured.

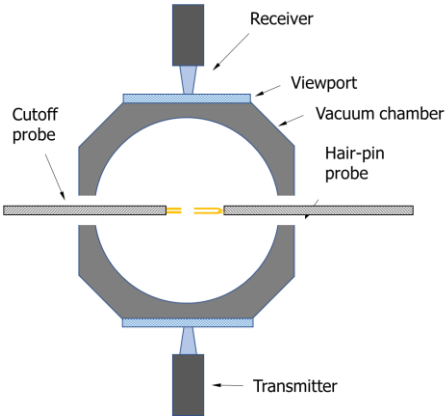



**Figure 1. A schematic of experimental setup.**

## References

[1] K. H. You et al., *Phys. Plasmas* **23**, 053515 (2016)
[2] B. H. Seo et al., *Phys. Plasmas* **24**, 123502 (2017).
[3] J. P. Booth et al., *J. Phys. D: Appl. Phys*. **45**, 195201 (2012).
[4] B. K. Na et al., *Rev. Sci. Instrum.* **83**, 013510 (2012)

# Nanosecond point-to-plane high-pressure discharge: PIC modelling and comparison with experiments

F. Taccogna, D. Aceto[1], P.F. Ambrico[1], F. Cichocki[2], P. Minelli and G. Dilecce[1,2]

[1] *Institute for Plasma Science and Technology – CNR via Amendola 122/D 70125 Bari - Italy*
[2] *Nuclear Department (NUC), ENEA, C.R. Frascati, via Fermi 45, 00044 Frascati, Italy*

Results of PICCOLO PIC code with spectroscopic and imaging measurements are compared for a point-to-plane nanosecond repetitively pulsed discharge in nitrogen, with the aim of setting-up a realistic code for the modelling of high-pressure plasma discharge.

## 1 General

In the frame of non-equilibrium discharge processing for $CO_2$ valorisation and nitrogen fixation, nanosecond repetitively pulsed (NRP) discharges have shown a promising set of performances. A modelling attempt must address microscopic time/space-resolved description of the physics and kinetics of the discharge. To this end, Particle-in-Cell (PIC) models seems to be the only option. The validation of the model must go as a first stage thorough experimental investigations in a well-defined geometry and diffused discharge condition.

## 2 Experimental device

The point-to-plane discharge is made of a tungsten needle and a SS plate with inter-electrode gap of 3 mm. The voltage and current plot at 100 Torr $N_2$ gas is shown in Fig. 1.

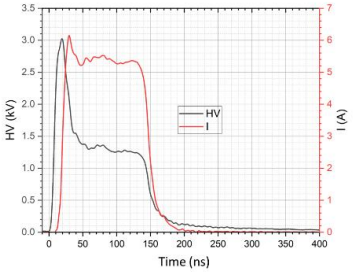



**Fig. 1** Applied voltage and current at 100 Torr.

## 2 Modelling

The modelling is achieved by the PICCOLO code, described in more detail in [2]. In Fig.2, an output of the Fig. 2, showing the axial-symmetric electron density at 20 ns after the pulse start.

## 3 Measurements

We have measured time resolved spectra of second positive system (SPS) and first negative system (FNS) with axial spatial resolution, to be compared with the outcomes of the model through a proper collisional-radiative (CR) model under development. Time resolved images have also been recorded, one of which is shown in the inset of Fig. 2, which is the spatial distribution of the FNS (0,0) band, which is representative of the excitation rate by electrons at energies above 18.7 eV. A direct comparison of these two pictures is not yet possible, since the model output must feed the CR model relevant to FNS excitation, but it shows the kind of work that will be presented.

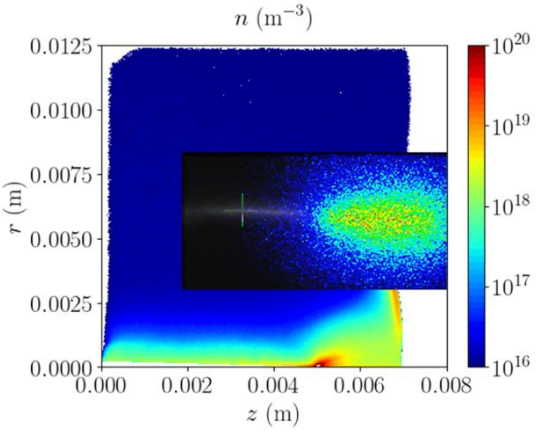



**Fig. 2** Electron density map in the 2D(r,z) axial-symmetric map of the needle-to-plane discharge, at 20 ns. The white region between 7 and 8 mm is the cathode fall, where the density is below $10^{16}$ $m^{-3}$. The inset picture is an image of the discharge acquired through an interference filter at 390 nm to select the (0,0) band of FNS emission system.

### 1.2 Acknowledgements

Work funded by the European Union under the National Recovery and Resilience Plan (NRRP) – NextGenerationEU, projects PRIN 2022 PLASMODD Prot. 2022J5NBBN and NEFERTARI – CUP B53C22003070006.

### References

[1] Montesano, C., Salden, T.P.W., Martini, L.M., Dilecce, G., Tosi, P., "$CO_2$ Reduction by Nanosecond-Plasma Discharges: Revealing the Dissociation's Time Scale and the Importance of Pulse Sequence" J. Phys. Chem. C, 127, 10045-10050 (2023).
[2] Taccogna, F., Minelli, P., Cichocki, F., "PICCOLO: a PIC code suite for low-temperature plasmas", this book of abstracts.

# Electrical characteristics of low-pressure radio frequency capacitively coupled discharges used for plasma polymer deposition

K. Polášková[1], N. Bolouki[1],T. Kristek[2], Š. Špánik[2], P. Drexler[2], L. Janů[1] and L. Zajíčková[1,3]

[1] *Plasma Technologies, CEITEC, Brno University of Technology, Brno, Czechia*
[2] *Faculty of Electrical Enginering, Brno University of Technology, Brno, Czechia*
[3] *Faculty of Science, Masaryk University, Brno, Czechia*

Deposition of plasma polymers by low-pressure radio frequency capacitively coupled plasma (RF CCP) discharges is a well-established method for enhancing surface biological properties. However, understanding the fundamentals of plasma deposition processes is still somewhat limited, not least thanks to the lack of information relevant to setup comparison. In this work, the electrical characteristics of two different RF CCP systems were measured by a VI probe. The results highlight how important it is to diagnose the plasma deposition setup.

## Introduction

Deposition of plasma polymers (PPs) by low-pressure radio frequency capacitively coupled plasma (RF CCP) discharges is a well-established method for enhancing the biocompatibility of various surfaces. PPs containing either primary amine ($NH_2$) or carboxyl (COOH) functional groups are typically prepared. Their properties can differ widely depending on the RF CCP setup and process parameters.

Despite the wide use, the fundamental understanding of the deposition processes is still somewhat limited. For example, deposition studies usually report only the power supplied by the generator, conveniently ignoring that part of it is lost (e.g., in the matching unit) before being delivered to plasma. This makes the comparison of results obtained in different setups and finding an explanation of differences difficult. In this work, we have used a VI probe to address this issue in our two RF CCP deposition reactors and to obtain information on their electrical parameters and ion fluxes.

## Experimental details

Two different-sized RF CCP reactors (small [1] and large [2]) with parallel plate electrodes were characterized. In both setups, the bottom electrode was capacitively coupled through a matching unit to an RF generator working at a frequency of 13.56 MHz. The showerhead upper electrode was grounded, and the gases were fed through it to the chamber. In the smaller RF CCP, both electrodes had the same diameter of 210 mm. In the larger RF CCP, the RF electrode had a diameter of 420 mm and the grounded electrode diameter was 380 mm. In both cases, the distance between the electrodes was kept constant at 55 mm. The electrical characteristics were measured for pure Ar (reference), Ar/cyclopropylamine (amine PPs), and $CO_2/C_2H_4$ (carboxyl PPs) discharges. The gas flow rates were set to keep the residence time in both setups the same.

The electrical parameters of both discharges were recorded using an OctIV Suite 2.0 probe from Impedans placed between the matching unit and the reactor feedthrough.

## Results and discussion

The RF CCP construction had a crucial impact on the electrical parameters of the discharge. For example, in the smaller RF CCP, the electrodes were situated relatively far from the chamber walls, and the expansion of plasma outside of the electrode region led to a significant increase in the grounded electrode area. Thus, higher self-bias values were observed for the smaller reactor, although the larger reactor has different-sized electrodes.

Using a depositing gas mixture led to a notable decrease in ion flux and self-bias. Instead of ionizing collisions, energy was lost in dissociation and excitation of numerous rotational and vibrational levels, resulting in the lower-density plasma that is more contained between the electrodes.

## References

[1] Michlíček, M. *Appl. Surf. Science*, **540**, 147979 (2021).
[2] Štrbkova, L. *Surf. Coat. Technology.*, **295**, 70–777 (2016).

# On Transient Nature of Polarized Emission from Laser Produced Plasma

Geethika B R[1,2], Jinto Thomas[1,2], Renjith Kumar R[1,2], Judhistir Shamal[1,2] and H C Joshi[1]

[1] *Institute For Plasma Research, Bhat, Gandhinagar, Gujarat, 382428, India.*
[2] *Homi Bhabha National Institute, Training School Complex, Anushaktinagar, Mumbai, 400094, India.*

Polarization of background radiation from laser-produced plasma has been used to selectively suppress background and enhance the signal-to-noise ratio in laser-induced breakdown spectroscopy (LIBS), a technique known as polarization-resolved LIBS (PRLIBS). However, the cause of this polarization remains unclear. Our study reveals that emission polarization significantly depends on both spatial location within the plasma as well as time of observation, which may greatly influence PRLIBS results. This work provides a detailed investigation into the spatio-temporal evolution of polarized emissions in laser-produced plasma and examines its impact on elemental analysis in PRLIBS.

## 1 Introduction

In the past few decades, Laser-Induced Breakdown Spectroscopy (LIBS) has garnered significant interest due to its applications in various fields, including fusion research, particularly in plasma-wall interactions, magnetic field quantification, and deuterium production analysis. Given its widespread use, various research groups have attempted to develop techniques to enhance the signal-to-noise ratio (SNR) in LIBS. One such technique is polarization-resolved LIBS (PRLIBS), which utilizes the polarized emission from plasma to suppress background noise.

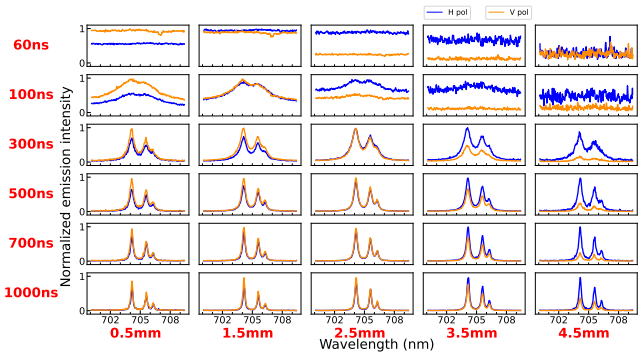



Figure 1: Spatio-temporal evolution of the emission spectra of Al II. Row-wise it shows the spectra with increasing time after the laser ablation and column-wise the spectra with increase in the distance from the target[1].

## 2 Results and Discussion

Polarized emissions from laser-produced plasma are particularly intriguing as they provide insights into the fundamental processes governing plasma formation and expansion. However, the mechanisms responsible for this polarization in laser-produced plasma (LPP) are still not well understood. This study presents a comprehensive spatio-temporal characterization of polarized emission from LPP, employing localized measurements of plasma parameters (ref fig 1) [1]. Our findings reveal an intriguing behavior in the degree of polarization (DOP) of emissions, specifically a sign reversal along the plume propagation axis. The study also explores potential explanations for this phenomenon.

These observations raise an important question: Does PRLIBS genuinely enhance the SNR, or does it overlook critical information about LPP?. Our findings can substantially improve the implementation of PRLIBS for elemental quantification [2].

## References

[1] B. R. Geethika, Jinto Thomas, Milaan Patel, Renjith Kumar R. and Hem Chandra Joshi Spatio-temporal dynamics of anisotropic emission from nano-second laser produced aluminium plasma. *JAAS*, **38**, 2477-2485 (2023).

[2] B.R. Geethika, Jinto Thomas, Renjith Kumar R, Janvi Dave and Hem Chandra Joshi. Effect of polarization on spectroscopic characterization of laser produced aluminium plasma. *Spectrochimica Acta Part B: Atomic Spectroscopy*, **221**, 107033 (2024).

# Stability of reactive species produced in plasma-activated water by various atmospheric air discharges and their antimicrobial properties combined with UV-A irradiation

R. Mehrabifard[1], A. Chithran[1], B.G. Kimani[1], and Z. Machala[1]

[1]*Faculty of Mathematics, Physics, and Informatics, Comenius University Bratislava, Slovakia*

Although extensive research has been carried out on various applications of plasma-activated water, this study focuses on measuring and understanding the stability and temporal evolution of reactive species therein. It also investigates the enhancement of antibacterial effects of PAW when combined with UV-A irradiation, which is not antibacterial by itself.

## 1 Introduction

Non-thermal plasma and plasma-activated water (PAW) are used in a vast variety of applications because of their reactive components, especially reactive oxygen and nitrogen species (RONS). PAW is mostly applied in agriculture and food safety, bio-medical applications, and surface treatment and modification. Although extensive research has been carried out on the PAW properties and applications [1], it is crucial to know the stability and temporal evolution of RONS in PAW.

In addition, based on some studies [2], antibacterial and chemical properties of PAW can be enhanced by UV-A radiation. The secondary objective of this study is to investigate the combined effects of plasma treatment with UV-A irradiation [3].

## 2 Experimental

Both tap and deionized (DI) water are used to produce PAW with three different plasma setups: Transient Spark (TS) batch water treatment, Transient Spark with water electrospray (TS-ES), and Fountain Dielectric Barrier Discharge (FDBD). TS and TS-ES run in pin-to-plane geometries, using a DC high voltage. The spark pulse frequency is fixed at 1 kHz for both, with 1 cm gap distance. 0.5 ml/min flow rate is set for TS-ES, while 10 mL water is treated for 10 min in batch TS. For FDBD a neon-sign AC high voltage supply was used with 15 kV pk-to-pk and 20 kHz, and 1 L of water was circulated during 20 min. Different modes of combined TS + UV-A treatment are examined including plasma alone, UV alone, TS and UV, TS followed by UV, and reverse.

## 3 Results

PAW characteristics, including the RONS concentrations ($H_2O_2$, $O_3$, $NO_2^-$ and $NO_3^-$), pH, electrical conductivity, oxidation reduction potential (ORP), temperature, and total dissolved solids (TDS), were measured in short and long time after plasma treatment. The PAW physiochemical characteristics were measured in the first 24 h (0, 2, 4, 8, 12, and 24 h) after treatment, and then 1, 2, 4, 8, 16, and 30 days after treatment for a long-time stability. The RONS in naturally buffering tap water are more stable than in DI water, however, most of RONS disappear after 10 days in tap water. All reactions between RONS occur faster in the acidified DI. $NO_3^-$ is the only species that stays in both tap and DI water after a long time.

A significant reduction in bacteria by TS PAW was detected (1.72 log). The combined TS PAW + UV-A treatments for TS+UV and TS then UV resulted in an even stronger log reduction by 2.49 and 2.63, respectively. For UV followed by TS, the result obtained was like that of TS alone. For UV alone, there was no bacterial reduction. These effects can by partly attributed to the UV-photolysis of $H_2O$ and $NO_2^-$, however, further investigations are required.

## 4 Summary

The findings obtained from this research are crucial for the post-production use of plasma-activated water in agriculture and disinfection and indicate a potential enhancement of PAW disinfection effects by combining with UV-A irradiation.

**Acknowledgment**

Funded by the EU NextGenerationEU through the Recovery and Resilience Plan for Slovakia under the project 09I03-03-V03-00033.

**References**

[1] Machala Z. et al. *Plasma Process. Polym.*, 10, 649–659 (2013)

[2] Pavlovich M. J. et al. *Plasma Process. Polym*. 10, 1051–1060 (2013)

[3] Mehrabifard R. et al. “Combined Antimicrobial Properties of Ultraviolet Radiation and Plasma-Activated Water,” (2024), *doi: 10.2139/SSRN.4961388*.

# Tuning properties of activated liquids produced by an atmospheric pressure plasma jet for application in plasma medicine

A. Marković[1], N. Škoro[1], N. Puač[1]

[1] *Institute of Physics, University of Belgrade, Pregrevica 118, 11080 Belgrade, Serbia*

We investigated the dielectric barrier discharge (DBD) type of atmospheric pressure plasma jet (APPJ) operating above the liquid samples to create plasma activated liquid (PAL). The device was used for treating of distilled water and RPMI 1640 cell culture medium. The working gases were He and mixture of He with water vapor. Optical characterization of the plasma showed that addition of water vapor to feed gas decreases the emission intensities of reactive species in the region above the treated liquid. However, the measurement of RONS in PALs showed that higher feed gas humidity increased concentrations of the measured RONS.

## 1 Introduction

The variety of atmospheric pressure plasma jets (APPJ) used in recent decades is really large. Depending on the specific application of plasma activated liquid (PAL), there are numerous operating parameters of plasma jets that should favour the generation of the desired reactive species, and the amount of reactive species should be adequate with respect to the application. The plasma jet used in this work effectively treated RPMI 1640 medium and distilled water, producing PAM for treatment of tumor cells [1] and PAW for wound healing in diabetic mice [2]. Therefore, providing reproducible plasma treatments for applications and desired reactive species in PAL is crucial for further application. Fine-tuning over PAL properties requires knowledge on links between the operating parameters of the APPJ system to enable precise control.

This work presents the effects of operating parameters such as power deposited in plasma, feed gas humidity, and liquid sample type on generation of reactive species both in gas and liquid phases.

## 2 Experimental setup and results

In this study, a dielectric barrier discharge (DBD)-type APPJ system with a two-electrode configuration (powered and grounded) was used. The Fig. 1 shows OES spectrum of detect excited and metastable species. He was used as the feed gas, with humidity controlled by gas flow using a bubbler. Treatments were conducted under three conditions: exposure to ambient air when a certain small constant amount of water molecules remained in the flow system (0-2 ppm) and with addition of water vapor (900 ppm and 1600 ppm). After plasma treatment, conductivity, pH, and concentrations of long-lived reactive species ($H_2O_2$, $NO_2^-$, and $NO_3^-$) were measured in PAL.

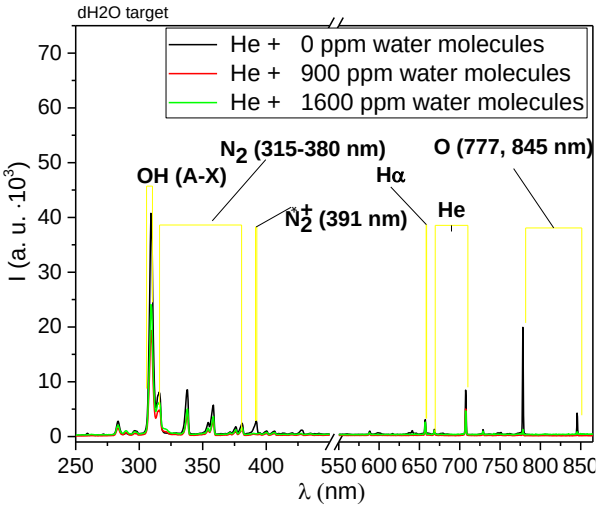



Fig. 1 The OES spectrum of He jet above the distilled water

## 3 Conclusion

It has been shown that the addition of water vapour in flow gas enhances the formation of RONS in the liquid, particularly $H_2O_2$. However, this modification in the gas flow requires operating at higher input voltages to achieve the same power delivered to the plasma.

**Acknowledgment**

This work was supported by MSTDI Republic of Serbia grant number 451-03-68/2025-14/200024.

## References

[1] S. Tomić, et al., Plasma-Activated Medium Potentiates the Immunogenicity of Tumor Cell Lysates for Dendritic Cell-Based Cancer Vaccines *Cancers*,**13**(7), 1626 (2021)

[2] J. Rajić, N.Grdović, et al., Plasma-Activated Water Improve Wound Healing in Diabetic Rats by Influencing the Inflammatory and Remodelling Phase, *Int. J. Mol. Sci*., **26**(3), 1265;( 2025)

# Influence of Pulsed Plasmas in Liquids on Copper Surfaces prepared for the XXXVI ICPIG

P. Pottkämper[1], N. Unteregge[1], S. Weller[1] and A. von Keudell[1],

[1] *Ruhr-University Bochum, Bochum, Germany*

18.03.25

One application of plasmas in liquids is the modification of metal surfaces. In this project a plasma is ignited at an electrode immersed in liquid using high voltages. Pulses with fast rise times in the nanosecond and microsecond range are urtilized. The plasma and plasma-activated liquid is then used to modify a coppper surface. The plasma causes a dissociation of water molecules, leading to the creation of many different reactive species with varying lifetimes such as oxygen, hydrogen, solvated electrons and hydrogen peroxyde. These species elicit different reactions that lead to the modification of the copper sample. It is possible to reduce the surface or to initiate growth of nanostructures depending on the experimental conditions.

## 1 General

One application of copper oxide nanocrystals is the catalytical electrochemical reduction of $CO_2$. During this reaction the activity of these catalysts decreases over time. The in-liquid plasma could be used to re-oxidize or create such catalytic surfaces. It is postulated that by combining an in-operando in-liquid plasma treatment with such a catalysis setup the lifetime of the catalytic surfaces can be extended.

We have observed the creation of uniform copper oxide nanocystals under certain conditions using a nanosecond-pulsed in liquid plasma. Using plasma activated water (PAW), copper oxide nanocrystals could be grown on copper surfaces. A possible growth mechanism is depicted in Fig. 1. The plasma creates many reactive species which oxidize the copper sample. The resulting $Cu(OH)_2$ dissolves into the liquid and precipitates onto the sample. Reducing reactive species then reduce the $Cu(OH)_2$ to $Cu_2O$ nanocrystals. In a cycle of oxidation and reduction, the crystals grow as more dissolved copper oxides attach to the initial seeds.

However, the plasma ignition mechanisms vary with pulse length. In the microsecond case, the liquid evaporates in the vicinity of the electrode tip due to Joule heating and the plasma ignites inside these bubbles. In the nanosecond case, the plasma ignites directly inside the liquid. Therefore, the resulting plasma-activared water may have different properties and effects on a copper sample. It is neccesary to compare the nanosecond-pulsed plasma effects on the PAW with the effects of the longer pulses in the microsecond range.

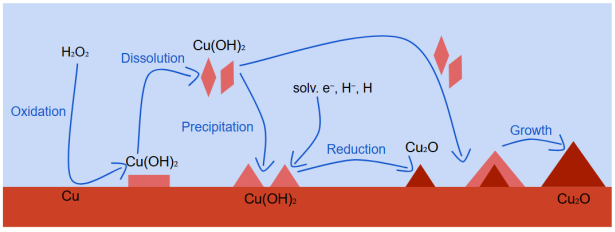



Figure 1: Proposed growth mechanism of $Cu_xO$ crystals from plasma-activated water, based on results produced from nanosecond-pulsed plasma in distilled water.

In our recent studies we have investigated the influence of pulse length on the reactivity of plasma-activated water. The effects of the PAW on copper in both cases was investigated using FTIR spectroscopy, SEM imaging and cyclic voltammetry.

## References

[1] Chauvet, L. and Nenbangkaeo, C. and Grosse, K. and von Keudell, A. Chemistry in nanosecond plasmas in water *Plasma Processes and Polymers*, **17**, (2019). DOI: 10.1002/ppap.201900192

[2] Pottkämper, P. and von Keudell, A. Plasma in liquids induced modification of Cu surfaces *Journal of Physics D: Applied Physics*, **57**, (2024). DOI: 10.1088/1361-6463/ad4b2d

# Penning mixture experiments in an inductively driven lamp

R. Anantharaman[1], C. Simon[1] and R. Kling[1]

[1] *Karlsruhe Institute of Technology, Light Technology Institute, Karlsruhe, Germany*

Penning mixtures are used to reduce the ignition voltage of gas discharge lamps. We measured ignition currents of five different Penning mixtures in inductively driven argon lamps, which were built for UV disinfection applications. A Penning mixture of 0.5% neon in argon shows a reduced ignition current in an inductively driven lamp similar to the Penning effect described in literature for lamps with electrodes.

## 1. Introduction

The "Penning effect" is named after Dr. Frans Michel Penning, who discovered that the breakdown voltage of the gas discharge in certain mixture ratios of neon, argon and mercury is lower than in pure noble gases, due to the creation of meta-stable states, which results in more ionisation reactions than in pure gases [2]. The Penning ionisation reduces the ignition voltage of gas discharge lamps and is caused by the ionization interaction between an excited molecule of the additional gas and the target molecule to eject a high energy electron [3]. In a series of experiments with xenon and argon [1], it was observed that Penning effect is at maximum for an 8% addition of xenon in argon and the effect is lower for other ratios.

## 2. Experimental setup

The setup consists of a high frequency inverter which drives a copper coil of 240 mm in length and 20.5 windings. The inverter operates at a frequency of about 3.125 MHz and adapts the frequency for current control. The input voltage to the inverter of the DC power supply is increased manually until the lamp ignites. As a result of the ignition, the controller notices a shift in the impedance of the lamp and records the lamp current at ignition time. We discuss our results of measured ignition currents of five different Penning lamps (length 60 mm, diameter 40 mm and a starting gas pressure of 40 Pa).

In this presentation, we investigate the Penning effect in inductively driven noble gas lamps. In electrode-based lamps, the charge carriers are accelerated due to the applied electric field between the electrodes. However, in the inductive (electrodeless) lamp, the applied current in the coil induces a magnetic field, which accelerates the charge carriers in the lamp. Therefore, we will compare the ignition currents in inductive lamps with Penning mixture filling to lamps with pure noble gas.

## 3. Results from ignition experiments

The data from the ignition experiments shown in Table 1 show that a 0.5% mix of neon in argon Penning mixture is useful in reducing the ignition current. This shows that the Penning effect of argon/neon pair in an inductive lamp setup helps in reducing the ignition current, similar to the argon/xenon pair in [4]. Any higher ratio of neon in argon and krypton in argon did not have a useful effect.

Table 1: Measured lamp current $I_{rms}$ (A, root mean square) necessary for igniting the hot lamp. T (°C) is the lamp temperature just before the ignition experiment as seen by an infrared camera.

| Lamp | Ar(%) | Ne(%) | Kr(%) | T(°C) | $I_{rms}$ (A) |
|---|---|---|---|---|---|
| 1 | 99.5 | 0.5 | 0 | 230 | 8.8 |
| 2 | 99 | 1 | 0 | 260 | 9.0 |
| 3 | 98 | 2 | 0 | 230 | 9.3 |
| 4 | 90 | 0 | 10 | 260 | 10 |
| 5 | 100 | 0 | 0 | 220 | 8.9 |

## References

[1] PC Agrawal and BD Ramsey. Penning gas mixtures for improving the energy resolution of proportional counters. *IEEE Transactions on Nuclear Science*, **36**(1):866–870, 1989.

[2] Chr. Meyer and H. Nienhuis. *DISCHARGE LAMPS*. Philips Technical Library, Kluwer Technische Boeken B.V. Deventer-Antwerpen, 1988.

[3] FM Penning. Über Ionisation durch metastabile Atome. *Naturwissenschaften*, **15**(40):818–818, 1927.

[4] Ö Şahin, I Tapan, Emin N Özmutlu, and R Veenhof. Penning transfer in argon-based gas mixtures. *Journal of Instrumentation*, **5**(05):P05002, 2010.

# Iron ore reduction in hydrogen-containing low-pressure plasma

M. Mayer[1], M. Pustylnik[1], C. Altenbach[1], U. Manzoor[2], I. R. Souza Filho[2,3], H. M. Thomas[1], D. Raabe[2], D. Zander[1]

[1] *DLR Institut für Materialphysik im Weltraum, Cologne, Germany*
[2] *Max-Planck-Institut for Sustainable Materials, Düsseldorf, Germany*
[3] *Institut Jean Lamour, CNRS, Université de Lorraine, Nancy, France*

Hydrogen-containing plasma is a promising alternative to coal coke for sustainable iron ore reduction. Hematite ($Fe_2O_3$) samples are reduced in a low-pressure inductively coupled plasma setup. Simultaneous monitoring of plasma parameters allows investigation of their impact on the reduction process.
**Keywords:** Hydrogen reduction, iron ore, metallurgy, inductively coupled plasma

## 1 Background

Since the iron and steel industry causes approximately 7 % of the global $CO_2$ emissions, considerable research is ongoing about sustainable iron- and steelmaking methods [1]. With $H_2O$ as product of the reduction reactions (e.g., $FeO + H_2 \rightarrow Fe + H_2O$) instead of $CO_2$, hydrogen plasma reduction of iron ores is a promising alternative to the traditional carbothermic process [1]. Reduction with hydrogen-containing arc discharges with the advantage of local heating of the reduction surface is currently investigated [2]. Hydrogen plasma reduction below the melting temperature of iron ore is also feasible [3] with better accessibility for plasma diagnostics in low-pressure plasma.

## 2 Setup and methods

Inductively coupled plasma is generated in a GEC RF reference cell with a 5-turn-coil antenna powered by a radiofrequency generator at 13.56 MHz [4]. Operating pressures in the argon-hydrogen (9:1) gas mixture are several tens of Pa. A sintered hematite ($Fe_2O_3$) sample is positioned 5 cm below the coil on a heater plate (Figure 1) with a temperature control up to several hundred °C.

Plasma diagnostics and reduction process monitoring are performed by means of optical emission spectroscopy, a current-voltage sensor, a microwave interferometer and a mass spectrometer.

The samples of hundred mg to a few g are analyzed by weighing, computed tomography scans, and energy dispersive X-ray spectroscopy.

## 3 Reduction experiments

In first attempts, a mass decrease of up to 4 % was achieved within 5-6 hours of processing compared to a mass decrease of 0.4 % by pure heating (thermogravimetric analysis up to 1000 °C).

The impact of the sample temperature and the radiofrequency power on the reduction process are investigated as well as the corresponding plasma parameters, e.g., the electron density and atomic hydrogen density. The analysis of the first reduction experiments will be shown in the contribution.

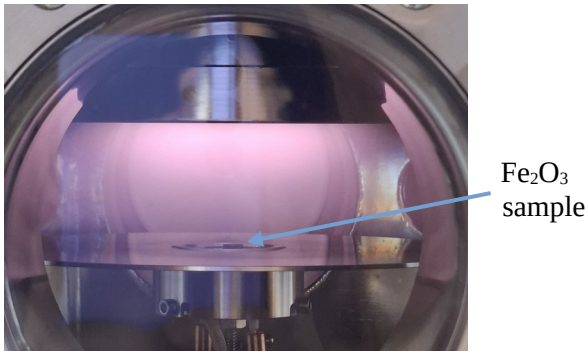



**Figure 1:** Plasma setup with hematite sample during reduction process in argon-hydrogen plasma.

**References**

[1] Sabat, K. C., Murphy, A. B. Hydrogen Plasma Processing of Iron Ore. *Metallurg. Mat. Trans.* **48B**, 1561-1594 (2017).
[2] Souza Filho, I. R., Ma, Y., Kulse, M., Ponge, D., Gault, B., Springer, H., Raabe, D. Sustainable steel through hydrogen plasma reduction of iron ore: Process, kinetics, microstructure, chemistry. *Acta Materialia* **213**, 116971 (2021).
[3] Rajput, P., Sabat, K. C., Paramguru, R. K., Bhoi, B., Mishra, B. K. Direct reduction of iron in low temperature hydrogen plasma. *Ironmaking & Steelmaking* **41**, 721-731 (2014).
[4] Miller, P. A., Hebner, G. A., Greenberg, K. E., Pochan, P. D., Aragon, B. P. An Inductively Coupled Plasma Source for the Gaseous Electronics Conference RF Reference Cell. *J. Res. Natl. Inst. Stand. Technol.* **100**, 427-439 (1995).

# Sputter epitaxy of ZnO films on lattice mismatched sapphire substrates using MgO buffer layers fabricated in Ar/$O_2$ discharges

K. Harada, T. Yunoue, H. Otsuyama, N. Yamashita, T. Okumura K. Kamataki, K. Koga, M. Shiratani, and N. Itagaki

*Graduate School of Information Science and Electrical Engineering, Kyushu University, Fukuoka, Japan*

Epitaxial ZnO films were successfully grown on 18%-lattice-mismatched sapphire substrates using wurtzite MgO buffer layers fabricated by radio-frequency magnetron sputtering. The buffer layers enabled the formation of atomically flat ZnO films with step-terrace structures, achieving a root-mean-square roughness as low as 0.11 nm. The ZnO films also exhibited excellent crystal quality, with a full width at half maximum of 0.006° for 0002 X-ray rocking curve. We attribute this to the MgO buffer layers providing lattice-relaxed nucleation centers, O-polar surfaces, and a small lattice mismatch with ZnO, all of which promote the 2D growth of subsequent ZnO films.

ZnO, a wide-band-gap semiconductor, is gaining renewed interest for its potential in space applications, ferroelectric and spintronic memories, and as an alternative to GaN in LEDs and power devices. However, its practical use remains limited by challenges in growing high-quality films on cost-effective substrates, primarily due to 18% lattice mismatch with sapphire. While buffer layers consisting of nanosized ZnO(N) islands have been developed for effective lattice strain relaxation [1], the approach has limitations, including a narrow process margin and nitrogen-induced defects. To address these issues, we here propose using MgO as a buffer layer. Though typically cubic, MgO can form nanosized islands with metastable wurtzite structure [2] and a small (~1%) lattice mismatch with ZnO especially under non-equilibrium processes such as magnetron sputtering, making it a suitable buffer layer. Additionally, its O-polar surface enhances Zn adatom migration, which can further improve the film quality. To optimize this approach, we also investigate effects of deposition temperatures for both the buffer layer ($T_{buffer}$) and ZnO layer ($T_{ZnO}$).

All layers were deposited by RF magnetron sputtering in Ar/$O_2$. First, MgO layers were deposited on c-plane sapphire at 750–850ºC. Then, 500-nm-thick ZnO layers were deposited at 800–900ºC.

We observed that MgO layers further improved the crystal quality of ZnO films compared to those using ZnO(N) buffer layers. Figure 1 shows atomic force microscopy (AFM) images of an MgO buffer layer and ZnO films. Like ZnO(N) buffers, MgO formed nanosized 3D islands, confirming its feasibility as a buffer layer. On MgO buffers, atomically flat ZnO films with step-terrace structures were grown. Notably, at $T_{ZnO}$ = 900ºC, root-mean-square roughness ($R_q$) was remarkably low at 0.11–0.15 nm, compared to 0.55 nm for a film grown at $T_{ZnO}$ = 800ºC. While ZnO film quality showed little dependence on $T_{buffer}$, suggesting a large process margin for MgO buffer layer. The ZnO films also exhibited excellent crystal quality, with a full-width at half maximum of 0.006° for the 0002 X-ray rocking curve. These outstanding properties are likely due to the wurtzite-structured MgO buffers consisting of O-polar nanosized islands, which effectively relax lattice strain and enhance adatom migration.

This work was supported by JSPS KAKENHI. JP22H05000, JP23K17752, JP24K00929, JST ASPIRE 1234505, and Tokyo Electron Ltd. (TEL).

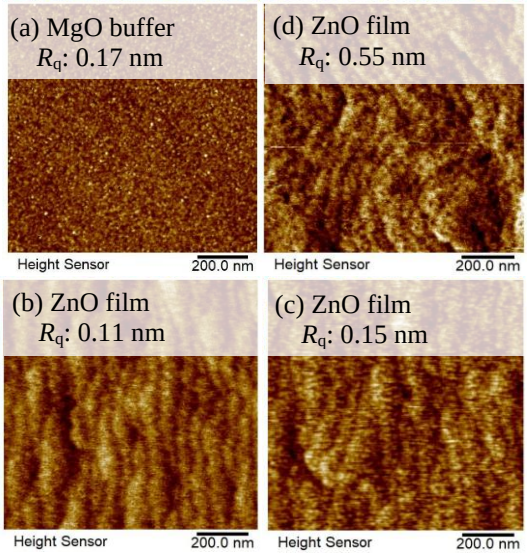



Fig. 1. AFM images. (a) MgO buffer layer ($T_{buffer}$: 750ºC). (b) ZnO film on buffer layer ($T_{buffer}$: 750ºC, $T_{ZnO}$: 800ºC). (c) ZnO film on buffer layer ($T_{buffer}$: 750ºC, $T_{ZnO}$: 900ºC). (d) ZnO film on buffer layer ($T_{buffer}$: 850ºC, $T_{ZnO}$: 900ºC).

## References

[1] N. Itagaki, et. al., Sci. Rep., 10 (2020), 4669.
[2] H. Kato, et al., Appl. Phys. Lett., 84 (2004), 4562.

# Synthesis of Chondrule-like Particles Based on Si-Fe in RF Discharge Conditions.

A. Baikaliyev[1,2], S. Orazbayev[1,2], B.Kyrykbay[3] and D. Batryshev[3]

[1]*Al-Farabi Kazakh National University, Almaty, Kazakhstan.*
[2]*Institute of Applied Science and Information Technologies, Almaty, Kazakhstan*
[3]*Kazakh-British Technical University, Almaty, Kazakhstan*

This paper presents experimental results on the synthesis of Si-Fe nanoparticles under HF discharge conditions. Ar/HMDSO/Ferocene gas mixture was used as initial components. SEM showed that the particle size varied in the range of 50-500 nm, while XRD and Mössbauer spectroscopy confirmed the presence of amorphous and crystalline Fe-Si phases similar to chondrite textures. Exposure to a pulsed plasma discharge resulted in partial melting and recrystallisation. The results demonstrate the possibility of laboratory modelling of chondrite formation processes in the early solar system.

Chondrites are primitive meteorites containing rounded structures called chondrules, which are considered to be among the oldest solid objects in the solar system. Their composition includes silicate and metallic components, indicating that complex thermal and physicochemical processes accompanied their formation. However, the exact mechanism of their origin is still a subject of scientific debate, and its laboratory modelling requires the development of special experimental techniques [1].

In this work, the laboratory synthesis of Si-Fe-based chondro-like particles under HF discharge conditions was carried out, which allowed us to reproduce the key stages of their formation in the protoplanetary disc. The experiments yielded nanoparticles of 50-500 nm in size, composed of silicon and iron, with characteristic spherical and aggregated morphologies. XRD and Mössbauer spectroscopy confirmed the presence of amorphous and crystalline phases such as $FeSi_2$ ($\beta$ -$FeSi_2$ - low temperature; $\alpha$ -$FeSi_2$ - high temperature), similar to the textures of chondrites in meteorites. These textures are characteristic of natural chondrites. In addition, the synthesised particles were exposed to a pulsed plasma discharge (T > 1500 K), which led to their partial melting and recrystallisation [2].

The results obtained allow us to reproduce in laboratory conditions the processes of aggregation, melting, and crystallisation of dusty material, which confirms the hypothesis about the possible formation of chondrites under the conditions of plasma processes in the early solar system.

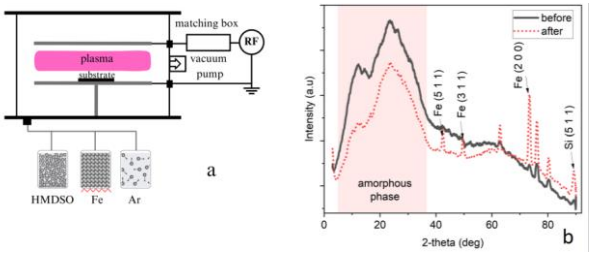



Figure 1. Experimental setup: (a) RF discharge plasma; (b) X-ray diffraction analysis before/after irradiation via the plasma accelerator

## References

[1] A.R. Abdirakhmanov et al. Physical Sciences and Technology, 10, 68-72 (2023)
[2] A. Baikaliyev et al. Appl. Sci. 14, 8714 (2024)

# Correlation between work function and $H^-/D^-$ production on C12A7 electride surface

M. Sasao[1], J.P. Broude[2], S. Inoue[1], Y. Inokuchi[1], Om Raval[2], J.M. Layet[2], G. Cartry[2]

[1] *Doshisha University, Kyotanabe, Kyoto 610-0321, Japan*
[2] *Aix-Marseille Université, CNRS, PIIM UMR 7345, Marseille, France*

The work function of a metallic plasma electrode in an $H^-$ / $D^-$ source has been considered as a key parameter for negative ion beam production, and a clear relationship has been confirmed experimentally and theoretically. In the case of some semiconducting or dielectric materials, however, the similar relationship has not been well studied. In the present paper, correlations between the work function and the surface production of $H^-/D^-$ yield on C12A7 electride were measured by changing the sample bias in a low-pressure deuterium plasma, and extracting the negative ions in a pulsed mode. The work function was measured by photoemission yield spectroscopy (PYS).

## 1 Introduction

Plasma-surface interaction of C12A7 electride, which is one of the most promising materials for Cs-free plasma electrodes of negative ion sources, is an important research subject for efficient source operation as well as from material science point of view for its various application [1,2]. The change of the work function of C12A7 electride by argon and hydrogen plasma bombardment has been reported [3,4], but details need to be understood.

## 2 Experiments and results

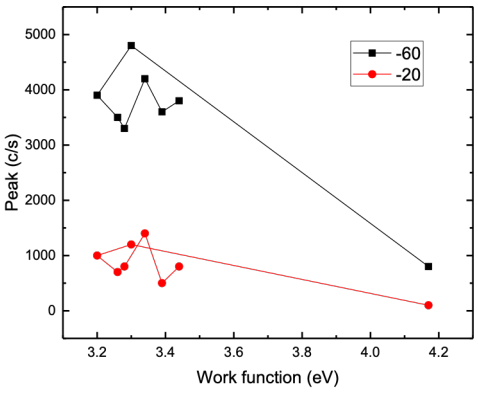



Figure 1.
Correlations between work function and $H^-/D^-$ peak counts observed in an energy resolved mass spectrometer from a C12A7 electride sample immersed in D plasma and positively and negatively biased. Black squares and red circles present the data extracted at -60 V and -20 V.

The experiments were carried out using a surface-produced negative ion measurement system and a photoelectron yield spectroscopy system installed on the plasma reactor at PIIM Aix-Marseille University [5]. Here, the sample bias in a low-pressure deuterium plasma was changed from +20V, +10V, +6V (floating), 0V, -10V, -20V, -40 V, and -60 V, in a pulsed mode [6]. Each measurement was composed of a 3min. floating in deuterium plasma and 5 min. DC biasing, and a DC biasing plus pulsed bias (-20 V or -60 V), and work function measurement by PYS. The results repeated this cycle twice and averaged are shown in Fig. 1. Changing the DC bias from -60 V to +10 V has little effect on the work function and negative ion yield, but +20 V significantly deteriorates the surface. The highest negative ion yield was obtained at +10 V, in the slow electron injection region

## 3 Discussions

Hydrogen plasma exposure might have 3 effects: 1) Hydrogen atoms and ions react with impurities on the surface, remove them [7], 2) but also create a H-doped C12A7 structure, 3) which might be kicked-off by electrons.

### References

[1] M Sasao et al, Applied Physics Express, 11(6), 2018
[2] H. Hosono and M.Kitano, Chemical Reviews 121.5 (2021): 3121-3185.
[3] F. Taccogna et al., Eur. Phys. J. D 75, 227 (2021)
[4] A. Heiler et al., AIP Conference Proceedings 2373, 020004 (2021)
[5] G. Cartry, et al., (2017). New Journal of Physics, 19(2), 025010
[6] G. Cartry, et al., presented at ICPIG2023, and ICPIG2024.
[7] M. Sasao et al., J. Phys.: Conf. Ser. 2743 012028.

# Electron surface scattering kernel in the few-eV energy range for plasma-facing dielectric solids

Franz X. Bronold and Felix Willert

*Institut für Physik, Universität Greifswald, D-17489 Greifswald, Germany*

Boltzmann-type kinetic modeling of spatially confined plasmas requires boundary conditions for the distribution functions of the species involved. We describe a computational approach for constructing a boundary condition for the electron distribution function in the few-eV energy range, which takes the electron microphysics inside the plasma-facing solid into account. It is based on an invariant embedding scheme and yields the electron surface scattering kernel to be used in the boundary condition of the plasma's electron Boltzmann equation. Infinitely thick halfspaces are discussed as well as dielectric slabs on top of metallic substrates.

Applying the invariant embedding principle, originally developed for albedo calculations of planetary and stellar atmospheres, we construct an electron surface scattering kernel $R(E,\xi|E',\xi')$ to be used in the boundary condition for the electron Boltzmann equation of a plasma confined by a solid. The kernel, connecting at the plasma-solid interface the distribution functions of the incoming and outgoing electrons via the relation (see Fig. 1)

$$F^{>}(E',\xi') = \int_0^\infty dE \int_0^1 d\xi\, F^{<}(E,\xi) R(E,\xi|E',\xi')\,,$$

takes the microphysics for electron emission and backscattering from the plasma-solid interface into account. To illustrate the approach we applied it to Si and Ge surfaces [1], using a semiempirical jellium model for the solid. It contains the quantum-mechanical transfer through the interface potential, encoded in the function $D(E,\xi)$, as well as the scattering cascades due to impact ionization and collisions with phonons and ion cores giving rise to the backscattering function $B(E,\xi|E',\xi')$. The latter satisfies a set of algebraic Riccati/Sylvester equations to be solved iteratively.

In order to describe dielectrically coated electrodes, we extended the formalism to layered structures. Whereas for halfspace geometries only electron backscattering (including secondary emission) matters, it is now also necessary to track electron transmission through the slab. Leaving aside, as a first step, the interaction of the transmitted electrons with the metallic substrate, we show how the slab's energy and angle-resolved transmission and backscattering function can be again obtained from the invariant embedding principle. Both functions enter the surface scattering kernel for the dielectric-metal structure, which also contains quantum-mechanical transfer functions due to the two interface potentials. Data as a function of layer thickness are shown for $SiO_2$. We also discuss the numerical scheme used for integrating the set of matrix Riccati/Sylvester differential equations which arise in the slab geometry in contrast to the algebraic equations appearing in the halfspace geometry.–Supported by Deutsche Forschungsgemeinschaft (DFG, German Research Foundation)–495729137.

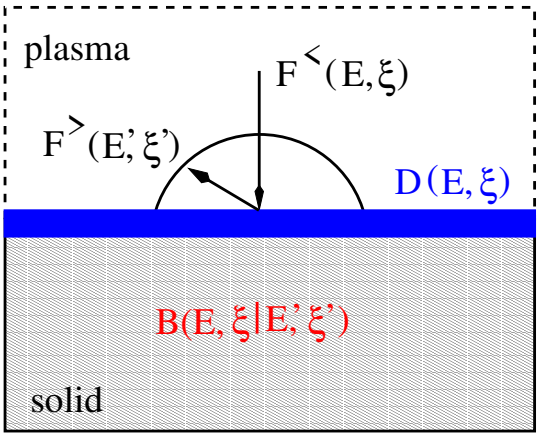



Figure 1: Illustration of the boundary condition connecting at the interface the distribution functions of the incoming and outgoing electrons, $F^{<}(E,\xi)$ and $F^{>}(E,\xi)$, respectively; $E$ and $\xi$ are the total energy and the direction cosine with respect to the surface normal. The surface scattering kernel $R(E,\xi|E',\xi')$ is obtained from the functions $D(E,\xi)$ and $B(E,\xi|E',\xi')$, encoding the quantum-mechanical transfer through the interface potential and the scattering cascades inside the solid, respectively.

## References

[1] Bronold, F. X. and Willert, F. Electron surface scattering kernel for a plasma facing a semiconductor. *Phys. Rev. E*, **110**, 035207 (2024).

# Influence of oxygen on arsenic containing inductively coupled plasma

R. Gudermanis[1], A. Abola[1], G. Revalde[1,2] and A. Skudra[1]

[1]*Institute of Atomic Physics and Spectroscopy, Faculty of Science and Technology, University of Latvia, Riga, Latvia*
[2]*Institute of Physics and Materials Science, Faculty of Natural Sciences and Technology, Riga Technical University, Riga, Latvia*

High-frequency electrodeless lamps with metal/rare gas fillings can be used for studies of processes happening in low-temperature inductively coupled plasma. Previous studies have shown that in certain conditions lamps can enter so-called impulse mode and start to emit pulse-like radiation. This phenomenon is not well understood. In this work, we look at the possible influence of oxygen atoms on the stability of radiation in As/Ar discharge. We registered the intensity of a number of Ar and O spectral lines at several different excitation generator voltages and calculated the intensity ratios. Our results showed gradual increase of oxygen emission followed by sudden decrease.

## 1 Introduction

Some of the applications for high-frequency electrodeless lamps (HFEDLs) with metal vapour/rare gas fillings include use as light sources in atomic absorption spectroscopy and low-temperature plasma diagnostics. The quality of the light sources depends on plasma-wall interaction.

We have previously observed that some HFEDLs in certain operating conditions start to pulsate – the emitted radiation intensity periodically changes [1]. The reasoning for this phenomenon is not well studied. In this work, we study the influence of oxygen atoms detached from the light source walls on the stability of HFEDL emission. For that, we chose several lamps in whose emission spectra oxygen triplet at 777 nm was observed and looked at the ratios between argon and oxygen spectral lines in stable and impulse emission modes.

## 2 Experiment

The study was done using As/Ar-containing HFEDLs. Lamps are made from quartz ($SiO_2$) and filled with As and Ar at low pressure. By placing the lamp in the coil of the excitation generator, an inductively coupled plasma is induced. Small amounts of oxygen atoms may enter the lamp bulb from the quartz walls.

Emission spectra of O 777.4 nm and Ar 772.6 nm and 763.2 nm spectral lines were registered at several excitation generator voltages using spectrometers Jobin Yvon 1000M and Ocean Optics HR-4000. Fig. 1 shows an example of O 777.4 nm and Ar 772.6 nm spectral line intensity changes in impulse mode.

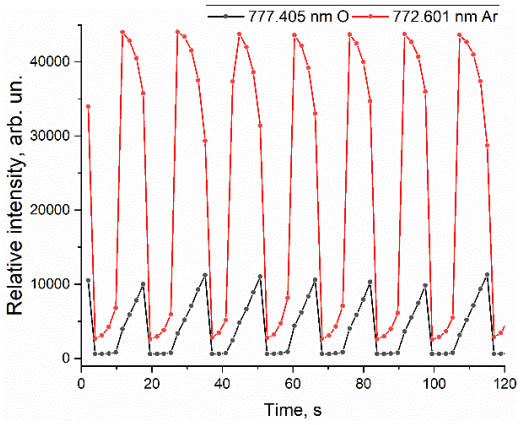



**Fig. 1** Intensity changes in time for O 777.4 nm and Ar 772.6 nm spectral lines during impulse mode.

## 3 Results and conclusions

We calculated the ratios between the relative intensities of oxygen and argon spectral lines. Our results showed the gradual increase of oxygen emission during the initiation phase of discharge, and the sudden decrease of discharge after reaching a certain amount confirms the hypothesis of oxygen as a main reason for discharge quenching

**Acknowledgements**

This work was partially supported by basic funding for scientific activities provided by the Faculty of Science and Technology, University of Latvia.

**Reference**

[1] Revalde G. et al. Investigation of Pulsed Mode Operation in Low-Temperature Arsenic Plasma Light Sources. *IEEE 14th International Conference Nanomaterials: Applications & Properties*, pp. 1-5 (2024),doi: 10.1109/NAP62956.2024.10739765.

# Is the use of the Sagdeev potential a legitimate way of deriving collisional Bohm criteria?

N. A. Almeida and M. S. Benilov

*Departamento de Física, FCEE, Universidade da Madeira, Largo do Município, 9000 Funchal, Portugal*
*Instituto de Plasmas e Fusão Nuclear, Instituto Superior Técnico, Universidade de Lisboa, 1041 Lisboa, Portugal*

A recent trend in the theory of the plasma-sheath transition and the Bohm criterion is to assume that the sheath edge is characterized by a maximum of the Sagdeev potential and to use this assumption to derive some or other form of the collisionally modified Bohm criterion. In this work, this approach is revisited and a significant issue has been identified.

## 1. Introduction

A lot of effort has been invested by able researchers over decades into the theory of the transition from quasi-neutral plasma to space-charge sheaths and related topics, in particular, the Bohm criterion; e.g., review [1] and references therein. Still, no universally accepted theory has emerged, in spite of the existence of results of a mathematical nature, including pure-mathematics results obtained in the course of the past two decades. In particular, there are many different versions of the so-called collisional Bohm criterion.

## 2. Assumption of a maximum of the Sagdeev potential at the sheath edge and the collisional Bohm criterion

In the framework of the classic Bohm's model of positive collision-free space-charge sheaths, the Bohm criterion is exactly equivalent to the condition $[d(n_i\text{-}n_e)/d\varphi]_{\varphi\,=\,0} < 0$. All designations here and further are conventional; $\varphi = 0$ corresponds to large distances from the surface, where the plasma is neutral. It follows that the Sagdeev potential $V(\varphi)$, which is defined by the formula $dV/d\varphi = e(n_i\text{-}n_e)$ (e.g., [2]), has a maximum at $\varphi = 0$.

In [3] and in a number of subsequent works, including very recent ones, it was assumed that the Sagdeev potential has a maximum at the edge of a collisional sheath. This leads to the sheath edge conditions

$$n_i = n_e, \qquad \frac{dn_i}{d\varphi} \le \frac{dn_e}{d\varphi} <=> \frac{dn_i}{dx} \le \frac{dn_e}{dx} \qquad (1)$$

Considering, as in [3], a slab of weakly ionized plasma with cold ions and ion-atom collisions and without ionization, using transport equations to evaluate the derivatives in the last relation in (1), and assuming the equality sign, one obtains

$$\frac{u_B^2}{v_i^2} - \frac{kT_e}{eE\lambda_i} = 1 \qquad (2)$$

Eq. (2) is equivalent to the lower limit of Bohm's sheath criterion for collisional sheaths derived in [3].

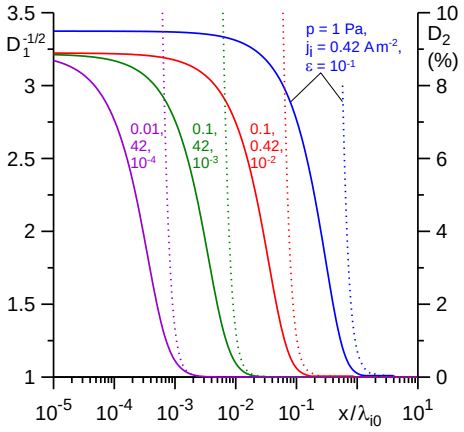



Fig. 1. Transition from a planar slab of a weakly collisional argon plasma to an absorbing negative surface. $\varepsilon = \lambda_D/\lambda_{i0}$.

In Fig. 1, $D_1$ (solid) designates the lhs of Eq. (2), $D_2$=1-$n_e/n_i$ (dotted), and $\lambda_D$ and $\lambda_{i0}$ are characteristic Debye length and ion-atom mean free path. One can see that the collisional Bohm criterion (2) is fulfilled at each point of the quasi-neutral region for all $\varepsilon$.

The latter is not surprising, since the last relation in Eq. (1), when written with the equality sign, represents a trivial corollary of the quasi-neutrality condition. In other words, the collisional Bohm criterion (2) represents a corollary of the transport equations written under the assumption of quasi-neutrality and thus does not provide any information concerning the ions leaving the quasi-neutral plasma and entering the sheath. In this sense, this criterion is no different from the quasi-neutrality condition itself and it is difficult to see how it could be useful.

This work was supported by FCT of Portugal under Project Nr. IPFN/UID/50010/2025.

## References

[1] Benilov, M. S. and Almeida, N. A. *Phys. Plasmas*, **32**, 030501 (2025).
[2] Chen, F. F. *Introduction to Plasma Physics and Controlled Fusion*, 3rd ed., Springer, Berlin (2015).
[3] Liu, J.-Y., Wang, Z.-X. and Wang, X. *Phys. Plasmas*, **10**, 3032 (2003).

# Investigation of H- surface-production in low-pressure plasma using a magnetized RFEA and in-situ photoemission

Theertha Matakkali Puthanpurayil[1], J.M. Layet[1], G. Cartry[1]
Max Kellermann-Stunt[2], Timo Gans[3] , James Dedrick[2]

[1] *Aix-Marseille Université, CNRS, PIIM UMR 7345, Marseille, France,*
[2] *University of York, York Plasma Institute, School of Physics, Engineering and Technology, York, UK,YO10 5DD,*
[3] *Dublin City University, National Centre for Plasma Science and Technology School of Physical Sciences, Faculty of Science and Health, Dublin, Ireland, D09 V209*

This study is dedicated to the investigation of negative-ion produced on a gadolinium surface in a low-pressure hydrogen plasma. Different technics to measure negative-ion with a magnetized retarding field energy analyser are first investigated. Then negative-ion surface production efficiency versus surface temperature is studied and correlated to changes of surface electronic properties.

## 1 Introduction

There are two main negative ion (NI) formation processes in low-pressure plasmas: volume production by dissociative attachment of electrons on molecules, and surface production through the electron capture by a neutral atom or an ion backscattered from a surface in contact with the plasma [1]. The later mechanism, which is used in most negative-ion sources, is efficient only when the surface is made of a low work-function material. The present study is dedicated to negative-ion production on Gadolinium (Gd) material which is a low work-function (WF) metal (WF = 2.9 eV). We first investigate different ways of using a Magnetized Retarding Field Energy Analyzer to measure the surface produced NI. We then study the Gd surface work-function changes due to plasma exposure and surface temperature, and compare with NI surface production efficiency variations.

## 2 Experimental set-up

Measurements are performed in an ICP reactor. The Gd sample is placed in the middle of the plasma chamber 40 mm away and facing a Magnetized Retarding Field Energy Analyzer which is basically made of a single grid Retarding Field Energy Analyzer plus a magnetic barrier [2]. The magnetic field (500 Gauss) is chosen to magnetized and trap electrons while letting NI passing through. The sample is negatively biased. Positive ions from the plasma are attracted toward the sample and form NI, which are then accelerated toward the plasma. Thanks to their acceleration NI can overcome the potential barrier due to the sheath in front of the MRFEA and are self-extracted from the plasma towards the MRFEA collector.

In order to measure the Gd surface work function upon exposure to the plasma, an in-situ photoemission yield diagnostic is employed. It consists in a tuneable light source, an optical fibre and collimation lenses to focus light onto the sample, as well as a light chopper, an ammeter and a lock-in detector. The photon energy is scanned from 1.12 eV (1200 nm) and 6.21 eV (200 nm). The photoemission threshold (i.e. the WF) is determined by measuring the sample current versus photon energy.

## 3 MRFEA measurements

The collector potential is scanned and I-V curves are obtained. The negative charge saturation current (positive collector bias) is not used to determine NI flux due to the possible presence of electrons escaping the barrier and secondary electrons generated by positive ion impact on the grounded grid. NI are detected in the negative collector region where they start to be electrostatically filtered when the collector reaches and goes below the sample bias value. Their presence is revealed by a step on the ion saturation. Different ways of detecting and measuring efficiently this small current step will be presented in this contribution.

## 4 NI production on Gd surfaces

The negative-ion surface production yield is measured for different Gd surface temperatures during plasma exposure (from room temperature to 750°C). After each plasma exposure to a given temperature, the WF is measured by photomemission. In this contribution, we will present possible correlations between WF variations and negative-ion surface production yield.

**References**

[1]: Bacal M., Physics aspects of negative ions, Nucl. Fusion 46 (2006) S250–S259.
[2]: D Rafalskyi et al Rev. Sci. Instrum., 86, 053302 (2015).

# Space Charge Structures on a Gridded Spherical Hollow Electrode

F. Enescu[1], D.G. Dimitriu[2], C. Ionita[1], and R. Schrittwieser[1]

[1] *Institute for Ion Physics and Applied Physics, University of Innsbruck, Austria*
[2] *Faculty of Physics, Alexandru Ioan Cuza University of Iasi, Romania*

We present investigations of the formation and behaviour of space charge structures in an Argon discharge plasma on and inside a gridded spherical hollow electrode of stainless steel. The experiments were conducted in a cylindrical stainless-steel chamber (inner length 92 cm and inner diameter 53,5 cm). Rows of strong permanent magnets with alternating polarity, magnetically fixed on the chamber's inner wall, increase the plasma density and its homogeneity, also reducing chaotic arc discharges to the chamber walls. As diagnostics we have used mainly optical emission spectroscopy to determine plasma density, electron temperature and particle composition.

## 1 Introduction

We have investigated space charge structures generated by negatively biasing a hollow spherical gridded electrode, which made it possible to observe the formation and behaviour of discharge structures also inside this electrode. These experiments were carried out in a vacuum chamber with an inner length of 92 cm and inner diameter of 53,5 cm (the former Innsbruck DP-machine). See also [1,2]

We focused on the behaviour of the plasma, in particular the creation, evolution, and dissolution of a hyperboloid structure inside and in front of the cathode's orifice. Especially the experimental arrangement producing hyperboloidal plasma structures offers interesting and useful applications, such as to spray heavy ions and create films on a substrate or to produce thrust (ionic or Hall thrusters).

As diagnostics we have used mainly optical emission spectroscopy to determine plasma density, electron temperature and particle composition.

In an accompanying contribution to this Conference the results of comparative experiments with two smooth spherical cathodes are presented [3].

### 1.1 Visual observations

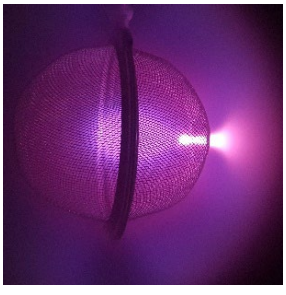


*Fig. 1 Plasma structure for V = –270 V.*

Argon plasma was produced at 0,1 mbar gas pressure by a spherical stainless-steel mesh cathode of 55 mm diam. (1 mm x 1 mm mesh width). The sphere had an orifice of 17 mm diameter on its horizontal axis.

The plasma structures inside, around the spherical mesh cathode, and inside its orifice, respectively, were observed for varying its bias $V$ in steps from 0 to –630 V and back to 0 V. At first, inside the spherical mesh cathode a spherical structure appears, another very weak one surrounds the grid, and one strong appears as a hyperboloid outside the orifice (Fig. 1). Emission spectra of the plasma were recorded using an Ocean Optics HR4000 spectrometer.

### 1.2 Analysis

Optical emission spectroscopy was performed at the centre of the gridded sphere and at the orifice level at –461 V and 0,1 mbar. We noticed similar temperatures in the centre of the plasma and in the orifice, whereas the electron density in the orifice was about three times higher than in the centre.

*Table 1. Electron temperature and plasma densities in gridded sphere (Fig. 1) calculated from Boltzmann plot and Saha equation, respectively:*

| | $T$ [K] | $n_e$ [cm$^{-3}$] |
|---|---|---|
| Centre of sphere | 5939 | $1{,}45 \cdot 10^9$ |
| In the orifice | 6000 | $3{,}56 \cdot 10^9$ |

**References**

[1] C.T. Teodorescu-Soare et al., *Int. J. Mass Spectrometry* 436 (2019) 83-90.
[2] C.T. Konrad-Soare et al., *Plasma Sources Sci. Techn.* 30 (2021), 085006 (9pp).
[3] F. Enescu, C. Ionita, D.G. Dimitriu, R. Schrittwieser, „Space Charge Structures on Smooth Spherical Hollow Electrodes", Poster contribution to this Conference.

# Space Charge Structures on Smooth Spherical Hollow Electrodes

F. Enescu[1], D.G. Dimitriu[2] C. Ionita[1] and R. Schrittwieser[1]

[1] *Institute for Ion Physics and Applied Physics, University of Innsbruck, Austria*
[2] *Faculty of Physics, Alexandru Ioan Cuza University of Iasi, Romania*

Investigations are presented of the formation and behaviour of space charge structures in an Argon discharge plasma on two smooth spherical hollow electrodes of stainless steel. Experiments were conducted at the University of Innsbruck (UIBK) in a cylindrical stainless steel chamber. Comparative investigations were carried out at the Alexandru-Ioan-Cuza University of Iasi (UAIC) (Romania) in a Pyrex vacuum chamber. For diagnostics we have used mainly optical emission spectroscopy to determine plasma density, electron temperature and particle composition.

## 1 Introduction

We have investigated space charge structures generated by two negatively biased spherical hollow electrodes of polished stainless steel with radii of 96 mm each (wall thickness 1 mm), placed at 5 cm distance from each other (surface to surface). These experiments were mainly carried out in a cylindrical vacuum chamber at the Univ. of Innsbruck (UIBK) (inner length and diameter of 92 cm and 53,5 cm, respectively, – the former Innsbruck DP-machine) (see Fig. 1). Comparative investigations were carried out at the Alexandru-Ioan-Cuza Univ. of Iasi (Romania) (UAIC) in a Pyrex vacuum chamber. See also [1,2].

Confer also to the accompanying contribution to this Conference dealing with the results of experiments with one gridded spherical cathode [3].

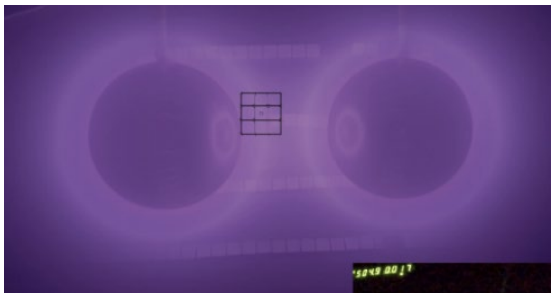


*Fig. 1. The two stainless-steel spheres and discharge around them* for $V = -500$ . *See also quadratic zone from which the spectroscopic data for Fig. 2 were derived.*

The cathodic discharges were created in Argon at 0,1 mbar. Both spheres were simultaneously biased negatively; the best conditions were found for $V = -500$ V for both spheres. For $V = -630$ V a strongly glowing plasma structure is seen around both electrodes simultaneously. Increasing the bias to $V = -396$ V we observe that the structures tend to split, encasing each sphere separately, but approaching each other, and overlapping for $V \cong -290$ V. Reducing the bias $V$ to negative values and re-increasing $V$, the current-voltage characteristic showed strong hysteresis.

### 1.1 Visual observations and analysis

From optical emission spectra electron temperature and density ($T_e$, $n_e$)were deduced from Boltzmann plots as mentioned in [3]. The spectral measurements were carried out at $V \cong -500$ V for both spheres with a current of 17 mA in both circuits. The spectra were evaluated at seventeen points near the LHS sphere as indicated in Fig. 1 by the quadratic zone. This made it possible to construct the two-dimensional $T_e$-profile, (Fig. 2).

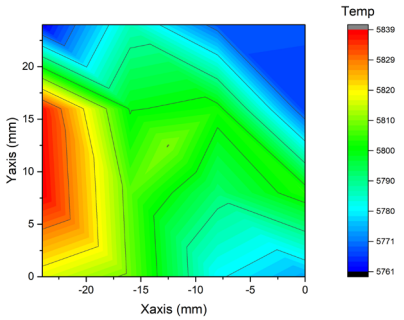



*Fig. 2. Zoomed-in $T_e$-map of the electron temperature determined from the spectra in the quadratic zone indicated in Fig. 1 on the LHS sphere.*

The highest value of $T_e$ was found near the surface of the spheres (Fig. 2, red zone, for $-24 \le X \le -22$ mm and $5 \le Y \le 17$ mm). There the $T_e$ reaches values up to $T_e \cong 5840$ K). However, around $Y \cong 0$, which is actually the region of closest approach between the two spheres, the electron temperature is again lower, even almost on the surface of the sphere ($T_e \cong 5820$ K).

**References**

[1] C.T. Teodorescu-Soare et al., *Int. J. Mass Spectrometry* 436 (2019) 83-90.
[2] C.T. Konrad-Soare et al., *Plasma Sources Sci. Techn.* 30 (2021), 085006 (9pp).
[3] F. Enescu, D.G. Dimitriu, C. Ionita, R. Schrittwieser „Space Charge Structures on Gridded Spherical Hollow Electrodes“, Poster contribution to this Conference.

# Comparison of Calculated Oxygen Thermodynamic Transport Properties with Literature

J. Dycke[1]
[1] *Karlsruhe Institute of Technology, Light Technology Institute, Karlsruhe, Germany*

We report a comparison of thermodynamic transport properties in thermal plasmas between a data set for oxygen acquired by calculation from the NASA CEA-program and literature. The data sets are benchmarked using finite element simulation and the results are used to evaluate for which situations and predictions the calculated data set is valid.

## 1 Introduction

Inductively coupled plasmas (ICP) have been known since the last century and are used in a wide spectrum of applications. Thermal ICPs offer high operating temperatures without the drawback of contamination from electrode materials. This makes them attractive for heating or spheroidization processes, with a high demand on material purity.

In the design process typically, numerical simulations are used, which assume local thermal equilibrium (LTE). Those are based on the curves of the thermodynamic transport properties over the temperature. This data can not be measured directly because the necessary temperature range often extends beyond 20000K. Instead it can be calculated from the interaction of the gas particles following the methods of Chapman and Enskog [1]. Unfortunately, this process is not only extensive and complex, but also requires detailed consideration for each new gas mixture. Thus, literature data for specific mixtures or uncommon operating regimes is hard to come by.

For this reason, we investigated the possibility of using the NASA chemical equilibrium with applications (CEA) program [2]. It can calculate the equilibrium composition and properties of complex gas mixtures as well as that of simple gases at a given pressure. Use of the program in an online interface is open and distributions of the program can be requested from NASA. This makes it an attractive simple to use option for simulation of gas mixtures or gases, where no literature is available. In this case, calculations and comparison are made for pure oxygen at atmospheric pressure.

## 2 Methods

The NASA CEA program calculates thermodynamic and fluid dynamic transport properties of a gas but not the electrical conductivity. Following [3] a simple estimation based on the transport cross sections of the electrons with the different species of the gas is implemented. The results are compared to tabled data from [4]. Both data sets are used to simulate an ICP torch under similar conditions, using COMSOL Multiphysics® as a basis for benchmarking them.

Simulations are carried out under the assumption of LTE, the use of magnetohydrodynamic force equations and the equations for heat transfer in fluids. Particle kinetics are not directly considered but represented by the thermodynamic transport properties over the temperature. The benchmarking is focused on temperature distribution, power input and resulting excitation coil impedance.

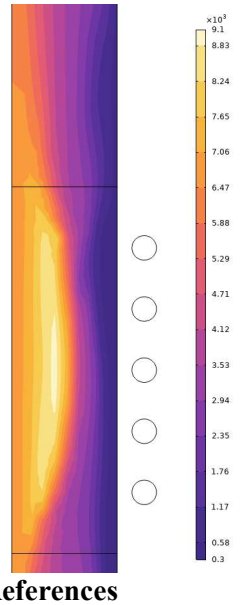



**Figure 1: Isothermal contours of a 2.4 MHz oxygen torch at a total volume flow of 150 L/min and a total power input of around 100 kW.**

**References**

[1] S. Chapman *et al*. The Mathematical theory of non-uniform gases: an account of the kinetic theory of viscosity, thermal conduction and diffusion in gases. *Cambridge Univ. Pr.* (1939)

[2] S. Gordon *et al*. Computer Program for Calculation of Complex Chemical Equilibrium Compositions and Applications. Part 1: Analysis. *NASA Lewis Research Center Cleveland* (1994)

[3] D. I. Yusupov *et al.* High-pressure ignition plasma torch for aerospace testing facilities. *J. Phys.: Conf. Ser.* **774**, 012185 (2016)

[4] M. I. Boulos *et al*. Thermal Plasmas. *Springer US* (1994)

# Diagnostic of DC arc plasmas in aeronautic conditions: application to detection

A. Hellé[1], R. Hugon[1], F. Brochard[1] and G. Marcos[1]

[1] *Université de Lorraine, CNRS, Institut Jean Lamour UMR 7198, Nancy, France*

Understanding the behavior of DC arc plasma and its electrical signature is crucial for detecting arc faults in DC systems. This study presents a detection approach based on the interaction between arc plasma and electrode surfaces, leading to the formation of metal bubbles. Accurately characterizing this phenomenon requires a thorough understanding of arc foot dynamics. Therefore, the second part of this contribution focuses on 3D plasma reconstruction using stereoscopic measurements, enabling a detailed study of arc foot behavior.

## 1 General

Detecting electric arc faults is a critical challenge for the electrification of transportation systems, particularly in the aeronautics sector, as well as for the widespread adoption of DC power systems. The ignition of a DC arc plasma within an electrical system can have severe consequences, releasing significant energy and potentially causing electrical fires. To mitigate this risk, promising detection methods utilize machine learning to identify arc plasma formation within complex cable networks, such as those found in aircraft. However, these methods rely on large, high-quality datasets, which are difficult to build and validate. Enhancing database reliability through a deeper physical understanding of arc behavior or by integrating hybrid detection approaches is therefore essential.

Our approach centers on the strong signal perturbations observed in electrical measurements following arc plasma ignition. By employing advanced plasma diagnostic techniques including fast-camera stereoscopy, optical emission spectroscopy, and electrical measurements, we aim to refine our understanding of arc plasma behavior under aeronautical fault conditions. This will enable the identification of key descriptors and their correlation with plasma dynamics, ultimately leading to more accurate and robust arc fault detection methods.

This approach already enables the correlation of electrical fluctuations with plasma-surface interaction phenomena. The surface of materials in contact with the arc foot undergoes intense energy exchange. The interface between the arc plasma and the electrode is predominantly composed of liquid metal, resulting in specific behaviors that can release material into the plasma and generate detectable electrical disturbances. In this presentation, the correlation between droplet ejection and current peaks will be discussed, along with a deeper understanding of this phenomenon achieved through object-tracking methods [1]. The signature of molten metal bubble explosions has also been identified, and we will demonstrate how it could be utilized for arc fault detection in aeronautic conditions using an initial detection algorithm approach. In order to investigate the dynamics of bubble formation and its connection to plasma-electrode interactions, the behavior of arc plasma has been analyzed using fast-camera stereoscopy and 3D reconstruction (figure 1). These measurements provide valuable insight into plasma-electrode interactions by tracking the movement of the arc foot and the resulting deformation of the plasma column.

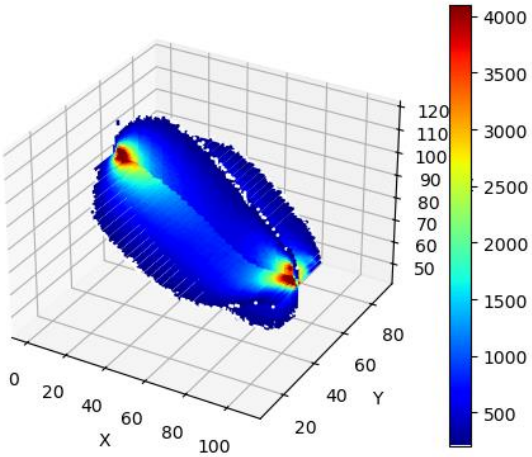



Figure 1: 3D reconstruction of an arc plasma using fast-camera stereoscopy. The color bar represents light intensity encoded in 12 bits.

**Reference**

[1] A. Hellé et al. Dynamics of the material ejection in a dipolar arc in continuous regime. Journal of Physics D: Applied Physics, **57**:425201 (2024).

# Calculation of the Radiative Properties of a Thermal Plasma $H_2O$-Air

Imane. Bendida[1,2], Yann. Cressault[1], Bachir. Liani[2] and Flavien. Valensi[1]

[1] *LAPLACE, University of Toulouse , CNRS, INPT, UPS, Toulouse, France*
[2] *LPT, University of Tlemcen, Tlemcen, Algeria*

The calculation of radiation emitted by thermal plasmas is a highly complex problem due to temperature gradients, species densities, and its intricate distribution. Moreover, it does not depend solely on spectral frequency, temperature, and the geometry of the medium.

Solving the radiative transfer equation is a fundamental approach to determining radiative flux, absorption, and emission within a plasma. Until recent years, the numerical treatment of radiative transfer has relied on simplifying assumptions whose validation has not always been justified.

The Net Emission Coefficient (NEC) represents a geometric simplification of the radiative transfer equation. In this work, we have calculated the NEC for a thermal plasma composed of $H_2O$-air mixtures at atmospheric pressure, over a temperature range from 300 K to 30,000 K, for various plasma thicknesses between 0 and 1 mm, under the assumption of local thermodynamic equilibrium. Through spectral simplification, the Mean Absorption Coefficients (MACs) divide the frequency range into several spectral intervals in which the total absorption is assumed to be constant. We present the calculated MACs for the $H_2O$-air mixture, considering multiple definitions of the mean coefficient as well as different spectral intervals, as a function of temperature, pressure, and plasma thickness.

# Evaluation of Plasma Fluctuation Using Stochastic Model Based on Relative Entropy

Y. Shimada[1,2] and H. Akatsuka[1]

[1] *Institute of Science Tokyo, 2-12-1, O-Okayama, Meguro-ku, Tokyo, 152-8550, Japan*
[2] *Kanagawa Prefectural Police Headquarters, Yokohama, Kanagawa, 236-0051, Japan*

New evaluation method is proposed using stochastic model for prediction of plasma fluctuation based on collisional-radiative model. Electron impact excitation of atoms is considered as a Wiener process, which is applied to analyze variation in excited-level populations in short time by Malliavin derivative. Relative entropy and fractional Brownian motion are introduced as indicators to evaluate how far a system is from its steady state, where both trend of entropy and contribution of radiative processes to the lifetime of excited states are taken into account. The high statistical weight of some excited states may act as a bottleneck in the energy relaxation throughout the system to a steady state.

Plasma fluctuations have been focused on as transient behavior in low-temperature plasmas. Analysis of excited states in plasmas has focused on the time change in number density, and collisional radiative (CR) models have been applied. In this study, the entropy generation rates of the excited states are being investigated at each level by using Malliavin analysis, based on sensitivity of temporal fluctuations in plasmas [1]. Now let $N_p$ be the number densities of $p$-th excited level with the ground-state density $N_1$, and consider temporal evolution of the excited-state density vector $\boldsymbol{N} = (N_2, N_3, \ldots, N_M)$ in non-equilibrium plasmas. In this study, $N_p$ is assumed to be described as summation of a term of the time-dependent general solution and a term expressed by the Wiener process as time-indepedent fluctuation. The time evolution of $\boldsymbol{N}(t)$ is approximately equivalent to the Malliavin derivative $D_t$. This approach is adopted when excluding the particular solution pertaining to the steady states:

$$\frac{\mathrm{d}N_p}{\mathrm{d}t} \sim D_t N_p(t) = -\xi_p N_p(t), \tag{1}$$

where $\xi_p$ corresponds to a differential coefficient for the Wiener process as random fluctuation. On the other hand, including the above fluctuating component, the CR model allows us to describe the population vector as

$$\frac{\mathrm{d}\boldsymbol{N}}{\mathrm{d}t} = \boldsymbol{a}\boldsymbol{N} + \boldsymbol{\xi}\boldsymbol{N} + \boldsymbol{\delta}, \tag{2}$$

where $\boldsymbol{a}$ is the collisional radiative matrix and $\boldsymbol{\delta}$ denotes the sum of recombination term and direct excitation from the ground state. For the steady state, the LHS of Eq. (2) equals zero. Hence, the straightforward expression for $\boldsymbol{N}$ is obtained as

$$\boldsymbol{N}(t) = -\boldsymbol{a'}^{-1}\boldsymbol{\delta}, \tag{3}$$

where $\boldsymbol{a'}$ consists of a sum of each matrix element of $\boldsymbol{a}$ and $\boldsymbol{\xi}$.

By employing the relative entropy method that analyzes non-adiabatic entropy, transient plasma behavior can be described through the CR model. The relative entropy $\sigma_{na}$ is formulated using following equation, which involves the time derivative of the Kullback-Leibler divergence.

$$\sigma_{na} = k \sum_{x,x'} W_{x,x'} P(x',t) \ln \frac{P^{SS}(x,\tau)P(x',t)}{P(x,t)P^{SS}(x',\tau)}, \tag{4}$$

where $k$ donotes the Boltzmann constant, $P(x,t)$ is the distribution function at time $t$, $P^{SS}(x,t)$ is that in the steady state, $W_{x,x'}$ is a state transition matrix, which, by heat exchange with a heat bath, corresponds to $\boldsymbol{a'}^{-1}\boldsymbol{\delta}$. The logarithm term in the summation on Eq. (4) can be interpreted as the weight of each transition rate, which is to be defined as $I(x,x')$. An example of the calculated value of $I$ is shown in Fig. 1 for argon excited states. This indicates that the parameter $I$ can be interpreted as an indicator to evaluate how far the level is from its steady state [2].

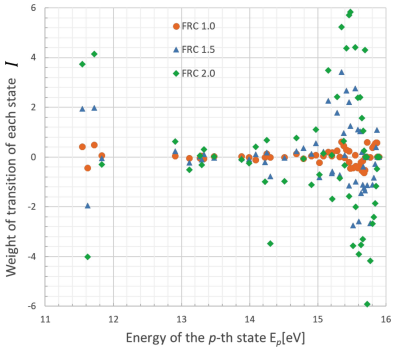



Figure 1: Non-adiabatic entropy weights $I$ for $T_\mathrm{e} = 1$ eV, $N_\mathrm{e} = 10^9$ cm$^{-3}$, $T_\mathrm{g} = 500$ K, pressure 133 Pa [2].

## References

[1] Shimada, Y. and Akatsuka, H. *Jpn. J. Appl. Phys.*, **63**, 05SP02 (2024).
[2] Shimada, Y. and Akatsuka, H. *Entropy*, **26**, [9], 782 (2024).

# Two-temperature modelling of ignition of high-current arc discharges on cold cathodes in atmospheric-pressure argon

D. F. N. Santos[1,2], M. D. Cunha[1,2], I. Stepanov[1,2] and M. S. Benilov[1,2]

[1]*Departamento de Física, Universidade da Madeira, 9000 Funchal, Portugal*
[2]*Instituto de Plasmas e Fusão Nuclear, Instituto Superior Técnico, 1041 Lisboa, Portugal*

This paper presents a study on the ignition of high-current arc discharges on cold cathodes in atmospheric-pressure argon using a two-temperature (2T) model. Results of the modelling of the quasi-stationary current increase from 1 mA to 200 A are reported. Three distinct modes of current transfer have been observed in the modelling: a glow-like mode, a mode with a hot arc spot on the cathode surface, and a diffuse mode with a uniformly hot cathode tip with the temperature around 3500 K.

## 1 Introduction

The study of high-current arc discharges, particularly the ignition phase on cold electrodes, is crucial for various industrial applications. Experimental investigations of these phenomena are often challenging due to the small spatial and temporal scales involved, as well as the extreme conditions typical of arc discharges. Therefore, numerical modelling plays a vital role in providing insights into the underlying physics.

In [1], the glow-to-arc transition in atmospheric-pressure argon was studied using a unified fully non-equilibrium description of the plasma in the discharge gap in the range of arc current $I$ up to 20 A. The aim of this work is to study $I$ up to 200 A. Since the unified description becomes impractical for high currents, a 2T ionization-equilibrium model is used.

## 2 Model and results

The model comprises mass and momentum conservation equations for the arc plasma, energy conservation equations for the heavy particles and the electrons, and a current continuity equation supplemented with a generalized Ohm's law. Ionization equilibrium is assumed. The interface between the 2T ionization-equilibrium plasma and the cathode is described by the model [2].

An atmospheric-pressure argon arc with a rod tungsten cathode and a plane water-cooled copper anode is studied. Results reported here refer to quasi-stationary variations of current $I$ across the range 1 mA to 200 A. Results concerning the cathodic part of the arc are shown in Fig. 1. Three distinct modes of current transfer are seen. The first one is a glow-like mode, which occurs for $I$ not exceeding a few hundred milliamps and is characterized by low temperatures of the cathode surface. The second one

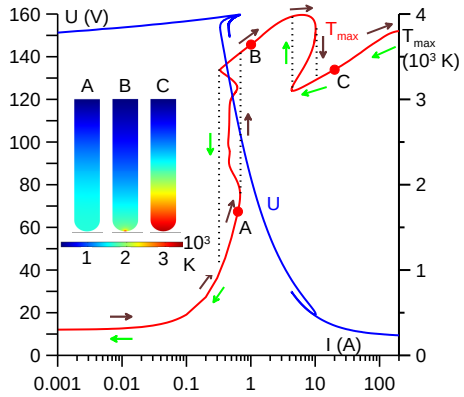



**Fig. 1.** The near-cathode voltage-drop and the maximum temperature of the cathode surface.

is a mode with a hot arc spot on the cathode surface, which occurs in the current range from a few hundred milliamps to a few amps and is characterized by the existence of a very hot (up to approximately 4000 K) small arc spot on the cathode surface, while the rest of the cathode surface is cold. The third one is a diffuse mode, which occurs for $I$ exceeding a few amps and is characterized by a uniformly hot cathode tip with the temperature around 3500 K. The transitions between these three modes are accompanied by hysteresis.

The transition between the first and second modes is a quasi-stationary glow-to-arc transition. The transition between the second and third modes is the well-known spot-diffuse transition on an arc cathode; e.g., review [3].

The work was supported by FCT of Portugal under Project Nr. IPFN/UID/50010/2025.

### References

[1] Saifutdinov, A. I. *Plasma Sources Scil Technol* **31** 094008 (2022).
[2] Santos, D. F. N. et al. *J Phys D: Appl Phys* **57** 405202 (2024).
[3] Benilov, M. S. *J Phys D: Appl Phys* **41** 144001 (2008).

# Program of Poster Session #4

| # | In Competition | Title | Speakers | Topic |
|---|---|---|---|---|
| F-1 | NO | Research on nonlinear phenomena concerning chaos control and synchronization in ionization waves | Fukuyama Takao | Collective and nonlinear phenomena |
| F-2 | NO | Unstable rotation of nanoparticles in conventional DC magnetron discharges | Arnas Cécile | Complex and dusty plasmas, ion-ion plasmas, mixed phase plasmas |
| F-3 | NO | Self-consistent simulation of nano dust with PLASIMO | Mihailova Diana | Complex and dusty plasmas, ion-ion plasmas, mixed phase plasmas |
| F-4 | NO | Investigation of carbon particles in the dusty plasma of a DC glow discharge | Ongaibergenov Zhanserik | Complex and dusty plasmas, ion-ion plasmas, mixed phase plasmas |
| F-5 | YES | Effect of Precursor Gas Molecules on the Deposition Characteristics of Hydrogenated Amorphous Carbon Films by Plasma Chemical Vapor Deposition | Ohara Shunpei | Elementary processes and fundamental data |
| F-6 | YES | Breakdown elementary mechanisms within controlled nanometer scale electrode gaps | Disson Baptiste | Elementary processes and fundamental data |
| F-7 | NO | Formation of electrodeless double-headed streamers (DHS) at sub-breakdown conditions | Disson Baptiste | Elementary processes and fundamental data |
| F-8 | NO | Notes on fluid and kinetic descriptions of the development of striations in the positive column plasma of rare gases | Boeuf Jean-Pierre | Elementary processes and fundamental data |
| F-9 | NO | Striations of the positive column in radiofrequency and direct current argon plasmas – Experiments and particle simulations | Dosbolayev Merlan | Elementary processes and fundamental data |

| # | In Competition | Title | Speakers | Topic |
|---|---|---|---|---|
| F-10 | YES | Improving the optical emission in the visible spectrum of CO2 streamers with trace Xe | Meekes Wouter | Elementary processes and fundamental data, High frequency and pulsed discharges, Plasma diagnostics methods |
| F-11 | NO | Experimental comparative study of the dc and ten-nanosecond electrical breakdown in air for flat and sharp electrodes | Demidov Vladimir | High frequency and pulsed discharges |
| F-12 | YES | On the Control and Design of Nanosecond Plasma Jets for Optimized Therapeutic Efficiency | Billeau Jean-Baptiste | High frequency and pulsed discharges |
| F-13 | NO | Rapid decomposition of bisphenol-A in water with pulsed arc discharge for developing novel wastewater Treatment Methods | Sasaki Mitsuru | High pressure and thermal plasma processing |
| F-14 | NO | Child–Langmuir law applicability for a cathode sheath description of dc glow discharge in acetylene | Lisovskiy Valeriy | Low pressure plasmas |
| F-15 | NO | Spatial variation of electron/ion heating mechanisms in Capacitively Coupled Discharges (CCDs) | Sharma Anuravi | Low pressure plasmas |
| F-16 | NO | Impact of non-equilibrium plasma treatment on selected properties of bovine milk | Pawlat Joanna | Medical, biological, environmental and aeronautical applications |
| F-17 | NO | In vivo tests of medical implant coatings deposited by plasma-activated reactive magnetron sputtering | Lisovskiy Valeriy | Medical, biological, environmental and aeronautical applications |
| F-18 | NO | Reactive species variation in gas and liquid phase irradiated through pulse modulated atmospheric pressure sub-RF plasma jet | Basu Mallick Aishik | Medical, biological, environmental and aeronautical applications |
| F-19 | NO | Effect of CO2 to CO conversion on bacteria and fungi inoculated onto the coat of wheat seed packed in a dielectric barrier discharge | El Shaer Mohamed | Medical, biological, environmental and aeronautical applications |

| # | In Competition | Title | Speakers | Topic |
|---|---|---|---|---|
| F-20 | YES | Plasma-Treated Soil for Sustainable Agriculture: Pesticide Removal, Enhanced Porosity, and Water Retention | Jangra Sushma | Medical, biological, environmental and aeronautical applications |
| F-21 | YES | Air atmospheric pressure plasma, a green approach for the sanitation of leafy greens vegetables | Aliyeva Zhanel | Medical, biological, environmental and aeronautical applications |
| F-22 | NO | Effects of high overvoltages on the treatment of PFAS in water | Brisset Alexandra | Medical, biological, environmental and aeronautical applications |
| F-23 | NO | Effects of cold plasma treatment on bio-chemical composition of argan kernel and oil (Argania Spinosa (L.) Skeels) | Saber Karim | Medical, biological, environmental and aeronautical applications |
| F-24 | NO | Plasma-enhanced bio-inspired photocatalytic fabrics for efficient micropollutant removal from wastewater | Tomas Homola | Medical, biological, environmental and aeronautical applications |
| F-25 | YES | Enhancing corrosion resistance of magnesium alloys with plasma treatment and electrospun biodegradable polymer coatings | Zahedi Leila | Medical, biological, environmental and aeronautical applications |
| F-26 | NO | Boundary Condition for the electron kinetics of a plasma using the microphysics of the wall | Willert Felix | Modelling and simulation techniques |
| F-27 | NO | MERLIN, an adaptative LTE radiative transfer model for any mixture | Favre Aurélien | Modelling and simulation techniques |
| F-28 | NO | Simulations of radio frequency capacitively coupled plasmas including external circuits | Yu Shimin | Modelling and simulation techniques |
| F-29 | NO | Discharge behaviour and chemistry of cold plasma jets | Murakami Tomoyuki | Modelling and simulation techniques |
| F-30 | NO | High-order gyrocoordinate transformations for electron dynamics in axisymmetric magnetic fields | Brinkmann Ralf Peter | Modelling and simulation techniques |

| # | In Competition | Title | Speakers | Topic |
|---|---|---|---|---|
| F-31 | NO | Comparison of 3D fluid and particle models for negative streamers in eco-friendly insulation gases. | Smits Thomas | Modelling and simulation techniques |
| F-32 | NO | Numerical Simulation of Partial Discharge Processes in Defects of Insulating Material | Gao Yuting | Modelling and simulation techniques |
| F-33 | NO | Mode Transitions in Micro Cavity Plasma Arrays: The Influence of Oxygen Admixtures on Discharge Dynamics | Steuer David | Non-equilibrium plasmas and microplasmas at high pressure |
| F-34 | NO | On the measurements of temperature by optical emission spectroscopy in nanosecond SDBD: check by calculations | Kreyder Geoffrey | Non-equilibrium plasmas and microplasmas at high pressure |
| F-35 | NO | How to obtain a Diffuse Dielectric Barrier Discharge in various molecular gases? | Naude Nicolas | Non-equilibrium plasmas and microplasmas at high pressure |
| F-36 | NO | Plasma-Catalytic Dry Reforming of Methane: on the Role of a Ni Catalyst at Room Temperature | Garcia Maria C | Non-equilibrium plasmas and microplasmas at high pressure |
| F-37 | NO | Study on DBD regimes in dry and wet air to produce ozone and nitrogen oxides | Stepanova Olga | Non-equilibrium plasmas and microplasmas at high pressure |
| F-38 | NO | Effect of H2O on the conversion of CH2O in a micro-capillary He plasma at atmospheric pressure | Gady Adrien | Non-equilibrium plasmas and microplasmas at high pressure |
| F-39 | NO | Optical radiation upon excitation of the Ar-N2 mixture by the products of the 6Li(n,$\alpha$)3H nuclear reaction | Khassenov Mendykhan | Non-equilibrium plasmas and microplasmas at high pressure |
| F-40 | NO | LIBS (Laser-Induced Breakdown Spectroscopy) applications for the Tritium measurement in tokamak plasma-facing components | Bultel Arnaud | Other applications such as low temperature plasma applications for magnetically confined fusion |

| # | In Competition | Title | Speakers | Topic |
|---|---|---|---|---|
| F-41 | NO | Towards time-resolved measurements for solvated electrons at the plasma/liquid interface | Light Adam D. | Plasma diagnostics methods |
| F-42 | YES | Towards calibration of picosecond O-TALIF | Shu Zhan | Plasma diagnostics methods |
| F-43 | NO | Imaging electric fields for cold plasma interacting with silica powders for catalysis applications | Munday Jack | Plasma diagnostics methods |
| F-44 | YES | Multielemental quantification by CF-LIBS assisted by an attention deep learning model trained on simulated spectra | Lemerle Luisa | Plasma diagnostics methods |
| F-45 | NO | Robust Emissive Probes for Hot Plasmas | Schrittwieser Roman | Plasma diagnostics methods |
| F-46 | NO | Effect of target on NO production in a kHz cold argon plasma jet measured by LIF | Shuai Zhao | Plasma diagnostics methods |
| F-47 | YES | Gas temperature distribution of atmospheric Argon glow discharge measured by Mach-Zehnder interferometer | Kimura Ren | Plasma diagnostics methods |
| F-48 | NO | Improvement of gas detection sensitivity of a self plasma-optical emission spectrometer | Kim Dae-Woong | Plasma diagnostics methods |
| F-49 | NO | Spectroscopy plasma characterization in an EM cavity in view of a Massive Open Online Laboratory | Fernandes Horacio | Plasma diagnostics methods |
| F-50 | NO | Probing aqueous | Polprasarn Kasidapa | Plasma diagnostics methods |
| F-51 | NO | 2D Measurement on single-filament dielectric barrier discharge by electric-field induced second harmonic generation | Wang Jianan | Plasma diagnostics methods |
| F-52 | YES | AI-Driven Langmuir and Cutoff Probe Diagnostics for Improved Data Consistency | Ko Jeonghun | Plasma diagnostics methods |

| # | In Competition | Title | Speakers | Topic |
|---|---|---|---|---|
| F-53 | NO | Three-dimensional characterization of the liquid surface deformation resulting from a pin-water discharge using free-surface synthetic Schlieren | Dyson Fredric | Plasma in/with liquids |
| F-54 | YES | Experimental and numerical study of CO2 discharges in contact with liquid water | Bois Sophie | Plasma in/with liquids |
| F-55 | NO | Fast Electron Promoting Geometry for Plasma Enhanced Thermionic Generators | Aleksander Clark | Plasma power and pulsed power technology, particle and radiation sources |
| F-56 | YES | Analysis of the correlation between TEOS plasma characteristics and $SiO_2$ thin film properties | Sato Yushi | Plasma processing of surfaces and particles |
| F-57 | NO | Understanding CF4/H2-based cryogenic etching mechanisms by monitoring radical densities with extended optical actinometry technique | Mo Michael | Plasma processing of surfaces and particles |
| F-58 | NO | Polymerization of EDOT into soluble PEDOT analogue by plasma inside bubble | Kaneko Yutaka | Plasma processing of surfaces and particles |
| F-59 | NO | High power impulse magnetron sputtering of a chromium target | Gudmundsson Jon Tomas | Plasma wall interactions, electrode and surface effects |
| F-60 | YES | Investigating early-stage helium-tungsten interactions: Retention and vacancy defects characterization | Alfazzaa Mounir | Plasma wall interactions, electrode and surface effects |
| F-61 | NO | Development and Investigation of a Miniature Pulsed Plasma Thruster Using Graphite Propellant | Suleimenova Assel | Plasma wall interactions, electrode and surface effects |
| F-62 | NO | Self-regulation in high-power impulse magnetron sputtering discharges and its effect on the metal ion escape | Gudmundsson Jon Tomas | Plasma wall interactions, electrode and surface effects |
| F-63 | NO | Effect of ion energy and magnetic shear on suprathermal ion transport in X-point plasmas in TORPEX | Sepulchre Cyrille | Thermodynamics and transport phenomena |

| # | In Competition | Title | Speakers | Topic |
|---|---|---|---|---|
| F-64 | NO | Discussion on the Definition of Excitation Temperature of Weakly Ionized Plasmas in a Non-equilibrium State | Akatsuka Hiroshi | Thermodynamics and transport phenomena |
| F-65 | NO | Study of the transport and optical properties of WDM taking into account local field correction | Kodanova Sandugash | Thermodynamics and transport phenomena |
| F-66 | NO | Plasma deposition of III-V semiconductors: sputtering and RPVPE approaches | Ouaras Karim | Low pressure plasmas |

# Presenter Index


- **Akatsuka Hiroshi**: F-64
- **Aleksander Clark**: F-55
- **Alfazzaa Mounir**: F-60
- **Aliyeva Zhanel**: F-21
- **Arnas Cécile**: F-2
- **Basu Mallick Aishik**: F-18
- **Billeau Jean-Baptiste**: F-12
- **Boeuf Jean-Pierre**: F-8
- **Bois Sophie**: F-54
- **Brinkmann Ralf Peter**: F-30
- **Brisset Alexandra**: F-22
- **Bultel Arnaud**: F-40
- **Demidov Vladimir**: F-11
- **Disson Baptiste**: F-6, F-7
- **Dosbolayev Merlan**: F-9
- **Dyson Fredric**: F-53
- **El Shaer Mohamed**: F-19
- **Favre Aurélien**: F-27
- **Fernandes Horacio**: F-49
- **Fukuyama Takao**: F-1
- **Gady Adrien**: F-38
- **Gao Yuting**: F-32
- **Garcia Maria C**: F-36
- **Gudmundsson Jon Tomas**: F-59, F-62
- **Jangra Sushma**: F-20
- **Kaneko Yutaka**: F-58
- **Khassenov Mendykhan**: F-39
- **Kim Dae-Woong**: F-48
- **Kimura Ren**: F-47
- **Ko Jeonghun**: F-52
- **Kodanova Sandugash**: F-65

- **Kreyder Geoffrey**: F-34
- **Lemerle Luisa**: F-44
- **Light Adam D.**: F-41
- **Lisovskiy Valeriy**: F-14, F-17
- **Meekes Wouter**: F-10
- **Mihailova Diana**: F-3
- **Mo Michael**: F-57
- **Munday Jack**: F-43
- **Murakami Tomoyuki**: F-29
- **Naude Nicolas**: F-35
- **Ohara Shunpei**: F-5
- **Ongaibergenov Zhanserik**: F-4
- **Ouaras Karim**: F-66
- **Pawlat Joanna**: F-16
- **Polprasarn Kasidapa**: F-50
- **Saber Karim**: F-23
- **Sasaki Mitsuru**: F-13
- **Sato Yushi**: F-56
- **Schrittwieser Roman**: F-45
- **Sepulchre Cyrille**: F-63
- **Sharma Anuravi**: F-15
- **Shu Zhan**: F-42
- **Shuai Zhao**: F-46
- **Smits Thomas**: F-31
- **Stepanova Olga**: F-37
- **Steuer David**: F-33
- **Suleimenova Assel**: F-61
- **Tomas Homola**: F-24
- **Wang Jianan**: F-51
- **Willert Felix**: F-26
- **Yu Shimin**: F-28
- **Zahedi Leila**: F-25

# Research on nonlinear phenomena concerning chaos control and synchronization in ionization waves

Takao Fukuyama

*Faculty of Education, Nagasaki University, 1-14 Bunkyo-machi, Nagasaki, 852-8521, Japan*

Nonlinear phenomena such as chaos and limit-cycle are observed in the time evolution of the intensity of ionization waves appeared in a positive column under a glow discharge in a laboratory plasma. When the time-delayed feedback method proposed by Pyragas was applied to oscillations exhibiting chaos, and the chaos was periodized. Conversely, when the same feedback was applied to periodic oscillations exhibiting limit-cycle, the limit-cycle underwent intermittency and transitioned to a chaotic state. Furthermore, it is found that a peculiar phenomenon called the devil's staircase appears in ionization waves, and that type-I intermittency exists, based on chaos theory.

## 1 Background

Ionization waves (propagation of wavefronts due to ionizing collisions with neutral particles) observed in the positive column of plasma generated under glow discharge are used as an experimental medium for nonlinear scientific research. The system can be controlled by the discharge current value, and various nonlinear oscillations such as chaos and limit-cycles are observed as patterns of light emission intensity from ionization wave.

We report on progress in experimental research on the control of chaos observed in ionization waves, on the excitation of chaos by applying feedback to limit-cycles, and on the synchronization of chaos by applying periodic external forces to it.

## 2 Experiments and results

A series of experiments are performed by generating ionization waves in a vacuum discharge tube. Typical electron and ion temperatures are 10 eV and 0.025 eV, respectively.

First, we report the results of chaos control using the time-delayed feedback method (Pyragas method). As shown in Fig. 1, a time series exhibiting a chaotic state can be controlled to a periodic state by the application of feedback [1].

Second, it is found that applying time-delayed feedback to limit-cycle oscillations (periodic oscillations) in ionization waves results in a transition to an intermittent chaotic state with bursts appearing in the laminar [1], as shown in Fig. 2, with the applied voltage as a parameter.

Third, a structure called the devil's staircase is discovered in which a periodic electric field as external force is applied to ionization wave that exhibit a chaotic state, and the waves are synchronized, repeating synchronization and desynchronization [1], as shown in Fig. 3.

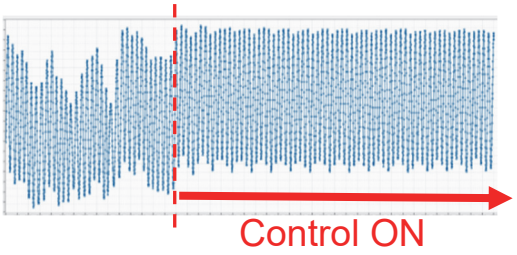



Fig. 1 Time series of chaos control by Pyragas method.

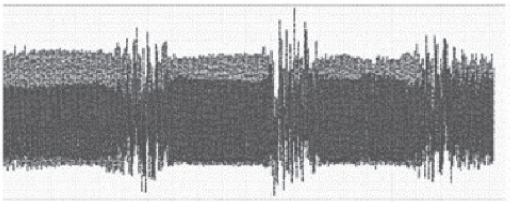


Fig. 2 Time series of intermittency caused by feedback.

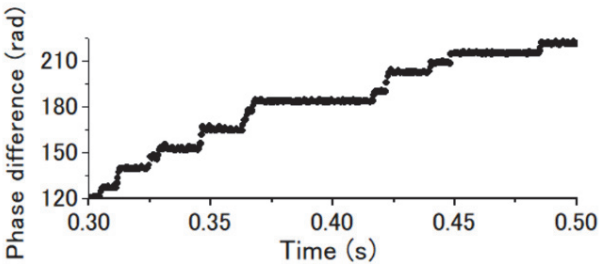



Fig. 3 Devil's staircase observed in ionization waves.

**Acknowledgments**

The author is grateful to Professor Dr. Nobuya Hayashi of Kyushu University for continuous warm support. This study was supported by the JSPS KAKENHI (Grant Number JP23K03355).

**References**

[1] See the list of papers in the following website: https://researchmap.jp/fukuyama-takao?lang=en

# Unstable rotation of nanoparticles in conventional DC magnetron discharges

M. Chekired, L. Couedel and C. Arnas

*Aix-Marseille Université, CNRS, PIIM, 13397 Marseille, France*

DC magnetron discharges with an aluminum cathode operating at pressures of 0.3-0.5 mbar are produced to generate nanoparticles from cathode sputtering. Under specific conditions, the rotation of the nanoparticle clouds is observed radially. These nanoparticle clouds exhibit complex patterns with the appearance of filaments, various stratifications and spatial modulations in the region of the last magnetic arches.

## 1 Introduction

Magnetron sputtering discharges are used at low pressure for etching and deposition of thin films for industrial applications. They operate with moderate magnetic fields where electrons are fully magnetized while ions are not or weakly magnetized. Electron confinement is efficient in the region where the cross fields ExB exist, B being the magnetic field due to permanent magnets and E, the electric field of the cathode sheath mainly and presheath. The cross fields generate a Hall current in the azimuthal direction of cylindrical symmetry devices. The resulting partially magnetized plasma is the place of instabilities early studied in DC magnetron plasmas from fluctuations of a Langmuir probe (LP) [1] and in HiPIMS with a LP array [2]. Light rotating structures called spokes were studied with fast cameras and photomultipliers in HiPIMS [3] and RF magnetron discharges [4].

In the present study, DC magnetron discharges operating at higher pressure than usual are produced to favor collisions between sputtered atoms giving rise to metallic clusters that grow until nucleation [5]. Under specific discharge conditions, the rotation of the nanoparticle clouds can be evidenced in lateral (radial) directions. They present complex patterns in the region of the last magnetic arches.

## 2 Experiments

Experiments are performed using an aluminium cathode of 3’ diameter. A grounded anode ring is placed all around. The Ar pressure is in the range of 0.3-0.5 mbar and the discharge current in the range of 400-500 mA. Scanning electron microscopy (SEM) allows to measure the sizes of the produced Al nanoparticles (NPs) collected on the anode at the end of the experiment. A cylindrical LP is used to measure the plasma parameters in regions where the magnetic field is weak enough to be neglected. A camera aiming the plasma radially, allows the direct visualization of the NP cloud to study the NP cloud azimuthal rotation.

## 3 Results

Langmuir probe measurements show that the electron temperature is quite low compared to typical argon discharges (around 0.9 eV) confirming the influence of sputtered Al atoms on the plasma parameters [6]. SEM measurements reveal two types of NPs: spherical and polyhedral particles with diameter up to ~150 nm when the plasma duration is less than 60 s. Video images show that under specific conditions the NP cloud can rotate counter clockwise. The cloud motion is visible with the naked eye and exhibits very complex patterns with filaments, various stratifications and spatial modulations in the region of the last magnetic arches (few centimeters from the cathode). This NP transport highlights the azimuthal plasma rotation. The observed “turbulent” nature should be the result of a competition between the usual forces applied on them in the rotating plasma such as the electric force, the ion drag and thermophoretic forces.

**References**

[1] E. Martines et al. Experimental investigation of low-frequency waves propagating in a DC planar magnetron plasma, *Phys. Plasmas* **11**, 1938 (2004)

[2] D. Lundin et al. Anomalous electron transport in HiPIMS. *Plasma Sci. Technol.* **17**, 025007 (2008)

[3] J. Winter et al. Instabilities in HiPIMS plasmas: from stochasticity to periodicity, *J. Phys. D: Appl. Phys.* **46**, 084007 (2013).

[4] M. Panjan et al. Self-organizing plasma behavior in RF magnetron sputtering discharges, *J. Appl. Phys.* **125**, 203303 (2019)

[5] C. Arnas et al. Forces applied to nanoparticles in magnetron discharges and the resulting size segregation, *Phys. of Plasmas* **29**, 073703 (2022).

[6] S. Mitic et al. Diagnostics of a high-pressure DC magnetron argon discharge with an aluminum cathode, *Eur. Phys. J. D* **75**, 240 (2021)

# Self-consistent simulation of nano dust with PLASIMO

D. Mihailova[1], K. van 't Veer[1], J. Janssen[1], W.Graef[1], R. Budé[1] and J. van Dijk[2]

[1] *Plasma Matters B.V., Eindhoven, The Netherlands*
[2] *Eindhoven University of Technology, Eindhoven, The Netherlands*

In order to simulate the transport of nano dust particles under plasma conditions, PLASIMO's particle tracker is being coupled to its drift-diffusion module. In this contribution we present preliminary results of this effort and provide an outlook to future work.

## 1 Introduction

In many plasma applications dust particles are critical sources of contamination that can deteriorate the product quality and lower the productivity of the manufacturing process. For example, in the semiconductor industry dust particles can lead to a yield loss of 100% if they land on the reticle of extreme ultra-violet (EUV) lithography systems.

A fundamental understanding of the formation, growth and transport of dust is of great importance for the control and minimization of contamination and for the successful and efficient deployment of nano-dusty plasma technologies.

Numerical plasma modeling of nano dust is a powerful tool that can help not only the research community for fundamental studies and interpreting experimental observations; it can also serve industry to answer technological questions promptly, cheaply and inspire the development of new plasma technologies.

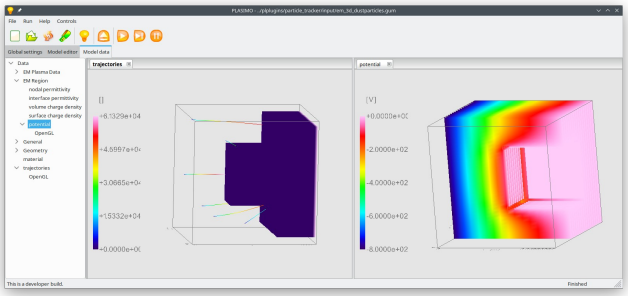
## 2 Model description

PLASIMO's [1, 2] particle tracker module calculates an electric field and follows the motion of a collection of test particles in that electric field. The electrostatic fields are calculated from the Poisson equation, based on user-specified applied voltages on the electrode materials.

The particle tracker module can be self-consistently coupled to a fluid plasma description in a hybrid simulation. The plasma module describes the evolution of the species by solving the particle balance, the momentum balance in drift-diffusion approximation and the electron energy balance equations. The electron energy distribution function is obtained from the built-in BOLSIG+ library [2] to calculate the electron transport coefficients and rate coefficients for the electron-impact reactions. These equations are coupled with the Poisson equation for the computation of the electric field.

## 3 Preliminary results

The figure below shows the trajectories of test particles (left) under the influence of a potential distribution (right). Present work aims at the bi-directional coupling of this functionality to PLASIMO's drift-diffusion module. Results of this effort will be presented.



## 4 Outlook

The model will be used to simulate the behavior of nano-size dust particles in low pressure argon plasma in parallel plate configuration. Results will be compared with experiments on this system that will be done at Eindhoven University of Technology.

**Acknowledgements**
This work is supported by the Chips Joint Undertaking and its members, including the top-up funding by RVO.

**References**

[1] https://plasma-matters.nl
[2] J. van Dijk, K.S.C. Peerenboom, M. Jimenez-Diaz, D.B. Mihailova and J.J.A.M. van der Mullen, *Journal of Physics D: Applied Physics*, **42**, 194012-1/14 (2009)
[3] G. J. M. Hagelaar and L. C. Pitchford, Solving the Boltzmann equation to obtain electron transport coefficients and rate coefficients for fluid models, *Plasma Sources Sci. Technol.* **14**, 722-733 (2005).

# Investigation of carbon particles in the dusty plasma of a DC glow discharge

Z. Onaibergenov[1,2], A. Utegenov[1,2] and A. Abdrakhmanov[1,2]

[1]*Al-Farabi Kazakh National University, Almaty, Kazakhstan.*
[2]*Institute of Applied Science and Information Technologies, Almaty, Kazakhstan*

In this paper, we present experimental results on the study of the characteristics of carbon nanoparticles synthesized in dusty plasma. Ar/C2H2 gas mixtures were used as the source of the dust component in the plasma medium. According to the experimental results, it was found by scanning electron microscope (SEM) that the size of the synthesized nanoparticles is within 100 nm. In addition, the results of the (XPS) analysis showed that the particles have a more amorphous and oxidized structure. EDAX confirmed the elemental composition, as well as the presence of carbon in the synthesized nanoparticles.

Dusty plasma, or complex plasma, as it is also called, is an ionized gas containing dust particles from nano to micro sizes. The study of dusty plasma began in the 1980s, and since then, scientists have begun to study the effect of micron-sized particles on plasma properties. The key moment was the discovery in 1986 of a phenomenon that was later called "plasma crystals" – ordered structures of dust particles formed in plasma under the influence of electrical and interparticle interactions [1,2]. Micron-sized particles are often exposed to gravity in laboratory conditions, which prevents the formation of a plasma crystal due to the gravitational effects. In this regard the "Plasma Kristall" experiments have been establishing on the board of ISS in order to prevent the gravity influence on the structural properties of the dusty plasma. The use of nanoparticles in laboratory conditions has become a solution in the study of dusty plasma in order to create volume bulk dust structure. Nanoparticles are synthesized by introducing precursor gases such as acetylene, methane, silane, etc. into plasma [3,4].

In this work, the properties of carbon nanoparticles synthesized in a DC glow discharge plasma using acetylene as a precursor were investigated. The size and morphological properties of the synthesized nanoparticles were evaluated using SEM. The average size of the synthesized nanoparticles was about 100 nm. The thickness of the films was also estimated using an atomic force microscope. The elemental composition of the nanoparticles was determined using EDAX. The density of the present elements and the chemical state of the surface of the nanoparticles were determined using X-ray photoelectron spectroscopy (XPS).

By controlling the plasma parameters such as pressure, gas flow, source power, and average temperature, it is possible to control the kinetics of nanomaterial growth, which makes it possible to obtain nanomaterials with specified properties.

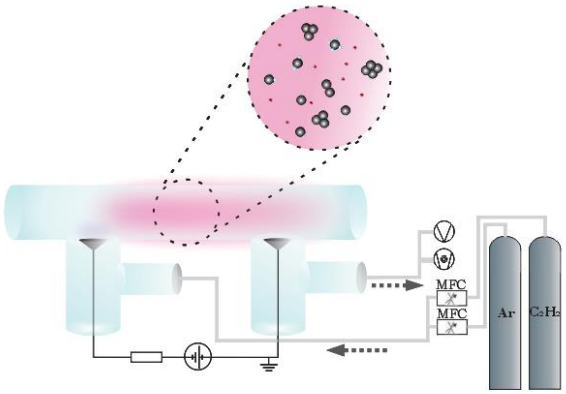



Figure 1. Experimental setup scheme

**References**

[1] Yasuaki, H. et. All. Observation of Coulomb-Crystal Formation from Carbon Particles Grown in a Methane Plasma. *The Japan Society of Applied Physics* **33**, L804 (1994).

[2] de Angelis, U. et. All. Dispersion properties of dusty plasmas. *Journal of Plasma Physics* **42**, 445-456 (1989).

[3] Orazbayev, S. et. All. Plasma with carbon nanoparticles: advances and application. *Nanotechnology* **32**, 455602 (2021).

[4] Utegenov, A. et. All. Investigation of the temperature of electrons in a glow discharge plasma at direct current Ar and Ar/C2H2. *Recent Contributions to Physics* **90(3)**, 2–37 (2024).

# Effects of Precursor Gas Molecules on the Deposition Characteristics of Hydrogenated Amorphous Carbon Films using Plasma Chemical Vapor Deposition

Shunpei Ohara[1], Shinjiro Ono[1], Manato Eri[1], Takamasa Okumura[1], Naho Itagaki[1], Kunihiro Kamataki[1], Kazunori Koga[1], and Masaharu Shiratani[1]

[1]*Graduate School and Faculty of Information Science and Electrical Engineering, Kyushu University, 744, Nishi-ku, Fukuoka 819-0395, Japan*

In this study, to achieve high-density and low-stress a-C:H films with a high deposition rate, we evaluated the deposition characteristics of plasma chemical vapor deposition (CVD) using $C_9H_{12}$ (cumene) and compared them using conventional precursor gases (methane and acetylene). Additionally, we studied the effect of incident ion energy on mass density. As a result, film deposition using cumene exhibited a higher deposition rate. Furthermore, it was suggested that mass density is determined by the ion energy per carbon atom, regardless of the precursor gas and discharge frequency. Moreover, we evaluated the etching resistance of the deposited films. The etching rate decreased as mass density increased, independent of the precursor gas molecule and deposition conditions.

Hydrogenated amorphous carbon (a-C:H) films serve as hard masks in high aspect ratio (HAR) etching for semiconductor manufacturing. Enhancing their properties requires high density, low compressive stress, and high deposition rates. In this study, cumene ($C_9H_{12}$) was used as the precursor gas, expecting to achieve both high-density films due to its low hydrogen-to-carbon ratio [1] and high deposition rates from its high carbon atom content [2]. Additionally, cumene is cost-effective (56 USD/L) [3]. To evaluate the effectiveness of cumene plasma CVD, we studied (1) deposition characteristics using methane, acetylene, and cumene, (2) effect of incident ion energy on mass density, and (3) evaluation of etching resistance of the deposited films.

A capacitively coupled plasma CVD system was used to deposit a-C:H films. Two parallel electrodes (115 mm apart) were placed at the center of the chamber. A 1 $cm^2$ Si substrate was placed on the lower electrode, and Ar diluted precursor gas was introduced. Plasma was generated by applying 13.56 MHz or 400 kHz high-frequency voltage to the lower electrode. For the 400 kHz discharge, the precursor gas was introduced at a total flow rate of 100 sccm with a precursor concentration of 5%, the total gas pressure was 0.02 Torr, and the discharge voltage was $V_{pp}$ = 1600 - 2400 V. For the 13.56 MHz, the flow rate was 100 sccm, the concentration 5 – 50%, pressure 0.02 – 0.3 Torr, and Vpp = 100 or 250 V.

First, at 13.56 MHz, films deposited using acetylene and cumene exhibited higher deposition rate than those deposited using methane. Additionally, at comparable mass density and stress levels between acetylene and cumene, the deposition rate for cumene increased by 20 nm/min compared to that for acetylene (~20 nm/min). At 400 kHz, films deposited using cumene also exhibited high density (~2 g/$cm^3$) and low stress (~1.0 GPa). Furthermore, at similar mass density and stress levels, the deposition rate for cumene was 10 nm/min higher than that of acetylene. In addition, at 13.56 MHz, while film stress generally correlated positively with mass density, it remained suppressed at around 1.0 GPa, independent of mass density.

Second, the correlation between ion energy and mass density was examined. By defining the ion energy index as $|V_{dc}|$ / pressure / $N_c$ (where $|V_{dc}|$ is the bias voltage, and $N_c$ is the number of carbon atoms per molecule), it was suggested that mass density is determined independently of precursor gas and discharge frequency. Moreover, the hydrogen content estimated from Raman spectroscopy exhibited a negative correlation with mass density, regardless of precursor gas or discharge frequency. On the other hand, the D/G peak ratio, an indicator of the $sp^2/sp^3$ ratio, correlated with mass density in regions where the total ion energy ($|V_{dc}|$ / pressure) was low (< 15 for acetylene, < 40 for cumene).

Third, the etching rate showed a decreasing trend as mass density increased, regardless of the precursor gas molecule or deposition conditions.

**References**

[1] J. Robertson, Mater. Sci. Eng. R37 (2002), 129.
[2] P. Koidl et al., Mater. Sci. Forum, 52 (1990), 41.
[3] https://www.chemicalbook.com/ChemicalProductProperty_EN_CB2191522.htm

# Breakdown elementary mechanisms within controlled nanometer scale electrode gaps

B. Disson[1], N. Bonifaci[2], R. Dussart[1], E. Manfé[2], O. Lesaint[2], C. Poulain[3], and S. Iseni[1]

[1] *GREMI , UMR 7344 CNRS / University of Orleans, Orleans, FRANCE,*
[2] *G2ELab UMR 5269 CNRS, Univ. Grenoble Alpes, Grenoble INP,, Grenoble, FRANCE,*
[3] *CEA, LETI, MINIATEC Campus, Grenoble, FRANCE*

This study reproduce the deviation from the Paschen's law in controlled conditions, in order to study the underlying elementary processes responsible for the breakdown in sub-micrometer gaps. This clarifies certain discrepancies in the very few experimental results published in the past. The point is also to suggest an empirical approach based on statistical analysis to describe the competition between the different breakdown processes.

## 1 General

Paschen's law is an empirical approach to estimate the minimum voltage (Vb) at which gas breakdown can occur taking into account the product of the pressure with the distance gap (p · d). This relation is convenient for determining Vb in various gases. The equation is based upon two elementary mechanisms: the Townsend electron avalanche in the gas and the secondary electron emission at the cathode surface.

However, numerous experimental, theoretical and simulation studies have shown deviations from the prediction of Paschen's law, particularly when the inter-electrode distance is very small, typically in the order of a micrometer and lower [1]. Those deviations result in a drop in Vb as the gap decreases at constant pressure. This raises many issues about the dielectric properties of gases [2]. The most promising theory to explain these discrepancies is the presence of an elementary mechanism not taken into account in the initial Pachen's law, namely the field emission.

### 1.1 Aim of the study

This experimental study follows on from previous work on Paschen's law deviations [3], but focuses on a more statistical approach to study the breakdown in dry argon. The aim is to discern the competing mechanisms involved responsible for the breakdown, in particular the field emission mechanism. To do this, the breakdown voltage measurements is repeated many times for each experimental condition in order to estimate a probability density law.

To do this, the breakdown voltage measurements will be repeated a large number of times for each experimental conditions in order to estimate a probability density law and highlight the competition between mechanisms.

### 1.2 Experimental setup

The experimental setup consists of a grounded silicon wafer acting as a cathode and a needle with a tip radius curvature of 20 µm used as the anode. Both electrodes are coated with a thin film of gold. A piezoelectric actuator controls the inter-electrode gap, from 100±25 nm to 6.0 µm. The experiments are carried out in a sealed chamber to control the pressure, the humidity and gas purity.

### 1.3 Application

To some extent, this study brings further insight in the field of nano-plasmas toward the development of pico-second switches for ultra-fast electronics [4].

**References**

[1] D B Go and A Venkattraman 2014 *J.Phys.D:Appl.Phys.* 47 503001
[2] C H Chen, J Andrew Yeh and P J Wang 2006 J. *Micromech. Microeng.* 16 1366–1373
[3] A Peschot, N Bonifaci, O Lesaint, C Valadares and C. Poulain 2014 *Appl. Phys. Lett.* 105
[4] Samizadeh Nikoo M, Jafari A, Perera N, et. al. 2020 *Nature.* 579(7800):534–9

*This research was fully supported by the French National Research Agency (ANR) with the project MIDICODE (ANR-22CE51-0022-01).*

# Formation of electrodeless double-headed streamers (DHS) at sub-breakdown conditions

B. Disson[1], 2, G. B. Sretenović[2], V. V. Kovačević[2], N. Bonifaci[3], C. Pichard[4], C. Cachoncinlle[1], A. Khacef[1] and S. Iséni[1]

[1] GREMI, CNRS / Université d'Orléans UMR7344, 45067 Orléans, France.
[2] Faculty of Physics, University of Belgrade, PO Box 44, 11000 Belgrade, Serbia.
[3] G2Elab CNRS / Grenoble INP / Université Grenoble Alpes UMR5269, 38042 Grenoble, France.
[4] Polytech Orléans, Université d'Orléans, 45067 Orléans, France.

Recent decades have seen significant advancements in understanding sprites and ionization waves. However, the natural occurrence of double-headed streamers (DHS) after breakdown remains unexplained. Extensive modeling studies have been conducted, but no experimental validation has been achieved until now. This work introduces the first experimental model of DHS using a primary plasma jet device at ground pressure. The experiment involves a noble gas flow (Helium or Neon) mixing with ambient air. Advanced diagnostics, such as optical emission spectroscopy (OES) and the Stark effect, were used to measure the electric field along the discharge axis. The results show that DHS can ignite under sub-breakdown conditions, highlighting the importance of pre-ionization. These findings align with previous modeling studies and provide insights into fundamental processes in atmospheric electricity.

This poster introduces an innovative experimental model that successfully replicates part of the natural atmospheric phenomenon of double-headed streamers (DHS) in a laboratory environment at atmospheric pressure. This pioneering effort marks the first time an electrodeless DHS has been reproduced, aligning with observations from the atmospheric electricity community in the late nineties [1]. The experiment employs guided ionization waves from an Atmospheric Pressure Plasma Jet (APPJ) device, namely the Electrodeless Atmospheric Secondary Induced Ionization Jet (EASII-jet) [2]. With this technique, one can achieve a high reproducibility and predictability in initiating DHS formation. The approach effectively mimics conditions such as maintaining an initial preionized column of free charges before breakdown, as assumed in various models, e.g. by Liu et al.[3]. The experimental results closely align with numerous simulation findings in the literature [3, 4]. Both positive and negative streamers were clearly identified, exhibiting simultaneous counter-propagation from the breakdown location. The stable discharge enabled advanced diagnostics, including time- and space-resolved optical emission spectroscopy, facilitating the first measurements of velocity growth, gas temperature, and electric field in a DHS. The electric field measurements confirmed the presence of positive and negative streamers and revealed that DHS can ignite under sub-breakdown conditions, underscoring the critical role of pre-ionization in their formation. This was priorly discussed in the predictive simulations results reported in [3]. These findings support existing theoretical predictions and open avenues for further research into the early stages of sprite discharges and other atmospheric electricity phenomena using cost-effective laboratory experiments. Part of this study has recently been pusblished in [5].

This research was partly supported by the French National Research Agency (ANR) with the project MIDICODE (ANR-22-CE51-0022-01).

## References

[1] V. P. Pasko, U. S. Inan, T. F. Bell, Geophys. Res. Lett. 1998, 25, 2123–2126.

[2] S. Iseni, A. Baitukha, N. Bonifaci, et al., Phys. Plasmas 2020, 27, 123504.

[3] N. Liu, B. Kosar, S. Sadighi, et al., Phys. Rev. Lett. 2012, 109, 025002.

[4] A. Luque, V. Ratushnaya, U. Ebert, J. Phys. D: Appl. Phys. 2008, 41, 234005.

[5] S. Iséni, G. B. Sretenović, V. V. Kovačević, et al., Phys. Rev. E 2025, 111, L023202.

# Notes on fluid and kinetic descriptions of the development of striations in the positive column plasma of rare gases

J.P. Boeuf and G.J.H. Hagelaar

*LAPLACE, Université de Toulouse, CNRS, INPT, UPS, 118 Route de Narbonne, 31062 Toulouse, France*

The stratification of the plasma in the positive column of rare gases has been recently described self-consistently with Particle-In-Cell simulations. It has also been shown that the growth rate, frequency and wavelength of the striations are relatively well predicted and understood by linearizing a fluid model of the plasma column, provided that the term proportional to the plasma density gradient is properly included in the electron energy flux, in addition to the classical thermal diffusion term. In this presentation, we use Monte Carlo simulations to show that the fluid approach effectively captures the mechanisms responsible for the onset of instability despite the presence of kinetic effects.

The stratification of positive column plasmas in rare gases has been known for many years; however, the underlying physical mechanisms driving the formation of striations remain incompletely understood. Particle-In-Cell Monte Carlo Collisions (PIC-MCC) can reproduce the formation and dynamics of the striations observed in experiments [1, 2], but a complete understanding of the phenomenon needs a more theoretical approach. In this presentation we consider low pressure conditions where metastable ionization is negligible.

Previous kinetic models based on solutions of the Boltzmann equation under a spatially oscillating electric field [3,4] have demonstrated the presence of resonances in the oscillations of plasma density and electron mean energy. It has been emphasized that instabilities responsible for the development of striations form under conditions where the electron energy relaxation length is not small with respect to the wavelength of the oscillations [5]. These considerations are consistent with the results of PIC-MCC simulations but do not provide a quantitative explanation of the phenomenon. A comprehensive investigation into the conditions that foster instability development should be based on dispersion relations derived from the linearization of the governing equations.

Fluid equations were used in Refs.[1-3] to derive a dispersion relation. The growth rate γ of the instability was found to be of the form:

$$\gamma = -D_{a0}k^2 + n_0\left(\frac{\partial \nu_i}{\partial T_e}\right)_0 \frac{\delta T_e}{\delta n}$$

where $\gamma$ is the growth rate of a perturbation, $D_a$ the ambipolar diffusion coefficient, $\nu_i$ is the ionization frequency, $n$ the plasma density and $T_e$ the electron temperature. The index 0 refers to the uniform solution. $\delta n$ and $\delta T_e$ are the perturbations of wavenumber $k$ in electron density and temperature. $\gamma$ can be positive only if $\delta T_e/\delta n > 0$.

It was shown in Refs. [1-3] that this is possible if the coefficient of the density gradient in the electron energy flux, $\chi_e = 3/2T_e(D_\varepsilon - (\mu_\varepsilon/\mu_e)D_e)$ is sufficiently negative ($D_e$ is the diffusion coefficient and $D_\varepsilon$ the energy diffusion coefficient, $\mu_e$ and $\mu_\varepsilon$ are the mobility and energy mobility).

In this presentation, we use a Monte Carlo (MC) simulation in a periodic spatially oscillating electric field (small perturbation) to study the sign of the $\chi_e$ coefficient and the validity of the fluid approach to describe the onset of the instability. We discuss the following points:

- In Refs [1-2], the $\chi_e$ coefficient was found to be negative. These studies employed transverse diffusion coefficients in the $\chi_e$ expression, as defined in swarm experiments. It is important to note that in rare gases, longitudinal and transverse diffusion coefficients can differ significantly. We explore the implications of choosing between transverse and longitudinal diffusion coefficients.
- Utilizing the MC simulation to evaluate the various components of the instability's growth rate as deduced from fluid equations, we demonstrate that despite the presence of kinetic effects, the fluid model accurately captures the underlying mechanism driving the onset of the instability. These kinetic effects arise because the electron energy relaxation length is not small compared to the wavelength of the developing instability.

**References**

[1] Boeuf, J.P. *Phys. Plasmas* **29**, 022105 (2022)
[2]Boeuf J.P., et al., *Phys. Plasmas* **31**, 073508 (2024)
[3] V. Desangles, et al., *Phys. Rev. Lett.* **123**, [2] 265001 (2019).
[3] Rohlena K et al. Czech., *J. Phys*. B **22** 920 (1972)
[4] Golubovskii et al., *Phys. Rev.* E **72**, 026414 (2005)
[5] Tsendin L.D., *Plasma Sources Sci. Technol.* **4** 200 (1995), *Physics-Uspekhi* **53**, 133 (2010).

# Striations of the positive column in radiofrequency and direct current argon plasmas – Experiments and particle simulations

M.K. Dosbolayev[1], S.A. Orazbayev[1,2], L. Boufendi[1,2], T.S. Ramazanov[1,2] and J.P. Boeuf[3]

[1]*NNLOT, Al-Farabi Kazakh National University, 71, Al-Farabi Av., Almaty 050040, Kazakhstan*
[2]*Institute of Applied Sciences and Information Technologies, Baizakov St. 280, Almaty 050040, Kazakhstan*
[3]*LAPLACE, Université de Toulouse, CNRS, INPT, UPS, 118 Route de Narbonne, 31062 Toulouse, France*

The conditions for the development of striations of a positive column plasma in argon under rf and dc voltages are experimentally investigated in a pressure range between 0.1 and 10 torr. Comparisons of the properties of the striations in RF and DC positive columns are presented and analyzed with the help of particle-in-cell simulations.

The positive column of a direct current (DC) glow discharge often has a striated structure, characterized by alternating light and dark areas [1]. Striated positive columns are also observed in radiofrequency (RF) capacitive discharges [2] and in hollow-cathode discharges [3].

To study the properties of striations of a RF capacitive discharge a glass tube with an internal diameter of 22 mm was used. A high-frequency (13.56 MHz) generator R101 with a matching device from Seren was used as a source of alternating voltage. Cylindrical electrodes made of aluminum foil were placed on the discharge tube and located at a fixed distance of 0.2 m from each other. One of the electrodes was connected to the output of the HF generator, and the second was grounded, Figure 1.

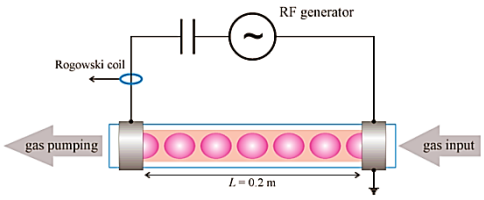



Figure 1. Schematic diagram of the experimental setup for a RF positive column plasma

Experiments revealed well-defined standing striations between 0.05 Torr and 1 Torr. Adding up to 10% hydrogen to the discharge does not affect striation in the region of 0.1 Torr and below. Since hydrogen is a good quencher of argon atoms in the metastable state, this indicates that the presence of metastable atoms plays no role in the striation of the positive column at this pressure and below. At higher pressures, the striations disappear when lower percentages of hydrogen are added in the experiment (less than 6% at 0.3 Torr and less than 3% at 1.1 Torr), showing that the presence of metastable atoms is necessary for the formation of the striations at sufficiently high pressures [4,5].

Stratification of the positive column of a DC discharge in argon was also studied. In this case a hollow cathode was used to reduce the applied voltage at high currents. We present a comparison of the domain of existence and of the properties of the striations in the RF and DC cases. In contrast with the DC case where fast-moving striations are present at low pressures, standing striations were more easily observed with the naked eye under RF conditions, provided that the electrode configuration and power coupling were symmetrical.

The Particle-In-Cell Monte Carlo Collisions (PIC-MCC) simulations are in qualitative agreement with the experiments and confirm that the contribution of metastable atoms to ionization becomes important and dominant above 0.5-1 torr. The simulations show that the electron energy distribution functions in the RF and DC cases are significantly different. Spectroscopic diagnostics will be used in the next future to confirm the simulations results.

**References**

[1] N. L. Oleson and A. W. Cooper. *Advances in Electronics and Electron Physics* **24**, 155 (1968).
[2] V. I. Kolobov, R. R. Arslanbekov, D. Levko and V. A. Godyak. Plasma stratification in radio-frequency discharges in argon gas. *Journal of Physics D: Applied Physics* **53**, 25lt01 (2020).
[3] L. He, F. He, Z. Bai and J. Ouyang. Observation of striations in RF hollow electrode discharge in argon. *Physics of Plasmas* **26** (2019).
[4] J. P. Boeuf, L. Boufendi, M. K. Dosbolayev, S. Orazbayev and T. S. Ramazanov. Striations in an argon positive column plasma. I. Theory. *Phys. Plasmas* **31**, 073508 (2024).
[5] M.K. Dosbolayev, S. Orazbayev, L. Boufendi, T. S. Ramazanov and J.P. Boeuf. Striations in an argon positive column plasma. II. Experiments and Particle simulations. *Phys. Plasmas* **31**, 073509 (2024)

XXXVI ICPIG, July 20-25, 2025, Aix-en-Provence, France Topic number 9

# Improving the optical emission in the visible spectrum of $CO_2$ streamers with trace Xe

W. Meekes[1], S. Nijdam[1], T.A. Smits[2]

[1] *Eindhoven University of Technology, Eindhoven, the Netherlands*
[2]*Research institute for mathematics and computer science, Amsterdam, the Netherlands*

The optical emission spectrum of $CO_2$ streamers lies mostly in the infrared region. This can lead to problems for spectroscopic methods which have a lower limit for the photon energy that can be detected, such as ICCD imaging. In this work, the optical emission of streamers in various $CO_2$/Xe ratios is measured and compared to pure CO2. If the signal is improved, it is important that the effect on the discharge is sufficiently limited. To this end, the electrical characteristics of the streamers in the different gas compositions will be compared.

## 1 General

Streamer discharges are the precursors to sparks such as lightning, and play an important role in the high-voltage industry. In high-voltage switchgear, electrical insulation starts with disrupting streamer propagation. As $SF_6$ is gradually phased out of such installations, $CO_2$ becomes an increasingly important gas for electrical insulation and arc quenching. To be able to use $CO_2$ most effectively, understanding the dynamics of streamer propagation in $CO_2$ is important.

However, $CO_2$ streamers emit most of their light in the infra-red region, with photons with too low energy to capture with an ICCD. As a result, capturing $CO_2$ streamers on such a camera and doing diagnostics on the morphology of the streamer – branches, velocity and width – is much more challenging than it is in air.

In this work, streamer discharges will be made in $CO_2$ mixed with Xenon, to investigate the impact of Xenon on the optical emission and streamer behaviour. Xenon is chosen in particular because it is a noble gas – which means it will likely interfere little with the $CO_2$ plasma – and has many transitions in the visible spectrum.

## 2 Measurement methods

Streamer discharges will be produced at pressures between 20 and 200 mbar, in $CO_2$ mixed with Xenon. Other trace gases will also be used for comparison, such as $N_2$, Ar and $O_2$.

The optical emission will be recorded using an ICCD, making directly clear any improvements to the optical emission.

However, as this work aims to improve diagnostics for $CO_2$ streamers, it is important that Xe does not interfere with the dynamics of the $CO_2$ streamers to too great a degree. To that end, for the different gas mixtures simple characteristics of the discharge will be compared, t.w. the voltage and current characteristics, as well as the ICCD images themselves.

This way, this research aims to find a concentration of Xe to mix with $CO_2$ that improves the optical emission sufficiently to allow advanced diagnostics on $CO_2$ streamers, without altering the discharges such that the streamer discharge can no longer be considered a $CO_2$ discharge.

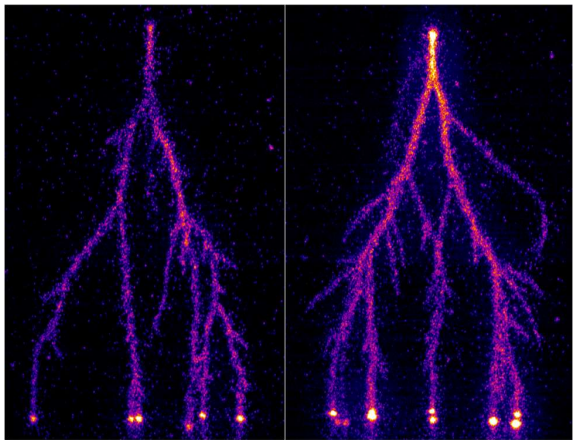


**Figure 1: Streamer discharge in pure $CO_2$ (left) and $CO_2$ with 10% Xe (right)**

# Experimental comparative study of the dc and ten-nanosecond electrical breakdown in air for flat and sharp electrodes

S. F. Adams[1] and V. I. Demidov[1,2]

[1] *Air Force Research Laboratory, WPAFB, OH 45433, USA*
[2] *West Virginia University, Morgantown, WV 26506, USA*

A comparison of experimental results for dc and 10-ns pulsed breakdown in air for flat and sharp electrodes is carried out. The features of such breakdowns are discussed.

## 1 General

In this study, we investigated 10-ns and dc breakdowns in air across a discharge gap with flat and sharp electrodes. The aim of the work was to understand what types of breakdown exist in such situations, how they are interrelated with each other and the corresponding Paschen curves. The study of breakdowns for electrodes of various shapes and time ranges is of interest both for analysis of the physics processes and for technical applications. Leaks of electrical energy and short circuits are of particular interest. Such short circuits are especially important in the conditions of more or all-electric aircraft.

Such breakdowns are characterized by large changes in both the breakdown parameters, including its time characteristics and the values of breakdown voltages, and the processes occurring during it. The latter can lead to a significant change in the radiation spectra during the breakdown. This phenomenon can be used to identify short circuits in electrical networks.

## 2 Results of the experiments

It was demonstrated (see, figure) that the Paschen curves in air for flat electrodes with a slowly changing voltage on them correspond well to similar curves for sharp electrodes (electrodes made of lanthanated tungsten, 1.6 mm in diameter, sharpened to a conical angle of 20 degrees) with $p \times d$ less than 0.04 atm×cm. Here $p$ is the air pressure, and $d$ is the distance between the electrodes. This situation does not change when the distance between the electrodes varied from 2 to 6 mm. At large $p \times d$, the breakdown voltage changes and is significantly lower than for flat electrodes. For comparison, it was shown that the Paschen curves for the 10-ns breakdown for flat electrodes have a breakdown voltage several times higher, and the breakdown minimum is shifted toward higher $p \times d$ relative to the previous curves. When using sharp electrodes, the breakdown voltages are higher than for electrodes, and the breakdown minimum is shifted even more toward higher $p \times d$.

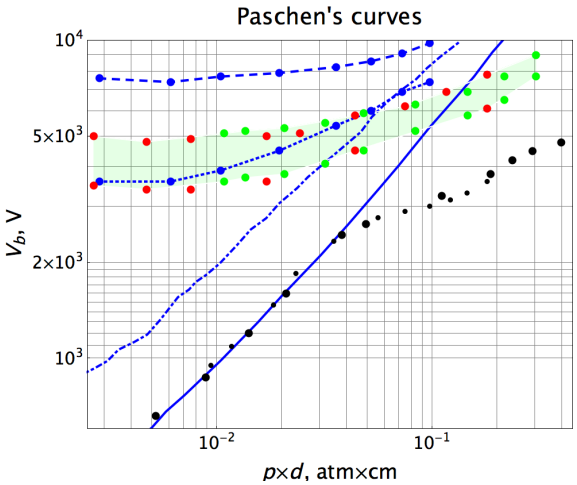



Figure: Paschen's curves for flat electrodes (blue curves and dots). Standard Paschen curve from [1] for air with a slow change in voltage on the electrodes (solid blue curve); Paschen curve for a microsecond time scale [2] (intermittent-dotted blue curve); experimental Paschen curve for a 10-nanosecond discharge obtained with increasing voltage (upper dashed blue line with dots showing experimental data); experimental curve for a 10-nanosecond discharge obtained with decreasing voltage (lower dotted blue line with dots showing experimental data). Paschen curve for sharp electrodes with a slow change in voltage (black dots). The same for a 10-nanosecond discharge, red and green dots (upper dots for increasing and lower dots for decreasing voltages). The upper and lower red and green dots are separated by green shading.

**References**

[1] Mesyats, G. A. Similarity laws for pulsed gas discharges. *Phys.- Usp.,* **49**, 1045 (2006).

[2] Babich, L. P. and Loko, T. V. Generalized Paschen law for overvoltage conditions. *IEEE Trans. Plasma Sci.*, **44**, 3243 (2016).

# On the Control and Design of Nanosecond Plasma Jets for Optimized Therapeutic Efficiency

Jean-Baptiste Billeau[1,3], Inna Orel[1], Joshua Crawford [1], Marc S. Saouda[1], Nazar Muliar[1], Svetlana Starikovskaia[1]
Nataliia Naumova[2], Lluis M. Mir[2], Franck André[2], Catherine Brenner[2]
Denis V. Seletskiy[4], Stephan Reuter[3]

[1]*Laboratory of Plasma Physics (CNRS, École Polytechnique, Univ. Paris-Sud, Observatoire de Paris, Sorbonne Université, Institut Polytechnique de Paris), École Polytechnique, Palaiseau, France*
[2] *Univ. Paris-Saclay, CNRS, Gustave Roussy, Metabolic and Systemic Aspects of Oncogenesis (METSY), Villejuif, France*
[3]*Plasma Physics and Spectroscopy Laboratory, Polytechnique Montréal, Montréal, Canada*
[4]*femtoQ Laboratory, Polytechnique Montréal, Montréal, Canada*

This study examines how pulsing parameters and reactor design influence reactive oxygen species generation, specifically hydrogen peroxide ($H_2O_2$) and ozone ($O_3$) for medical plasma application. Experiments with a custom-designed nanosecond plasma jet reveal that electric pulse duration does not directly correlate with $H_2O_2$ production, while higher frequencies enhance both $H_2O_2$ and $O_3$ levels. These findings emphasize the need for better control over plasma parameters to optimize therapeutic efficacy, highlighting the importance of advanced diagnostics for refining treatments.

From targeting cancer cells to accelerating healing processes, precise control and understanding of cold plasma properties are essential in medical contexts. Despite its promising potential, the impact of plasma reactor design on the production of reactive species remains largely unknown. Understanding how various plasma parameters influence the generation of reactive oxygen species (ROS) and reactive nitrogen species (RNS) is crucial for optimizing the therapeutic efficacy of plasma-based treatments. This study investigates the relationship between electrical pulsing parameters and plasma jet reactor design on ROS production, particularly hydrogen peroxide ($H_2O_2$) and ozone ($O_3$), to refine plasma-based treatment strategies.

Experiments were conducted using a custom-designed cold atmospheric pressure plasma jet operating with helium gas and powered by a nanosecond generator (3-30 ns). Hydrogen peroxide ($H_2O_2$) production in phosphate-buffered saline (PBS) was monitored using a chemo-fluorescent probe based on the Amplex Red reagent. Ozone ($O_3$) density near the plasma jet nozzle was quantified at a single point using an ozone analyser.

Our findings reveal two key observation: **(1)** pulse duration does not directly correlate with increased $H_2O_2$ production, and **(2)** high $H_2O_2$ levels are observed at long treatment times. Ozone measurements confirmed theoretical predictions, demonstrating that increased interaction surface, frequency, and voltage contribute to higher $O_3$ density. In contrast to the response of ozone production to electrical pulse duration variation, shorter pulse suggest that $H_2O_2$ production is more likely to be enhanced.

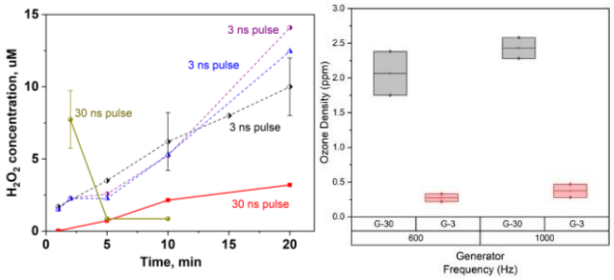



**Figure 1:** Comparison of $H_2O_2$ (left) and $O_3$ (right) concentration for different plasma parameters

The findings highlight the need for more precise control over plasma parameters to optimize the generation of ROS and RNS for therapeutic applications. To address these challenges, further investigations incorporating advanced diagnostic optical techniques are needed.

## Acknowledgement

The authors acknowledge the financial support from the FRQNT and NSERC (RGPIN-06820).

# Rapid decomposition of bisphenol-A in water with pulsed arc discharge for developing novel wastewater Treatment Methods

Mitsuru Sasaki[1,2*], Ryohei Mori[3], Tetsu Sakakibara[4], Katsuyuki Takahashi[4,5], Olivier Boutin[2,6]

[1] *Institute of Industrial Nanomaterials, Kumamoto University, Kumamoto Japan*
[2] *International Research Organization for Adv. Sci. and Technol., Kumamoto Univ., Kumamoto, Japan*
[3] *Graduate School of Science and Technology, Kumamoto University, Kumamoto, Japan*
[4] *Faculty of Science and Engineering, Iwate University, Japan*
[5] *Agri-Innovation Center, Iwate University, Iwate, Japan*
[6] *Aix-Marseille Univ., CNRS, Centrale Med, M2P2 UMR 7340, Marseille, France*

The authors studied factors affecting bisphenol-A decomposition, including discharge time, location, gas conditions, pH, and frequency. They found that longer discharge times improved conversion rates, with TOC measurements indicating carbon was released as $CO_2$. Gas-liquid discharge outperformed underwater discharge, though initial pH significantly impacted efficiency, with lower pH enhancing decomposition. The optimal conditions were a pH of 2 and a discharge frequency of 100 pps, achieving 100% bisphenol-A conversion in 2 min. LC/MS analysis identified phenol and cresol as products, while hydrogen peroxide measurements suggested that OH radicals played a key role in the reaction. The authors proposed a reaction pathway for bisphenol-A decomposition via pulsed arc discharge at the air-aqueous interface.

The authors investigated the effects of discharge time, discharge location, gas-phase conditions, initial pH, and discharge frequency on bisphenol-A (BPA) decomposition. The conversion rate improved with the discharge time, and a decrease in the amount of carbon in the solution was confirmed by TOC measurement. This is thought to have been released outside as carbon dioxide. Compared to underwater discharge, the performance of BPA decomposition was lower than that of gas-liquid discharge. However, after 4 min, the discharge energy value per shot was higher. However, as the purpose was to treat it quickly, it was thought to be unsuitable. Next, when argon replacement was performed, the decomposition efficiency of BPA did not improve, even though the discharge was strong, the discharge energy was high, and the discharge efficiency was good. At this time, the decrease in pH was suppressed, so the initial pH was adjusted, and experiments were performed. The effects of physical properties and discharge current/voltage on the BPA decomposition rate were investigated. As a result, the more acidic the initial pH, the higher the conductivity of the reaction solution and the higher the BPA decomposition rate. The peak voltage during pulse discharge was about 20 kV at pH 4-12, while it was 10-12 kV at pH 2. The peak current value increased with decreasing pH, and was 360-380 A at pH 2. It can be surmised that the BPA decomposition reaction was promoted because the higher the concentration of ions as the acidity increased, making it easier to pass electricity. In addition, the results showed that the higher the discharge frequency, the better the BPA decomposition efficiency. Based on these results, the pH was adjusted to 2 with nitric acid, and the discharge frequency was 100 pps under air, and discharge at the gas-liquid interface was determined as the optimal condition. In these conditions, the BPA conversion rate was 100% with a 2-min discharge. The TOC value at this time was reduced by 26% from the untreated raw aqueous solution. Next, the reaction pathways for BPA decomposition on the pulsed discharge were predicted on the basis of the LC/MS and HPLC analyses. In addition, since it is difficult to quantify the active species OH radicals generated by pulse discharge, the amount of OH radicals were estimated by quantifying the hydrogen peroxide generated by the recombination of OH radicals. An increase in the hydrogen peroxide concentration was confirmed, and the conversion of BPA also increased accordingly, so it was considered that OH radicals were mainly involved in the reaction. Based on the above findings, the authors proposed the possible reaction pathway for BPA decomposition on the air-aqueous solution interfacial pulsed arc discharge.

**References**

[1] H. Sarma et al., *Environm. Sci. and Pollution Res.*, 25(18), 17227–17239, **2018**.
[2] F. Cheng, et al., *Journal of Colloid and Interface Science*, 580, 540–549, **2020**.
[3] D. Chen et al., *Environm. Sci. and Technol.*, 50(11), 5438–5453, **2016**.
[4] D. K. A. Barnes, et al., *Philosophical Transactions of the Royal Society B: Biological Sciences*, 364, no. 1526, 1985–1998, **2009**.

# Child–Langmuir law applicability for a cathode sheath description of dc glow discharge in acetylene

V. Lisovskiy, S. Dudin, A. Shakhnazarian, S. Rezunenko, V. Yegorenkov

*V.N. Karazin Kharkiv National University, 4 Svobody Sq., Kharkiv, 61022, Ukraine*

The processes in the cathode sheath of a DC discharge in acetylene have been experimentally investigated, considering the effect of plasma-stimulated gas pumping. It has been shown that in the entire investigated range of the discharge current and the initial pressure of acetylene, the law for constant mobility of positive ions must be used to describe the parameters of the cathode sheath. Its implementation in a cathode sheath with a strong electric field is possible due to the movement of positive ions under conditions when the charge-exchange process at collisions with gas molecules is obstructed.

In this work, the regularities of the formation of the cathode layer of a dc discharge in acetylene were studied experimentally, taking into account the effect of plasma-stimulated gas pumping (the initial gas pressure decreases significantly due to the consumption of gas molecules for the deposition of polymer films). The dynamics of changes in gas pressure $p$, voltage between electrodes $U$, and discharge current $I$ for different values of initial gas pressure in the range of 0.03–0.2 Torr were investigated using an oscilloscope. Also, the discharge was photographed with subsequent determination of the thickness of the cathode layer. Based on the obtained results, the applicability of the Child-Langmuir laws was verified for the movement of positive ions through the cathode layer.

The Child-Langmuir laws for the motion regimes through the cathode sheath without collisions with gas molecules, as well as with collisions in regimes with a constant mean free path $\lambda_i$ and constant ion mobility $\mu_i$, have the following form, respectively:

$$J = K_i \varepsilon_0 \left(\frac{2e}{M}\right)^{1/2} \frac{U^{3/2}}{d^2 p^0}, \quad (1)$$

$$J = 1.68\, \varepsilon_0 \left(\frac{2e\lambda_{i1}}{M}\right)^{1/2} \frac{U^{3/2}}{d^{5/2} \cdot p^{1/2}}, \quad (2)$$

$$J = \frac{9}{8} \varepsilon_0 \mu_{i1} \frac{U^2}{d^3 \cdot p^1}. \quad (3)$$

The three Childe-Langmuir laws have the general form:

$$I = C \cdot \frac{U^m}{d^n \cdot p^k}, \quad (4)$$

where $I = J \cdot S$ is the discharge current, $S$ is the cathode area. In the collisionless Child-Langmuir law (1) $m = 1.5$, $n = 2$, $k = 0$; in the law with a constant mean free path of ions (2) $m = 1.5$, $n = 2.5$, $k = 0.5$, and in the law for constant ion mobility (3) $m = 2$, $n = 3$, $k = 1$. If for some triple of values of $m$, $n$ and $k$ the experimental dependence of $I\,(U^m/(d^n p^k))$ is well described by a straight line drawn from the origin, then the corresponding Child-Langmuir law can be used to analyze the processes in the cathode layer of a glow discharge.

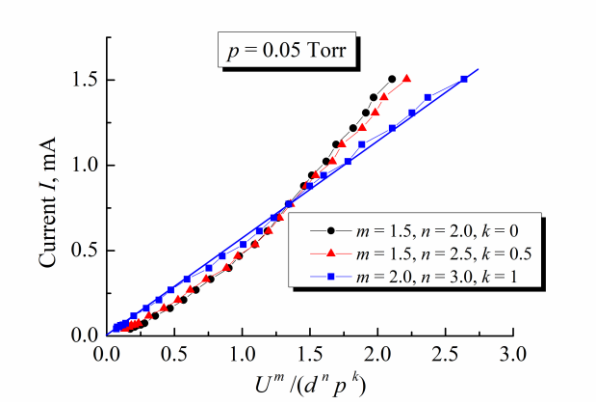



Figure. Dependences of the discharge current on the ratio $U^m/(d^n p^k)$ for the initial acetylene pressure of 0.05 Torr, taking into account the influence of gas pressure.

We found out that in the entire studied range of initial acetylene pressure and discharge current, the law for the constant mobility of positive ions must be used to describe the parameters of the cathode layer (see Figure). A proposed scheme of processes in the cathode layer involves the predominant transport of heavy positive ions, such as $C_4H_2^+$ and $C_6H_2^+$, through the region. These ions are unable to re-charge upon collisions with acetylene molecules because their ionization potentials are significantly lower than those of acetylene molecules.

## Acknowledgment

This research was supported by the National Research Foundation of Ukraine in the framework of the project 2021.01/0204.

# Spatial variation of electron/ion heating mechanisms in Capacitively Coupled Discharges (CCDs)

Anuravi Sharma[1], A. Rawat[2], R. Narayanan[1], A. Ganguli[3]

[1] *Indian Institute of Technology Delhi, Hauz Khas, New Delhi-110016*
[2]*Plasma Impedans Ltd,* [3]*Retired Faculty*

This work explores power absorption mechanisms in Capacitively Coupled Discharges (CCDs), a widely used plasma source in semiconductor processing. Studies confirmed the widespread presence of stochastic heating across various pressures. Spatial plasma variations were incorporated into an existing model, to better understand spatial dynamics of ion and electron power absorption mechanisms across different pressure regimes.

## 1. Introduction

The increased miniaturization and reduced feature size of semiconductor chips implies that the requirement of uniformity over larger areas and precise control of the energy distribution of the species involved during semiconductor processing is becoming more stringent with time. In this context, plasma-based technology has become an important process tool in the semiconductor industry with its ability to manufacture sophisticated electronic devices with accuracy, scalability, and high efficiency. The major advantage of plasma technology lies in its inherently high-energy, quasi-neutral state; governed by the power coupling mechanism, defined boundary conditions, and collisional dynamics within the specific process gas composition. Hence, the plasma parameters can be tuned to control energy distribution of processing species, optimizing interactions with the substrate for end-use application requirements. Among the different types of plasma sources used, Capacitively Coupled Discharges (CCDs) are found to be the most widely adopted and highly effective configurations in industry. Their ability to deliver uniform and regulated plasma processing is essential for advancing semiconductor scaling and ensuring high-performance microelectronics [1].

## 2. Experimental Set-up

To explore the above-mentioned challenges, Plasma Lab, IIT Delhi, has been undertaking studies in a Capacitively Coupled Discharge (CCD) system using argon gas that includes a stainless-steel vacuum chamber (25 cm dia,30 cm height) having an asymmetric parallel plate electrode geometry with the top electrode being powered at RF (13.56 MHz) whereas the bottom electrode being grounded. The two electrodes are separated by a distance $d$ =7.5 cm.

## 3. Results & Discussions

This work presents a comprehensive analysis of the power absorption mechanisms in CCDs to address the above-mentioned key challenges. Earlier studies confirm the importance of energy distribution within the discharge in governing plasma spatial dynamics, allowing precise control over ion energies and densities bombarding the substrate. Recent experiments conducted in the lab revealed the ubiquitous nature of the stochastic mechanism, which operates efficiently across a broad pressure range ($p_{fill}$~ 5mTorr - 400mTorr). This finding was based on an in-house developed model that assumed uniform radial and axial plasma profiles [2, 3]. In the present work, the effect of spatial variation of plasma parameters is incorporated into the model and compared with the uniform 0-D profiles. Theoretical modelling has been used to establish a correlation between power absorption mechanisms and experimentally acquired plasma parameters, thereby enabling the spatial visualization of ion power absorption and electron power absorption (*Ohmic and Stochastic heating*) mechanisms in different pressure regimes.

**References**

[1] Liu, Y. X., Zhang, Q. Z., Zhao, K., Zhang, Y. R., Gao, F., Song, Y. H., & Wang, Y. N. Fundamental study towards a better understanding of low-pressure radio-frequency plasmas for industrial applications. *Chinese Physics* B, **31**(8), 085202 (2022).

[2] Rawat, A., Ganguli, A., Narayanan, R., & Tarey, R. D. Correlation of stochastic and ohmic power absorption with observed RF harmonics and plasma parameters in capacitively coupled discharges. *Plasma Research Express*, **2**(3), 035015 (2020).

[3] Rawat, A., Ganguli, A., Narayanan, R., & Tarey, R. D. A new JE probe for measurement of spatial profiles of power absorption in RF produced plasma. *Review of Scientific Instruments*, **94**(6) (2023).

# Impact of non-equilibrium plasma treatment on selected properties of bovine milk

J. Pawłat[1], A. Starek-Wójcicka[2], M. Krajewska[2], P. Terebun[1], D. Zarzeczny[1], M. Kwiatkowski[1], B. Budzyńska[3], Ł. Kurach[3], K. Gołębiowska[4], E. Grządka[4]

[1] *Lublin University of Technology, Nadbystrzycka 38a Str., 20-618 Lublin, Poland*
[2] *University of Life Sciences in Lublin, Akademicka 13 Str., 20-612 Lublin, Poland*
[3] *Medical University of Lublin, Chodźki 1 Str., 20‑093 Lublin, Poland*
[4] *Maria Curie-Skłodowska University, M. Skłodowskiej - Curie 3 Sq., 20-031 Lublin, Poland*

Glide-arc (GAD) plasma treatment was applied for fresh cow's milk hygienization and proposed method was compared with pasteurization in terms of microbiological and toxicological safety, nutritional content, physicochemical properties, colloidal stability and chemical alterations. Plasma treatment improved microbial safety of fresh milk. Compared to thermal methods, cold plasma treatment better preserved vitamins, minerals, and polyphenols.

## 1 Introduction

Milk is a widely consumed beverage that provides nourishment, hydration, and immune support, with cow's milk being the most common source. It also plays a key role in dairy products like yogurt, butter, containing essential nutrients such as vitamins and minerals. While processing methods like pasteurization and UHT sterilization ensure safety, they can reduce certain nutrients and alter flavour. This highlights the need for new non-thermal processing techniques that preserve nutritional value, minimize physical and chemical changes while maintaining safety. Non-thermal plasma could be a promising solution for treatment of milk.

## 2 Methods and results

30 mL of fresh bovine milk was treated in as set up with GAD working with air and nitrogen gases (440 l/h flow rate) at 50 Hz frequency and 40 W of active power from the network. Magnetically stirred sample was placed 10 mm from the electrodes and treated for 5, 10 or 20 min. Temperature of sample did not exceed 36°C. The microbial studies based on surface inoculation using the plate count method on agar media, in accordance with standard procedures (ISO 4833-2, n.d.; ISO 21527-2, n.d.). Toxicological study focused on zebrafish larvae at four days post-fertilization (4 dpf), assessing mortality and heartbeat rates after exposure to different milk dilution ratios (1:150-1:25). For minerals' content and total polyphenol content CEM Mars Xpress apparatus with spectroscopic absorption method and the Singelton method were used, respectively. Chromatography was utilized to measure the vitamins B content.

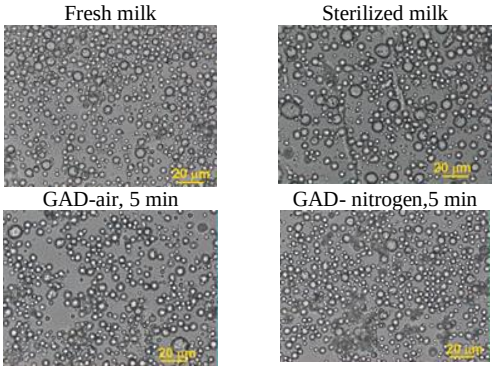



Fig. 1. Microscopic photos of the structure of milk samples

Total aerobic mesophilic bacteria/yeasts and molds counts of fresh and 20 min air plasma treated milk were 4.23/3.91 log CFU/ml and 3.26/2.71 log CFU/ml, respectively; showing noticeable reduction of tested microorganisms correlated with treatment time. According to toxicological studies, GAD milk treatment resulted in higher zebrafish survival rates compared to traditional processing methods. Plasma treatments shorter than 20 min did not lead to worsening of nutritional properties maintaining the content of Ca, Zn and Se, while 10 min air or nitrogen GAD treatment contributed to slight improvement of polyphenol content. Traditional milk treatment methods cause serious decrease of all vitamin from B group while in case of GAD ($N_2$) losses did not exceed 11%. Proposed treatment did not cause coalescence of fat particles (Fig. 1), colloidal stability was slightly improved and the brightness (L* parameter) of the milk sample was enhanced.

# In vivo tests of medical implant coatings deposited by plasma-activated reactive magnetron sputtering

V. Lisovskiy[1], S. Dudin[1], S. Yakovin[1], O. Nakonechna[2] and O. Kyslov[2]

[1] *V.N. Karazin Kharkiv National University, 4 Svobody Sq., Kharkiv, 61022, Ukraine*
[2] *Khariv National Medical University, 4 Nauky avenue, Kharkiv, 61022, Ukraine*

In this research, we investigate the possibility of using tantalum compounds to cover polypropylene prosthetic meshes used in hernia surgery. The tantalum-based coatings were deposited by plasma-activated reactive magnetron sputtering. The biological response of the organism to the implant coatings was estimated *in vivo* that allows to prove the efficiency of tantalum-based coatings to improve the biomedical implants.

Today, a pressing problem is the creation of modern materials for hernioplasty. These materials will help prevent complications in the postoperative period, thereby accelerating the convalescence period. Polypropylene hernioplasty mesh prostheses are usually used to replace aponeurotic and muscle tissue. However, such meshes can cause a serious foreign body reaction over time.

Experimental studies have demonstrated that the application of an additional titanium coating to polypropylene filaments resulted in improved biocompatibility compared to an identical mesh without coating [1]. Further progress in this direction can be expected through the use of tantalum-based coatings, which are known as excellent biomaterials with exceptional biocompatibility. Based on many years of positive experience in the use of tantalum compounds in the field of endoprosthetics, in this research, we investigate the possibility of using this material to cover polypropylene prosthetic meshes used in hernia surgery. The tested coating materials were tantalum oxide, nitride, and oxynitride as well as metallic tantalum.

The tantalum coating deposition was performed using DC magnetron sputtering, while for the synthesis of high-quality transparent tantalum oxide and nitride films, we used plasma-activated reactive magnetron sputtering [2]. This technology involves a dedicated plasma source activating the reactive gas being passed through the dense plasma.

The application of a hard coating to a soft plastic substrate by magnetron sputtering was studied, which faces the typical problem of coating delamination if its thickness exceeds 50-100 nm. The problem was solved for the deposition of tantalum-based coating to polypropylene substrates, focusing on the optimal deposition modes that allow applying a thicker coating without delamination.

The physical, mechanical and biological properties of the synthesized coatings were studied. The surface morphology and topography of the deposited coatings were observed using scanning electron microscopy with elemental composition assessment by energy dispersive X-ray analysis. The phase composition of the coatings was studied by X-ray diffraction. The hardness and elastic modulus of the coated surfaces were evaluated by nanoindentation. It was found that the oxide and oxynitride coatings are amorphous while tantalum and its nitride have a crystalline phase.

The organism response to the parameters of implant coatings was estimated by *in vivo* studies using laboratory animals. Morphological studies were conducted on the quality of wound healing on the anterior abdominal wall; the presence and severity of general pathological processes in the dermis, hypodermis, muscle and connective tissue layers; angiogenesis, apoptosis and proliferation processes in granulation tissue overgrowing the surgical mesh; adhesion formation processes. It has been proven that the use of implants coated with tantalum compounds does not cause pathomorphological changes in the abdominal organs and does not provoke purulent-septic processes in the postoperative period, which confirms the possibility of their use to improve the longevity and stability of use as biomedical implants.

## Acknowledgment

This research was supported by the National Research Foundation of Ukraine in the framework of the project 2021.01/0204.

## References

[1] F. Kockerling, and C. Schug-Pass, Hernia, vol. 18, pp. 445–457, 2014.
[2] S.V. Dudin, S.D. Yakovin, A.V. Zykov, East Eur. J. Phys. 3, 606 (2023), https://doi.org/10.26565/2312-4334-2023-3-72

# Reactive species variation in gas and liquid phase irradiated through pulse modulated atmospheric pressure sub-RF plasma jet

Aishik Basu Mallick, G. Veda Prakash, Satyananda Kar and Ramesh Narayanan

*Department of Energy Science and Engineering, Indian Institute of Technology Delhi, Hauz Khas, New Delhi, India.*

This study aims to highlight the influence of excitation parameters such as applied voltage and pulse modulation frequency of an in-house developed sub-RF plasma jet on distribution of reactive oxygen and nitrogen species in gas and liquid phase. The species efficacy in liquid phase is analyzed through dye degradation of aqueous dye solution over different treatment times. Optical emission spectra show signature of Argon lines with $OH^{\bullet}$, $O^{\bullet}$ and nitrogen radicals. A substantial variation in the relative yield of different ions over the wide range of excitation parameters has been observed. Physico-chemical properties of treated solutions show dissolution of reactive species in the liquid media. This work may provide significant insight into optimization of electrical excitation towards production and transport of RONS in a plasma-liquid system.

## 1 Introduction

Atmospheric Pressure Plasma Jets (APPJs) are known for producing various reactive oxygen and nitrogen species (RONS) viz., $OH^{\bullet}$, $O_3$, $NO_3^-$, $H_2O_2$ *etc.*, making APPJs a suitable candidate for various applications. In recent years, one has observed plasma chemical treatment studies gaining importance, considering plasma's synergetic effect on degrading the persistent and recalcitrant chemicals. The efficient degradation of the chemical compounds such as dyes in water-based solutions [1] largely depends on the generation and transfer of radicals from the plasma to the bulk liquid. The control of charge particles and species concentrations in the gas phase region can be effectively regulated by electrical excitation. However, the penetration depth of such species is up to several μm from the liquid surface posing major rate limiting step in these applications [2]. Further studies are required to understand and address these limitations, aiming to control species concentration in the plasma-liquid interaction region and the bulk liquid.

## 2 Experimental Setup

A DBD plasma jet with tapered glass nozzle is used in a cross-field configuration. An in-house developed pulse modulated power source oscillating in a sub-RF frequency is applied across the jet [3]. The experiments were performed for different applied voltages (6-9 $kV_{pp}$), pulse modulation frequency (10-30 kHz) for varying treatment time for a fixed argon flow rate, dye concentration and volume. Applied power across jet and gas temperature of plume were measured. Gas phase RONS is monitored through optical emission and molecular beam mass spectrometric techniques. Qualitative analysis of concentration of dyes in terms of absorption spectra analyzed by UV-VIS spectroscopy has been undertaken. Physico-chemical properties of water such as pH, solution conductivity, TDS and solution temperature of water were measured for different operating conditions. Dissolved species such as $OH^{\bullet}$, $H_2O_2$ and $NO_3^-$ in water are measured through chemical dosimetry and ion selective electrodes respectively.

## 3 Results and Discussion

Applied power across jet varies proportionally with rise in voltage and pulse modulation frequency with a maximum ≈ 43W; corresponding gas temperature ≈ 50°C indicative of its non-thermal nature. Emission profile of $OH^{\bullet}$ and $O^{\bullet}$ and Argon lines increases with applied power with highest intensity at $9kV_{pp}$ and 30 kHz. Similar trend for relative yield of $OH^-$ ≈ 0.95-3.94%, $O^-$ ≈ 3.71-9.40%, and $OH^+$ ≈ 1.47-7.67%, $O^+$ ≈ 1.85-9.90%. The pH of treated water sharply decreases whereas solution conductivity and TDS increases in water with treatment time along with marginal rise in temperature up to 35°C. Dissolved $OH^{\bullet}$, $H_2O_2$ and $NO_3^-$ concentration increase with treatment time and power. It was found that plasma treated samples operated at higher applied power showed better dye degradation for a particular treatment time. This can be attributed due to enhanced production rate of RONS due to heightened energy deposition into the plasma at higher pulse frequency and applied voltages thereby stimulating plasma chemistry.

**References**

[1] D. Joshi, G.V. Prakash, S.Z. Ahammad, S. Kar, and T.R. Sreekrishnan, *Plasma Sci. Technol*. **24**, 105501 (2022).

[2] P. Vanraes, and A. Bogaerts, *J. Appl. Phys.* **129**, 220901 (2021).

[3] A.B. Mallick, G.V. Prakash, S. Kar, and R. Narayanan, *Rev. Sci. Instrum*. **94**, (2023).

# Effect of $CO_2$ to CO conversion on bacteria and fungi inoculated onto the coat of wheat seed packed in a dielectric barrier discharge

M. El Shaer, H. Gabr, A. Zaki, M. Awad, M. Abdel-azim, H. Fayed, M. Mobasher

*Plasma & Energy Applications Research Laboratory, Department of Engineering Physics and Mathematics, Faculty of Engineering, Zagazig University, 44519, Zagazig, Egypt*

Wheat seeds (*Triticum aestivum* L.) of the local variety Egaseed 22 are packed in a plasma dielectric barrier discharge under the flow of a $CO_2$/Ar gas mixture. The conversion of $CO_2$ to CO is investigated under different operating conditions. The combined effects of plasma and the generated CO are evaluated to determine their effectiveness in seed disinfection under varying operating frequencies and inlet gas mixture flow rates. A few minutes of exposure to the combined plasma and CO treatment enhances germination parameters and eliminates bacteria and fungi more effectively than plasma alone. This effect is maximized at lower frequencies and lower $CO_2$ concentrations in the $CO_2$/Ar gas mixture.

## 1 Materials and methods

A seed packed dielectric barrier discharge (DBD), has been found to be effective for plasma seed treatment [1]. Figure 1 illustrates a DBD occurring in a quartz tube with an outer diameter of 16 mm and an inner diameter of 13 mm. Inside the tube, a stainless-steel rod with a 6 mm diameter serves as the inner high-voltage electrode, while a copper foil wrapped around the tube acts as the grounded outer electrode. This configuration creates a 3.5 mm gap, which is packed with wheat seeds along a length of 5 cm. The discharge operates at a peak-to-peak voltage of approximately 7 kV. The combined effects of plasma and CO, produced by $CO_2$ dissociation under the influence of reactive species generated within the plasma discharge, have been reported to be beneficial for pathogen elimination [2]. In this work this effect is analyzed for two types of bacteria—gram-negative *Escherichia coli* and gram-positive Staphylococcus aureus—as well as one type of fungus, *Aspergillus flavus*, inoculated onto the coat of wheat seeds.

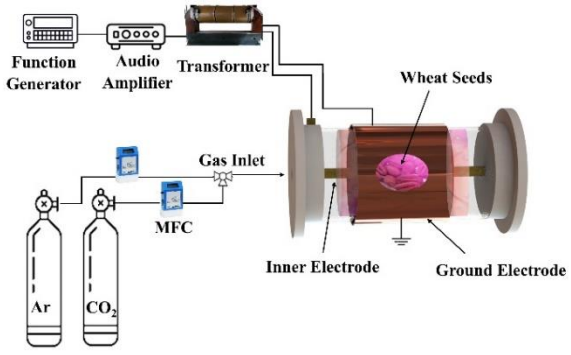



Figure 1: DBD discharge Packed with wheat seeds

The experimental investigations are performed for a constant total inlet gas flow rate of 500 ccm. First, at 20% $CO_2$ concentration in $CO_2$/Ar gas mixture for different frequencies of 3.6 kHz, 4 kHz, 5 kHz, and 6 kHz. Second, at constant frequency of 3.6 kHz and variable $CO_2$ concentration in $CO_2$/Ar gas mixture of 10%, 20%, and 30%.

## 2 Results

Seed germination parameters increase with rising frequency and $CO_2$ concentration in $CO_2$/Ar gas mixture. The highest bacterial and fungal death rate is observed at the lowest frequency of 3.6 kHz and decreases as the frequency increases up to 6 kHz. Similarly, the maximum bacterial and fungal death rate occurs at the lowest $CO_2$ concentration of 10% in the $CO_2$/Ar gas mixture and decreases as the $CO_2$ concentration increases up to 30%."

## 3 Conclusion

Using $CO_2$/Ar gas mixture in seed packed DBD increase seed germination and causes bacterial and fungal death more rapidly than with Ar plasma alone.

**Acknowledgements:** Authors acknowledge the support during this work of the Science, Technology & Innovation Funding Authority (STDF), Egypt, under grant number: Applied Science Grant- 45970.

**References**

[1] Judée, F., Dufour, T. Seed-packed dielectric barrier device for plasma agriculture: Understanding its electrical properties through an equivalent electrical model. *J. Appl. Phys*. **128**, 044901. (2020).
[2] Mestre, E., Orel, I., Henze, D., Chauvet, L., Burhenn, S., Dozias, S., Brulé-Morabito, F., Golda, J., Douat, C. Comparison of CO production and Escherichia coli inactivation by a kHz and a MHz plasma jet, *Plasma Process Polym*. **21,** 3. (2023).

# Plasma-Treated Soil for Sustainable Agriculture: Pesticide Removal, Enhanced Porosity, and Water Retention

Sushma Jangra, and Ram Prakash

*Department of Physics, Indian Institute of Technology Jodhpur, Jodhpur, Rajasthan, India*

*e-mail (speaker): sushma.1@iitj.ac.in*

Recent research has explored the potential of cold plasma in agricultural applications [1], [2] . Cold plasma offers several benefits for sustainable farming, including the suppression of pathogens, pests, weeds, and the degradation of pesticides in soil. The presence of pesticide residues in soil poses significant environmental and health concerns, which can be effectively addressed through non-thermal plasma technology [3], [4]. In this study, a Dielectric Barrier Discharge (DBD)-based cold atmospheric pressure plasma system is employed to facilitate pesticide degradation in soil. Several factors influence the degradation efficiency, including electrode gap, applied voltage, frequency, initial pesticide concentration, soil moisture content, and pH levels. The primary reactive species responsible for pesticide breakdown include nitrogen oxides ($NO_x$), ozone ($O_3$ ), and hydroxyl radicals (•OH) generated during plasma discharge.

To gain deeper insights into the process, the electrical characteristics and temperature variations within the DBD plasma source have been analysed. The pesticide concentration in soil has been quantified using UV-Vis spectrophotometry, High-Performance Liquid Chromatography (HPLC), and Gas Chromatography-Mass Spectrometry (GC-MS). Additionally, the impact of plasma treatment on soil nitrite levels post-degradation has been investigated. Plasma treatment has shown significant enhancement in nutrient bioavailability in soil by breaking down complex organic matter and transforming nutrients into more accessible forms. Moreover, it also alters the soil's physical and chemical properties, as confirmed by Field Emission Scanning Electron Microscopy (FESEM) and Fourier Transform Infrared Spectroscopy (FTIR), leading to improved porosity, water retention, and aeration. Plasma-based agricultural technologies hold significant promise for advancing sustainable farming practices. The comprehensive findings of this study will be presented in detail.

## References

[1] S. Jangra, A. Mishra, R. Mishra, S. Pandey, and R. Prakash, "Transformative impact of atmospheric cold plasma on mung bean seeds: Unveiling surface characteristics, physicochemical alterations, and enhanced germination potential," *AIP Adv*, vol. 14, no. 7, Jul. 2024, doi: 10.1063/5.0211662.

[2] S. Jangra, R. Mishra, A. Mishra, S. Pandey, and R. Prakash, "Analysis of short-term treatment effects of dielectric barrier discharge plasma to improve germination characteristics of wheat seeds," *Radiation Effects and Defects in Solids*, vol. 179, no. 7–8, pp. 1023–1031, Jul. 2024, doi: 10.1080/10420150.2024.2378437.

[3] J. Zhan *et al.*, "Gasoline degradation and nitrogen fixation in soil by pulsed corona discharge plasma," *Science of The Total Environment*, vol. 661, pp. 266–275, Apr. 2019, doi: 10.1016/j.scitotenv.2019.01.183.

[4] M. Gavahian, C. Sarangapani, and N. N. Misra, "Cold plasma for mitigating agrochemical and pesticide residue in food and water: Similarities with ozone and ultraviolet technologies," *Food Research International*, vol. 141, p. 110138, Mar. 2021, doi: 10.1016/j.foodres.2021.110138.

# Air atmospheric pressure plasma, a green approach for the sanitation of leafy greens vegetables

Zh. Aliyeva[1], T. Maho[1], Ph. Guillot[1], C. Muja[1]

[1]*DPHE Laboratory, Toulouse University, INU J.F. Champollion, Place de Verdun, Albi, France*

Non-thermal plasma technology has emerged as a promising alternative to conventional sterilization methods due to its energy efficiency and reduced environmental impact. This study explores the use of an air atmospheric pressure plasma system for the sanitation of leafy green vegetables. A surface dielectric barrier discharge (SDBD) device was employed, and its discharge characteristics were analyzed through electrical, optical, and chemical diagnostics. The system's antimicrobial potential was evaluated using *Escherichia coli* O157:H7 as a model microorganism. Bacterial inactivation kinetics were determined on both metallic carriers and leafy greens, highlighting the impact of plasma parameters and substrate effects. The results demonstrate the effectiveness of non-thermal plasma for microbial reduction, supporting its potential as a green sanitation technology for fresh produce.

## 1 Introduction

Inactivation of microorganisms using non-thermal plasma technology has emerged as a promising alternative to conventional sterilization methods, offering advantages in terms of energy efficiency and environmental impact [1].

This study investigates the suitability of an air atmospheric pressure plasma system as a green technology for the sanitation of leafy greens vegetables.

## 2 Experimental set-up

The experimental setup consists of a surface dielectric barrier discharge (SDBD) device comprising two stainless steel electrodes separated by an $Al_2O_3$ alumina disk. The high-voltage electrode is powered by a pulse generator (U = 1–10 kV, f = 20 kHz, duty cycle = 1–30%). The device operates in ambient air at atmospheric pressure and is enclosed in a sealed 5 L glass chamber to maintain controlled relative humidity (30-85%) and confined RONS.

## 3 Plasma system characterisation

Through a parametric study, an in-depth characterization of the discharge was performed from electrical, optical, and chemical diagnostics. The power dissipated in the plasma was evaluated using voltage (Tektronix P6015A) and current (PEARSON™) measurements. Optical Emission Spectroscopy (PI-HRS-750 coupled with a PIMAX4) was employed to analyse plasma emissions. Additionally, $O_3$ and $NO_2$ concentrations in the chamber were monitored over time via absorption spectroscopy based on Beer-Lambert's law. The discharge dynamics, homogeneity, and stability were further assessed using an intensified camera (PI-MAX1). These comprehensive analyses were used to define the optimum operating parameters.

## 4 Sanitation potential

*Escherichia coli* O157:H7 (ATTC 700728) was used in this study as model microorganism to evaluate the plasma system sanitation potential. Metallic carriers inoculated with bacteria were treated in for 2 to 30 minutes in the reaction chamber and different plasma parameters. After the treatment bacteria were recovered their survival rate was determined by classical colony forming unit (CFU) counting on TSA agar media. Obtained data were used to determine the kinetics of microbial inactivation. Furthermore, inactivation of *E. coli* inoculated on green salad was examined to assess the matrix effect on sanitation potential.

**References**

[1] Harikrishna, S et al. Cold plasma as an emerging non-thermal technology for food processing: A comprehensive review. *Journal of Agriculture and Food Research* **14**, 100747 (2023).

# Effects of high overvoltages on the treatment of PFAS in water

A. Brisset[1], R. Prastiko[2], X. Duten[2], H. Budzinski[3], P. Labadie[3], G.D. Stancu[1] and A. Vega-Gonzalez[2]

[1]*Laboratoire EM2C, CNRS, UPR 288, CentraleSupélec, Université Paris-Saclay, 3 rue Joliot Curie, 91192, Gif-sur-Yvette, France*
[2]*Laboratoire LSPM, CNRS, UPR 3407, Université Sorbonne Paris Nord, 93430 Villetaneuse, France*
[3]*EPOC, EPHE, CNRS, UMR 5805, Université Bordeaux, 33600 Pessac, France*

The chemical structure of per-polyfluoroalkyl substances (PFAS), based on strong C-F bonds makes them extremely stable in the natural environments. Plasma technologies have a strong potential for degrading PFAS in water. Understanding of the plasma removal mechanisms is necessary to improve the efficiency and to better control the by-products. Here three types of discharges with the same deposition energy were investigated for plasma removal of PFAS. An AC and a nanosecond high voltage pulse discharge were used in a wire-to-water surface configuration, whereas an atmospheric pressure fast ionization wave was generated in a 3-pins configuration over the liquid surface. Faster initial decomposition rates and large differences in the by-products production were observed. The 3-pins geometry questions the role of contact surface as well as gas versus liquid chemistry.

## 1 Cold plasmas for water treatment

Non equilibrium discharges in contact with water produce high yields of reactive radicals such as H•, OH•, reactive oxygen and nitrogen species (RONS), aqueous electrons with $E°(H2O/e_{aq}^-) = –2.77$ V, but also (V)UV light, soft X-rays and induce hydrodynamic processes like shock waves that may contribute to the removal of organic molecules. For water treatment, the removal efficiency of many reactor configurations and plasma sources (DC, AC, RF, MW or pulsed discharges) were tested. For instance, the removal yield of pharmaceutical organic compounds presented in [1] ranged from a fraction of g/kWh to a more than a hundred g/kWh, authors highlighting the importance of the plasma source design.

## 2 Results of PFAS removal

In this work, we focus on two key elements that influence the treatment efficiency, namely the gas phase electron mean energy and the plasma-water contact surface. Particularly, the contaminant removal rate seems directly proportional to the contact area for plasmas above liquids [2].

First, we compared the removal of PFOS ($C_8F_{17}SO_3H$), PFOA ($C_7F_{15}COOH$) and some by-products after treatment with a 15-kV AC and a high voltage nanosecond pulsed discharge at 1.2 kHz repetition frequency. The high voltage pulse is characterised by a rise time of 1 ns, a 4 ns duration and 41 kV peak voltage. We ensured here that the same energy is deposited in the system and that the reactor design is kept the same. A UV-Vis spectroscopic method for routine measurement of PFOS was combined with liquid chromatography coupled to tandem mass spectrometry (LC-MS/MS). This allows to identify and follow the concentration of some PFAS after plasma treatment. Figure 1 compares the removal of a couple of by-products of PFOS by AC and ns discharges. When switching from AC to the ns-discharge, a shift of the absolute concentration of by-products from the longest to the shortest carbon chain species is observed. This shift is accompanied by a twice larger concentration of F- in the solution.

Second, for the atmospheric pressure fast ionization wave discharges generated in a 3-pins configuration over the liquid surface, we have demonstrated a similar removal efficiency of PFOS compared to the AC discharge despite reducing the plasma-water contact surface by about a factor ten.

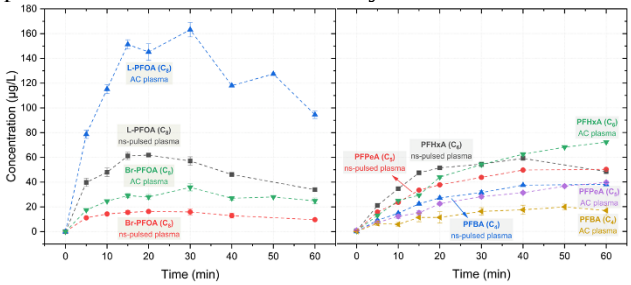



Figure 1: PFAS by-products removal with AC and ns discharges.

### Acknowledgments

This research was funded by MITI project STOP - PFAS 2024.

### References

[1] Banaschik *et al.* 2015, *Water Research*, **84**, 127–135.
[2] Stratton *et al.* 2015, *Chem. Engin. J.l*, **273**, 543–550.

# Effects of cold plasma treatment on bio-chemical composition of argan kernel and oil (Argania Spinosa (L.) Skeels)

K. Saber[1], A. Asbbane[2], A. Hani[1], M. Nid Ahmed[2], A. Abahazem[3], K. Wen Goh[4], A. Bouyahya[5], N. Merbahi[6], S. Gharby[2]

[1]*Materials and Renewable Energies Laboratory, Physics Department, Cité Dakhla BP 8106, Ibn Zohr University, Agadir, Morocco*
[2] *Biotechnology, Analytical Sciences and Quality Control Team, Polydisciplinary Faculty of Taroudant, Ibn Zohr University, Agadir, Morocco.*
[3] *Lasdis, Crmef-sm, Avenue Mly Abdellah, BP 106, Inezgane, Morocco*
[4]*Faculty of Data Science and Information Technology, INTI International University, Nilai, Malaysia*
[5]*Laboratory of Human Pathologies Biology, Faculty of Sciences, Mohammed V University in Rabat, Rabat 10106, Morocco.*
[6]*Laplace umr 5213-CNRS, 118 Route de Narbonne, Bât. 3R2, 31062 Toulouse Cedex 9, Paul Sabatier University, France*

**Abstract**

This study investigates the effects of cold plasma on argan kernels and oil quality. Four samples were analyzed: untreated (AKC0) and plasma-treated for 3 min (AKP3), 6 min (AKP6), and 12 min (AKP12). After 12 min, oil content increased, while protein content slightly decreased (3.40%). Significant changes in mineral composition were observed. Plasma treatment enhanced antioxidant capacity and polyphenol content. Free fatty acids decreased by 28.65%, while chlorophyll and carotenoid levels increased by 50.9% and 30.1%. No significant impact was found on the fatty acid profile, iodine, or saponification values. Cold plasma improves argan oil's nutritional and oxidative stability.

**Keywords:** Cold plasma, Argan oil, Kernels, Antioxidant activity, Oxidative stability, Fatty acid**.**

# Plasma-enhanced bio-inspired photocatalytic fabrics for efficient micropollutant removal from wastewater

T. Homola[1], A.P. Drdanová[1], A. Fatima[2] F. Zažímal[2], J. Ryba[3], A. V. Staňová [4,5], T. Mackuľak[1]

[1]*Department of Environmental Engineering, Slovak University of Technology in Bratislava, Slovakia*
[2]*Department of Plasma Physics and Technology, Masaryk University Brno, Czech Republic*
[3]*Department of Polymer Processing, Slovak University of Technology in Bratislava, Slovakia*
[4]*South Bohemian Research Center of Aquaculture and Biodiversity of Hydrogenases, University of South Bohemia in České Budejovice, Czech Republic*
[5]*Department of Analytical Chemistry, Comenius University in Bratislava, Slovakia*

Plasma-treated photocatalytic fabrics were engineered to improve wastewater treatment efficiency. SEM/EDX and BET analyses assessed their morphology and surface properties. Plasma modifications enhanced adhesion, stability, and photocatalytic performance. HPLC and LC-MS confirmed the effective degradation of micropollutants, including pharmaceuticals. Real wastewater testing demonstrated their practical applicability. Activated under 450 nm blue light, the fabrics efficiently removed contaminants, highlighting their potential for quaternary wastewater treatment and large-scale sustainable water purification.

The rapid increase in the global population coupled with ongoing advancements in societal development has intensified a critical water contamination issue, particularly when wastewater is released into natural water resources. Even after conventional treatment processes, wastewater still contains micropollutants, including pharmaceuticals, in concentrations reaching nanograms per liter (ng/L). These persistent contaminants pose severe environmental and health risks, with antibiotics contributing to the development of antibiotic resistance—an escalating global health crisis. The accumulation of such pollutants in aquatic ecosystems can lead to long-term adverse effects on biodiversity and human well-being. Recently, graphitic carbon nitride (g-$C_3N_4$) has attracted significant interest as a photocatalyst for pollutant degradation in wastewater, owing to its non-toxic properties, cost-effectiveness, environmentally benign precursor materials, and photocatalytic activity under visible light (bandgap of 2.7 eV). However, the practical application of g-$C_3N_4$ faces limitations due to weak substrate adhesion and structural instability upon continuous water exposure, resulting in delamination and subsequent release into aquatic environments.

The research focuses on the development of bio-inspired, photocatalytic functionalized fabrics designed to mimic the structural characteristics of spider webs. These fabrics incorporate g-$C_3N_4$ within their matrix and are produced through electrospinning of synthetic polymers. This fabrication approach enhances the mechanical stability of the materials while preserving the photocatalytic efficiency of g-$C_3N_4$. To further improve the surface properties of both the polymeric fibers and g-$C_3N_4$ itself, atmospheric pressure plasma treatment plays a crucial role in enhancing the stability, adhesion, and overall performance of these photocatalytic fabrics.

Comprehensive characterization was conducted employing SEM/EDX, XPS BET to analyze the morphology, elemental composition, and surface properties of the modified materials. The effectiveness of plasma-treated fabrics in degrading selected micropollutants was rigorously evaluated using HPLC and LCMS. The fabrics that demonstrated the most effective plasma-induced enhancements were further tested under real wastewater conditions, highlighting the transformative potential of plasma treatment in advancing photocatalytic wastewater remediation technologies.

Our findings demonstrate that the developed photocatalytic fabrics exhibit a high efficiency in removing and degrading a wide range of micropollutants from wastewater effluents when exposed to 450 nm blue light. This photocatalytic activation facilitates the breakdown of persistent contaminants, including pharmaceuticals and other organic pollutants, which are otherwise difficult to eliminate through conventional wastewater treatment methods. Given their strong performance, these fabrics have significant potential as an advanced solution for quaternary wastewater treatment, addressing the urgent need for effective removal of trace pollutants.

# Enhancing corrosion resistance of magnesium alloys with plasma treatment and electrospun biodegradable polymer coatings

L. Zahedi, P. Ghourchi Beigi, M. Stupavská and D. Kováčik

*Department of Plasma Physics and Technology, CEPLANT – R&D Centre for Plasma and Nanotechnology Surface Modifications, Faculty of Science, Masaryk University, Kotlářská 2, 602 00 Brno, Czech Republic*

A novel method for enhancing the corrosion control of magnesium-based implants has been studied using Diffuse Coplanar Surface Barrier Discharge (DCSBD). While magnesium is a crucial biodegradable element in the human body, it rapidly corrodes in body fluid, increasing pH and releasing $H_2$. A coating layer must serve as an effective barrier with strong adhesion while mimicking the extracellular matrix (ECM) to minimize corrosion consequences. In this study, the barrier properties of the electrospun nanofibers were studied while the polymer was functionalized using DCSBD before the electrospinning. Also, plasma treatment of the Mg substrate results in better adhesion of the protective nanofibrous layer. This two-step plasma treatment significantly improved the features of the electrospun coating and its barrier performance on Mg alloy, yielding a lowered corrosion rate implant suits orthopedic applications. This advancement eliminates the removal surgery and aims to bring comfort to patients using a biodegradable implant.

## 1 Introduction

Traditional metallic orthopedic implants, like stainless steel and titanium alloys, are non-degradable and often require removal due to complications such as toxic ion release and immune reactions. Magnesium (Mg) alloys offer a promising alternative with biocompatibility and controlled biodegradability, but their rapid corrosion leads to mechanical failure, hydrogen evolution, and pH disturbances. Electrospun biodegradable polymeric coatings serve as protective barriers, slowing degradation while enhancing cell adhesion and drug delivery. Electrospinning creates ECM-like 3D fibrous membranes for better tissue integration than dip-coating. Plasma activation of the Mg substrate can further improve polymer coating adhesion by increasing its hydrophilicity and incorporation of functional groups. Combining electrospun coatings with plasma treatment significantly enhances corrosion resistance and biocompatibility.

## 2 Experimental

This research used a low-temperature atmospheric-pressure plasma source, Diffuse Coplanar Surface Barrier Discharge (DCSBD), to modify the Mg substrate and functionalize the Polyhydroxybutyrate (PHB) powder. The PHB powder was treated for 2 minutes using DCSBD before preparing the electrospinning solution. DCSBD functionalized the polished Mg substrates for 5 seconds for better adhesion of the protective layer. The final sample was studied via SEM/EDX, ATR-FTIR, LCM, EIS, WCA, and SFE. The coated Mg was evaluated in Simulated Body Fluid (SBF) for seven days to monitor the evolution of hydrogen gas and pH changes.

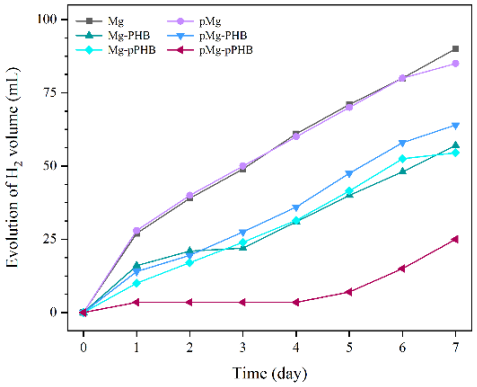



Figure 1: Hydrogen evolution of samples in SBF. The prefix "p" means plasma-treated.

## 3 Results and Discussion

Fig. 1 shows the evolution of $H_2$ of the bare- and coated-Mg submerged in SBF within 7 days. As the trends present, the creation of hydrogen from the reaction between magnesium and oxygen has the highest rate for the untreated and treated bare-Mg. The electrospun nanofibers show the barrier effect by decreasing the slope of this trend, which has been proved in previous studies. Moreover, interestingly, the two-step plasma-treated sample has the lowest released hydrogen, which is in agreement with pH change and reduction of corrosion rate.

**References**

[1] Rivero, P. J. *et al. Metals* **10**, 350 (2020).
[2] Zhu, Y. *et al. Journal of Polymer Science* **60**, 32-51 (2022).
[3] Fang, H. *et al. Corrosion Science* **168**, 108466 (2020).

# Boundary Condition for the electron kinetics of a plasma using a microphysical description of the wall

Felix Willert[1], Clemens Hoyer[1] and Franz X. Bronold[1]

[1] *Universität Greifswald, Institut für Physik, Felix-Hausdorff-Straße 6, D-17489 Greifswald, Germany*

For an electron Boltzmann equation we derive a Marshak type energy- and angle-dependent boundary condition, containing the electron microphysics inside the wall. It uses the electron surface scattering kernel, describing electron reflection as well as secondary emission from a microscopic solid-state physics point of view. We incorporate the kernel within an Legendre polynomial expansion approach for solving the electron Boltzmann equation, but the kernel can be also used for PIC-MCC simulations. Numerical results for an argon plasma in contact with a silicon surface are presented, showing the significance of the microphysics-based boundary condition.

In this work we show how to employ a surface scattering kernel (SSK), as calculated in [1], in the boundary condition of a Boltzmann equation. The SSK is the kernel of the integral equation, relating the in- with the outgoing electron flux at a boundary. The kernel describes the microphysics inside the wall, including reflection at the wall, impact ionization, scattering with phonons and image charge effects. The kernel was calculated using the invariant embedding approach.

The newly constructed boundary condition was integrated into an existing code [2], describing a dc-discharge, using a hydrodynamical description for the heavy species and a Boltzmann equation for the electrons. The latter one is being expanded in terms of Legendre polynomials up to arbitrary order. The Marshak-type boundary conditions are derived by relating the odd-order moments of the distribution function of the in- and outgoing electrons at the anode and the cathode. Hereby the expansion coefficients are connected to macroscopic quantities, like the flux. These well-defined quantities allow us to correctly implement the microscopic processes inside the wall.

The microphysics-based boundary condition—even though it covers a lot more effects than a phenomenological one—only leads to modifications of some values in the discretized transport equation with values taken from the SSK. Thus, almost no additional numerical effort is needed to solve the equation compared to common boundary conditions. These types of boundary conditions can be straightforwardly adapted to other deterministic simulations of the electron kinetics, but the SSK and the underlying physics can be used for PIC simulations as well.

Our numerical results for an Argon plasma in contact with a silicon wall show a significant change in the densities and fluxes in the plasma sheath and in their angular and energetic distribution. These changes lead to smaller, but eventually important changes in the bulk as well. For example the electron flux from the anode into the system is stronger and shifted towards lower energies, see Fig. 1. - Supported by Deutsche Forschungsgemeinschaft (DFG)–495729137.

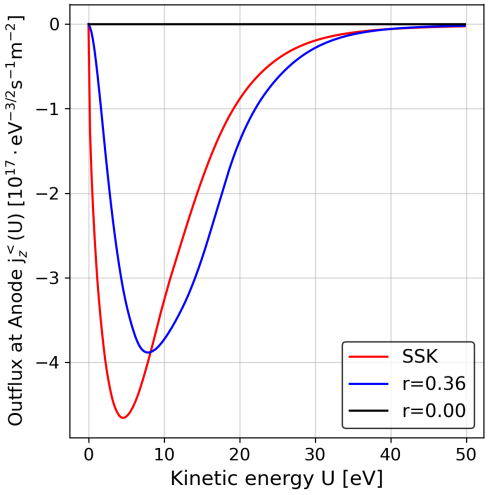



Figure 1: The flux of electrons entering the plasma from the anode. Due to the inelastic effects inside the solid, a higher flux at lower energies appears, compared to common boundary conditions.

## References

[1] Bronold, F.X. and Willert, F. Electron surface scattering kernel for a plasma facing a semiconductor. *Phys. Rev. E* **110**, 035207 (2024).

[2] Becker, M.M., Grubert, G., and Loffhagen, D. Boundary conditions for the electron kinetic using expansion technique. *Eur. Phys. J. Appl. Phys.* **51**, 11001 (2010).

# MERLIN, an adaptative LTE radiative transfer model for any mixture

A. Favre[1], A. Bultel[1], V. Morel[1], L. Gosse[1], L. Lemerle[1] and M. Lesage[2]

[1] *CORIA UMR 6614, Université de Rouen - Normandie, 76801 Saint-Etienne du Rouvray, France*
[2] *R. Tech, Parc Technologique Delta Sud, 09340 Verniolle, France*

The MERLIN (MultiElemental Radiative equiLibrIum emissioN) code is designed to simulate any thermal plasmas emission at Local Thermodynamic Equilibrium (LTE). The main application is the chemical quantification of plasma species via Calibration-Free Laser-Induced Breakdown Spectroscopy (CF-LIBS).

Laser-Induced Breakdown Spectroscopy (LIBS) technique allows to measure the elemental composition of a sample irradiated by a laser pulse. When the objective is to characterize a known alloy or to analyze the sample semi-quantitatively, standards can be used. This method refers to the ‘‘calibrated LIBS’’. When the studied sample is complex (for instance unknown alloy [1] and/or concentration gradients [2]), the modeling of the experimental emission spectra leads to the determination of the laser-induced plasma characteristics including its composition. This second method refers to the ‘‘Calibration-Free LIBS’’ (CF-LIBS).

In this communication, we present the radiative transfer code MERLIN (MultiElemental Radiative equiLibrIum emissioN) aiming at modelling experimental spectra of a laser-induced plasma in Local Thermodynamic Equilibrium (LTE) conditions for calibration-free LIBS [3]. MERLIN provides the simulated spectra for any elementary mixture thanks to queries from spectral databases available online. The code is optimized and modular to allow outputs even for a high number of species. The validation of MERLIN is based on a thorough analysis of the plasma emission performed on the alloy Eurofer97 in experimental conditions providing the LTE. The reconstruction of the observed spectra is performed with MERLIN (see Figure 1). No adjusted variable is required since all the necessary parameters are derived from experiments. The spectra of interest exhibits several Fe II and Cr II lines which are strongly self-absorbed (black body saturation). The simulation of the emission centered around 275 nm thus allows to validate a) the LTE computation, b) the radiative transfer resolution and c) the convolution method of several broadening mechanisms.

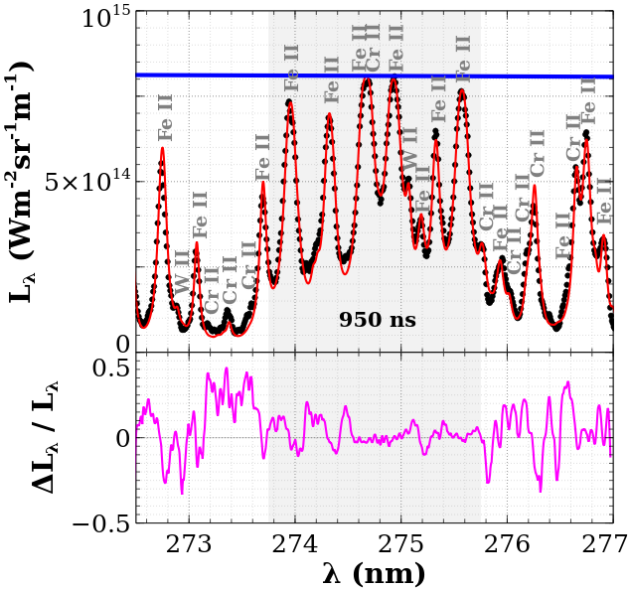



**Fig. 1** : Eurofer97 laser-induced plasma experimental emission (in black) compared to MERLIN simulation (in red). Black body radiation is exposed in blue.

**References**

[1] Favre, A. *et al.*, *Phys. Src.*, **99**, 035609 (2024).
[2] Favre, A. *et al.*, *J. Nucl. Mat.*, **591**, 154924 (2024).
[3] Favre, A. *et al.*, *JQSRT*, **330**, 109222 (2025).

# Simulations of radio frequency capacitively coupled plasmas including external circuits

S. Yu[1,2], J. Schulze[2], Y. Zhang[3] and W. Jiang[4]

[1] *School of Electrical and Electronic Engineering, Huazhong University of Science and Technology, Wuhan 430074, People's Republic of China*
[2] *Chair of Applied Electrodynamics and Plasma Technology, Ruhr University Bochum, Germany*
[3] *Department of Physics, Wuhan University of Technology, Wuhan 430070, People's Republic of China*
[4] *School of Physics, Huazhong University of Science and Technology, Wuhan 430074, People's Republic of China*

A self-consistent method that couples capacitively coupled plasmas (CCPs) with generalized external circuits is proposed, enabling accurate modelling and optimization of power transfer in CCP systems. This work systematically studies the impedance matching under various conditions, including single-frequency and tailored voltage waveform (TVW) excitation as well as plasmas considering RF transmission line effects. Furthermore, the effect of impedance matching on the electron heating mode transition is investigated, which provides new insights into the power coupling dynamics and plasma behaviours. These results can help optimize the design and operation of advanced plasma processing systems.

## 1 Introduction

Plasma technology is playing an increasingly critical role in a wide range of industrial applications, including semiconductor manufacturing, materials processing, surface modification, and environmental protection [1]. In these applications, radio-frequency (RF) and microwave discharges such as inductively coupled plasma (ICP) and capacitively coupled plasma (CCP) are widely employed due to their ability to generate high-density, low-temperature plasmas under controllable conditions.

In practical systems, plasma sources are not isolated but rather integrated into complex electrical environments that include matching networks, RF generators, transmission lines, and other circuit components. The interaction between the plasma and the external circuit strongly affects discharge behaviours. Accurate modelling and design of this interaction are crucial for improving energy efficiency and ensuring stable, repeatable operation in industrial applications.

In this work, impedance matching for plasmas excited by single frequency and tailored voltage waveforms is investigated based on our self-consistent model. The computational description of the plasma utilizes an improved 1d3v implicit PIC/MCC code. The discharge is maintained in pure argon at a pressure of 200 mTorr.

## 2 Results and discussion

For single frequency CCPs, a L-type impedance matching network with two adjustable capacitors and one adjustable inductor is used. By calculating the plasma impedance and the matching equations, the circuit parameters were iteratively updated to find the best matching parameters. By adjusting the capacitance and the inductance of the circuit, the reflection coefficient can be significantly reduced from 0.913 to 0.004. Meanwhile, the electron density increases from the initial $1 \times 10^{15}\ m^{-3}$ to $1.1 \times 10^{16}\ m^{-3}$, and the fraction of the power provided by the RF source and absorbed in the increases from less than 10% to about 39% [2].

For CCPs excited by TVW, a similar LC resonant network of Foster's 2nd form for multi-frequency impedance matching is proposed. The simulation results show that the addition of a serial multi frequency IMN with well-designed matching parameters can greatly improve the energy efficiency of plasma generation via TVW. The reflection coefficients of all three frequency components can be reduced to below 0.01 after matching. Additionally, a change in the quality of the impedance matching is found to cause an electron heating mode transition from ohmic heating-dominated to pressure/ambipolar electron heating-dominated [3].

**References**

[1] Lieberman Michael A. and Lichtenberg A. J. Principles of Plasma Discharges and Materials Processing 2nd Edition. *Wiley* (2005)

[2] Yu, Shimin, et al. Best impedance matching seeking of single-frequency capacitively coupled plasmas by numerical simulations. *Journal of Applied Physics* **132**.8 (2022).

[3] Yu, Shimin, et al. Kinetic simulations of capacitively coupled plasmas driven by tailored voltage waveforms with multi-frequency matching. *Plasma Sources Science and Technology* **33**.7 075003 (2024)

# Discharge behaviour and chemistry of cold plasma jets

T. Murakami[1], S. Okada[1] and I. Saito[1]

[1] *Seikei University, Musashino, Tokyo, Japan*

Two-dimensional numerical simulation is conducted focusing on the behavior of ionization wave propagating from a kHz-powered cold plasma jet operated in dry air. The ionization wave initiated in the discharge core region propagates to ambient air, which induce ionization and excitation of air components, such as $N_2^+$, $O_2^+$ and O even in the afterglow region.

## 1 Introduction

Atmospheric pressure dielectric barrier discharge jets are one of the typical examples of low temperature plasma sources. The plasma is ignited by a pulsed discharge and passed through a guided helium jet. The luminous zone (plasma plume) extending into the open air is not continuous, but actually consists of a series of streamer-like ionization waves [1,2]. In this work, we developed a two-dimensional numerical model of a helium-based plasma jet and simulated the ionization propagation phenomenon and the chemical reactions induced.

## 2 Modelling

The two-dimensional plasma-fluid dynamics model consists of a steady-state fluid dynamics part (Navier-Stokes and heat transfer equations), a plasma mechanics part (drift-diffusion and Poisson equations) and chemical kinetics. The *dV/dt* of the applied voltage is approximately $4.5\times10^9$ V/s, with a peak value of 6 kV. Chemical species, He, $He^+$, $He(2^3S)$, $He(2^1S)$, $He_2^*$, $He_2^+$, $N_2$, $N_2^*$, $N_2^+$, $O_2$, $O_2^*$, $O_2^+$, $O_2^-$, $O_3$, $O_3^-$, O, $O(^1D)$ and $O^-$, and electrons, are considered. The model includes 60 electron collision reactions, 15 chemical reactions and 19 surface reactions.

## 3 Results

Figure 1 shows a numerically derived 2D map of the ionization frequency of helium atoms, which allows us to understand the propagation of ionizing waves. Ionizing waves travel upward from the electrode toward the open end of the discharge tube. A streamer-like structure forms on the outside of the tube. The propagation velocity is up to 50 km/s.

Figure 2 shows the spatial distribution of the maximum values of number densities and reaction rates. The number densities of electrons, $He^+$, $He(2^3S)$, and $He_2^*$ are between $10^{18}$ and $10^{20}$ $m^{-3}$ inside the discharge tube. They increase to about $10^{20}$ $m^{-3}$ within an approximately 5 mm from tube exit. The ionization and excitation rates of helium atoms are significant even outside the tube. This leads the ionization ambient oxygen and nitrogen molecular and production of reactive species (atomic oxygen).

## 4 Conclusion

Numerical simulation clarifies that the ionization wave initiated in the discharge core region propagates to ambient air, which induce ionization and excitation of air components, such as $N_2^+$, $O_2^+$, and O even in the afterglow region.

This work was partially supported by JSPS KAKENHI 20KK0089, 23H01404, 24H00036, 24H02246 and 24H02249.

### References

[1] J-P. Boeuf, et al. J. Phys. D: Appl. Phys. **46**, 015201 (2013).
[2] C. McDonnell, et al. J. Plasma Phys. **88**, 905880316 (2022).

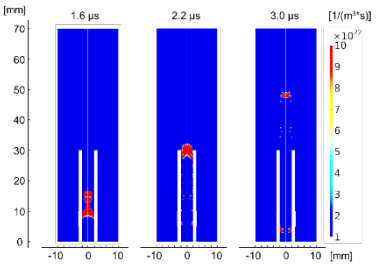



Fig.1 Propagation of ionization waves from a jet.

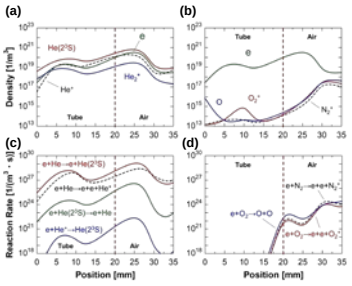



Fig.2 Spatial distribution of species number densities (a, c) and reaction rates (b, d).

# High-order gyrocoordinate transformations for electron dynamics in axisymmetric magnetic fields

R.P. Brinkmann[1], L. Vogelhuber[1], K. Köhn[1], D. Krüger[1], J. Kallähn[1], L. Xu[1,2], Y. Sharova, D. Eremin[1]

[1] *Theoretical Electrical Engineering, Ruhr-University Bochum, 44701 Bochum, Germany*
[2] *Physical Science and Technology, Soochow University, Suzhou 215006, PR China*

Low-pressure gas discharges with axisymmetric magnetic fields play a crucial role in surface engineering, electric propulsion, and related technologies. This study analyzes the electron motion in such discharges, assuming that the Larmor radius $r_L$ is much smaller than a characteristic scale $L$ (magnetic curvature radius). A transformation is constructed as a power series in $r_L/L$ that relates cylindrical coordinates $(r,\theta,z,v_r,v_\theta,v_z)$ to a set of newly defined gyrocoordinates $(\psi,\vartheta,s,\chi,\varphi)$. By construction, the guiding center magnetic flux $\psi$ and the speed $v$ are exact constants of motion, while the gyrophase $\varphi$ evolves on the gyro time scale $r_L/v$, the guiding center arc length $s$ and the pitch angle $\chi$ on the bounce time scale $L/v$, and the guiding center azimuth $\vartheta$ on the drift time scale $L^2/r_L v$. The formalism is general enough to accommodate all magnetic fields but can easily be specialized to the case of current-free vacuum fields.

## 1 Partially magnetizes gas discharges

Partially magnetized low pressure gas discharges with axisymmetric magnetic fields play a crucial role in thin film deposition and other surface engineering. They are widely used in, e.g., DC, RF, and high-power impulse magnetron sputtering (DC/RFMS, HiPIMS). Magnetic fields of 10 to 100 mT confine the electrons and enable operation on the left of the Paschen curve. Pressures are 0.1 - 1 Pa, densities $10^{18}$ - $10^{20}$ $m^{-3}$ [1].

## 2 Research objective

Issues of electron confinement, plasma transport, and overall discharge stability have been at the center of research for several decades [2]. For deeper insight one needs to understand how the electron dynamics emerges from a superposition of gyration around, motion along, and drift across the magnetic field lines. We aim to contribute by exploiting the very essence of magnetization itself, the smallness of the electron gyroradius $r_L$ compared to the system scale length L. Similar theories, called driftkinetics or gyrokinetics, were very successful in fusion and space research [3]. We seek an approach tailored to our own specifics.

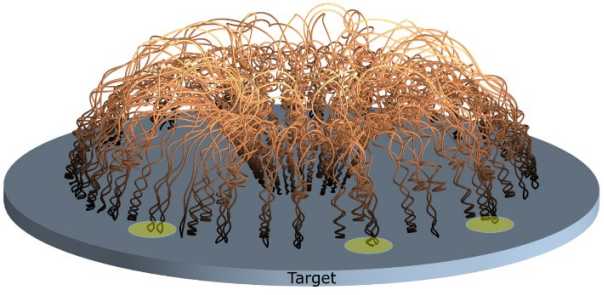



Fig 1: Trajectory of a single electron in a magnetron field, showing a superposition of gyration, bouncing, and drift.

## 3 A gyro-coordinate transformation

A coordinate transformation is set up to express the electron position and velocity in standard cylindrical kinetic coordinates $(r,\theta,z,v_r,v_\theta,v_z)$ in terms of a newly developed system of gyrocoordinates $(\psi,\vartheta,s,v,\chi,\varphi)$. The names/symbols of the new coordinates are meant to evoke associations but are defined in a novel way:

- The flux value $\psi$ of the guiding center is a measure of the canonical angular momentum $p_\theta$.
- The speed $v$ is a measure of the electron energy.
- The azimuth angle $\vartheta$ and the arc length parameter $s$ of the guiding center, as well as the pitch angle $\chi$ and the gyrophase $\varphi$ are power series in $r_L/L$.

By construction, the guiding center magnetic flux $\psi$ and the total speed $v$ are exact constants of motion. The gyrophase $\varphi$ evolves on the gyro time scale $r_L/v$; arc length s and pitch angle $\chi$ on the bounce scale $L/v$, and the azimuth $\vartheta$ on the drift time scale $L^2/r_L v$.

## 4 Conclusion and outlook

An innovative formalism was presented to describe the electron dynamics in low pressure gas discharges with axisymmetric magnetic fields. A comparison with standard guiding center theories will be given.

Support by DFG via PN 550860775 is acknowledged.

**References**

[1] J.T. Gudmundsson, Magn. sputtering discharges, *Plasma Sources Sci. Technol.* **29,** 113001 (2020)
[2] A. Hecimovic, A. von Keudell, Spokes in HiPIMS plasmas, *J. Phys. D: Appl. Phys.* **51**, 453001 (2018)
[3] J.R. Cary and B. Brizard, Hamiltonian theory of guiding-center motion, *Rev. Mod. Phys.* **81**, 693 (2009)

# Comparison of 3D fluid and particle models for negative streamers

Thomas Smits[1], Jannis Teunissen[1] and Ute Ebert[1,2]

[1]*Centrum Wiskunde & Informatica, Amsterdam, The Netherlands*
[2]*Eindhoven University of Technology, Eindhoven, The Netherlands*

This work focusses on comparing numerical models of negative streamers in mixtures of $CO_2$ and $C_4F_7N$, which is a high-voltage insulation gas that is proposed to replace the commonly used $SF_6$, as $SF_6$ is the most potent greenhouse gas. We focus on the initial stage of discharge, studying negative streamers without free electron sources. Previous numerical work has been focussed on 2D fluid or 3D particle models, but we compare and verify 3D fluid models against particle simulations. Additionally, is it studied how different cross-section datasets for $CO_2$ and $C_4F_7N$ and different Boltzmann solvers affect transport and reaction coefficients. The goal of this study is to determine a numerical setup for 3D fluid modelling of stochastic negative streamers in mixtures of $CO_2$ and $C_4F_7N$.

$SF_6$ is commonly used in high-voltage equipment as an insulating gas. However, $SF_6$ is also the most potent greenhouse gas, making its replacement with more eco-friendly alternatives, such as mixtures of $CO_2$ and $C_4F_7N$, necessary. Insulating gases require a high electron attachment coefficient and breakdown field.

Our focus is on the initial stage of discharge, known as streamer discharges. Streamers are non-stationary, transient, and often precede other discharges. We study negative streamers, which propagate against the direction of the electric field. Previous modelling work on negative streamers in mixtures of $CO_2$ and $C_4F_7N$ has primarily focused on 2D fluid simulations [2,3,4] or 3D particle simulations [1]. We have compared and verified 3D fluid models against the 3D particle model of [1]. It is crucial to verify that fluid models can quantitatively describe negative streamers in mixtures of $CO_2$ and $C_4F_7N$, to enable long-time-scale simulations.

The input transport and reaction coefficients for the fluid model are calculated from cross-sections using Boltzmann solvers. Different cross-section datasets for $CO_2$ and $C_4F_7N$, as well as different solvers, exist. We study the sensitivity of the transport and reaction coefficients to the choice of cross-section dataset and Boltzmann solver

The results of these studies provide a numerical fluid model setup of negative streamers in stochastic 3D fluid simulations of $CO_2$ and $C_4F_7N$ mixtures.

## References

[1] Guo, B. et al., **Plasma Sources Sci. Technol.** 32, 115001 (2023)
[2] Yan, X. et al., **AIP Adv.** 13, 03 (2023)
[3] Simonović, I. et al., **Plasma Sources Sci. Technol.** 33, 085012 (2024)
[4] Wang, F. et al., **IEEE Trans. Plasma Sci**. 49, 2048-2054 (2021)

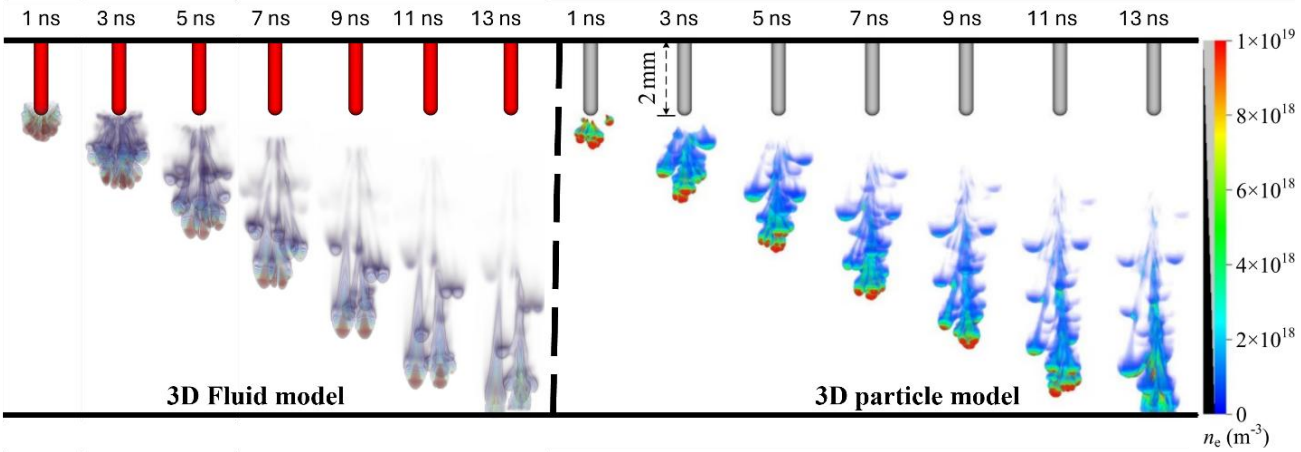



**Figure 1: Comparison of electron density in negative streamers between the fluid model (left) and the particle model [1] (right). Both models use a stochastic initial seed of electrons and ions at the electrode tip. No photoionization or background ionization is present.**

# Numerical Simulation of Partial Discharge Processes in Defects of Insulating Material

Y. Gao[1], U. Ebert[1,2], and J. Teunissen[1]

[1] *Centrum Wiskunde & Informatica (CWI), Amsterdam, the Netherlands*
[2] *Eindhoven University of Technology, Eindhoven, the Netherlands*

## 1 Introduction

The insulation of coils in high-voltage devices must withstand high voltages and strong electric fields. Defects in the insulation are critical sites for partial discharges (PDs) and potential failure points in the system. We consider a coil where enameled wires are embedded in epoxy resin. Defects can degrade the insulation. Voids inevitably form in the epoxy resin during curing[1], and thermal expansion or mechanical stress may cause delamination between the epoxy and enameled wire, leading to cracks. These defects have much lower dielectric strength than the epoxy resin, making them likely sites for PD initiation and propagation, which accelerates material aging and increases the risk of failure. Significant potential differences exist between coil layers, creating an uneven electric field[2]. A defect located in such a high-field region is more likely to trigger PDs.

### 1.1 Aims

The highly non-uniform electric field around the coil makes discharge processes difficult to predict, and the criteria for streamer initiation remain debated. We aim to numerically simulate the discharge process within defects to study PD initiation and propagation, improve PD inception voltage prediction, and refine streamer initiation criteria. Additionally, by comparing simulation results with experimental data, we seek to infer properties of the gas inside defects, such as gas type and pressure, providing insights for practical applications. Furthermore, we will explore the impact of various factors on defect-induced PDs and provide advice for the operating conditions of the coil.

### 1.2 Methods

Our study will begin with Particle-in-Cell (PIC) simulations, starting from simple structures with uniform fields and gradually extending to more complex conditions with non-uniform fields and defect structures. The discharge gas will initially be air and later expand to other gases.

**References**

[1] Deng, Y., et al. The combined impact of voids and thermal aging on the mechanical reliability of epoxy resin evaluated by statistical analysis. *Polymer Degradation and Stability* **215** (2023): 110455.
[2] Shishavan, Arvin P., et al. A Study on Electrical Stress Distribution of Racetrack Coils Used in Ironless Linear Actuators with a Hybrid Modeling Approach. *2024 International Conference on Electrical Machines (ICEM)*. IEEE (2024).

# Mode Transitions in Micro Cavity Plasma Arrays: The Influence of Oxygen Admixtures on Discharge Dynamics

D. Steuer[1], H. van Impel[1], R. Labenski[1], V. Schulz-von der Gathen[2], M. Böke[2] and J. Golda[1]

[1]*Plasma Interface Physics, Ruhr-University Bochum, D-44801 Bochum, Germany*
[2]*Experimental Physics II: Physics of Reactive Plasmas, Ruhr-University Bochum, D-44801 Bochum, Germany*

This study investigates the mode transition in a micro cavity plasma array reactor operating with helium and oxygen admixtures (0–5%) at atmospheric pressure. Optical emission spectroscopy, power measurements, and electric field diagnostics reveal a transition from a homogeneous glow discharge to a filamentary mode at oxygen concentrations above 1%. This shift is accompanied by changes in pulse characteristics, electric field distribution, and atomic oxygen formation, providing crucial insights into optimizing discharge processes e.g. for plasma catalysis.

Dielectric barrier discharges (DBDs) are a well-established technology for plasma-based gas conversion and surface treatment. Their ability to generate reactive species under atmospheric pressure makes them highly relevant for oxidation processes. However, the addition of small amounts of molecular gases, in this case oxygen, is known to significantly alter the discharge dynamics. Depending on the application, these changes may be undesirable or require adjustments to the reactor geometry and discharge parameters to maintain optimal operating conditions. In this study, a micro cavity plasma array reactor is used to investigate how small molecular oxygen admixtures (0–5%) in a helium discharge influence plasma behaviour.

The experimental setup consists of a micro cavity plasma array with a dielectric barrier configuration [1], operated at atmospheric pressure with controlled gas flows. Optical emission spectroscopy (OES) is used to monitor the discharge structure [2], reactive species formation [3,4] and electric field dynamics based on Stark splitting [5]. Electrical measurements allow for precise characterization of power dissipation and ignition behaviour.

In the absence of oxygen, the plasma remains in a homogeneous atmospheric pressure glow discharge (APGD) mode, with continuous or quasi-pulseless emission. With small oxygen admixtures up to 0.5%, a pseudo-glow regime is observed, where individual pulses become distinguishable. At higher oxygen concentrations (≥1%), the plasma transitions into a filamentary discharge, characterized by localized ionization channels and increased pulse-to-pulse variability. The measured electric field distribution confirms a significant change in discharge structure, with localized regions of high field strength corresponding to the emergence of filamentary modes. This transition is also reflected in the power measurements, which show a non-linear dependence on oxygen admixture and a sharp increase in ignition voltage.

The formation of atomic oxygen is closely linked to the discharge mode. In the homogeneous glow regime, oxygen is efficiently dissociated, leading to high atomic oxygen densities. However, as the discharge transitions into a filamentary state, dissociation efficiency decreases due to increased recombination and spatial inhomogeneity of the plasma. Time-resolved OES measurements further indicate that the majority of atomic oxygen is produced during the distinct discharge pulses, highlighting the role of pulse dynamics in reactive species generation.

These results provide important insights for the optimization of plasma-based oxidation processes. By controlling the discharge mode through gas composition and external electrical parameters, plasma reactors can be tuned to maximize conversion efficiency while minimizing thermal load and unwanted filamentary behaviour.

**Ackknowledgments**

This work is funded by the Deutsche Forschungsgemeinschaft (DFG, German Research Foundation) via CRC 1316 (project A6).

**References**

[1] S. Dzikowski *et al*. *Plasma Sources Sci. Technol.* **29** 035028 (2020)
[2] D. Steuer *et al. J. Phys. D: Appl. Phys.* **58** 085211 (2025)
[3] D. Steuer *et al. Plasma Sources Sci. Technol.* **32** 025013 (2023)
[4] D. Steuer *et al. Plasma Sources Sci. Technol.* **33** 125007 (2024)
[5] H. van Impel *et al. Plasma Sources Sci. Technol.* **33** 105008 (2024)

# On the measurements of temperature by optical emission spectroscopy in nanosecond SDBD: check by calculations

B. Zhang[1], G. Kreyder[2], N. Popov[3] and S. M. Starikovskaia[2]

[1] College of Automation Engineering, Nanjing University of Aeronautics and Astronautics, Nanjing 211106, People's Republic of China
[2] Laboratory of Plasma Physics (CNRS, Ecole Polytechnique, Sorbonne Université, LPP), route de Saclay, 91128 Palaiseau, France
[3] Skobeltsyn Institute of Nuclear Physics, Moscow State University, Moscow, 119991, Leninsky gory, Russia

This work investigates nanosecond surface dielectric barrier discharge (nSDBD) in atmospheric pressure air using experiments and 2D numerical modelling. Measurements include current, energy input, ICCD imaging, and gas heating during discharge and afterglow. The properties of a weaker probe discharge, formed by a reflected pulse 500 ns later, are analysed. The feasibility of using this secondary pulse for post-discharge gas temperature diagnostics is discussed.

The nanosecond surface DBD discharge is studied in classical airflow configuration. High-voltage and low-voltage electrodes, produced from 0.1 mm copper foil, are glued on the opposite side of a 0.5 mm PVC layer. Key parameters of the high-voltage pulse are the following: rise time of 4 ns, pulse duration at FWHM of 20 ns, and a voltage amplitude on the electrode U $= +27.5$ kV.

Spectrally integrated plasma images of streamers were captured by an ICCD camera (PIMax4, Princeton Instruments). The emission in UV-vis corresponds mainly to the $N_2(C^3\Pi_u) \rightarrow N_2(B^3\Pi_g)$ SPS transition. High-resolution images were taken with a long-distance microscope (LDM-1UV, LaVision). The temperature is measured by collecting the SPS emission in the direction perpendicular to the plane of the discharge.

Analysing obtained experimental data and 2D numerical modelling, it was concluded that the measured value of temperature is influenced not only by the actual gas temperature but also by the spatial distribution of SPS emission intensity, integrated over the detector's depth of field (DOF). In numerical modelling, the expected to be measured temperature $T_m(t)$ was calculated by the convolution of the gas temperature $T_g$ and the spatial distribution of SPS emission intensity.

In the figure, the black dot-dashed curve represents calculated gas temperature $T_g(t)$ at the point (x;y) = (1 mm; 25 $\mu$m), $x = 0$ which corresponds to the edge of the high-voltage electrode. Red curve describes the dynamics of $T_m(t)$ at x = 1 mm from the edge of the high-voltage electrode. The dashed part of the curve corresponds to the time interval when the measurements of the temperature are not possible

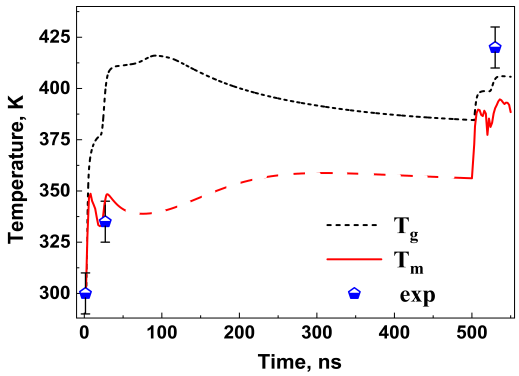



Figure 1: Temperature as a function of time (see text)

because of the absence of the population of $N_2(C^3\Pi_u)$ state by electron impact. Experimental data are given by symbols.

At the falling edge of the high-voltage pulse, the measured temperature is much lower than the calculated temperature. This effect illustrates that OY (vertical) profiles of the temperature and of the SPS emission are significantly different and as a result, provide a distortion of the measured temperature.

Another effect is observed in the afterglow, 500 ns later. In the secondary pulse, differently from the main pulse, the calculated OY-profiles of the gas temperature and the emission intensity are similar. The observed difference at 500 ns is due to the hydrodynamic expansion of the gas after the first pulse.

## Acknowledgements

The work was partially supported by AID/CIEDS PPRINCE (3335), E4C (ANR-18-EUR-0006-02), Russian Science Foundation, Project No. 23-17-00264.

# How to obtain a Diffuse Dielectric Barrier Discharge in various molecular gases?

N. Naudé[1], A. Belinger[1], S. Dap[1]

[1] *LAPLACE, Université de Toulouse, CNRS, INPT, UPS, Toulouse, France*

This contribution investigates the conditions to obtain a diffuse Dielectric Barrier Discharge at atmospheric pressure in various molecular gases ($N_2$, $N_2$-O mixtures, $CO_2$, $N_2O$). The pre-ionization mechanisms leading to a Townsend breakdown and then to a diffuse discharge will be described and discussed.

## 1 Introduction

Dielectric Barrier Discharges (DBDs) can be used for many atmospheric pressure applications, including thin-film coating, sterilisation, treatment of flue and toxic gases, aerodynamic flow control, and energy-efficient lighting devices [1-3]. Depending on the gas, electrical parameters, and electrode configuration, these discharges can operate in the classical filamentary mode or in a homogeneous mode [4-5]. The filamentary mode can be very restrictive for some applications (*e.g.* surface coating). Nevertheless, conditions to obtain a diffuse DBD can also be restrictive. Diffuse DBDs at atmospheric pressure have been obtained in helium, argon, neon and nitrogen [5]. Contrary to noble gases, in nitrogen, the ionisation level is too low to allow the formation of a cathode fall. Thus, the electrical field is quasi-uniform over the discharge gap, like in low-pressure Townsend discharges, and the obtained discharge is called Atmospheric Pressure Townsend Discharge (APTD) [5]. For a Townsend discharge to occur, a production source of secondary electrons is necessary to sustain the APTD when the electric field is low.

## 2 Results and Discussion

The different mechanisms responsible for the memory effect in APTDs and their quantification depending on the experimental conditions are summed up in Figure 1. In Figure 1(a), they are compared as a function of the oxidising gas concentration added to $N_2$, for a fixed power supply frequency of a few kHz. In Figure 1(b), they are compared as a function of the power supply frequency for gas mixture of nitrogen with a small concentration of oxidising gas (a few $10^{th}$ of ppm). It shows that the dominant physical and chemical mechanisms involved in the memory effect are strongly related to the experimental conditions. Then, the seed electrons necessary to obtain an APTD are created through a combination of different mechanisms on the dielectric surfaces and in the gas gap.

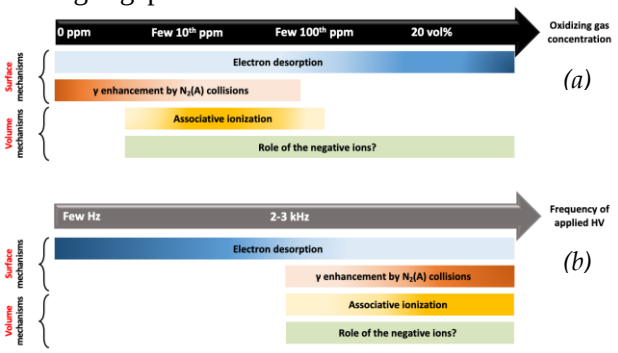



**Fig. 1**. Schematic representation of the dominant memory effect mechanisms as a function of: (a) the oxidizing gas concentration at a fixed frequency of a few kHz, and (b) the frequency in $N_2$-O mixtures

This work aims to summarise what could be the origin of the production of seed electrons in various molecular gases and to understand how to promote the occurrence of a Townsend discharge in various molecular gases. The presented results will be illustrated by data for APTD obtained in various gases such as $N_2$, $N_2$ + oxidizing gases ($O_2$, NO, $N_2O$), Air, $CO_2$, and $N_2O$ [6-8].

## Acknowledgement

This work was supported by Agence Nationale de la Recherche (DECAIR project ANR-20-CE08-0014).

## References

[1] S. Samukawa *et al.*, J. Phys. D: Appl. Phys. 45 (2012) 253001
[2] I Adamovich *et al.*, J. Phys. D: Appl. Phys. 55 (2022) 373001
[3] U. Kogelschatz, Plasma Chem Plasma P 23 (1), 1-46 (2003)
[4] R. Brandenburg, Plasma Sources Sci. Technol. (2017) 26 053001
[5] F. Massines *et al.*, Eur. Phys. J. Appl. Phys. 47, 22805 (2009)
[6] C. Bajon *et al.*, Plasma Sources Sci. Technol. (2023) 32 045012
[7] A. Belinger *et al.*, J. Phys. D: Appl. Phys., 2022, 55 (46), pp.465201
[8] H. Höft *et al.*, Eur. Phys. J. D 77, 35 (2023)

# Plasma-Catalytic Dry Reforming of Methane: on the Role of a Ni Catalyst at Room Temperature

A. Megías-Sánchez[1,2], P. Navascués[1], M. Ruiz-Martín[1,2], S. Marín-Meana[1,2], M.C. García[3], A. González-Elipe[1], M. Oliva-Ramírez[1,2], A. Gómez-Ramírez[1,2]

[1] *Instituto de Ciencia de Materiales de Sevilla (CSIC-U. Sevilla), Av. Américo Vespucio 49, 41092 Sevilla, Spain*
[2] *Dpto Física Atómica, Molecular y Nuclear, Fac. Física, U. Sevilla, Av. Reina Mercedes s/n, 41012 Sevilla, Spain*
[3] *Dpto. de Física Aplicada, Rad. y Medicina Física, Campus de Rabanales, Univ. de Córdoba, 14071 Córdoba, Spain*

Plasma-assisted dry reforming of methane is a promising process for converting $CH_4$ and $CO_2$ into value-added products under mild conditions. This study investigates the role of a Ni catalyst in a ferroelectric-moderated packed-bed reactor. By comparing the behaviour of PZT pellets with and without Ni-$Al_2O_3$ coatings, we examine the impact of the Ni catalyst on the plasma electrical properties and product distribution. The findings here aim to clarify the debated synergies between plasma and catalysis.

## 1 Introduction

Utilizing $CH_4$ and $CO_2$ mixtures through plasma-assisted dry reforming (DRM) offers a promising pathway for greenhouse gas valorization and valuable chemical production.[1] However, the role of catalysts in plasma-assisted reactions remains a subject of debate. Recent studies suggest that the observed plasma-catalysis synergies may arise from changes in the reactor electrical behavior instead of classical catalytic mechanisms.[2] In this context, we investigate the effect of a Ni catalyst in a ferroelectric-moderated packed-bed reactor to assess its influence on the plasma electrical properties and the reaction product distribution.

## 2 Methods

The experiments were conducted in a packed-bed reactor by using Lead Zirconate Titanate (PZT) pellets as packing material. Plasma discharges were generated by an AC electrical signal (3.15 kV, 5 kHz). Optical emission spectroscopy and quadrupole mass spectrometry were used to characterize the plasma light emission and reaction products, respectively. Gas feed ratios ($CH_4$:$CO_2$) were varied from 1:1 to 4:1 at a total flow rate of 20 sccm. The reactor walls were cooled to maintain a temperature of 40°C.

## 3 Results

$CH_4$ + $CO_2$ mixtures in PZT moderated packed bed reactor produces $H_2$, CO, $C_2$, $C_3$, and traces of $H_2O$. Figure 1 shows the absolute conversion rates obtained as a function of the $CH_4$:$CO_2$ ratio. The highest conversion rates, 34% for $CH_4$, and 22% and for $CO_2$, were obtained for a 3:1 ratio. The presence of Ni produces higher power consumption, but the negligible presence of oxygenated compounds suggests no relevant catalytic effects. The amount produced of $H_2$ follows a similar tendency to the $CH_4$ conversion rate as expected from the fact that methane is the unique source of hydrogen atoms available in the system. Our results suggest that $CH_4$ and $CO_2$ follow parallel plasma reactions pathways that do not significantly interact and that the presence of Ni does not alter the reaction mechanism, at least at room temperature. Thus, formation of high added value oxygenated compounds would require a different strategy.

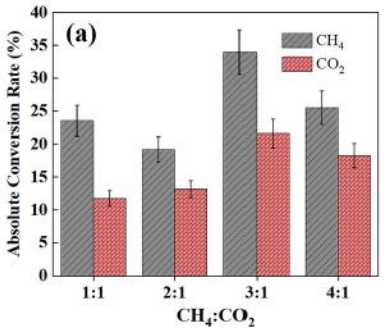



Figure 1. $CH_4$ and $CO_2$ conversion rates vs. $CH_4$:$CO_2$

**Acknowledgements**

The authors acknowledge projects PID2020-114270RA-I00, PID2023-147916NA-I00 and PID2020-112620GB-I00 funded by MCIN/AEI/10.13039/501100011033, project TED2021-130124A-I00 funded by AEI/10.13039/501100 011033/Unión Europea Next Generation EU/PRTR. M. M. Oliva-Ramírez received support from Grant IJC2020-045087-I, and S. Marín Meana from Grant PRE2021-100465, both funded by MCIN/AEI and the European Union NextGeneration EU.

**References**

[1] Navascués, P. et al, Fuel Processing Technology 2023, 248, 107827.

[2] Ruiz-Martín M., et al. Current Opinion in Green and Sustainable Chemistry 2025, 51:100990.

# Study on DBD regimes in dry and wet air to produce ozone and nitrogen oxides

O. Stepanova[1], V. Snetov[1], O. Grushko[1], A. Dyachenko[1], I. Ruchkin[1,2] and M.Pinchuk[1]

[1] *Istitute for Electrophysics and Electric Power, Russian Academy of Sciences, St.Petersburg, Russia*
[2] *Ioffe Institute, Russian Academy of Sciences, St.Petersburg, Russia*

The study contains data on the amounts of ozone and nitrogen oxides measured in a flow of dielectric-barrier discharge products produced in dry and wet air at different applied voltage values. Species concentrations are analysed in correspondence with a plasma gas temperature and heating-up of a chemical plasma reactor. Non-linear dependence of ozone and nitrogen oxides concentrations on the applied voltage was revealed in experiments. This has been checked with numerical simulations of plasma chemical kinetics of ozone production in DBD.

## 1 Introduction

A dielectric-barrier discharge (DBD) in air is well-known as a source of ozone [1], and ozone generation is historically considered to be the main application of air DBD. But, nevertheless authors are currently posing a question on optimal conditions of ozone and nitrogen oxides production, in particular the issue on gas temperature dependence and its controlling [2].

The presented study contains data on ozone and nitrogen oxides concentrations measured in a flow of dielectric-barrier discharge products produced in dry and wet air at the applied voltage peak-to-peak values of 9, 10 and 12 kV. The experimentally obtained dependence has been compared with numerical study results on plasma chemical kinetics of ozone production.

## 2 Experiment and its results

An original experimental setup includes a coaxial DBD electrode system applied by a sinusoidal power supply with a signal frequency of 26.5 kHz, gas supply system with control of temperature and humidity of the air passing through the discharge gap.

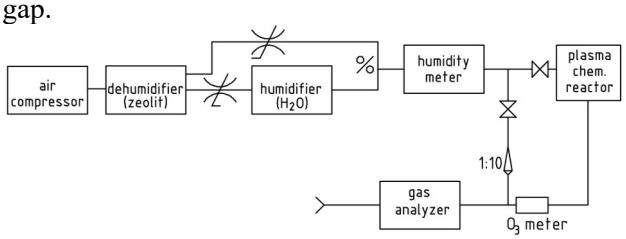



Fig. 1. A schematics of air supply system with controlling gas temperature and humidity

The chemical composition of DBD products (the amount of ozone and nitrogen oxides) was measured using a MEDOZON-254/5 gas analyzer (Medozon, Russia) and a gas analyzer GAZOTEST (POLIGAZ PLUS, Russia) (Fig. 2).

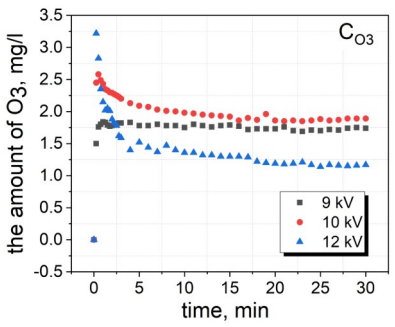



Fig. 2. Ozone concentrations measured in dry air DBD products flow

In experiments, we revealed a non-linear dependence of species concentrations on a peak-to-peak value of applied voltage. This has been checked with numerical simulations of plasma chemical kinetics with taking into account of plasma gas temperature measured with optical emission spectroscopy based on the spectral band profile $N_2$ 0-0 (337.13 nm).

The study has been supported by a grant from the Russian Science Foundation № 24-29-00816, https://rscf.ru/en/project/24-29-00816/.

**References**

[1] Stucki, S., and Kogelschatz, U. Advanced Ozone Generation. *Process technologies for water treatment,* 87-118 (1988).

[2] Bang, S., Snoeckx, R. and Cha, M.S. Temperature-dependent kinetics of ozone production in oxygen discharges. *Plasma Chemistry and Plasma Processing* **43**(6), 1453-1472 (2023).

# Effect of $H_2O$ on the conversion of $CH_2O$ in a micro-capillary He plasma at atmospheric pressure

G.Bauville[1], A. Gady[1,2], C. Rudolf-D'Alexis[2], M. Heninger[2], P. Jeanney[1], J. Lemaire[2], J. Santos Sousa[1], A. Pallandre[2], S. Pasquiers[1]

[1] *Université Paris-Saclay, CNRS, Laboratoire de Physique des Gaz et des Plasmas, UMR8578, Orsay, France*
[2] *Université Paris-Saclay, CNRS, Institut de Chimie Physique, UMR8000, Orsay, France*

**Abstract:** We investigate the effect of water vapor on the conversion of formaldehyde in a He plasma created in a micro-capillary tube using a DC-pulsed micro-dielectric barrier discharge (µDBD). The concentration of $CH_2O$ is measured with real-time mass spectrometry Fourier Transform Ion Cyclotron Resonance with Chemical Ionization (CI-FTICR). It is found that $H_2O$ has a detrimental effect on the formaldehyde removal rate.

## 1 Introduction

Volatile Organic Compounds have an impact on the atmosphere and therefore on our everyday-life environment. Cold plasmas allow efficient removal of such molecules, in particular for the formaldehyde [1]. This compound is a significant concern due to its prevalence in indoor and outdoor air, its toxicity causing serious health issues [2]. Besides, plasma micro-reactors constitute a new developing subject of study for the conversion or synthesis of organic molecules [3]. The present work aims to determine the effect in the conversion of $CH_2O$ of adding $H_2O$ to a micro-capillary He plasma.

## 2. Experiment

The set-up and protocols are identical to what was published in [3]; the method for creating mixtures with a controlled $CH_2O$ concentration is given in [1]. Using a DC-pulsed µDBD, we ignite a plasma inside a tube with an inner diameter of 800 $\mu m$ in He at 1 ln/min flow, with $CH_2O$ at an inlet concentration around 180 ppm; the mixture can be completed with 1% of $H_2O$. A stainless-steel needle is inserted inside the tube, playing the role of the high voltage electrode, while the counter electrode is a copper tape wrapped around the tube. The plasma is ignited with voltage pulses of 3 µs of duration at a frequency of 10 kHz, with amplitudes in the range 2 kV up to 5 kV. To follow the concentration of $CH_2O$, a real-time mass spectrometer CI-FTICR [4] is set up at the tube outlet [3].

## 3. Results

A typical example of results is given in Figure 1, highlighting the impact of the plasma in the conversion of $CH_2O$ for the two gas mixtures studied. The molecule is not only removed but also transformed into other products, potentially including $H_2$, CO, or even HCOOH for the wet mixture.

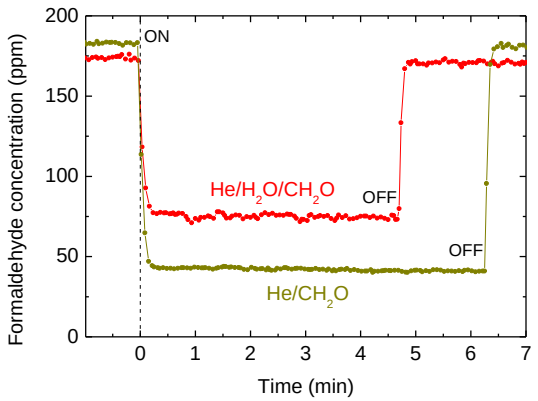



Figure 1 – Outlet $CH_2O$ concentration for a voltage of 4 kV. ON/OFF: time interval for the plasma. Input energy per pulse and plasma length: 520 µJ and 135 mm for the dry mixture, 580 µJ and 20 mm for the wet one.

## 4. Conclusion

$H_2O$ has a detrimental effect on the $CH_2O$ removal rate, at fixed electrical parameters of the µDBD. It suggests that He species, metastable states and ions, should be more efficient for the removal of $CH_2O$ than OH radicals coming from the dissociation of $H_2O$. Further studies will elucidate reaction pathways and identify by-products.

**Acknowledgement**

This project has received financial support from the CNRS through the MITI interdisciplinary programs through its exploratory research program (MoPlasMic project).

**References**

[1] N. Blin-Simiand *et al.*, *J. Phys. D.* **49**, 195202 (2016).
[2] A.H. Khoshakhlagh *et al.*, *Environ. Geochem. Health* **46**, 206 (2024).
[3] G. Bauville *et al.*, *J. Phys. D* **58**, 015207 (2025).
[4] M. Heninger *et al.*, *Anal. Chem.* **90**, 7517 (2018).

# Optical radiation upon excitation of the Ar-$N_2$ mixture by the products of the $^6Li(n,\alpha)^3H$ nuclear reaction

M. Khasenov[1], Yu. Gordienko[1], E. Batyrbekov[2], Yu. Ponkratov[1], K. Samarkhanov[1], Ye. Tulubayev[1], V. Bochkov[1]

[1] *Institute of Atomic Energy Branch of the National Nuclear Center of the Republic of Kazakhstan, Kurchatov 071100, Kazakhstan*
[2] *National Nuclear Center of the Republic of Kazakhstan, Kurchatov 071100, Kazakhstan*

The optical emission spectra of an argon-nitrogen mixture excited by the products of the $^6Li(n,\alpha)^3H$ nuclear reaction at temperatures of 375-730 K were studied. The temperature dependence of the emission intensity of argon atoms, nitrogen molecules, lithium atoms and alkali metal impurities were determined. The main processes leading to emission on transitions of the argon atom and bands of the second positive system of nitrogen were described.

The study of optical (laser and spontaneous) radiation of nuclear-excited plasma is of interest for the development of a method for extracting energy from a nuclear reactor, as well as for monitoring and regulating the parameters of nuclear reactors [1]. Selective energy transfer from an excited Ar* atom to an $N_2$ molecule makes it possible to obtain an effective light source in the near UV-region of the spectrum. The emission of an argon-nitrogen mixture is also of interest for the methods used to measure the efficiency of converting nuclear energy into light. This is based on comparing the intensity of the investigated line and the second positive system of nitrogen in the Ar-$N_2$ mixture [2].

The studies were conducted at the IVG.1M nuclear reactor at a thermal neutron flux density of $3 \cdot 10^{13}$ n/cm$^2$s. The experimental technique and methodology are described in detail in [3]. The emission spectrum of the Ar-$N_2$ mixture at a temperature of 375 K is represented by the lines of the 4p-4s transitions of the argon atom in the IR-region and the bands of the second positive system of nitrogen in the UV-region. At temperatures above 520 K, lines of lithium appear, as well as of sodium and potassium, contained in lithium as impurities. The appearance of alkali metal lines in the emission spectra is associated with evaporation during the emission of α-particles and tritium nuclei from the deposited lithium layer. When the lithium layer is sputtered by nuclear particles, the density of lithium vapours is generated, which is significantly higher than the density of saturated vapours [3].

At mixture temperatures of 375-470 K, the intensity of the emission bands of the second positive nitrogen system decreases by approximately 5 times (Figure 1). Thus, the argon-nitrogen mixture is not of interest as a source of optical radiation from a nuclear reactor. The use of the Ar-$N_2$ mixture in determining the efficiency of converting nuclear energy into light is possible at a mixture temperature of ~300 K, at which the rate constants of processes in the plasma are fairly well-known.

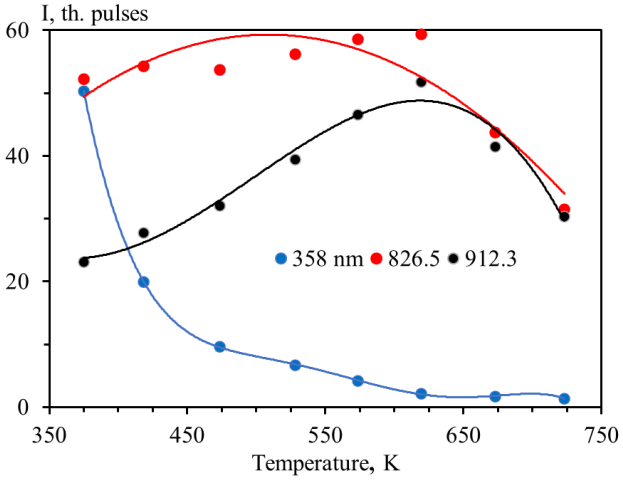



Fig. 1. Dependence of the intensity of the nitrogen band at 358 nm and the argon atom lines in the Ar-$N_2$ mixture on temperature. Integration time of the spectrometer: 1 s (358 nm) and 300 ms (826.5, 912.3 nm).

**Acknowledgments**

This research is funded by the Science Committee of the Ministry of Science and Higher Education of the Republic of Kazakhstan (Grant No. AP26102955).

**References**

[1] Mel'nikov, S.P., Sinyanskii, A.A., Sizov, A.N., Miley, G.H. *Lasers with Nuclear Pumping*. Springer, New York, 2015.

[2] Batyrbekov E., Gordienko Yu., Khasenov M., Ponkratov Yu., *Science and Technology of Nuclear Installations*, 2015, V. 2015, Article ID 161535.

[3] Batyrbekov E., Khasenov M., Gordienko Yu., Samarkhanov K., Ponkratov Yu. *Journal of Luminescence*, 2020, V. 220, 116973.

# LIBS (Laser-Induced Breakdown Spectroscopy) applications for the Tritium measurement in tokamak plasma-facing components

A. Bultel[1], A. Favre[1], V. Morel[1]
F. Montupet Leblond[2], M. Payet[2], M. Missirlian[2], S. Vartanian[2], E. Bernard[2], C. Grisolia[2]

[1]*Université de Rouen-Normandie, CNRS, CORIA UMR 6614, Saint-Étienne du Rouvray, France*
[2]*IRFM, CEA Cadarache, Saint-Paul-lèz-Durance, France*

Various experiments are performed to test the LIBS capacity to measure T in tokamak plasma-facing components. These experiments focus on the technique itself as well as its implementation in real situations.

The LIBS (Laser-Induced Breakdown Spectroscopy) technique is a method for determining the multi-elemental composition from the spectroscopic analysis of a thermal plasma produced by laser-matter interaction.

Among many others, one of the advantages of LIBS is its ability to provide the composition *in situ*. This is a key point considering the Plasma-Facing Component (PFC) within a tokamak that may contain Tritium. Indeed, sampling is then unnecessary, the nuclear safety can be easily ensured and results can be obtained between shocks without delay. These advantages make LIBS a serious candidate for implementation in ITER.

To go further in the validation of LIBS for tokamak applications, we have developed a strategy based on the following steps.

**1. T measurement in metallic sample by LIBS**

Since Tritium and Deuterium are both used as fuel in tokamak, they can diffuse within the PFC. Spectra obtained by LIBS then reveal the lines of the Balmer series. The $T_\alpha$ and $D_\alpha$ lines are the most intense on the visible spectral range and very close to each other (difference $\Delta\lambda = 0.054\,nm$). Since the lines are broadened by Stark effect, electron density within the LIBS plasma must then be low to allow the isotopic discrimination (on figure 1, a test for a sample with H and T) [1]. The spectra can be completely recalculated [2].

**2. LIBS implementation in WEST using AIA**

To test the implementation of LIBS within a tokamak, a specific device using optical fibres has been elaborated and validated in laboratory. Then, its installation has been performed within WEST at the end of the Articulated Inspection Arm (AIA) for inner measurements [3]. Figure 2 illustrates the composition profile obtained at the same location with successive shots.

**3. Remote LIBS implementation in WEST**

The previous device is limited in terms of laser energy due to the fibres. A remote system is currently in test to increase the fluence on the PFC by direct transmission from outside of the laser pulse through an optical window.

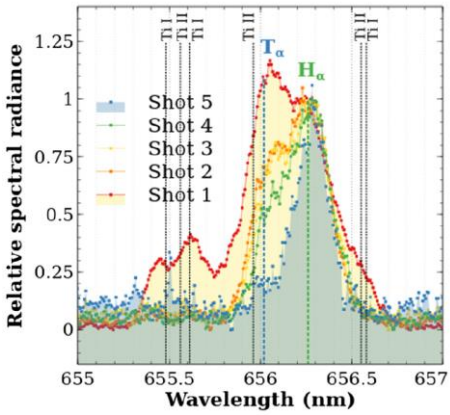



**Figure 1**. LIBS spectra obtained on a sample charged with H and T [1].

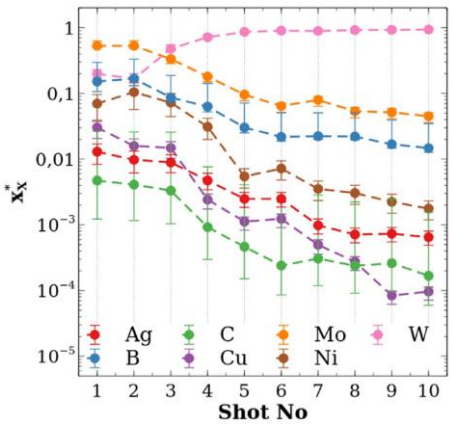



**Figure 2**. Metallic mole fraction profiles of a PFC within WEST [3].

**References**

[1] A. Favre, A. Bultel et al., J. Nucl. Mater. 591 (2024) 154924.
[2] A. Favre, A. Bultel et al., J. Quant. Spectrosc. Radiat. Transfer 330 (2025) 109222.
[3] A. Favre, A. Bultel et al., Phys. Scr. 99 (2024) 035609.

# Towards time-resolved measurements for solvated electrons at the plasma/liquid interface

A.D. Light[1], M.B. Gardner[1*], E.A. Biesiada[1*], and M.S. Jacka[1*]

[1] *Colorado College, 14 E Cache la Poudre St, Colorado Springs, CO USA*
**Denotes undergraduate researcher*

Free electrons dissolved in liquid ("solvated electrons") are hypothesized to be a key part of plasma/liquid chemistry but are difficult to measure in water. We are developing a broadband transient absorption diagnostic to measure time-resolved concentration of solvated electrons at the plasma/liquid interface.

## 1 Motivation

Contamination of groundwater by poly-fluoroalkyl substances (PFAS) is increasingly recognized as a major environmental issue [1]. Sometimes called "forever chemicals," these compounds bioaccumulate, can cause adverse health outcomes, and are difficult to break down. Plasma technologies offer promising avenues toward remediation, but the mechanisms remain largely opaque [2–6]. The role of solvated electrons is of particular interest in plasma-mediated PFAS breakdown, but their short lifetime in water makes detection difficult. The Go and Rumbach groups at Notre Dame have measured time-average concentration of solvated electrons produced by a DC discharge at the water/plasma interface [7–11], but few similar measurements exist. By replacing the continuous-wave lasers in their protocol with a pulsed light source, we are working to add time resolution to their absorption technique.

## 2 Diagnostic

We use light from a sub-nanosecond, pulsed supercontinuum (FYLA Iceblink) and the total internal reflection geometry of Rumbach, et. al [10] to sample a broad absorption feature in the thin layer immediately underneath the liquid surface (Fig. 1). Low-jitter timing allows us to localize the measurement relative to the start of the discharge. A student-designed, inexpensive multichannel detector records time-resolved intensity in the 500-950nm wavelength band and we use multi-channel lock-in detection to recover the small signals. We describe the status of the diagnostic, results to date, and planned improvements.

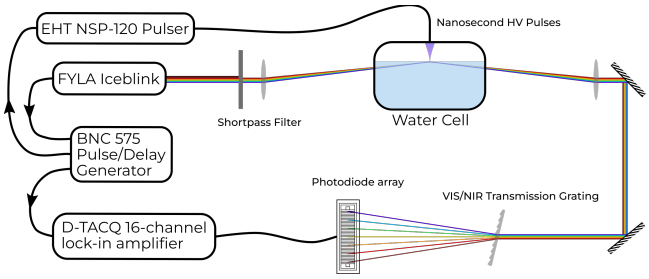



**Figure 1**: Schematic of measurement.

**References**

[1] H. Ryu *et al.*, J. Hazard. Mater. 124437 (2020).
[2] M. J. Bentel *et al.*, Environ. Sci. Technol. **53**, 3718 (2019).
[3] J. Cui, P. Gao, and Y. Deng, Environ. Sci. Technol. **54**, 3752 (2020).
[4] L. Huang, W. Dong, and H. Hou, Chem. Phys. Lett. **436**, 124 (2007).
[5] S. S. R. K. C. Yamijala, R. Shinde, and B. M. Wong, Phys. Chem. Chem. Phys. **22**, 6804 (2020).
[6] B. N. Nzeribe *et al.*, Crit. Rev. Environ. Sci. Technol. **49**, 866 (2019).
[7] H. E. Delgado *et al.*, J. Appl. Phys. **129**, 083303 (2021).
[8] R. Gopalakrishnan *et al.*, J. Phys. Appl. Phys. **49**, 295205 (2016).
[9] D. C. Martin *et al.*, Plasma Sources Sci. Technol. (2021).
[10] P. Rumbach *et al.*, Nat. Commun. **6**, 7248 (2015).
[11] P. Rumbach, D. M. Bartels, and D. B. Go, Plasma Sources Sci. Technol. **27**, 115013 (2018).

# Towards calibration of picosecond O-TALIF

Z. Shu[1], S. Latorre[1], J. B. Billeau[1,2], J. P. Booth[1],
D. V. Seletskiy[3], S. Reuter[2], N. A. Popov[4] and S. M. Starikovskaia[1]

[1] *Laboratory of Plasma Physics (CNRS, Ecole Polytechnique, Univ. Paris-Sud, Observatoire de Paris,* Sorbonne Université, l'Institut Polytechnique de Paris), Ecole Polytechnique, route de Saclay, 91128 Palaiseau, France
[2] *PPSL Laboratory, Department of Engineering Physics, Polytechnique Montréal, Montréal, Québec H3T 1J4, Canada*
[3] *femtoQ Laboratory, Department of Engineering Physics, Polytechnique Montréal, Montréal, Canada*
[4] *Skobeltsyn Institute of Nuclear Physics, Moscow State University, Moscow, 119991, Leninsky gory, Russia*

Experimental procedure of obtaining the Xe/O two-photon absorption cross-section ratio is discussed for nanosecond and picosecond TALIF experiments. The same nanosecond capillary discharge with 100% oxygen dissociation at 30 mbar pressure is used as a source of O-atoms.

## 1 Nanosecond TALIF experiments

TALIF calibration on noble gas was proposed 20 years ago by Niemi *et al* who measured the two-photon absorption cross-section ratio $\sigma^{(2)}_{\mathrm{Xe}}/\sigma^{(2)}_{\mathrm{O}}$. Recent work [2] validated this value of this cross-section ratio using a nanosecond capillary discharge with 100% dissociation of oxygen and refining the accuracy to $1.8 \pm 0.2$. Note that the absolute value of the two-photon absorption cross-section of Xe measured in [3, 4] appears to be more than a factor of 2 smaller than what had been deduced from the measured $\sigma^{(2)}_{\mathrm{Xe}}/\sigma^{(2)}_{\mathrm{O}}$ [1] and the measured two-photon cross-section of O [5]. The mentioned discrepancy indicates the importance of independently verifying, in the future, the absolute two-photon absorption cross-section of O-atoms and answering the question of this inconsistency. Still, using nanosecond discharge with a known O-atoms density allows for analyzing picosecond TALIF.

## 2 Picosecond TALIF experiments

In the experimental context, the present work is close to paper [2]: the same nanosecond capillary discharge in a mixture of $N_2$ with a few percent $O_2$ at 30 mbar was used. The difference was using a picosecond laser system to get the two-photon absorption cross-section ratio $\sigma^{(2)}_{\mathrm{Xe}}/\sigma^{(2)}_{\mathrm{O}}$ (in both ns and ps experiments we mean the cross sections integrated over the frequency scale). The 355 nm output of a ps Nd:YAG laser (EKSPLA PL2251A) was used to pump the optical parametric generator (EKSPLA PG401) to produce the UV beam at 10 Hz with the energy around 100 $\mu$J, used for O (225.65 nm) and Xe (224.31 nm) excitation. The ps TALIF spectrum exhibited a spectral width 10 times broader than that of the ns case; the duration of the ps laser pulse was $< 26$ ps, while the duration of the ns laser pulse was 6.5 ns. The decay rate of the ps TALIF signal was obtained directly from the measurements. The high peak intensity of the ps laser system allowed the use of significantly lower pulse energies compared to ns experiments [2]: 9 $\mu$J for O-atom excitation (250 $\mu$J in ns) and 6 $\mu$J for Xe (130 $\mu$J in ns). The integrated ps TALIF signal at the same laser energy (9 $\mu$J and 6 $\mu$J) was about 40 times higher than that of the ns system. Using the rate equation model, the calibrated Xe/O two-photon absorption cross-section ratio remains at 1.8, though with a larger uncertainty due to laser intensity fluctuations. A refined model is currently under development to further elucidate the complexities of the underlying processes.

## Acknowledgements

This work was partially supported by E4C IP Paris (ANR-18-EUR-0006-02) and Engie Foundation. The support for Z. Shu by the China Scholarship Council (CSC) program for PhD students is acknowledged. The authors are thankful to C. Blondel and C. Drag for numerous discussions and for sharing their remarkable experience in laser diagnostics.

## References

[1] Niemi, K., Schulz-Von Der Gathen, V. and Döbele, H. F. *Plasma Sources Sci. Technol.*, **14**, 375 (2005).
[2] Shu, Z., Popov, N. A. and Starikovskaia, S. M. *Plasma Sources Sci. Technol.*, **33**, 025019 (2024).
[3] Blondel, C., Alkhoury, J., Jannaud, T. and Drag, C. *J. Phys. Conf. Ser.*, **1412**, 142012 (2020).
[4] Drag, C., Marmuse, F. and Blondel, C. *Plasma Sources Sci. Technol.*, **30**, 075026 (2021).
[5] Bamford, D.J., Dyer, M. J., and Bischel, W. K. *Phys. Rev. A*, **36**, 3497 (1987).

# Imaging electric fields for cold plasma interacting with silica powders for catalysis applications

J. Munday[1], E. Slikboer[1]

[1] *School of Science and Technology, Nottingham Trent University, NG11 8NS, Nottingham, UK*

Electric fields are an important parameter in characterizing any plasma-surface interaction, but they are non-trivial to detect or image. Polarimetric techniques can be used to achieve this. Some of these techniques require non-complex, non-depolarizing samples, limiting their use for in-situ analysis. Others account for these more complex targets. In this work, depolarization is induced by added different densities of silica powder to the target surface. Two polarimetric setups were used to investigate these powder spots under plasma jet exposure and quantitatively image the electric fields for plasma catalysis applications.

## 1 General

Cold atmospheric pressure plasma jets (CAPPJs) are becoming increasingly relevant for many applications. The benefit for these applications lies within the plasma-surface interaction, involving a cocktail of electrons, ions, radiation, radicals and electric fields. This mix is dynamic, with each aspect influenced by the others. For this reason, diagnostic techniques for investigating each element of the plasma-surface interaction are important for the understanding and reproducibility of plasma jets and progressing their applications. When a jet is impinged on a surface, charges deposited on the surface induce a local electric field. This influences the surface dynamics of the plasma, the surface chemistry that takes place, and the coupling between the surface and the plasma. It is important that this local electric field is investigated to better understand these interactions.

Polarimetry, utilizing electro-optic crystals (e.g. BSO) to take advantage of the Pockels effect, can enable the imaging of electric fields induced on a surface by CAPPJs.[1-2] The Pockels effect describes the linear change in refractive index due to applied electric field. This induces a change in birefringence that can be imaged and used to calculate the applied electric field and surface charge. Combined with iCCD imaging, the time-dependent induced electric field can be captured to study the plasma-surface interaction, conventionally this relates to interactions with the non-depolarizing BSO surface. In reality, the interaction with the actual samples must be studied, meaning complex targets need to be added that cause depolarization of the polarized light beam. For the field of plasma medicine, an initial study has shown it is possible to still capture the plasma induced field through a single layer of onion cells [3]. In this work, the applicability of Mueller polarimetry is examined for the field of plasma catalysis, where heterogeneous powders are added to the interaction.

## 2 Results

Electric field induced by plasma interacting with silica powder is measured using two polarimetry setups: The Sénarmont Compensator and the more complex Mueller Polarimeter. A cold helium atmospheric pressure plasma jet was used, operating at 30kHz, which interacts with the silica powder that has been deposited on a BSO crystal to form complex targets with varying packing densities. Both polarimetry techniques allow for the detection of electric fields at significantly low powder densities. When the powder density is increased, the electric field is not accurately detected with the simplified Sénarmont setup due to the increased level of depolarization. Mueller polarimetry separates the effects of depolarization and birefringence, allowing to detect induced electric fields during plasma-surface interactions with significantly higher powder densities. This highlights new diagnostics opportunities for difficult to measure fields like cold plasma catalysis.

## References

[1] E. Slikboer et al., Imaging axial and radial electric field components in dielectric targets under plasma exposure *J. Phys. D: Appl. Phys.*, **51**, 115203 (2018).

[2] B. Zhang et al., Visualization of electrical interaction among close-packed atmospheric pressure plasma jets *Phys. Plasmas*, **31**, 053503 (2024).

[3] E. Slikboer et al., In-situ monitoring of an organic sample with electric field determination during cold plasma jet exposure *Sci. Rep.*, **10**, 13580 (2020).

# Multielemental quantification by CF-LIBS assisted by an attention deep learning model trained on simulated spectra

L. Lemerle[1], A. Favre[1], A. Poux[1], V. Morel[1] and A. Bultel[1]

[1] *Université de Rouen Normandie, CORIA UMR 6614, Saint-Etienne du Rouvray, France*

Automatic learning codes that assist LIBS quantification are usually trained on a database of experimental spectra. In our case, we have developed an attention model trained using simulated spectra. In addition to reporting the results of plasma composition and parameter predictions, we have also analyzed the impact of the noise level of the spectra on the prediction error.

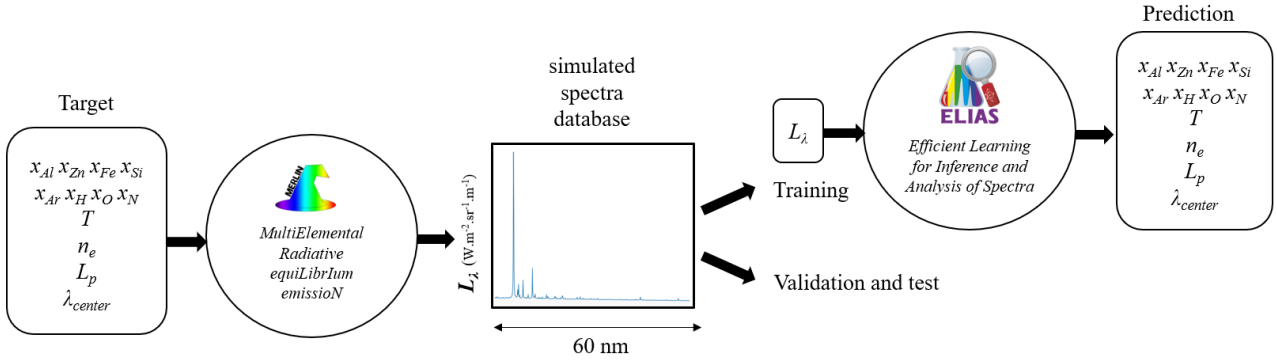



Fig. 1 : Overall approach from database creation to training

LIBS (Laser-Induced Breakdown Spectroscopy) is an elemental quantification technique based on the study of atomic emission spectra obtained from samples irradiated by a laser pulse [1]. CF-LIBS (Calibration Free Laser Induced Breakdown Spectroscopy) enables element concentrations to be determined without calibration [2]. It requires the simulation of emission spectra, and therefore the modeling of radiative transfer, taking into account line profile broadening caused by various physical phenomena (Doppler effect, Stark effect, apparatus function, etc.). One way of overcoming this issue is the use of artificial intelligence, including deep learning from labeled data [3, 4]. Successful learning of the network relies mainly on the database, which must be large enough in terms of the number of spectra to cover the full range of possible conditions. However, assembling millions of labelled experimental spectra, i.e. spectra whose plasma parameters and emitter proportions have already been determined, is a time-consuming and demanding task. For this reason, the database can be simulated using the modeling tools developed for CF-LIBS [5, 6]. We present the results of a multi-species quantification test case using a deep learning tool. This work follows on from the team's work on the quantification of 9 species using a convolutional neural network trained on a simulated database [7]. Training and tests are performed using over a million simulated spectra generated by the MERLIN (MultiElemental Radiative equiLibrIum emissioN) code which models LIBS spectra at Local Thermodynamic Equilibrium (LTE) [8]. Spectral radiances are processed by a neural network, this time based on an attention model [9]. This type of architecture is usually used for language processing, but in our case, it enables the prediction of homogeneous plasma composition and physical variables (electron density, temperature, plasma length and spectral range).

## References

[1] Kunze, H.J. *Springer Ser. Atomic, Opt., Plasma Phys.* **56** (2009).
[2] Ciucci, A. et al. *Appl. Spectrosc.* **53**, 960-964 (1999).
[3] Castonera, J. et al. *Spectrochim. Acta B* **178**, 106125 (2021).
[4] Niu, C. et al. *Anal. Chem.* **93**, 2281-2290 (2021).
[5] D'Andrea, E. et al. *Appl. Phys. B-Lasers O.* **118**, 353–360 (2015).
[6] Gąsior, P., Gromelski, W., Kastek, M. *Spectrochim. Acta B* **199**, 106576 (2023).
[7] Favre, A. et al. *Spectrochim. Acta B* **224**, 107082 (2025).
[8] Favre, A. et al. *J. Quant. Spectroscop. Ra.* **330**, 109222 (2025).
[9] Vaswani, A. et al. *Adv. Neur. In.* **30** (2017).

# Robust Emissive Probes for Hot Plasmas

F. Enescu, C. Ionita and R. Schrittwieser

[1] *Institute for Ion Physics and Applied Physics, University of Innsbruck, Austria*

The plasma potential $\Phi_{pl}$ is the space potential of the plasma and is therefore one of the most important plasma parameters. Its reliable determination is not an easy task especially in high temperature plasmas. Electron-Emissive plasma probes (EEP) have a floating potential which ideally is equal to the plasma potential since EEPs compensate the incoming electron flux from the plasma by its own electron emission flux. We report on the development of an EEP that is sufficiently robust and emissive to be used even in the edge plasma of toroidal plasma experiments.

## 1 Introduction

The plasma potential $\Phi_{pl}$ is a very important parameter which should be determined with high reliability, accuracy and temporal resolution. According to Poisson's equation, $\Phi_{pl}$ depends solely on the charge carrier densities – but not on their velocity distributions and thus also not on possible electron drifts.

A conventional Cold Langmuir Probe (CLP) is easy to construct and to handle. The easiest accessible parameter is its floating potential $V_{fl}$. However, the floating potential of a CLP is not useful since in most plasmas (of electrons and only positive ions) $V_{fl}$ is more negative than $\Phi_{pl}$ due to the higher mobility of the electrons. This is also the reason that the current-voltage characteristic of a CLP is asymmetric with respect to the plasma potential.

However, an Electron-Emissive Probe (EEP) can balance the electron current from the plasma by an equal electron emission current from the probe into the plasma, thereby making the current-voltage characteristic of an EEP symmetric and shifting its floating potential to the real plasma potential $\Phi_{pl}$.

We present the latest progress of a new type of EEP which is strong and robust enough for the use in the edge region of toroidal fusion experiments [1,2].

### 1.1 Probe construction

Usually an EEP has been constructed by a loop of tungsten wire, heated by a current to electron emission. The disadvantage is that there is a voltage drop along the wire which might falsify the measurement.

We have developed two methods to heat an EEP indirectly, either by an IR laser [3,4] or by heat conduction. The principle of the latter probe is shown in Fig. 1 (for more details cf. [1,2]). Probe legs and probe pin are made of HOPG (Highly Oriented Pyrolytic Graphite):

The electric resistivity of HOPG along the principal of its lattice axis (001) is $0{,}25 \cdot 10^{-2}\ \Omega\,\mathrm{m}$. Along the layer plane (002) it is $5 \cdot 10^{-7}\ \Omega\,\mathrm{m}$. Therefore, when a heating current is passed through the HOPG "loop" mainly the upper short "bridge" between the two legs will be heated to yellowish glow. The heat produced there will be transported up to the probe tip which eventually will be heated to electron emission.

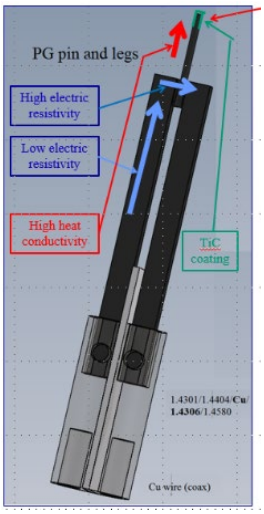



*Fig. 1. The probe is heated by heat conduction originating from a „loop" of HOPG (Highly Oriented Pyrolytic Graphite) [2].*

This effect will work since also the heat conductivity of HOPG is strongly different for the two lattice directions so that the heat produced in the "bridge" will be transported to the top of the probe which eventually will be coated by TiC (Titanium Carbide).

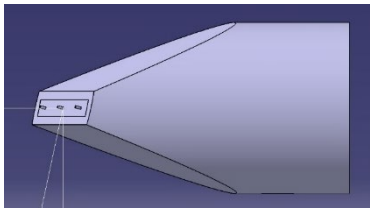


*Fig. 2. Side view of a New Probe Head for W 7-X. The centre probe will be an EEP, the two other probes are CLPs.*

This heating principle will also be utilized for a New Probe Head under development for the Stellarator Wendelstein 7-X at the Max-Planck-Institute for Plasma Physics, Greifswald Branch (Fig. 2).

**References**

[1] B.S. Schneider, et al., Plasma Phys. Control. Fusion 61 (2019), 054004 (12pp).

[2] C. Ionita, et al., European Physical J. D 73 (2019), 73 (16pp), Topical Review.

[3] R. Schrittwieser et al., *Physica Scripta* T123 (2006), 94-98.

[4] R. Schrittwieser et al., *Rev. Sci. Instrum.* 79 (2008), 083508 (9pp).

# Effect of target on NO production in a kHz cold argon plasma jet measured by LIF

S.Zhao, R. van de Wege and A. Sobota

*Eindhoven University of Technology, 5600 MB, Eindhoven, The Netherlands*

This work presents the characteristics of nitric oxide (NO) production in a kHz pulse-driven atmospheric pressure argon plasma jet, operated in the open air, including the investigation of both the free jet and the jet with targets. Laser-induced fluorescence (LIF) is employed to measure the absolute density of the ground state NO. Both time-resolved and space-resolved measurements are conducted to explore the temporal evolution and spatial distribution of NO in the plasma plume region. Results indicate that, in the region above the target, the distance between the jet and the target affects the target contribution to NO density. A closer target leads to a greater increase in the NO generation. Compared to the glass target, water has a larger influence possibly due to the OH radicals in the plasma and the change in discharge morphology.

## 1 Introduction

Atmospheric pressure plasma jets (APPJs) demonstrate broad prospects in biomedical applications due to the production of reactive species. Cold APPJs are more practical in applications where a low-temperature feature is required to prevent samples from thermal damage. Among these reactive species, nitric oxide (NO), plays an important role and is more likely to interact sufficiently with the treated sample, thanks to its longer lifetime. To take full advantage of NO in APPJs, it is imperative to have a thorough grasp of the NO generation process with the presence of target and control its production within the plasma jet under demand.

Laser-induced fluorescence (LIF) is an in *situ* spatially resolved diagnostic approach, with which the absolute NO density can be probed with high precision. The ground state NO($X^2\Pi$, $v = 0$) is excited to NO($A^2\Sigma^+$, $v = 0$) by a laser beam in the vicinity of 226 nm. The fluorescence signal can be detected when the excited state falls back to the NO($X^2\Pi$, $v = 2$) state, in which transition emits light at around 247 nm [1-2]. In this work, using LIF, we conducted the NO measurement in a kHz pulsed Ar plasma jet operated in the open air to trace the NO density variation with the presence of glass or demineralized water.

## 2 Experimental setup

The LIF system consists of the laser, the plasma jet and the detector. A Nd: Yag pump laser with a dye laser is used to generate the laser beam at around 226 nm, with a 5 kHz repetition frequency and 9 ns pulse length. A DC high-voltage power supply combined with a high-voltage pulse generator is used to drive the plasma jet, operating at 5 kHz. The fluorescence signal is perpendicularly collected by a monochromator and PMT and read out by a photon counter. Each LIF measurement is performed by accumulating 5000 laser shots to get a relatively stronger signal. A delay generator is used to synchronize the laser beam, the discharge and the gate of the photon counter so as to obtain time-resolved signals. An iCCD camera is used to capture the plasma ionization wave propagation. The absolute density is calibrated by using a gas mixture of Ar with a known concentration of NO.

## 3 Results

The distance between the plasma jet nozzle and the target was respectively set as 10 mm and 15 mm for each target case. At 10 mm, the presence of both glass and water significantly leads to the increase in NO density in the region near the target surface. Water contributes more to NO compared to glass probably due to the increase of OH radicals and the change in discharge morphology. At 15 mm, target plays a less significant role in NO production.

**References**

[1] Van Gessel A, Alards K and Bruggeman P NO production in an RF plasma jet at atmospheric pressure. *Journal of Physics D: Applied Physics* **46,** 265202 (2013).

[2] Van Gessel A, Hrycak B, Jasi´nski M, Mizeraczyk J, Van Der Mullen J and Bruggeman P Temperature and NO density measurements by LIF and OES on an atmospheric pressure plasma jet. *Journal of Physics D: Applied Physics* **46,** 095201 (2013).

# Gas temperature distribution of atmospheric pressure Argon glow discharge measured by Mach-Zehnder interferometer

R. Kimura[1], Y. Nakagawa[1] and F. Tochikubo[1]

[1] *Tokyo metropolitan university, 6-6 Asahigaoka, Hino, Tokyo, Japan*

In non-thermal plasma, the gas temperature distribution is an important parameter that affects chemical reaction and discharge regime. In this study, the gas temperature of atmospheric pressure DC argon glow discharge was measured using Mach-Zehnder interferometer. The discharge was generated between nozzle and sphere electrodes. In nozzle cathode condition, the gas temperature increased near anode and cathode. The gas heating near the cathode is explained with Joule heating caused by sheath formation, and the gas heating near the anode can be attributed to air mixing near anodic sphere.

## 1 Introduction

The gas temperature is an important parameter which predominates chemical reaction rates, discharge regime, and gas-phase particle transport. Atmospheric pressure glow discharge with noble gas is applicable to various fields, whereas, its gas temperature is not investigated in detail yet. In this study, the 2-D gas temperature distribution of Argon glow discharge was measured using Mach-Zehnder interferometer.

## 2 Experimental setup

Mach-Zehnder interferometer measures the refractive index changes corresponding to the gas temperature changes of the interference fringes [1]. In this study, the nozzle-sphere electrodes with 3 mm gap were used. A stable glow discharge was generated by flowing argon gas from the nozzle electrode into air and applying a DC-high voltage between the electrodes.

## 3 Result and discussion

Figure 1 shows the obtained gas temperature distribution with discharge current of 11 mA, gas flow rate of 0.5 L/min, and the nozzle cathode. In this figure, R is a radical position and Zis a distance from the nozzle. The gas temperature increased to 1000 K near the cathode, dropped to the room temperature as the position approached to the anode, then increased to 800 K again. The glow discharge typically forms a strong electric field in the cathode sheath Joule heating. However, the gas heating near the anode cannot be explained by Joule heating due to its weak electric field. A possible reason will be air mixing into the argon flow. Since the argon gas comes from the nozzle cathode into the air, the air mixing ratio increase as the position approaches to the anode. With higher air-mixing ratio, the electron energy can be transferred to gas temperature via vibrational translational relaxations, or an increase in the plasma resistance due to negative ions formation enhances Joule heating.

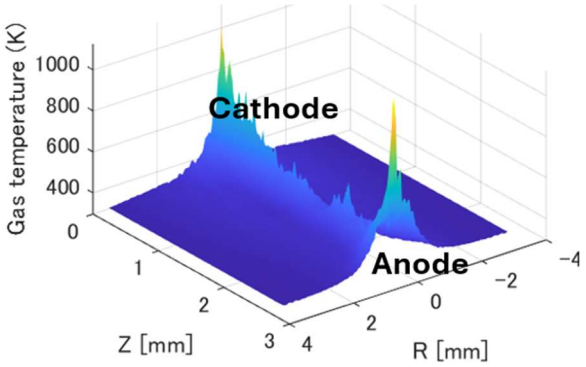



Fig. 1 Gas temperature distribution with sphere electrode as anode

To validate the effect of air mixing, the gas temperature distribution with different gap length (1, 2, and 3 mm) was measured with the discharge current of 17 mA and the gas flow rate of 0.5 L/min. The gas temperature near the cathodic nozzle remained almost constant at 1500 K with each gas length. However, the gas temperature near the anodic sphere increased to 1000, 1500, and 2000 K as the discharge gap became wider. Because the air-mixing ratio increases as the discharge gap becomes wider, the gas hearing near the anode is explained by the effect of air mixing effect. This result implies that the molecular gas mixing ratio into the noble gas strongly affects the gas temperature as well as the generations of atmospheric-pressure plasma and radicals.

Part of this research was supported by JSPS Grant-in-Aid for Scientific Research JP21H01075.

**References**

[1] J. A. Lopez *et al*, Gas Temperature Determination of an AC Arc Discharge at Atmospheric Pressure in Air Using a Mach-Zehnder Interferometer. *IEEE TRANSACTION ON PLASMA SCIENCE*, **34**, 115-120 (2006).

# Improvement of gas detection sensitivity of a self plasma-optical emission spectrometer

Dae-Woong Kim[1], Geon-Woong Eom[1,2], InYong Park[1,2], Sang-Ho Lee[1,2], Jin Young Lee[1], Shin-Jae You[2], Min Hur[1], Woo-Seok Kang[1]

[1] *Korea Institute of Machinery and Materials, Republic of Korea*
[2] *Chungnam National University, Republic of Korea*

A self plasma-optical emission spectrometer (SP-OES) is utilized for real-time residual gas detection in semiconductor manufacturing processes due to its contamination resistance and efficiency. As semiconductor devices shrink, accurate trace gas detection becomes important, requiring improved SP-OES sensitivity. This study quantitatively evaluated and optimized SP-OES detection sensitivity using an $N_2$ and Ar gas-mixing system. Various parameters that affect the detection sensitivity of SP-OESs were analyzed and optimized using the gas-mixing system to determine the dependence of the sensitivity on a predetermined gas-mixing ratio. The limit of detection was obtained to evaluate the sensitivity of SP-OESs. We believe that this study provides insights into enhancing SP-OES performance for advanced semiconductor process monitoring.

As semiconductor processes continue to shrink, detecting even minute changes in the composition of process gases or by-products becomes imperative. Therefore, identifying gas species and measuring their exact proportions within a process chamber has become important. A self plasma optical emission spectrometer (SP-OES) analyses residual gases in an exhaust line by detecting the intrinsic wavelengths of species excited by the self plasma module.

In this study, various parameters affecting the detection sensitivity of an SP-OES were analysed and optimised using a gas mixing evaluation system. Nitrogen ($N_2$) was used as a background gas and argon (Ar) as a trace gas. The concentration of the trace gas was precisely varied from 0.1% to 1.8%. The limit of detection (LoD), defined as the minimum concentration that can be reliably detected, was measured to quantify the sensitivity of the SP-OES. Parameters such as integration time for photon collection, operating pressure under the self-plasma module and selected emission wavelengths were systematically investigated to improve sensitivity.

Analysis of the emission wavelengths revealed that despite the highest emission intensity at 750.57 nm, the detection sensitivity at this wavelength was lowest due to spectral interference from $N_2$ at a nearby wavelength. In contrast, minimal interference from $N_2$ resulted in optimal detection sensitivity at 811.55 nm. This indicates that the selection of emission wavelengths with minimal background gas interference is critical to improve detection sensitivity.

In addition, the investigation of the operating pressure showed that the detection sensitivity decreased as the pressure increased from 0.2 Torr to 3.5 Torr. The highest sensitivity was achieved at the lowest pressure tested, suggesting that changes in electron density, electron temperature and electron energy distribution function with pressure influence SP-OES sensitivity. Therefore, optimal plasma discharge pressure and electrode configurations need to be considered for efficient plasma excitation of gas species.

Finally, evaluation of the effects of integration time showed that increasing the integration time improved detection sensitivity by increasing signal intensity and decreasing LoD. However, excessively long integration times could limit real-time monitoring capabilities; therefore, selection of an appropriate integration time is critical in practical semiconductor process applications.

In conclusion, this study has quantitatively demonstrated that the sensitivity of SP-OES is highly dependent on controllable parameters such as emission wavelength selection, operating pressure and integration time. The selection of appropriate wavelengths with minimal interference and the optimisation of operating conditions are essential strategies for improving the sensitivity of SP-OES.

**References**

[1] G. W. Eom Analysis of gas detection sensitivity of a self plasma-optical emission spectrometer using an N2 and Ar gas-mixing evaluation system Appl. Sci. Converg. Technol. 33, 130-134 (2024)

# Spectroscopy plasma characterization in an EM cavity in view of a Massive Open Online Laboratory

M. Santos[1], G. Torres[3], J. Brotankova[2], H. Fernandes[3]

[1] *Instituto Superior Técnico, Universidade de Lisboa, Portugal*
[2]*Faculty of Nuclear Sciences and Physical Engineering, Czech Technical University, Prague, Czech Republic*
[3]*Instituto de Plasmas e Fusão Nuclear, Instituto Superior Técnico, Universidade de Lisboa, Portugal*

The electromagnetic cavity (EM) existing at e-lab is a freely accessible experimental apparatus as part of a remotely controlled laboratory enabling the study of plasma physics and was recently upgraded with a broadband spectrometer. In this communication, we present the advance on the EM cavity in which plasmas can be created through a Penning discharge in view of its integration in a MOODLE course, producing a Massive Open On-line Laboratory with learner's self-assessment.
It's expected that by using the new setup, students will be able to grasp how factors such as the spectrometer sensor integration time and electronic gain, window transmissibility, and plasma density impact the measurements made.

## 1. Introduction

Remote Controlled Laboratories (RCLs) as an educational resource started to emerge in the beginning of this century. elab, a remote controlled laboratory at IST, Lisbon, came to life by the year 2000 and since then has served various physic experiments. Recently, with contributions from IAEA and Fusenet, two remote experiments have been deployed on the advanced laboratory, namely a Langmuir probe and an Electromagnetic Cavity [1]. Both are based on a low frequency RF high voltage power source (50 kHz, 1kV, 2-3W).

## 2. The Electromagnetic Cavity

Recently, the EM cavity was upgraded with a broadband spectrometer in the visible range, ranging from 180 to 1100 nm. This upgrade is intended to introduce learners to spectroscopy studies and how they allow them to identify the plasma composition. Included in the possible studies, a method is introduced to use spectroscopy as a quality process for leak detection and to study the balance between line intensities according to the plasma density, external magnetic field and deposited power.

With the advance in the EM cavity, it is now possible to illustrate for instance how a gas chromatography detector works.

## 3. MOODLE integration

The apparatus remote control room is accessed through a web browser, without the need to install additional software. By integrating it with the FREE platform into a Content Management System (CMS) connected through a Learning Tools Interoperability channel, it leads to an embedded platform that creates a transparent and fluid student experience between the laboratory and the CMS.

The equipment allows the selection of the gas, between Helium, Nitrogen, or Argon, the control of the gas pressure inside the chamber, the selection of the discharge power, and the setting of current in a Helmholtz coil to confine the plasma.

The apparatus was equipped with a microwave spectrum analyzer that allowed the determination of plasma electron density. Experimental results show that by using the installed spectrometer, it's possible to match the peaks measured with each gas to the strong spectral lines available in NIST's database. Furthermore, it is also possible to identify the presence of impurities that get into the cavity through a slow leak by noting the existence of spectral lines that do not match those of the used gases.

In this communication we will characterise (i) this plasma source (ii), its plasma density for different gases and (iii) the conception of a MOOL including students self-assessment using a MOODLE framework.

## References

[1] J Oliveira *et all,* An accessible microwave cavity experiment for plasma density determination, *Eur. J. Phys.* **42** 035203, (2021)
[2] P. Rossa *et al*, A Massive Online Plasma Physics Course Using Remote Controlled Laboratories in Open edX, *6th Experiment@ International Conference* (2023)

# Probing aqueous $NO_3^-$ at the Plasma-Water Interface of a Plasma Electrochemical Reactor by *In-situ* Raman Spectroscopy

K.Polprasarn and D. Z. Pai

*Laboratoire de Physique des Plasmas, CNRS, Sorbonne Université, École Polytechnique, Institut Polytechnique de Paris, 91120 Palaiseau, France*

A major challenge in the synthesis of nanomaterials such as graphene quantum dots (GQDs) using Plasma Electrochemical Reactor (PEC) is the direct and detailed experimental investigation of the plasma-liquid interfacial region. Diagnostics of the plasma-liquid interaction at the interface are necessary for understanding how the plasma transforms the carbon precursor into GQDs [1]. In this work, we have used *in situ* Raman spectroscopy to investigate the aqueous environment using the symmetric stretch vibrational mode of the nitrate anion ($NO_3^-$) as a convenient probe molecule otherwise produced naturally by the PEC reactor.

## 1 Introduction

*In-situ* Raman spectroscopy has been successfully applied to investigating plasma-water interactions[2]. Near the interface, where the detection volume (DV) is low, both the $NO_3^-$ concentration and the spectral width of its Raman spectrum increased relative to the bulk liquid[1]. However, the production of nitrate anions by the plasma was low, resulting in low signal-to-noise ratio. To improve the signal, $NaNO_3$ 500 mM has been introduced in the current work.

## 2 Experimental setup and methods

A PEC was operated at 2.5 kV and 4 mA with a positive-polarity discharge generated in Ar flowing into ambient air at atmospheric pressure, while the solution was grounded using a Pt electrode. Over the course of the 2.5-hour experiment, four cycles of increasing/decreasing detection volume (DV) were controlled by a syringe pump, while plasma heating simultaneously caused the DV to decrease due to evaporation.

The Raman spectra of the symmetric stretching vibrational mode of the nitrate anion ($NO_3^-$) and OH bending mode of water were observed near the plasma-liquid interface. *OH* bend helped us to determine the DV of a given measurement as well as the concentration of $NO_3^-$ upon calibration with reference solutions of known concentration.

## 3 Results and Discussion

Raman spectra of $NO_3^-$ symmetric stretch were acquired *in-situ* at various DV representing the depth below the plasma-liquid interface over which signal is collected. Fits of the Raman spectra of $NO_3^-$ stretch and *OH* bend are obtained using Lorentzian and Gaussian functions, respectively. Fig. 1 compares the Raman spectra of the symmetric stretch mode of $NO_3^-$ at DV values of 18.5%, 45%, 68%, and 100%, which indicate measurements integrated from the plasma-liquid interface down to depths of 49, 119, 180, and 265 µm, respectively. At DV=18.5% the Raman signal appears narrower, with a width of 5.2 $cm^{-1}$ compared to 8.3 $cm^{-1}$ at higher DV. The width of this Raman spectrum is known to depend on liquid temperature. The spectrum broadens at any DV after switching on the plasma, consistent with gradual heating of the liquid. However, the spectral narrowing at low DV would point to cooling of the liquid near the plasma interface, unless another cause is responsible for this observation.

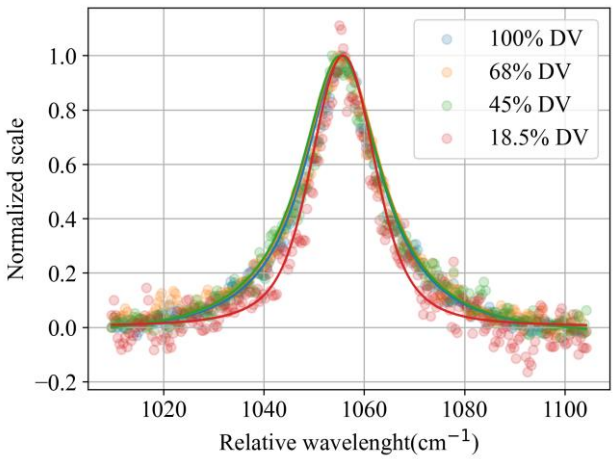



Fig. 1. Normalized Raman spectra of the symmetric stretching mode of $NO_3^-$ measured at different DV, along with corresponding Lorentzian fits.

## References

[1] Kurniawan, D., Caielli, F., Thyagajaran, K., Ostrikov, K. K., Chiang, W. H., & Pai, D. Z. *Nanoscale* **16**, 15104 – 15112 (2024).

[2] Pai, D. Z. *J. Phys. D: Appl. Phys.* **54**, 355201 (2021).

[3] Perrot, M. *J. Phys. Chem.* **87**, 5193–5197(1983)

# 2D Measurement on single-filament dielectric barrier discharge by electric-field induced second harmonic generation

Jianan Wang[1], Hans Hoeft[2], Yihao Guo[1], Anne Limburg[1], and Sander Nijdam[1]

[1]*Eindhoven University of Technology, Eindhoven. The Netherlands*
[2]*Leibniz Institute for Plasma Science and Technology (INP), Greifswald, Germany*

This study investigates the electric field along the propagation of a streamer in a dielectric barrier discharge (DBD) using picosecond electric-field induced second harmonic (E-FISH) generation. A pulsed-driven, double-sided DBD featuring a 1 mm gas gap was investigated using binary $N_2$-$O_2$ gas mixtures at atmospheric pressure. Utilizing an ICCD camera to measure the induced second harmonic signal improves the efficiency of the electric field measurement since no scanning is needed for spatial resolution.

## 1 General

Understanding streamers in low-temperature plasma is important for research and engineering, as the electric field plays a key role in discharge breakdown, streamer propagation, and plasma channel formation [1]. A non-intrusive technique for measuring the electric field is electric-field induced second harmonic (E-FISH) generation [2]. This methodology involves focusing a beam on the plasma and measuring the corresponding induced signal at half the wavelength, which is related to the external electric field strength. However, this method lacks spatial resolution and requires an additional scanning process. To improve the measurable range, an ICCD camera can replace the photomultiplier tube (PMT), allowing an instant 2D image of the signal. In this work, we use E-FISH to measure the electric field along the propagation of a streamer in a dielectric barrier discharge (DBD) and use an ICCD camera to capture the 2D results. In addition, the camera's relatively low sensitivity is also taken into consideration.

## 2 Methodology and primary results

We deployed a high-voltage pulse (10 kV, 200 ns, 10 kHz) dielectric barrier discharge (DBD) in a 1 mm gap, fed with a gas mixture of $N_2$ with 0.1 vol% $O_2$ at 1 bar [3]. The generated streamer propagates along the gap, where the E-field measurement is applied. A picosecond Nd: YAG laser provides the fundamental wavelength at 1064 nm. The laser beam travels through several optical components, becoming a near-collimated beam with a diameter of less than 1 mm. The high pressure enhances the intensity of the E-FISH signal, meeting the sensitivity requirements of the ICCD. This signal is separated from the fundamental wavelength by a dichroic mirror and prism and finally directed to an ICCD camera with a bandpass filter (Figure 1).

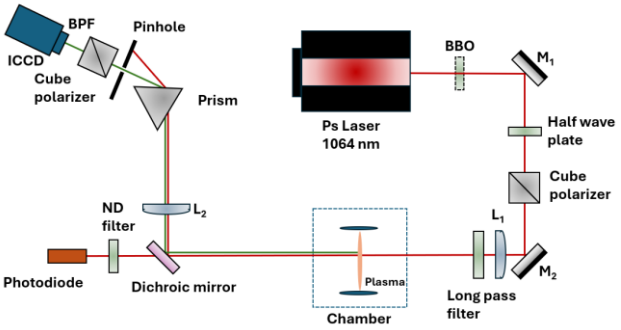



Figure 1. Experimental setup.

The primary results of the E-FISH signal generated from a static electric field (10 kV/cm) are shown in Figure 2. The test condition is close to the minimum field strength during streamer propagation. Further diagnostics will be conducted to solve spatial resolution and E-field calibration. Furthermore, it enhances the understanding of the streamer propagation phase of a DBD.

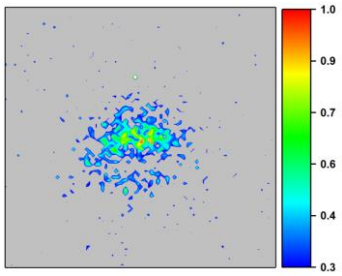



Figure 2. Primary results on ICCD image of raw E-FISH.

This work is supported by the German Research Foundation (DFG) - project number 535827833.

**References**

[1] Nijdam, Sander, et al. Plasma Sources Science and Technology 29.10 (2020): 103001.
[2] Guo, Yihao, et al. Physical Review Research 7.1 (2025): 013051.
[3] Höft, H., et al. Journal of Physics D: Applied Physics 55.42 (2022): 424003.

# AI-Driven Langmuir and Cutoff Probe Diagnostics for Improved Data Consistency

Jeonghun Ko[1], Jongchan Kim[1], June Young Kim[2], and Sanghoo Park[1]*
[1] *Korea Advanced Institutde of Science and Technology (KAIST), Daejeon, Republic of Korea*
[2] *Korea University, Sejong, Republic of Korea*

Electron density and temperature of an argon capacitively coupled plasma at 13.56 MHz were measured radially using a Langmuir probe and cutoff probe. When scanning the probes in the plasma chamber, consistency and reliablity of the probes' data become poor. Here, we report that AI-based data fitting will open a new era of plasma diagnostics.

## 1 Introduction

Langmuir probes have been in use for nearly a century and remain a foundational diagnostic tool in plasma research. Measurements of fundamental plasma parameters, such as electron density and temperature, derived from probe signals are essential for investigating plasmas of interest. Consequently, ensuring the reliability of these parameters via rigorous data processing is critical. However, the inherent sensitivity of probe signals and their strong dependence on human interpretation often compromise consistency. Indeed, even among experienced researchers, large discrepancies can arise when interpreting the same dataset. Here, we present how artificial intelligence (AI) can reduce human bias in post-processing and enhance the reliability of both Langmuir probe (LP) and cutoff probe (CP) data. By employing machine learning techniques for signal analysis, we aim to improve the consistency of LP/CP measurements in capacitively coupled plasma (CCP).

## 2 Method

Our approach is demonstrated using an argon CCP generated between two parallel electrodes ($\phi = 200$ mm) driven by a 13.56 MHz power supply. We employed an in-house, RF-compensated LP integrated with a commercial DAQ system (Impedans Ltd.). For the CP, a microwave cylindrical antenna was designed and optimized (e.g., tip and gap lengths from 7 to 15 mm) according to operating conditions and chamber geometry.

The 'cutoff' (plasma) frequency in measured microwave spectra of CP directly corresponds to electron density based on the wave dispersion relation in unmagnetized plasmas [1]. In practice, significant noise can occur in CCPs, especially when the probe is scanned over the electrodes. This variability complicates determination of the cutoff frequency and thus the inferred electron density.

The LP was used to determine $n_e$ and $T_e$ from the current–voltage (I–V) characteristic via the ion-current analysis and Druyvesteyn method, respectively [2]. Because the I–V curve typically involves multiple regimes (ion saturation, electron saturation, and a nonlinear transition region), fitting procedures strongly affect the extracted plasma parameters. We developed a machine learning-based noise-reduction and curve-fitting framework for LP data to improve precision and consistency. In the future, we anticipate that additional experimental artifacts—stemming from non-ideal behaviors of plasma or probes—will be further mitigated using this AI-based approach.

## 3 Results

Figure 1 presents the radial profile of electron density measured using the LP and CP under a representative condition of 100 mTorr and 300 W. The measured $n_e$ exhibited a bell-shaped distribution, while $T_e$ varies inversely in the range of 1.0–1.5 eV. Although the CP and LP results are broadly consistent, discrepancies in electron density measurements arise at higher pressures, where local plasma perturbations and altered sheath formation can diminish the reliability of CP data.

Addressing these discrepancies through additional experimental optimization and advanced data processing techniques remains as future work to further improve the probes' reliability.

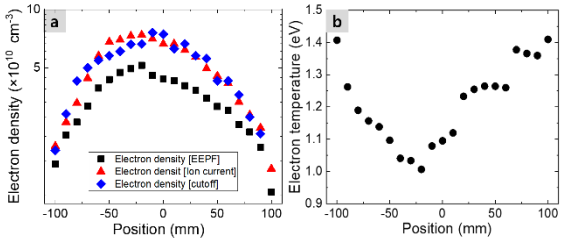



Figure 1. Radial distribution of (a) electron density and (b) effective temperature in the test CCP under conditions of 100 mTorr working pressure and 300 W power.

### References

[1] Kim, S. J. et al. *Plasma Sources Science and Technology* **28**, 055014 (2019).
[2] Godyak, V. A. and Demidov, V. I. *Journal of Physics D: Applied Physics.* **44,** 269501 (2011).

# Three-dimensional characterization of the liquid surface deformation resulting from a pin-water discharge using free-surface synthetic Schlieren

F. Dyson[1], E. Moreau[1] and T. Orriere[1]

[1] *Institut PPrime, Université de Poitiers-ENSMA, CNRS, UPR 3346, Poitiers, France*

This study deals with a three-dimensional measurement of the water surface during a pin-water plasma interaction. This is achieved using free-surface synthetic Schlieren (FS-SS). The discharge regimes studied range from onset corona to stable glow by applying a slow triangular waveform. As well as the effect of different liquid conductivities.

Plasma discharges in contact with liquids can generate reactive species at low energy costs. For this reason, plasma-liquid interactions have gathered a lot of attention in many areas of research [1]. Reactive species are first created in the gas phase and must be transferred by convection or diffusion to the liquid phase before they recombine. In a pin-water electrode geometry with a DC power supply we observed three distinguishable discharge regimes: corona, unstable glow and stable glow [2]. Understanding the interface could provide useful insight for optimizing the aforementioned transfer or regime transitions. Indeed, the liquid electrode in many configurations is deformed, by the electric field, ionic wind or other phenomena. Few papers have studied experimentally the shape of the interface and these rely on 2D methods. By using the free-surface synthetic Schlieren (FS-SS) method developed by Moisy et al. [3], it is possible to measure the topography of the interface in three dimensions.

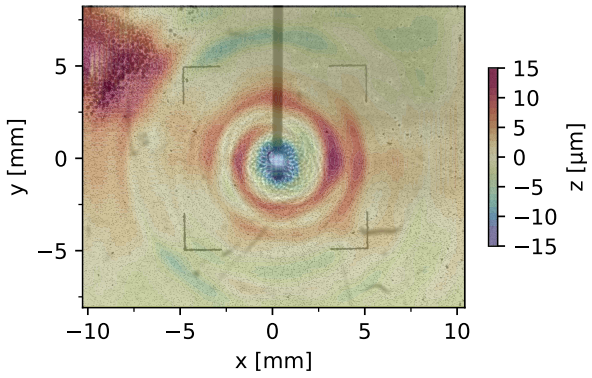



Figure 1: Instantaneous height map of the water surface during unstable glow of 1 mS.cm$^{-1}$ at 1.7 kV and 2.5 mA.

Our reactor consists of a tungsten needle with a 100 $\mu$m radius of curvature placed 2 mm above water contained in a glass cuvette (35x35x32 mm$^3$). The conductivity of the solution is varied from 0.2 $\mu$S.cm$^{-1}$ to 10.0 mS.cm$^{-1}$ by adding $H_2SO_4$. For the FS-SS measurements, collimated light is shone through a motif situated above the water and reaches the lens of the camera below the cuvette. The method is validated by observing a vertical slice of the water. To favour the repeatability of the experiment, a near-DC triangular wave is applied to the pin and the liquid is grounded with a platinum wire. A delay generator is used to synchronise the oscilloscope, the voltage, the light source and the camera. Figure 1 shows the instantaneous shape of the water surface measured with a diluted $H_2SO_4$ aqueous solution of 1 mS.cm$^{-1}$ at 1.7 kV. Capillary waves at the surface originate from the center and propagate outwards with a wavelength of 1.8 mm. In the top left corner bubbles formed from electrolysis perturb the measurement. Omitting this, the surface reaches a high of 13 $\mu$m and a low of -12 $\mu$m underneath the needle. During the positive half cycle, a Taylor cone appears at onset voltage, but soon after the surface is pushed inwards due to the presence of ionic wind. During the negative half cycle, the surface is pushed down with a wider depression than during positive voltage.

This study aims to show the effect of conductivity on the deformation of the liquid electrode at different voltages in a pin-water plasma geometry. Also will be discussed are the limits of the method as we show that steeper deformations are impossible to measure.

## References

[1] Bruggeman, P. J. et al. *Plasma Sources Sci. Technol.*, **25**, 053002 (2016).

[2] Alomari, L., Orriere, T., Batiot-Dupeyrat, C. et al. *Plasma Chem Plasma Process*, 1-29 (2025).

[3] Moisy, F., Rabaud, M. & Salsac, K. *Exp Fluids*, **46**, 1021–1036 (2009).

# Experimental and numerical study of $CO_2$ discharges in contact with liquid water

S. Bois[1], A. Herrmann[1], E. Nicol[2] and O. Guaitella[1]

[1] *Laboratoire de Physique des Plasmas, CNRS, UMR 7648, Univ. Paris-Saclay, SorbonneUniversité, Ecole Polytechnique, France*
[2] *Laboratoire de Chimie Moléculaire, CNRS, UMR 9168, Ecole Polytechnique, France*

Hydrogenation of $CO_2$ is at the core of any $CO_2$ recycling process. Converting $CO_2$ using $H_2O$ would avoid the energy costly step of producing $H_2$. In this work two plasma-liquid interaction configurations are studied. In the first one, streamers are generated above the liquid surface, and in the second one a plasma enhanced electrolytic system is investigated. The first one provides intense transient electric fields while the second one provides continuous electrolytic current and solvated electrons in the liquid. For these two configurations, both the plasma development and the molecules induced in the liquid phase are studied.

## 1 Introduction

Plasma discharges in contact with liquids have been shown to induce chemical reactions in the liquid phase, especially in the case of air plasmas interacting with water. The processes taking place at the plasma-liquid interface are extremely complex: the transfer of plasma-activated species into the liquid phase enables new chemical paths to be induced. This could be a way of efficiently recycling $CO_2$, by providing a cheap and abundant source of hydrogen to convert $CO_2$ into value added products, therefore responding to the climate emergency. Among the plasma-liquid interaction configurations likely to generate the most reactive species for synthesizing molecules dissolved in the liquid phase, two very different configurations are often used: streamer configurations above a liquid, and plasma-assisted electrolysis reactor configurations. In this work, both configurations are used with a $CO_2$ atmosphere to evaluate the possibility of generating organic molecules in the liquid phase.

## 2 Pulsed nanosecond discharges in contact with water

The experimental protocol used in this part is greatly inspired by [1], and has been adapted for $CO_2$ atmosphere. A schematic representation of the experimental setup used in this part is shown in Figure 1. A pulsed power supply generating pulses of 100-500 ns, with rise time ~20 ns and frequency up to 5kHz is used to ignite discharges under air or $CO_2$ atmosphere in a point-plane configuration. A ground electrode is immersed in the water reservoir filled with MilliQ water. An iCCD camera mounted vertically enables to image the streamers propagation on the water surface. The evolution of water conductivity and pH are also monitored as function of the time of exposure to the plasma. Analysis of current peaks correlated with the fast imaging provides information on the energy deposited in each streamer branch.

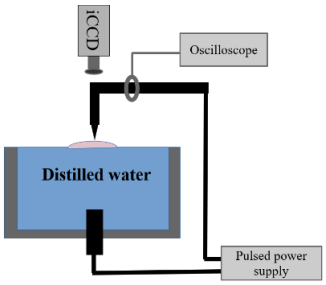



**Figure 1:** experimental setup of the pin to plane discharge configuration

A statistical study enables to determine the number of streamers created on the liquid surface and their propagation speed. These results are then compared with the model developed previously [1]. After plasma exposure the liquid is analysed using high resolution mass spectrometry (HR-MS) and headspace gas chromatography mass spectrometry (HS GC-MS).

## 3 Plasma enhanced electrolysis

This configuration consists in creating a negatively biased DC discharge under $CO_2$ atmosphere above MilliQ water (similar as [2]). An anode (grounded) plunges in the water as well. Various materials are tested for the electrodes because of the catalytic capacity of some metals. Like for the pin to plane configuration, conductivity and pH evolution are monitored and the liquid phase are analysed using MS for different exposure times to the plasma.

### References

[1] A. Herrmann, Étude expérimentale et modélisation de la dynamique spatiotemporelle de décharges nanosecondes impulsionnelles en contact avec l'eau (2024).
[2] R. Hawtof et al, Science advances (2019).

# Fast Electron Promoting Geometry for Plasma Enhanced Thermionic Generators

A. Clark[1], V. Demidov[2], S. Adams[2] and Z. Zhang[1]

[1] *University of Tennessee, Knoxville, TN, USA*
[2] *Air Force Research Laboratory, Wright-Patterson Air Force Base, OH, USA*

It is proposed in this text that bounding geometry between thermionic electrodes in a plasma enhanced system can improve power density of the thermionic energy converter. This text explores a conical shaped boundary for a pulsed plasma across a tungsten-cerium boride electrode pair and the current generation at 1400°C emitter temperature. The concept shows applicability of pulsed plasma thermionic enhancment optimized by specific geometry promoting high velocity electrons.

## 1 Introduction

This work applies concepts of thermionic generation at emitter cathode temperatures of 1400°C enhanced by argon plasma between the thermionic electrodes generated by a pulsed bias. Previous work has shown that thermionic generation can be enhanced using pulsed plasma discharge [1] where enhancement occurs just after discharge in the plasma afterglow. The additional concept of promoting fast electrons via conical gemoetry was performed by V. Demidov *et al.* [2] using a continuous DC plasma in helium. Additionally, work has been ongoing using a tungsten-ceriumboride electrode pair with injected argon plasma to observe argon plasma enhancement between the two [3].

The plasma enhancement uses a pulser capable of up to 300kHz and 10kV, though the experiment only utilizeses between 200V and 600V similar to that in [1]. Observations are made just after the bias voltage is terminated during the plasma afterglow between each pulse. This is to maximize thermionic electron flow, while minimizing power input for the pulsed plasma generation. This is also to limit the number of electrons collected due to the plasma discharge. A conical boundary is carries the same polarization as the emitter cathode so to promote electrons to remain in the gap and only terminate on the cold collector plate. The combination of tungsten and a boride collector has shown to be capable of thermionic generation [1,3] at extreme temperatures above 1400°C.

Cerium boride is used in this case as it ongoing work using injected plasma enhancement in argon has shown higher current generation at temperatures between 1500°C and 1800°C. The graph in table 1 shows a comparision of the two borides in such a case with varying injected plasma enhancement voltages and an additional 25 volt bias applied across the thermionic electrodes. By altering how the plasma is generated and bounding the plasma in the conical geometry, it is this configuration that can be optimized for greater thermionic generation.

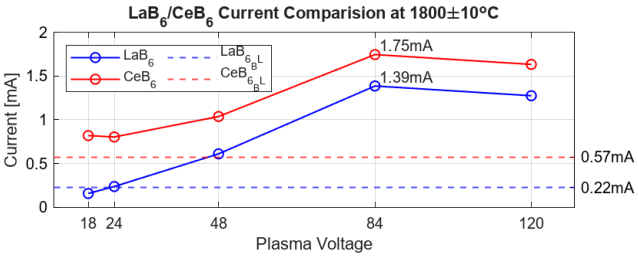



Figure 1: Comparison of lanthanum hexaboride and cerium boride collectors paired with a tungsten emitter of various injected plasma enhancement voltages. Thermionic electrodes have a 25 volt bias applied to the circuit.

Continued optimization of this device has the potential to improve power output with minimal power input resulting in a safe way to plasma enhance a thermionic generator. Extreme temperature applications of this could be done in atmosphere and be able to utilize waste heat, or other direct heat to electricity applications.

## References

[1] Alderman, B. A., *et al.* Pulsed Thermionic Power Conversion with Positive Work Function Difference. *48th AIAA Aerospace Sciences Meeting*, **AIAA 2010-1344**, (2010).

[2] Demidov, V. I., *et al.* Gas-discharge Plasma Sources for NPT. *Applied Physics Letters*, **91**, 201503 (2007).

[3] Clark, A. M., *et al.* Application of a Plasma Based Thermionic Generator for High-Temperature Surfaces *AIAA SciTech 2024 Forum*, **AIAA 2024-2245**, (2024)

# Analysis of the correlation between TEOS plasma characteristics and $SiO_2$ thin film properties

Yushi Sato[1], Sukma Wahyu Fitriani[1], Yousei Kurosaki[1], Kunihiro Kamataki[1], Daisuke Yamashita[1], Takamasa Okumura[1], Naoto Yamashita[1], Naho Itagaki[1], Kazunori Koga[1], and Masaharu Shiratani[1]

[1]*Graduate School and Faculty of Information Science and Electrical Engineering, Kyushu University, 744 Motooka, Nishi-ku, Fukuoka, 819-0395, Japan*

We studied a method to estimate silicon dioxide ($SiO_2$) thin film quality through plasma parameter measurements. By using the Insulated Pulse Probe (IPP), we enable plasma parameter measurements even in reactive plasmas to estimate the quality of deposited $SiO_2$ films. In this study, we successfully measured plasma parameters in TEOS plasma, a reactive plasma, and observed a strong correlation between deposition rate and plasma density ($n_p$).

This study explores the relationship between TEOS plasma parameters and $SiO_2$ thin film quality in Plasma-enhanced chemical vapor deposition using tetraethylorthosilicate (TEOS-PECVD), a key technique in semiconductor fabrication. Using the Insulated Pulse Probe (IPP), we measure electron density ($n_e$) and temperature ($T_e$) in reactive plasma to clarify their impact on film quality.

Experiment was conducted using a capacitively coupled plasma reactor [3] with a showerhead RF electrode (diameter: 75 mm), a ground electrode (diameter: 60 mm), and an electrode spacing of 10 mm (gas: TEOS, $O_2$, and Ar, RF frequency: 13.56 MHz, pressure: 0.3~2 Torr). Plasma parameters were measured using IPP installed at the position of the plasma bulk. For verification of the IPP measurement results, we compared them with results obtained by the Langmuir Probe (LP) method in Ar plasma.

Figure 1 shows RF power dependence of $n_e$ and $T_e$ in Ar plasma (0.3 Torr, 10 sccm Ar, 20-60 W) using IPP and LP methods. This figure demonstrates that increasing RF power leads to an increase in $n_e$ and a decrease in $T_e$, as indicated by similar values obtained from both probes.

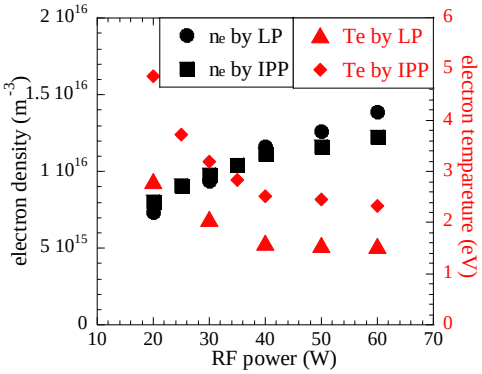



Figure 1: RF power dependence of $n_e$ and $T_e$ in Ar plasma measured by IPP and LP

Figure 2 shows $O_2$ flow rate dependence of $n_p$ and $T_e$ in TEOS/$O_2$/Ar Plasma measured by IPP (2 Torr, 10 sccm TEOS and Ar, 10-100 sccm $O_2$, 40 W). This figure shows $n_p$ increased from $1.19\times10^{16}$ $m^{-3}$ to $1.25\times10^{16}$ $m^{-3}$ and then decreased to $1.23\times10^{16}$ $m^{-3}$, while the deposition rate increased from 50 nm/min to 220 nm/min and then decreased. These results suggest that plasma density is, to some extent, correlated with radical flux and deposition rate under these conditions [4]. Further details will be presented at the conference.

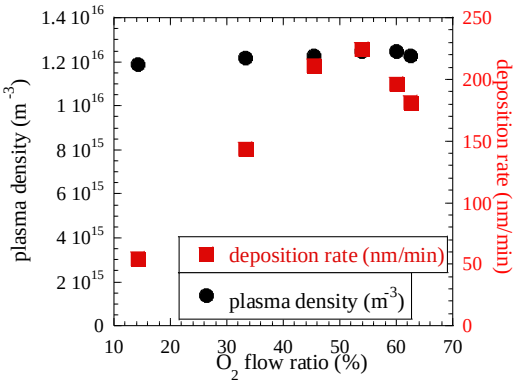



Figure 2: $O_2$ flow ratio dependence of $n_p$ in TEOS/$O_2$/Ar Plasma measured by IPP and deposition rate of $SiO_2$

This work was partly supported by JSPS KAKENHI (Grant No. JP24H00205 and No. JP23K03368).

## References

[1] M. Deguchi, Ph.D thesis, Kyoto Univ. (2003).
[2] M. Deguchi, et al., Jpn. J. Appl. Phys., 37, 970 (1998).
[3] K. Kamataki, et al., 2022 AIP advance, 12, 085220 (2022).
[4] M. Hori, et al., J. Plasma Fusion Res., 91, 5, 317 (2015).

# Understanding $CF_4/H_2$-based cryogenic etching mechanisms by monitoring radical densities with extended optical actinometry technique

M. K. T. Mo[1], S.-N. Hsiao[1], M. Sekine[1], M. Hori[1], and N. Britun[1]

[1]*Center for low-temperature plasma sciences, Nagoya University, Nagoya, Aichi, Japan*

The etching of silicon nitride with reduced substrate temperatures was studied using optical emission spectroscopy to better understand changes in etching mechanisms during cryogenic plasma processing. Actinometry using multiple argon line-ratios were used to obtain absolute densities of key reactive species, F and H, and relative densities of etch products, CN and NH. Consequently, contrasting behaviour of these products with decreasing substrate temperature was found, with an increase in NH being favoured. This indicates that the etching mechanism changes as a result of low temperature enabling particular surface reactions.

## 1. Introduction

Fabrication of 3D NAND flash storage devices requires highly selective etching between layers of $SiO_2$ and SiN. Consequently, etching at cryogenic temperature is of interest since it improves etching characteristics [1]. Under these conditions, the etch rate (ER) of SiN decreases at lower temperatures [2,3] unless given sufficient bias voltage [3,4]. Fluorinated gases with added hydrogen can also lead to formation of $(NH_4)_2SiF_6$, resulting in a different etch pathway [4]. In this work, optical actinometry is applied to measure both absolute and relative radical densities, and the specific etching mechanisms and its influence on ER that occur with reduced substrate temperature.

## 2. Experimental

A plasma of $CF_4/H_2$ (total 50sccm, 3.3Pa) was generated in a dual-frequency industrial-grade reactor as described in [5], with up to 4% trace rare gases added for both actinometry and electron temperature, $T_e$, determination. $H_2$ content (20-70%) and substrate temperature, $T_{sub}$ (25ºC to -60ºC) were varied while emission of radical species, F(703nm) and H(486nm), and etch products of CN(385nm), NH(336nm) and $N_2$(337nm) were measured. Absolute densities of F and H were calculated using multiple actinometric pairs to minimise the uncertainty [5], whereas N-containing molecule densities were estimated relative to F. Similarly, multiple line ratios of krypton and xenon with argon were used to obtain an average $T_e$.

## 3. Results and discussion

F and H densities appear unaffected by $T_{sub}$, but up to twice the amount of NH was obtainable as seen in fig. 1. The lower substrate temperature reduces the volatility of $(NH_4)_2SiF_6$ formed on SiN, and NH is released through subsequent ion interactions with this layer. The ER also increased by up to 40% overall at -60ºC. With increasing $H_2$%, the relative density of all etch products reduces – since less $CF_4$ is available, so too are ions e.g. $CHF_2^+$ that carry out reactive ion etch.

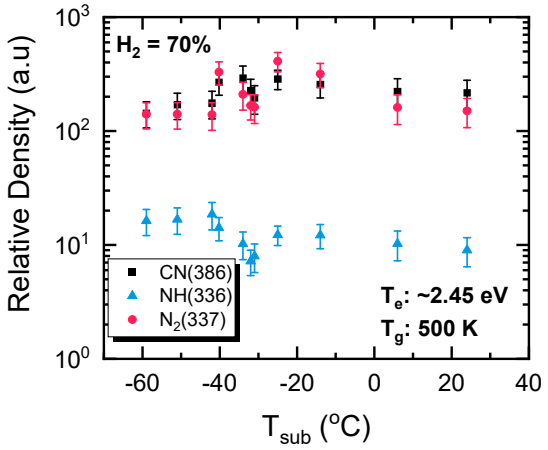



Figure 1: Relative densities of CN, NH and $N_2$ as a function of substrate temperature and $H_2$ = 70%, using electron excitation cross-section for F($^2p^o$ 3/2).

**References**

[1] S. Tachi et al., *Appl. Phys. Lett.*, **52** (1988) 616
[2] S.-N. Hsiao, et al., *Vacuum*, **210** (2023) 111863
[3] R. Dussart, et al., *J. Appl. Phys.*, **133** (2023) 113306
[4] S.-N. Hsiao, et al., *ACS Appl. Electron. Mater.*, **5** (2023) 6797
[5] N. Britun, et al., *J. Appl. Phys.*, **136** (2024) 111101

# Polymerization of EDOT into soluble PEDOT analogue by plasma inside bubble

Y. Kaneko[1], S. Kawai[2] and H. Takana[1]

[1] *Institute of Fluid Science, Tohoku University, Miyagi, Japan*
[2] *Graduate School of Mechanical and Aerospace Engineering, Tohoku University, Miyagi, Japan*

Poly(3,4-ethylenedioxythiophene) (PEDOT) is a conductive polymer synthesized by the polymerization of 3,4-ethylenedioxythiophene (EDOT). Conventional chemical synthesis adds non-conductive additives to impart water-solubility, which in turn lowers conductivity. In this study, a new synthesis of soluble PEDOT analogue via radical polymerization induced by plasma inside bubbles is demonstrated. FT-IR and mass spectrometry confirmed the successful synthesis of PEDOT oligomers from dimers to pentamers. Furthermore, there is an optimal $O_2$ concentration in plasma forming gas for the conductivity of the PEDOT film.

## 1 Introduction

Poly(3,4-ethylenedioxythiophene) (PEDOT), one of the conductive polymers, is synthesized by the polymerization of 3,4-ethylenedioxythiophene (EDOT) [1]. Despite PEDOT exhibits high conductivity, thermal and chemical stability, and transparency, insolubility of PEDOT causes poor processability. A conventional chemical synthesis method requires non-conductive additives to impart water-solubility, which in turn lowers conductivity [2]. In this study, radical polymerization of EDOT into soluble PEDOT analogue is demonstrated by plasma inside bubbles.

## 2 Method

An EDOT dispersion (1.0 wt.%) is prepared by ultrasonic emulsification of EDOT in pure water. Ar and $O_2$ mixture as a plasma forming gas is introduced through a glass tube with a hole, which is inserted into a reactor tube filled with the EDOT emulsion, and bubbles are generated from the hole. Applying an AC high-voltage (2.4 $kV_{pp}$, 50 kHz, duty ratio of 50%) between a rod electrode inside the glass tube and mesh electrode surrounding the test tube, barrier-discharge is generated inside a bubble for radical polymerization of EDOT. The conductivity of the PEDOT film prepared by drop casting of the processed dispersion is measured using four-point probe method.

## 3 Results

Molecular structure analysis by FT-IR and mass spectrometry confirmed that the proposed method successfully synthesizes PEDOT oligomers from dimers to pentamers with water-solubility. Figure 1 shows the conductivity of the PEDOT film for $O_2$ concentration in the plasma forming gas. An optimal concentration for maximizing conductivity clearly exists. More disruption of the molecular structure is caused by higher energy electrons as $O_2$ concentration increases, which leads to a deterioration in PEDOT film conductivity.

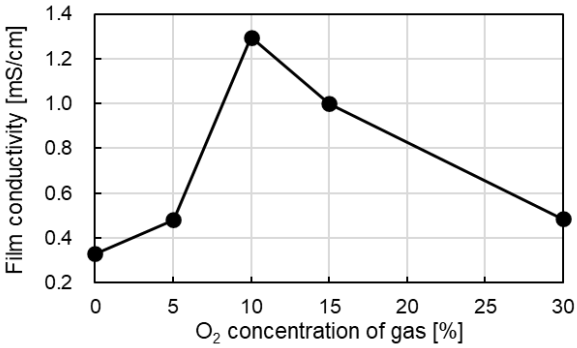



Fig. 1 PEDOT film conductivity as a function of $O_2$ concentration in plasma forming gas.

## 4 Conclusions

This study demonstrated synthesis of soluble PEDOT analogue using plasma inside bubble. The experimental results show that there is an optimum $O_2$ concentration in plasma forming gas to maximize the conductivity of the fabricated PEDOT film.

**References**

[1] Kayser, L. V. and Lipomi, D. J. Stretchable conductive polymers and composites based on PEDOT and PEDOT: PSS *Advanced Materials* **31**, 1806133 (2019).

[2] Fan, X., Nie, W., Tsai, H., Wang, N., Huang, H., Cheng, Y., Wen, R., Ma, L., Yan, F., and Xia, Y. PEDOT:PSS for flexible and stretchable electronics: modifications, strategies, and applications. *Advanced Science* **6**, 1900813 (2019).

# High power impulse magnetron sputtering of a chromium target

Kateryna Barynova[1], Tetsuhide Shimizu[2], Daniel Lundin[3], Martin Rudolph[4], and Jon Tomas Gudmundsson[1,5]

[1] *Science Institute, University of Iceland, Dunhaga 3, IS-107 Reykjavik, Iceland*
[2] *Department of Mechanical Systems Engineering, Graduate School of Systems Design, Tokyo Metropolitan University, 6-6, Asahigaoka, Hino-shi, 191-0065 Tokyo, Japan*
[3] *Plasma and Coatings Physics Division, IFM-Materials Physics, Linköping University, SE-581 83 Linköping, Sweden*
[4] *Leibniz Institute of Surface Engineering (IOM), Permoserstraße 15, 04318 Leipzig, Germany*
[5] *Division of Space and Plasma Physics, School of Electrical Engineering and Computer Science, KTH Royal Institute of Technology, SE-10044 Stockholm, Sweden*

High power impulse magnetron sputtering (HiPIMS) discharges with a chromium target are studied experimentally and by applying the ionization region model (IRM). The $Cr^+$ is found to be the dominating ion in the discharge. The back-attraction probability of the sputtered species decreases with decreasing pulse length, and with increasing peak discharge current density.

High power impulse magnetron sputtering (HiPIMS) discharges [1] with a chromium target are studied experimentally and by applying the ionization region model (IRM) [2]. For a given pulse length the deposition rate decreases and the ionized flux fraction increases with increased discharge current density in the range 0.4 – 1.0 A/cm$^2$. The measured chromium ionized flux fraction is in the range 10 – 50 %, highest for the highest peak discharge current density, and the shortest pulse length studied. The deposition rate increases as the pulse length is reduced from 200 $\mu$s, exhibits a maximum for pulse length of around 50 $\mu$s, and then decreases as the pulse length is further reduced to 25 $\mu$s. It is found that the singly charged chromium ion is the dominant ion at the target surface and consequently the discharge operates in the self-sputter operating regime.

Two internal discharge parameters, the probability of ionization, and the probability of back-attraction of the sputtered species provide a quantitative insight into the quality of a deposition process and its efficiency are shown in Figure 1 versus pulse length. We see in Figure 1 (a) that the probability of ionization $\alpha_t$ increases at first and then decreases as the pulse length is increased. Figure 1 (b) shows that the back-attraction probability $\beta_t$ increases with increasing pulse length and decreases with increased peak discharge current density as had been hinted [3]. Recall that a decrease in the back-attraction of the sputtered species has positive influence on both the deposition rate and the ionized flux fraction. The back-attraction probability of the sputtered species decreases with decreasing pulse length, and with increasing peak discharge current density.

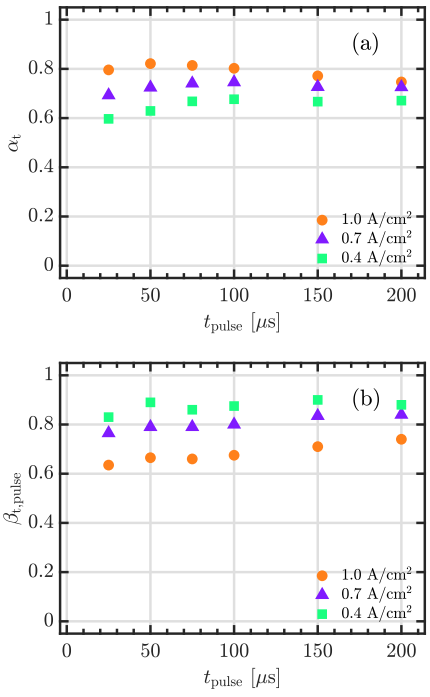



Figure 1: (a) The ionization probability $\alpha_t$ and (b) the back-attraction probability $\beta_{t,pulse}$ determined by the IRM versus the pulse length. The working gas was argon at 0.3 Pa and the target was 150 mm diameter chromium disk.

## References

[1] J. T. Gudmundsson et al., *J. Vac. Sci. Technol. A*, **30**, 030801 (2012).
[2] C. Huo, et al., *J. Phys. D: Appl. Phys.*, **50**, 354003 (2017).
[3] N. Brenning et al., *J. Vac. Sci. Technol. A*, **38**, 033008 (2020

# Investigating early-stage helium-tungsten interactions: Retention and vacancy defects characterization

M. Alfazzaa[1], Z. Hu[1], T. Sauvage[1], F. Foucher[1], O. Wendling[1], P. Desgardin[1], J. Joseph[1], and M-F Barthe[1]

[1] *CNRS, Université d'Orléans, CEMHTI UPR 3079, Orléans, France*

In this study, the retention of helium in tungsten and the formation of vacancies are investigated at a fundamental level. Polycrystalline and monocrystalline W samples are exposed to low-pressure $^3$He plasmas with fluxes as low as $1.0\times10^{16}$ $m^{-2}s^{-1}$. Preliminary results of NRA, AFM, and positron annihilation spectroscopy are combined to explore the mechanisms of He self-trapping in W.

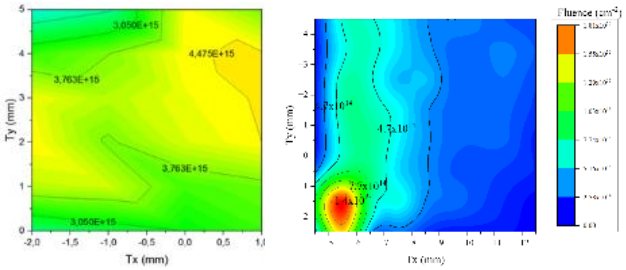
## 1 Context

In future nuclear fusion reactors like ITER, the tungsten (W) divertor will withstand hydrogen isotopes and helium (He) ion fluxes of the order of $10^{24}$ $m^{-2}s^{-1}$ at the strikeline [1]. In particular, He atoms being not soluble in W, they tend to agglomerate, leading to the formation of He-filled nanovoids (bubbles) [2]. Notably, most models of Helium retention assume that He is a mobile species that accumulates at pre-existing defects, such as grain boundaries, vacancies, and vacancy clusters, a process referred to as "trap-mutation". However, an alternative mechanism, known as He self-trapping, is also possible, where under a sufficient $He^+$ flux, mobile $He_n$ clusters can form in W [3]. Once the cluster size exceeds a temperature-dependent threshold, the lattice stress displaces a W atom, creating a vacancy (V) and a self-interstitial atom (SIA). This self-trapping process can thus be described by the reaction: $He_n \rightarrow He_nV + SIA$ [4]. Recent thermal desorption results reveal a self-trapping threshold flux of He in monocrystalline W at about $7\times10^{16}$ $m^{-2}s^{-1}$ at an energy of 130 eV [5]. Furthermore, a saturation of the total retained He fluence in the crystalline matrix at a given incident ion energy has already been observed in both simulations and experiments [6]. Understanding helium retention and defect formation under low-flux He exposure at a fundamental level is critical, as it represents the initial stage of interaction and the precursor to bubble formation. These processes can also ultimately lead to alterations in macroscopic properties such as swelling, hardening, and changes in thermal conductivity.

## 2 Methods and Findings

In this work, re-crystallized polycrystalline and monocrystalline W samples are exposed to $^3$He plasmas at room temperature using maximum incident ion energies of ~300 eV (below the He sputtering threshold), fluxes as low as $1.0\times10^{16}$ $m^{-2}s^{-1}$ and an incident fluence of about $1.0\times10^{20}$ $m^{-2}$ (corresponding to the saturation of the W matrix with He at this energy).

Nuclear Reaction Analysis (NRA) with a 900 keV $D^+$ beam is used to quantify the $^3$He-implanted dose via the reaction: $^3He(^2H,^4He)^1H$. 2D mapping across the entire sample surface are performed to evaluate the homogeneity of the plasma (e.g, Figure 1). On the other hand, Atomic Force Microscopy (AFM) is employed to assess the roughness-induced modifications of the sample and also reveals the presence of non-burst He bubbles at the surface. Furthermore, Doppler Broadening - Positron Annihilation Spectroscopy (DB-PAS) permits probing vacancies, vacancy clusters and He-vacancy complexes generated by He self-trapping.




a/ b/

Figure 1: 2D maps of the $^3$He implanted fluence acquired from a W monocrystalline sample using NRA under fluxes of: (a) $3\times10^{17}$ $m^{-2}s^{-1}$ (homogeneous) and (b) $1.3\times10^{16}$ $m^{-2}s^{-1}$ (inhomogeneous).

**References**

[1] R. A. Pitts et al., *Journal of Nuclear Materials* **438**, S48–S56 (2013).
[2] M. Ialovega et al., *Nuclear Fusion* **62**, 126022 (2022).
[3] L. Pentecoste et al., *Acta Materialia* **141**, 47-58 (2017).
[4] W. D. Wilson et al., *Phys. Rev. B* **24**, 5616 (1981).
[5] A. Dunand et al., *Nuclear Materials and Energy* **34**, 101324 (2023).
[6] L. Pentecoste et al., *Journal of Nuclear Materials*, **470**, 44-54 (2016).

# Development and Investigation of a Miniature Pulsed Plasma Thruster Using Graphite Propellant

A.Kh. Suleimenova[1], Zh.B. Igibayev[1], M.K. Dosbolayev[1]

[1]*Institute of Experimental and Theoretical Physics, al-Farabi Kazakh National University, Almaty, Republic of Kazakhstan*

To achieve miniaturization, a pulsed plasma thruster with graphite propellant for nanosatellites was developed and investigated in a vacuum environment simulating space conditions.

## 1 General

With the rapid advancement of miniature space technologies, a compact pulsed plasma thruster has been developed and investigated as a continuation of previous research [1,2]. Graphite was selected as the propellant, which simultaneously serves as the igniting electrode. A potential of 100 V was applied to the igniting electrode relative to the cathode (Figure 1).

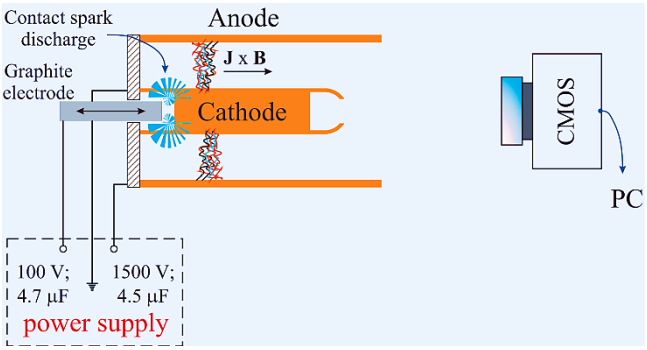



Figure 1. Schematic diagram of the experimental setup

The study focused on the electrical, thrust-energy, and plasma structural characteristics of the thruster [3,4]. The operating voltage ranged from 800 to 1500 V, with a capacitor capacitance of 4.5 μF and a discharge current of 1.3 kA. At a discharge energy of 4.5 J, the impulse bit was measured at 9 μN·s.

The plasma plume structure was analyzed using spectroscopic methods, revealing the presence of fuel ions in various ionization states. The plasma flow velocity was evaluated using high-speed imaging and probe diagnostics [5].

This work was supported by the Ministry of Education and Science of the Republic of Kazakhstan (project no. IRN AP19576858).

**References**

[1] Levchenko I., Bazaka K., Ding Y., Raitses Y., Mazouffre S., Henning T., Klar P.J., Shinohara S., Schein J., Garrigues L., Kim M., Lev D., Taccogna F., Boswell R.W., Charles C., Koizumi H., Shen Y., Scharlemann C., Keidar M., Xu S. Space micropropulsion systems for Cubesats and small satellites: From proximate targets to furthermost frontiers. *Applied Physics Reviews* **5**, 011104 (2018).

[2] Dosbolayev M.K., Igibayev Z.B., Tazhen A.B., et al. Preliminary Study of the Solid-State Pulsed Plasma Thruster Model with Graphite as a Propellant. *Plasma Physics Reports* **48**, 263-270 (2022).

[3] Li Z., Zhang Q., Zhang Y., et al. A review on plasma diagnosis technology of pulsed plasma thruster. *Journal of Physics: Conference Series* **1952**, 032087 (2021).

[4] Riazantsev A., Jakubczak M., Cichorek O., Kurzyna J. Side and front fast imaging of solid and liquid fed ablative pulsed plasma thruster's discharge. *Acta Astronautica* **225**, 583–591 (2024).

[5] Tazhen A.B., Dosbolayev M.K., Igibayev Z.B., et al. Generation and Diagnostics of Pulse Plasma Flows. *Plasma Physics Reports* **46**, 393-400 (2020).

# Self-regulation in high-power impulse magnetron sputtering discharges and its effect on the metal ion escape

Kateryna Barynova[1], Nils Brenning[2,3], Swetha Suresh Babu[1], Joel Fischer[3], Daniel Lundin[3], Michael A. Raadu[2], Jon Tomas Gudmundsson[1,2], and Martin Rudolph[1,2]

[1] *Science Institute, University of Iceland, Dunhaga 3, IS-107 Reykjavik, Iceland*
[2] *Division of Space and Plasma Physics, School of Electrical Engineering and Computer Science, KTH Royal Institute of Technology, SE-10044 Stockholm, Sweden*
[3] *Plasma and Coatings Physics Division, IFM-Materials Physics, Linköping University, SE-581 83 Linköping, Sweden*
[4] *Leibniz Institute of Surface Engineering (IOM), Permoserstraße 15, 04318 Leipzig, Germany*

The impact of self-sputter yields on high power impulse magnetron sputtering discharges has been studied for a number of target materials. The electron temperature and the ion-back attraction probability are found to decrease with increased self-sputter yield of the target material.

In high power impulse magnetron sputtering (HiPIMS) discharges a significant fraction of the sputtered atoms becomes ionized as they pass through the dense plasma of the ionization region [1]. The impact of self-sputter yields in 35 HiPIMS discharges operated in argon is studied, for 7 different target materials, using the ionization region model (IRM) [2]. We find the electron temperatures to be correlated inversely with the self-sputter yield of the target material. This can be explained by the atomic composition in the ionization region shifting from argon-dominated at low sputter yields to metal-rich at high sputter yields. This has implications for the metal ion escape in a HiPIMS discharge, since the ionization mean free path of sputtered atoms depends on the electron temperature. As a result, ionization in metal-rich discharges (lower electron temperature) occurs, on average, further away from the target surface, where the remaining potential hill they have to climb to escape, is lower [3]. Metal ions in those discharges can therefore escape more easily to the substrate region compared to metal ions in metal-poor discharges. The ion back-attraction in the IRM is formally described as the probability that an ion created in the ionization region is back-attracted toward the target during the pulse. Figure 1 shows the back-attraction probability $\beta_{\mathrm{t,pulse}}$, for the discharges studied here, as a function of the sputter yield. The trend clearly shows a significant decrease, with values starting at around 0.95 for low sputter yield carbon discharges and dropping to approximately 0.55 for high sputter yield copper.

To conclude, discharges with high target materials, such as chromium or copper, can be sustained at a lower electron temperature because they are rich in easily ionized metal atoms and the sputtered species are ionized further away from the cathode where the electric potential is flatter compared to the target vicinity. Discharges with low sputter yieled target materials, such as carbon or titanium, are argon-dominated and metal-poor, and higher electron temperature is needed to sustain the observed high discharge currents. As a side effect, sputtered metals ionize close to the target vicinity where they are subjected to strong back-attracting fields, increasing the loss in deposition rate.

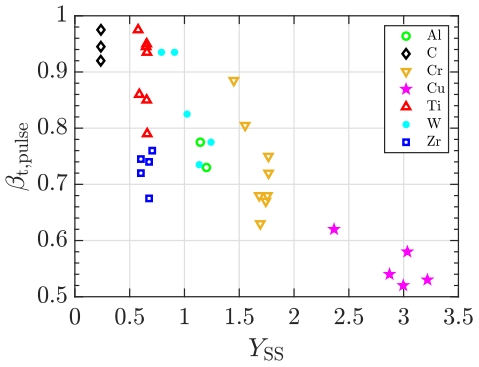



Figure 1: The target ion back-attraction probability as a function of self-sputter yield.

## References

[1] J. T. Gudmundsson, N. Brenning, D. Lundin, and U. Helmersson, *J. Vac. Sci. Technol. A*, **30**, 030801 (2012).

[2] C. Huo et al.D. Lundin, J. T. Gudmundsson, M. A. Raadu, J. W. Bradley, and N. Brenning, *J. Phys. D: Appl. Phys.*, **50**, 354003 (2017).

[3] J Held, V. Schulz-von der Gathen and A. von Keudell, *Plasma Sources Sci. Technol.*, **32**, 065006 (2023).

# Effect of ion energy and magnetic shear on suprathermal ion transport in X-point plasmas in TORPEX

C. Sepulchre[1], S. P. H. Vincent[1], M. Baquero-Ruiz[1], and I. Furno[1]

[1] *École Polytechnique Fédérale de Lausanne (EPFL), Swiss Plasma Center (SPC), CH-1015 Lausanne, Switzerland*

The transport of suprathermal ions is studied in TORPEX, a low temperature toroidal plasma device, around a magnetic X-point. The ions are injected close to the maximum of plasma density fluctuations and the ion transport is studied for two ion energies. This talk presents experimental results showing that the suprathermal ion transport depends on the ion energy, and that the magnetic shear, modifying the background plasma profiles and characteristics, has an effect on the beam shape.

## 1 Motivation

Understanding the transport of suprathermal ions (or fast ions, FI) in plasmas is crucial in tokamaks, and of major interest in astrophysics. Since extensive spatio-temporal characterization (both in tokamaks and outer space) is challenging, low temperature plasma devices, such as TORPEX, a toroidal basic plasma experiment (R = 1 m, a = 0.2 m), are essential for fundamental FI transport studies.

## 2 Experimental setup

In this work, hydrogen plasmas (base pressure $\sim 5.10^{-5}$ mbar) are produced and sustained in an X-point magnetic geometry, with the toroidal magnetic field $B_{tor}$ being much larger than the poloidal magnetic field $B_{pol}$. Plasmas are characterized with four sets of *in-situ* Langmuir probes. The plasma parameters (density and potential time averaged and fluctuation profiles), the dominant modes of the fluctuations, and the turbulent transport are presented [1]. The magnetic shear $s$, defined as the sharpness of the change in the pitch angle of a field line, is varied and is shown to significantly modify several plasma properties.

$^6Li^+$ ions are produced using a miniaturized thermo-emitter and are injected in the area of the plasma where the dominant plasma modes are propagating. The FI injection energy is $E_{ion} \simeq 30$ or 70 eV, being much larger than the background plasma electron temperature ($T_e \lesssim 5$ eV). The emitter is toroidally moved to vary the propagation time $t$ of the beam. FI are detected by a gridded energy analyzer (GEA) placed at a fixed toroidal position but moving in the poloidal plane ($X$,$Z$) during a discharge to reconstruct the FI beam profile. By combining ($X$,$Z$) data for several $t$, the 3D FI beam is reconstructed and transport properties are computed.

## 3 Suprathermal ion results

The suprathermal ion transport is investigated in X-point plasmas. The transport is quantified by fitting $\sigma_X^2 \propto t^\gamma$, where $\sigma_X^2$ is the horizontal variance of the FI beam and $\gamma$ is the transport exponent. It is shown that $\gamma$ depends on $E_{ion}$, with a transition from super- to sub-diffusive when $E_{ion}$ increases (i.e. a decrease from $\gamma > 1$ to $\gamma < 1$). These results are compared with previous studies conducted in TORPEX in a simple magnetic geometry [2].

The impact of the background plasma profiles on FI propagation is also studied, by varying the magnetic shear $s$. While the impact on the FI transport is observed to be negligible, there is a significant influence of the background plasma profiles on the beam shape.

## 4 Outlook

This study will be extended to other injection positions to observe the interaction between suprathermal ions and the X-point, and to quantify the effect of turbulent cross-field transport on the FI propagation.

## References

[1] C Sepulchre, S. P. H. Vincent, P. Quigley, M. Baquero-Ruiz, and I. Furno. Impact of the magnetic shear on plasma equilibrium and turbulent transport at the vicinity of an x-point in torpex. *submitted to Physics of Plasmas*, 2025.

[2] A. Bovet, A. Fasoli, P. Ricci, I. Furno, and K. Gustafson. Nondiffusive transport regimes for suprathermal ions in turbulent plasmas. *Phys. Rev. E*, 91:041101, Apr 2015.

# Discussion on the Definition of Excitation Temperature of Weakly Ionized Plasmas in a Non-equilibrium State

K. Kikuchi and H. Akatsuka

*Institute of Science Tokyo, 2-12-1-N1-10, O-Okayama, Meguro-ku, Tokyo, 152-8550, Japan*

In non-equilibrium plasmas, the electron energy distribution function (EEDF) and excited state number density distribution generally do not follow the Boltzmann distribution. Even for such non-equilibrium states, it may be possible to define the temperature $T$ as $1/T = \partial S/\partial U$ using the entropy $S$ and internal energy $U$ in statistical mechanics. In this calculation, however, the principle of entropy maximization should be applied. In the case of non-equilibrium, non-extensive Tsallis entropy is one of the candidates rather than Gibbs entropy. This study focuses on the excited-state density distribution in hydrogen plasma and the EEDF in low-temperature weakly-ionized plasma, by various temperatures newly defined using the non-extensive entropy.

The collisional-radiative (CR) model gives the number density of excited states of the $i$-th excited level, using electron temperature $T_\mathrm{e}$ and density $N_\mathrm{e}$, and the number density of the atomic ground state [1]. Even for such non-equilibrium plasma, the temperature $T$ of the excited-state distribution should be defined as $1/T = \partial S/\partial U$, where $S$ and $U$ denote the entropy and the internal energy, respectively, from a statistical mechanical perspective [2]. However, if the Gibbs entropy is applied, the principle of entropy maximization is not taken into account, which cannot be tolerated from the viewpoint of statistical physics. In the present study, the excited state density distribution in hydrogen plasma is focused on with the CR model calculation, and various temperatures newly defined from its Tsallis entropy $S_q$ are reconsidered, which is defined as follows [3]:

$$S_q \equiv k\frac{1-\sum_i p_i^q}{q-1}. \tag{1}$$

Under the following constraints

$$\sum_{i=1}^{w} p_i = 1, \quad \frac{3}{2}\frac{\sum_{i=1}^{w} p_i^q \epsilon_i}{\sum_{j=1}^{w} p_j^q} = U_q \equiv \frac{3}{2}kT_{\langle U_q\rangle}, \tag{2}$$

the Lagrange multiplier method mathematically proved that maximizing the Tsallis entropy $S_q$ gives the probability distribution $p_i$ as follows [3]:

$$p_i = \frac{1}{Z_q}\exp_q\left[-\frac{\beta}{\sum_{j=1}^{w} p_j^q}(\epsilon_i - U_q)\right] \tag{3}$$

where $Z_q$ is the $q$-partition function given as

$$Z_q(\beta) = \sum_{i=1}^{w}\exp_q\left[-\frac{\beta}{\sum_{j=1}^{w} p_j^q}(\epsilon_i - U_q)\right]. \tag{4}$$

with the Lagrange multiplier $\beta$ and the $q$-exponential function as $\exp_q$. When $\beta_q$ is defined as $\beta_q \equiv \beta/(\sum_{j=1}^{w} p_j^q)$, the temperature of the system is also consistently defined as $T_{q-\beta} \equiv 1/(k\beta_q)$. The obtained $T_{q-\beta}$ coincides with the physical temperature derived in accordance with the zero-th law of thermodynamics, which is calculated as $T_{q-\mathrm{Tsallis}}$ as follows:

$$T_{q-\mathrm{Tsallis}} = \left(1 + \frac{1-q}{k}S_q\right)\left(\frac{\partial S_q}{\partial U_q}\right)^{-1}. \tag{5}$$

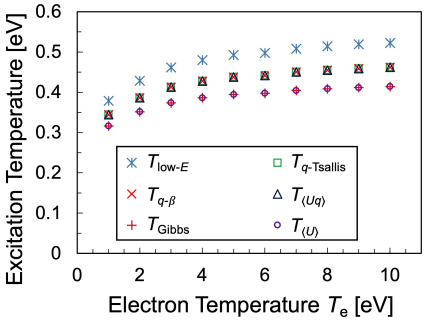



Figure 1: Excitation temperatures plotted against $T_\mathrm{e}$ [3].

Under the preparation described above, the excited level populations of atomic-hydrogen plasma were calculated with hydrogen CR model [4]. It is shown that the excited-state distribution is better fitted with the $q$-distribution function than with the Boltzmann distribution function. Figure 1 shows the comparison between various temperatures defined for the hydrogen plasma. The calculation also shows that the temperatures $T_{\langle U_q\rangle}$, $T_{q-\beta}$ and $T_{q-\mathrm{Tsallis}}$ are in good agreement, and it is possible to derive a consistent Tsallis temperature $T_{q-\mathrm{Tsallis}}$ [3].

## References

[1] Akatsuka, H. *Adv. Phys. X*, **4**, 1592707 (2019).
[2] Akatsuka, H. and Tanaka, Y. *Entropy*, **25**, 276 (2023).
[3] Kikuchi, K and Akatsuka, H. *Entropy*, **25**, 1400 (2023).
[4] Shimizu, Y. *et al. IEEE TPS*, **43**, 1758 (2015).

# Study of the transport and optical properties of WDM taking into account local field correction

S. Kodanova[1,2], M. Issanova[1,2], N. Djienbekov[1,2], A. Uderbayeva[1,2] and N. Turekul[1,2]

[1] *Al-Farabi Kazakh National University, Almaty, Kazakhstan*
[2] *Institute of Applied Sciences and Information Technology, Almaty, Kazakhstan*

A combination of an effective potential approach and the molecular dynamics (MD) method was employed to investigate the influence of the local field correction on ion transport properties in the warm dense matter regime. As an example, we considered hydrogen dense plasma. The MD simulations were performed within a microcanonical ensemble, and the analysis included calculating the mean squared displacement (MSD) and velocity autocorrelation function (VAF) of the particles. The MSD and VAF are used to compute the diffusion coefficient of ions. The results are compared with the data computed neglecting the electronic exchange-correlation effects. Furthermore, the viscosity coefficient of ions was evaluated using the Green-Kubo relation, which links viscosity to the stress autocorrelation function. The optical properties of hydrogen at different temperatures and densities were also investigated.

## 1 General

The study of matter at high densities in astrophysical objects and modern experiments with high-intensity lasers is of great interest for many applications. Confirmation of the existence of dense hydrogen under high pressure will allow the development of theories about new states of matter. This, in turn, can find application in describing the state of matter in extreme conditions, such as the cores of planets and stars at different stages of their evolution [1-2]. Theoretical and experimental studies of dense hydrogen are also motivated by interest in the problems of warm dense matter in condensed matter physics and applications to research on inertial confinement thermonuclear fusion [3]. Also, the dense hydrogen medium at various temperatures is actively studied experimentally, where knowledge of the transport and optical properties is important for understanding the experimental results [4-5].

In the states of a heated dense matter, ions are usually strongly correlated and nondegenerate. The use of the exact theory of exchange-correlation effects is of decisive importance for many interesting physical phenomena, such as the calculation of material properties, electrical and thermal conductivity, stopping power, etc. As a result of using the expansion of the reciprocal of the electron permittivity with the use of the local field correction, which contains all the exchange-correlation effects, the effective potential was obtained [6]. To study the influence of electronic exchange-correlation effects on the transport and optical properties of hydrogen at high densities using the molecular dynamics method, this work is supposed to use this potential.

## 2 Results and discussion

The transport and properties of hydrogen at high pressures can be calculated accurately taking into account the correction of the local field correction based on ab initio Quantum Monte-Carlo simulations data. The local field function (LFC) contains all the exchange-correlation effects in a wide range of densities and temperatures. Using the local field correction approach, we have computed diffusion, viscosity, thermal conductivity. We used the MSD of ions to compute the diffusion coefficient at long time scales. Additionally, we used the VACF of ions to find the diffusion coefficient employing the Green-Kubo relation connecting the VACF with the diffusion coefficient. These two methods allowed us to crosscheck our results for the diffusion coefficient. Similar analysis of the viscosity coefficient computed using corresponding Green-Kubo relations. Optical properties of hydrogen at different temperatures and densities were also obtained using the structure factor of the ion component from molecular dynamics and the quantum theory of electron-ion collisions. The impact of electronic exchange-correlations effects on transport and optical properties are discussed and compared with available experimental data.

**References**

[1] Clérouin J. et al, *Phys.Rev.Lett.* **116**, 115003 (2016)
[2] Fortney J. J. et al, *Space Sci. Rev.* **152**, 423 (2010)
[3] Tahir N.A., *Phys. Rev.E*. **63**, 016402 (2000)
[4] Craxton R.S. et al, *Phys. Plasmas* **22**, 110501 (2015).
[5] Hurricane O.A. et al, *Nature* **506**, 343 (2014)
[6] Moldabekov Z.A. et al, *Contrib. Plasma Phys.* 202000176 (2022).

# Plasma deposition of III-V semiconductors: sputtering and RPVPE approaches

L. Srinivasan[1,2], L. Watrin[1,2], A. Eurosi[1,2], D. Meurice[1], P. Roca i Cabarrocas[1,2], K. Ouaras[1,*]

[1] *LPICM, CNRS, Ecole polytechnique, Institut polytechnique de Paris, Route de Saclay, 91128 Palaiseau, France.*
[2] *IPVF, Institut Photovoltaïque d'Ile-de-France (IPVF), 91120, Palaiseau, France.*
**Correspondence: karim.ouaras@polytechnique.edu*

We develop plasma processes to synthesize III-V thin films at both lower temperature and cost than conventional MOCVD or MBE techniques. We show room-temperature growth of polycrystalline GaN using reactive sputtering, and high-quality GaAs epitaxy at 500 °C via Remote Plasma VPE, supported by both materials and plasma analysis.

## 1 Introduction

The semiconductor (SC) industry is facing increasingly complex and demanding requirements, driven by the growing global need for high-performance devices. At the same time, ongoing economic and ecological challenges call for more affordable, energy-efficient, and environmentally friendly SC growth processes. In response, LPICM has launched a new research initiative focused on developing low-temperature, low-cost plasma processes for depositing III-V materials (GaN and GaAs), which offer superior yet complementary optoelectronic properties to silicon. Leveraging the advantages of plasmas, we developed two in-house plasma reactors, namely Reactive Sputtering and Remote-Plasma Vapour Phase Epitaxy (RPVPE), detailed in [1] and [2], respectively. This approach contrasts with conventional epitaxial techniques like MBE and especially MOCVD [3] that require high growth temperatures (600–1000 °C), which hinder hetero-epitaxy with mismatched materials due to thermal stress leading to defect formation. Moreover, MOCVD—widely used in the industry—operates at near-atmospheric pressure and consumes large volumes of toxic and costly gases to ensure uniform precursor distribution, contributing to the high production cost of III-V materials, restricting their use.

## 2 Results

Figure 1.a&b shows some features of the GaN and GaAs thin films synthetized by sputtering and RPVPE, respectively. As far as GaN is concerned, the growth was performed at room temperature, on Si substrates as shown in the TEM image (Figure 1.a). Under these conditions, we successfully produced polycrystalline films. When it comes to GaAs, we used RPVPE at 500°C to achieve excellent homo-epitaxy as shown in the cross-section SEM micrograph in Figure 1.b. The main findings related to spectroscopic investigations of the plasma along with further results related to the properties of the synthetized films will be presented in this talk.

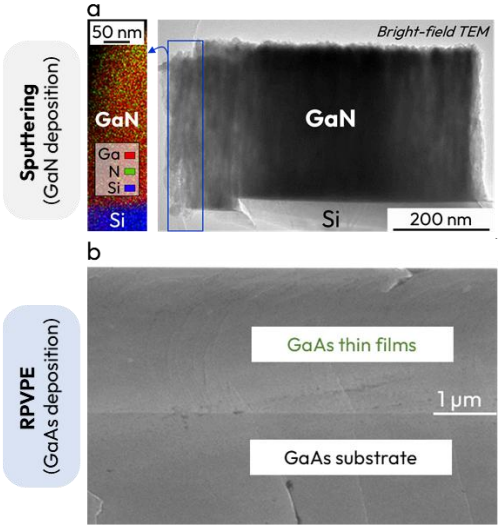



Figure 1. Typical images of the III-V growth.

### References

[1] L Srinivasan, C Jadaud, F Silva, J-C Vanel, J-L Maurice, E Johnson, P Roca i Cabarrocas, K Ouaras. Reactive Sputtering Deposition of Polycrystalline GaN Thin Films on Silicon Substrates at Room Temperature. *Journal of Vacuum Sci. and Technology A*, 41, 053407 (2023).

[2] L Watrin, F Silva, L Largeau, N Findling, M Al Katrib, M Bouttemy, K Dembélé, N Vaissière, C Jadaud, Pl Bulkin, J-C Vanel, EV Johnson, K Ouaras, P Roca i Cabarrocas. Homoepitaxial growth of device-grade GaAs using low-pressure remote plasma CVD. *Materials Science in Semiconductor Processing*, 186, 109069 (2025).

[3] R D Dupuis, Metalorganic Chemical Vapor Deposition of III-V Semiconductors. *Science* 226, 623-629 (1984).